Australian National University

Research School of Chemistry

College of Science

Carbidos, Carbonyls, Carbenes, and Carbynes – The Reactivity of the Bridging C_1 Ligand

Harrison J. Barnett

Submitted in partial fulfilment of the requirements for the degree of Doctor of Philosophy (PhD) at the Australian National University

January 27, 2022

George: *You can't stop modern science. Can't stop it, you can't stop it. Can't stop science. Can't be stopped, no way, no how, science just marches--*

Elaine: *Shut up, George.*

George: *Shut up?*

Elaine: *Yeah.*

George: …*Interesting.*

- *Seinfeld*, S03E09

ABSTRACT

Dimetallacumulenic μ-carbido complexes have appeared sporadically in the literature over a number of years. Their scarcity in the literature reflects the lack of generalisable synthetic routes, their syntheses having been largely serendipitous. These issues have precluded any attempt to understand the chemistry of the μ-carbido ligand or explore any potential reactivity. The work described herein sets out to lay the foundation for μ-carbido reactivity studies.

Chapter One provides a comprehensive overview of dimetallacumulenic μ-carbido chemistry to date. The introduction focusses on the historical development of pathways for their synthesis and examines key characterisational information including their ^{13}C NMR features and solid-state molecular structures. The scant reactivity studies performed previously are outlined thereby highlighting current limitations of the knowledge base.

Chapter One continues with results pertaining to ligand-based reactivity starting from **$[Rh_2(\mu\text{-}C)Cl_2(PPh_3)_4]$**. The replacement of the monodentate phosphine ligands with bridging bidentate phosphines provided the complexes **$[Rh(\mu\text{-}C)Cl_2(L_2)_2]$** ($L_2$ = dppm, dcpm, dcpe, dppp, dppf). The installation of polydentate ligands bearing both hard and soft donor atoms was achieved with success found for both 2,2'-bipyridyl (**$[Rh_2(\mu\text{-}C)(bipy)_2(PPh_3)_2](PF_6)_2$**) and trithiacyclononane ligands (**$[Rh_2(\mu\text{-}C)(9S3)_2(PPh_3)_2](PF_6)_2$**). The first successful functionalisation in this work of the cumulenic μ-carbido ligand was achieved upon addition of sulfur and selenium, forming the μ_2-chalcocarbonyl complexes **$[Rh_2(\mu\text{-}CE)Cl_2(\mu\text{-}dppm)_2]$** (E = S, Se). Reactivity of these μ_2-chalcocarbonyl complexes with both HBF_4 and MeOTf was explored, forming μ-hydride **$[Rh_2(\mu\text{-}CE)H(FBF_3)Cl_2(\mu\text{-}dppm)_2]$** and μ-alkylselenolatocarbyne **$[Rh_2(\mu\text{-}CSeCH_3)Cl_2(\mu\text{-}dppm)_2]OTf$** products, respectively.

Chapter Two is centred around oxidation addition processes using halogen sources. Halogenation of **$[Rh_2(\mu\text{-}C)X_2(\mu\text{-}dppm)_2]$** using $PhICl_2$ (X = Cl) or pyridinium tribromide (X = Br) successfully oxidised both rhodium centres to rhodium(III), though inferred migration of a halide onto the μ-carbido ligand led to the formation of the first structurally characterised μ_2-halocarbyne complexes in **$[Rh_2(\mu\text{-}CX)(\mu\text{-}X)X_4(\mu\text{-}dppm)_2]$ (X = Cl, Br)**. The halocarbyne ligand could successfully undergo nucleophilic substitution with TMS-imidazole to furnish an imidazole carbyne complex **$[Rh_2(\mu\text{-}CIm)(Im)(HIm)Br_2(\mu\text{-}dppm)_2]$**. The chlorination of the sterically

more encumbering complex **[Rh_2(μ-C)Cl_2(μ-dppf)$_2$]** yielded the diamagnetic rhodium(II) species **[Rh_2(μ-C)Cl_4(μ-dppf)$_2$]**.

Chapter Three describes the synthesis of the first isolable and structurally authenticated bent μ-carbido complexes which could be achieved through addition of activated alkynes RC≡CR' (R, R' = CF_3, CO_2Me, CO_2Et) to **[Rh_2(μ-C)Cl_2(μ-dppm)$_2$]**. The formation proceeds via formal [3+2] cycloaddition reactions to generated five-membered metallacycles that include a bent μ-carbido ligand (Rh–C–Rh: 124.7(10)°−128.4(2)°). The bent carbido ligands in **[Rh_2(μ-C:)(μ-RCCR'))Cl_2(μ-dppm)$_2$]** have properties reminiscent of an Arduengo N-heterocyclic carbene (NHC), which was exemplified through coordination to linear coinage metal addenda, forming rare examples of trigonal $μ_3$-carbido complexes **[Rh_2(μ-C-M)(μ-RCCR')Cl_2(μ-dppm)$_2$]** (R = R' = CO_2Me; M = AuCl, CuCl, Au(C_6F_5)). Addition of sulfur and selenium generated further examples of m_2-chalcocarbonyl compounds **[Rh_2(μ-CE)(μ-DMAD)Cl_2(μ-dppm)$_2$]** (E = S, Se) in reactions that parallel those of Arduengo carbenes with chalcogens to afford chalcourea derivatives. Chlorination of the μ-carbido complex yielded the cationic $μ_2$-halocarbyne complex **[Rh_2(μ-CCl)(μ-DMAD)Cl_2(μ-dppm)$_2$]$^+$**.

To further interrogate the NHC/MHC analogy, Chapter Four provides an in-depth quantification of the electronic properties of MHCs. The selenium adducts **[Rh_2(μ-CSe)(μ-RCCR')Cl_2(μ-dppm)$_2$]** were explored and the ^{77}Se NMR chemical shifts compared to the framework previously developed for NHC/selenourea chemistry. This led to the discovery that the stabilisation of the 'carbene' by the metal centres causes it to have high π-acidity relative to more conventional NHCs.

Chapter 5 demonstrates that the μ-carbido ligand could be directly involved in cycloaddition reactions across the Rh=C bond. The [2+2] cycloaddition of benzyne across one of the Rh=C bonds was achieved, which formed a rare example of a metallacyclobutadiene or cyclometallated benzylidyne species **[Rh_2($μ_2$:$κ^2$-CC_6H_4)(μ-Cl)(Ph)Cl_2(μ-dppm)$_2$]**. The oxidative cyclometallation of a cyclopropenium salt [*cyclo*-C_3Ph_3]PF_6 was accomplished, resulting in the formation of a metallacyclopentadiene salt **[Rh_2($μ_2$:$κ^2$-CC_3Ph_3)Cl_2(μ-dppm)$_2$]PF_6**. Following only a single prior report of a group 9 $μ_2$-carbyne complex **[Rh_2(μ-CC_6H_4Me-4)(CO)($η^5$-C_5Me_5)$_2$]$^+$**, these metallacyclic carbynes join the halo, imidazolyl and alkylselenolato carbynes described in previous chapters to significantly broaden the field.

Difficulties in the NMR characterisation of dirhodium μ-carbido complexes are addressed in Chapter Six with recourse to selective enrichment and multi-dimensional multinuclear NMR protocols. The development of a suitable ^{31}P-^{13}C HMQC and a new three-dimensional ^{1}H-^{31}P-^{13}C NMR pulse sequence was achieved, which successfully and indirectly detected the μ-carbido resonance for a number of complexes. The prevalence of phosphines as co-ligands in organorhodium chemistry offers many other avenues for these techniques to be of use. Optimisation of the synthesis for **$[Rh(^{13}CS)Cl(PPh_3)_2]$** allowed for the cost-effective generation of **$[Rh_2(\mu\text{-}^{13}C)Cl_2(PPh_3)_4]$**. Indirect detection of the ^{103}Rh resonances for a range of μ-carbido complexes was possible using ^{31}P-^{103}Rh HMQC NMR.

ACKNOWLEDGEMENTS

There are a decent amount of people I need to thank for helping me finish this thesis. Let's start with the obvious. Tony (Prof. Hill if we're getting all formal), you've been an outstanding supervisor over the last 4/5 years. Few have the intellect you possess, and I've never been afraid of approaching a problem because I know you'll have a solution. Thank you for trusting me with the ever-expensive rhodium supply, and to make my own research pathway decisions.

To Dr Ben Frogley, or Froggles as he likes to be called by his best friends. You thankfully arrived a few months into my failing honours project and have been the most amazing postdoc ever since. Not only are you probably the most talented chemist I know, but you've definitely influenced my outside of the lab life, including my music taste and career pathways. I know you're not pursuing academia and it is their loss, not yours. I will miss being in the lab with you.

To the Hill Group. The old gentry (Kathy, Yong-Shen, Chee, and Richie) who helped me sort my life and lab skills out when I was an appalling chemist at the start of Honours. And the new guard; Ray Ray, Stevie, Lachlie, and Burty. You've made the lab an incredible experience and made academia a fun and enjoyable place to be, which is hard to say for the rest of the department. You'll all do great, and I know the lab is in safe hands (probably safer) with me leaving.

To the collaborators and technical staff who made data analysis and acquisition a breeze. Hugo, you're a comp wizard and I'm ever grateful you agreed to hop on board and beep boop the things that I never could. To Dr Gareth Nealon in UWA, getting ^{103}Rh NMR data was a crazy idea that only worked because you could do it. At the ANU, to Anitha, Mike, Jo, and Doug, thank you for keeping the machines running and helping throughout my studies.

To my family and friends. You largely just put up with me saying random technical terms and didn't ask too often what I actually research or when I would finish. Your ongoing support and gaming sessions have been crucial to my success. To Jess, you've been my go-to for everything and my rock when I needed someone to lean against. I wouldn't be here without your love and care, and I know I'll be reading a similar passage in your thesis in the not-too-distant future.

And finally, to my parents. You've supported my journey through university and a PhD without doubting me or my capabilities. I always know you have my back if I ever need it, and your love and encouragement to let me pursue this will never be forgotten. I owe all of this to you two.

DEDICATION

This statement confirms that all the work presented in this thesis, unless otherwise appropriately referenced, is my own.

Harrison John Barnett

27/01/22

CONTENTS

Episode Three: Revenge of the NHCs

Episode Four: A New Class

Episode Five: The Alkyne Strikes Back

Episode Six: Return of the Resonance

ABBREVIATIONS

{^{1}H} - protium decoupled NMR

BINAP - 2,2'-bis(diphenylphosphino)-1,1'-binaphthyl

Bp - hydrobis(pyrazol-1-yl)borate

Bp* - hydrobis(3,5-dimethylpyrazol-1-yl)borate

CCDC - Cambridge Crystallographic Data Centre

Cp - cyclopentadienyl

Cp* - pentamethyl cyclopentadienyl

DBT – dibenzothiophene

dcpe – bis(dicyclohexylphosphino)ethane

dcpm - bis(dicyclohexylphosphino)methane

dmpm - bis(dimethylphosphino)methane

dppe - 1,2-bis(diphenylphosphino)ethane

dppf - 1,1'-bis(diphenylphosphino)ferrocene

dppm – bis(diphenylphosphino)methane

DCM – dichloromethane (methylene chloride)

ECP – Effective Core Potential

ESI – Electrospray Ionisation (Mass Spectrometry)

HBF_4 – tetrafluoroboric acid

HCl - hydrochloric acid

HMQC – Heteronuclear Multiple Quantum Correlation

IR - Infrared (spectroscopy)

$^{n}J_{AB}$ - n-bond coupling constant between two nuclei A and B

MHC – *Metalla*-Heterocyclic Carbene

MS – Mass Spectrometry

NHC – *N*-Heterocyclic Carbene

NMR - Nuclear Magnetic Resonance (spectroscopy)

OTf – triflate

Ph – phenyl

PMe_3 - trimethylphosphine

PPh_3 - triphenylphosphine

r.t. – room temperature

SR DFT – Scalar Relativistic Density Functional Theorem

SO – Spin Orbit Coupling

TBAF – tetrabutylammonium fluoride

TBAT – tetrabutylammonium triphenyl fluorosilicate

tBu – tertiary butyl

THF - tetrahydrofuran

Tp - hydrotris(pyrazol-1-yl)borate

Tp* - hydrotris(3,5-dimethylpyrazol-1-yl)borate

EPISODE ONE – THE PHANTOM CARBON

PART ONE:

REVIEW OF DIMETALLACUMULENIC μ-CARBIDO COMPLEXES

1.1 PREFACE

The aim for the prefaces to each chapter is to have the abstract from a paper that the work has been published in. Due to its size, this chapter diverges into a few avenues of reactivity. The abstract chosen is from the paper that started it all:

H. J. Barnett, L. K. Burt, A. F. Hill, *Dalton Trans.,* **2018**, 47, 9570.

The reaction of **[RhCl(CS)(PPh$_3$)$_2$]** with excess catecholborane affords the cumulenic carbido complex **[Rh$_2$(μ-C)Cl$_2$(PPh$_3$)$_4$]** which undergoes phosphine and halide substitution to afford a range of complexes in which the Rh=C=Rh spine remains intact. Amongst these, the reactions with K[L] (L = $H_2B(pz)_2$, $H_2B(pzMe_2)_2$, $HB(pz)_3$; pz = pyrazol-1-yl) afford **[Rh$_2$(μ-C)(PPh$_3$)$_2$(L)$_2$]** whilst with K[$HB(pzMe_2)_3$] the unsymmetrical complex **[Rh$_2$H(μ-C)(μ-C$_6$H$_4$PPh$_2$-2){HB(pzMe$_2$)$_3$}$_2$]** is obtained in which the carbido ligand spans d^6-Rh(III) and d^8-Rh(I) centres.

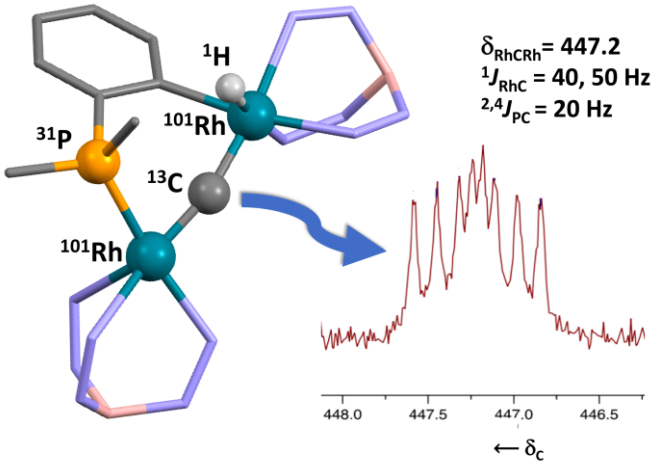

Figure 1.0: Abstract graphic

1.2 INTRODUCTION

It should be noted that the following introduction had been written as part of a larger literature review in partnership with L. K. Burt on the entirety of μ-carbido chemistry. It was intended to be submitted to Chem. Rev., however, an excellent review was (rather poorly timed) quite recently published on the same topic by Reinholdt and Bendix.[1] *The introduction presented here focuses primarily on Class A μ-carbido chemistry and none of this work that has been published to date.*

1.2.1 The μ-carbido ligand

The interstitial carbon atoms in metal carbide compounds are referred to as 'carbido' ligands. Monoatomic carbon in these structures can be described by one of two alternate forms; as either a tetra-anionic carbon (C^{4-}), or the neutral or zerovalent bis-carbene form (:C:).[i] The carbido ligand can bridge several metal atoms in a variety of modes {μ_n: n = 2, 3, 4, 5, 6}, thus being described as high-nuclearity (μ_4–μ_6) or low-nuclearity (μ_2 or μ_3). High-nuclearity carbido compounds have been implicated as functional, albeit ill-defined, components in chemical processes such as the reductive incorporation of carbon monoxide into hydrocarbons by the Fischer–Tropsch fuel synthesis,[2] and the nitrogen fixation capabilities of the FeMo nitrogenase cofactor in bacterial enzymes.[3] In contrast, lower nuclearity carbido complexes (μ_2 and μ_3) have been far less explored, yet have been suggested as models to study fundamental reactivity that may occur on the surface of metal carbides.[4]

1.2.2 Classification of μ_2-carbido complexes

Prior to the beginning of this work, the lowest nuclearity (μ_2-) carbido complexes could be described by one of three bonding forms (**Chart 1.1**), and the bonding description reflects the electronic requirements of the bonded metal termini. The canonical forms consist of the symmetrical Class A with two metal-carbon double bonds, and the asymmetric Classes B and C

[i] Since oxidation state is defined as the charge left on an element when bonding electrons are transferred to the more electronegative element, if we employ Pauling's electronegativity scale then it seems appropriate to also defer to his concept of electroneutrality and eschew assigning implausibly high charges to donor atoms in these highly covalent compounds. Accordingly, throughout, and especially for rhodium complexes (PE(Rh) = 2.28) since the electronegativity difference with carbon (PE(C) = 2.55) is small, we shall arbitrarily, but for consistency, consider a Class A carbido ligand as neutral.

with a metal-carbyne ligand and single or dative (polar-covalent) coordination to a second metal centre, respectively.

This introduction will focus on compounds that fall within the Class A dimetallacumulenic bonding description, as it is the focus of this work. An introduction to Class B and C carbido complexes is provided below, but a more in-depth analysis of the synthesis and reactivity of Class B and C complexes can be found in the review of Reinholdt and Bendix.

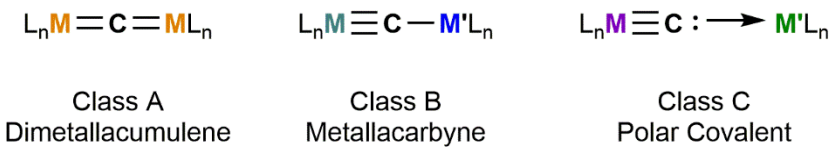

Chart 1.1: Bonding descriptions of μ_2-carbido complexes

1.2.3 Class B – Metallacarbynes

When the metal termini of a μ_2-carbido complex differ, a model consistent with class B is often most appropriate. A difference between metal termini provides an electronic inequity, relaying the difference through the carbido ligand with simultaneous bond elongation and contraction. These species have been labelled as 'metallacarbynes' alluding to carbyne chemistry pioneered by Fischer and Schrock, denoting the coexistence of formal triple and single metal-carbon bonds in the one molecule, that best accommodate the Effective Atomic Number (EAN) requirements (1 vs 3 valence electrons) of the disparate metals. Indeed, some examples have arisen via modification of a pre-formed carbyne ligand. The first metallacarbyne species, **[WRu(μ-C)(O^{t}Bu)$_3$(CO$_2$)(Cp)]** was reported by Selegue and co-workers in 1987, some years after the development of Class A μ-carbido chemistry.[4]

Synthesis

Although the total number of metallacarbynes currently forms the minority of the classes A–C, they benefit from a significant number of available synthetic pathways. A metallacarbyne,

$[(tBuO)_3W{\equiv}C–Ru(CO)_2(\eta\text{-}C_5H_5)]$,[ii] was first achieved by Selegue through an alkyne scission between the carbyne complex **[W(≡CEt)(O^{t}Bu)$_3$]** and the alkynyl species **[Ru(-C≡CMe)(CO)$_2$(Cp)]**. Since then, numerous methods have emerged such as: nucleophilic substitution,[5] Umpolung,[6] transmetallation,[7] selenium extrusion from isoselnocarbonyls,[8] and oxidative addition (**Scheme 1.1**),[9] as well as a methylidene ligand decomposition for which intimate mechanistic details have yet to emerge.[10] One of the two metal termini in this class are comprised mainly of group 6 elements, largely reflecting their predominance in bearing carbyne motifs, and the general, though perhaps merely historical, decrease in prevalence for later transition metal carbynes.

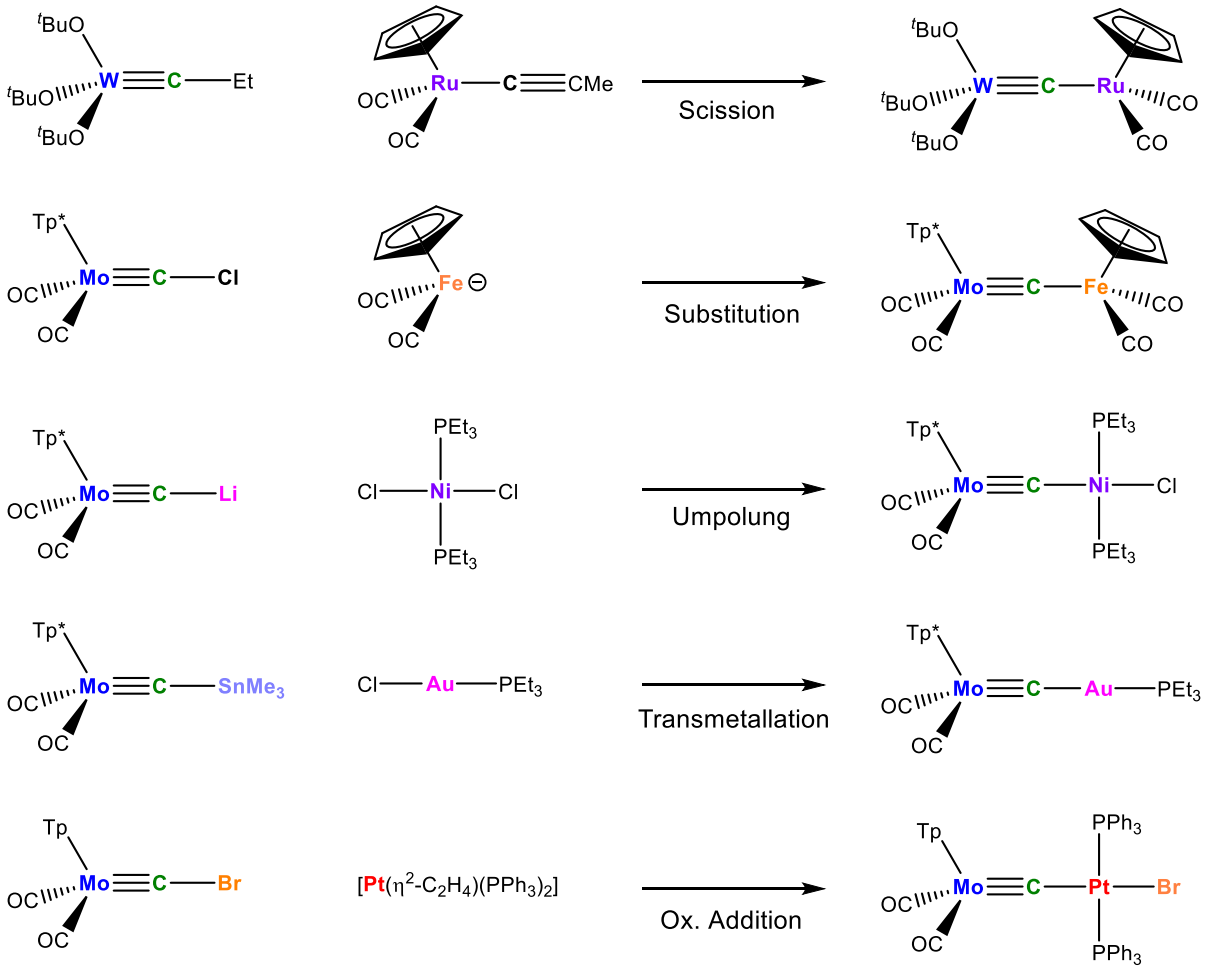

Scheme 1.1: Selected synthetic pathways to metallacarbyne complexes

[ii] To avoid ambiguity, herein non-systematic line formulae for Class B μ-carbido complexes will take the form [$L_nM{\equiv}C–M'L_n'$] rather than [$MM'(\mu\text{-}C)L_nL_n'$].

Reactivity

The reactivity of the Class B μ-carbido ligand has been briefly explored by Templeton on the molybdenum-iron complex **[(Tp*)(CO$_2$)Mo≡C-Fe[iii](Cp)(CO)$_2$]**.[11] Photolysis in the presence of CS_2 resulted insertion into the Fe-C bond to form **[MoFe(CCS$_2$)(Cp)(CO)$_4$(Tp*)]**. The carbido ligand could also be protonated using tetrafluoroboric acid to generate the μ-methylidyne salt **[MoFe(μ$_2$-CH)(Cp)(CO)$_4$(Tp*)]** (**Scheme 1.2**) which was suggested to contain methylidyne ligand with an agostic C–H–Mo interaction on the basis of spectroscopic data (δ_H = 1.94, $^1J_{CH}$ = 72 Hz). It should perhaps be noted that the data do not entirely exclude a conventional μ-methylidyne bridging an iron-tungsten bond.

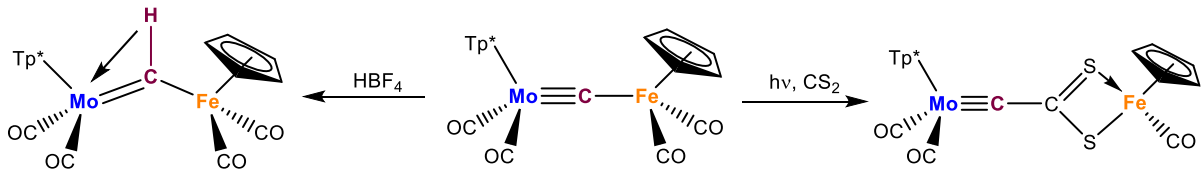

Scheme 1.2: Reactivity of the metallacarbyne complex **[(Tp*)(CO$_2$)Mo≡C-Fe(Cp)(CO)$_2$]**

Transformation of a μ-carbido ligand into a μ$_2$-methylidyne ligand has been repeated more recently by Frogley and co-workers in 2019.[6c] In an effort to form the "half-sandwich" cyclobutadiene complex **[(η^4-C$_4$Me$_4$)Pt{C≡W(CO)$_2$(Tp*)}$_2$]**, the tungsten lithiocarbyne species **[W(CLi)(CO$_2$)(Tp*)]** was treated with **[PtCl$_2$(η^4-C$_4$Me$_4$)]**. The product of the reaction unusually contained a central platinum atom bridged by two carbonyl and two μ-methylidyne ligands in **[W$_2$Pt(μ-CH)$_2$(μ-CO)$_2$(CO)$_2$(Tp*)$_2$]**. The detection of minor amounts of the ditungstabutadiyne species **[W$_2$(μ-C$_2$)(CO)$_4$(Tp*)$_2$]** suggests a competitive reductive elimination pathway from the desired tungsten-platinum metallacarbyne complex prior to methylidyne generation.

[iii] Throughout the literature, there is a tendency to describe the μ-carbido ligand in line formula as either [MM'(μ-C)L$_n$] or [L$_n$MCM'L$_n$], and it is interchangeably used in this work to reflect the original publications.

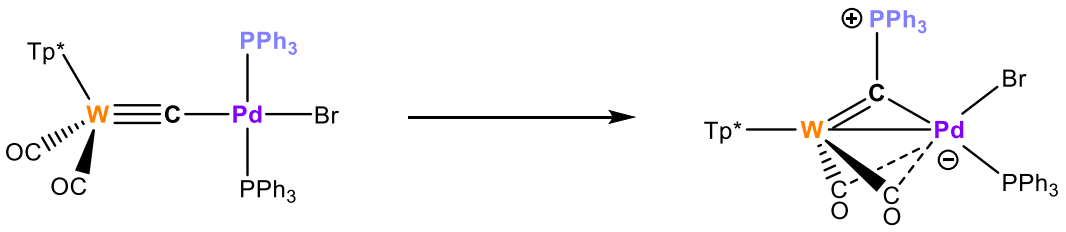

Scheme 1.3: Migration of a phosphine ligand to form a phosphinocarbyne complex

The tungsten-nickel carbido **[(Tp*)(CO)$_2$W≡C-NiCl(PEt$_3$)$_2$]** was found to spontaneously rearrange at room temperature to afford a μ-phosphoniocarbyne complex **[WNi(μ-CPEt$_3$)Cl(CO)$_2$(PEt$_3$)]**[12] and more recently Burt *et al.*, saw the migration of a PPh$_3$ ligand from palladium onto a Class B μ-carbido ligand, forming a μ$_2$-phosphoniocarbyne complex, **[WPd(μ-CPPh$_3$)Br(μ-CO)$_2$(PPh$_3$)(Tp*)]**.[13] The phosphoniocarbyne complex could also be synthesised from the oxidative addition of the pre-formed tungsten phosphoniocarbynecarbyne salt **[W(≡CPPh$_3$)(CO)$_2$(Tp*)]Br** to the palladium(0) species **[Pd$_2$(dba)$_3$]**. The phosphoninocarbyne complex was the result of a gradual migration of a terminal palladium PPh$_3$ ligand in the Class B μ-carbido complex **[MoPd(μ-C)Br(CO)$_2$(PPh$_3$)$_2$(Tp*)]** (**Scheme 1.3**). The complex was first encountered as a catalyst decomposition product in palladium-mediated nucleophilic substitution (cross-coupling) reactions of bromocarbynes with terminal alkynes to afford propargylidynes,[14] for which Class B μ-carbido complexes of the form **[MPd(μ-C)Br(CO)$_2$(PPh$_3$)$_n$(Tp*)]** (M = Mo, W; n = 1,2) are presumed to be intermediates. The same Class B carbido complexes are also key intermediates in the conversion of bromocarbyne complexes **[M(≡CBr)(CO)$_2$(Tp*)]** to carbynes bearing 1° and 2° phosphinosubstituents[15] and a diverse range of polycyclic aromatic compounds decorated with 1-4 carbyne units.[16] By analogy with the phosphine migration, a similar process involving μ-carbido-isonitrile migratory coupling afforded the first examples of iminoketenylidene (CCNR) complexes.[17]

1.2.4 Class C – Polar Covalent

The polar covalent μ-carbido ligand is in some respects quite similar to the metallacarbyne description, as it bridges two disparate metal centres, and the two metal-carbon bonds are quite distinct in their character. The distinction for Class C complexes is that all derive from rather

unique the terminal carbido complex **[Ru(C)Cl$_2$(PCy$_3$)$_2$]**,[iv] the carbido ligand of which displays somewhat modest nucleophilic character. This nucleophilic lone pair is able to coordinate to a second metal centre in what Frenking suggests is best described as a dative (polar-covalent) bond (*cf.* CO coordination).[18a] That said, one might envisage an extreme, zwitterionic canonical description akin to a Class B carbido complex and as more examples are identified beyond those based on the 'RuCl$_2$(PCy$_3$)$_2$' terminus alone, perhaps a continuum between Classes B and C may emerge.

Synthesis

The distinction, and discovery, of a Class C carbido complex was originally presented by Grubbs and co-workers in 2002, utilising the terminal carbido **[Ru(≡C:)Cl$_2$(PCy$_3$)$_2$]**.[18b,c] Grubbs demonstrated the terminal carbido ligand could displace labile ligands such as SMe$_2$ from **[PdCl$_2$(SMe$_2$)$_2$]** and NMe$_3$ from **[Mo(NMe$_3$)(CO)$_5$]** to afford the polar covalent complexes **[(PCy$_3$)$_2$Cl$_2$Ru≡C:PdCl$_2$(SMe$_2$)]** and **[(PCy$_3$)$_2$Cl$_2$Ru≡C:Mo(CO)$_5$]** (**Scheme 1.4**).

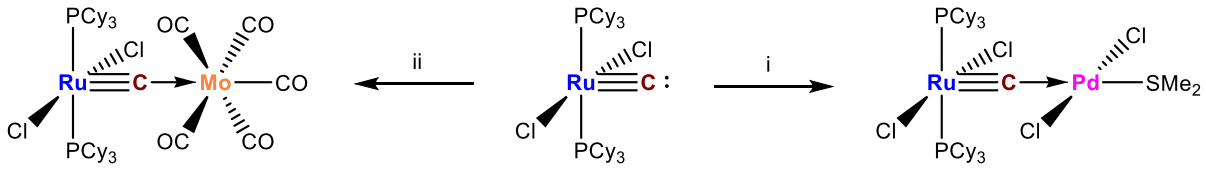

Scheme 1.4: Grubb's archetypical synthesis of polar covalent complexes utilising a terminal ruthenium carbide. (i) **[PdCl$_2$(SMe$_2$)$_2$]**, (ii) **[Mo(NMe$_3$)(CO)$_5$]**

These palladium and molybdenum adducts could be spectroscopically characterised, recording carbido signals in the $^{13}C\{^1H\}$ NMR spectra (δ 381.2 and 446.3 respectively), with upfield chemical shifts compared to the parent carbido complex (δ 471.8). A key observation that circumstantially lends weight to the polar-covalent description is that the molybdenum example reacts with CO under mild conditions to reform the terminal carbido precursor and **[Mo(CO)$_6$]**. Thus in the classical view of polar-covalent bonding, the Mo–C bond is cleaved *heterolytically* with

[iv] The osmium analogue is also known but has not been explored in this context.

the departing carbido complex (re)taking its electron pair with it. Class C chemistry has been largely developed since 2015 by Bendix and co-workers, continuing with the free carbido scaffold in **[Ru(≡C:)Cl_2(PCy_3)$_2$]**.[19] Coordination of the carbide to a variety of middle and late transition metal fragments have furnished a library of Class C μ-carbido complexes and this extensive body of work has recently been comprehensively reviewed (see **Chapters 1.2** and **6.1**).

Reactivity

The reactivity of Class C complexes has been scarce and largely centred around co-ligand transformations on the metal centres. Analogues of the ruthenium-platinum complex **[(PCy_3)$_2$$Cl_2$Ru≡C:$PtCl_2$(L)]** (L = $AsPh_3$, CNCy, PCy_3, PPh_3, bipy, μ-Cl) were developed in order to use the carbido ligand as a measure of the coordinated ligands' *trans*-effect.[20]

One standout reaction is the transformation of a Class C μ-carbido complex into a Class B ligand (**Scheme 1.5**). The reaction of **[Ru(C)Cl_2(PCy_3)$_2$]** with **[$PtCl_2$(py)$_2$]** results in the formation of the Class B μ-carbido complex **[(PCy_3)Cl_3Ru≡C–PtCl(py)$_2$]** presumably via an intermediate Class C complex **[(PCy_3)$_2$$Cl_2$Ru≡C:$PtCl_2(py)_n$]** (n = 1, 2) that undergoes halide transfer from platinum to ruthenium upon loss of phosphine. This complex undergoes ligand replacement when the bidentate diphosphine bis(diphenylphosphino)methane (dppm) is added. The bidentate phosphine bridges the Ru-Pt linkage, acting as a donor to both metal centres. The consequence is the product **[RuPt(μ$_2$-C)Cl_4(μ-dppm)$_2$]**, which formally contains a d^8-square planar platinum(II) metal centre and d^6-ruthenium(II) centre (CR^+ formalism), and is therefore best described as a μ-carbido ligand of the metallacarbyne bonding form.[19c] This complex is of particular relevance to Class A complexes **[Rh_2(μ$_2$-C)Cl_2(μ-dppm)$_2$]** and **[Rh_2(μ$_2$-C)Cl_n(μ-dppf)$_2$]** (n = 2,4) which will appear often in the work to follow. Taken together, these topologically similar complexes elegantly demonstrate the impact of varying the metal termini on the delineation of Class A and B μ-carbido complexes.

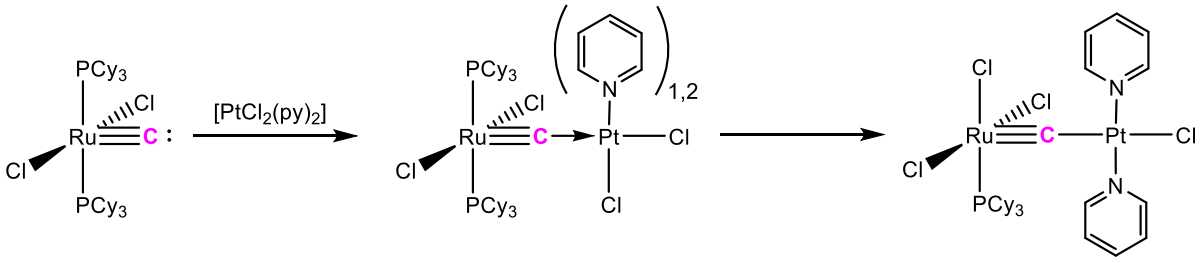

Scheme 1.5: Class C to Class B μ-carbido transformation

1.2.5 Synthesis of Class A μ-carbido complexes

Class A μ-carbido complexes, known as dimetallacumulenes, have undergone significant development over recent years after what can be described as a history of serendipity and scarcity. Previously referred to 'cumulenic' until this concept was refined, the three-atom system is easily distinguished by two, in most cases often identical metal-carbon double bonds, *viz.* M=C=M. The scarcity and limited diversity of the Class A complexes throughout the literature is a natural consequence of limited viable synthetic pathways that offer generality, with early synthetic progress arising sporadically from small molecule activation by two or more identical metal reagents, with direct palindromic implications. It is because of this that the vast majority of complexes are homometallic, with only three published exceptions.

Synthesis of macrocyclic complexes

The cumulenic μ-carbido history starts with Nobel predictions. Hoffmann, a couple of years before presenting his Nobel Prize lecture on the isolobal analogy in 1981, proposed the viability and calculated the stability of μ-carbido complexes, specifically focussing on iron porphyrin systems.[v,21] The real world of μ-carbido complexes officially began in 1980 when Mansuy and co-workers reported the synthesis of the prototypical μ_2-carbido complex **[$Fe_2(\mu_2$-C)$(TPP)_2$]**.[23] Using the same iron porphyrin system which was previously mooted to be theoretically viable by Hoffmann, **[FeCl(TPP)]** (TPP = tetraphenylporphyrinato) Mansuy

[v] Though a tin-rhenium μ-carbido complex was reported in 1979,[22] Hoffman suggested that it was in fact a μ-oxo complex on the basis of EAN arguments.

showed that it was capable of small molecule activation under reductive conditions, in this case carbon tetrahalides (**Scheme 1.6**).

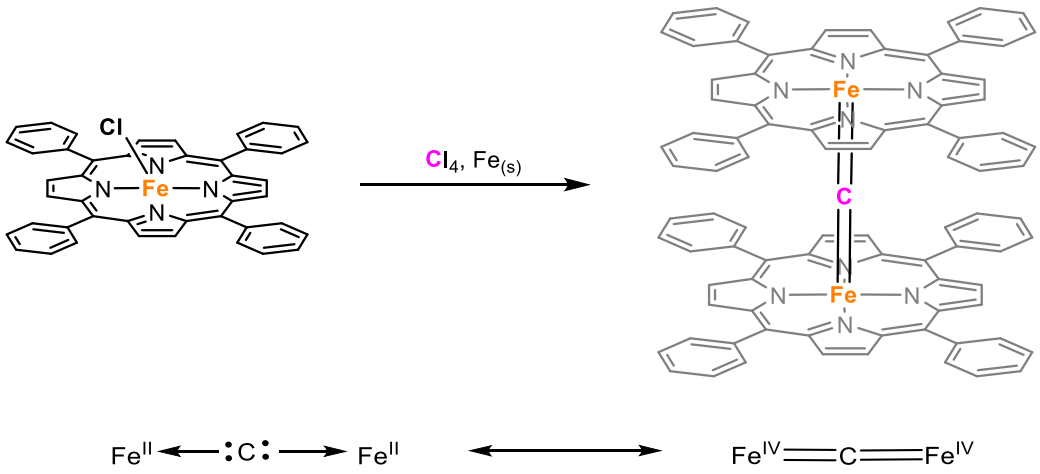

Scheme 1.6: (top) Mansuy *et al.* activation of CI_4 to give the first μ-carbido complex**.** (below) presented Class A coordination modes of dative or covalent character

It is with the first synthesis of a μ-carbido complex that the recurrent role of serendipity in their formation can be first seen. In the presence of a reducing agent, **[FeCl(TPP)]** reductively cleaves off two halogens from CCl_4 and CBr_4, furnishing early examples of dihalocarbene complexes **[Fe(CX$_2$)(TPP)]** (X = Cl, Br). However, when the same reaction was repeated with the heavier halogen iodine, the formation of the diiodocarbene was not seen. Rather, further reduction at the carbon atom results in the loss of all four iodine groups and the coordination of the carbene to a second iron moiety, forming the symmetrical μ-carbido species **[Fe$_2$(μ$_2$-C)(TPP)$_2$]**. The failure in isolating a diiodocarbene complex is rationalised by their presumed instability due to the higher reactivity of the C–I bonds, and to date still no structurally characterised examples of dibromo- or diiodocarbene complexes exist. The μ-carbido complex could also be formed slowly when the dibromocarbene complex **[Fe(CBr$_2$)(TPP)]** was mixed with excess reducing agent.

Though unable to be immediately structurally characterised, the presence of the μ-carbido ligand was supported through detailed infrared comparison to known μ-oxo and μ-nitrido analogues of the FeTPP system. Comparing the three systems, the asymmetric $\nu_{Fe=E=Fe}$ stretching mode decreases with increasing atomic weight of the bridging nucleus (C = 940 cm^{-1}, N = 910 cm^{-}

[1], O = 885 cm^{-1}). Though not published in its original synthesis, the molecular structure was elucidated by Goedken and co-workers (See **Figure 1.1**).[24] The highly symmetric structure supported the presence of the cumulenic μ-carbido ligand, with two identical (symmetry generated) Fe=C bonds of 1.673 Å,[vi] which fall within the accepted range for an iron-carbon double bond. The linear nature of the μ-carbido species was also confirmed with the symmetry generated Fe=C=Fe linkage by necessity aligning perfectly at 180 °.

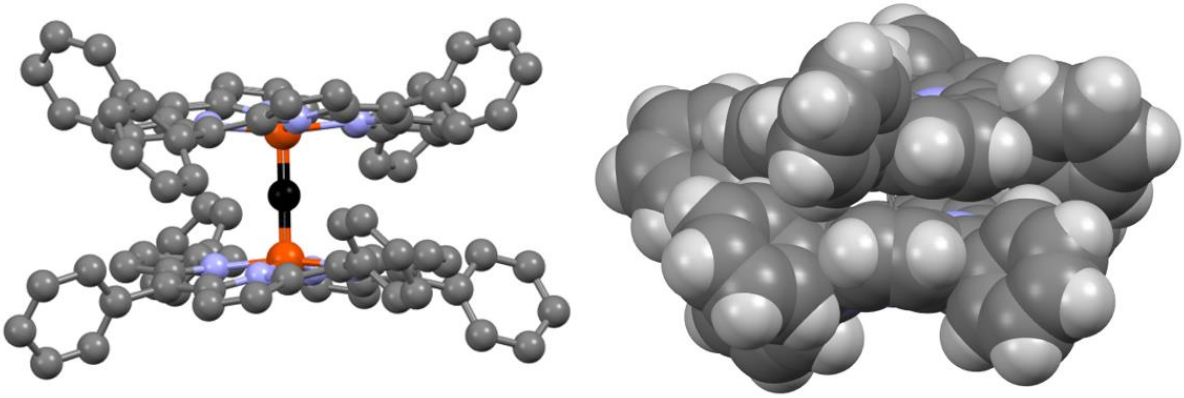

Figure 1.1: Simplified molecular structure of **$[Fe_2(\mu_2\text{-}C)(TPP)_2]$**.
Inset: space-filling diagram showing packing

Further testing of this complex examined the potential for metal-metal communication across the π-bound cumulenic carbido linkage. If the porphyrin π system was connected across this bridging ligand, then cyclic voltammetry would be expected to show two distinct oxidation events, as the iron centres would not behave independently towards electron transfer. This was indeed the case, with two oxidation events separated by ~0.4 V, supporting possible metal-metal communication across the μ-carbido ligand.[24] The initial synthesis of this complex also started the debate of electronic representation, with Mansuy displaying **1** as a resonating form with a dative carbon ligand and iron(II) centres on one hand, and a C^{4-} ligand coordinated to two iron(IV) centres. Early Mössbauer spectroscopy studies from Hendrickson and co-workers support the latter representation, with iron(IV) centres and non-dative bonds.[25]

[vi] e.s.d. values for the bond-lengths were not published, though models with acceptable precision for this and related derivatives have since appeared.

The reliance of a macrocycle ancillary ligand became a common feature in Class A carbido synthesis throughout the following 40 years. In 1988 Rossi and co-workers utilised an identical procedure used by Mansuy to synthesis another iron-macrocycle μ-carbido complex, except replacing the porphyrin co-ligands with phthalocyanine (pc).[26] The new μ-carbido complex **[(pc)Fe=C=Fe(pc)]** was again compared to the corresponding nitrido and oxo analogues and found to have a higher wavenumber infrared absorption for the lighter carbido atom (990 cm^{-1} *cf.* 910 and 852 cm^{-1}, respectively), which was attributed to a higher conjugation capability of the carbon. The Fe=C bond lengths were similar to the TPP species at 1.70(1) Å. The only notable reactivity of **[(pc)Fe=C=Fe(pc)]** was the facile coordination of *N*-methylimidazole groups *trans* to the carbido ligand and increased stability towards pyridine than its TPP analogue.

Complex	M=C (Å)	as. $\upsilon_{M=C=M}$ (cm^{-1})	M=C=M (°)
[(TPP)Fe=C=Fe(TPP)]	1.675*	940	180[a]
[(TPP)Fe=C=Fe(TPP)]·THF	1.683(1)	-	180[a]
[(TPP)Ru=C=Ru(TPP)]	-	-	-
[(pc)Fe=C=Fe(pc)]	1.70(1)	990	178(1)
[(pc)Fe=C=Fe(pc)]·Me_2CO	-	940	-
[(pc)Fe=C=Fe(pc)]·$(4\text{-mepy})_2$	-	888	-
[(pc)Fe=C=Fe(pc)]·$(1\text{-meim})_2$	1.69(1)	940	178(1)
[(pc)Ru=C=Ru(pc)]	-	1050	-
[(pc)Ru=C=Ru(pc)]·$(py)_2$	1.78(1) 1.77(1)	974	177.4(6)
[(TPP)Fe=C=Fe(pc)]·$(THF)_3$	1.71(1) 1.65(1)	948	179(1)
[(OEP)Fe=C=Fe(OEP)]	1.6638(9)	976	179.5(3)
$(NBu_4)_2$[(F)(pc)Fe=C=Fe(pc)(F)]	1.687(4)	917	179.5(3)
[(TPP)Fe=C=$Re(CO)_4Re(CO)_5$]	Fe: 1.605(13) Re: 1.957(12)	-	172.8(4)

Table 1.1: Selected bond lengths, angles and IR stretches for macrocyclic μ-carbido complexes. Note: * no e.s.d. was provided of found in the cif files. [a] symmetry constrained bond angle of exactly 180 °

Expansion beyond iron complexes was first explored by Homberg *et al.* with the first ruthenium Class A complex.[27] Though the metal changes, the μ-carbido complexes synthesised once again require a macrocycle co-ligand, in this case both TPP and pc furnish ruthenium analogues. However, both the octaethyl porphyrin (OEP) derivate **[(OEP)Fe=C=Fe(OEP)]**, and the mixed-porphyrin complex with TPP and pc macrocycles were also produced.[28] In addition to this, both pyridine and THF adducts were isolated and crystallised as six-coordinate complexes.[29] The ν_{RuCRu} stretch for **[Ru$_2$(μ-C)(pc)$_2$]** (1050 cm^{-1}) appears anomalously high (*cf.* 990 cm^{-1} for the iron analogue) based on simple Redlich-Teller arguments such that it might be concluded that covalency makes a significant contribution to the M-C bond strength.

Homburg developed a more general "one-pot" synthesis for the macrocyclic complexes, with reduction of both the macrocycle precursor and $CHCl_3$ by potassium hydroxide under anaerobic conditions, proceeding via a proposed *in-situ* condensation and redox reaction of the dichlorocarbene intermediate with another equivalent of reduced macrocycle to furnish the μ-carbido species, though the authors make no claim to elucidating the proposed mechanism. Their detailed studies on the μ-carbido complexes included crystallography,[30] identification of the symmetric $\nu_{M=C=M}$ stretch in the Raman spectra (**[(TPP)Fe=C=Fe(TPP)]** at 443 cm^{-1}, **[(OEP)Fe=C=Fe(OEP)]** at 460 cm^{-1}) and confirmation of metal-metal electronic communication through cyclic voltammetry. Further development of macrocyclic μ-carbido complexes include substituted phthalocyanine rings,[31] and most notably the synthesis of an anionic species with a coordinated halo ligand, for example **(^{n}Bu$_4$N)$_2$[{Fe(F)(pc)}$_2$(μ-C)]·3H$_2$O**. [32]

Both research groups explored the reactivity of these phthalocyanine compounds including oxidation with iodine, derivatisation to the ruthenium(IV) analogue, production of alkyl-substituted phthalocyanine rings, and mixed porphyrin/phthalocyanine species.[33] Ercolani and co-workers also recounted μ_2-carbidos in a review of phthalocyanine chemistry in 2003.[34]

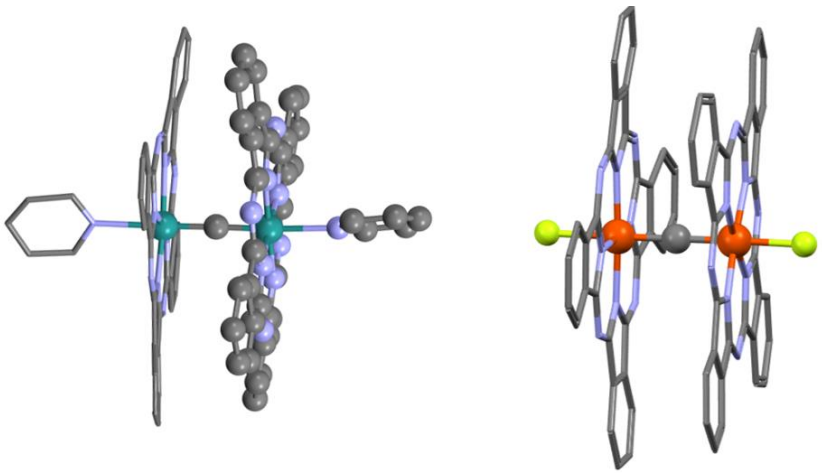

Figure 1.2: (left) Simplified molecular structure of **[(pc)Ru=C=Ru(pc)]·(py)$_2$**. (right) Simplified molecular structure of the dianion of **(^{n}Bu$_4$N)$_2$[{Fe(F)(pc)}$_2$(μ-C)]·3H$_2$O**

All of the macrocycle complexes presented have consisted of homometallic systems, *i.e.*, both metal complexes bound to the μ-carbido ligand are identical. The detailed Mössbauer spectroscopy performed on macrocyclic complexes all support the presence of two electronically identical metal nuclei in terms of oxidation state. This did not change until 10 years after Mansuy's original synthesis, when in 1990 Beck published work on the preparation of the first asymmetric μ-carbido complex.[35] Beck's work commenced with the stable dichlorocarbene species that Mansuy had first isolated, **[(TPP)Fe=CCl$_2$]**, however, cleavage of the chloride groups from the carbene was achieved through nucleophilic attack by a separate metal complex, namely **[Re(CO)$_5$]$^-$**. This furnished the unsymmetrical trimetallic μ-carbido complex, **[(TPP)Fe=C=Re(CO)$_4$Re(CO)$_5$]** in which the carbido coordinate to both 'Fe(TPP)' and 'Re$_2$(CO)$_9$' units (**Figure 1.3**). The molecular structure was confirmed through X-ray crystallography, which suggested that even with the lack of symmetry, the μ-carbido ligand contained a formal double bond to both metals (Fe-C = 1.605(13) Å, Re-C = 1.957(12) Å) though it must be noted that the Fe-C bond length is considerably shorter (~0.06 Å) than **[(TPP)Fe=C=Fe(TPP)]**.

The μ-carbido resonance was tentatively assigned to a resonance at 211.7 ppm in the ^{13}C{^{1}H} NMR spectrum, however, this lies more than 100 ppm upfield of the common μ-carbido region and is likely a carbonyl resonance, as only a single environment was assigned in the NMR despite three chemically distinct environments appearing on the complex. It should however be

noted that (i) the many studies on $[M_2(\mu\text{-}C)(\text{macrocycle})_2]$ compounds have rather neglected NMR as a means of characterisation providing few useful comparative data and (ii) the ring currents associated with porphyrin-type ligands have a profound effect on shielding and the resulting chemical shifts or proximal nuclei.

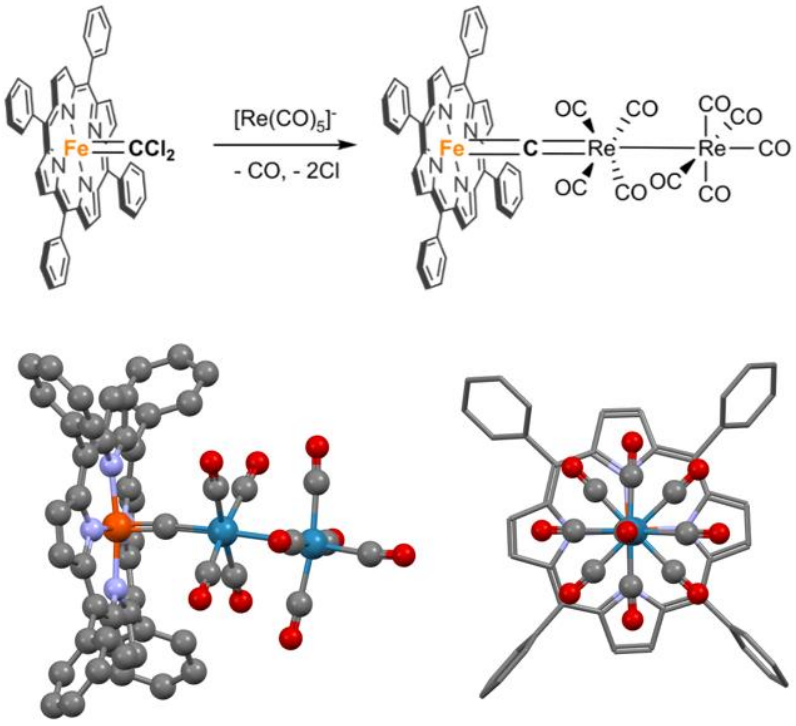

Figure 1.3: Reaction scheme and simplified molecular structure of **$[(TPP)Fe{=}C{=}Re(CO)_4Re(CO)_5]$**

Almost 20 years later, Beck reported the same experimental approach but expanded on both the porphyrin co-ligand and nucleophilic metal carbonylate species.[36] Using tetracarbonyl ferrate **$[Fe(CO)_4]^{2-}$** as the nucleophile, both the TPP and TCNP (tetrakis(*p*-cyanophenyl)porphyrin) bimetallic μ-carbido complexes were readily made **$[(L)Fe{=}C{=}Fe(CO)_4]$**. With manganese and chromium, the corresponding carbido complexes **$[(TCNP)Fe{=}C{=}Mn_2(CO)_9]$** and **$[(L)Fe{=}C{=}Cr(CO)_5]$** (L = TPP, TCNP) were obtained, though the formulations of these complexes rest entirely upon elemental composition and UV-Vis data and would benefit from more extensive characterisation. Regardless, this method provided the first insight into expansion of μ-carbido complexes beyond the macrocycle framework and a potentially generalisable route towards unsymmetrical complexes.

The final contribution to macrocyclic Class A μ-carbido complexes appeared more recently in 2015.[37] Sorokin and co-workers had been examining the catalytic activity of phthalocyanine ruthenium complexes, and serendipitously discovered the formation of a μ-carbido complex when attempting to generate a ruthenium phthalocyanine complex using the **[Ru$_3$(CO)$_{12}$]** cluster as the source of ruthenium – a common entry protocol for ruthenium porphyrin chemistry. The desired monometallic macrocycle **[Ru(CO)$_2${(^{n}BuO)$_8$pc}$_2$]** was the major species, containing terminal ruthenium carbonyl ligands, but the μ-carbido complex **[Ru$_2$(μ-C){(^{n}BuO)$_8$pc}$_2$]** was also formed (**Scheme 1.7**). The μ-carbido ligand was confirmed through ESI-MS, IR spectroscopy (as. $\nu_{Ru=C=Ru}$ at 1013 cm^{-1}) and the now-diastereotopic nature of the OCH_2 hydrogens in the O^{n}Bu groups evident in the ^{1}H NMR spectra. It was stated that the μ-carbido ligand was sourced from thermolysis of **[Ru$_3$(CO)$_{12}$]** resulting is dissociation of a CO bond. Unfortunately, the complex was not structurally characterised, nor was the μ-carbido resonance detected in the ^{13}C{^{1}H} NMR studies, though its catalytic activity was explored in a later publication.[38] It might be argued that the alternative formulation, **[Ru$_2$(μ-O){(^{n}BuO)$_8$pc}$_2$]**, is neither implausible nor adequately discounted, though carbonyl ligands certainly have served as μ-carbido ligand precursors in high-nuclearity ruthenium cluster chemistry, albeit under rather forcing conditions.[39]

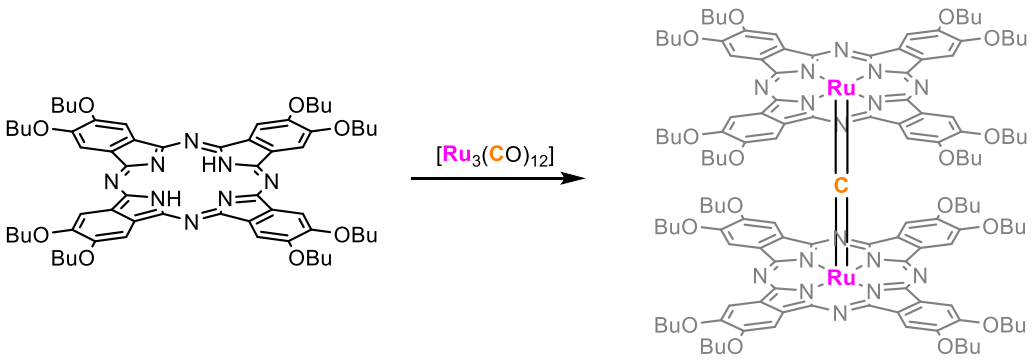

Scheme 1.7: Thermolysis of **[Ru$_3$(CO)$_{12}$]** to give μ-carbido complex **[Ru$_2$(μ-C){(BuO)$_8$pc}$_2$]**

The synthesis of these macrocyclic μ-carbido complexes by and large resulted from the reduction of haloalkanes to form reactive halocarbene intermediates which could further be reduced in the presence of a second metal complex. Though this synthetic preparation has not

been successfully applied to non-macrocyclic complexes, these works confirmed experimentally what was first predicted by Hoffmann concerning the existence of stable sandwich μ-carbido complexes.

Non-macrocyclic complexes - CO Bond Activation

With the synthesis of the first unsymmetrical cumulenic μ-carbido complex, Beck showed Class A compounds were no longer limited to the bis(macrocyclic) framework which had so far hindered complex diversity. The first example of a completely non-macrocyclic Class A μ-carbido species came shortly after Beck's work in 1993, when Wolczanksi and Miller synthesised the tungsten complex **[(silox)$_2$(O)W=C=WCl$_2$(silox)$_2$]** (silox = OSi*t*Bu$_3$).[vii,40] The synthetic route to this tungsten complex was unique to the system, as it involved thermal scission of ligated carbon monoxide across a W-W triple bond. The di-tungsten starting material **[(silox)$_2$Cl(CO)W]$_2$** undergoes thermolysis at 120 °C, losing one carbonyl ligand and breaking apart the second, forming the bridging carbido ligand and an oxo ligand on one tungsten, forming an unsymmetrical species (**Scheme 1.8**).

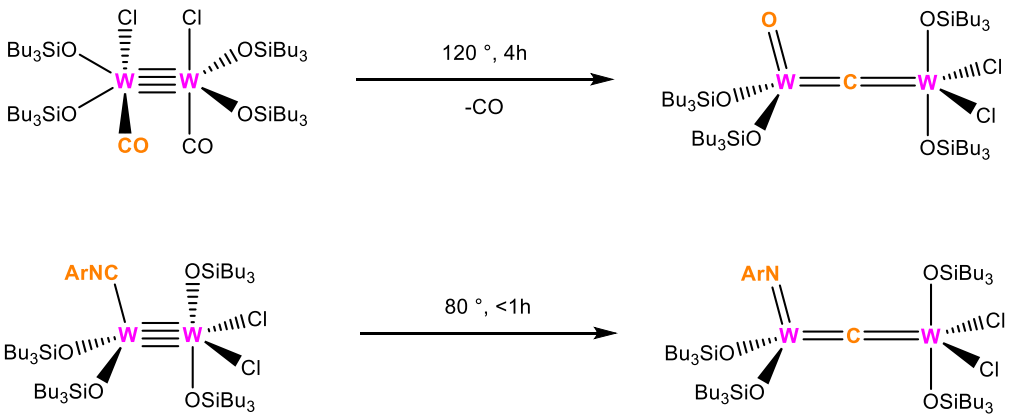

Scheme 1.8: Thermolysis of CO and CNR to produce μ-carbido complexes

[vii] The silox ligand OSi*t*Bu$_3$ is mooted as providing a mimic for metals bound to a silica or general metal oxide surface.

The presence of the μ-carbido ligand was confirmed in the IR spectra (as. $\nu_{W=C=W}$ at 1155 cm^{-1}) while the resonance in the $^{13}C\{^1H\}$ NMR spectrum showed coupling to the disparate tungsten centres (δ_C = 379.1, $^1J_{WC}$ = 200, 187 Hz). The scission of CO could also be reproduced for the CN bond of mesityl isocyanide. The analogous species **[(silox)$_4$Cl$_2$W$_2$(CNAr)]** underwent C-N dissociation to form the μ-carbido and imido ligand in **[(silox)$_2$(ArN)W=C=WCl$_2$(silox)$_2$]**. Once again, the asymmetric μ-carbido stretch was identified in the IR spectra at 1120 cm^{-1}, along with a downfield shift of the carbido resonance which appeared at δ_C = 406.3 ($^1J_{WC}$ = 194 Hz). To confirm the cumulenic nature, both molecular structures were determined (although only data for **[(silox)$_2$(ArN)W=C=WCl$_2$(silox)$_2$]** were provided). The asymmetric nature of the ditungsten species, with tetrahedral and trigonal bipyramidal metal centres, is evident when examining the W-C bond lengths. The carbido bond to the tetrahedral complex is significantly longer than its five-coordinate counterpart (1.99(2) *cf.* 1.77(2) Å). Wolczanski explained this disparity with two alternate resonance descriptions that are Class B in nature, containing a W-C≡W bonding mode, though the impact of also including the W–N multiple bond perhaps plays a role (without the need to invoke heptavalent tungsten). Though unsymmetrical, these di-tungsten complexes satisfy the Class A μ-carbido description.

The cleavage of carbon monoxide across a metal-metal multiple bond was extended at the turn of the millennium by Floriani and co-workers.[41] Taking the calix[4]arene niobium dimer, **[(Nb=Nb){*p*-^{t}Bu-calix[4]-(O)$_4$}$_2$Na$_2$]**, the reaction with carbon monoxide breaks apart the niobium coordination and forms a bridging oxalkylidyne ('isocarbonyl') species (**Scheme 1.9**). The oxalkylidyne ligand could be reduced further using sodium to form interstitial carbido and oxo ligands, and further again to isolate the μ-carbido ligand in **[{Nb(p-^{t}Bu-calix[4]-(O)$_4$)}$_2$(μ-C)Na$_3$]**.

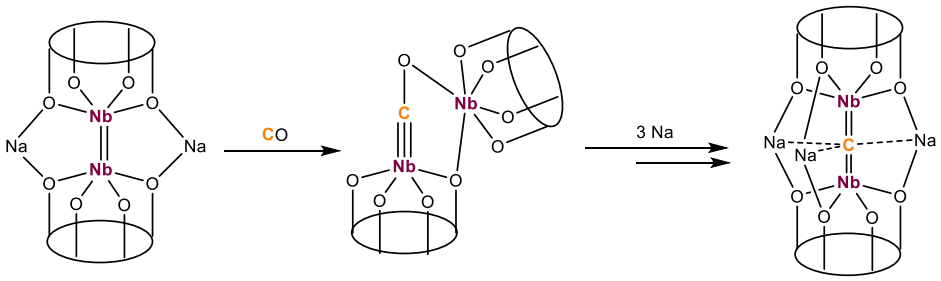

Scheme 1.9: Stepwise reduction of CO to form a μ-carbido complex **[{Nb(p-^{t}Bu-calix[4]-(O)$_4$)}$_2$(μ-C)Na$_3$]**

The paramagnetic species was structurally characterised (**Figure 1.4**), with the average Nb=C bond length of 1.922(4) Å being of comparable length to alkylidene complexes of niobium and supporting the formation of a cumulenic μ-carbido species, though it remains coordinated to the three sodium ions (Na--C = 2.698(4) and 2.876(4) Å).

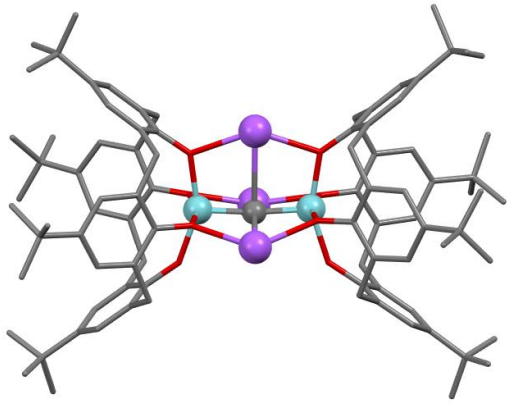

Figure 1.4: Side-on view of **[{Nb(p-^{t}Bu-calix[4]-(O)$_4$)}$_2$(μ-C)Na$_3$]**

C≡C Bond Activation

An alternative source of the μ–carbido carbon was demonstrated years later, by Severin and co-workers in 2007.[42] By examining the reactivity of a ruthenium cymene complex (**[(*p*-cymene)Ru(μ-Cl)$_3$RuCl(C$_2$H$_4$)(PCy$_3$)]**) with acetylenes with respect to atom transfer radical addition catalysis, it was found that substituted acetylenes replaced the coordinated ethene and underwent conventional ligand rearrangement to form vinylidene ligands. However, when the parent species ethyne was utilised, the isolated product was the tetrametallic μ-carbido species **[({(P-cymene)Ru(μ-Cl)$_3$}RuCl(PCy$_3$))$_2$(μ-C)]** (**Scheme 1.10**). It was substantiated through ^{13}C labelling that ethyne was the source of the μ-carbido ligand (δ_C = 430.5), though detailed spectroscopic analysis could not be completed due to poor solubility and a mechanism was not proposed. Structural analysis revealed two symmetry-generated halves, with the Ru=C bond length of 1.7877(9) Å similar to the ruthenium macrocycle complexes isolated previously.

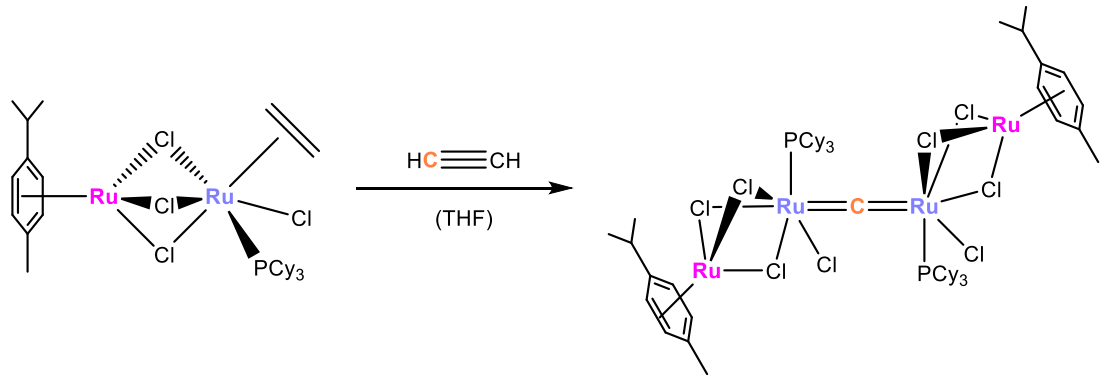

Scheme 1.10: Synthesis of **[({(p-cymene)Ru(μ-Cl)$_3$}RuCl(PCy$_3$))$_2$(μ-C)]** from acetylene activation

C-Chalcogen Bond Activation

The role of serendipity in the emergence of Class A carbido chemistry continued when in 2013 in an effort to repeat Butler's published synthesis the rhenium thiocarbonyl species **[Re(CO)$_2$(CS)(Cp)]**,[43] the reactive *solvento* complex **[Re(THF)(CO)$_2$(Cp)]** was treated with carbon disulfide and triphenyl phosphine, in a process analogous to Wilkinson's prototypal thiocarbonyl complex **[RhCl(CS)(PPh$_3$)$_2$]**.[44] In addition to the desired thiocarbonyl complex, a low-yielding second species was identified as the μ-carbido complex **[{Re(CO)$_2$(Cp)}$_2$(μ-C)]** (**Scheme 1.11**).[45] Once recognised as such, it was shown that the yield of the μ-carbido complex could be improved through a direct reaction between the pre-isolated thiocarbonyl complex and THF *solvent* complex.

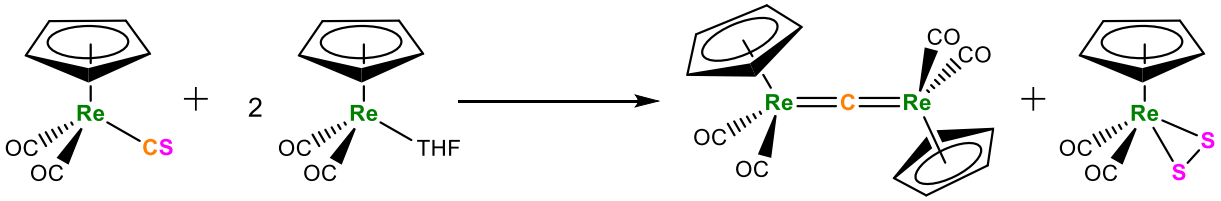

Scheme 1.11: Synthesis of **[Re$_2$(μ-C)(CO)$_4$(Cp)$_2$]** through cleavage of the thiocarbonyl C=S bond

The μ-carbido resonance was detected downfield in the ^{1}H-^{13}C HMBC spectrum at 436.4 ppm and the asymmetric $\nu_{Re=C=Re}$ stretch was found in the infrared spectrum at 1019 cm^{-1} (calculated to be at 1004 cm^{-1}). The crystallographically unique but almost colinear Re=C bonds

(1.881(14) and 1.882(14) Å) fall in the range accepted for a formal bond order of two (*cf.* rhenium carbene and vinylidene complexes with similar ancillary ligands) but fell slightly shorter than in Beck's Fe=C=Re porphyrin complex. Notably, a remarkably low barrier to rotation of the rhenium termini was suggested, and computationally substantiated, to arise from a 3-centre, 12-electron orbital manifold for the Re=C=Re spine rather than the 3-centre, 8-electron description that might superficially arise from an isolobal analogy with allenes. The authors posited the possibility for a more generalisable μ-carbido synthesis through thiocarbonyl activation.

Around the same time, it was also shown that the putative isoselenocarbonyl complex **[MoIr(μ-CSe)(CO)$_3$(PPh$_3$)$_2$(Tp*)]** evolved to the first group 9 μ-carbido complex diiridadiselenatetrahedrane **[Mo$_2$Ir$_2$(μ-C)$_2$(μ-Se$_2$)(CO)$_6$(PPh$_3$)$_2$(Tp*)$_2$]**, albeit of the Class B nature.[8] Taken together, these observations suggest that, further to Wolczanski's CO activation, the heavier chalcocarbonyls CS and CSe would appear to potentially serve as carbido precursors, given the weakening of C–chalcogen bonding upon descending group 16.

A further example of reductive cleavage of a thiocarbonyl ligand arose in 2015 when Braun and co-workers reported that for the square-planar rhodium(I) boryl complex **[Rh(Bpin)(PEt$_3$)$_3$]** (pin = pinacolato), it was discovered that the boryl co-ligand played a key role in the activation of small molecules such as CO_2 and N_2O.[46] When treated with carbon disulfide, the rhodium boryl complex underwent C-S activation to form a spectroscopically observable thiocarbonyl complex **[Rh(CS)(SBpin)(PEt$_3$)$_2$]** that reacted with further **[Rh(Bpin)(PEt$_3$)$_3$]** to ultimately form the μ-carbido complex **[Rh$_2$(μ-C)(SBpin)$_2$(PEt$_3$)$_4$]** (**Scheme 1.12**).

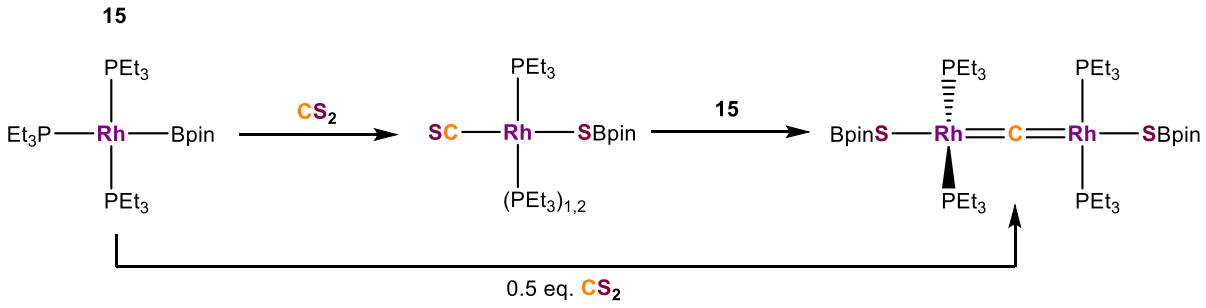

Scheme 1.12: CS bond activation on rhodium boryl complex to form a μ-carbido species

Braun was able to use ^{13}C enrichment to form the isotopologue of **[Rh_2(μ-^{13}C)(SBpin)$_2$(PEt_3)$_4$]** with an enriched μ-carbido ligand and detected the ^{13}C resonance at 439.4 ppm in the ^{13}C NMR spectrum. The μ-carbido resonance appeared as a triplet of pentets, coupled to both the ^{103}Rh and ^{31}P nuclei in the AM_2X_4 spin system ($^1J_{RhC}$ = 45 Hz, $^2J_{PC}$ = 11 Hz). The asymmetric $\nu_{Rh=C=Rh}$ stretch was detected in the infrared spectra at 978 cm^{-1} (946 cm^{-1} for ^{13}C isotopologue). The cumulenic nature of the μ-carbido ligand follows from the homometallic system and was confirmed with the observation of two crystallographically identical Rh=C bond lengths (1.790(7) and 1.776(7) Å, 2 e.s.d.) that correspond well to rhodium-carbon double bonds in related 4-coordinate rhodium carbene and vinylidene complexes. The boryl thioester ligands could be replaced with sulfhydryl (SH) groups upon addition of methanol, though no other reactivity was observed.

Braun and co-workers put forward that the weakening of the CS bond through metal coordination and the formation of the strong B-S bond underpinned the formation of the μ-carbido complex, and the procedure was repeated two years later with a germyl analogue, **[Rh($GePh_3$)(PEt_3)$_3$]**.[47] The germyl species could undergo an identical formation of thiocarbonyl species through addition of CS_2, forming a germylthiolato co-ligand. The boryl-induced cleavage of the thiocarbonyl ligand was seen again when the intermediate thiocarbonyl species was combined with **[Rh(Bpin)(PEt_3)$_3$]**, forming a spectroscopically observable but inseparable mixture of all three μ-carbido complexes **[Rh_2(μ-C)($SGePh_3$)$_2$(PEt_3)$_4$]**, **[Rh_2(μ-C)(SBpin)$_2$(PEt_3)$_4$]** and the unsymmetrical **[Rh_2(μ-C)($SGePh_3$)(SBpin)(PEt_3)$_4$]** (δ_C = 425.8, 429.3, 432.6). Despite failure to isolate a single product for spectroscopic analysis, the bis(germylthiolato) analogue **[Rh_2(μ-C)($SGePh_3$)$_2$(PEt_3)$_4$]** was crystallographically characterised, confirming two Rh=C double bonds of 1.788(4) and 1.798(4) Å.

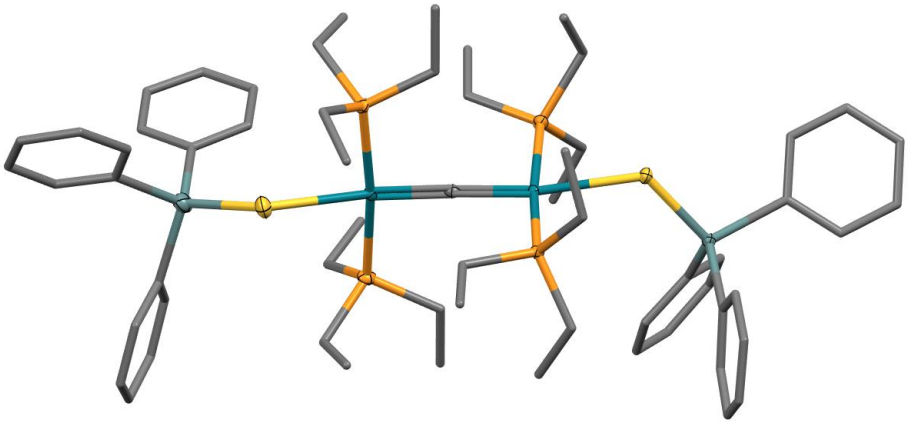

Figure 1.5: Simplified molecular structure of **[$Rh_2(\mu\text{-}C)(SGePh_3)_2(PEt_3)_4$]**

The oxidative addition of boranes to **[$MCl(CO)(PPh_3)_2$]** (M = Rh, Ir) had been previously investigated by Marder,[48] however, the only involvement of boranes in thiocarbonyl chemistry involved a report in the secondary literature of the reaction of **[$RuCl(Ph)(CS)(PPh_3)_2$]** with HBCat to afford **[$Ru(BCat)Cl(CS)(PPh_3)_2$]**, carbonylation of which resulted in migratory insertion of boryl and thiocarbonyl ligands to provide **[$RuCl(\eta^2\text{-}SCBCat)(CO)(PPh_3)_2$]**.[49] Following the unusual activation of a rhodium-coordinated thiocarbonyl by a bis(methimazolyl)borate $H_2B(mt)_2$ (mt = *N*-methyl-2-mercaptoimazolyl) ligand[50] the reactivity of the rhodium thiocarbonyl complex **[$RhCl(CS)(PPh_3)_2$]** with a variety of borane reagents (HBpin, HBCat, B_2Cat_2, B_2pin_2) was investigated. It was discovered that the reaction of the thiocarbonyl complex with catecholborane resulted in cleavage of the thiocarbonyl ligand to form the μ-carbido complex **[$Rh_2(\mu\text{-}C)Cl_2(PPh_3)_4$]** (**Scheme 1.13**).[51] The synthesis proved to be unsuccessful when even modest variations were made to the phosphine co-ligands (PCy_3, $P(4\text{-}C_6H_4Me)_3$), and the reaction of the iridium analogue **[$IrCl(CS)(PPh_3)_2$]** also failed to provide a stable analogue.

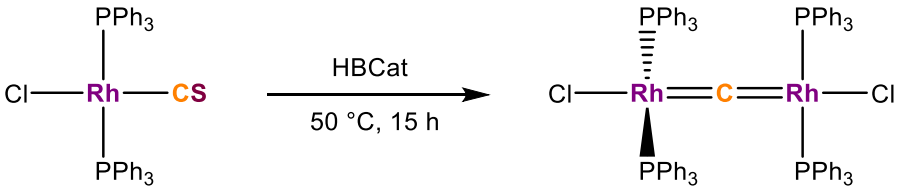

Scheme 1.13: Synthesis of the rhodium μ-carbido complex through CS activation by an extraneous boryl reagent

The presence of the μ-carbido ligand was inferred from ESI-MS and infrared spectra (asymmetric $\nu_{Rh=C=Rh}$ at 1011 cm^{-1}) data, and through ^{13}C labelling the μ-carbido ligand was directly detected through a resonance appearing at 424.4 ppm ($^{1}J_{RhC}$ = 47 Hz), showing broad coupling to the two rhodium and four phosphorus nuclei. The cumulenic nature was supported by the molecular structure determination (**Figure 1.6**), which revealed two crystallographically identical Rh=C double bonds (1.773(3), 1.780(3) Å). The mechanism by which the μ-carbido ligand forms remains obscure, though it is inferred to proceed through oxidative addition of catecholborane, prior to activation of the CS bond. The complex **$[Rh_2(\mu\text{-}C)Cl_2(PPh_3)_4]$** is central to the work to follow and further features of interest will be discussed in later sections.

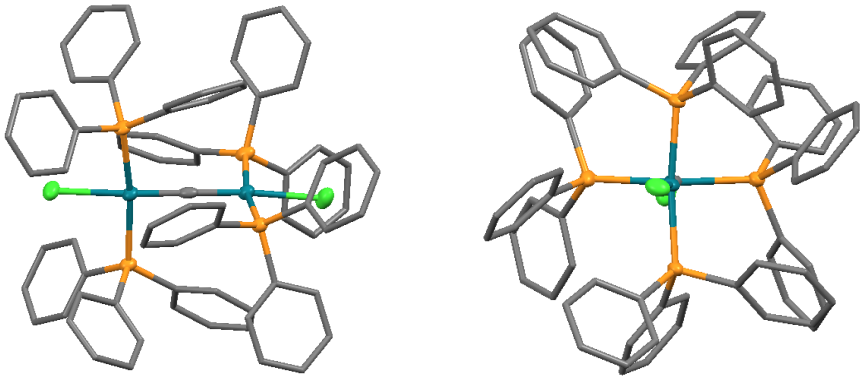

Figure 1.6: (left) simplified structure of **$[Rh_2(\mu\text{-}C)Cl_2(PPh_3)_4]$**. (right) view along the Rh=C=Rh vertex showing the retention of square-planar rhodium(I) geometry

Examining the structures of the three rhodium μ-carbido complexes, the retention of the square-planar geometry at the rhodium centres implies the retention of the 16-electron, d^8 rhodium(I) oxidation state using the neutral carbide formalism. In order to satisfy this electronic requirement, the Class A μ-carbido ligand must act as a two-electron donor to both metal centres, in a similar fashion to carbonyl or thiocarbonyl ligands. This presents an alternative viewpoint to that presented in early macrocycle Class A chemistry, which considered the μ-carbido as a C^{4-} ligand, which is perhaps more acceptable for carbido complexes of the less electronegative element iron (PE(Fe) = 1.83).

A further example of chalcocarbonyl activation involving the heavier element selenium appeared in 2019,[52] in which the neutral tungsten selenocarbonyl species **[W(NO)(CSe)(CO)(Tp*)]** was treated with the same rhenium *solvento* species **[Re(THF)(CO)$_2$(Cp)]** used to synthesis **[Re$_2$(μ-C)(CO)$_4$Cp$_2$]**. Addition of the two complexes resulted in abstraction of selenium and the coordination of the resulting carbido fragment to the rhenium complex, forming one of the scarce heterometallic cumulenic μ-carbido complexes **[WRe(μ-C)(CO)$_3$(NO)Cp(Tp*)]**.[viii] The synthesis was presumed to involve selenium abstraction by the rhenium complex, partially supported by the isolation of a rhenium μ-selenido complex (**Scheme 1.14**).

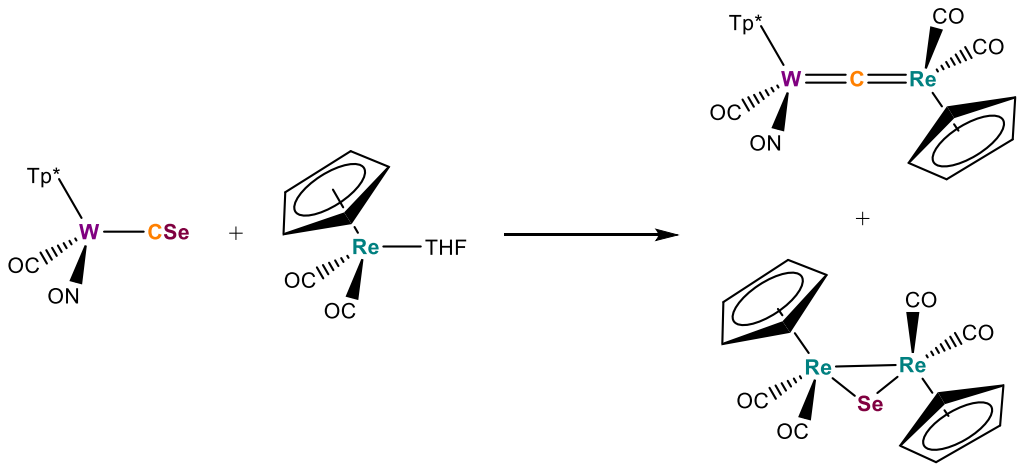

Scheme 1.14: CSe bond cleavage and synthesis of a heterometallic Class A μ-carbido

The most notable characterisational feature was the downfield shift of the μ-carbido resonance in the ^{13}C NMR spectra, appearing at 508.8 ppm, making it the lowest field Class A resonance to date. The asymmetric vibration band in the infrared for $\nu_{W=C=Re}$ was detected at 1019 cm^{-1} (calculated at 1004 cm^{-1}). The heterometallic nature of the complex results in two distinct bonds from the carbido ligand (W = 1.966(6), Re = 1.893(6) Å), though both remain classified for

[viii] Analogies between Cp, Cp*, Tp and Tp* ligands are regularly drawn in the literature, as is the isoelectronic relationship between ReCO and WNO units. The complexes **[Re$_2$(μ-C)(CO)$_4$(Cp)$_2$]** and **[WRe(μ-C)(CO)$_3$(NO)(Cp)(Tp*)]** are therefore considered to be isoelectronic.

electronic inventory purposes as M=C double bonds, classifying it as a Class A cumulenic μ-carbido complex.

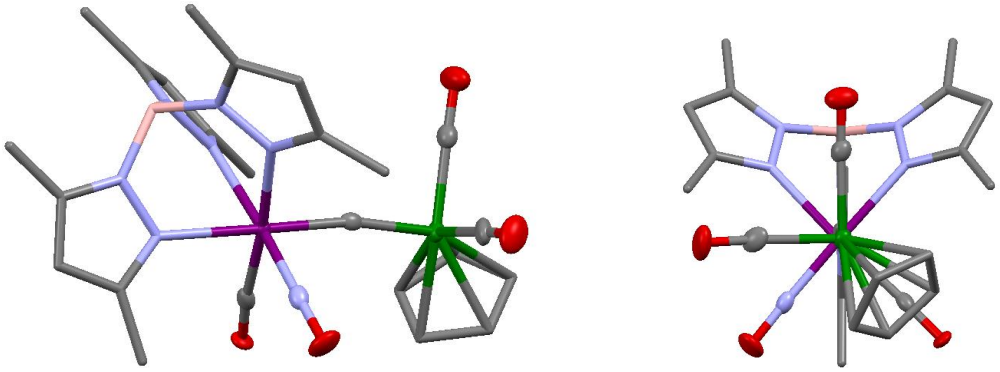

Figure 1.7: (left) Simplified molecular structure of **[WRe(μ-C)(CO)$_3$(NO)Cp(Tp*)]**. (right) view down Re=C=W axis

C-Halogen Reduction

The most recent addition (and published after majority of the work described herein) to the dimetallacumulene synthetic pathway is the reduction of a carbon-halogen bond from Takao and Seki.[53] Taking the ruthenium μ-chloromethylidyne species **[{(Cp*)RuCl}$_2$(μ-CCl)(μ-Cl)]**,[ix] reduction with zinc in the presence of ethene formed the μ-ethylidyne-μ-propylidyne complex **[(Cp*Ru)$_2$(μ-CMe)(μ-CEt)(μ-ZnCl$_2$)]**. The chlorocarbyne reduction was inferred to proceed through a μ-carbido ligand, and when the reduction with zinc was performed in the presence of diethyl maleate, the μ-carbido complex could be isolated as **[(Cp*Ru)$_2$(μ-C){μ-η$_1$:η$_2$-ZnCl(−OC(OEt)CH=CHC(OEt)O−}$_2$]** (**Scheme 1.15**).

[ix] Bridging halocarbyne chemistry is discussed in more detail in **Section 2.1**

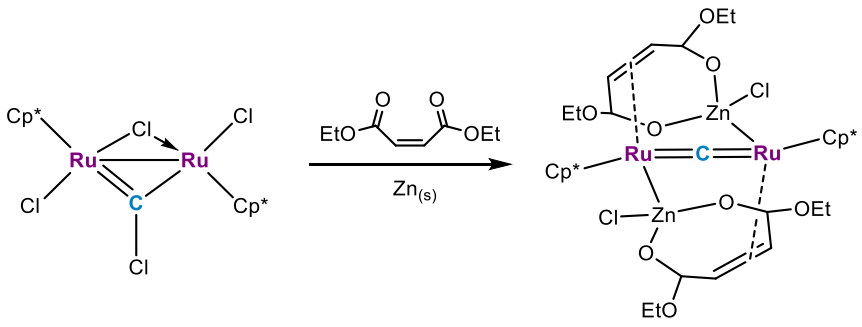

Scheme 1.15: Reduction of μ-chloromethylidyne to μ-carbido ligand

The average Ru=C bond length of 1.84 Å was noted by the authors to be slightly longer than the previous ruthenium μ-carbido complexes, which is perhaps not surprising given the associated bridging assemblies. Carbon-13 NMR studies performed on **[(Cp*Ru)$_2$(μ-C){μ-η$_1$:η$_2$-ZnCl(−OC(OEt)CH=CHC(OEt)O−}$_2$]** identified the μ-carbido signal at 458.7 ppm, at a lower field than the μ-ethylidyne and μ-propylidyne signals in **[(Cp*Ru)$_2$(μ-CMe)(μ-CEt)(μ-ZnCl$_2$)]**.

The synthesis of non-macrocyclic Class A μ-carbido complexes have, with only two exceptions, been achieved through activation of chalcocarbonyl ligands. The weakening of the carbon-chalcogen bond after metal coordination enables cleavage through addition of an abstracting agent, and it is likely this process will continue to be developed to produce more generalisable synthetic routes to these complexes. Unfortunately, a readily accessible, high yielding and readily functionalisable μ-carbido complex was, prior to the outset of this project, out of reach.

1.2.6 Class A Properties

M=C=M Rotation Barrier

One of the defining areas of interest in Class A carbido chemistry is the rotation barrier of the μ-carbido core. Unlike Classes B and C, the two formal double bonds of Class A in principle might be expected to result in restrict rotation much like their organic counterparts (allenes). Allenes, due to the directionality of the carbon p-orbital π-bonds, have a severe rotation barrier peaking at 90 ° with rotation barrier energies in the order of 200 kJ.mol^{-1}. Metal carbenes (alkylidenes) display a remarkably wide range of rotation barriers because unlike the methylene

termini of allenes which have a single *p*-orbital for sustaining C–C multiple bonding, the π-component of metal-carbon multiple bonding arises from interaction of 't_{2g}-type' *d*π orbitals, two of which have π-symmetry with respect to the metal-carbon vector. Depending on the nature of ancillary ligands, these may be of different energies and occupancies, and it is these variables that contribute to the broad range of rotation barriers observed, and even the co-existence of discreet rotamers.[x]

This was first noted by Wolczanski on the ditungsten complexes.[40] Based on NMR coalescence of the silox resonances in the ^{1}H NMR spectra, the rotation barrier of the W=C=W spine were calculated to be 70.1 kJ.mol^{-1} for **[(silox)$_2$(O)W=C=WCl$_2$(silox)$_2$]** but only 46 kJ.mol^{-1} for **[(silox)$_2$(NAr)W=C=WCl$_2$(silox)$_2$]**. Notwithstanding the very substantial steric encumbrance of the ancillary ligands, adopting the neutral carbide formalism would allocate each tungsten a d^2 configuration, *i.e.*, with only a single orbital for contribution to W–C π-bonding, being more akin to an allene. The Wolczanski carbido complexes are however at present unique in possessing such low d-occupancies, with all other Class A examples being d^6-d^6 or d^8-d^8 such that all d_{xy}, d_{xz} and d_{yz} orbitals are occupied and available for retrodonation.

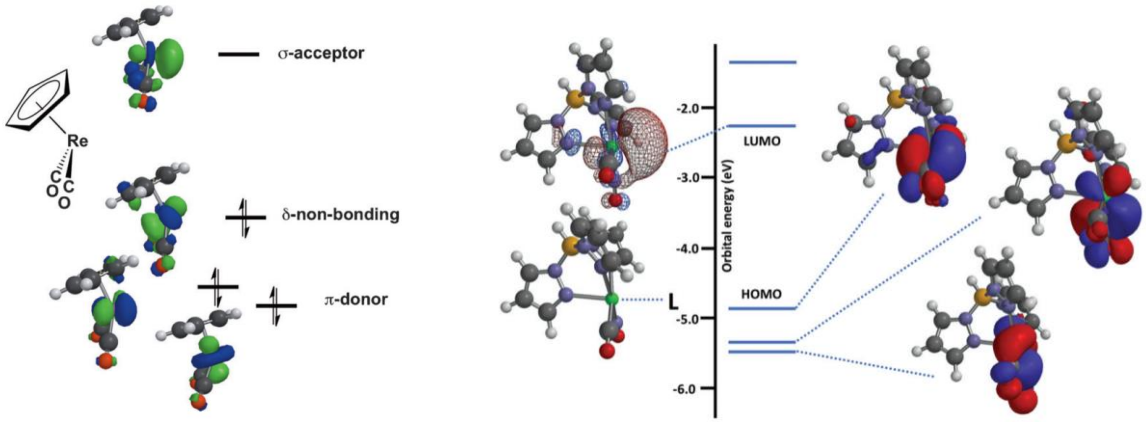

Figure 1.8: (left – from [45]) Relevant orbitals of **[Re(CO)$_2$Cp]** fragment. (right – from [52]) Relevant orbitals of **[W(Tp)(NO)(CO)]**

[x] For two occupied and degenerate metal *dp* orbitals, π-bonding can be sustained through any angle of rotation, leaving only steric factors to contribute.

The simplicity of the rhenium μ-carbido complex **[{Re(CO)$_2$(Cp)}$_2$(μ-C)]** makes it especially amenable to both experimental and computational investigation. The high symmetry inferred from the ^{1}H and ^{13}C NMR spectra suggested magnetic equivalence of the four carbonyl and two cyclopentadienyl ligands, which could only be possible through either a static C_{2h} geometry with anti-periplanar cyclopentadienyl groups or a low rotation barrier about the cumulenic carbido. Theoretical interrogation revealed a 3-centre, 12-electron bonding system of Class A carbidos, in comparison to the 3-centre, 8-electron bond of the allene. Taking the rhenium fragment **'Re(CO)$_2$Cp'**, there are four possible orbitals on the metal centre that point towards the μ-carbido ligand. The two low-lying near-degenerate orbitals were characterised as π-retrodonating, one was non-bonding and the highest in energy was the σ-acceptor orbital (empty for d^6-occupancy). This would allow for σ-donation from the carbido ligand to the metal, and two near degenerate, orthogonal metal orbitals capable of π-retrodonation back to the carbido. Because of this, a linear combination of atomic orbitals can be surmised to describe the π-bonding of the carbido ligand at any angle (See **Figure 1.8**) as the metal orbitals can interact with both the p_x and p_y orbital on the central carbon. In this respect the bonding is more akin to O=C=O than H$_2$C=C=CH$_2$. The experimental and theoretical studies that have been performed on Class A carbido complexes support a clear distinction from the organic cumulene analogue. With a more intricate and complex bonding system at the transition metal, the inorganic μ-carbido complexes do not suffer from the high rotation barriers that allenes do and may lead to unforeseen chemistry. This was again confirmed recently with the asymmetric species **[WRe(μ-C)(CO)$_3$(NO)(Cp)(Tp*)]**, as the orbitals of the tungsten fragment again displayed isolobal orbital representations.

^{13}C{^{1}H} NMR

For a ligand consisting of a single carbon the primary discussion point μ$_2$-carbido complexes provide to explore their properties resides with the data provided by ^{13}C{^{1}H} NMR spectroscopy. Compared to other common nuclei such as ^{1}H, ^{31}P and ^{19}F, the spin active nucleus of carbon (^{13}C) is only 1.1% naturally abundant making it more challenging to measure under normal circumstances even though most modern spectrometers are optimised for this particular nucleus. The issue of measurement compounds when a 'quaternary' μ$_2$-carbido ligand does not have any hydrogens attached, thus signal intensity is reduced akin to a tertiary carbon in the absence of nuclear Overhauser effect enhancement. Secondly, the presence of spin-active nuclei (both

metal and co-ligand) may further reduce the signal intensity. As the two bound termini of these nuclei are both metals, the paramagnetic deshielding contribution towards the carbon nucleus is greatly enhanced and thus the chemical shift of such a carbon is likely to be well outside the normal range – both a help and a hindrance. Finally, a significant number of the μ-carbido population are of the form $[M_2(\mu\text{-C})(\text{macrocycle})_2]$ for which perhaps the macrocycle aromatic ring current is responsible for such resonances not yet being reported. Despite these challenges, many compounds have had their carbido chemical shifts measured and their implications are discussed in this section.

The first use of $^{13}C\{^1H\}$ NMR data to characterise a μ-carbido complex was demonstrated by Selegue and co-workers with their Class B metallacarbyne **$[(Me_3CO)_3W{\equiv}C{-}Ru(CO)_2(Cp)]$** which displayed a downfield resonance at δ_C of 273.3.[4] By contemporary standards, this is rather shielded. The tungsten terminus also contains a spin active nucleus [^{183}W, I = ½, 14% abundance], such that Selegue also detected clear satellites straddling the carbido resonance ($^1J_{CW}$ = 290 Hz) not dissimilar to the values observed for convention alkylidyne complexes $L_nW{\equiv}CR$. Selegue's complex, although not the first species produced in the μ_2-carbido family, demonstrated the use of $^{13}C\{^1H\}$ NMR spectroscopy as a viable technique to measure these unique carbon atoms.

In the years prior, several studies had already begun on class A μ-carbido complexes beginning with Mansuy's porphyrin species **[(TPP)Fe=C=Fe{TPP)]**, yet $^{13}C\{^1H\}$ NMR data were not reported. It is for the aforementioned paramagnetic contributions that not only are the chemical shifts of these early species presumably much further downfield than what may be expected, it is likely they were unable to be detected at all due to low signal/noise achievable with magnets of the day. Many more class A species have been produced in the interim and aided by technological advancements, many of their $^{13}C\{^1H\}$ resonances have been assigned and therefore interclass comparisons with classes B and C can be drawn.

Except for the questionable assignment of the iron-rhenium complex **$[(TPP)Fe{=}C{=}Re(CO)_4Re(CO)_5]$**,[35] almost all of the μ-carbido resonances appear at shifts greater than 350 ppm and with 508.8 ppm as the contemporary boundary. Coordination to the metal centre can also result in unique coupling, such as the triplet of pentet multiplicity recorded for the dirhodium complexes. Unfortunately, the unique environments these carbido ligands often confounds (or deters) detection in NMR studies, and as **Table 2.2** below details, only 13 resonances have been found to date. Regardless, the complexity of the origins of the downfield shift calls for a more sophisticated analysis of the shielding tensor than the simple

inductive/mesomeric deshielding arguments used to interpret simple shifts in typical ^{1}H and ^{13}C NMR spectra.[xi]

Complex	δ_C	as. $\upsilon_{M=C=M}$ (cm^{-1})	M=C=M (°)
[(TPP)Fe=C=Re(CO)$_4$Re(CO)$_5$]	211.7*	-	173.3(9)
[{Nb(p-^{t}Bu-calix[4]-(O)$_4$)}$_2$(μ-C)Na$_3$]	257	-	-
[(silox)$_2$(O)W=C=WCl$_2$(silox)$_2$]	379.1	1155	-
[(silox)$_2$(NAr)W=C=WCl$_2$(silox)$_2$]	406.3	1120	176.0(12)
[Rh$_2$(μ-C)Cl$_2$(PPh$_3$)$_4$]	424.4	1011	173.4(2)
[Rh$_2$(μ-C)(SGePh$_3$)$_2$(PEt$_3$)$_4$]	425.8	-	175.6(2)
[Rh$_2$(μ-C)(SGePh$_3$)(SBpin)(PEt$_3$)$_4$]	429.3	-	-
[({(p-cymene)Ru(μ-Cl)$_3$}RuCl(PCy$_3$))$_2$(μ-C)]	430.5	-	178.8(9)
[{Re(CO)$_2$(Cp)}$_2$(μ-C)]	436.4	1019	173.3(7)
[Rh$_2$(μ-C)(SBpin)$_2$(PEt$_3$)$_4$]	439.4	978	176.1(4)
[Rh$_2$(μ-C)H(κ$_c$-2-C$_6$H$_4$PPh$_2$)(Tp*)$_2$]	447.2	-	165.9(3)
[Ru$_2$(μ-C){μ-ClZn(DEM)}$_2$(Cp*)$_2$][A]	458.7	-	172.1(1)
[(Tp*)(ON)(CO)W=C=Re(CO)$_2$Cp]	508.8	1019	169.3(3)

Table 1.2: Relevant ^{13}C NMR, infrared and structural data for μ-carbido complexes

([a] DEM = diethylmaleate)

Trans-effect of μ$_2$-carbido ligands

One of the defining features of a ligand class is the impact it has on the bonding (*trans* influence) and lability (*trans*-effect) of the ligand to which it is coordinated *trans* on the metal centre. In its simplest form, two occupied σ-donor ligand orbitals combine with the same empty metal orbital in a 3-centre, 4-electron σ-bonding manifold such that the middle orbital swells in the

[xi] This challenge will be addressed in more detail in **Chapters 4** and **6**.

vicinity of the bond to the more electronegative donor atom. The bond is thereby preferentially weakened which may be evident in the ground-state structure (X-ray crystallography *r*(M–L), IR ν_{M-L} or NMR $^{1}J_{ML}$) and this may be manifest in a kinetic labilisation ("*trans* effect"[xii]). Accordingly, strong trans influences are characteristic of stong σ-donor ligands based on electropositive donors (hydrides, σ-organyls, silyls and boryls). Is also, however, a recurrent feature of π-acidic C_1 ligands such as carbenes, carbynes, chalcocarbonyls and vinylidenes and might therefore be expected for μ-carbido ligands.

The most effective means of quantifying the *trans*-influence of the μ-carbido ligand involves examining the bond lengths of molecular structures for elongation since infrared and NMR data are somewhat more equivocal. The earliest work for Class A complexes where this is possible is the tetrametallic ruthenium complex **[({(P-cymene)Ru(μ-Cl)$_3$}RuCl(PCy$_3$))$_2$(μ-C)]**.[42] The complex contains two identical sets of three bridging chloride ligands, which are position *trans*- to the carbido, terminal chloride, and phosphine ligand respectively (**Figure 1.9**). Because of this, the *trans*- influence of these three ligands can be directly and internally compared. The chloride ligand *trans*- to the terminal chloride was unsurprisingly the shortest at 2.439(3) Å, followed by the phosphine ligand at 2.548(3) Å. The longest Ru-Cl bond length was observed for the chloride *trans*- to the carbido ligand (2.685(3) Å), a full 0.1 Å longer than the chloride *trans*- to the phosphine. This implies the μ-carbido ligand has a significantly stronger *trans* influence than the PCy_3 and chloride ligand.

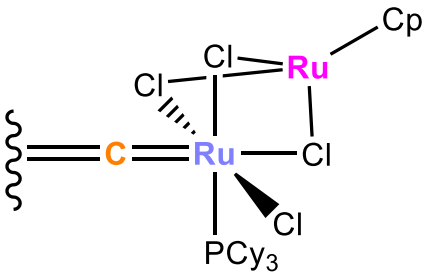

Figure 1.9: Simplified structure of **[({(P-cymene)Ru(μ-Cl)$_3$}RuCl(PCy$_3$))$_2$(μ-C)]**, highlighting μ-chloride *trans* ligands

[xii] The *trans* effect is not limited to ground-state *destabilisation* (*trans* influence) but may also originate from transition state *stabilisation* , *e.g.*, by π-donor ancillary ligands.

This analysis may be repeated with the unsymmetrical tungsten rhenium carbido complex **[(Tp*)(NO)(CO)W=C=Re(CO)$_2$Cp]**. The tungsten centre contains the tridentate scorpionate 'reporter' ligand Tp*, with nitrogen donors positioned *trans-* to the carbonyl, nitrosyl and carbido ligands. Examining the W-N bond lengths, again the nitrogen positioned *trans-* to the carbido has the most elongated bond length at 2.278(4), which is 10 e.s.d. longer than the nitrosyl ligand and 14 e.s.d. longer than the nitrogen *trans-* to the carbonyl group.[xiii] This again confirms experimentally the strong *trans-* effect of the μ-carbido ligand.

Perhaps the easiest form of comparison has come with the detailed work into the rhodium μ-carbido complexes, as they can invoke direct comparisons to carbonyl and thiocarbonyl analogues. Braun's germyl thioether complex **[Rh$_2$(μ-C)(SGePh$_3$)$_2$(PEt$_3$)$_4$]** was formed alongside the corresponding thiocarbonyl species **[Rh(SGePh$_3$)(CS)(PEt$_3$)$_2$]**.[47] Comparing the Rh-S bond to the thioether, the thiocarbonyl and μ-carbido ligand can be directly compared. The thiocarbonyl species, a strong π-acceptor with strong ligand-field effects, has a Rh-S bond length of 2.4389(5) Å. Comparing the Class A carbido, the Rh-S bond length increases marginally to 2.4903(10) Å. In a similar manner with the rhodium μ-carbido species **[Rh$_2$(μ-C)Cl$_2$(PPh$_3$)$_4$]**, comparing the μ-carbido ligand to the structurally characterised thiocarbonyl and carbonyl analogues **[RhCl(CE)(PPh$_3$)$_2$]** (E = O, S), the μ-carbido complex contains considerably elongated Rh-Cl bond lengths.[51] The carbonyl and thiocarbonyl bond lengths are essentially comparable at 2.395(4) and 2.3872(7) Å, respectively, but the average Rh-Cl bond length for the μ-carbido species is 2.4288(7), owing to the stronger *trans-* influence of the μ-carbido ligand in comparison to carbonyl and thiocarbonyl ligands.[xiv]

[xiii] Nitrosyl and carbonyl ligands are themselves considered to exert strong *trans* influences such that the variations are less pronounced than in the tetraruthenium example.

[xiv] Chemical manifestations of the *trans*-labilisation of this halide will be encountered in subsequent discussions.

1.2.7 Reactivity of Class A complexes

Ligand Substitutions

One of the issues associated with Class A carbido chemistry prior to this study is the lack of diversification of co-ligands and their amenability towards further modification. Of all of the complexes presented, only two have be shown to undergo co-ligand transformation following carbido installation. For the rhodium carbido complex **[Rh$_2$(μ-C)(SBpin)$_2$(PEt$_3$)$_4$]**, although no carbido-centred reactivity was reported, the B–S bond of the borylthiolato ligand could be hydrolysed with methanol to form the terminal sulfhydryl ligand in **[Rh$_2$(μ-C)(SH)$_2$(PEt$_3$)$_4$]**. The thiol ligand is potentially a more useful ligand for further reactivity studies, though none were performed.

The bulk of the work into co-ligand transformation have come from the rhodium μ-carbido complex **[Rh$_2$(μ-C)Cl$_2$(PPh$_3$)$_4$]**. The readily functionalised chloride and triphenylphosphine co-ligands were seen to individually and collectively be replaced with monodentate and polydentate ligands. This synthetic versatility may be traced to the coordinative unsaturation of the 16-electron rhodium centres allowing access to associative substitution pathways in combination with the *trans* effect (*vide supra*) of the carbido ligand and the steric bulk of the phosphine ligands. Addition of a silver salt (such as silver(I) triflate) in acetonitrile selectively abstracts chloride from the rhodium centres, forming the dicationic complex **[Rh$_2$(μ-C)(MeCN)$_2$(PPh$_3$)$_4$](OTf)$_2$**.

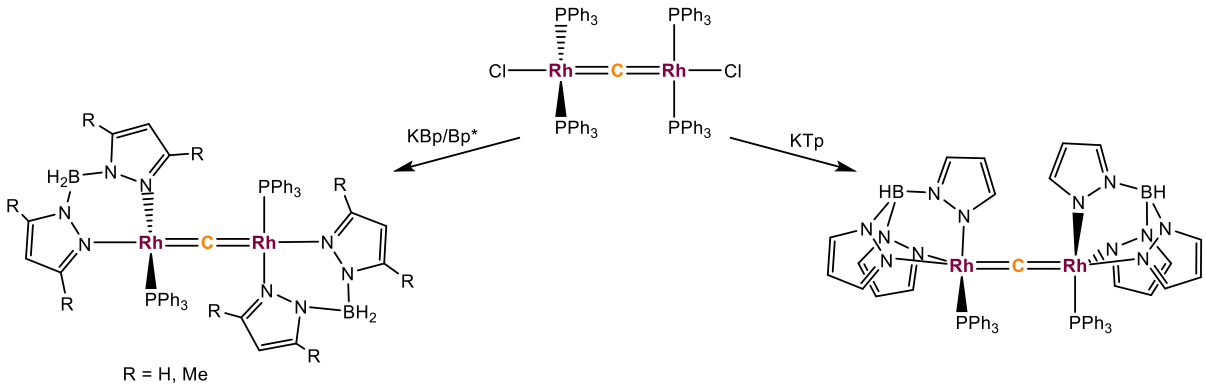

Scheme 1.16: poly(pyrazolyl)borate ligand substitution to **[Rh$_2$(μ-C)Cl$_2$(PPh$_3$)$_4$]**

The phosphine and halide co-ligands could be removed to coordinate bidentate and polydentate ligands (**Scheme 1.16**).[51] The geometric effects on the μ-carbido ligand were assessed by installing a series of poly(pyrazolyl)borates ligands. The coordination of bidentate borates and tridentate tris(pyrazolyl)borate led to the expected symmetrical complexes **[Rh$_2$(μ-C)(PPh$_3$)$_2$(L)$_2$]** (L = Bp, Bp*, Tp). The increase in coordination number from the bidentate Bp to tridentate Tp is evident in the smaller $^1J_{RhP}$ coupling constant (212 Hz *cf.* 166 Hz), though ^{13}C NMR studies were unsuccessful in locating the μ-carbido resonance.

The most sterically cumbersome of these pyrazolyl borate ligands, Tp*, did not produce the intended compound **[Rh$_2$(μ-C)(PPh$_3$)$_2$(Tp*)$_2$]**. Rather, the ^{1}H NMR spectrum included a high-field resonance (-12.86 ppm) that displayed a ddd multiplicity ($^1J_{RhH}$ = 29, $^3J_{RhH}$ = 25, $^4J_{PH}$ = 3 Hz), which suggested a terminal hydride ligand present on a complex with distinct rhodium chemical environments and a single phosphine ligand. The molecular structure confirmed that the *ortho*-hydrogen of one phenyl ring on the phosphine ligand had undergone C–H activation with the rhodium centre, forming as asymmetric phosphine bridging ligand (**Scheme 1.17**).

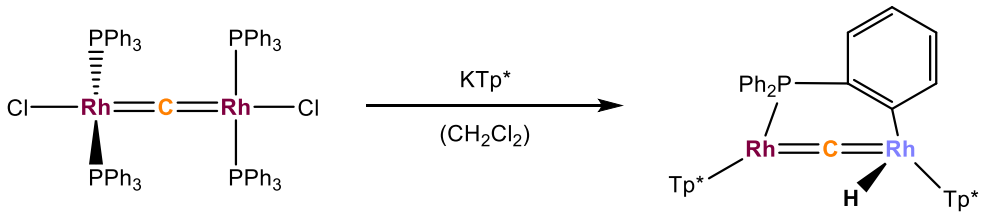

Scheme 1.17: *ortho*-metalation of PPh$_3$ to form asymmetric homometallic μ-carbido complex

The complex **[Rh$_2$H(μ$_2$-C)(μ:κ^2-*C,P*-C$_6$H$_4$PPh$_2$-2)(Tp*)$_2$]** features two distinct rhodium environments: a five-coordinate rhodium(I) centre, and a six-coordinate rhodium(III) centre. Despite the changes in oxidation state and coordination number, the formal bonding system of the μ-carbido ligand is still classified as Class A, as the two Rh=C bond lengths (1.818(6) and 1.740(6) Å) fall within the range observed for a bond order of two, and the six-coordinate rhodium(III) bond length to the carbido ligand is longer as expected when shifting to higher coordination number. Isotopic labelling of the μ-carbido ligand by employing ^{13}CS$_2$ in the formation of the thiocarbonyl precursor revealed the presence of the μ-carbido environment in the ^{13}C{^{1}H} NMR spectrum, downfield at 447.2 ppm and displaying distinct coupling to the two

rhodium and one phosphorus nuclei ($^1J_{RhC}$ = 50, 40 Hz, $^2J_{PC}$ = 20 Hz). The juxtaposition of both hydride and σ-aryl groups cis to the carbide is of note in that both these ligands are often prone to migratory insertion to C_1-π-acid ligands. Exposure to CO failed to induce any reaction to form putative **[Rh$_2$(μ$_2$-C)(CO)(PPh$_3$)(Tp*)$_2$]**, providing circumstantial evidence that the C–H activation process does not appear to be spontaneously reversible.

Redox Chemistry

Though not directly carbido-centred reactivity, one of the reactions investigated for Class A complexes has been their redox chemistry. The earliest work comes from Wolczanski with the ditungsten complex **[(silox)$_2$(O)W=C=WCl$_2$(silox)$_2$]**.[40] In an effort to reduce the μ-carbido species, it was treated with a sodium/mercury amalgam and H_2, and the result of the reduction included a hydrogenation of the μ-carbido ligand (**Scheme 1.18**). The reduced species, **[{(silox)$_2$W}$_2$(μ-CH)(μ-O)(μ-H)]**, was believed to contain bridging oxo and hydride ligands, in addition to the hydrogenated μ-methylidyne ligand. The μ-methylidyne ligand was detected at 319.5 in the ^{13}C NMR spectrum, with the hydrogen resonance appearing at a remarkably low field chemical shift of 19 ppm in the ^{1}H NMR spectrum, and unusually the μ-hydride was reported at a low field shift of 11.77 ppm. This process is intriguing in the context of what roles surface bound carbidos ligands might play in Fischer Tropsch processes.

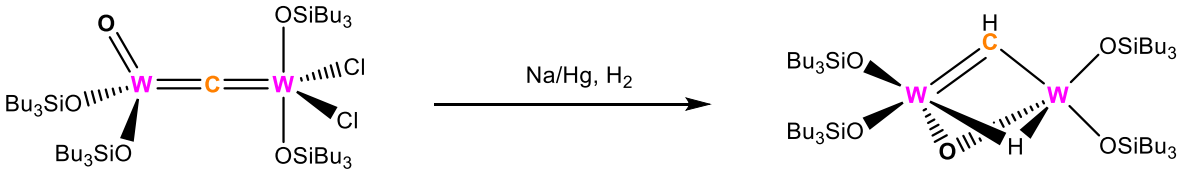

Scheme 1.18: Reduction and hydrogenation to produce μ-methylidyne ligand

Oxidation of a μ-carbido complex was also described by Floriani and co-workers, however, the oxidation process did not intimately involve the μ-carbido ligand.[41] The niobium complex **[{Nb(p-^{t}Bu-calix[4]-(O)$_4$)}$_2$(μ-C)Na$_3$]** is paramagnetic and contains three μ-Na nuclei which have a weak affinity for the μ-carbido ligand. Oxidation of this complex was achieved with ferrocenium

and resulted in a diamagnetic species (hence the identification of the μ-carbido resonance at ~257 ppm) which was believed to contain only two bridging sodium nuclei. The μ-carbido ligand and remainder of the complex remained unchanged, and no further characterisation or reactivity was explored. A further oxidation process was explored by Ercolani and co-workers, who used iodine as an oxidant to form the partially oxidised μ-carbido phthalocyanine complex **[{(pc)Fe}$_2$(μ-C)](I$_3$)$_{0.66}$**.[34] Once again, the oxidation reaction displays no chemical consequences at the μ-carbido ligand, being apparently[xv] a strictly metal-centred process.

Reactivity at the μ-carbido ligand

The serendipitous nature of dimetallacumulenic synthesis, combined with the steric encumbrance of the co-ligands, has resulted in the field being largely untouched. Tantalisingly, there has yet to be a documented example of successful directed reactivity at a Class A μ-carbido ligand. The indirect reduction and hydrogenation to form a μ-methylidyne ligand presented by Wolczanski and co-workers remains the only example of any observed functionalisation.

One plausible reason for this lack of chemistry is the prophylactic steric encumbrance commonly associated with the majority of known μ-carbido complexes. Braun and co-workers reported in their synthesis of **[Rh$_2$(μ-C)(SBpin)$_2$(PEt$_3$)$_4$]** that attempts to observe reactivity at the μ-carbido ligand had been unsuccessful and stated that the steric bulk of the four triethylphosphine (Tolman Cone Angle = 132°) co-ligands is a likely culprit behind its inactivity. In the case of **[Rh(μ-C)Cl$_2$(PPh$_3$)$_4$]** (TCA = 145°) this is also likely to be a key factor.

1.2.8 Rationale for this work

As sections of the preceding introduction highlighted, there exist significant gaps in the emerging literature of Class A carbido complexes. Due to the rather serendipitous nature behind many of the μ-carbido synthetic pathways, these processes have been exceptionally specific to the molecule and fail to provide a more generalisable route to Class A complexes. Indeed, the generally

[xv] In metal porphyrin and phthalocyanine redox chemistry, the potentially non-innocent role of the heterocyclic chelate is often a matter for debate.

substitution-inert nature of many of the metal-ligand coordination spheres employed may well have played a role in such complexes even being successfully isolated. This has so far limited the expansion of the Class, and efforts towards a more generalised route should be undertaken to achieve this.

The second omission from the literature is the subsequent reactivity of these complexes. The dimetallacumulenic μ-carbido ligand presents a unique chemical environment for carbon; π-bound to two metal centres. It has been seen from the ^{13}C NMR studies that these carbon environments are significantly deshielded compared to metallacarbynes, carbenes and organic analogues.

The very limited reactivity studies attempted have largely been thwarted by the steric encumbrance of the co-ligands, essentially in many cases blocking access to the μ-carbido itself. In addition to this, many of the complexes shown do not possess a ligand set that lends itself to easy modification following carbido installation. This is yet another issue that has not been overcome in the field but is the most important challenge to address. Possible functionalisation of the Class A μ-carbido ligand may lead to further unexplored organometallic chemistry.

The work to be described arises from the rhodium complex **$[Rh_2(\mu\text{-}C)Cl_2(PPh_3)_4]$**, the initial synthesis and preliminary ligand substitutions of which were explored during the author's brief Honours research project, much of which has been published (see **Supporting Information**). This complex, alongside suitably engineered derivatives to be described, provide an ideal and versatile platform to address the challenges and omissions discussed above. The work aims to take Class A complexes beyond their status as laboratory curiosities and begin to define a reactivity profile for the cossetted lone carbon atom *en route* to functional utility.

EPISODE ONE - THE PHANTOM CARBON

PART TWO:

SYNTHESIS OF DIMETALLACUMULENIC μ-CARBIDO COMPLEXES

1.3 Results and Discussion

1.3.1 μ-carbido Bonding Analysis

Before delving into the reactivity and substitution patterns of the μ-carbido complex **[Rh$_2$(μ-C)Cl$_2$(PPh$_3$)$_4$]**, examination of the Frontier Molecular Orbitals (FMOs) of the complex is a useful step in understanding the π-bonding system of the μ-carbido ligand. It was discussed previously in **Section 1.2.4** that the μ-carbido rotation barrier is significantly lower when compared to allene species, and this was primarily due to the presence of multiple low-lying occupied metal *d*-orbitals with π-symmetry to the carbon.

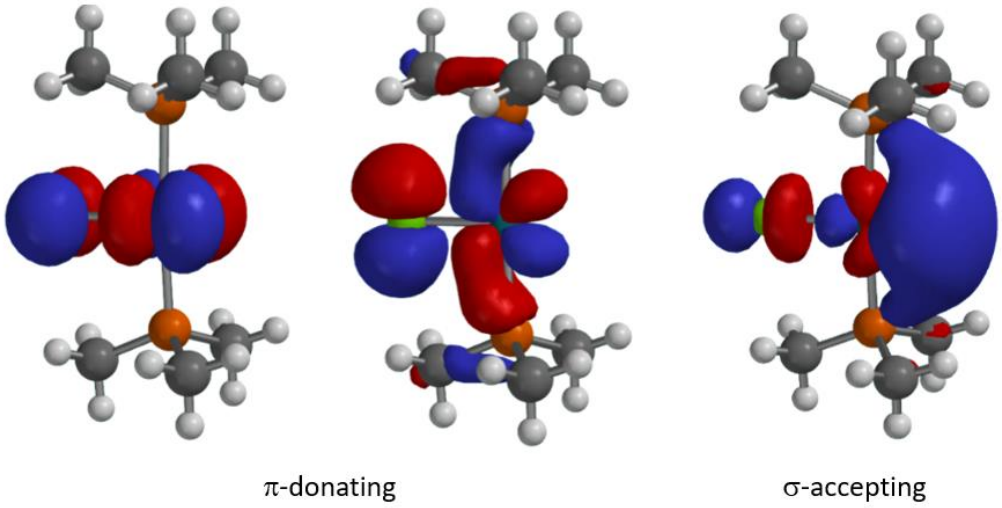

Figure 1.10: (left-middle) Occupied fragment orbitals of **[RhCl(PPh$_3$)$_2$]**, which have π-symmetry to the μ-carbido. (right) rhodium virtual σ-acceptor orbital

Examining the simplified dirhodium complex **[Rh$_2$(μ-C)Cl$_2$(PMe$_3$)$_4$]**, the bonding system becomes more sophisticated than that of an isolobally related allene. Looking at the molecular orbitals of the rhodium centre (modelled as the fragment **[RhCl(PMe$_3$)$_2$]**[xvi]), it contains two

[xvi] These orbitals, provided for illustrative purposes, were derived by optimising the geometry of **[RhCl(CO)(PMe$_3$)$_2$]**, removing the CO ligand and generating FMOs from the frozen geometry.

primarily[xvii] *d*-orbitals that have the correct symmetry to act as π-retrodative orbital to the central carbon (d_{xy} and d_{xz}, defining the P-Rh-P axis as z). Excavating the FMOs (**Figure 1.10**), there are four occupied metal-ligand fragment orbitals, within 1 eV of one another, directed along the Rh=C vector, one with σ-symmetry and two that present the required π-symmetry to presumably interact with the $p_{x,y}$ orbitals on the central carbon atom.

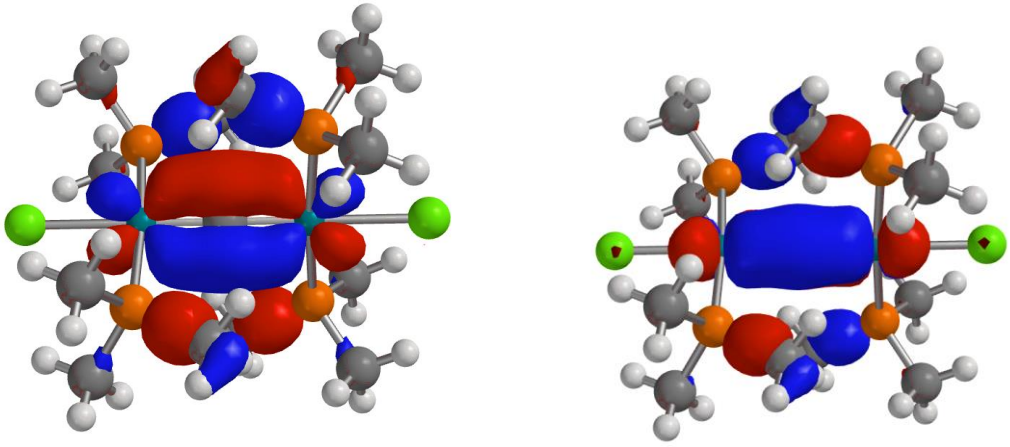

Figure 1.11: Rh=C=Rh π-bonding molecular orbitals for **[Rh$_2$(μ-C)Cl$_2$(PMe$_3$)$_4$]**

The molecular orbitals of the rhodium cumulenic carbido species are more complex but give credence to the previously calculated low rotation barrier of the M=C=M linkage.[xviii] The π-system of the cumulenic μ-carbido complex **[Rh$_2$(μ-C)Cl$_2$(PMe$_3$)$_4$]**, arises from six atomic orbitals (4x Rh, 2x C), which subsequently contribute to six molecular orbitals. An 'allene-esque' π-bonding is present in the degenerate HOMO-1 and -2 orbitals, which consist of one in-phase and out-of-phase Rh=C π-bond. The two systems are orthogonal to each other, as each rhodium interacts with a different carbon *p*-orbital.

[xvii] Although the discussion here is focused on the Rh=C=Rh unit, the clear involvement of halide *p*-orbitals in these retrodative fragment orbitals indicates that the *trans* ligand is also an avenue for modification of the bonding.

[xviii] The geometry of **[Rh$_2$(μ-C)Cl$_2$(PMe$_3$)$_4$]** optimised at the B3LYP/6-31G* level of theory gives a dihedral angle of 90.00° between the two rhodium coordination planes, *cf.* 90.09(2)° observed experimentally for the PPh$_3$ complex.

Buried much further down in the molecular orbital framework (HOMO-14 and -15) are two π-bonding molecular orbitals, except both are completely in-phase across the entire Rh=C=Rh linkage (**Figure 1.11**). The two molecular orbitals are orthogonal relative to each other and interact with the two *p*-orbitals on the μ-carbon. The rotation of one rhodium centre would not break the π-system, as a LCAO (Linear Combination of Atomic Orbitals) could be written to account for any dihedral angle.

One of the key features of the μ-carbido complexes is the heavy metal presence in the FMOs. Examining the HOMO reveals that the molecular orbital is rhodium centred, consisting largely of the d_{z2} orbitals with almost negligible contribution from the central carbon atom (**Figure 1.12**). Unlike allenes, in which reactivity is heavily based on the C=C π system, the reactivity of these square planar rhodium μ-carbido complexes may exhibit both metal- and carbon-centred reactivity.

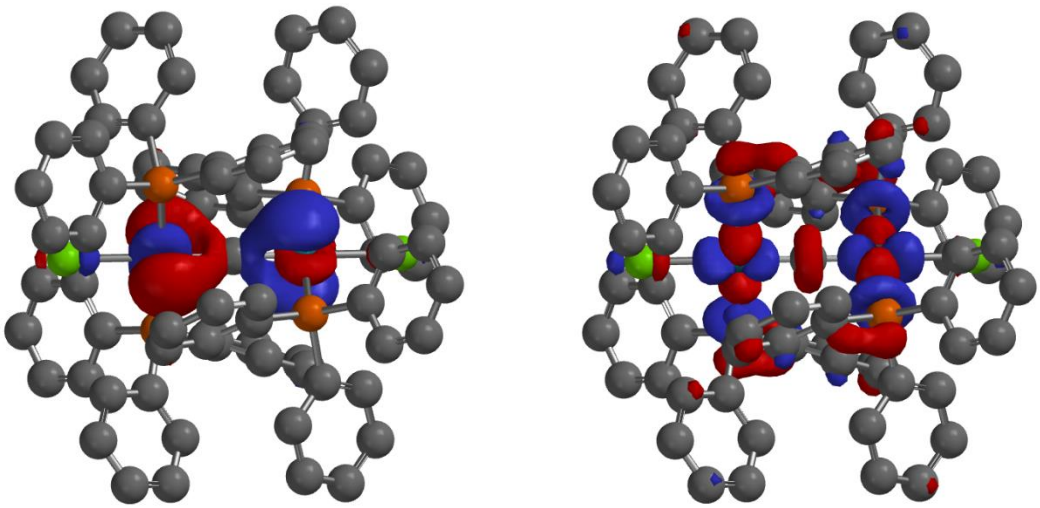

Figure 1.12: (left) HOMO and (right) LUMO of **[Rh_2(μ-C)Cl_2(PPh_3)$_4$]**

1.3.2 Reactivity of Mono and Bidentate Phosphines

Previous reactivity with PCy_3 and P(4-C_6H_4F)$_3$

Previous work by the author explored the reactivity of the parent μ-carbido species **[Rh_2(μ-C)Cl_2(PPh_3)$_4$]** with monodentate phosphines. Complete replacement of the four phosphine ligands was successful when the fluorine analogue P(4-FC_6H_4)$_3$ was utilised. A

chloroform solution with heating at reflux undergoes complete conversion to the new μ-carbido complex **[Rh$_2$(μ-C)Cl$_2$(P{4-C$_6$H$_4$F}$_3$)$_4$]** (**Scheme 1.19**).

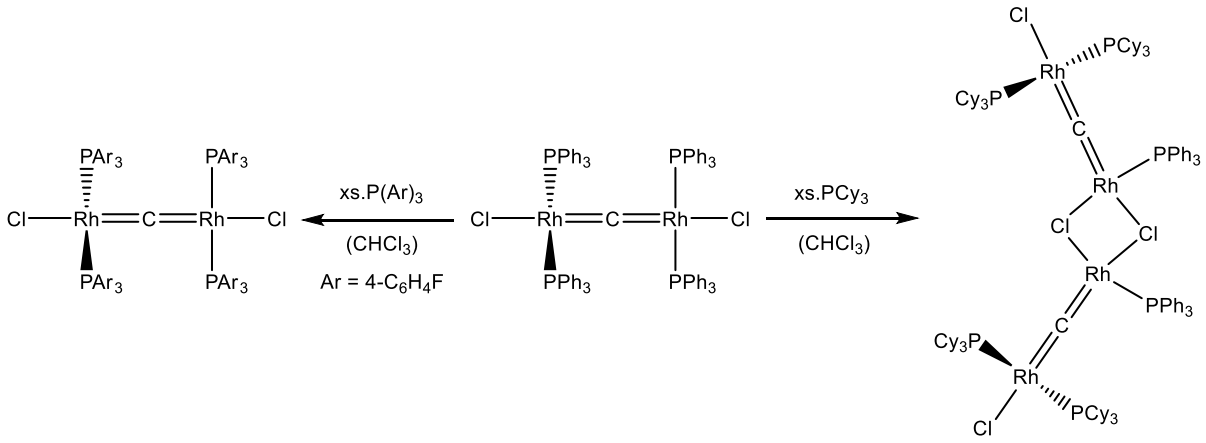

Scheme 1.19: monodentate phosphine substitution to **[Rh$_2$(μ-C)Cl$_2$(PPh$_3$)$_4$]**

When the more sterically encumbering phosphine PCy$_3$ was used, a simple phosphine substitution was not observed. Instead, a μ-dichloride tetrametallic species **[Rh$_2$(μ-C)Cl(PCy$_3$)$_2$(PPh$_3$)]$_2$(μ-Cl$_2$)** was formed as the major species, which retains one PPh$_3$ ligand on each dirhodium half. The incomplete substitution could be rationalised by the significantly larger cone angle of PCy$_3$ (170° *cf.* 145°), which is too large to accommodate four around the μ-carbido framework. This was supported by the corresponding thiocarbonyl complex **[Rh(CS)Cl(PCy$_3$)$_2$]** failing to form the μ-carbido complex in the presence of catecholborane.

Reaction with diphenylphosphinomethane

Aside from the discovery of the initial synthetic pathway to the cumulenic carbido, perhaps the most significant outcome of the authors' previous studies was the intriguing *ortho*-metalation of triphenylphosphine that coincided with the installation of the sterically intrusive Tp* ligand. Cyclometallation of PPh$_3$ on mono- and bimetallic systems is itself unremarkable and has a long history, not least from the pioneering studies of Prof. Martin A. Bennett, in this school. What distinguishes the complex **[Rh$_2$(μ-C)H(κC-2-C$_6$H$_4$PPh$_2$)(Tp*)$_2$]** from all before is however that when a C$_6$H$_4$PR$_2$ groups bridges two metals, they are either directly bonded, or when accompanied by a bridging ligand, this ligand lies off the M···M vector. The observation that the three-atom C–C–P bridge could geometrically accommodate a linear M–X–M unit was rather unexpected. This

result was of chemical importance as it showcased the ease of which a ligand could bridge the Rh=C=Rh core, while sustaining the linear carbido geometry, opening up the possibility of including other triatomic bridges.

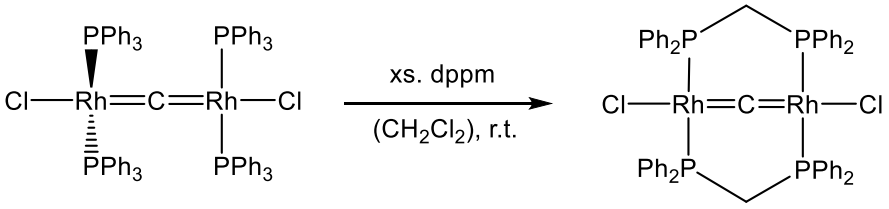

Scheme 1.20: Synthetic route to **[Rh_2(μ-C)Cl_2(μ-dppm)$_2$] (1)**

Though bidentate diphosphines (dppe, dppf, dppb *etc.*) are widely deployed as chelating ligands, dppm (bis(diphenylphosphino)methane) has a propensity for serving as a bridging ligand to form 5-membered dimetallacycles rather than the more strained 4-membered monometallic chelates. Amongst the plethora of dppm bridged bimetallic complexes, a subset with sufficiently distinctive properties are those involving two dppm bridges which are collectively referred to as A-frame complexes.[54] This principle has most recently been applied to μ-carbido chemistry by Bendix *et. al.*, with the successful installation of both dppm and the cyclohexyl analogue dcpm attended by the conversion of a Class C to B carbido species, in the 'A-frame' species **[PtRu(μ-C)(PCy_3)$_2$$Cl_4(py)_n$]** (n=1, 2).[19]

The dichloromethane solution of **[Rh_2(μ-C)Cl_2(PPh_3)$_4$]** and excess (*ca* five equivalents) of dppm underwent a rapid colour change to red when stirred at room temperature (**Scheme 1.20**). Using $^{31}P\{^1H\}$ NMR to monitor the reaction, the typical doublet corresponding to the triphenylphosphine starting material had completely disappeared after five hours, supported with the appearance of free triphenylphosphine.

Dilution of the red solution with hexane precipitated a red/brown product, which could be easily isolated and separated from the residual free phosphines. The $^{31}P\{^1H\}$ NMR spectrum of the product revealed at sole doublet of doublet resonance at 19.12 ppm, with an observed $^1J_{RhP}$ coupling of 191 Hz, and the $^3J_{RhP}$ of 38 Hz respectively. The ^1H NMR spectrum became usefully diagnostic due to the presence of the methylene hydrogens on dppm which in this case could be

seen as a broad peak at 2.90 ppm.[xix] The single phosphorus environment in the NMR spectrum suggested a complete substitution and with formation of a symmetrical product, **[Rh_2(μ-C)Cl_2(μ-dppm)$_2$] (1)**, and this was further confirmed in the ESI-MS, with the $[M+H+MeCN]^+$ (acetonitrile as matrix) ion appearing at 1099.0352 *m/z* (calc. for $C_{53}H_{48}{}^{35}Cl_2NP_4Rh_2$: 1098.0224 *m/z*). Slow evaporation of a dichloromethane/hexane solution gave rise to bright red plates of **1**, which were subjected to single X-ray diffractometry to determine the crystal structure (**Figure 1.13**).

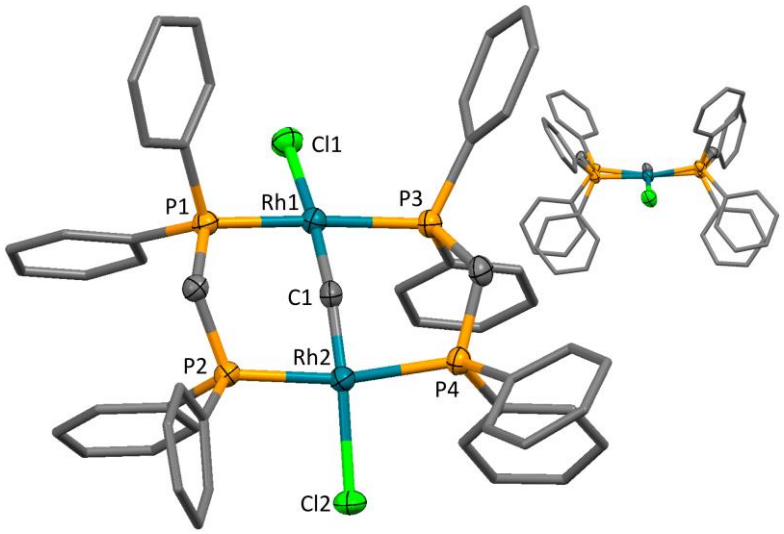

Figure 1.13: Molecular structure of **1** (50% displacement ellipsoids, solvent, hydrogen atoms omitted, phenyl groups simplified). Selected bond lengths (Å) and angles (°): Rh1-C1 1.732(11), Rh2-C1 1.757(11), Rh1-P3 2.328(3), Rh1-Cl1 2.418(3), Rh1-C1-Rh2 162.6(7), C1-Rh1-P3 84.6(3)

The Class A nature of the carbido ligand was confirmed with two statistically identical (< 3 e.s.d.) Rh=C bond lengths of 1.732(11) and 1.757(11) Å, which show negligible change from the precursor. The deviation of the Rh=C=Rh from the expected 180° (162.6(7)°) mimics what has occasionally been observed for previous carbido structures and can be attributed to solid state effects rather than a legitimate chemical deviation. Using ^{31}P-^{13}C HMQC NMR spectroscopy (see **Chapter 6**), the μ-carbido resonance could be detected at 411.7 ppm.

[xix] In future derivatives, the appearance of one or two chemical shifts provided information regarding the symmetry of the molecules.

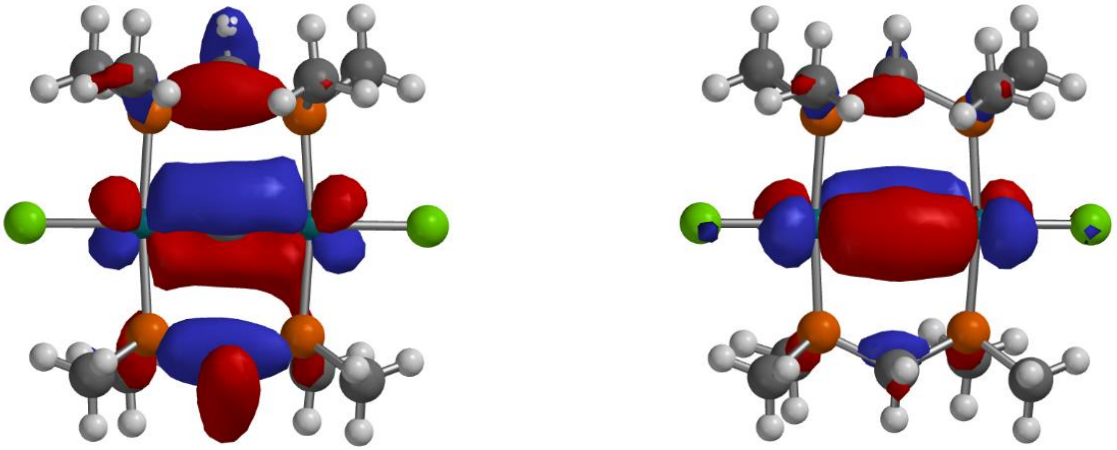

Figure 1.14: π–bonding orbitals of the Rh=C=Rh ligand in **[Rh$_2$(μ-C)Cl$_2$(μ-dmpm)$_2$]**[xx]

Due to the limited bite angle and flexibility of the dppm ligand (which typically coordinates as a *cis*- ligand on a single metal centre), the rhodium coordination spheres are positioned coplanar, rather than the orthogonal geometry adopted by the precursor (P-Rh···Rh-P torsional angles of 1.44(5) and 4.45(6)°). For reasons that will become apparent, the adoption of the A-frame geometry would appear to reflect the geometric constraints imposed by the short methylene bridges rather than being of electronic origin. Nevertheless, molecular orbital analysis supports the retention of Rh-C multiple bonding in non-orthogonal geometries.

Examining the π-bonding system of the simplified coplanar species **[Rh$_2$(μ-C)Cl$_2$(μ-dmpm)$_2$]**, the same in-phase Rh=C=Rh π-bonds can be detected (**Figure 1.14**). The π-bonding orbitals of interest are no longer degenerate, as the nodal plane of one coincides with the RhL$_4$ coordination planes while the second is orthogonal. Significantly, however, the π-bonding orbitals again utilise the two-rhodium d-orbitals ("d_{xz}", "d_{yz}" if the z-axis is defined by the Cl-Rh-C-Rh-Cl spine) such that both interact with the carbon *p*-orbitals.

Reaction with dicyclohexylphosphinomethane

Given that the A-frame dirhodium complex could be supported by the methylene linked dppm ligands, replacing the phenyl rings with cyclohexyl would provide a useful comparison for

[xx] The smaller analogue dimethylphosphino methane is routinely employed for theoretical calculations to significantly reduce computational time.

steric factors and also the electronic effect of introducing a more σ-basic trialkylphosphine.[xxi] A dichloromethane solution of **[Rh$_2$(μ-C)Cl$_2$(PPh$_3$)$_4$]** and excess dcpm turns the same dark red colour seen for dppm. The difference in reactivity with the bulkier dcpm ligand is immediately noticeable in the ^{31}P NMR spectrum of the reaction mixture. Whereas the dppm reaction cleanly converts to the bisphosphine complex **1**, the number of environments present clearly suggested an intermediate product persisting. The presence of a complex that contained both dcpm and PPh$_3$ could be clearly seen (**Figure 1.15**) with an equal intense cluster of peaks in the PPh$_3$ and PCy$_2$ region with strong *trans* P-P coupling {δ_P = 21.20 (dd, $^1J_{RhP}$ = 166 Hz, $^2J_{PP}$ = 280 Hz), 45.84 (dd, $^1J_{RhP}$ = 210 Hz, $^2J_{PP}$ = 278 Hz). The two $^1J_{RhP}$ and $^2J_{PP}$ couplings were able to be accurately simulated using gNMR (278, 216 and 164 Hz, respectively), however, the higher order $^3J_{RhP}$ and multiple $^4J_{PP}$ couplings could not be accurately discerned.

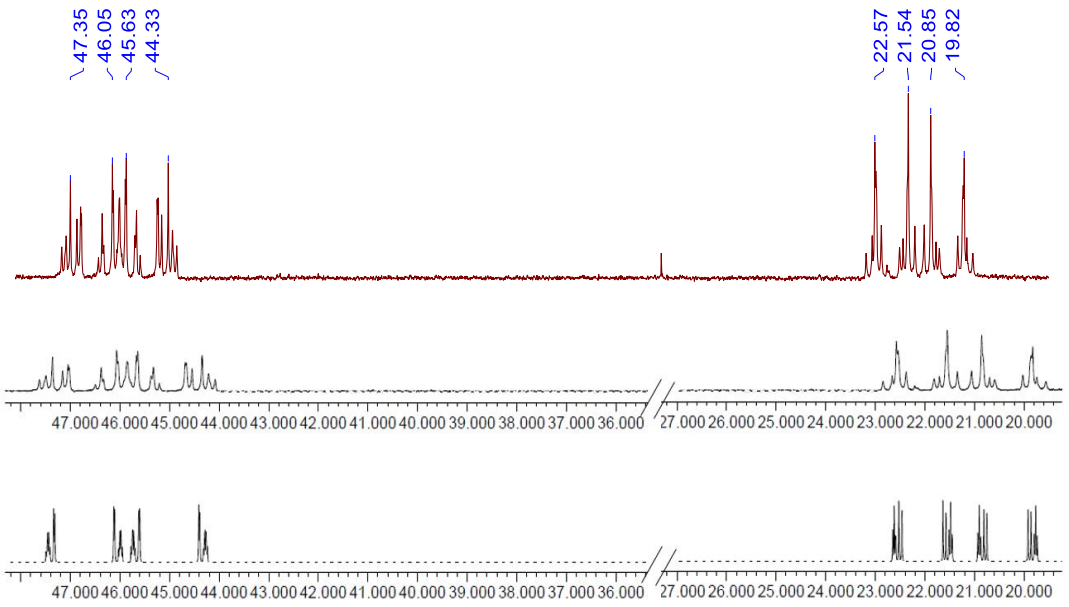

Figure 1.15: (top) ^{31}P{^{1}H} NMR spectrum and (bottom) gNMR simulated ^{31}P NMR spectrum of **[Rh$_2$(μ-C)Cl$_2$(PPh$_3$)$_2$(μ-dcpm)] (2)**

The ^{1}H NMR spectrum confirmed the presence of both phenyl and cyclohexyl rings, with the former integrating for 30 hydrogens appearing between 7.11-7.51 ppm and the latter (44

[xxi] The Tolman Electronic Parameter (TEP) is not available for the ligands dppm and dcpm, however as a first approximation the values for Ph$_2$PMe (2067.3) and Cy$_2$PMe (2058.9) provide an indication of the enhanced basicity upon Ph/Cy replacement: TEP = 2056.1 + S_ic_i; c_i = 0.1(Cy), 4.3(Ph), Me (2.6).

hydrogens) between 0.60 and 2.73 ppm. The major fragment in the mass spectrum corresponded to the expected $[M\text{-}Cl]^+$ of **$[Rh_2(\mu\text{-}C)Cl_2(PPh_3)_2(\mu\text{-}dcpm)]$**,[xxii] which appeared at 1185.2667 m/z (*cf.* 1185.2697 for $C_{62}H_{76}{}^{35}ClP_4Rh_2$). The intermediate species **$[Rh_2(\mu\text{-}C)Cl_2(PPh_3)_2(\mu\text{-}dcpm)]$** could be cleanly isolated by reacting **$[Rh_2(\mu\text{-}C)Cl_2(PPh_3)_4]$** with only one equivalent of dcpm. The molecular structure of **$[Rh_2(\mu\text{-}C)Cl_2(PPh_3)_2(\mu\text{-}dcpm)]$** (**Figure 1.16**) confirms that the coordination of a single dcpm ligand has occurred across the Rh-C-Rh linkage, rather than chelating onto one rhodium centre.

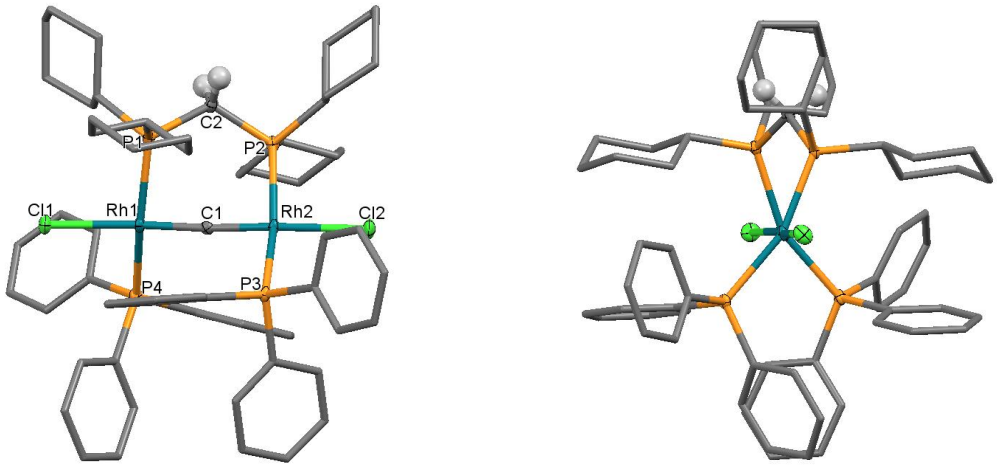

Figure 1.16: Molecular structure of **$[Rh_2(\mu\text{-}C)Cl_2(PPh_3)_2(\mu\text{-}dcpm)]$ (2)** (50% displacement ellipsoids, solvent, hydrogen atoms omitted, rings simplified, alternative enantiomer generated by crystallographic symmetry: inversion centre in $P\bar{1}$ space group). Selected bond lengths (Å) and angles (°): Rh1-C1 1.753(4), Rh2-C1 1.756(4), Rh1-P1 2.318(1), Rh1-P4 2.351(1), Rh2-P2 2.314(10), Rh2-P3 2.355(1), Rh1-Cl1 2.411(2), Rh1-C1-Rh2 175.2(3), P1-Rh1—Rh2-P2 39.05(4), P4-Rh1—Rh2-P3 81.31(5)

The two Rh-C bonds that make up the μ-carbido ligand in **2** are well within the range for a cumulenic bonding mode (1.753(4) and 1.756(4) Å). The two bonds to the dcpm phosphine are slightly shorter than the triphenylphosphine ligands, and in contrast to the *ca* D_{2h} symmetry of the dppm analogue the excessive inter-ligand steric repulsion results in a twisting of molecule from ideal C_{2v} to C_2 symmetry (P3-Rh2—Rh1–P4 dihedral angle of 39.05(4) ° *cf.* 81.31(5) °).

[xxii] Throughout, ESI-MS was performed using either a methanol or acetonitrile matrix and accordingly when halides were present ionisation to $[M\text{-}Cl]^+$ was commonly observed or on occasion $[M\text{-}Cl+MeCN]^+$.

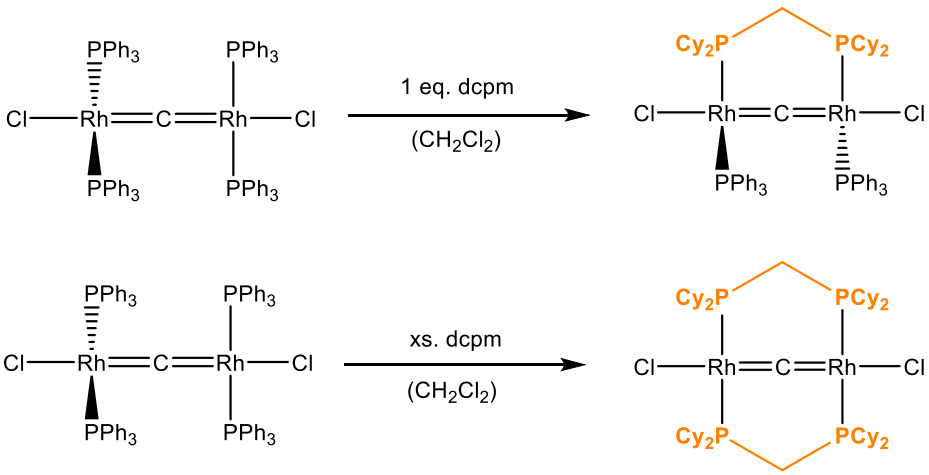

Scheme 1.21: Synthesis of **[Rh₂(μ-C)Cl₂(μ-dcpm)(PPh₃)₂]** and **[Rh₂(μ-C)Cl₂(μ-dcpm)₂]**

In addition to the presence of this singly substituted intermediate, a phosphorus resonance with a similar appearance to that for the dppm complex **[Rh₂(μ-C)Cl₂(μ-dppm)₂]** was observed at 40.3 ppm (**Figure 1.17**, **Scheme 1.21**). Unfortunately, the presumed bis-dcpm complex had physical characteristics similar to the free dcpm ligand, which made purification through crystallisation or chromatography exceedingly difficult and wasteful.

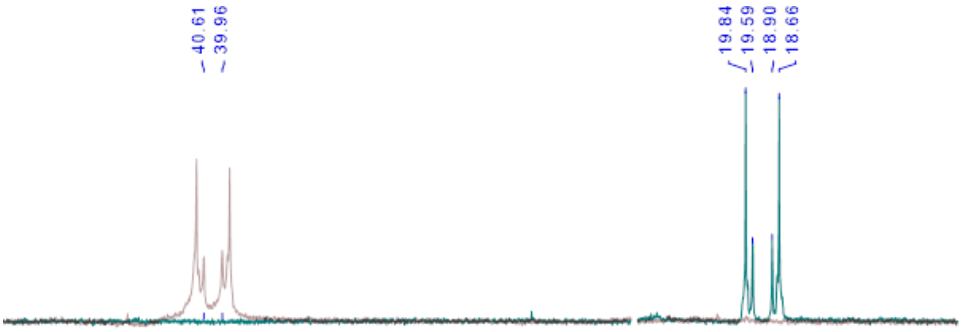

Figure 1.17: ^{31}P NMR comparison of **[Rh₂(μ-C)Cl₂(μ-R₂PCH₂PR₂)₂]** (Red = Cy, Blue = Ph)[xxiii]

The presence of a symmetrical environment and the large $^{1}J_{RhP}$ and $^{3}J_{RhP}$ couplings of 190 and 43 Hz respectively is indicative of the coplanar alignment of the rhodium coordination planes.

[xxiii] The magnetic inequivalence of the phosphine environment resulted in most A-frame complexes in this study giving rise to second order AA'A"A"'XX' spectra which were simulated using the gNMR program to extract couplings.

The complex **[Rh$_2$(μ-C)Cl$_2$(μ-dcpm)$_2$] (3)** was deceptively hard to purify, as its solubility and polarity index is practically identical to the free phosphine and attempts to synthesise **3** through addition of precisely two equivalents of dcpm failed. Crystals were acquired fortuitously from the crude oil of complex and phosphine, through the cubic unit cell and high disorder led to an exceptionally fraught solution process. The structural model of **3** (**Figure 1.18**) confirmed that the bis phosphine species retained the near D_{2h} idealised geometry that was seen for the dppm analogue, with the Ph-Rh—Rh-P torsion angle of 18.6(2) °.

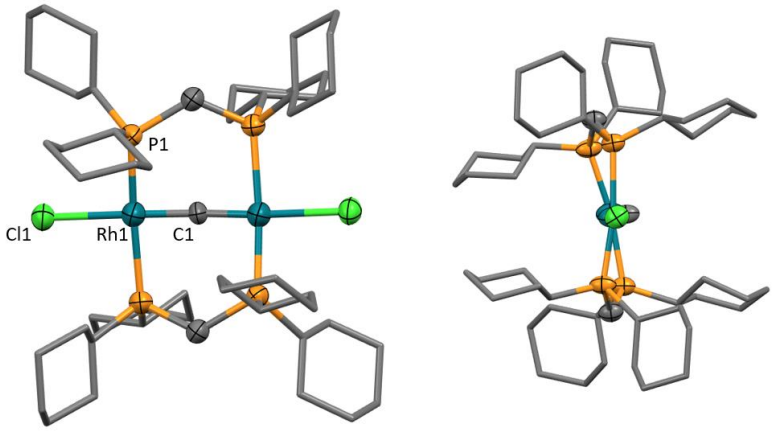

Figure 1.18: Molecular structure of **[Rh$_2$(μ-C)Cl$_2$(μ-dcpm)$_2$] (3)** (50% displacement ellipsoids, solvent, hydrogen atoms omitted, rings simplified, half the molecule is crystallographically unique due to an inversion centre at C1). Selected bond lengths (Å) and angles (°): Rh1-C1 1.759(12), Rh1-P1 2.405(5), Rh1-Cl1 2.459(6), Rh1-C1-Rh1 150(3), P1-Rh1—Rh1-P1 18.6(2). Insert: alternate view along Rh=C=Rh bonds.

Due to the disorder and low quality of the structural model, geometric parameters associated with the μ-carbido are of limited precision. The Rh1-C1 bond length of 1.759(12) still falls within double bond norms, and although the ligand is apparently bent in the solid-state to 150(3) °, difficulties in modelling the associated disorder deter over-interpretation . Due to the frustrating purification issues, and the increased size of the cyclohexyl rings, **[Rh$_2$(μ-C)Cl$_2$(μ-dcpm)$_2$]** was not pursued further in favour of less recalcitrant derivatives.

Reactions with dcpe and dppe

Fundamentally, the importance of **[Rh$_2$(μ-C)Cl$_2$(μ-R$_2$PCH$_2$PR$_2$)$_2$]** (R = Ph, Cy) rests on discarding the view that the rhodium centres would by default remain orthogonal due to the classic combination of steric effects and residual adherence to an electronically based allene analogy. With the electronic effects actually being made irrelevant due to the availability of two orthogonal rhodium atomic orbitals for compiling the μ-carbido π-system, the geometric preference of mutually orthogonal rhodium centres can be overcome by ligands with predetermined geometric constraint. The next step in this series was to expand the bidentate phosphine ligands to those with a longer and more flexible linker, and therefore a larger bite angle.

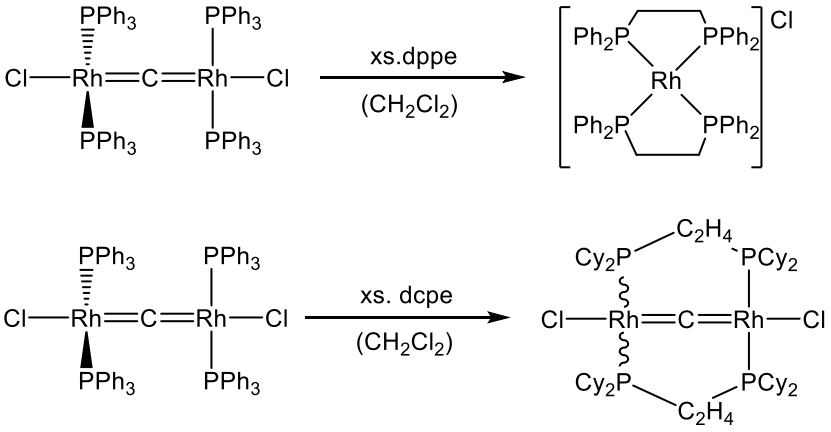

Scheme 1.22: Synthesis of **[Rh(dppe)$_2$]Cl** and **[Rh$_2$(μ-C)Cl$_2$(μ-dcpe)$_2$] (4)**

Taking dppm as the starting point, the next ligand explored was dppe (1, 2-bis(diphenylphosino)ethane), as the only alteration was the addition of an extra methylene unit between the two phosphine groups. The expectation would be that under similar circumstances the 'A frame' species **[Rh$_2$(μ-C)Cl$_2$(μ-dppe)$_2$]** might be formed readily (**Scheme 1.22**). Instead, the appearance of a doublet far downfield in the $^{31}P\{^1H\}$ NMR spectrum at 57.47 ppm ($^1J_{RhP}$ = 133 Hz) was vastly outside the expected range of the desired product based on the previous examples. The ESI-MS of the yellow product came to 899.1772 *m/z*, which is a perfect match for the bisphosphine rhodium complex **[Rh(dppe)$_2$]$^+$**, and this was confirmed with a comparison of the ^{31}P NMR data to those in the literature.[55] The loss of the bridging carbido carbon under such mild conditions was completely unexpected, and any attempts to locate it on a separate rhodium species or organic side product were unsuccessful.

Unfortunately, no conditions were identified to divert the process away from formation of the cationic species, which was attributed to the strong cis-chelating nature of dppe towards a single metal centre. To try and prevent this, the larger dcpe ligand (1, 2-bis(dicyclohexylphosphino)ethane) was used, as it was presumed that the larger cyclohexyl rings would retard the formation of the, albeit known, cation **[Rh(dcpe)$_2$]$^+$**.[56] Under identical reaction conditions, the $^{31}P\{^1H\}$ NMR spectrum revealed two Rh-P environments. The unwanted cationic species was detected at 66.42 ppm; however, it was a minor product (approximately 1:10) accompanied by an intense doublet resonance seen at 33.38 ppm. Although this displayed a similar $^1J_{RhP}$ value to the dppm species (172 Hz), the anticipated $^3J_{RhP}$ coupling was not observed. This was nevertheless tentatively attributed to a species with an 'A frame' geometry.

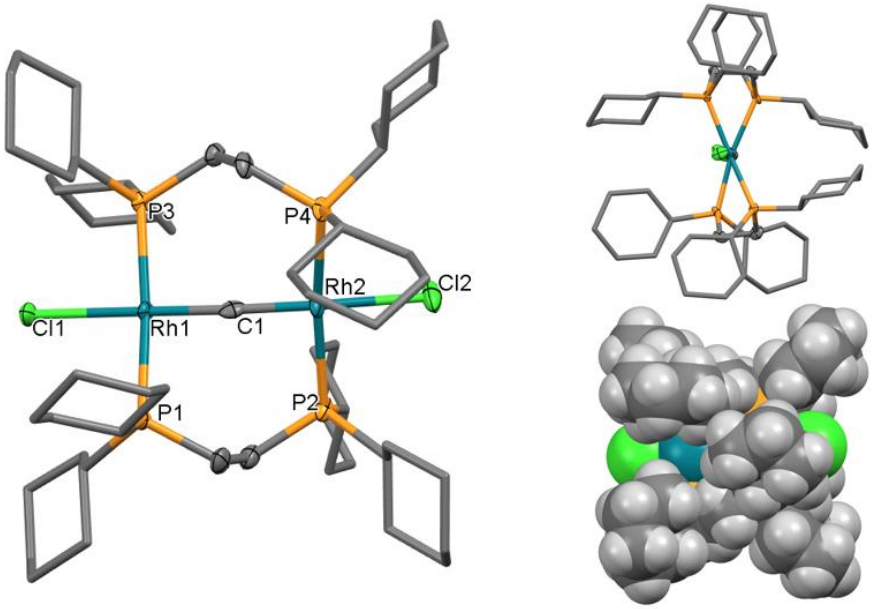

Figure 1.19: Molecular structure of **[Rh$_2$(μ-C)Cl$_2$(μ-dcpe)$_2$] (4)** (50% displacement ellipsoids, solvent, hydrogen atoms omitted, phenyl groups simplified). Selected bond lengths (Å) and angles (°): Rh1-C1 1.777(5), Rh2-C1 1.774(5), Rh1-P3 2.341(2), Rh1-C1-Rh2 177.6(4), P1-Rh1···Rh2-P3 37.78(5), P2-Rh1···Rh2-P4 48.07(5). (right) Insert: alternate view along Rh=C=Rh bonds and spacefill of **4**

Separation of the salt and neutral complex on a silica gel column isolated this major doublet complex, which showed only resonances in the cyclohexyl and methylene regions of the ^1H NMR spectrum, suggesting a complete substitution. The ESI-MS showed a major fragment at 531.2281 *m/z*, which corresponded accurately to the *dicationic* fragment $[M - 2Cl]^{2+}$ (calc. for $C_{53}H_{96}P_4Rh_2$ = 531.2286 *m/z*) with two dcpe ligands. The molecular structure was determined through single

crystal X-ray diffractometry, confirming the successful synthesis of **[Rh_2(μ-C)Cl_2(μ-dcpe)$_2$] (4)** (**Figure 1.19**). The only previous structurally authenticated examples of bimetallic species bridged by two dcpe ligands are the d^{10}-d^{10} species [M_2(μ-dcpe)$_2$] M = Pd^0, Au^+.[57] The μ-carbido environment could be indirectly detected again using ^{31}P-^{13}C HMQC studies, appearing at 415.1 ppm. Interestingly, the inclusion of cyclohexyl rings on the phosphine leads to only a marginal shift in the carbido resonance in thee ^{13}C NMR spectrum.

Once again, the indirect effect the phosphine has on the Rh=C=Rh core of the complex remains negligible, with identical Rh=C bond lengths of approximately 1.77 Å (1.777(5) and 1.774(5) Å), only slightly longer than the previous dppm analogue. The Rh=C=Rh bond angle lies much closer to the ideally expected 180° (177.6(4)) than previously, but once again this cannot be assigned to a chemical change but rather solid-state packing effects.

The value of interest at this point was the dihedral angle of the adjacent phosphine ligands. Compared to **1**, the two P-Rh···Rh-P dihedral angles were calculated to be closer to 45° (37.78(5) and 48.07(5)). These dihedral angles suggest that the increased flexibility provided by the additional methylene unit on the bridging phosphine increases the bite angle, while the rhodium orbitals allow the centres to be neither coplanar nor orthogonal to each other, but halfway in between requiring the Rh=C=Rh bonding to involve helical coarctate character.[58]

Reaction with dppp

Considering that complexes **1** and **3** with a single methylene unit contained coplanar rhodium coordination planes, while two methylene units allowed these in **4** cant by approximately 45°, it was presumed that extending the phosphine backbone to three methylene units with dppp (1, 3-bis{diphenylphosphino}propane) would have a sufficiently long tethers to allow the rhodium centres to revert to mutually orthogonal positioning (**Scheme 1.23**) to minimise steric interactions between adjacent interdigitated PPh_2 units. The dichloromethane solution of **[Rh_2(μ-C)Cl_2(PPh_3)$_4$]** with excess dppp turns yellow quite rapidly, and an orange powder can be easily separated from the phosphines by diluting the mixture with alkanes resulting in precipitation over a few hours. The orange precipitate curiously showed three ^{1}H NMR multiplets for the three methylene units of dppp (4.21, 1.85 and 1.27 ppm, each integrating for 4 protons), which would normally only be two environments in a 2:1 ratio. This can be rationalised when examining the molecular structure (see H94A and H94B in **Figure 1.20**), as the methylenic protons adjacent to the phosphine atom are diastereotopic due to the C_2 molecular symmetry. This suggests that the

steric bulk of the PCy_2 units prevents the molecule from inverting by twisting along the Rh–C–Rh axis on the ^1H NMR timescale.

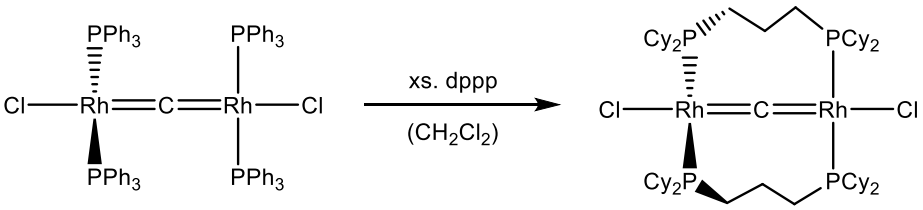

Scheme 1.23: Synthesis of **$[Rh_2(\mu\text{-}C)Cl_2(\mu\text{-}dppp)_2]$ (5)**

Once again, the ESI-MS confirmed the presence of two dppp ligands and two chloride ligands, with the $[M - 2Cl]^{2+}$ detected at 521.0569 *m/z* (*c.f.* $C_{55}H_{52}P_4Rh_2$ of 521.0565 *m/z*). The μ-carbido resonance was detected at 411.5 ppm, suggesting an almost identical environment to **1**. The $^{31}P\{^1H\}$ NMR spectrum of **5** once again displayed only a single doubled doublet resonance at 3.21 ppm, with the observed $^1J_{RhP}$ and $^3J_{RhP}$ coupling constants 161 and 8 Hz respectively. It is interesting at this point to observe the difference in the $^3J_{RhP}$ values. In the orthogonal carbido **$[Rh_2(\mu\text{-}C)Cl_2(PPh_3)_4]$** it was observed to be approximately 7 Hz, but the coplanar complex **1** has a much larger value of 38 Hz, which suggests that the relative geometry of the rhodium centres has Karplus-type influence of this value. With the observed coupling constant for this product being 8 Hz, it might be loosely argued that it should correspond to an orthogonal species.

Yellow crystals of analytical quality were grown by a slow evaporation of a CH_2Cl_2/hexane mixture. The single crystal X-ray molecular structure of **5** (**Figure 1.20**) confirmed both the continuing trend and gave support to the NMR $^3J_{RhP}$ coupling constant supposition, as the rhodium centres are now positioned close to the archetypical orthogonal geometry. Although the two P-Rh···Rh-P dihedral angles are still smaller than the expected 90° (73.90(3) and 65.19(3)), this can be attributed to the restriction of free rotation and bite angle from the bidentate phosphine in comparison to four single isolated phosphine ligands. That said, the two dihedral angles show a clear jump from the smaller bidentate phosphines towards an orthogonal species.

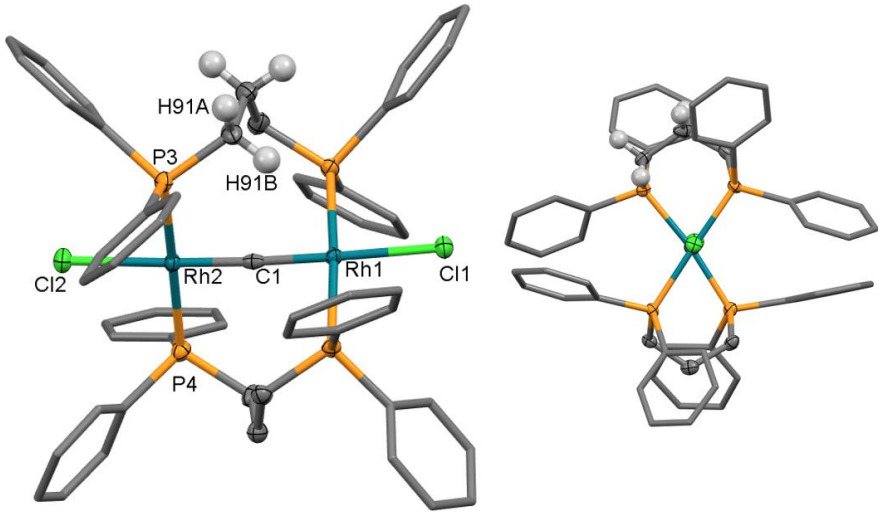

Figure 1.20: Molecular structure of **[Rh_2(μ-C)Cl_2(μ-dppp)$_2$] (5)** (50% displacement ellipsoids, solvent, hydrogen atoms and disorder omitted, phenyl groups simplified). Selected bond lengths (Å) and angles (°): Rh1-C1 1.764(3), Rh2-C1 1.772(3), Rh2-P3 2.325(1), Rh1-C1-Rh2 177.1(2), P1-Rh1···Rh2-P3 73.90(3), P2-Rh1···Rh2-P4 65.19(3). Insert: alternate view along Rh=C=Rh bonds.

Reaction with 1,1'-bis(diphenylphosphino)ferrocene

In an effort to use an especially flexible bidentate phosphine species, attention turned towards the use of the metallophosphine dppf (1, 1' – bis(diphenylphosphino)ferrocene). A dichloromethane solution of **[Rh_2(μ-C)Cl_2(PPh_3)$_4$]** and dppf turns a bright orange over a period of 30 minutes, and the residual phosphine and carbido product are rapidly separated on a silica gel column eluted with neat CH_2Cl_2. The ^{1}H NMR spectrum of the bright orange powder displayed the typical aromatic peaks, but also two broad peaks at 4.17 and 4.12 ppm which integrated to the 16 hydrogens on the Cp rings of two dppf ligands. The Cp rings are also manifest in the $^{13}C\{^1H\}$ NMR spectrum, with the α, β and γ carbons detected at 76.3, 73.3 and 70.9 ppm respectively. The Infrared spectrum was of diagnostic use for the first time in this project, with the characteristic mode of ferrocene-diyl appearing as a strong band at 693 cm^{-1}. The ESI-MS again included the dicationic species $[M - 2Cl]^{2+}$ at 663.0049 *m/z* (Calc. for $C_{69}H_{56}Fe_2P_4Rh_2$: 663.0071 *m/z*).

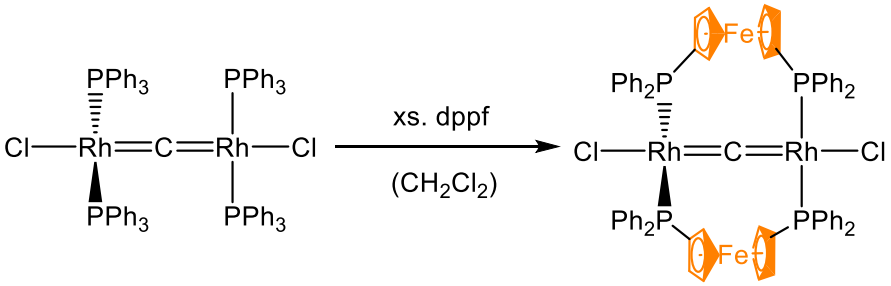

Scheme 1.24: Synthesis of **[Rh$_2$(μ-C)Cl$_2$(μ-dppf)$_2$] (6)**

The $^{31}P\{^{1}H\}$ NMR spectrum of the presumed tetrametallic species **[Rh$_2$(μ-C)Cl$_2$(dppf)$_2$] (6)** (**Scheme 1.24**) contained a very broad doublet resonance at 18.9 ppm, similar to the characteristic broader singlet peak of free dppf (δ_P = -16.8, hhw = 38 Hz). The $^{1}J_{RhP}$ value (191 Hz) was clearly evident, but the smaller three-bond coupling could not be resolved from the broad peaks. Regardless, the spectroscopic data pointed to the bis-phosphine species **6** being successfully made. This was supported with a new μ-carbido resonance in the $^{13}C\{^{1}H\}$ NMR spectrum, which was identified at 418.6 ppm using the enriched isotopologue **6'** since the broadness of the ^{31}P resonance precluded the indirect 2 or 3-dimesnsional techniques developed in **Chapter 6**.

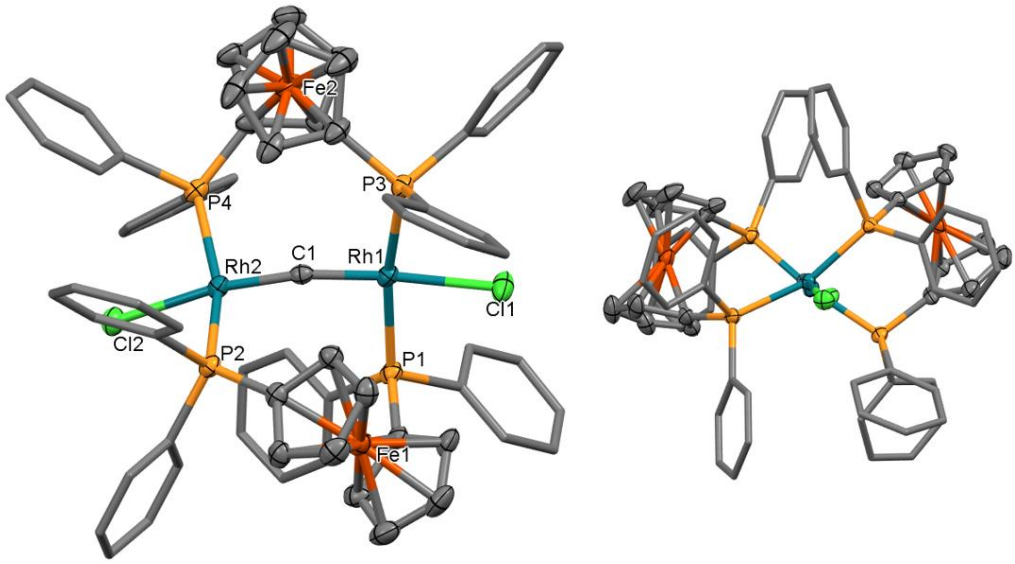

Figure 1.21: Molecular structure of **[Rh$_2$(μ-C)Cl$_2$(μ-dppf)$_2$] (6)** (50% displacement ellipsoids, solvent, hydrogen atoms and disorder omitted, phenyl groups simplified). Selected bond lengths (Å) and angles (°): Rh1-C1 1.783(4), Rh2-C1 1.766(4), Rh2-P2 2.331(1), Rh1-C1-Rh2 168.4(3), P1-Rh1···Rh2-P2 75.96(4), P4-Rh2···Rh1-P3 67.20(4). Insert: alternate view along Rh=C=Rh bonds.

Although there are over three hundred structurally characterised bi- or polymetallic complexes in which two metals are bridged by a single ddpf ligand, those in which an '$M_2(\mu\text{-dppf})_2$' core has been confirmed with two bridging dppf ligands are limited to a small number of coinage metal halides, alkynyl and *pseudo*-halides of the form **$[M_2X_2(\mu\text{-dppf})_2]$** (M = Cu, Ag)[59] and the dipalladium species **$[Pd_2Cl_2(C_6F_3Cl_2)_2(\mu\text{-dppf})_2]$**.[60] The molecular structure of **6** (**Figure 1.21**) continues the trend developed above for bridging bidentate phosphine. The size and bite angle of the dppf ligands allow the rhodium coordination planes to be orthogonal, with dihedral angles of 75.96(4) and 67.20(4)° respectively. There is once again no appreciable difference in the Rh=C bond lengths, which are only slightly longer than the previous structures (1.783(4) and 1.766(4) Å).

The introduction of bidentate phosphine ligands has allowed detailed study of the changing relative geometry of the two rhodium coordination planes. As **Figure 1.22** shows, the two rhodium coordination planes can readily adopt geometries that range from mutually coplanar through to orthogonal. Furthermore, the geometries of the complex appear to be solely dictated by the bite angle of the phosphine installed and the various geometries have little or no impact on the Rh-C bond length and by cautious inference, their strength of interaction.

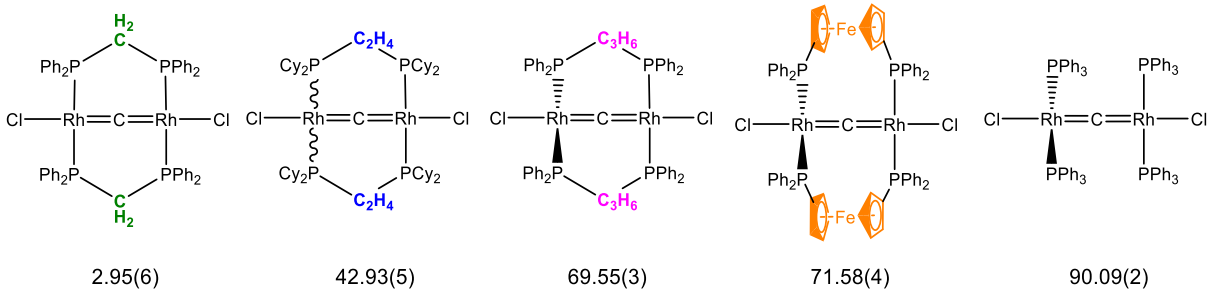

Figure 1.22: Synthesised A-frame complexes and average P-Rh···Rh-P dihedral angles (°)

Comparing the μ-carbido core of the phosphine-substituted complexes (**Table 1.3**), it becomes clear that the rigidity of the Rh=C=Rh linkage retains its Class A character. Across the seven complexes analysed, the Rh=C bond lengths do not deviate by more than 0.05 Å, and almost all can be classified as technically crystallographically equivalent, with bond length variation being typically < 6 e.s.d. All of the complexes contain a Rh=C=Rh bond angle with deviation from linear, though this can be attributed to packing effects in the solid-state. The only geometrical

property that changes significantly is the torsional angle, which is reflective of the bite angle of the phosphine installed.

Phosphine	Rh=C a (Å)	Rh=C b (Å)	Rh=C=Rh (°)	P-Rh—Rh-P (°)
dppm	1.732(11)	1.757(11)	162.6(7)	2.95(6)
dcpm+PPh_3	1.753(4)	1.756(4)	175.2(3)	39.05(4), 81.31(5)
dcpm	1.759(12)	-	150(3)	18.6(2)
dcpe	1.777(5)	1.774(5)	177.6(4)	42.93(5)
dppp	1.764(3)	1.772(3)	177.1(2)	69.55(3)
dppf	1.783(4)	1.766(4)	168.4(3)	71.58(4)
PPh_3	1.773(2)	1.782(2)	173.36(14)	90.09(2)

Table 1.3: Selected bond lengths and angles for dirhodium μ-carbido complexes

What this study of bidentate phosphines and their molecular structures demonstrates is the flexibility of rotation about the μ-carbido ligand. The ability for the rhodium coordination spheres to coexist in any number of geometries relative to each other is only possible though the unique bonding and low rotation barrier present in the μ-carbido ligand.

1.3.2 Nitrogen-based Ligands

Coordination of acetonitrile

When examining the μ-carbido complex **$[Rh_2(\mu\text{-}C)Cl_2(PPh_3)_4]$**, removal of the terminal chloride ligands with the addition of silver(I) triflate rapidly forms the dicationic species **$[Rh_2(\mu\text{-}C)(PPh_3)_4](OTf)_2$**. When performed in the presence of acetonitrile, the solvent is able to coordinate to the rhodium centres *trans-* to the μ-carbido ligand, forming **$[Rh_2(\mu\text{-}C)(MeCN)_2(PPh_3)_4](OTf)_2$** (**Scheme 1.25**). However, this species is unable to be isolated from solution, as the solid immediately turns dark and decomposes upon solvent removal. Addition of excess LiBr to the MeCN causes the red solution to turn orange again, and the bromine analogue is easily formed.

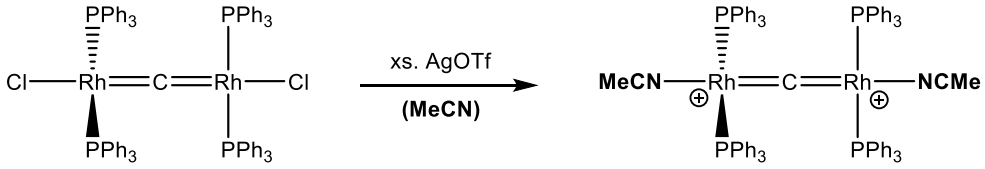

Scheme 1.25: Chloride abstraction with silver to form **[Rh$_2$(μ-C)(CH$_3$CN)$_2$(PPh$_3$)$_4$](OTf)$_2$** (triflate ions excluded for clarity)

The reactivity of the bridging phosphine complex **[Rh$_2$(μ-C)Cl$_2$(μ-dppm)$_2$]** behaved in an analogous fashion. Addition of silver triflate to a dichloromethane solution slowly causes a dark colour change and precipitation of AgCl. Conducting the reaction, however, in the presence of acetonitrile results in a clean conversion to a red compound. The $^{31}P\{^1H\}$ NMR spectrum of the filtered reaction mixture shows a characteristic downfield shift typical of formation of a cation, with the new ddd environment at 23.83 ppm ($^1J_{RhP}$ = 184 Hz, $^3J_{RhP}$ = 44 Hz, $^4J_{PP}$ = 2 Hz). The dicationic species was stable enough to be crystallised, and the solid-state structure of **[Rh$_2$(μ-C)(MeCN)$_2$(μ-dppm)$_2$](OTf)$_2$ (7)** could be elucidated (**Figure 1.23**). Addition of a bromide source to the acetonitrile adduct causes an instant colour change to orange, and the phosphorus resonance in the NMR spectrum returns back to the vicinity of that of the chloride complex, forming **[Rh$_2$(μ-C)Br$_2$(μ-dppm)$_2$] (1b**, see **Section 2.2)** in quantitative yields.

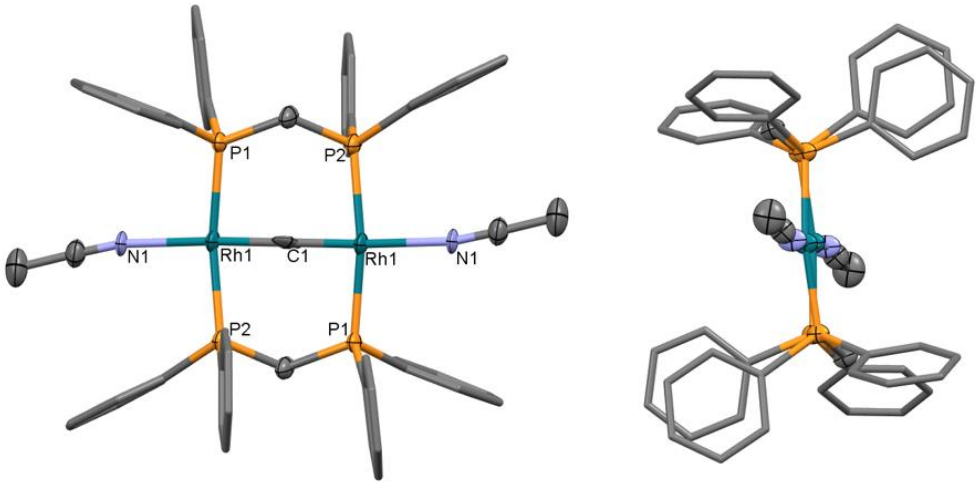

Figure 1.23: Molecular structure of **[Rh$_2$(μ-C)(MeCN)$_2$(μ-dppm)$_2$](OTf)$_2$ (7)** (50% displacement ellipsoids, phenyl rings simplified, hydrogen atoms and triflates removed). Selected bond lengths lengths (Å) and angles (°): Rh1-C1 1.7443, Rh1-N1 2.168(7), Rh1-P1 2.324(2), Rh1-C1-Rh2 180.0

Reaction with bipy

The carbido core was already seen to be maintained when the harder anionic N-bound pyrazolylborate chelates were installed, however the steric bulk of even the smaller Bp and Bp* ligands hindered access to the μ-carbido ligand when examining the molecular structures. This steric occlusion is implicit in their formation in that phosphine, albeit a large one, was available in principle for the formation of 18-electron complexes **[Rh_2(μ-C)L_2(PPh_3)$_4$] (L = Bp, Bp*)**. The possibility of extending the range of nitrogen ancillary ligands was briefly explored by beginning with neutral bipyridyl (bipy) (**Scheme 1.19**). Bipyridyl-ligated carbide complexes were previously limited to the Class B example **[WPt(μ-C)(bipy)(CO)$_2$(PPh_3){Tp*)]**$^+$.[61] Installation of the bidentate ligand was expected to proceed in a similar manner to the borates, with replacement of the halide and a single phosphine ligand furnishing the dicationic complex **[Rh_2(μ-C)(bipy)$_2$(PPh_3)$_2$]$^{2+}$**, though in the absence of KCl precipitation as a driving force, the possibility of forming neutral derivatives **[Rh_2(μ-C)Cl_2(bipy)$_2$(PPh_3)$_n$]** (n = 0, 2) was also considered plausible.

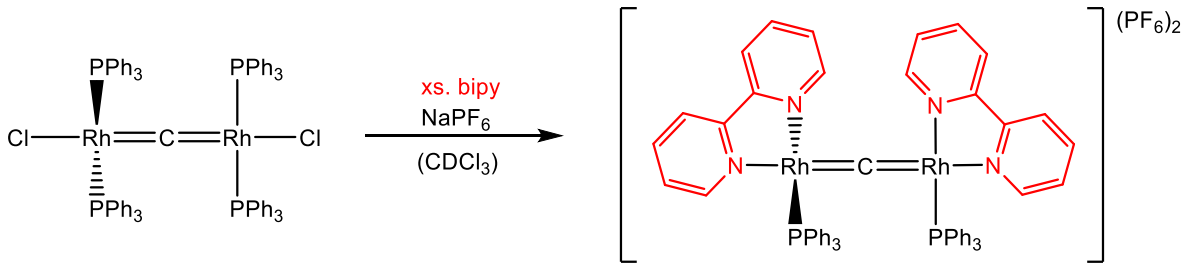

Scheme 1.26: Synthesis of **[Rh_2(μ-C)(bipy)$_2$(PPh3)$_2$][PF_6]$_2$ (8)**

Addition of excess bipy to a chloroform solution of **[Rh_2(μ-C)Cl_2(PPh_3)$_4$]** saw a colour change to bright red and monitoring the reaction through ^{31}P NMR spectroscopy indicated the appearance of a new resonance at 37.8 ppm in addition liberated phosphine (-5.6) ppm. The doublet at 37.8 ppm displayed a larger $^1J_{RhP}$ value of 208 Hz, which corresponds well to the increase seen with the installation of the N-bound pyrazolyl ligands. The presumed product **[Rh_2(μ-C)(bipy)$_2$(PPh_3)$_2$](Cl)$_2$** was confirmed in the high-resolution mass spectra, with the [M]$^{2+}$ dication being detected at 527.06467 *m*/*z* (*cf.* 527.06484 for $C_{57}H_{46}N_4P_2Rh_2^{2+}$). Whilst ionisation of chloride

from a neutral complex **[Rh_2(μ-C)Cl_2(bipy)$_2$(PPh_3)$_2$]** under ESI conditions might in principle also provide the same result, the 1:2 salt formulation could be confirmed *via* counter-anion metathesis (excess $NaPF_6$ in 1:1::CH_2Cl_2:MeOH) to provide **[Rh_2(μ-C)(bipy)$_2$(PPh_3)$_2$][PF_6]$_2$ (8)** (**Scheme 1.26**), the ^{31}P NMR spectrum of which was identical to that of the chloride salt other than the inclusion of the characteristic high frequency PF_6^- heptet resonance.

The ^1H NMR spectrum of the red product **8** contained key downfield multiple resonances (δ_H = 8.70 (4H), 8.40 (1H), 8.30 (1H), 8.14 (3H), 8.01 (1H)) that correspond well with other examples of bipy coordinated to rhodium, though with significant overlap with PPh_3 aromatic environments for the remaining resonances.[62] The number of resonances observed reflects the unsymmetrical coordination of the ligand, with the rings being *trans* to either the μ-carbido or phosphine ligand.

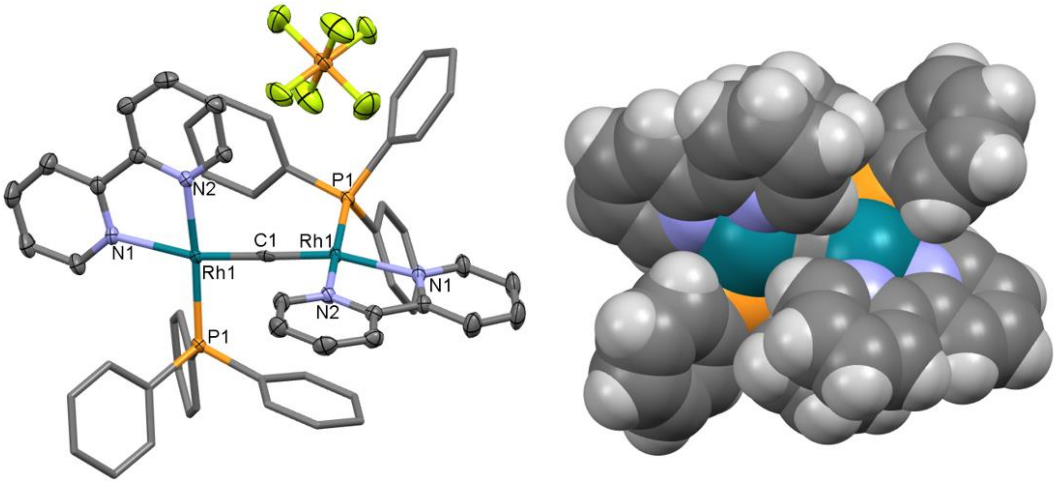

Figure 1.24: Simplified molecular structure (left) and spacefill (right) of one enantiomer of **[Rh_2(μ-C)bipy$_2$(PPh_3)$_2$][PF_6]$_2$ (8)**. 50% displacement ellipsoids, phenyl rings simplified, and hydrogen atoms removed. Selected bond lengths lengths (Å) and angles (°): Rh1-C1 1.76783(18), Rh1-N1 2.201(2), Rh1-N2 2.114(2), Rh1-C1-Rh1 176.9(2)

Only one half of the chiral complex (**Figure 1.24**) is crystallographically unique due to the μ-carbido atom lying on a crystallographic two-fold rotation axis while the alternative enantiomer is generated by an inversion centre. The Rh=C=Rh bond angle is 176.9(2) degrees but both bond lengths are axiomatically equal (1.76783(18) Å). The bite angle of the *cis* bipy ligand is acute (76.52(7)°), to accommodate within reason the geometric requirements of the sp^2 hybridised

nitrogen atoms. The strong *trans* influence of the μ-carbido ligand is manifest in a longer Rh-N bond length to the *trans cf. cis* pyridyl groups (2.201(2) *cf.* 2.114(2) Å, 44 e.s.d.).

As the molecular structure shows, the coordinated bipy ligands retain their expected planarity, in contrast to the boat shaped geometries of the Bp and Bp* chelates which allows the BH_2 groups in **$[Rh_2(\mu\text{-}C)L_2(PPh_3)_4]$ (L = Bp, Bp*)** to shield one face of each rhodium. The planar nature of the bipy ligand in contrast leaves the carbido core more exposed, which along with the dicationic nature, makes **8** a possible candidate for further reactivity studies.

The reactivity with the tridentate analogue terpyridine (terpy) was briefly explored, however, CH_2Cl_2 reaction mixtures of **$[Rh_2(\mu\text{-}C)Cl_2(PPh_3)_4]$** or **$[Rh_2(\mu\text{-}C)(PPh_3)_4](OTf)_2$** turn immediately dark in the presence of added terpy and monitoring the reaction using ^{31}P NMR and ESI-MS detected only complex degradation.

1.3.3 Sulfur-based Ligands

Reaction with the thiocrown ether 9S3

Perhaps one of the most surprising results to emerge from the studies of the nitrogenase MoCo co-factor was the discovery that the interstitial atom long known to reside within the trigonal prismatic $(MoS_{10})Fe_6$ core was not eponymously nitrogen, but actually a μ_6-carbido.[3] This unexpected result provides impetus for exploring small-molecule carbido chemistry within a sulfur-rich coordination environment, prompting Reinholdt and Bendix to investigated the reactions of the terminal ruthenium carbido complex **$[Ru(\equiv C:)Cl_2(PCy_3)_2]$** with a range of metal sulfido clusters.[12] Beyond that single study, and the Braun complexes for which the formation of thiolato ligands underpins CS_2-activation, however, there are no other reports of μ_2-carbido complexes involving sulfur-based ligands. Accordingly, the first ligand chosen for investigation was the thiacrown ether 9S3 (1,4,7-trithiacyclononane). This facially tridentate capping ligand has previously been installed on rhodium, including the dicationic Rh(III) species **$[Rh(9S3)_2]^{2+}$** and **$[Rh(CO)(9S3)(PPh_3)]PF_6$**.[63] Furthermore, the salt **$[Rh(9S3)(PPh_3)_2]PF_6$** has been shown to catalytically demercurate organomercurials.[64] The 9S3 ligand is pre-organised to adopt facial coordination to metal centres leading to analogies being mooted with anionic Tp and Cp ligands, however the neutral charge would (as with bipy) render the rhodium species cationic if installed on a rhodium carbido complex (**Scheme 1.27**).

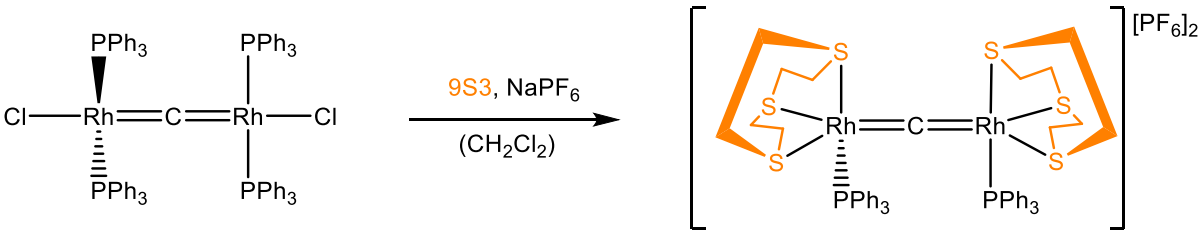

Scheme 1.27: Synthesis of **[Rh$_2$(μ-C)(9S3)$_2$(PPh$_3$)$_2$][PF$_6$]$_2$ (9)**

When excess 9S3 was added to **[Rh$_2$(μ-C)Cl$_2$(PPh$_3$)$_4$]** in dichloromethane, the solution turned yellow overnight. The resulting salt, **[Rh$_2$(μ-C)(9S3)$_2$(PPh$_3$)$_2$]Cl$_2$** was precipitated upon dilution of the reaction mixture with hexane. The ^{31}P{^{1}H} NMR spectrum showed a single symmetrical environment at 37.2 ppm, which showed strong one and three bond couplings to rhodium ($^1J_{RhP}$ = 202 Hz, $^3J_{RhP}$ = 14 Hz) and the normally elusive four bond P-P coupling ($^4J_{PP}$ = 8 Hz), which supported the installation of two 9S3 ligands on adjacent rhodium centres. The ^{1}H NMR spectra showed two multiplets for the 9S3 C_2H_4 backbone (δ_H = 1.94, 3.13) despite the molecular C_2 symmetry that would result in 12 chemical environments for a static structure.[65] This indicates that the ligand is fluxional on the ^{1}H NMR timescale, most likely due to weak coordination of the individual thioether donors allowing site exchange *via* favourable d^8-square-planar rhodium intermediates with κ^2-*S,S'* binding of the macrocycle.

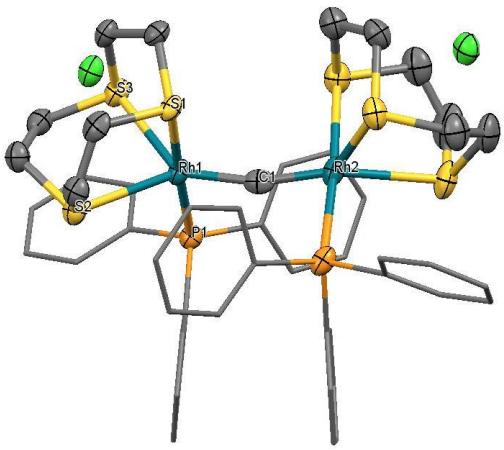

Figure 1.25: Simplified molecular structure of one enantiomer of **[Rh(μ-C)(9[ane]S$_3$)$_2$(PPh$_3$)$_2$](Cl)$_2$ (9a)**. 50% displacement ellipsoids, phenyl rings simplified, and hydrogen atoms removed; enantiomer

generated by an inversion centre in space group P_{-1}. Selected bond lengths lengths (Å) and angles (°): Rh1-C1 1.82(1), Rh2-C1 1.78(1), Rh1-S1 2.492(3), Rh1-S2 2.492(3), Rh1-S3 2.356(3), Rh1-C1-Rh2 164.1(7)

The chloride ligand that dissociates is retained as the counter ion, forming **$[Rh_2(\mu\text{-}C)(9S3)_2(PPh_3)_2]Cl_2$ (9a)**, however, when the reaction was completed with addition of $NaPF_6$, the PF_6 salt **$[Rh_2(\mu\text{-}C)(9S3)_2(PPh_3)_2](PF_6)_2$ (9b)** could be readily isolated. The issue presented with the installation of the 9S3 ligand, whilst successful, was that the steric features around the central carbido ligand presented a similar problem to the facially coordinating Tp complex **$[Rh_2(\mu\text{-}C)(Tp)_2(PPh_3)_2]$**. The molecular structure of **9** (**Figure 1.25**) displays the two chloride counter ions nestled near the 9S3 ligand, and as commonly observed, the C–H bonds of 9S3 coordinated to cationic centres are sufficiently polarised as to readily enter into hydrogen-bonding with ionic halides (C–H···Cl = 2.502 Å). Consistent with a d^8-configuration, the geometry at each crystallographically unique rhodium is best described as trigonal bipyramidal with the carbido ligand of interest assuming an equatorial site due to it being the only π-acidic ligand present. The *trans* influence of the μ-carbido ligand is therefore obscured by the adopted geometry, though the two equatorial Rh-S bond (2.492(3) Å) are significantly longer than that of the axial thioether which is trans to the PPh_3 ligand (2.356(3) Å). Though cationic and five-coordinate, the two Rh=C bond lengths in **9** fall within the norms emerging for the double bonds of a Class A description, at 1.82(1) and 1.78(1) Å.

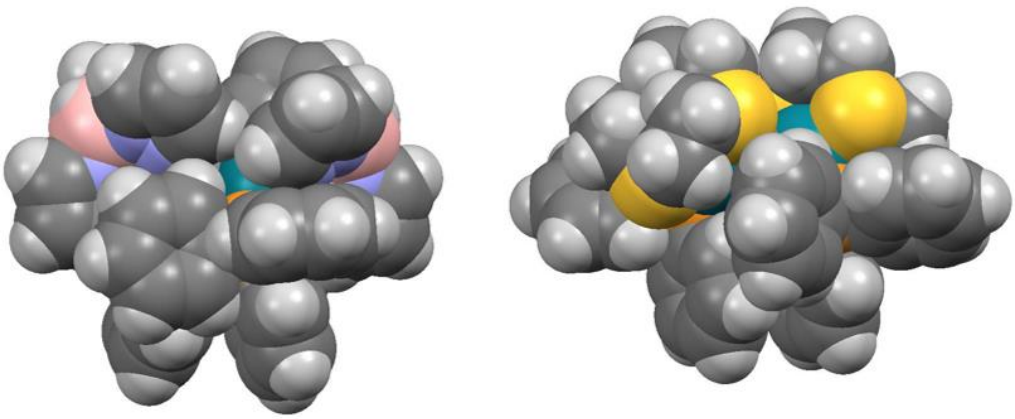

Figure 1.26: Spacefill diagrams of **$[Rh_2(\mu\text{-}C)(Tp)_2(PPh_3)_2]$** (left) and **9** (right)

The space-filling representations shown above (**Figure 1.26**) highlight how sterically encumbering the tridentate ligands Tp and 9S3 are in conjunction with the phosphines. The central carbido ligand is substantially blocked and would therefore be relatively inert to external reagents. Efforts to replace the remaining triphenylphosphines in **$[Rh_2(\mu\text{-}C)(9S3)_2(PPh_3)_2](PF_6)_2$** with the smaller dppm chelating ligand ultimately failed, with the bidentate phosphine binding more strongly than the coordinated 9S3 ligands and replacing them, forming **$[Rh_2(\mu\text{-}C)(dppm)_2](PF_6)_2$**. Because of this steric encumbrance, complex **9** was not pursued for further studies. It should be noted that with the data for **9** in hand, the reactions of the known salt **$[Rh(CS)(PPh_3)(9S3)]Cl$** with HBCat were explored under a range of conditions but in no instance did the $^{31}P\{^1H\}$ NMR spectrum of the reaction mixture indicate formation of **9**.

1.3.4 Terminal chloride reactivity

Reactivity towards lithium reagents

When examining the reactivity difference between the μ-carbido ligand and the well-known carbonyl complex **$[RhCl(CO)(PPh_3)_2]$**, the behaviour of the terminal chloride ligand towards acetylide nucleophile is notable. Whether through direct reactivity with the lithioacetylide, or elimination of an organic moiety, the framework of **$[Rh(C{\equiv}C\text{-}R)(CO)(PPh_3)_2]$** remains quite stable, even with inclusion of the tungsten tricarbido species **$[W(\equiv C\text{-}C\equiv C\text{-})(CO)_2(Tp^*)]$** (**Scheme 1.28**).[66] The carbonyl ligand appears to stabilise the inclusion of the *trans*-alkynyl ligand through its strong π-acidity.

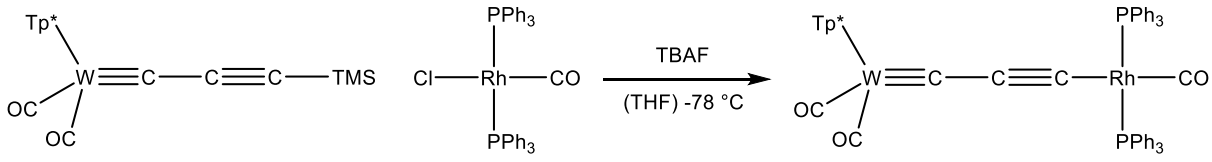

Scheme 1.28: Synthesis of rhodium(I) acetylide complexes with carbonyl co-ligand

Unfortunately, all attempts to explore this aspect of the reactivity of the μ-carbido complex ultimately failed, and the discussion here will be brief. The first route explored was through lithiation (**Scheme 1.29**). Lithiated (^{n}BuLi) THF solutions of common acetylenes (phenylacetylene,

TMS-acetylene, *p*-nitro phenylacetylene) at -78°C cause the rhodium carbido solution to turn dark in colour when slowly warmed to room temperature. A $^{31}P\{^{1}H\}$ NMR spectra of the solutions always displayed the characteristic singlets at 29 or 25 ppm, which unfortunately are the resonances of the free phosphine ligand (PPh_3 and dppm respectively) undergoing decomposition. The same outcomes were observed with common lithium reagents such as methyl lithium and phenyl lithium.

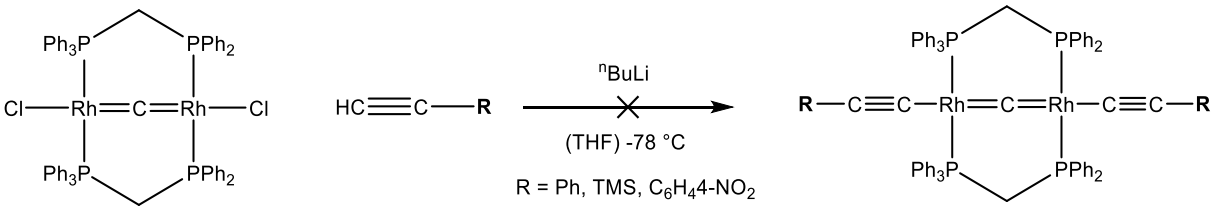

Scheme 1.29: Unsuccessful reactions of **1** with lithiated acetylenes

Attempts to use the tungsten alkynyl species **[W(≡CBr)(CO)$_2$(Tp*)]**, either alone or in combination with ^{n}BuLi to generate the lithiocarbyne species **[W(≡CLi)(CO)$_2$(Tp*)]** also had similar decomposition pathways with no identifiable products detected.

Attempted reactivity through desilation

Attempts to use a milder source of acetylide anions turned towards desilation (**Scheme 1.30**). Both the commercially available trimethylsilyl acetylene and the organometallic complex **[W(≡C-C≡C-TMS)(CO)$_2$Tp*]** were examined, with TBAF used as the source of fluoride. The instant the TBAF solution is added to the solution, it immediately turns dark. Once again, working up the reaction and examining the ^{31}P NMR spectrum shows only ligand decomposition products and **1** in solution.

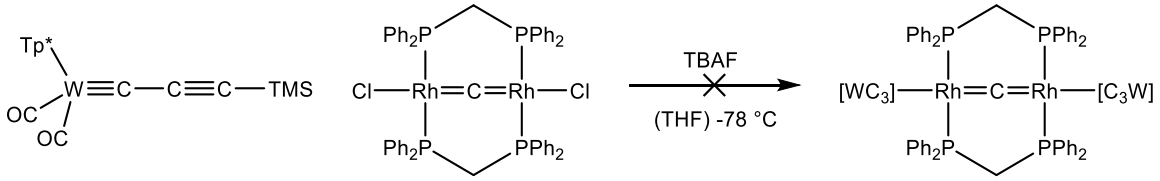

Scheme 1.30: Unsuccessful desilation and coordination of **[W(≡C-C≡C-TMS)(CO)$_2$(Tp)*]** to **1**

Catalytic Coupling of Ag and Hg

When examining the reactivity with acetylides, transfer agents such as mercury and silver acetylides were employed. Alkynyl mercurials have proven to serve as mild alkynyl transfer reagents to transition metals, lanthanides, and main group elements.[67] It was envisioned that metal halogen metathesis could take place, exchanging the R group on mercury or silver with the halide on rhodium.

Utilising the silver alkynyl complex **[W(≡C-C≡C-Ag.AgNO$_3$)(CO)$_2$(Tp)*]**,[68] the dichloromethane solution with **1** develops a silver mirror over the course of half an hour at room temperature. The deposition of metallic silver does not support the halide metathesis taking place, which would instead be reflected in the precipitation of colourless silver chloride. Subjecting the solution to silica gel chromatography, a green band was isolated, and the ^{1}H NMR analysis of the complex revealed it to be the previously synthesised ditungsten C_6 species **[W$_2$(μ-C$_6$)(CO)$_4$(Tp)*$_2$]**, which is the result of the coupling of the two C_3 complexes mediated by the rhodium species.

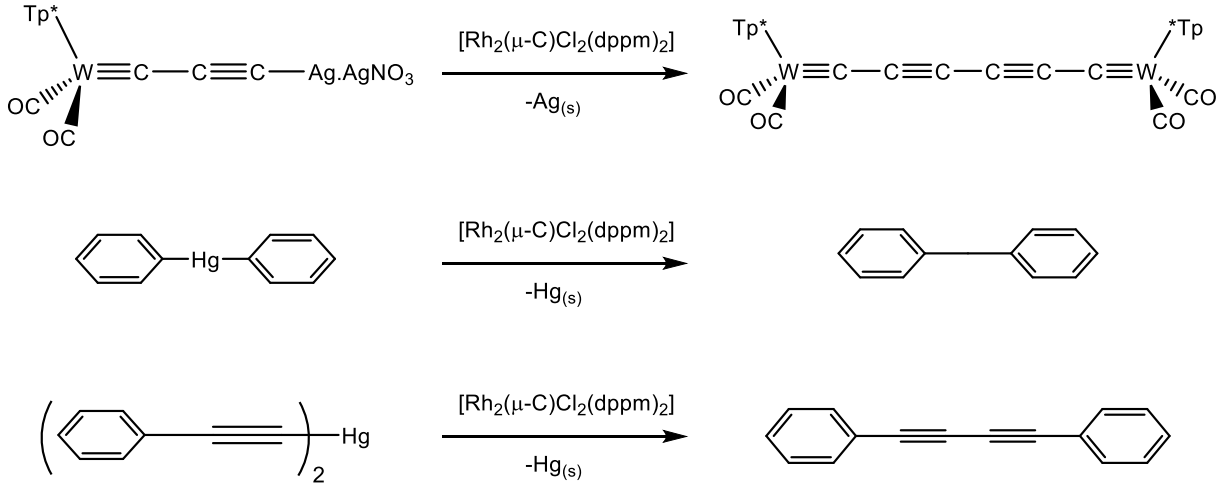

Scheme 1.31: Catalytic coupling of silver and mercury compounds with **1**

A similar procedure was attempted using mercury(II) compounds (**Scheme 1.31**). Rhodium complexes are well known to catalyse the coupling of mercury acetylides and using both diphenyl mercury(II) and bis(phenylacetylene)mercury(II) resulted in the deposition of metallic mercury and the generation of the coupled organic groups.[69] In all cases, the μ-carbido complex **1** ultimately remains unchanged and can be recovered through chromatography, owing to its catalytic

behaviour and stability. This presents the first use of well-defined μ-carbido complexes in a catalytic process (C-C coupling, though the mechanism is unlikely to differ from that involving more conventional co-ligands on rhodium.

Whilst there is no obvious reason why complexes of the form **[Rh$_2$(μ-C)(R)$_2$(PR'$_3$)$_4$]** would not be viable, the synthetic routes explored above failed to provide access. The class of compound nevertheless remains a desirable target, given that the only example of a μ$_2$-carbido complex with a σ-organyl co-ligand[xxiv] remains the cyclometallated species **[Rh(μ-C)H(C$_6$H$_4$PPh$_2$-2)(Tp*)$_2$]**.

1.3.5 Chalcogen Reactivity – μ$_2$-chalcocarbonyls

Reaction of [Rh$_2$(μ-C)Cl$_2$(PPh$_3$)$_4$] with carbon disulfide

Amongst the early work performed largely by Cowie and co-workers with the dirhodium A-frame complex **[Rh$_2$(μ-CO)Cl$_2$(dppm)$_2$]**, one standout mode of reactivity involved carbon chalcogenide species such as CS_2, which undergoes a two-fold addition to form **[Rh$_2$(μ-CO)(C$_2$S$_4$)Cl$_2$(dppm)$_2$]** (**Scheme 1.32**).[70] One of the benefits of using chalcogens to probe reactivity is their useful spectroscopic handles, with chalcocarbonyls containing strong and unique bands in the infrared spectrum, and in the case of ^{77}Se, a potentially useful NMR signature.

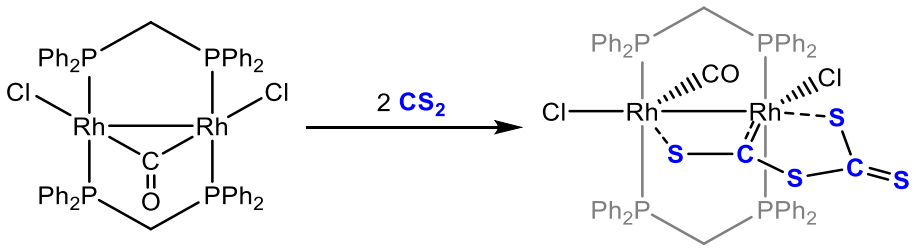

Scheme 1.32: Reactivity of CS_2 with **[Rh$_2$(μ-CO)Cl$_2$(dppm)$_2$]**

[xxiv] Colleagues have isolated the Class B complexes **[MPt(μ-C)(CH$_3$)(CO)$_2$(PPh$_3$)$_2$(Tp*)]** (M = Mo, W): L. K. Burt and R. Shang, unpublished results.

To initially test the reactivity of the carbido ligand to a chalcogen, sulfur was used as the starting point. The addition of elemental chalcogens to metal-carbon multiple bonds has been widely documented for carbyne, carbene and vinylidene ligands (**Scheme 1.33**).[71]

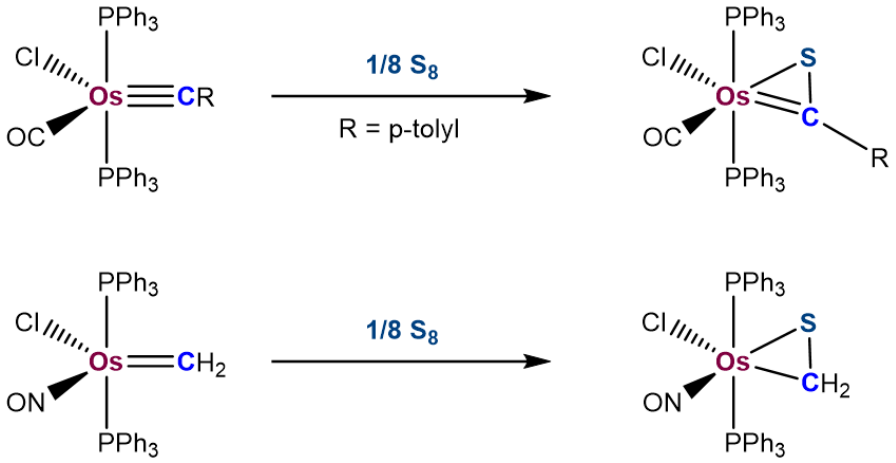

Scheme 1.33: Sulfur coordination across (top) carbyne bond and (bottom) methylene bond

The complex initially chosen was the parent complex **[$Rh_2(\mu\text{-}C)Cl_2(PPh_3)_4$]**, which although containing larger phosphine co-ligands, would hopefully produce a readily identifiable product. The reaction would include the addition of CS_2, which would ideally undergo a [2+2] cycloaddition of Rh=C and C=S multiple bonds in a manner akin to heteroatomic olefin metathesis to reform two equivalents of the rhodium thiocarbonyl precursor **[$RhCl(CS)(PPh_3)_2$]**. A similar cycloaddition of CS_2 across the Ru≡C bond of a benzylidyne complex **[$Ru(\equiv CPh)Cl(CO)(PPh_3)_2$]** has been proposed to account for the formation of the thiobenzoyl-thiocarbonyl complex **[$Ru(\eta^2\text{-}SCPh)Cl(CS)(PPh_3)_2$]**.[72] Given the product is well known, monitoring the reaction for its appearance in the ^{31}P NMR and IR spectra would be simple.

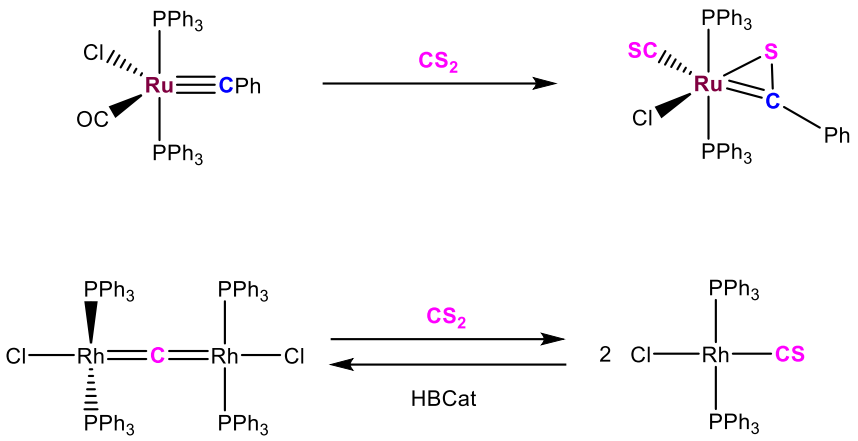

Scheme 1.34: (top) [2+2] cycloaddition of CS2 to **[Ru(≡CPh)Cl(CO)(PPh$_3$)$_2$].** (bottom) Reactivity pathways to and from the thiocarbonyl complex **[RhCl(CS)(PPh$_3$)$_2$]**

The $^{31}P\{^1H\}$ NMR spectrum of a $CDCl_3$ solution of **[Rh$_2$(μ-C)Cl$_2$(PPh$_3$)$_4$]** was first acquired to exclude the possibility of any residual precursor thiocarbonyl complex being present. Upon addition of CS_2, the yellow solution turned orange quite rapidly and after 30 minutes, the ^{31}P NMR spectrum of the mixture indicated a residual amount (*ca* 20% by integration) of the carbido complex however, the major doublet at 31 ppm corresponded to the thiocarbonyl complex **[RhCl(CS)(PPh$_3$)$_2$]**. After 3 hours, the ^{31}P NMR spectrum shows complete conversion into the thiocarbonyl species (**Scheme 1.34**).

Although the reaction was accompanied by further phosphine sequestration (as the sulfide), the reversal of the μ-carbido synthesis back to the thiocarbonyl complex gives strong support to the ligand being able to undergo further cycloaddition processes (see **Chapter 5**).

Reactions of [Rh$_2$(μ-C)Cl$_2$(μ-dppm)$_2$] with sulfur

Given the cleavage of the dirhodium complex into two mononuclear species, it was surmised that a similar process commencing with the A-frame analogue **[Rh$_2$(μ-C)Cl$_2$(dppm)$_2$]** might result in a product **[Rh$_2$(CS)$_2$Cl$_2$(μ-dppm)$_2$]** in which the binuclear integrity was retained by virtue of the bridging dppm buttresses (**Scheme 1.35**).

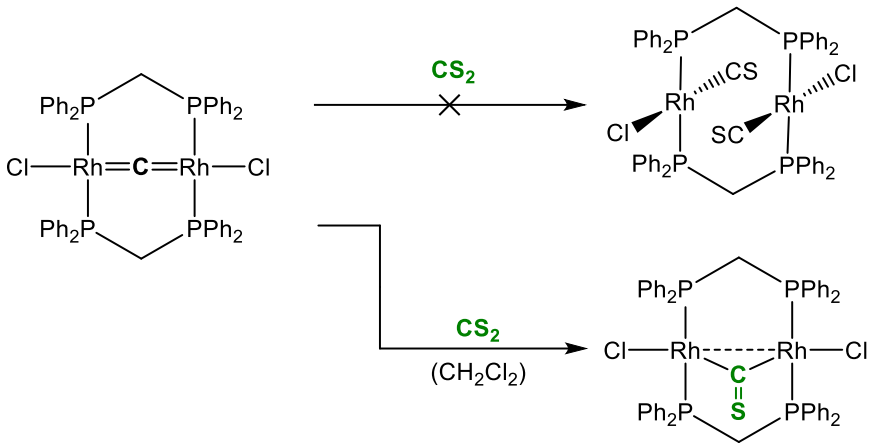

Scheme 1.35: Synthesis of **[$Rh_2(\mu\text{-}CS)Cl_2(dppm)_2$] (11)** from CS_2 addition to **1**

Addition of excess CS_2 to a red solution of **[$Rh_2(\mu\text{-}C)Cl_2(dppm)_2$]** gradually resulted in a change colour to green and monitoring the reaction *via* $^{31}P\{^1H\}$ NMR spectroscopy revealed complete conversion to a new compound after 12 hours. Subjecting the mixture to silica gel chromatography led to the elution of a dark green band, which produces dark green crystals upon standing. The NMR spectra of the green product did not, however, point to the synthesis of the desired dithiocarbonyl product.[xxv] The resonance for the product observed at 17.2 ppm in the $^{31}P\{^1H\}$ NMR spectrum displayed a reduced $^1J_{RhP}$ coupling constant of 118 Hz, which is typically indicative of an increase in the coordination number at the rhodium centres from four to five. The symmetric nature of the product indicated from the phosphorus resonance was also inferred from the ^1H NMR spectra. That being said, the presence of two highly coupled resonances at 3.02 and 3.58 ppm indicate the methylene protons on the dppm linker are in two distinct non-exchangeable chemical environments. This was supported through couplings detected in the ^1H-^1H COSY NMR and correlation to the same carbon group at 27.4 ppm in the ^{13}C NMR spectra. For the methylene hydrogens to be in distinct environments while the phosphorus nuclei are all in a single environment, the product must contain two (C_{2v}) but not three (D_{2h}) internal mirror planes, i.e., that one face of the rhodium must be different to the other whilst retaining symmetry elsewhere.

The IR spectra showed the presence of a single strong absorption at 1093 cm^{-1} attributed to the thiocarbonyl C=S stretch in a region indicative of a bridging rather than terminal coordination mode. The presence of a single stretch does not necessarily indicate formation of a

[xxv] The reaction of **[$RhCl(CS)(PPh_3)_2$]** with dppm might have been expected to also afford **[$Rh_2Cl_2(CS)_n$(m-dppm)$_2$]** (n = 1, 2), however, the $^{31}P\{^1H\}$ NMR spectrum acquired 2 hours after combination revealed only resonances corresponding to complex decomposition.

complex with a single thiocarbonyl ligand, because the symmetric stretching mode would be infrared silent unless the $M_2(\mu\text{-}CS)_2$ unit is non-planar, e.g., **$[Co_2(\mu\text{-}CS)_2(PMe_3)(\eta\text{-}C_5H_5)_2]$** has ν_{CS} = 1157, 1121 cm^{-1}.[73] In the present complex this seemed unlikely and would in any event render the phosphorus nuclei chemically inequivalent.

After many frustratingly futile attempts (including recourse to the Australian Synchrotron), crystals large enough for single crystal X-ray analysis were formed through evaporation of a CH_2Cl_2-toluene solution. The molecular structure derived from a toluene monosolvate was consistent with the formulation proposed on the basis of spectroscopic and analytical data (**Figure 1.27**), viz. a symmetrical bridging (thioketonic) *mono*-thiocarbonyl species **$[Rh_2(\mu\text{-}CS)Cl_2(dppm)_2]$ (10)**.

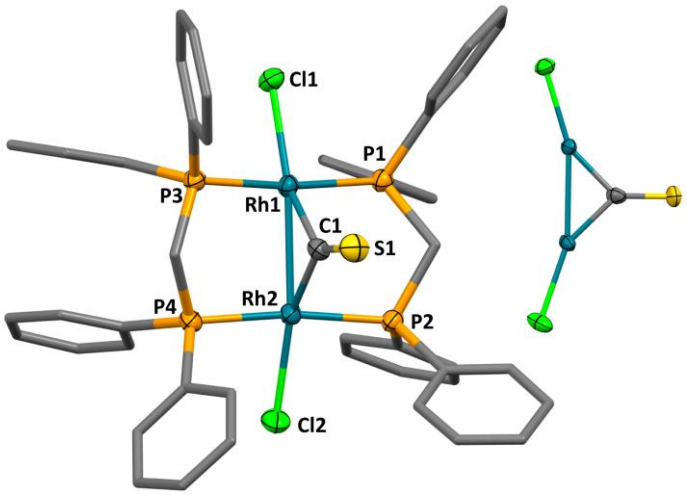

Figure 1.27: Molecular structure of **$[Rh_2(\mu\text{-}CS)Cl_2(dppm)_2]$ (10)** (50% displacement ellipsoids, selected hydrogen atoms and solvent omitted, phenyl groups simplified for clarity). Selected bond lengths (Å) and angles (°): Rh1-C1 1.915(4), Rh2-C1 1.913(4), Rh1-Rh2 2.7060(4), Rh1-P1 2.314(1), Rh1-Cl1 2.359(1), C1-S1 1.618(4), H4A-S1 3.290(1), Rh1-C1-Rh2 90.0(2), Cl1-Rh1···Rh2-Cl2 157.31(1)

The addition of a single sulphur atom to the bridging carbido ligand has a number of geometric and electronic consequences for the rhodium complex. The oxidation of the carbido to the thiocarbonyl ligand changes the electronic requirements at the metal centres, with symmetrical bridging thiocarbonyl ligands (as with their chalcogen counterparts) formally providing one electron to each metal centre. The rhodium centres with the bridging thiocarbonyl ligand would become 15 electron complexes, and as a result of this, the introduction of a formal rhodium-

rhodium bond occurs to satisfy the EAN Rule (16 valence electrons) and account for the diamagnetism. The Rh-Rh distance in **10** is reduced to 2.7060(4) Å, which is now shorter than the sum of covalent radii ($2r_{cov}$ = 2.84 Å for Rh-Rh[xxvi]) supporting the presence of a bonding interaction. A similar situation arises for the structurally characterised carbonyl analogue previously reported by Cowie, Stephan and Loeb (Rh1-Rh2 = 2.726(3) Å).[74]

The formal rhodium-rhodium interaction results in the complexes undergoing a minor geometrical change. The previously square-planar coplanar rhodium centres now adopt a distorted trigonal bipyramidal geometry to incorporate the rhodium-rhodium bond. However, it is far from the idealised geometry, with the internal RhCRh core adopting a near-perfect right-angle triangle, with the Rh1-C1-Rh2 angle at 90.0(2)° and the two C1-Rh1/2-Rh2/1 angles both at 45.0(1)°. The terminal chloride ligands are bent away from the thiocarbonyl ligand, with the Cl1-(Rh1-Rh centroid)-Cl2 angle out at 157.31(1)°.

The two hydrogens environments on the methylene linker of dppm evident in the ^{1}H NMR spectrum can be easily rationalised when examining the molecular structure. So long as the dppm ligand remains coordinated through both donors, there is no way for the two hydrogen atoms to exchange sites, such that one hydrogen atom of each methylene is constrained on the same face of the complex as the thiocarbonyl ligand (H4A-C1 distance = 3.007(1) Å, H4A-S1 = 3.283(1) Å), which although is too far away to contain any formal short contacts, places the hydrogen in a distinctly different chemical environment to its geminal counterpart.

Examining the thiocarbonyl ligand, accurate comparisons can be made between **10** and the monometallic rhodium terminal-thiocarbonyl complex **[RhCl(CS)(PPh$_3$)$_2$]**. The C-S bond length in the bridging thiocarbonyl complex (1.618(4) Å) is notably longer (0.06 Å, 16 e.s.d.) than the for the terminal thiocarbonyl in the mononuclear species (1.556(2) Å) which parallels the more general observation for bridging vs terminal carbonyl ligands.

Although CS_2 is the most ubiquitous source molecule for installation of a thiocarbonyl ligand,[76] the mechanism in most cases involves an initial η^2 coordination of CS_2 to a metal centre before elimination of a sulfur atom typically through phosphine abstraction. The addition of a single sulfur atom to the already present carbido ligand is considerably more ostentatious and has

[xxvi] Covalent radii of certain nuclei are repeatedly mentioned throughout this text, and in all cases come from the published work of Cordero and co-workers.[75]

on one previous occasion been observed in the reaction of a transient μ-carbido complex **[Ru$_2$(μ-C)(μ-N^{t}Bu)(η-C$_5$Me$_5$)$_2$]** with sulfur to afford **[Ru$_2$(μ-CS)(μ-N^{t}Bu)(η-C$_5$Me$_5$)$_2$]**.[77]

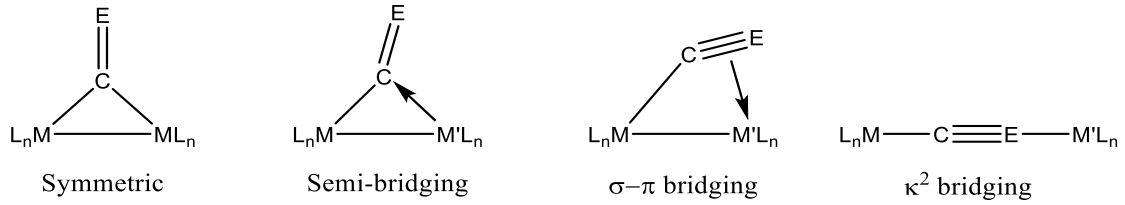

Figure 1.28: Possible bonding modes of a μ$_2$-CE ligand

The nature of bridging chalcocarbonyl ligands is understood well enough to describe them by four distinct bonding modes, three of which contain a μ$_2$-bridging carbon. The three bonding modes all respond to different electron requirements of the metal centres and donation ability of the carbon and chalcogen atoms (**Figure 1.28**). Because of the equidistant positioning of the sulfur atom to both rhodium centres, and the requirement of both rhodium centres to need only a single electron from the bridging ligand, the only suitable bonding mode to describe the ligand is the symmetrical bridging which intuitively makes sense, as the remaining two bonding modes are only seen with complexes of disparate metals.

Because of the lack of precedent, the mechanism for the reaction is not well understood. Monitoring of the reaction progress shows no intermediate structures enduring sufficiently to become apparent in the $^{31}P\{^1H\}$ NMR spectra, with a clean conversion over time of the only two resonances present, those being the carbido starting material to the thiocarbonyl product. Even when the reaction is incomplete, the NMR data only show the two complexes existing in solution in observable amounts (**Figure 1.29**).

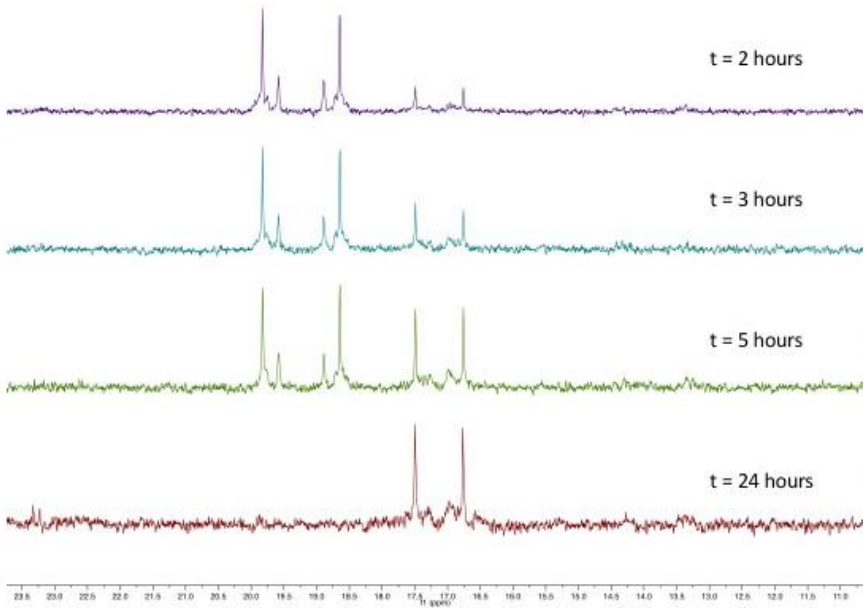

Figure 1.29: $^{31}P\{^{1}H\}$ NMR time-lapse spectra for the conversion of **1** (left) into the thiocarbonyl species **10** (right)

With no identifiable intermediate, the mechanism is open to uninformed conjecture. Computational analysis of the dppm starting material show that the valence electron density of the HOMO is localised on the Rh=C bonds, but that the LUMO is also substantially centralised on the μ-carbido ligand. Because the carbon atom has considerable amphoteric character contributing to both the HOMO and LUMO, it could in theory be the site of nucleophilic attack by the CS_2 sulfur atom, or, the CS_2 could first coordinate to the rhodium centre[78] prior to a [2+2] cyclo-addition as inferred for the PPh_3 derivative above.

The latter option involving direct addition from the carbido ligand is less likely, as no observable reactivity to date has behaved in this fashion, though CO_2 reacts with the transient bent carbido complex via C–C bond formation to provide **$[Ru_2(\mu\text{-}CCO_2)(\mu\text{-}N^tBu)(\eta\text{-}C_5Me_5)_2]$**.[79] There has been a single example of *intact* CS_2 coordinating across a M-M linkage, when the palladium dimer **$[Pd_2(\mu\text{-}P\,^tBu_2)(PPh_3)_3][BF_4]$** in excess CS_2 forms the stable yellow species **$[Pd_2(\mu\text{-}P\,^tBu_2)(\kappa^3\text{-}CS_2)(PPh_3)_3][BF_4]$**, consisting of formal interactions between the carbon and sulfur atoms to both palladium centres (**Scheme 1.36**).[80]

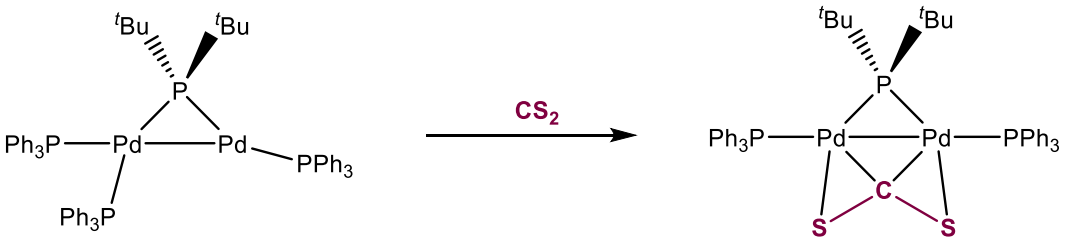

Scheme 1.36: κ^3 coordination of CS_2 across a Pd-Pd bond

There are however numerous instances of CS_2 cleavage across M–M bonds, including examples from 'A-Frame' systems, e.g., the reaction of **$[Re_2Cl_4(\mu\text{-dppm})_2]$** with CS_2 to afford the μ-sulfido complex **$[Re_2(\mu\text{-S})(CS)Cl_4(\mu\text{-=dppm})_2]$**.[81] Being said, a κ^3 coordination of CS_2 to the μ-carbido species would likely generate a cyclo-addition product, either producing the dithiocarbonyl product predicted or a thioketenylidene (CCS) and sulfido ligand.

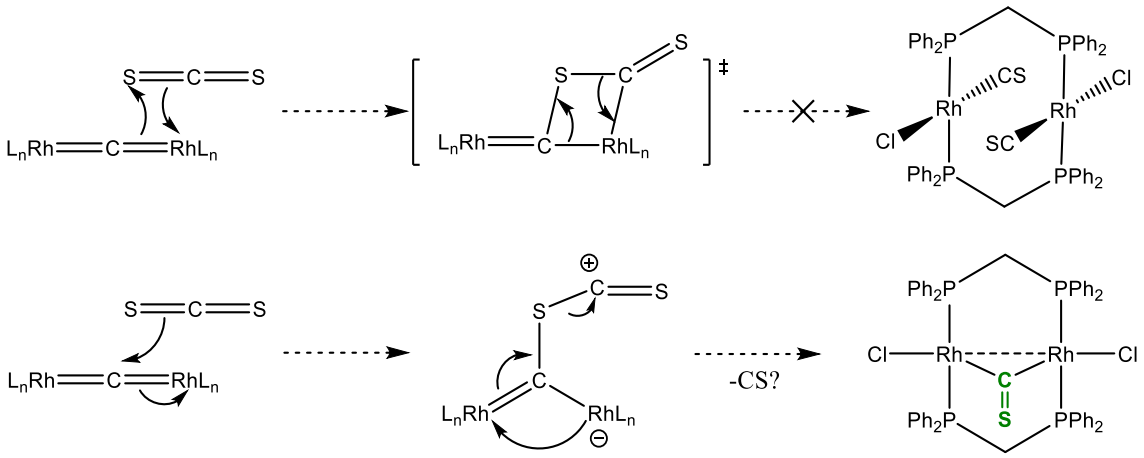

Scheme 1.37: Potential mechanistic pathways for CS_2 addition

The remaining mechanistic possibility is the nucleophilic attack of sulfur to the central carbido, forming a thioether intermediate. With a stoichiometric loss of CS seemingly unlikely, it is more probable that a mechanism involving more than one equivalent of CS_2 is taking place. It should be emphasised that loss of free CS would seem to represent a high energy process in that the molecule is exceedingly reactive and has only been observed in cryogenic matrices or the inter-stellar medium.[82]

With symmetric bridging μ_2-thiocarbonyl complexes still remaining comparatively scarce in the literature, especially when compared to the almost 6000 hits for structurally characterised bridging carbonyl complexes, this complex marks the first to bridge two rhodium centres. Due to its central importance, the ^{13}C enriched species was prepared using the isotopologue of **1**, cleanly forming **[Rh$_2$(μ-^{13}CS)Cl$_2$(dppm)$_2$]** (**10'**) under identical conditions (see **Chapter 6** for further ^{13}C NMR details). The $^{13}C\{^1H\}$ NMR spectrum of the enriched complex **10'** (in an approximately 1:1 mixture with **10**) included the resonance for the thiocarbonyl ligand at 322.1 ppm. This resonance (**Figure 1.30**) neatly displays the expected triplet of pentet splitting due to the ^{103}Rh and ^{31}P couplings, respectively ($^1J_{RhC}$ = 39 Hz, $^2J_{PC}$ = 7 Hz). The presence of the enriched ^{13}C nuclei has no noticeable effect on the ^{31}P or ^1H NMR spectrum of **10'**, appearing identical to **10**.

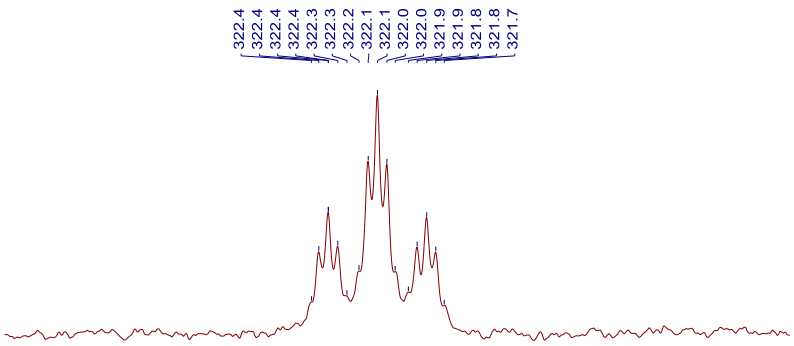

Figure 1.30: $^{13}C\{^1H\}$ NMR spectrum extract of the μ-CS resonance for **[Rh$_2$(μ-^{13}CS)Cl$_2$(dppm)$_2$]**

To investigate if the reaction could be repeated with a simpler form of sulfur, an NMR scale reaction was undertaken with **[Rh$_2$(μ-C)Cl$_2$(μ-dppm)$_2$]** and propylene sulfide, which has been occasionally used as a mild monoatomic sulfur delivery agent. Much to our dismay, the reaction is accompanied by complete dissociation of the phosphine ligands with formation of dppm sulfide, decomposing the starting material entirely. This did not help shed light on the mechanism of formation as the reactivity of S_8 is often radical based and hard to predict.

Reaction of $[Rh_2(\mu\text{-}C)Cl_2(\mu\text{-}dppm)_2]$ with selenium

Although initially the extension into the heavier chalcogens was deferred due to the difficulties in preparing or buying CSe_2 for obvious village-evacuation reasons,[xxvii] the success of the reaction with S_8 provided some hope. Studies on the reactivity and synthesis of selenocarbonyl complexes is fairly uncharted territory, has progressed rather sporadically and seemed unlikely to be as amenable as sulfur analogues.

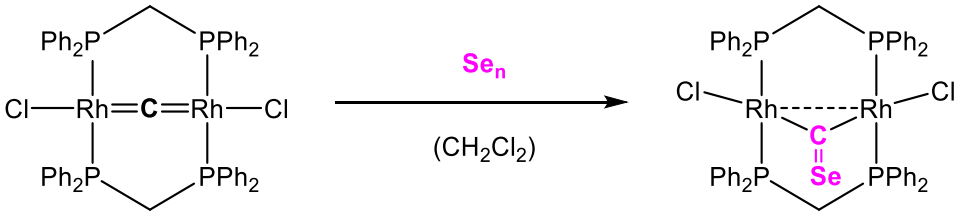

Scheme 1.38: Synthesis of **$[Rh_2(\mu\text{-}CSe)Cl_2(dppm)_2]$ (11)** from selenium addition to **1**

The insolubility of grey selenium proved to be one of the barriers to overcome, with the initial addition of equimolar selenium to a dichloromethane solution of **$[Rh_2(\mu\text{-}C)Cl_2(\mu\text{-}dppm)_2]$** showing no reactivity over 24 hours. Changing the reaction conditions to include five atom equivalents and increasing the solvent volume proved successful and filtering out the undissolved selenium powder left behind a dark green solution after 24 hours (**Scheme 1.38**). Once again, a stable complex could be isolated using column chromatography, and the green product thus isolated had an attractive metallic sheen to it.

Examining the spectroscopic data available, it was instructive to make comparisons to the thiocarbonyl complex **$[Rh_2(\mu\text{-}CS)Cl_2(dppm)_2]$**. The second-order $^{31}P\{^1H\}$ NMR pattern of the symmetrical complex is centred at 14.6 ppm, only 2 ppm upfield from the thiocarbonyl complex. More importantly, the fine structure of the peaks is rather characteristic (see **Figure 1.31**) which supports the synthesis of a complex with identical geometries at the rhodium centres.

[xxvii] See: https://www.science.org/content/blog-post/things-i-won-t-work-carbon-diselenide

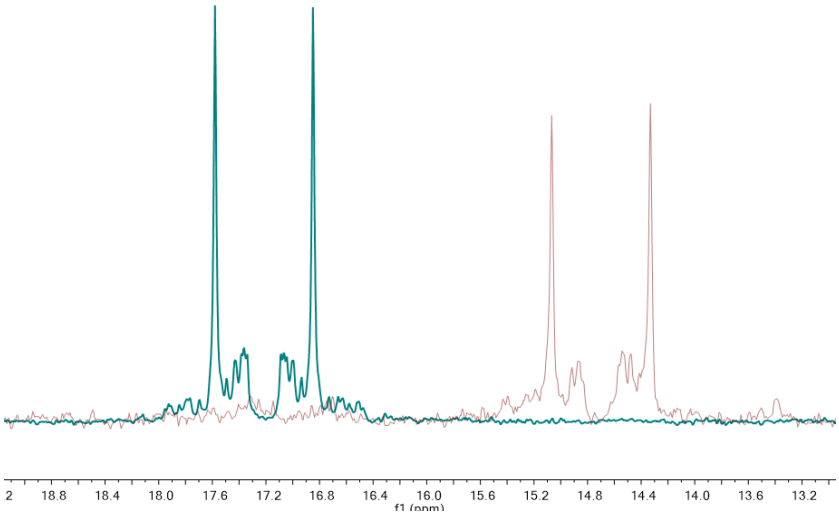

Figure 1.31: $^{31}P\{^{1}H\}$ NMR spectra comparison of **[Rh_2(μ-CE)Cl_2(μ-dppm)$_2$]** (Blue = S, Red = Se)

The two distinct hydrogen environments on the methylene dppm linkers are again seen in the ^{1}H NMR spectrum, at 2.96 and 3.68 ppm respectively. The addition of one selenium atom to the complex is unambiguously obvious in the mass-spectrum, reflecting the distinct selenium isotopic envelope centred at 1100.9379 *m/z* (*cf.* 1100.9360 for $C_{51}H_{44}{}^{35}ClP_4Rh_2{}^{77}Se$). Identifying the expected C=Se stretch in the infrared spectrum becomes slightly more difficult than its lighter chalcogens, as it would be expected to appear as a weaker band in the fingerprint region around 900 wavenumbers. The only known symmetrical μ-CSe complex is **[Ru_2(μ-CSe)(μ-N^{t}Bu)(η-C_5Me_5)$_2$]** for which no infrared data were provided.[77] Fortunately, an absorption stretch of moderate intensity centred on 957 cm^{-1} was detected and using a difference IR spectrum subtracting data for the thiocarbonyl analogue, to reveal a stretching mode only present in the selenocarbonyl complex.

Though all of the data pointed towards the symmetrically bridging selenocarbonyl complex **[Rh_2(μ-CSe)Cl_2(dppm)$_2$] (11)** being the product, the bridging selenocarbonyl ligand was unambiguously established in the X-ray molecular structure determination (**Figure 1.32**). The symmetrically bridging C=Se bond stands at 1.747(8) Å, and the distorted sp^2 geometry at carbon is again constrained close to 90° (91.8 °). Comparing **11** to **[Ru_2(μ-CSe)(μ-NPh)(Cp*)$_2$]**, the C=Se bond is significantly shorter (*cf.* 1.802 and 1.843 Å), suggesting more multiple bonding character present. It is also shorter than the range observed for isoselenocarbonyls (1.770 - 1.867 Å).[83] The replacement of sulfur with selenium has no effect on the electronic requirements of the two rhodium centres, which form a Rh-Rh single bond (2.7577(8) Å) to remain as five-coordinate, 16-electron species.

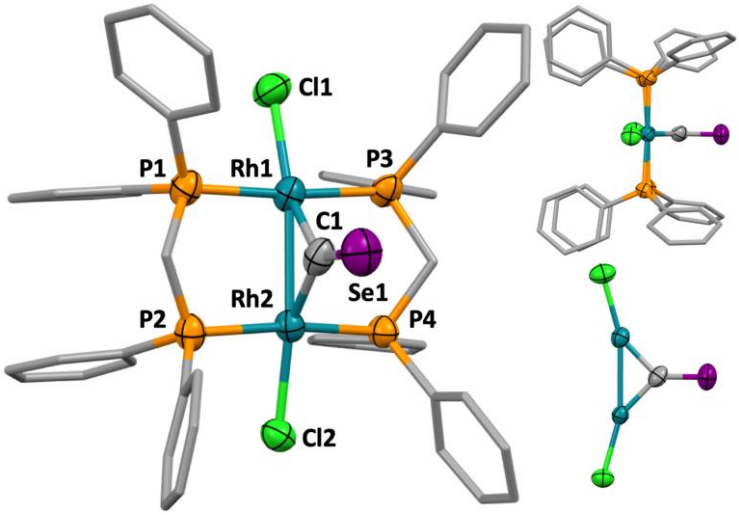

Figure 1.32: Molecular structure of **11** (50% displacement ellipsoids, solvent and hydrogen atoms omitted, dppm groups simplified. Selected bond lengths (Å) and angles (°): Rh1–Rh2 2.7577(8), Rh1–Cl1 2.351(2), Rh1–C1 1.911(9), Rh2–C1 1.928(8), Se1–C1 1.747(8), C1–Rh1–Rh2 43.8(3), Rh2–C1–Rh1 91.8(4), Se1–C1–Rh1 134.0(6)

Because of the uniqueness of the bridging selenocarbonyl ligand, the synthesis was repeated with the ^{13}C isotopologue to form the enriched isomer **[Rh$_2$(μ-^{13}CSe)Cl$_2$(dppm)$_2$]**. Though the selenocarbonyl resonance was not detected in the conventional 1D $^{13}C\{^1H\}$ NMR spectrum due to the high multiplicity, the enriched complex presented a highly coupled downfield resonance at 341.3 ppm. Running a long scan ^{77}Se NMR, the selenocarbonyl environment appeared unexpectantly as a sharp singlet at 1116.2 ppm. Complex **11** presents the first structural characterisation for a group 9 selenocarbonyl species.

Protonation of [Rh$_2$(μ-CE)Cl$_2$(μ-dppm)$_2$] (E = O, S, Se)

As previously mentioned, the bridging carbonyl complex **[Rh$_2$(μ-CO)Cl$_2$(μ-dppm)$_2$]** was synthesised back in the 1980s by Cowie and co-workers.[84] The bridging carbonyl complex stems from an entirely different synthetic route, with the decarbonylation of the dicarbonyl complex *trans*-**[Rh$_2$Cl$_2$(CO)$_2$(dppm)$_2$]** requiring refluxing toluene to form the red complex **[Rh$_2$(μ-CO)Cl$_2$(μ-dppm)$_2$]**. Having the chalcogen series of oxygen through to selenium allows for some analytical comparisons of the NMR and structural data (**Table 1.4**).

Property	CO[a]	CS	CSe
δ ^{31}P ($^{1}J_{RhP}$)	19.7 (116)	17.2 (118)	14.7 (119)
δ PCH_2	3.21, 3.26	3.02, 3.58	2.96, 3.68
C=E (Å)	**1.22(3)**	**1.619(4)**	**1.747(8)**
Rh-C (Å)	**1.90(3)**	**1.914(4), 1.913(4)**	**1.911(9), 1.928(8)**
Rh-Rh (Å)	2.726(3)	2.7059(4)	2.7577(8)
Rh-C-Rh (°)	92(1)	90.0(2)	91.8(4)

Table 1.4: NMR and crystallographic data analysis for **$[Rh_2(\mu\text{-}CE)Cl_2(dppm)_2]$** (E = O, S, Se).
[a] data taken from Cowie[78]

What is notable about the solid-state structures is the unchanging Rh_2C core. Though the carbon-chalcogen bond length undergoes significant elongation moving down group 16, the two Rh-C bond lengths only differ at most by 0.03 Å (or ~5 e.s.d.), and the distorted sp^2 geometry at the chalcocarbonyl remains very close to 90° across the series.

One of the questions that arises with the synthesis of the heavier chalcocarbonyls was to what extent this affect the reactivity of the complex? One of the initial reactions performed by Cowie and co-workers on the carbonyl analogue was an attempted protonation of the complex using HCl. Instead of protonation occurring at the carbonyl ligand, the hydrogen instead adds across the Rh-Rh bond and forms a μ-hydrido ligand, with the chloride conjugate base coordinating to one rhodium centre to form a neutral complex **$[Rh_2(\mu\text{-}CO)(\mu\text{-}H)Cl_3(dppm)_2]$** (**Scheme 1.39**).[85] This process was repeatable with triflic acid and tetrafluoro boric acid, with the less nucleophilic anion participating in a dynamic coordination process. In the context of models for the Fischer-Tropsch process, a surface-bound hydroxycarbyne 'COH' is an intriguing species to consider and whilst no bimetallic μ_2-COH complexes have been structurally characterised, there are a number of μ_3-COH examples, e.g., **$[Co_3(\mu_3\text{-}COH)(CO)_9]$** and **$[Ru_5(\mu_3\text{-}COH)(\mu\text{-}H)_2(CO)_{14}]^-$**.[86]

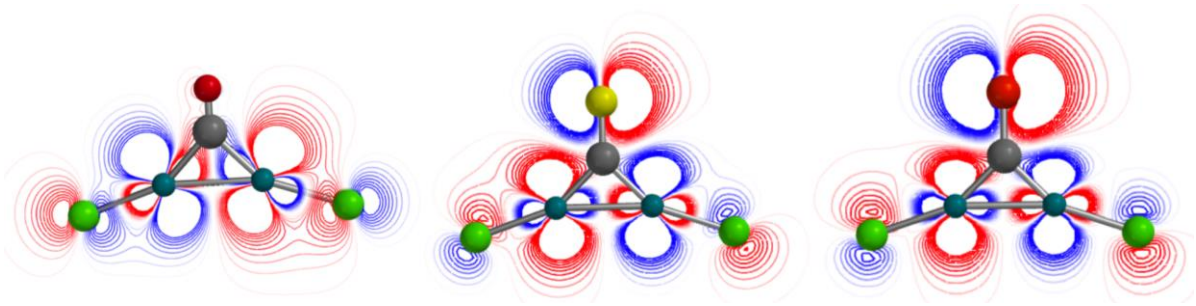

Figure 1.33: HOMO cross-sections for **[Rh$_2$(μ-CE)Cl$_2$(dmpm)$_2$]** (E = O, S, Se from L to R) (DFT: ωB97X-D/6-31G*/LANL2Dζ)

Though protonation did not occur at the carbonyl ligand, the progression down Group 16 results in some key changes to orbital energies. Most notably, both CS and CSe have calculated HOMOs of significantly higher energy than CO, and the LUMO of lower energy. The energy differences allow CS and CSe to be better σ-donors and π-acceptors than CO. This distinction becomes profound when considering the results of DFT studies performed on the trimmed model compounds **[Rh$_2$(μ-CE)Cl$_2$(dmpm)$_2$]** (E = O, S, Se) (**Figure 1.33**). The calculated HOMO of the three complexes shows a stark difference between CO and CS/Se. Protonation of the carbonyl complex in retrospect was likely to occur across the Rh-Rh bond because the HOMO contains almost no carbonyl character, and instead primarily comprises rhodium *d*-orbitals. However, the heavier chalcogens contain significant *p*-orbital character in the corresponding HOMOs, suggesting that protonation might occur at the chalcogen itself to form a thiolato or selenolato carbyne. It should be noted that protonation at hetero-atoms with lone pairs does not involve a rehybrisation or geometry change that might contribute to a kinetic barrier and are in general very rapid relative to proton transfers to and from carbon. Norton has suggested protonation/deprotonation of transition metals is in contrast to heteroatoms rather slow, being more comparable to carbon.[87] Accordingly, insights that follow from **Figure 1.33** relate to the most likely site of *kinetic* protonation, the caveat being that slow, thermodynamically favoured, and irreversible metal protonation may conceal the operation of rapid but reversible chalcogen protonation.

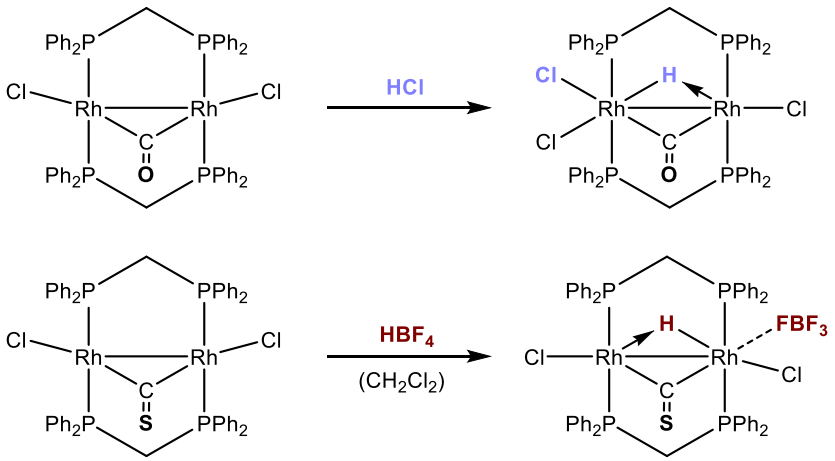

Scheme 1.39: Rh-Rh bond protonation for **[Rh$_2$(μ-CO)Cl$_2$(dppm)$_2$]** and **[Rh$_2$(μ-CS)Cl$_2$(dppm)$_2$]**

To examine the possibly different reactivity, the thiocarbonyl and selenocarbonyl complexes were both treated with anhydrous HBF_4 in CH_2Cl_2. The green solution of the thiocarbonyl complex immediately turns bright yellow upon addition of HBF_4. Precipitation of a yellow powder with petrol unfortunately detected a *ca* 1:1 ratio with the starting material. The symmetrical phosphorus resonance at 25.3 ppm ($^1J_{RhP}$ = 96 Hz) had the same downfield shift and reduction of coupling constant as observed for the μ-hydrido carbonyl species. The presence of a hydrido ligand was clearly evident in the ^{1}H NMR spectrum, with a highly structured triplet of pentet resonance at -16.46 ppm. Utilising ^{1}H-^{13}C HMBC NMR analysis revealed informative correlations between both the μ-hydride and the dppm methylene linker to a resonance at 300.0 ppm which may been assigned confidently as the μ-thiocarbonyl resonance. The ^{19}F NMR spectrum measured in CD_2Cl_2 did not show a sharp singlet (or quartet[xxviii]) as would be expected at *ca* –151 ppm for the uncoordinated anion. Rather, two broadened resonances (indicative of reduced local symmetry[xxix]), each with their ^{10}B and ^{11}B components are observed (see **Figure 1.34**), suggesting coordination to the complex is not only detectable, but also that exchange with free BF_4^- is slow on the ^{19}F NMR timescale given the sharp nature of the resonance that is

[xxviii] Though not normally observed due to the quadrupolar nature of ^{10}B (I = 3) and ^{11}B (I = $^3/_2$), $^1J_{BF}$ may under favourable conditions be observed (*ca* 5 Hz), e.g., when the boron nucleus is in an isotropic cubic electric field such as for a free tetrahedral BF_4^- anion. The natural abundances of these two isotopes results in principle in the observation of two signals in the approximate ration of 1:4 due to isotopic shift.

[xxix] The quadrupolar moment of a nucleus typically couples to the local electric field gradient resulting in extensive broadening, the exception being when the electric field has cubic (T_d, O_h) symmetry such that there is no nett effect on the non-spherical nucleus. Line-sharpening by thermal decoupling, i.e., by heating the sample, would be expected to invalidate the observations due to perturbing the dissociation equilibrium.

adventitiously present due a trace of residual free $^{11}BF_4^-$ (150.0 ppm, resonance due to $^{10}BF_4^-$ obscured). This dynamic inner-sphere coordination of BF_4 has been recorded previously on gold(I) NHC complexes by Nolan and co-workers.[88]

Unfortunately, the reversible nature of the Rh-Rh protonation results in an equilibrium being established with the dark green starting material, and even working the reaction mixture up with solvents such as diethyl ether causes rapid deprotonation. In order to acquire complete spectroscopic data, excess HFB_4 was kept in the CD_2Cl_2 NMR vial, which maintained the bright yellow colour of the solution, allowing for analysis of the μ-hydride product **[Rh_2(μ-CS)(μ-H)Cl_2(dppm)$_2$(FBF_3)] (12)**.

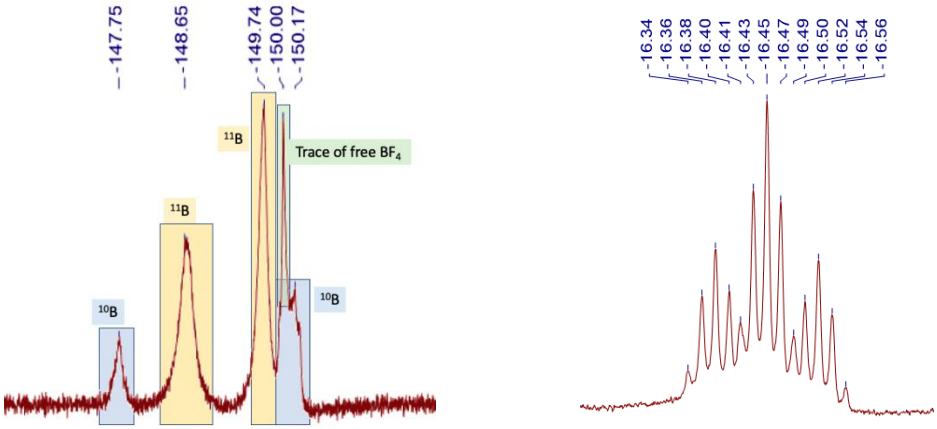

Figure 1.34 (left) ^{19}F NMR and (right) ^1H NMR extract of **[Rh_2(μ-CS)(μ-H)Cl_2(FBF_3)(μ-dppm)$_2$]**

In their work on the bridging carbonyl complex, Cowie and co-workers noted the dynamic coordination of the anion and deprotonation of the hydride ligand in coordinating solvents. Subjecting the thiocarbonyl complex to either silica gel chromatography or addition of any solvent (*e.g.*, Et_2O, THF) to the dichloromethane solution resulted in the clean decomposition to a dark yellow powder (**Scheme 1.40**). The hydride ligand of **12** was no longer detected in the ^1H NMR spectrum, and the phosphorus resonance had relocated upfield to 11.8 ppm, but with a similar $^1J_{RhP}$ coupling constant of 95 Hz.

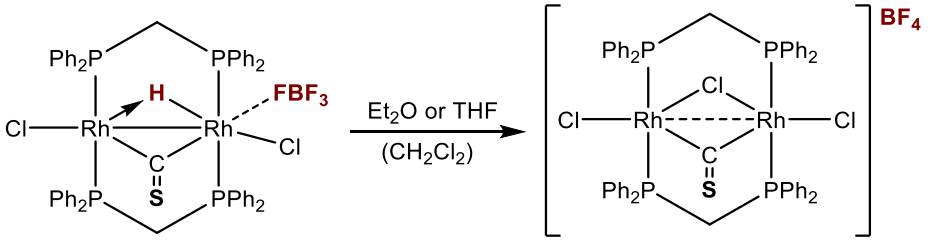

Scheme 1.40: Hydride removal of **[Rh$_2$(μ-CS)(μ-H)Cl$_2$(FBF$_3$)(μ-dppm)$_2$]** to form **[Rh$_2$(μ-CS)(μ-Cl)Cl$_2$(μ-dppm)$_2$][BF$_4$] (13)**

The BF_4 counter ion is still present but is now evident as a sharp singlet (δ_F = -150.97) in the $^{19}F\{^1H\}$ NMR spectrum as expected for an uncoordinated anion (this could also be seen as the antisymmetric T_2 B-F stretch appeared at 1055 cm^{-1} in the ATR IR spectrum). Resonances for the two methylene hydrogens on dppm appear at different chemical shifts (δ_H = 3.20, 4.24), implying the retention of symmetry (C_{2v}) across two of the three faces of the complex. The ESI-MS detected a cationic complex of formula **[Rh$_2$(CS)Cl$_3$(dppm)$_2$]$^+$** (1122.9277 *m/z*, *cf.* 112.9290 for $C_{51}H_{44}{}^{35}Cl_3P_4Rh_2S^+$), with the increased complexity of the isotopomeric envelope corresponding to an addition of a $^{35/37}$Cl atom. The spectroscopic yield of conversion was sufficient to implicate the dichloromethane solvent as the source of the additional chloro ligand. The presence of a chloride ligand and retention of C_{2v}-symmetry implies the chloride assumes the bridging position previously occupied by the hydride ligand. This was crystallographically confirmed in the molecular structure of the salt **[Rh$_2$(μ-CS)(μ-Cl)Cl$_2$(μ-dppm)$_2$][BF$_4$] (13)** (**Figure 1.35**).

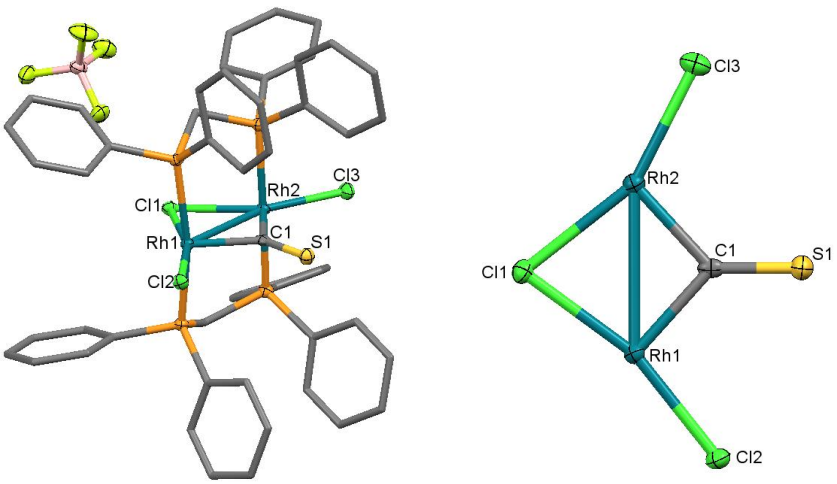

Figure 1.35: Molecular structure of **[Rh$_2$(μ-CS)(μ-Cl)Cl$_2$(μ-dppm)$_2$][BF$_4$] (13)** (50% displacement ellipsoids, solvent and hydrogen atoms omitted, dppm groups simplified). Selected bond lengths (Å) and angles (°): Rh1-C1 1.971(4), Rh2-C1 1.964(5), Rh1-Rh2 2.9117(5), C1-S1 1.552(4), Rh1-Cl1 2.384(1), Rh2-Cl1 2.436(1), Rh1-Cl2 2.308(1), Rh2-Cl3 2.321(1), Rh1-C1-Rh2 95.5(2), S1-C1-Cl1 178.7(2)

Upon oxidation, the bridging thiocarbonyl ligand undergoes a slight geometric change from the precursor **[Rh$_2$(μ-CS)Cl$_2$(μ-dppm)$_2$]**, with the Rh-C bonds being slightly elongated (1.971(4) and 1.964(5) Å) and the C=S bond being contracted (1.552(4) *cf.* 1.618(4) Å), suggesting increased multiple bond character for the CS bond at the expense of retrodonation through the Rh-C linkage. For the precursor, in the solid state the methylene groups points towards the thiocarbonyl ligand however in 13 these have flipped so as to allow weak incipient hydrogen bonding to both the bridging chloride ligand (C–H···Cl = 2.764(1) Å) and the tetrafluoroborate counter anion (C–H···F = 2.628(1) Å). The most interesting feature of **13**, however, is the Rh-Rh distance of 2.9117(5) Å. This distance lies on the boundary for formal metal-metal interactions to take place ($2r_{cov}$Rh = 2.84 Å), though EAN rules do not necessitate the need for a Rh-Rh bond. Canonical forms that would invoke d^7 rhodium(II) centres are discounted, given the diamagnetism that follows from the spectroscopic studies.

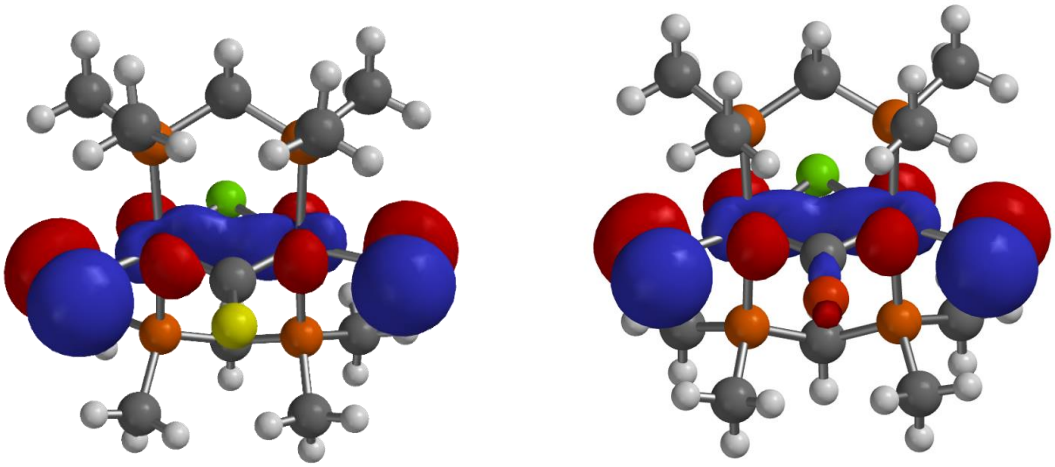

Figure 1.36: (left) HOMO-4 of **[Rh$_2$(μ-CS)(μ-Cl)Cl$_2$(μ-dmpm)$_2$]$^+$** and (right) HOMO-6 of **[Rh$_2$(μ-CSe)(μ-Cl)Cl$_2$(μ-dmpm)$_2$]$^+$** (DFT: ωB97X-D/6-31G*/LANL2DZ)

Computational exploration of the simplified analogues **[Rh$_2$(μ-CE)(μ-Cl)Cl$_2$(μ-dmpm)$_2$]$^+$** (E = S, Se, **Figure 1.36**), reveals that the HOMO-4 (and HOMO-6 for E = Se) do indeed suggest a rather modest constructive overlap of *d*-orbitals on adjacent rhodium centres, though the calculated Löwden bond order (0.474 for CSe) falls short of a full bond. Thus, whilst the geometry and calculations point towards a Rh-Rh interaction, this at best weak and more likely reflects that with four bridging ligands, the rhodium centres have little option but to acknowledge each other.

The selenocarbonyl complex, with the largest percentage of heteroatom *p*-orbital character in the HOMO, was expected to offer the best chance of perhaps observing chalcogen protonation. The addition of anhydrous HBF_4 saw the dark green solution not turn the bright yellow colour seen for the oxygen and sulfur analogues, but instead a deep pink (**Scheme 1.41**). In a similar fashion to the thiocarbonyl species, the selenium complex undergoes rapid colour change when placed in coordinated solvents or during attempts to precipitate with ether. In order to secure useful NMR data, the reaction was performed in CD_2Cl_2 with excess HBF_4 to sustain the bright pink colouration. The $^{31}P\{^1H\}$ NMR spectrum showed clean conversion to a new downfield environment at 20.83 ppm, and the expected reduction in coupling constant $^1J_{RhP}$ of 95 Hz. The ^{19}F NMR spectrum was dominated by a strong resonance for the requisite excess BF_4^- (δ_F = -150.17), but with shoulders corresponding to the likely FBF_3 coordination (δ_F = -147.51, -153.41).

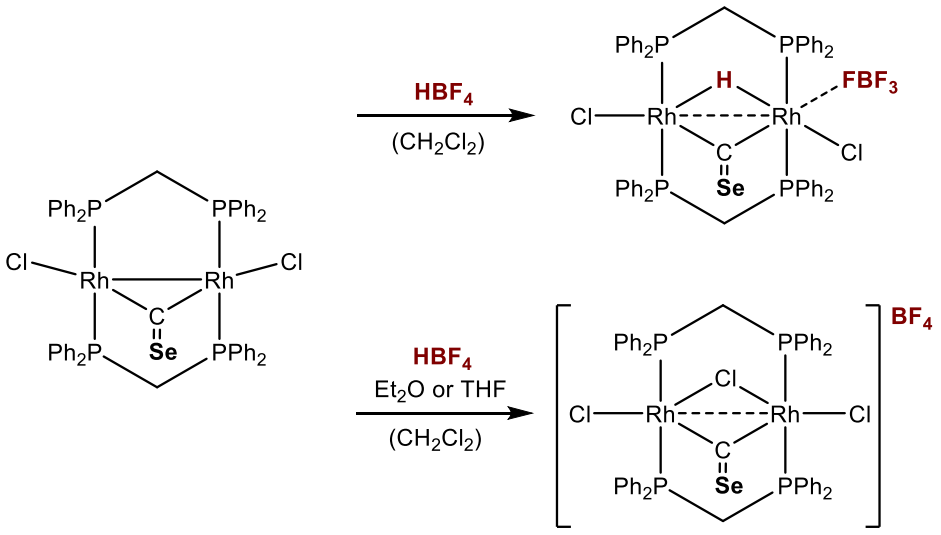

Scheme 1.41: Protonation and subsequent decomposition of the selenocarbonyl complex **[Rh$_2$(μ-CSe)Cl$_2$(μ-dppm)$_2$]**

The ^{1}H NMR spectrum provided the most unequivocal evidence for the location of the added proton. The highly structure triplet of pentet resonance at -15.13 ppm ($^{1}J_{RhH}$ = 30 Hz, $^{2}J_{PH}$ = 7.7 Hz) confirmed that protonation had occurred symmetrically across the Rh-Rh linkage again, rather than protonation of the selenocarbonyl, forming **[Rh$_2$(μ-CSe)(μ-H)Cl$_2$(FBF$_3$)(dppm)$_2$] (14)**. The methylene linkers manifested as two distinct resonances (3.17 and 3.58 ppm) showing the doublet of (virtual) pentet fine-structure ($^{2}J_{HH}$ = 15 Hz, J_{PH} = 5 Hz) due to the strongly coupled magnetically inequivalent *trans*-coordinated phosphorus nuclei.

The 'decomposition' product that developed upon attempts to work up or purify **[Rh$_2$(μ-CSe)(μ-H)Cl$_2$(FBF$_3$)(dppm)$_2$]** could be isolated as a dark pink powder upon addition of excess ether or petrol. The new symmetrical phosphorus resonance, as with the thiocarbonyl analogue, undergoes an upfield shift to 9.94 ppm, with the $^{1}J_{RhP}$ coupling remaining at 95 Hz. The free BF_4 counter ion could be detected in the ^{19}F{^{1}H} spectrum, appearing as a sharp singlet, confirming no enduring coordination to the rhodium centre(s). Most conspicuously, no hydride resonance could be detected in the high field region of the ^{1}H NMR spectrum. The μ-chloro cation **[Rh$_2$(μ-CSe)(μ-Cl)Cl$_2$(μ-dppm)$_2$]$^+$ (15)** could be detected as a cationic species in the mass spectrum, appearing as a complex isotopic envelope centred on 1170.8734 *m*/*z* (*cf.* 1170.8734 *m*/*z* for $C_{51}H_{44}{}^{35}Cl_3P_4Rh_2{}^{80}Se$). The infrared spectrum saw no Rh-H band but the presence of the unbound BF_4 $\nu_{B\text{-}F}$ at 1054 cm^{-1}. Unfortunately, the anticipated $\nu_{C\text{-}Se}$ absorption was calculated to fall in the range 950-1000 cm^{-1} (968cm^{-1} for **[Rh$_2$(μ-CSe)(μ-Cl)Cl$_2$(μ-dmpm)$_2$]$^+$**), which includes the intense BF_4 T_2 mode and dppm overtones and was therefore unable to be unambiguously identified. These data all taken together indicate that protonation of the selenocarbonyl complex has proceeded in an analogous manner to that observed for the thiocarbonyl analogue.

Alkylation of [Rh$_2$(μ-CSe)Cl$_2$(μ-dppm)$_2$]

Even though protonation of the selenocarbonyl complex did not (ultimately) occur at the heteroatom as initially hoped, the next logical step to examine its reactivity was through alkylation. Though the μ_2-CSeH or μ_2-CSH ligands were not expected to be overly stable, alkylation to a selenoether was anticipated to be more successful. The alkylation of a terminal selenocarbonyl complex had already been demonstrated with the terminal anionic selenocarbonyl complex **Li[Mo(CSe)(CO)$_2${HB(pzMe$_2$)$_3$}]** which reacted with methyl iodide to furnish the neutral methylselenolatocarbyne product **[Mo(≡CSeCH$_3$)(CO)$_2${HB(pzMe$_2$)$_3$}]**.[89] In a similar manner,

there are many examples of the alkylation of μ_2- or μ_3-thiocarbonyl ligands.[90] The only known μ_2-selenatocarbyne complexes have recently been reported, however, these arise from the addition of 'AuCl' to pre-formed terminal alkyl- or alkynytlselenolatocarbynes.[91] Within A-frame chemistry, Gladfelter has shown that alkylation of **$[Ru_2(CO)_5(dmpm)_2]$** with MeOTf takes one of two courses. Methylation of a bridging carbonyl ligand provides the μ_2-methoxycarbyne complex **$[Ru_2(\mu\text{-}COMe)(CO)_4(\mu\text{-}dmpm)_2]^+$** (33%) or alternatively direct attack at the metal centre followed by migratory insertion affords the μ-acyl complex **$[Ru_2(\mu\text{-}OCMe)(CO)_4(\mu\text{-}dmpm)_2]^+$** (45%) (**Scheme 1.42**).[92]

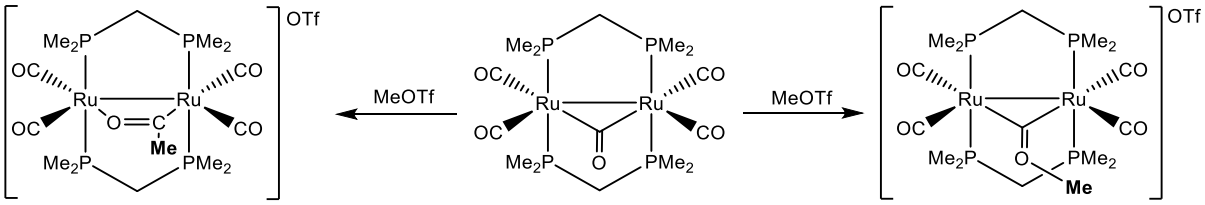

Scheme 1.42: alkylation of (right) μ-carbonyl ligand and (left) ruthenium centre of **$[Ru_2(CO)_5(dmpm)_2]$**

The first alkylation agent chosen was trimethyl oxonium tetrafluoroborate ($[Me_3O][BF_4]$). In a CD_2Cl_2 NMR-scale test reaction, the dark green solution turns dark red/pink upon addition of the colourless crystals. After an hour, monitoring the ^{31}P NMR spectrum displayed complete loss of the starting material but the appearance of two very distinct environments. The minor of the two appeared as a sharp doublet at 20.7 ppm ($^1J_{RhP}$ = 95 Hz), which perfectly matched the μ-hydride complex seen earlier. It was rationalised that the aged sample of $[Me_3O][BF_4]$ was most likely contaminated with HBF_4, causing the protonation. However, the major product consisted of a very broad doublet at 15.9 ppm ($^1J_{RhP}$ = ~90 Hz). The broad doublet suggested an incipient fluxionality, as both the selenocarbonyl starting material and the μ-hydride protonation product present noticeably sharp phosphorus peaks and defined second order splitting.

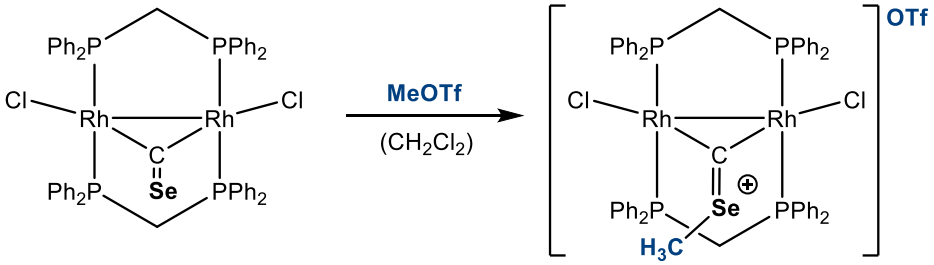

Scheme 1.43: Alkylation of the selenocarbonyl species **[Rh$_2$(μ-CSe)Cl$_2$(μ-dppm)$_2$]**

Moving away from the questionably anhydrous oxonium salt, the cleaner and slightly more toxic methylating source methyl triflate (MeOTf) was used (**Scheme 1.43**). An NMR scale reaction in CD_2Cl_2 resulted in the dark green solution remaining dark upon addition of MeOTf. Addition of toluene and removal of all solvents (and remaining methyl triflate) under high vacuum yielded a dark yellow residue of formulated as **[Rh$_2$(μ-CSeCH$_3$)Cl$_2$(μ-dppm)$_2$]OTf (16)**.

Monitoring the changes by $^{31}P\{^1H\}$ NMR revealed a remarkably a clean conversion to the same broad doublet environment at 15.9 ppm ($^1J_{RhP}$ = 83 Hz). The ^{1}H NMR spectrum included two doublet of pentets resonances at 3.23 and 3.51 ppm ($^2J_{HH}$ = 15 Hz, J_{PH} = 4 Hz) due to the PCH_2 methylene groups in a locally C_{2v}-symmetric complex. The high-field region of the NMR spectrum was devoid of any resonances that might suggest that if the methyl group resided on one or both rhodium centres. Instead, a broad singlet was identified at 2.78 ppm integrating for 3 hydrogens and didn't correspond to any residual solvents or MeOTf. The presence of a triflate counter ion was clearly detected in the ^{19}F NMR spectrum, as a singlet at -78.00 ppm.

In further NMR analysis of **16**, the singlet at 2.78 ppm showed no correlation to any other hydrogen environments in the ^{1}H-^{1}H COSY spectrum while the ^{1}H-^{13}C HSQC spectrum clearly detected the expected correlation between the methylene hydrogens at 2.23 and 3.51 ppm and the same PCH_2 carbon resonance at 25.0 ppm. The resonance at 2.78 ppm in the ^{1}H dimension correlated with a carbon environment nearby at 25.4 ppm, which corresponds to a selenoether methyl group.

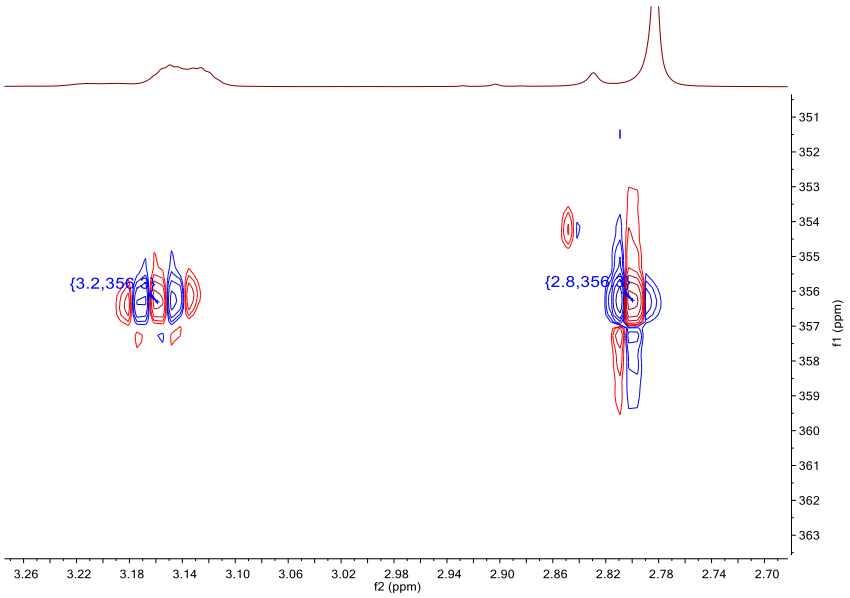

Figure 1.37: Extract of the ^{1}H-^{13}C HMBC for **[Rh$_2$(μ-CSeCH$_3$)Cl$_2$(μ-dppm)$_2$]OTf (16)**, depicting correlations between methyl and methylene resonance with that for the selenocarbonyl resonance

The ^{1}H-^{13}C HMBC spectrum revealed the final pieces to the puzzle. The resonance originally due to the selenocarbonyl was replaced by a new resonance shifted downfield to 356.3 ppm which curiously showed a strong correlation (^{4}J) to one of the dppm methylene resonances (**Figure 1.37**). This same carbon resonance was also correlated to the singlet peak at δ_H = 2.78, strongly supporting the case for the latter being assigned to the selenium-coordinated methyl group. The ^{13}C{^{1}H} NMR spectrum detected the methyl environment clearly at 25.4 ppm, just downfield of the observed triplet resonance due to the methylene linker.

The cationic complex of the salt **[Rh$_2$(μ-CSeCH$_3$)Cl$_2$(μ-dppm)$_2$]OTf** was easily detected in the high-resolution ESI-MS, with the isotopic envelope centred at an m/z of 1150.9287 (*cf.* 1150.9281 for $C_{52}H_{47}{}^{35}Cl_2P_4Rh_2{}^{80}Se$). Unfortunately, crystals suitable for X-ray analysis were not successfully obtained, however, even without the molecular structure, the spectroscopic data available points towards successful alkylation on the selenium.

Reactivity of [Rh$_2$(μ-CSe)Cl$_2$(μ-dppm)$_2$] to [AuCl(SMe$_2$)]

With the alkylation of the selenocarbonyl successful, testing the coordinate ability of the selenium atom towards a metal was next explored, given that selenoureas are known to serve as

ligands towards a range of metals, including gold,[93] in particular to the AuCl moiety. The reaction of the selenocarbonyl complex towards **[AuCl(SMe$_2$)]** was therefore investigated.

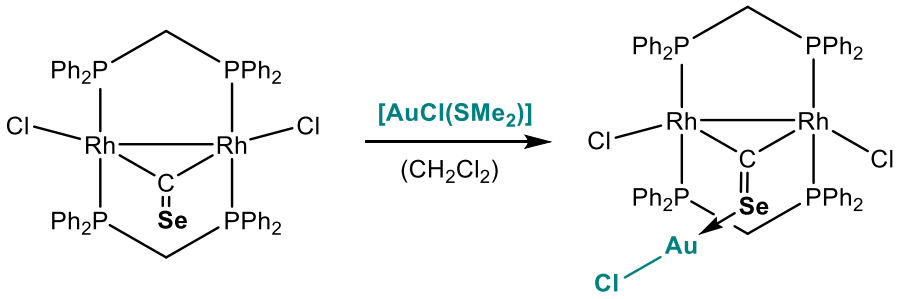

Scheme 1.44: Coordination selenocarbonyl species **[Rh$_2$(μ-CSe)Cl$_2$(μ-dppm)$_2$]** to **[AuCl(SMe$_2$)]**

The yellow colour change upon addition of excess **[AuCl(SMe$_2$)]** to **[Rh$_2$(μ-CSe)Cl$_2$(μ-dppm)$_2$]** supported the desired reaction taking place (**Scheme 1.44**). Chromatographic purification eluted a yellow band, which produced a yellow microcrystalline complex. The $^{31}P\{^1H\}$ NMR spectrum indicated the formation of an unsymmetrical species, with two neighbouring resonances centred at 0.56 ($^1J_{RhP}$ = 142 Hz) and -0.05 ppm ($^1J_{RhP}$ = 149 Hz). Unlike the methylation product, the two distinct phosphorus chemical environments implies that the AuCl is unable to freely rotate around the selenium, most likely due to its significantly larger size.

The two dppm methylene linker hydrogens of **[Rh$_2$(μ-CSeAuCl)Cl$_2$(μ-dppm)$_2$] (17)** again give rise to resonances indicative of distinct chemical environments, appearing as a broad doublet at 2.90 ($^2J_{HH}$ = 14 Hz) and the expected doublet of virtual pentets downfield at 4.30 ppm ($^2J_{HH}$ = 14 Hz, J_{PH} = 5 Hz). The methylene resonance appears at 23.4 ppm in the ^{13}C NMR spectrum, which is downfield relative to its usual shift of ~16 ppm. Without the coordinated 'reporter' methyl group, the μ$_2$-selenocarbonyl environment was unable to be identified through either 1D or ^1H-^{13}C HMBC studies. The high-resolution mass spectrum of **17** featured a major fragmentation at 1367.8394 *m/z*, which is a strong match for the expected $[M\text{-}Cl]^+$ fragment ($C_{51}H_{44}Au^{35}Cl_2P_4Rh_2{}^{80}Se^+$) at 1367.8400 *m/z*. Unfortunately, the AuCl adduct **17** could not be cleanly crystallised, but the data present support the selenium displaying sufficient nucleophilicity to undergo coordination to AuCl, in a similar fashion to a selenourea.[94]

1.3.6 Summary

This opening chapter largely explored the ligand transformations possible starting from the parent μ-carbido complex **[Rh_2(μ-C)Cl_2(PPh_3)$_4$]**. The replacement of the phosphine ligands with bidentate phosphines was a facile and in general successful process. The bidentate phosphines with small bit angles, such as dppm and dcpm, provided the first examples of a coplanar dirhodium μ-carbido species in **[Rh_2(μ-C)Cl_2(μ-dRpm)$_2$]** (R = Ph, Cy). The installation of phosphines with a larger bite angle (dcpe, dppp, dppf) resulted in the bridging complexes approaching mutually orthogonal arrangement of the two rhodium coordination planes to the extent allowed by geometric constraints of the diphosphine tether.

A selection of alternative ligands to phosphines was explored. The nitrogen-based bipyridine ligand could be successfully installed on the μ-carbido complex to form the dicationic species **[Rh_2(μ-C)(bipy)$_2$(PPh_3)$_2$]Cl_2**. The softer donor atom sulfur was also incorporated, with the thiacrown ether 1,4,7-trithiacyclononane, which could be installed as a facially capping ligand onto each rhodium in **[Rh_2(μ-C)(9S3)$_2$(PPh_3)$_2$]Cl_2**.

The terminal chloride ligands on the lead compound **[Rh_2(μ-C)Cl_2(μ-dppm)$_2$]** could be removed by addition of silver(I) trifluoromethanesulfonate, forming the acetonitrile adduct **[Rh_2(μ-C)(MeCN)$_2$(μ-dppm)$_2$](OTf)$_2$** in solution. The chlorides could be successful replaced with bromine ligands, though any attempt to replace the chlorides through nucleophilic substitution with carbon nucleophiles failed. Addition of silver(I) or mercury(II) acetylides led to the catalytic coupling of the acetylide groups by the μ-carbido species.

The μ-carbido ligand underwent its first documented functionalisation in the presence of chalcogens. Addition of CS_2 to the parent species **[Rh_2(μ-C)Cl_2(PPh_3)$_4$]** furnished two equivalents of the thiocarbonyl precursor **[Rh(CS)Cl(PPh_3)$_2$]**, however, addition of CS_2 or S_8 to **[Rh_2(μ-C)Cl_2(μ-dppm)$_2$]** led to the formation of the green μ_2-thiocarbonyl species **[Rh_2(μ-CS)Cl_2(μ-dppm)$_2$]**, and the first rhodium selenocarbonyl species could be made in an identical reaction with grey selenium. Attempted protonation of the chalcogen with HBF_4 led instead to the formation of the μ-hydrido complexes **[Rh_2(μ-CE)(μ-H)Cl_2(μ-dppm)$_2$(FBF_4)]** (E = S, Se), which decomposed in the presence of dichloromethane to furnish the μ-chloro complex **[Rh_2(μ-CS)(μ-Cl)Cl_2(μ-dppm)$_2$]BF_4**. The selenocarbonyl species could be successfully methylated using methyl triflate to form the cationic methylselenolatocarbyne complex **[Rh_2(μ-CSeCH_3)Cl_2(μ-**

dppm)$_2$](OTf). Addition of **[AuCl(SMe$_2$)]** to the selenocarbonyl species formed a gold adduct **[Rh$_2$(μ-CSeAuCl)Cl$_2$(μ-dppm)$_2$]**, in a similar fashion to gold adducts of cyclic selenourea species.

The exploratory research in this chapter paved the way for further functionalisation in the coming chapters, which are centred around the μ-carbido complex **[Rh$_2$(μ-C)Cl$_2$(μ-dppm)$_2$]**.

1.4 EXPERIMENTAL

General Experimental

Unless otherwise stated, experimental work was carried out at room temperature under a dry and oxygen-free argon atmosphere using standard Schlenk techniques with dried and degassed solvents. NMR spectra were obtained on a Bruker Avance 400 (^{1}H at 400.1 MHz, ^{13}C at 100.6 MHz, ^{31}P at 162.0 MHz), a Bruker Avance 600 (^{1}H at 600.0 MHz, ^{13}C at 150.9 MHz) a Bruker Avance 700 (^{1}H at 700.0 MHz, ^{13}C at 176.1 MHz), or a Bruker Avance 800 (^{1}H at 800.0 MHz, ^{13}C at 201 MHz) spectrometers at the temperatures indicated. Chemical shifts (δ) are reported in ppm with coupling constants given in Hz and are referenced to the solvent peak, or external references (H_3PO_4 in H_2O for ^{31}P, $CFCl_3$ for ^{19}F, $SeMe_2$ for ^{77}Se, [Rh(acac)$_3$] for ^{103}Rh). The multiplicities of NMR resonances are denoted by the abbreviations s (singlet), d (doublet), t (triplet), m (multiplet), br (broad) and combinations thereof for more highly coupled systems. In some cases, distinct peaks were observed in the ^{1}H, ^{31}P{^{1}H} and ^{13}C{^{1}H} NMR spectra, but to the level of accuracy that is reportable (i.e. 2 decimal places for ^{1}H NMR, 1 decimal place for ^{13}C and ^{31}P NMR) they are reported as having the same chemical shift. The abbreviation 'C_6H_5' is used to refer to the phenyl rings on the (diphenylphosphino)methane ligand. Due to solubility issues, a number of ^{13}C environments were discerned using indirect techniques, and coupling information is not available. Spectra provided generally correspond to samples obtained directly from chromatography and may contain residual solvent as recrystallised samples often display reduced solubility. NMR solvents were stored under nitrogen with molecular sieves.

Infrared spectra were obtained using a PerkinElmer FTIR spectrometer. Bands in the IR spectrum are recorded in wavenumbers (cm^{-1}) to the nearest integer. Elemental microanalytical data were provided the London Metropolitan University. Elemental analysis results with solvent present were confirmed where possible with ^{1}H NMR studies. High-resolution electrospray ionisation mass spectrometry (ESI-MS) was performed by the ANU Research School of Chemistry mass spectrometry service with acetonitrile as the matrix. When giving isotopomeric composition for accurate mass simulations, unless otherwise stated the common isotopes ^{1}H, ^{13}C, ^{103}Rh, etc. are implied.

Data for X-ray crystallography were collected with an Agilent Xcalibur CCD diffractometer and an Agilent SuperNova CCD diffractometer using Mo-Kα radiation (λ = 0.71073 Å) or Cu-Kα radiation (λ = 1.54184 Å) at 150 K using the CrysAlis PRO software. The structures were solved by direct or Patterson methods and refined by full-matrix least-squares on

F^2 using the SHELXS or SHELXT and SHELXL programs. Hydrogen atoms were located geometrically and refined using a riding model. Diagrams were produced using the CCDC visualisation program Mercury.

The compounds dppf,[95] $PhICl_2$,[96] [AuCl(THT)],[97] [$Au(C_6F_5)$(THT)],[98] [$Hg(CF_3)_2$][99] and [$Ni(CO)_4$][100] were prepared from literature methods. The remaining reagents were used as received from commercial suppliers.

Optimised Synthesis of [$Rh_2(\mu$-C)$Cl_2(PPh_3)_4$]

The complex [RhCl(CS)$(PPh_3)_2$] (550 mg, 0.778 mmol) was partially dissolved in dry benzene (50 mL). A solution of HBcat in THF (4.0 mL, 1.0 M, 4.0 mmol) was added and the solution stirred with heating at 50°C for fifteen hours. The solution was concentrated under reduced pressure and 50 mL of a 1:1 solution of ethanol and *n*-hexane added to precipitate out a dark orange product. Yield 214 mg (0.160 mmol, 41%). ^{1}H NMR ($CDCl_3$, 400 MHz) δ_H = 7.13-7.17 [m, 24 H, $H^{2,6}(C_6H_5)$], 7.27-7.30 [m, 12 H, $H^4(C_6H_5)$], 7.39-7.44 [m, 24 H, $H^{3,5}(C_6H_5)$]. $^{13}C\{^1H\}$ NMR ($CDCl_3$, 176 MHz) δ_C = 424.4 (t.br, μ- C, $^1J_{RhC}$ = 47), 134.9 [t^v, $C^4(C_6H_5)$, J = 6], 133.1 [t^v, $C^{2,6}(C_6H_5)$, J = 22], 129.4 [t^v, $C^{3,5}(C_6H_5)$, J = 5 Hz], 127.9 [$C^4(C_6H_5)$]. $^{31}P\{^1H\}$ NMR ($CDCl_3$, 162 MHz) δ_P = 21.61 (dd, $^1J_{RhP}$ = 180, $^3J_{RhP}$ = 7 Hz). IR (ATR, cm^{-1}) ν_{max} = 1011 ($\nu_{Rh=C=Rh}$). MS-ESI(+): m/z = 1301.14 [M-Cl]$^+$, 1039.05 [M-Cl-PPh_3]$^+$. Accurate mass: found 1301.1438 [M–Cl+H]$^+$. Calc. for $C_{73}H_{60}{}^{35}ClP_4Rh_2$: 1301.1444. Anal. found: C, 62.90; H, 4.62%. Calcd for $C_{73}H_{60}Cl_2P_4Rh_2.CH_2Cl_2$: C, 62.47; H, 4.39%. The compound was structurally characterised as a dichloromethane monosolvate through single crystal X-ray crystallography. *Crystal data for* $C_{73}H_{60}Cl_2P_4Rh_2.CH_2Cl_2$: M_w = 1422.73 g.mol^{-1}, triclinic, *P*-1 (No. 2), a = 12.5983(2), b = 13.8742(3), c = 20.5650(4) Å, α = 85.461(2), β = 84.238(1), γ = 75.285(1)°, V = 3453.74(12) Å^3, Z = 2, T = 150.0(1) K, μ(Cu Kα) = 6.47 mm^{-1}, D_{calcd} = 1.368 Mg.m^{-3}, 29219 reflections measured (7.8° ≤ 2Θ ≤ 133.2°), 13963 unique (R_{int} = 0.027) which were used in all calculations. The final R_1 was 0.0345 ($I > 2\sigma(I)$) and wR_2 was 0.090 (all data) for 757 parameters. CCDC 1834291.

Synthesis of [$Rh_2(\mu$-C)$Cl_2(\mu$–dppm)$_2$] (1)

A mixture of [$Rh_2(\mu$-C)$Cl_2(PPh_3)_4$] (100.0 mg, 0.075 mmol) and dppm (150 mg, 0.390 mmol) was dissolved in dry CH_2Cl_2 (10 mL). The red solution was stirred at room temperature for

24 hours. The solution was concentrated under reduced pressure, and n-hexane added until a red precipitate formed. The precipitate was isolated *via* vacuum filtration, washed with cold hexane and ether, and dried in vacuo. The complex could be recrystallised from a mixture of CH_2Cl_2 and *n*-hexane, however the crude material was found to be spectroscopically pure ($^{31}P\{^1H\}$ NMR) and was generally used, as obtained, for subsequent investigations. Yield: 77 mg (0.073 mmol, 97% yield) of yellow product. ^1H NMR (400 MHz, $CDCl_3$) δ_H = 2.90 (s, 4 H, PCH_2), 7.25-7.31 (m, 24 H, C_6H_5), 7.78 (br. s, 16 H, C_6H_5). $^{13}C\{^1H\}$ NMR (201 MHz, $CDCl_3$) δ_C = 411.7 (μ-C), 134.2 [t^v, $^2J_{PC}$ = 6 Hz, $C^{2,6}(C_6H_5)$], 132.2 [p^v, $^1J_{PC}$ = 11 Hz, $C^1(C_6H_5)$], 130.5 [$C^{3,5}(C_6H_5)$], 128.4 [$C^4(C_6H_5)$], 22.0 (^vp, $^1J_{PC}$ = 11 Hz, CH_2). $^{31}P\{^1H\}$ NMR (162 MHz, $CDCl_3$) δ_P = 19.12 (dd, $^1J_{RhP}$ = 191 Hz, $^3J_{RhP}$ = 38 Hz). IR ν_{max} (ATR, cm^{-1}): 2935, 999 (ν_{as} Rh=C=Rh).[xxx] MS (ESI, *m/z*) Accurate mass: Found 1099.0352 $[M+H+MeCN]^+$, Calcd for $C_{53}H_{48}{}^{35}Cl_2NP_4Rh_2$: 1098.0224. Anal.: Found: C, 57.98; H, 4.25%. Calcd for $C_{51}H_{45}Cl_2P_4Rh_2$: C, 57.92; H, 4.19%. *Crystal data for* $^2/_3(C_{51}H_{44}Cl_2P_4Rh_2)\cdot 4/5(CH_2Cl_2)$: M_w = 775.18 g.mol^{-1}, tetragonal, $P4_1$ (no.76) $a = b =$ 21.2680(4) Å, c = 14.3108(4) Å, V = 6473.2(3) Å^3, Z = 6, D_{Calcd} = 1.193 Mg.m^{-3}, T = 150.0(1) K, 13165 independent reflections, F^2 refinement, R_1 = 0.059, wR_2 = 0.183 for 10742 reflections with $I > 2\sigma(I)$, θ_{max} = 26.4°, 587 parameters, CCDC 1867971.

Synthesis of $[Rh_2(\mu\text{-}C)Cl_2(\mu\text{-dcpm})(PPh_3)_2]$ (2)

A mixture of $[Rh_2(\mu\text{-}C)Cl_2(PPh_3)_4]$ (100.0 mg, 0.075 mmol) and dcpm (150 mg, 0.390 mmol) was dissolved in dry DCM (10 mL). The red solution was stirred at room temperature for 24 hours. The solution was concentrated under reduced pressure and subjected to silica gel chromatography. An orange band was eluted with neat CH_2Cl_2 and an orange powder forms upon removal of solvent. Yield: 85 mg (0.032 mmol, 93% yield) of orange product. ^1H NMR (400 MHz, $CDCl_3$) δ_H = 0.73-0.77 (m, 2 H, C_6H_{11}), 0.93-0.97 (m, 2 H, C_6H_{11}), 1.07-1.11 (m, 2 H, C_6H_{11}), 1.27-1.37 (m, 12 H, C_6H_{11}), 1.41-1.51 (m, 7 H, C_6H_{11}), 1.68 (br. s, 4 H, C_6H_{11}), 1.83 (br. s, 3 H, C_6H_{11}), 1.99 (s, 4 H, C_6H_{11}), 2.25-2.32 (m, 4 H, C_6H_{11}), 2.84 (t, $^2J_{PH}$ = 12 Hz, 2H, PCH_2), 7.23 (t, J = 7.4 Hz, 12 H, C_6H_5), 7.30 (t, J = 7 Hz, 6 H, C_6H_5), 7.59-7.62 (m, 12 H, C_6H_5). $^{31}P\{^1H\}$ NMR (162 MHz, $CDCl_3$) δ_P = 21.20 (dd, $^1J_{RhP}$ = 166 Hz, $^2J_{PP}$ = 280 Hz, PPh), 45.84 (dd, $^1J_{RhP}$ = 210 Hz, $^2J_{PP}$ = 278 Hz PCy). $^{13}C\{^1H\}$ NMR (151 MHz, $CDCl_3$) δ_C = 134.9 (dd, J = 6, 6 Hz, C_6H_5) 134.4 (d, J = 11 Hz, C_6H_5), 132.2 (d, J = 10 Hz, C_6H_5), 132.1 (d, J = 10 Hz, C_6H_5), 129.6 (br. s, C_6H_5), 128.5

[xxx] Although not specifically listed for all subsequent derivatives, the fingerprint region of complexes of the form $[Rh_2L_n(\mu\text{-dppm})_2]$ typically displayed the following common absorptions: 1435, 798.

(d, J = 12 Hz, C_6H_5), 128.1 (dd, *J* = 5, 5 Hz, C_6H_5), 128.0 (d, *J* = 10 Hz, C_6H_5), 39.9 (br. d, *J* = 17 Hz, C_6H_{11}), 31.2 (br. s, C_6H_{11}), 29.6 (br. s, C_6H_{11}), 28.8 (br. s, C_6H_{11}), 3.7 (t, $^1J_{PC}$ = 22 Hz, PCH_2). IR ν_{max} (ATR, cm^{-1}): 2935, 999 (ν_{as} Rh=C=Rh). MS (ESI, *m/z*) Accurate mass: Found 1185.2667 $[M\text{-}Cl]^+$, Calcd for $C_{62}H_{76}{}^{35}ClP_4Rh_2$: 1185.2697. *Crystal data for* $C_{62}H_{76}ClP_4Rh_2$: M_w = 1221.82 $g.mol^{-1}$, triclinic, *P*-1 (No. 2), *a* = 13.3374(3), *b* = 13.9316(4), *c* = 17.0486(6) Å, *V* = 3120.37(16) $Å^3$, *Z* = 2, D_{Calcd} = 1.300 $Mg.m^{-3}$, *T* = 150.0(1) K, 20467 independent reflections, F^2 refinement, R_1 = 0.072, wR_2 = 0.202 for 15068 reflections with $I > 2\sigma(I)$, θ_{max} = 32.5°, 631 parameters.

Synthesis of $[Rh_2(\mu\text{-}C)Cl_2(\mu\text{–}dcpm)_2]$ (3)

A flask containing $[Rh_2(\mu\text{-}C)Cl_2(PPh_3)_4]$ (100.0 mg, 0.075 mmol) and dcpm (150 mg, 0.390 mmol) was charged with dry CH_2Cl_2 (20 mL). The red solution was stirred at room temperature for 24 hours. The solution was concentrated under reduced pressure, and *n*-hexane added until a red oil formed. The oil was subject to silica gel chromatography, isolating a red band with neat petrol as the eluent. The solution was concentration under vacuum, and a red oil isolated. Yield: 77 mg (0.069 mmol, 93% yield) of red oil $[Rh_2(\mu\text{-}C)Cl_2(\mu\text{-}dcpm)_2]$ (3). ^1H NMR (400 MHz, $CDCl_3$) δ_H = 3.19 (br., 4 H, PCH_2), 2.15 (t^v, *J* = 12 Hz, 8 H, C_6H_{11}), 2.02 (d, *J* = 13 Hz, 14 H, C_6H_{11}), 1.66-1.72 (m, 30 H, C_6H_{11}), 1.41 (q, *J* = 12 Hz, 8 H, C_6H_{11}), 1.15-1.27 (m, 28 H, C_6H_{11}). $^{31}P\{^1H\}$ NMR (162 MHz, $CDCl_3$) δ_P = 40.29 (dd, $^1J_{RhP}$ = 190 Hz, $^2J_{RhP}$ = 44 Hz). $^{13}C\{^1H\}$ NMR (151 MHz, $CDCl_3$) δ_C = 36.3 (s, C_6H_{11}), 34.8 (s, C_6H_{11}), 29.2 (s, C_6H_{11}), 27.0 (br. m, C_6H_{11}), 28.8 (br. s, C_6H_{11}), 3.8 (m, PCH_2). IR ν_{max} (ATR, cm^{-1}): 2940, 2936 ν_{CH}. $\nu_{Rh=C=Rh}$ obscured by aromatic overtones. MS (ESI, *m/z*) Accurate mass: Found 1110.4223 $[M+H+MeCN]^+$, Calcd for $C_{53}H_{95}{}^{35}ClNP_4Rh_2$: 1110.4214. Satisfactory elemental microanalyrtical data not acquired due to oil formation. Crystals of questionable quality for analysis grew from the crude oil at -20 °C. *Crystal data for* $2(C_{25.5}H_{46}ClP_2Rh)$: M_w = 1105.84 $g.mol^{-1}$, cubic, *Fd*-3 (No 203), *a* = 43.0368(2) Å, *V* = 79711.1(13) $Å^3$, *Z* = 48, *T* = 150.0(1) K, μ(Cu Kα) = 5.86 mm^{-1}, D_{calc} = 1.106 $Mg.m^{-3}$, 112841 reflections measured (9.0° ≤ 2Θ ≤ 133.2°), 5881 unique (R_{int} = 0.054) which were used in all calculations. The final R_1 was 0.081 ($I > 2\sigma(I)$) and wR_2 was 0.240 (all data) for 527 refined parameters with 855 restraints. It should be noted that structural data for **3** was exceptionally difficult to acquire due to poor quality crystals and is likely solved in an unideal space group.

Synthesis of [$Rh_2(\mu\text{-}C)Cl_2(\mu\text{-}dcpe)_2$] (4)

A mixture of [$Rh_2(\mu\text{-}C)Cl_2(PPh_3)_4$] (51.0 mg, 0.038 mmol) and dcpe (102 mg, 0.241 mmol) was dissolved in dry CH_2Cl_2 (10 mL). The red solution was stirred at room temperature for 24 hours. The solution was subjected to a silica column with a CH_2Cl_2 eluent, and the red band collected. An orange precipitate formed upon removal of CH_2Cl_2 under reduced pressure. The precipitate was isolated *via* vacuum filtration, washed with pentane, and dried *in vacuo*. Yield: 39 mg (0.034 mmol, 90%) of orange product. ^{1}H NMR (400 MHz, $CDCl_3$) δ: 1.22-1.36 (m, 32 H, C_6H_{11}), 1.67-1.76 (m, 16 H, C_6H_{11}), 1.82-1.88 (m, 20 H, C_6H_{11} + PC_2H_4P), 1.98 (br. s, 8 H, C_6H_{11}), 2.06 (br. m, 4 H, PC_2H_4P) ,2.17 (br. s, 8 H, C_6H_{11}), 2.49 (d, $^2J_{PH}$ = 42 Hz, 8 H, *ispso*-C_6H_{11}). ^{31}P{^{1}H} NMR (162 MHz, $CDCl_3$) δ: 32.82 (d, $^1J_{RhP}$ = 172 Hz). ^{13}C{^{1}H} NMR (151 MHz, $CDCl_3$) δ_C = 415.1 (μ-C – detected using ^{31}P-^{13}C HMQC), 36.54 (br. s, ipso-C_6H_{11}), 32.1 (s, C6H11), 31.8 (br. s, *ipso*-C_6H_{11}), 31.1 (s, C_6H_{11}), 29.2 (s, C_6H_{11}), 28.3 (s, C_6H_{11}), 27.4 (s, C_6H_{11}), 27.3 (s, C_6H_{11}), 26.9 (s, C_6H_{11}), 26.6 (s, C_6H_{11}), 13.2 (t^v, J_{CP} = 9 Hz, PCH_2). IR ν_{max} (ATR, cm^{-1}): 2920, 2848, 1447. MS (ESI, *m/z*) Accurate mass: Found 531.2281 [M – 2Cl]$^{2+}$, Calc. for $C_{53}H_{96}P_4Rh_2$: 531.2286. Anal.: Found: C, 51.93; H, 8.05%. Calc for $C_{53}H_{96}Cl_2P_4Rh_2.CH_2Cl_2$: C, 51.90; H, 7.91%. *Crystal data for* $C_{53}H_{96}Cl_2P_4Rh_2{\cdot}0.11(CH_2Cl_2)$ (M_w = 1143.31 g.mol^{-1}): triclinic, space group *P*-1 (No. 2), a = 14.9284(2), b = 21.7368(3), c = 29.6511(3) Å, α = 70.545(1)°, β = 82.086(1)°, γ = 80.039(1)°, V = 8902.3(2) Å^3, Z = 6, T = 150.0(1) K, μ(Cu Kα) = 6.66 mm^{-1}, D_{calc} = 1.280 Mg.m^{-3}, 386549 reflections measured (8.2° ≤ 2Θ ≤ 147.2°), 115705 unique (R_{int} = 0.098) which were used in all calculations. The final R_1 was 0.069 ($I > 2\sigma(I)$) and wR_2 was 0.186 (all data) for 1675 refined parameters with 3 restraints.

Synthesis of [$Rh_2(\mu\text{-}C)Cl_2(\mu\text{-}dppp)_2$] (5)

A mixture of [$Rh_2(\mu\text{-}C)Cl_2(PPh_3)_4$] (30 mg, 0.022 mmol) and dppp (69 mg, 0.17 mmol) was dissolved in dry dichloromethane (15 mL). The bright orange solution was stirred at room temperature for 24 hours and then concentrated under reduced pressure. The mixture was loaded on a silica gel chromatography column and eluted with CH_2Cl_2, and a yellow/orange band was collected. Dilution with n-hexane resulted in an orange precipitate upon removal of CH_2Cl_2 under reduced pressure. The precipitate was isolated *via* vacuum filtration, washed with n-pentane, and dried *in vacuo*. Yield: 0.020 g (0.018 mmol, 82%) of orange product [$Rh_2(\mu\text{-}C)Cl_2(\mu\text{-}dppp)_2$] (5). ^{1}H NMR (400 MHz, $CDCl_3$) δ: 1.27, 1.85 (2x br. s, 8 H, PCH_2), 4.21 (br. s, 4H, -CCH_2C-), 7.26-7.28 (m, 14 H, C_6H_5), 7.38-7.40 (m, 10 H, C_6H_5), 7.57 (t^v, J = 6 Hz, 8 H, C_6H_5), 7.74 (t^v, J = 6 Hz, 8 H,

C_6H_5). $^{31}P\{^1H\}$ NMR (162 MHz, $CDCl_3$) δ: 3.21 (dd, $^1J_{RhP}$ = 161 Hz, $^3J_{RhP}$ = 8 Hz). $^{13}C\{^1H\}$ NMR (151 MHz, $CDCl_3$) δ_C = 411.5 (μ-C , detected using ^{31}P-^{13}C HMQC), 135.4 (t^v, *J* = 6 Hz, C_6H_5), 135.0 (t^v, *J* = 21 Hz, C_6H_5), 132.6 (t^v, *J* = 6 Hz, C_6H_5), 131.0 (t^v, *J* = 22 Hz, C_6H_5), 130.2 (s, C_6H_5), 129.4 (s, C_6H_5), 128.8 (t^v, *J* = 4 Hz, C_6H_5), 128.0 (t^v, *J* = 5 Hz, C_6H_5), 23.0 (t^v, *J* = 16 Hz, P*C*H_2-), 18.3 (s, C*C*H_2C). IR ν_{max} (ATR, cm^{-1}): 3051, 2924, 1433. MS (ESI, *m/z*) Accurate mass: Found 521.0569 $[M - 2Cl]^{2+}$, Calc. for $C_{55}H_{52}P_4Rh_2$: 521.0565. Anal.: Found: C, 56.12; H, 4.54%. Calc. for $C_{55}H_{52}Cl_2P_4Rh_2.CH_2Cl_2$: C, 56.25; H, 4.82%. *Crystal data for* $0.67(C_{55}H_{52}Cl_2P_4Rh_2)\cdot 2(CH_2Cl_2)$ (M_w = 912.23 $g.mol^{-1}$): triclinic, space group *P*-1 (No. 2), *a* = 12.2332(4), *b* = 15.2365(5), *c* = 18.0549(5) Å, *α* = 86.740(2)°, *β* = 76.500(2)°, *γ* = 76.077(3)°, *V* = 3176.15(18) $Å^3$, *Z* = 3, *T* = 150.0(1) K, μ(Mo Kα) = 0.99 mm^{-1}, D_{calc} = 1.431 $Mg.m^{-3}$, 38022 reflections measured (7.6° ≤ 2Θ ≤ 57.8°), 12941 unique (R_{int} = 0.051) which were used in all calculations. The final R_1 was 0.046 ($I > 2\sigma(I)$) and wR_2 was 0.121 (all data) for 673 refined parameters with 126 restraints.

Synthesis of $[Rh_2(\mu\text{-}C)Cl_2(\mu\text{-}dppf)_2]$ (6)

A flask with $[Rh_2(\mu\text{-}C)Cl_2(PPh_3)_4]$ (77.0 mg, 0.058 mmol) and dppf (104 mg, 0.188 mmol) was charged with CH_2Cl_2 (10 mL). The bright orange solution was stirred at room temperature for 24 hours. The solution was then concentrated under reduced pressure. The orange mixture was subjected to a silica gel chromatography column eluting with neat CH_2Cl_2, and an orange band collected. Ethanol was added, and an orange precipitate formed upon removal of volatiles under reduced pressure. The precipitate was isolated *via* vacuum filtration, washed with ethanol, and dried *in vacuo*. Yield: 0.079 g (0.057 mmol, 98% yield) of the orange product $[Rh_2(\mu\text{-}C)Cl_2(\mu\text{-}dppf)_2]$ (6). ^1H NMR (400 MHz, $CDCl_3$) δ: 3.74 (br., 4 H, C_5H_4), 4.12 (s, 4 H, C_5H_4), 4.17 (s, 4 H, C_5H_4), 6.24 (br., 4 H, C_5H_4), 7.16 (br., 7 H, C_6H_5), 7.22 (t, J_{HH} = 8 Hz, C_6H_5), 7.28-7.32 (br. m, 9 H, C_6H_5), 7.45 (br. s, 8 H, C_6H_5). $^{31}P\{^1H\}$ NMR (162 MHz, $CDCl_3$) δ: 18.90 (br. d, $^1J_{RhP}$ = 191 Hz). $^{13}C\{^1H\}$ NMR (176 MHz, $CDCl_3$) δ_C =.6 (br., μ-C), 134.9 (br. m, $C^1\{C_6H_5\}$), 133.7 (t^v, J_{PC} = 5 Hz, $C^{3,5}\{C_6H_5\}$), 129.5 (s, $C^4\{C_6H_5\}$), 128.0 (t^v, J_{CP} = 5 Hz, $C^{2,6}\{C_6H_5\}$), 127.0 (t^v, J_{CP} = 4 Hz, $C^{2,6}\{C_6H_5\}$), 76.3 (t^v, J_{CP} = 23 Hz, Cα), 73.3 (s, Cβ), 70.9 (s, C_y). IR ν_{max} (ATR, cm^{-1}): 3055, 1432, 693 (ν_{FeC}). MS (ESI, *m/z*) Accurate mass: Found 663.0049 $[M–2Cl]^{2+}$, Calc. for $C_{69}H_{56}Fe_2P_4Rh_2$: 663.0071. Anal.: Found: C, 54.42; H, 3.96%. Calc. for $C_{69}H_{56}Cl_2Fe_2P_4Rh_2.2CH_2Cl_2$: C, 54.41; H, 3.86%. *Crystal data for* $C_{69}H_{56}Cl_2Fe_2P_4Rh_2\cdot 2(CH_2Cl_2)$ (M_w = 1567.29 $g.mol^{-1}$): monoclinic, $P2_1/c$, *a* = 13.1742(3), *b* = 26.8362(6), *c* = 18.2963(3) Å, β = 90.747(2)°, *V* = 6468.0(2) $Å^3$, *Z* = 4, D_{calcd} = 1.609 Mgm^{-3}, *T* =

150.0(1) K, 13206 independent reflections, F^2 refinement, R_1 = 0.048, wR_2 = 0.109 for 10044 reflections with $I > 2\sigma(I)$, θ_{max} = 26.4°, 794 parameters. CCDC 1867970.

Synthesis of $[Rh_2(\mu\text{-}C)(MeCN)_2(dppm)_2](OTf)_2$ (7)

A mixture of $[Rh_2(\mu\text{-}C)Cl_2(dppm)_2]$ (100 mg, 0.095 mmol) and AgOTf (50 mg, 0.20 mmol) were dissolved in acetonitrile (10 mL). The red solution was stirred at room temperature for two hours. Monitoring by $^{31}P\{^1H\}$ NMR spectroscopy confirmed 100% *in situ* conversion. Toluene (10 mL) was added, and the solution concentrated under reduced pressure. Red crystals of the product were isolated *via* filtration and washed with ether. Isolated yield: 13 mg (0.010 mmol, 11%) of red crystals. ^1H NMR (400 MHz, CD_3CN) δ_H = 1.93-1.95 (br.m, MeCN – exchanging with d_3-MeCN), 7.32-7.37 (m, 14 H, C_6H_5), 7.40-7.43 (m, 12 H, C_6H_5), 7.66-7.67 (br. m, 14 H, C_6H_5). $^{31}P\{^1H\}$ NMR (162 MHz, CD_3CN) δ_P = 23.83 (d, $^1J_{RhP}$ = 184 Hz). $^{13}C\{^1H\}$ NMR (101 MHz, CD_3CN) δ_C = 134.4 [br., $C^{2,6}(C_6H_5)$], 132.4 [br., $C^{3,5}(C_6H_5)$], 131.5 [m, $C^1(C_6H_5)$], 129.9 [br., $C^4(C_6H_5)$], 122.2 (q, $^1J_{CF}$ = 321 Hz, CF_3), 119.0 (CN), 19.7 (p^v, J_{PC} = 14 Hz, PCH_2), CH_3 obscured by solvent. IR ν_{max} (ATR, cm^{-1}): 2284 ν_{CN}, 1224 ν_{CF}, 1160 ν_{CF}, 1026 ν_{SO}. MS (ESI, *m/z*) Accurate mass: Found 493.0245 $[M–2MeCN]^{2+}$, Calcd for $C_{51}H_{44}P_4Rh_2$: 493.0252. Inadequate amounts of analytically pure sample could be isolated for elemental analysis. *Crystal data for* $C_{27.5}H_{25}NP_2Rh\cdot CF_3O_3S\cdot C_7H_8$ (M_w = 775.54 $g.mol^{-1}$):, monoclinic, $P2_1/c$, a = 11.7284(3), b = 23.9123(7), c = 12.0420(3) Å, b = 95.506(3)°, V = 3370.89(16) $Å^3$, Z = 4, D_{Calcd} = 1.528 $Mg.m^{-3}$, T = 150.0(1) K, 5954 independent reflections, F^2 refinement, R_1 = 0.099, wR_2 = 0.275 for 5149 reflections with $I > 2\sigma(I)$, θ_{max} = 66.6°, 423 parameters, CCDC 1880641.

Synthesis of $[Rh_2(\mu\text{-}C)(bipy)_2(PPh_3)_2][PF_6]_2$ (8)

An NMR vial containing $[Rh_2(\mu\text{-}C)Cl_2(PPh_3)_4]$ (0.015 g, 0.011 mmol) was charged with 1.0 mL of $CDCl_3$. Excess 2,2'-bipyridyl (0.010 g, 0.064 mmol) was added and the solution immediately turned red in colour. A methanol solution of $NaPF_6$ was added and the mixture left to stir for three hours. The solvents were removed under vacuum, and the red precipitate isolated *via* a CH_2Cl_2/hexane extraction, filtration, and concentration. Yield: 0.007 g (0.005 mmol, 50%). Limited spectroscopic data available presented here due to low and unreproducible yield. ^1H NMR (400 MHz, $CDCl_3$) δ_H: 6.97 (br. s, 2 H, C_6H_5), 7.44-7.48 (m, 11 H, C_6H_5), 7.53-7.57 (m, 6 H, C_6H_5),

7.64-7.69 (m, 11 H, C_6H_5), 8.01 (t, J = 8 Hz, bipy), 8.09-8.16 (2 x m, 3 H, bipy), 8.30 (d, 1 H, J = 8 Hz, bipy), 8.40 (d, 1 H, J = 8 Hz, bipy), 8.70 (br., 4 H, bipy). $^{31}P\{^1H\}$ NMR (162 MHz, $CDCl_3$) δ: 37.77 (dd, $^1J_{RhP}$ = 208 Hz, $^3J_{RhP}$ = 7 Hz), -144.3 (hept., $^1J_{PF}$ = 712 Hz, PF_6). IR (ATR, cm^{-1}) = 3053, 1564 ν_{CN}, 1432, 891 ν_{PF}. MS (ESI, *m/z*) Accurate mass: Found 527.06467 $[M]^{2+}$, Calc. for $C_{57}H_{48}N_4P_2Rh_2^{2+}$: 527.06484. Crystals suitable for analysis were grown from evaporation of a $CHCl_3$ solution. *Crystal data for* $C_{57}H_{46}N_4P_4Rh_2 \cdot 2(F_6P)$ (M_w = 1344.68 $g.mol^{-1}$): monoclinic, space group *C2/c*, *a* = 24.7593(3), *b* = 9.2408(1), *c* = 23.6559(2) Å, *β* = 90.773(1)°, *V* = 5411.88(10) $Å^3$, *Z* = 4, *T* = 150.0(1) K, μ(Cu Kα) = 6.80 mm^{-1}, D_{calc} = 1.650 $Mg.m^{-3}$, 14576 reflections measured (7.2° ≤ 2Θ ≤ 141.6°), 5132 unique (R_{int} = 0.023) which were used in all calculations. The final R_1 was 0.027 ($I > 2\sigma(I)$) and wR_2 was 0.071 (all data) for 357 refined parameters without restraints.

Synthesis of $[Rh_2(\mu_2\text{-}C)([9]aneS_3)_2(PPh_3)_2]Cl_2$ (9)

A mixture of $[Rh_2(\mu\text{-}C)Cl_2(PPh_3)_4]$ (55 mg, 0.041 mmol) and 1,4,7-trithiacyclononane (9S3: 20 mg, 0.11 mmol) was dissolved in dichloromethane (15 mL) and the resulting dark orange solution was stirred at room temperature for 2 hours. The solution was concentrated under reduced pressure and an orange product precipitated upon addition of n-hexane. The product was filtered and washed with n-hexane and dried *in vacuo*. Yield: 45 mg (0.038 mmol, 93%). ^1H NMR (400 MHz, $CDCl_3$) δ: 1.95 (br. d, $^3J_{RhH}$ = 8 Hz, 12 H, SCH_2), 3.14 (d, $^3J_{RhH}$ = 6 Hz, 12 H, SCH_2), 7.30 (t, J_{HH} = 8 Hz, 10 H, C_6H_5), 7.30 (t, J_{HH} = 8 Hz, 6 H, C_6H_5), 7.52-7.69 (m, 14 H, C_6H_5). $^{31}P\{^1H\}$ NMR (162 MHz, $CDCl_3$) δ: 37.24 (ddd, $^1J_{RhP}$ = 201 Hz, $^3J_{RhP}$ = 13 Hz, $^5J_{PP}$ = 7 Hz).$^{13}C\{^1H\}$ NMR (176 MHz, $CDCl_3$) δ: 134.7 (d, $^1J_{PC}$ = 11 Hz, C_6H_5), 132.3 (d, $^3J_{PC}$ = 10 Hz, C_6H_5), 128.7 (d, $^2J_{PC}$ = 12 Hz, C_6H_5), 128.4 (d, J_{PC} = 10 Hz, C_6H_5), 34.6 (s, SCH_2 – correlates to δ_H = 1.95 and 3.14 in ^1H-^{13}C HSQC NMR). MS (ESI, *m/z*) Accurate mass: Found = 551.0041 $[M\text{-}2Cl]^{2+}$, Calc. for $C_{49}H_{54}P_2P_2Rh_2S_6$: 551.0062. *Crystal data for* $C_{49}H_{54}P_2Rh_2S_6.2(Cl).4(CHCl_3)$ (M_w = 1651.41 $g.mol^{-1}$):, triclinic, *P*1 (No. 1), *a* = 13.6655(5), *b* = 14.1961(8), *c* = 22.9053(6) Å, *α* = 86.106(3)° *β* = 87.971(3)°, *γ* = 71.149(4)°, *V* = 4195.1(3) $Å^3$, *Z* = 2, D_{Calcd} = 1.307 $Mg.m^{-3}$, *T* = 150.0(1) K, 15559 independent reflections, F^2 refinement, R_1 = 0.081, wR_2 = 0.217 for 12704 reflections with $I > 2\sigma(I)$, θ_{max} = 70.0°, 694 parameters.

Synthesis of $[Rh_2(\mu\text{-}CS)Cl_2(\mu\text{-}dppm)_2]$ (10)

To a flask containing $[Rh_2(\mu\text{-}C)Cl_2(\mu\text{-}dppm)_2]$ (0.020 g, 0.017 mmol) in CH_2Cl_2 (20 mL), CS_2 was added (0.50 mL, 8.4 mmol). The resulting red solution was stirred for 5 hours, becoming dark green in colour. After this time the volatiles were removed *in vacuo* and the residue was subjected to column chromatography (10 x 1 cm silica gel column), eluting with neat CH_2Cl_2. A green band was collected, and the volatiles were removed under reduced pressure to give a green microcrystalline solid $[Rh_2(\mu\text{-}CS)Cl_2(\mu\text{-}dppm)_2]$ (10) (0.016 g, 0.015 mmol, 88%). ^{1}H NMR (400 MHz, $CDCl_3$, 298 K): δ_H = 3.02 (dp^v, J_{PH} = 11, J_{HH} = 4 Hz, 2 H, PCH_2), 3.58 (dt, $^2J_{PH}$ = 14, $^2J_{HH}$ = 5 Hz, 2 H, PCH_2), 7.07-7.09 (m, 8 H, C_6H_5), 7.21–7.24 (m, 4 H, C_6H_5), 7.31–7.32 (m, 12 H, C_6H_5), 7.68 (br s, 16 H, C_6H_5). ^{13}C{^{1}H} NMR (151 MHz, $CDCl_3$, 298 K): δ_C = 322.1 (tp, $^1J_{RhC}$ = 39 Hz, $^2J_{PC}$ = 7 Hz, μ_2-CS), 136.1 (s, C_6H_5), 134.1 (p^v, J_{PC} = 14 Hz, C_6H_5), 132.5 (br., C_6H_5), 130.6 (s, C_6H_5), 130.0 (p^v, J_{PC} = 12 Hz, C_6H_5), 129.9 (br., C_6H_5), 128.2 (br., C_6H_5), 128.1 (br., C_6H_5), 27.4 (p^v, J_{CP} = 10 Hz, PCH_2). ^{31}P{^{1}H} NMR (162 MHz, $CDCl_3$, 298 K): δ_P = 17.2 (d, $^1J_{RhP}$ = 118 Hz). IR ν_{max} (ATR, cm^{-1}): 1093 s ν_{CS}. MS (ESI, *m/z*) Accurate mass: Found 1052.9895 $[M–Cl]^+$. Calcd for $C_{51}H_{44}{}^{35}ClP_4Rh_2S$ $[M–Cl]^+$: 1052.9913. Anal. Found: C, 52.86; H, 3.79%. Calcd for $C_{51}H_{44}Cl_2P_4Rh_2.CH_2Cl_2$: C, 53.18; H, 3.95%. A crystal of a toluene solvate suitable for structure determination was grown by slow evaporation of CH_2Cl_2 from a CH_2Cl_2/toluene solution. *Crystal data for* $2(C_{51}H_{44}Cl_2P_4Rh_2S)\cdot 2.5(C_7H_8)$ (M_w = 2409.37 g.mol^{-1}): triclinic, space group *P*-1 (No. 2), *a* = 16.3139(3), *b* = 19.5375(3), *c* = 22.4893(4) Å, α = 71.332(2)°, β = 72.996(2)°, γ = 79.948(2)°, *V* = 6468.1(2) Å^3, *Z* = 2, *T* = 150.0(1) K, μ(Cu Kα) = 22.258 mm^{-1}, D_{calc} = 1.237 Mg.m^{-3}, 25086 reflections measured (7.2° ≤ 2Θ ≤ 141.6°), 19891 unique (R_{int} = 0.067) which were used in all calculations. The final R_1 was 0.073 ($I > 2\sigma(I)$) and wR_2 was 0.225 (all data) for 1235 refined parameters with 263 restraints. CCDC 2013308.

Synthesis of $[Rh_2(\mu\text{-}CSe)Cl_2(\mu\text{-}dppm)_2]$ (11)

To a flask containing $[Rh_2(\mu\text{-}C)Cl_2(\mu\text{-}dppm)_2]$ (0.050 g, 0.047 mmol) in CH_2Cl_2 (50 mL), excess grey selenium was added (0.014 g, 0.173 mg.atom). The resulting red/black suspension was stirred for 15 hours, during which time the supernatant became dark green in colour. After this time volatiles were removed *in vacuo* and the residue was subjected to column chromatography (10 x 1 cm silica gel column), eluting with neat CH_2Cl_2. A green band was collected, and the volatiles were removed under reduced pressure to give a green microcrystalline solid $[Rh_2(\mu\text{-}CSe)Cl_2(\mu\text{-}$

dppm)$_2$] (0.028 g, 0.025 mmol, 52%). ^{1}H NMR (400 MHz, $CDCl_3$, 298 K): δ_H = 2.96 (br. d, J = 14 Hz, 2 H, PCH_2), 3.68 (dt, J = 14, 4 Hz, 2 H, PCH_2), 7.04-7.08 (m, 7 H, C_6H_5), 7.15–7.23 (m, 5 H, C_6H_5), 7.31–7.33 (m, 12 H, C_6H_5), 7.66-7.71 (m, 16 H, C_6H_5). ^{13}C{^{1}H} NMR (151 MHz, $CDCl_3$, 298 K): δ_C = 341.3 (br. m, μ_2-CSe), 136.1 (t^v, J_{PC} = 5 Hz, C_6H_5), 133.9 (t^v, J_{PC} = 15 Hz, C_6H_5), 132.5 (t^v, J_{PC} = 3 Hz, C_6H_5), 130.6 (s, C_6H_5), 129.9 (s, C_6H_5), 129.8 (t^v, J_{PC} = 12 Hz, C_6H_5), 128.2 (t^v, J_{PC} = 3 Hz, C_6H_5), 128.1 (t^v, J_{PC} = 3 Hz, C_6H_5), 26.3 (p^v, $^1J_{CP}$ = 11 Hz, PCH_2). ^{31}P{^{1}H} NMR (162 MHz, $CDCl_3$, 298 K): δ_P = 14.7 (d, $^1J_{RhP}$ = 119 Hz). ^{77}Se{^{1}H} NMR (134 MHz, $CDCl_3$, 298 K) δ_{Se} = 1116.2 (br.). IR ν_{max} (ATR, cm^{-1}): 957 s ν_{CSe}. MS (ESI, *m/z*) Accurate mass: Found 1100.9379 [M–Cl]$^+$. Calcd for $C_{51}H_{44}{}^{35}ClP_4Rh_2{}^{80}Se$ [M–Cl]$^+$: 1100.9360. A crystal of a toluene solvate suitable for structure determination was grown by slow evaporation of CH_2Cl_2 from a toluene solution. *Crystal data for* $2(C_{51}H_{44}Cl_2P_4Rh_2Se)\cdot 3(C_7H_8)$ (M_w = 2549.24 g.mol^{-1}): triclinic, space group *P*-1 (No. 2), a = 16.2884(4), b = 20.0388(5), c = 22.3244(6) Å, α = 70.671(2)°, β = 75.071(2)°, γ = 80.200(2)°, V = 6615.0(3) Å^3, Z = 2, T = 150.0(1) K, μ(Cu Kα) = 22.258 mm^{-1}, D_{calc} = 1.280 Mg.m^{-3}, 38393 reflections measured (7.0° ≤ 2Θ ≤ 141.8°), 18074 unique (R_{int} = 0.036) which were used in all calculations. The final R_1 was 0.083 ($I > 2\sigma(I)$) and wR_2 was 0.260 (all data) for 1201 refined parameters with 459 restraints. CCDC 2013309.

Generation of [Rh$_2$(μ$_2$-CS)(μ$_2$H)Cl$_2$(FBF$_3$)(μ-dppm)$_2$] (12)

To an NMR vial containing [Rh$_2$(μ-CS)Cl$_2$(μ-dppm)$_2$] (0.010 g, 0.009 mmol) was added CD_2Cl_2 (1.0 mL). To this dark green solution was added HBF_4 (1.0 M in ether, 0.01 mL, 0.01 mmol) upon which the solution immediately turned yellow in colour. The solution was stored in the NMR vial to avoid decomposition. ^{1}H NMR (800 MHz, CD_2Cl_2, 298 K): δ_H = -15.48 (tp, $^1J_{RhH}$ = 30 Hz, $^2J_{PH}$ = 8 Hz, 1 H, μ-H), 3.23 (br. d, $^2J_{HH}$ = 15 Hz, 2 H, PCH_2), 3.51 (dp^v, $^2J_{HH}$ = 15 Hz, J_{PH} = 5 Hz, 2 H, PCH_2), 7.27 (t, J = 8 Hz, 8 H, dppm C_6H_5), 7.44 (q, J = 7 Hz, 12 H, dppm C_6H_5), 7.50-7.55 (m, 20 H, dppm C_6H_5). ^{13}C{^{1}H} NMR (151 MHz, CD_2Cl_2, 298 K): δ_C = 300.0 (μ-CS), 135.0, 132.8, 132.0, 129.3, 128.8, 128.7, 125.5, 125.4 (C_6H_5), 25.9 (PCH_2). The ^{13}C resonances were detected using ^{1}H-^{13}C HSQC/HMBC to avoid decomposition timeframes, couplings unavailable. ^{19}F{^{1}H} NMR (376 MHz, $CDCl_3$, 298 K): δ_F = -147.75 (^{10}BF), -148.65 (^{11}BF), -149.74 ($^{11}BF_3$), -150.17 ($^{10}BF_3$). ^{31}P{^{1}H} NMR (162 MHz, CD_2Cl_2, 298 K): δ_P = 25.3 (d, $^1J_{RhP}$ = 96 Hz). IR, ESI-MS and X-ray diffraction data unavailable due to complex stability.

Synthesis of $[Rh_2(\mu_2\text{-}CS)(\mu_2\text{-}Cl)Cl_2(\mu\text{-}dppm)_2]BF_4$ (13)

A CH_2Cl_2 solution of $[Rh_2(\mu\text{-}CS)(\mu\text{-}H)Cl_2(FBF_3)(dppm)_2]$ (*ca.* 0.011 g, 0.009 mmol) prepared as described above was subjected to silica gel chromatography. A 1:19 THF:CH_2Cl_2 mixture eluted a dark yellow band, which produced a dark yellow powder upon addition of ether. The powder was filtered and washed with ether. Drying *in vacuo* gave a yellow/orange powder of pure $[Rh_2(\mu_2\text{-}CS)(\mu_2\text{-}Cl)Cl_2(\mu\text{-}dppm)_2]BF_4$ (13) (0.006 g, 0.005 mmol, 60%). ^{1}H NMR (800 MHz, $CDCl_3$, 298 K): δ_H = 3.32, 4.32 (2x m, 4 H, PCH_2), 7.06 (m, 8 H, C_6H_5), 7.16 (m, 6 H, C_6H_5), 7.34 (m, 10 H, C_6H_5), 7.50 (m, 8 H, C_6H_5), 7.77 (m, 8 H, C_6H_5). ^{13}C{^{1}H} NMR (201 MHz, $CDCl_3$, 298 K): δ_C = 135.4 (t^v, J_{PC} = 4 Hz, C_6H_5), 132.4 (t^v, J_{PC} = 4 Hz, C_6H_5), 132.0 (s, C_6H_5), 129.6 (s, C_6H_5), 128.6 (s, C_6H_5), 128.5 (br. s, C_6H_5). ^{31}P{^{1}H} NMR (283 MHz, $CDCl_3$, 298 K): δ_P = 7.09 (d, $^1J_{RhP}$ = 133 Hz). ^{11}B{^{1}H} NMR (225 MHz, $CDCl_3$, 298 K): δ_B = -0.85 (br. s). ^{19}F{^{1}H} NMR (376 MHz, $CDCl_3$, 298 K): δ_F = -150.97 (br. s). IR ν_{max} (ATR, cm^{-1}): 1102s ν_{CS}, 1055s ν_{BF}. MS (ESI, *m/z*) Accurate mass: Found 1122.9277. Calcd for $C_{51}H_{44}{}^{35}Cl_3P_4Rh_2S^+$ $[M]^+$: 1122.9290. A crystal suitable for structure determination was grown by slow evaporation of a CH_2Cl_2/toluene mixture. *Crystal data for* $C_{51}H_{44}Cl_3P_4Rh_2S.BF_4.2(C_7H_8)$ (M_w = 1396.05 gmol^{-1}): triclinic, space group *P*1, *a* = 12.1438(10), *b* = 14.2658(13), *c* = 19.1968(17) Å, α = 91.861(7), β = 92.063(7)°, γ = 107.991(8)°, *V* = 3157.7(5) Å^3, *Z* = 2, *T* = 150.0(1) K, μ(MoKα) = 0.84 mm^{-1}, D_{calc} = 1.468 Mg.m^{-3}, 34471 reflections measured (7.4° ≤ 2Θ ≤ 48.8°), 13415 unique (R_{int} = 0.081) which were used in all calculations. The final R_1 was 0.066 ($I > 2\sigma(I)$) and wR_2 was 0.134 (all data) for 728 refined parameters with 96 restraints.

Generation of $[Rh_2(\mu_2\text{-}CSe)(\mu_2\text{-}H)Cl_2(FBF_3)(\mu\text{-}dppm)_2]$ (14)

To an NMR vial containing $[Rh_2(\mu\text{-}CSe)Cl_2(dppm)_2]$ (0.005 g, 0.004 mmol) was added CD_2Cl_2 (1 mL). To this dark green solution was added HBF_4 (1.0 M in ether, 0.01 mL, 0.01 mmol). The resulting green solution immediately turned pink in colour. The solution was stored in the NMR vial with excess HBF_4 to avoid decomposition. ^{1}H NMR (800 MHz, CD_2Cl_2, 298 K): δ_H = -15.11 (tp, $^1J_{RhH}$ = 30 Hz, $^2J_{PH}$ = 7.7 Hz, 1 H, μ-H), 3.17 (br. d, $^2J_{HH}$ = 15 Hz, 2 H, PCH_2), 3.58 (dp^v, $^2J_{HH}$ = 15 Hz, J_{PH} = 5 Hz, 2 H, PCH_2), 7.25 (t, *J* = 8 Hz, 8 H, C_6H_5), 7.40-7.43 (m, 12 H, C_6H_5), 7.48-7.56 (m, 20 H, C_6H_5). ^{13}C{^{1}H} NMR (151 MHz, CD_2Cl_2, 298 K): δ_C = 317.0 (μ-CSe – from HMBC coupling with μ-H), 135.6, 133.9, 132.8, 131.7, 131.0, 130.9, 128.2, 127.8 (C_6H_5), 25.8 (PCH_2). The ^{13}C resonances were detected using ^{1}H-^{13}C HMBC and HSQC spectroscopies to avoid

decomposition timeframes, couplings unavailable. $^{19}F\{^{1}H\}$ NMR (376 MHz, CD_2Cl_2, 298 K): δ_F = -147.51 (^{10}BF), -150.17 ($^{11}BF_3$), 153.41 ($^{10}BF_3$). $^{31}P\{^{1}H\}$ NMR (162 MHz, CD_2Cl_2, 298 K): δ_P = 20.8 (d, $^{1}J_{RhP}$ = 95 Hz). IR, ESI-MS and X-ray diffraction data unavailable due to complex stability.

Synthesis of $[Rh_2(\mu_2\text{-}CSe)(\mu_2\text{-}Cl)Cl_2(\mu\text{-}dppm)_2]BF_4$ (15)

A CH_2Cl_2 solution of $[Rh_2(\mu\text{-}CSe)(\mu\text{-}H)Cl_2(FBF_3)(dppm)_2]$ (*ca.* 0.010 g, 0.008 mmol) prepared as described above was subjected to silica gel chromatography. A 1:19 THF:CH_2Cl_2 mixture eluted a dark yellow band, which produced a dark pink powder upon addition of ether. The powder was filtered and washed with ether. Drying *in vacuo* gave a dark pink residue of $[Rh_2(\mu_2\text{-}CSe)(\mu_2\text{-}Cl)Cl_2(\mu\text{-}dppm)_2]BF_4$ (0.004 g, 0.004 mmol, 41%). ^{1}H NMR (400 MHz, $CDCl_3$, 298 K): δ_H = 4.15-4.22 (m, 2 H, PCH_2), 7.01-7.23 (m, 10 H, dppm C_6H_5), 7.33-7.65 (m, 24 H, C_6H_5), 7.85-7.91 (m, 6 H, C_6H_5). $^{31}P\{^{1}H\}$ NMR (162 MHz, $CDCl_3$, 298 K): δ_P = 9.94 (d, $^{1}J_{RhP}$ = 95 Hz). $^{19}F\{^{1}H\}$ NMR (376 MHz, $CDCl_3$, 298 K): δ_F = -150.96 (br.). IR ν_{max} (ATR, cm^{-1}): 1057s ν_{BF}. MS (ESI, *m/z*) Accurate mass: Found *m/z* = 1170.8734. Calcd for $C_{51}H_{44}{}^{35}Cl_3P_4Rh_2{}^{80}Se^+$ $[M]^+$: 1170.8734. Insufficient material could be isolated to obtain accurate ^{13}C NMR data and elemental analysis.

Synthesis of $[Rh_2(\mu_2\text{-}CSeCH_3)Cl_2(\mu\text{-}dppm)_2](OTf)$ (16)

To a dark green dichloromethane solution (20 mL) containing $[Rh_2(\mu\text{-}CSe)Cl_2(\mu\text{-}dppm)_2]$ (0.021 g, 0.018 mmol) was added MeOTf (1.0 M in ether, 0.01 mL, 0.10 mmol). The resulting green solution immediately darkened. Subjecting the solution to silica gel chromatography eluted a dark red band using a 1:19 mixture of THF in CH_2Cl_2. Addition of petrol and removal of solvent under vacuum produced a purple product of pure $[Rh_2(\mu_2\text{-}CSeCH_3)Cl_2(\mu\text{-}dppm)_2](OTf)$ (16) (15 mg, 0.012 mmol, 63%). ^{1}H NMR (800 MHz, CD_2Cl_2, 298 K): δ_H = 2.78 (s, 3 H, SeCH_3), 3.12-3.16 (m, 2 H, PCH_2-), 3.64 (dp^v, $^{2}J_{HH}$ = 14 Hz, J_{PH} = 5 Hz, 2 H, PCH_2), 7.13 (t, J = 8 Hz, 8 H, C_6H_5), 7.33 (t, J = 8 Hz, 4 H, C_6H_5), 7.42 (br. s, 12 H, C_6H_5), 7.54 (br. s, 8 H, C_6H_5), 7.67 (br. s, 8 H, C_6H_5). $^{13}C\{^{1}H\}$ NMR (151 MHz, CD_2Cl_2, 298 K): δ_C = 356.3 (μ-CSe – from HMBC), 136.3 (t^v, J_{PC} = 6 Hz, C_6H_5), 135.6 (br. m, C_6H_5), 132.4 (br. s, C_6H_5), 131.7 (s, C_6H_5), 131.2 (s, C_6H_5), 128.9 (s, C_6H_5), 128.6 (s, C_6H_5), 125.6 (s, C_6H_5), 25.4 ($SeCH_3$), 25.2 (p^v, J_{PC} = 12 Hz, PCH_2). $^{19}F\{^{1}H\}$ NMR (376 MHz, CD_2Cl_2, 298 K): δ_F = -78.9. $^{31}P\{^{1}H\}$ NMR (162 MHz, CD_2Cl_2, 298 K): δ_P = 16.0 (br.

d, $^{1}J_{RhP}$ = 94 Hz). IR ν_{max} (ATR, cm^{-1}): 1250br, s ν_{SO}, 1222s ν_{CF}. MS (ESI, *m/z*) Accurate mass: Found 1150.9287. Calcd for $C_{52}H_{47}{}^{35}Cl_2P_4Rh_2Se$ $[M]^+$: 1150.9282.

Synthesis of $[Rh_2(\mu_2\text{-}CSeAuCl)Cl_2(\mu\text{-}dppm)_2]$ (17)

To a dark green dichloromethane solution containing $[Rh_2(\mu\text{-}CSe)Cl_2(dppm)_2]$ (0.025 g, 0.022 mmol) was added $[AuCl(SMe_2)]$ (0.009 g, 0.30 mmol). The resulting green solution immediately turned yellow. Subjecting the solution to silica gel chromatography, a yellow band was eluted with a 1:19 mixture of THF and CH_2Cl_2. Addition of petrol and removal of solvent under vacuum produced a light-yellow powder of pure $[Rh_2(\mu_2\text{-}CSeAuCl)Cl_2(\mu\text{-}dppm)_2]$ (23 mg, 0.017 mmol, 76%). ^{1}H NMR (800 MHz, CD_2Cl_2, 298 K): δ_H = 2.90 (d, $^{2}J_{HH}$ = 14 Hz, 2 H, PCH_2), 4.30 (dp^v, $^{2}J_{HH}$ = 14 Hz, J_{PH} = 5 Hz, 2 H, PCH_2), 6.96-7.06 (m, 5 H, C_6H_5), 7.10-7.18 (m, 5 H, C_6H_5), 7.33-7.44 (m, 12 H, C_6H_5), 7.50-7.53 (m, 4 H, C_6H_5), 7.60-7.69 (m, 10 H, C_6H_5), 7.80-7.85 (m , 4 H, C_6H_5). $^{13}C\{^{1}H\}$ NMR (201 MHz, CD_2Cl_2, 298 K): δ_C = 136.4, 132.6, 132.2 131.0, 130.8, 130.4, 129.3, 128.2, 127.9, 127.8, 127.6, 124.8, 124.2 (C_6H_5), 23.4 (PCH_2). ^{13}C resonances identified though ^{1}H-^{13}C HSCQ/HMBC studies due to solubility issues, couplings unavailable. $^{31}P\{^{1}H\}$ NMR (162 MHz, CD_2Cl_2, 298 K): δ_P = 0.57 (ddd, $^{1}J_{RhP}$ = 152 Hz, $^{3}J_{RhP}$ = 13 Hz, $^{2}J_{PP}$ = 9 Hz), -0.04 (ddd, $^{1}J_{RhP}$ = 160 Hz, $^{3}J_{RhP}$ = 13 Hz, $^{2}J_{PP}$ = 9 Hz). IR ν_{max} (ATR, cm^{-1}): 3052 ν_{CH}, 1435 ν_{CC}. MS (ESI, *m/z*) Accurate mass: Found 1367.8394. Calcd for $C_{51}H_{44}Au^{35}Cl_2P_4Rh_2Se$ $[M\text{-}Cl]^+$: 1367.8400.

EPISODE TWO – ATTACK OF THE CARBYNES

SYNTHESIS AND REACTIVITY OF THE FIRST STRUCTURALLY CHARACTERISED μ_2-HALOCARBYNE COMPLEXES

2.1 PREFACE

Abstract taken from H. J. Barnett, A. F. Hill, *Chem. Commun.,* **2019**, 55, 1734.

The reaction of **[$Rh_2(\mu\text{-}C)Cl_2(PPh_3)_4$]** with bis(diphenylphosphino)methane (dppm) affords the A-frame μ-carbido complex **[$Rh_2(\mu\text{-}C)Cl_2(\mu\text{-}dppm)_2$]**, halide metathesis of which provides **[$Rh_2(\mu\text{-}C)Br_2(\mu\text{-}dppm)_2$]**. The reactions of the former with $PhICl_2$ or the latter with [pyH][Br_3] provide rare examples of μ_2-halocarbyne ligands in the complexes **[$Rh_2(\mu\text{-}CX)(m\text{-}X)X_4(\mu\text{-}dppm)_2$]** (X = Cl, Br).

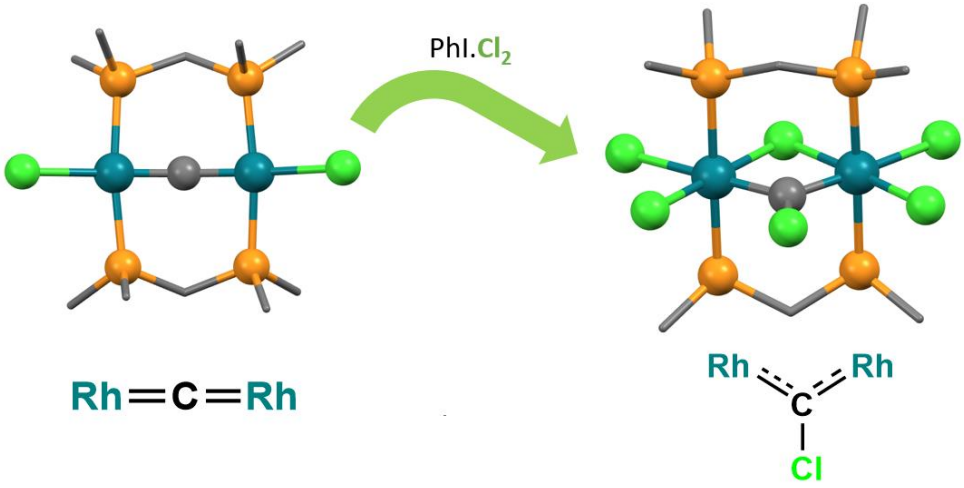

Figure 2.0: Simplified transformation from μ-carbido to μ_2-halocarbyne ligand

2.2 INTRODUCTION

2.2.1 The Carbyne Ligand

The carbyne ligand, formally (IUPAC) known as a metal alkylidyne, consists simply of a metal-carbon triple bond. In a similar fashion to other ligands which form multiple bonds to transition metals, the triple bond may be viewed as comprising a σ bond from the HOMO of the carbon atom donating to the metal, and in this case, two π bonds from occupied d-orbitals on the metal undergoing retrodonation to the unoccupied *p*-orbitals on the *sp* hybridised carbon atom, giving the carbyne ligand both σ-donor and π-acceptor characteristics.[xxxi]

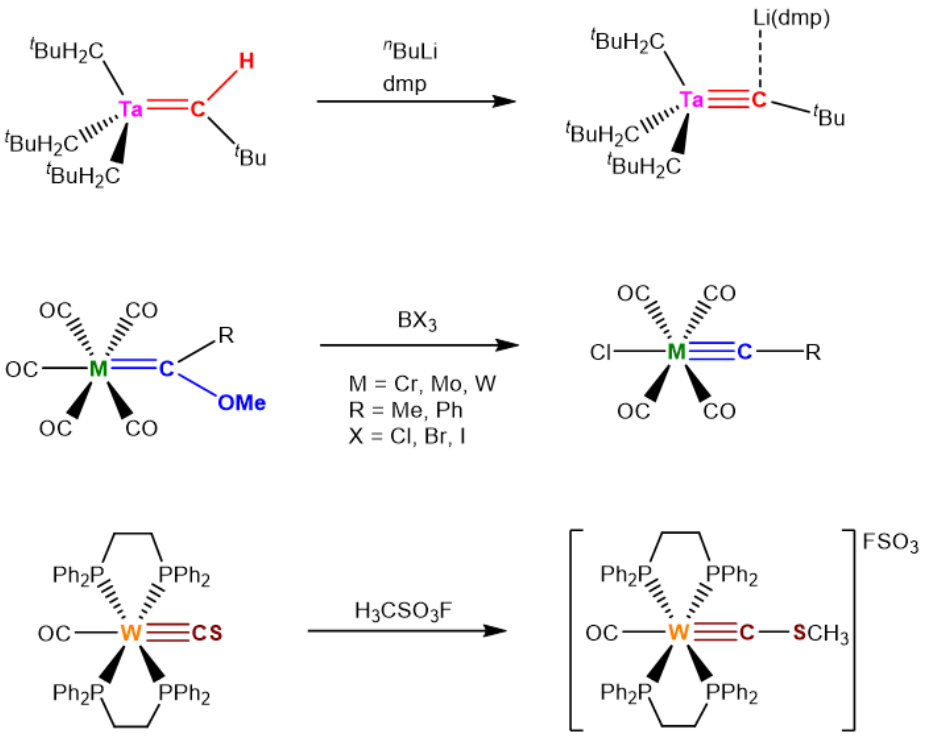

Scheme 2.1: Synthesis of a Schrock, Fischer and Angelici metal carbyne complex[102]

[xxxi] This perspective arbitrarily deconstructs the M≡C bond by considering the carbyne as a cationic fragment (*i.e.*, $[CR]^+/[M]^-$) with an occupied sp_z orbital (σ-donor) and empty p_x/p_y (π-acceptor) orbitals to emphasise the isoelectronic relationship between CO, $[CF]^+$ and $[NO]^+$. Alternative ways of conceptually partitioning charges between hypothetical constituent fragments (*e.g.*, sp^3-$[CR]^{3-}/[M]^{3+}$) also have their advocates. Both formalisms are widely employed in the literature, the only caveat arising when, artificial by nature, metal oxidation states are assigned. Group 9 carbyne complexes are exceedingly rare but the few examples illustrate this dichotomy *e.g.*, **$[Ir(\equiv CPh)(PMe_3)(\eta\text{-}C_5Me_5)]^+$** and **$[Rh(\equiv CF)\{N(C_6H_3MeP^iPr_2\text{-}2)_2\}]^+$** may be designated as involving metals in the +I or +V oxidation states.[101]

Since the synthesis of the first carbyne complexes by Fischer and two years later by Angelici and Schrock (**Scheme 2.1**),[102] the field of carbyne chemistry has flourished. This has been aided by the discovery that transition metal alkylidyne complexes can be useful catalysts for alkyne metathesis reactions, the same way metal alkylidene complexes are for alkene metathesis.[103]

The Fisher and Schrock Carbynes

As was the case initially with carbene chemistry, carbyne chemistry[xxxii] was pioneered by groups led by Fischer and Schrock based on different metal centres with disparate ancillary ligands resulting in contrasting electronic features for the metal centres. In retrospect, it is perhaps not surprising that dichotomous reactivity patterns emerged on such distinct platforms, however at the time carbynes came to be viewed as belonging to either the Fisher- or Schrock-type categories. Thus, although both types of carbynes contain the same metal-carbon triple bond, the electronic requirements of the metal centres vastly differ, and this has a significant impact on the reactivity and stability of the carbyne complex and ligand in particular.

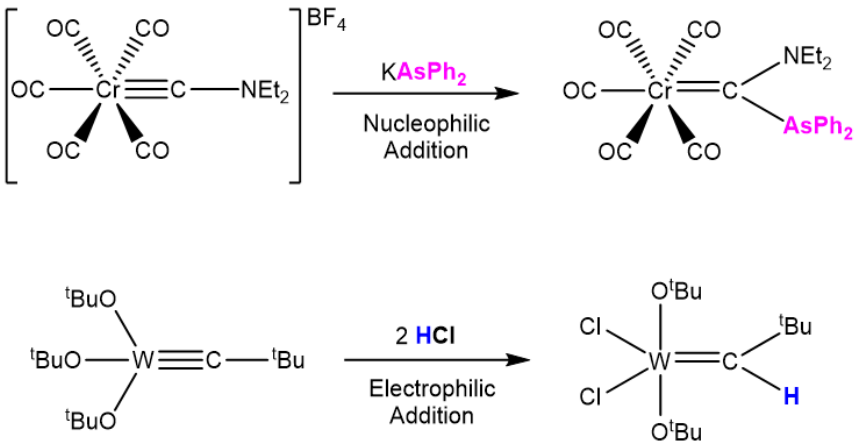

Scheme 2.2: Electrophilic and Nucleophilic behaviour of Fischer and Schrock carbynes, respectively[104]

[xxxii] The terms carbene/carbyne and alkylidene/alkylidyne are all used throughout the literature, often interchangeably. Whilst the former calls to mind an analogy between the ligand and free molecules, the latter (recommended by IUPAC) emphasises the group as a covalently bound metal substituent.

Fisher carbyne complexes, like the archetype presented in **Scheme 2.1** above, consist of low-oxidation state, mid to late transition metals that are relatively electron rich (*i.e.*, higher d-occupancies) and co-ordinately saturated.[105] Accompanying the carbyne ligand are typically π-acceptor ligands, such as carbonyl ligands. The strong π-acidic co-ligands reduce electron density around the carbyne carbon, causing it to exhibit electrophilic behaviour.

The Schrock carbynes are diametrically opposite. Schrock carbynes typically utilise earlier, co-ordinately unsaturated transition metals in high oxidation states and are typically (increasingly) supported by strong electron donating ligands, which are often anionic with π-dative capacity (alkoxide, amido) to ameliorate the high oxidation state (low d-occupancy) of the metal. Often being the lone π-acceptor ligand, the carbyne sequesters electron density and displays nucleophilic character at the carbon atom. The nucleophilic attack, either from the Schrock carbyne or to the Fisher carbyne, ultimately results in reforming a carbene complex (**Scheme 2.2**).

This tidy picture, arising historically from studies of extreme classes, eventually gave way to a unified view of a spectrum of reactivity for which Fischer and Schrock types provided the extremes. This followed the emergence of intermediate counter examples, *e.g.*, the low-valent, coordinatively saturated and nucleophilic carbyne **[Os(≡CC$_6$H$_4$Me-4)Cl(CO)(PPh$_3$)$_2$]**[106] *cf.* the high-oxidation state complex **[Os(≡CC$_6$H$_4$NMe$_2$-4)Cl$_2$(OH$_2$)(PPh$_3$)$_2$]$^+$** which reacts with nucleophiles at the carbyne carbon.[107] The position a carbyne assumes along this continuum therefore reflects a combination of factors that impact upon the energy match between the metal and carbyne orbitals.

Functionalising the Carbyne Ligand

As with any carbon-based moiety, functionalisation becomes a key area of synthetic work. For terminal carbyne species [M]≡C–R specifically, the early work of Fisher and Schrock employed fairly tame hydrocarbyl carbyne substituents (R = aryl, alkyl[xxxiii]) which leave significant room for development.

Recent developments have ensured that functionalised carbynes exist that include substituents based on almost all the *p*-block elements. Excluding hydrocarbyl carbynes, some 200 carbyne ligands bearing heteroatomic substituents have been structurally characterised.[108] By far

[xxxiii] Early α-hydride elimination/abstraction approaches were attended by additional restrictions on the choice of alkyl substituent (R) to obviate more facile β-hydride elimination processes.

the largest subset is that of the amino carbynes, which account for around 25% of the characterised structures, but notable examples also include Group 14 carbynes,[109] phosphinocarbynes,[110] and the family of chalcolatocarbyne ligands.[111] Amongst this latter class, the alkoxycarbynes $L_nM{\equiv}COR$ have, following early studies by Lippard,[112] attracted particular attention in part because of the relevance they have to understanding the value-added reductive activation of diatomic molecules such as CO and, by analogy, iso-electronic N_2. A welcome corollary of more recent studies by Peters is that they have afforded carbyne complexes of metals (iron, cobalt) for which conventional carbynes have yet to be established.[113] Each of these unique functionalised carbynes bring with it new vistas of uncharted reactivity and untapped potential to carbyne chemistry.

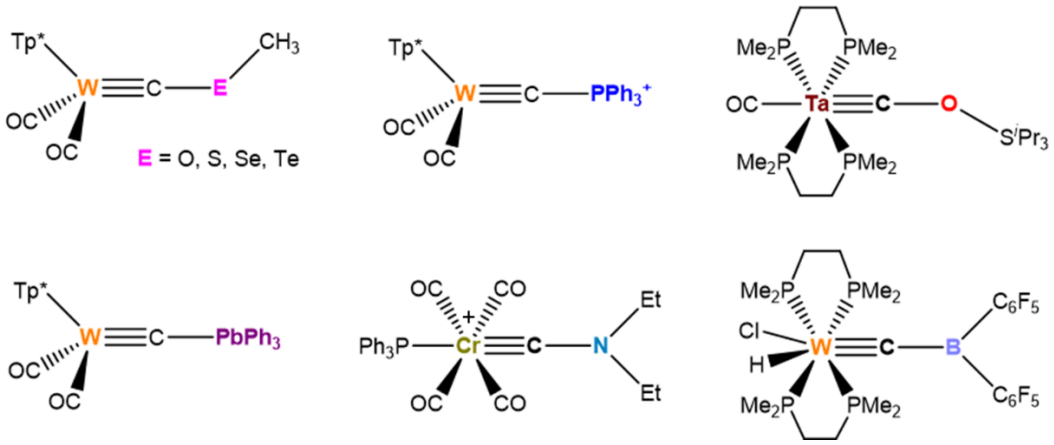

Figure 2.2: Examples of main-group functionalised carbyne ligands[114]

The ongoing issue that has plagued the development of functionalised carbyne ligands is the lack of available and generalisable synthetic routes. Because complexes of the terminal carbido ligand, M≡C: , are with a few exceptions (namely **[Ru(≡C)Cl$_2$(PCy$_3$)$_2$]**, **[Os(≡C)Cl$_2$(PCy$_3$)$_2$]**, and **K[Mo(≡C){N^{t}Bu(C$_6$H$_3$Me$_2$-3,5)}$_3$]**)[115] unstable and non-isolable, the pathways taken to install diversity at the carbyne ligand are arduous and specific to the complex. The need to incorporate the carbyne substituent early in a synthetic sequence leaves it vulnerable to conditions or reagents required in later steps. However, that problem has been largely overcome with the development of halocarbyne ligands.

2.2.2 Halocarbynes

Arguably the most useful functionalisation of the carbyne ligand would be the incorporation of a halogen to form halocarbynes. These, however, remain relatively scarce, as they are not synthetically viable products *via* the classical Fischer or Schrock carbyne protocols. Fisher's early synthesis of the carbyne ligand came from attempts to create a chlorocarbene using BCl_3, however, the halides did not coordinate to the carbene but instead at the metal centre (see **Scheme 2.1**).[xxxiv]

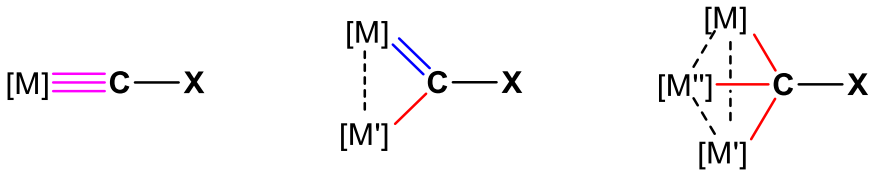

Figure 2.3: (left to right) the possible coordination modes of the halocarbyne ligand; linear terminal coordination, μ (otherwise denoted μ_2), and μ_3 bridging coordination

Halocarbyne ligands, like carbynes in general, may be divided into three classifications which are dependent on the bonding mode of the carbyne carbon. All bonding forms exhibit three metal-carbon interactions; however, the number of metal nuclei involved may vary from one to three (**Figure 2.3**).

Trinuclear halocarbynes have a long history beginning with **$[Co_3(\mu_3\text{-}CX)(CO)_9]$** (X = Cl, Br), predating terminal halocarbynes by some two decades. Prior to the commencement of this body of work, there were 29 structurally characterised μ_3-halocarbynes (containing F, Cl and Br but lacking I), 18 examples of terminal halocarbynes, and most importantly, and no structurally characterised examples of μ_2-halocarbyne complexes.

Terminal Halocarbynes

The field of terminal halocarbyne chemistry began in 1983 with Lalor's synthesis of the first halocarbyne complexes, **$[M(\equiv CCl)(CO)_2(Tp^*)]$** (M = Mo, W) (**Scheme 2.3**). [117] It had been previously discovered that an unusual redox reaction of the carbonyl metallate **$[M(CO)_3(Tp^*)]^-$**

[xxxiv] Fischer and Lappert did go on to make halocarbene complexes, e.g., **$[Cr\{=CCl(NMe_2)(CO)_5]$** [116]

with aryl diazonium salts ([ArNN]BF_4) form novel complexes featuring an η^2-COAr ligand.[118] When this reaction was performed in CH_2Cl_2, the outer-sphere electron transfer process produced instead the chlorocarbyne complex as the major product.

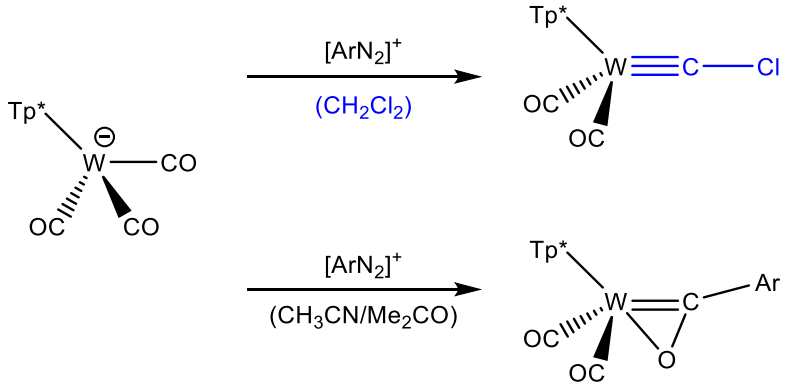

Scheme 2.3: Lalor's initial chlorocarbyne synthesis and η^2-aroyl formation (M = Mo, W)

The rather specific synthetic pathway relies heavily on the sterically encumbering Tp* co-ligand, which prevents direct nucleophile-electrophile coupling in favour of outer-sphere electron transfer and fails for smaller co-ligands such as cyclopentadienyl or even tris(pyrazolyl)borate (Tp). The terminal halocarbyne has assumed impressive synthetic importance due to its rather versatile reactivity. The similarly obtained tungsten bromocarbyne complex **[W(≡CBr)(CO)$_2$(Tp*)]** through combination of the polarity of the $^{\delta+}$C–Br$^{\delta-}$ bond and the nucleofugacity of the bromine atom, makes the bromocarbyne susceptible to nucleophilic substitution, easily furnishing a range of nucleophile functionalised carbyne complexes.

What makes this tungsten bromocarbyne complex so versatile is that the polarity of the carbyne can be switched (**Scheme 2.4**) via lithium-halogen exchange to generate *in-situ* a lithiocarbyne species.[xxxv] The resulting *nucleophilic* lithiocarbyne species is prone to reactions with a diverse range to electrophiles.[120] The bromocarbyne complex and its molybdenum analogue effectively unlocked much organometallic chemistry that was previously inaccessible

[xxxv] This species, and preliminary demonstrations of its synthetic versatility, were previously described by Templeton, arising less conveniently *via* a multi-step procedure involving thermolabile intermediates.[119]

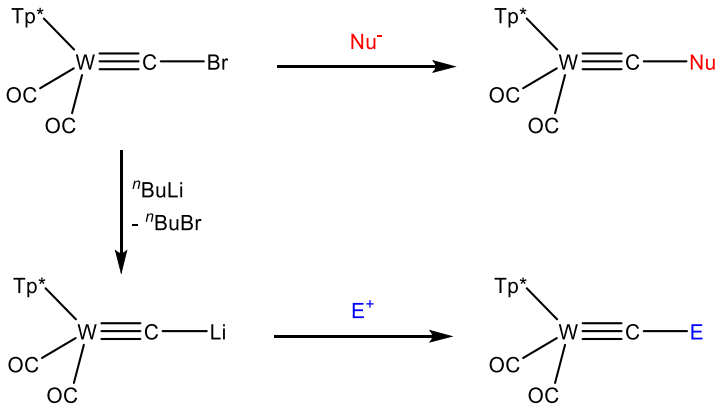

Scheme 2.4: Synthetic versatility of the terminal bromocarbyne **[W(≡CBr)(CO)$_2$(Tp*)]** towards both nucleophiles and electrophiles

. Examples of functionalised carbynes accessible through this bromocarbyne species include all of the tungsten and molybdenum functionalised carbynes in **Figures 2.1** and **2.2**, expansions into heavier chalcogens, pnictogens,[121] and even coordination to a second transition metal complex to form μ$_2$-metallacarbyne complexes.[122] The versatility of this rather simple starting material has allowed for a significant broadening of heteroatom functionalised- and metalla-carbyne chemistry.

μ$_3$-Halocarbynes

The face-capping, bridging μ$_3$-halocarbyne is the oldest and most commonly seen structural motif of the three binding modes. The field developed at a similar time, with the first structurally characterised example appearing on cobalt in 1981 from Schmid,[123] though its synthesis dates back to 1962[124] and its chemistry was extensively developed the 70's by Seyferth (**Scheme 2.5**).[125] Though μ$_3$-carbyne complexes are scattered in the literature, the mere 30 characterised μ$_3$-halocarbyne complexes are remarkably dispersed amongst cobalt, iron, osmium, ruthenium, molybdenum, platinum, and recently chromium.[126]

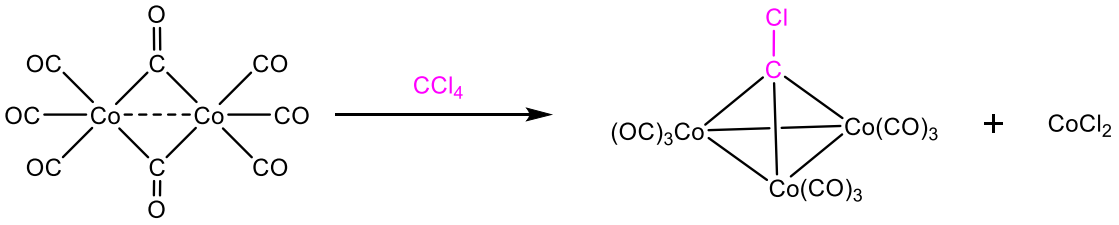

Scheme 2.5: Synthesis of **[$Co_3(\mu_3\text{-}CCl)(CO)_9$]** through CCl_4 addition to **[$Co_2(CO)_8$]**

The sp^3-hybridised halocarbyne ligand is still susceptible to nucleophilic substitution reactions *via* palladium-mediated processes or with the aid of a Lewis Acid such as $AlCl_3$, though these transformations are often more mechanistically complex than conventional S_N1 or S_N2 prtocesses. For example, for the μ_3-bromocarbyne cluster, **[$Co_3(\mu_3\text{-}CBr)(CO)_9$]**, addition of $AlCl_3$ followed by anhydrous methanol results in the formation of a methoxycarbonyl carbyne **[$Co_3(\mu_3\text{-}CCO_2Me)(CO)_9$]** (**Scheme 2.6**),[127] *via* the intermediacy of a ketenylidene ligand arising from carbide/carbonyl coupling.

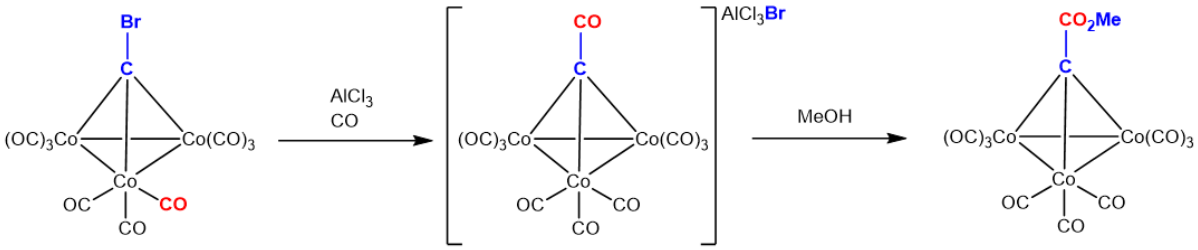

Scheme 2.6: Lewis Acid activation of a μ_3-bromocarbyne

Considering heterogenous materials are the backbone of most industrial-scale catalysis, very little is actually understood about the mechanisms and structures of species that form on metal or metal oxide surfaces that control and define the reactivity. To better understand and inform development of this field, discrete molecular metal cluster complexes have been suggested since the 1970s as reasonable molecular models for metal surfaces,[128] and μ_3-carbyne complexes have played a role in helping understand important C-C bond formation and C–O bond cleavage processes such as those involved in the Fischer-Tropsch process.[129]

μ_2-Halocarbynes

Though μ_2-carbyne ligands are prevalent in the field, that is not the case for halocarbynes. Prior to the start of this work, there existed only one polymeric example that had been structurally characterised, and the strategic synthesis and spectroscopic inference of this bonding mode was limited to a single example from Wolfgang Beck as late as 2008; decades after the other bonding modes were already structurally characterised and studied.

The polymeric example reported by Johannes Beck back in 2002 arose from the rather simple albeit curious reaction of tungsten hexachloride, carbon tetrachloride, and arsenic, heated to 250 °C (2 days) and 100 °C (6 weeks) under solvothermal conditions. From this, black crystals of the polymeric species **$[W_2Cl_7(CCl)]_n$** formed in unspecified yield.[130] The polymeric species, bridged by chlorides, contains a μ_2-CCl ligand. The two W-C bond lengths (1.94(1) and 1.94(2) Å) fall within the accepted range for a μ_2-alkylidyne ligand.

Taking the terminal bromocarbyne complex **$[Mo(\equiv CBr)(CO)_2(Tp^*)]$** and the reactive platinum(0) species **$[Pt(\eta^2\text{-}C_2H_4)(PPh_3)_2]$**, loss of the labile alkene and oxidative addition of the C-Br bond to platinum ultimately forms the Class B μ_2-carbido complex **$[(Tp^*)(CO)_2Mo\equiv C\text{-}PtBr(PPh_3)_2]$**.[131] However, it was observed that the intermediate species might involve carbyne coordination to the platinum centre before oxidative addition of the C-Br bond, which would form a transient μ_2-bromocarbyne species **$[MoPt(\mu\text{-}CBr)(CO)_2(PPh_3)_2(Tp^*])$** (**Scheme 2.7**). The ^{13}C NMR data for the intermediate species agree well with a similar μ_2-arylcarbyne **$[WPt(\mu\text{-}CC_6H_4Me\text{-}4)(CO)_2(PMe_3)_2(Tp^*])$** described by Stone,[132] with the presumed halocarbyne resonance at 315.9 ppm (*cf.* 332 ppm for Stone's arylcarbyne), which is downfield of the linear terminal halocarbyne, suggesting an increased paramagnetic contribution to the shielding from a second metal. Though strong evidence was provided for the intermediacy of this μ_2-halocarbyne species, its evolution to the μ-carbido complex *via* spontaneous but slow oxidative addition prevented structural data being acquired at the time. No reactivity of the halocarbyne intermediate was described aside from this oxidative addition.

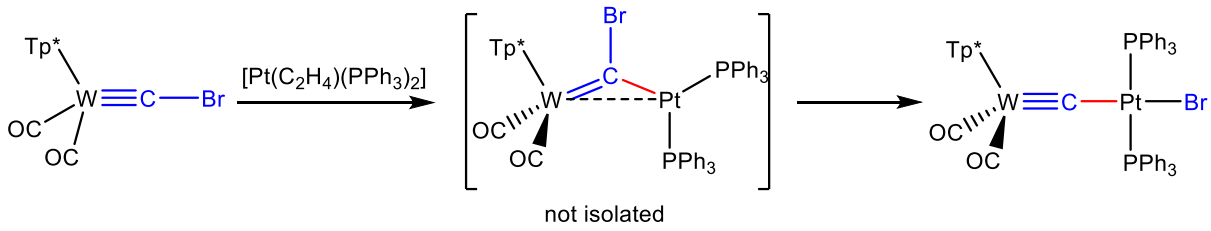

Scheme 2.7: Observed asymmetric μ_2-halocarbyne complex

The only other structurally characterised example of a molecular μ_2-halocarbyne complex appeared in 2021 after publication of the work to be described herein from Takao and Seki.[53] In an effort to form a tri-ruthenium μ_3-chlorocarbyne, the reaction between the ruthenium cluster **[{(Cp*)Ru(μ-H)}$_3$(μ$_3$-H)$_2$]** and carbon tetrachloride was examined. Rather than forming the anticipated μ_3-chlorocarbyne, one ruthenium terminus was lost, resulting in the formation of the unexpected μ_2-chlorocarbyne species **[{(Cp)*RuCl}$_2$(μ-CCl)(μ-Cl)]** (**Scheme 2.8**). The ruthenium-ruthenium distance (2.7523(6) Å) and electron requirements call for a formal intermetallic bonding interaction, and the two ruthenium-carbon bond lengths (average of 1.892 Å) lie well within the range observed for typical ruthenium μ_2-alkylidyne complexes. The ^{13}C resonance of the chlorocarbyne appears downfield at δ 323.4, close to the value observed by Beck for the heterobimetallic molybdenum-platinum example above.

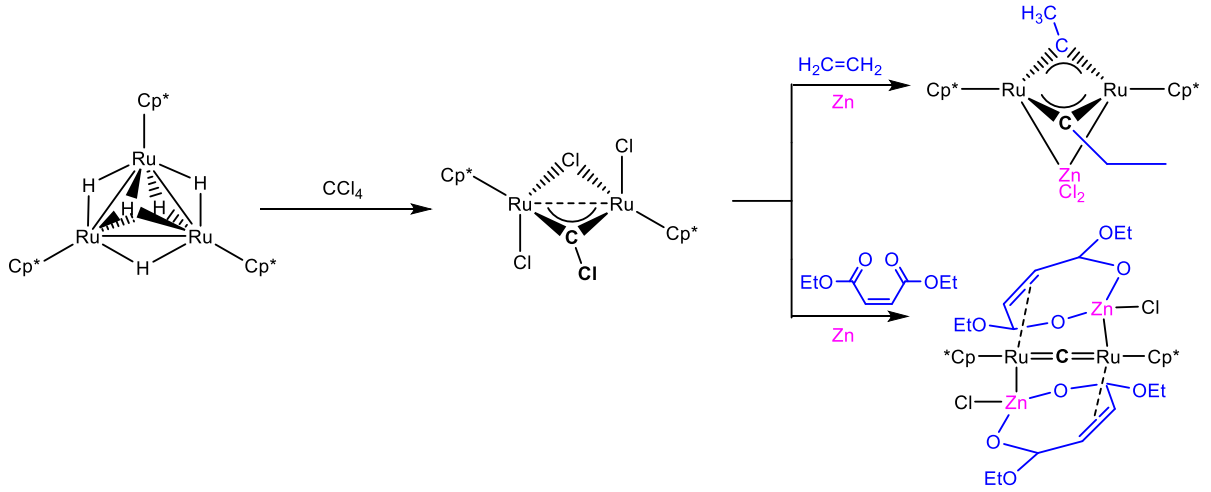

Scheme 2.8: Synthesis and subsequent reduction of a di-ruthenium μ_2-chlorocarbyne ligand

The preliminary reactivity explored for this chlorocarbyne ligand was focussed on reduction using zinc powder. Though no isolable products could be identified from the reduction alone, the presence of trapping agents ethene and diethyl maleate lead to the isolation of a μ-ethylidyne-μ-propylidyne species and the presumed μ-carbido reactive intermediate, respectively. The formation of the μ-propylidyne ligand was suggested to go through a μ-carbido intermediate which reacts further with two equivalents of ethene (See **Section 1.2**).

2.2.4 Rationale for this work

The carbyne ligand provides multiple forms of reactivity and an almost endless potential for functionalisation. Of these, the halocarbyne ligand is by far the most versatile starting point to access a range of unseen chemistry, as amply demonstrated for terminal and μ_3-halocarbynes.

The one caveat of the halocarbyne chemistry is the underdeveloped field of μ_2-halocarbynes. With no small molecule examples prior to the undertaking of this work, the gap in the field is notable. With the highly plausible formulation by Beck of a sole unstable μ_2-halocarbyne complex as a reactive intermediate,[xxxvi] the synthesis and documented reactivity of stable μ_2-halocarbyne complexes provides a timely addition to the field of carbyne chemistry. The work presented in this chapter helps fill that void.

[xxxvi] Since publication of the work described herein, ANU colleagues have structurally authenticated a range of μ_2-halocarbynes, e.g., **[MoPt(μ-CCl)(CO)$_2$(dppe)(Tp*)]** and **[W$_2$Pt(μ-CCl)(CO)$_4$(Tp*)$_2$]**: L. K. Burt, R. Y. Kong and C. S. Onn, unpublished results

2.3 RESULTS AND DISCUSSION

2.3.1 Oxidative Addition – μ_2-halocarbyne synthesis

Reactions with $PhICl_2$

Considering the carbido bridge as a neutral ligand, the complexes in the previous chapter might be viewed as involving conventional d^8-square planar rhodium, the classical venue for exploring oxidative addition processes, by analogy with Vaska's textbook complex **[IrCl(CO)(PPh$_3$)$_2$]**. As noted at the beginning of this Chapter, the reactivity of an alkylidyne/alkylidene is intimately governed by the electronic nature of the metal centre, including oxidation state, *d*-occupancy, and coordination number. To explore the extension of this principle to μ-carbido ligands would call for a platform that allowed the factors to be systematically varied and prior to the advent of the rhodium complexes described herein, no such opportunity existed. Accordingly, the oxidative addition reactions of these μ-carbido complexes are now discussed.

The initial oxidative addition reactions were investigated with the progenitor carbido complex **[Rh$_2$(μ-C)Cl$_2$(PPh$_3$)$_4$]**. Chlorination was chosen as the halogenation to be attempted as not only are they not too sterically encumbering like bromine and iodine, but they are also present on the starting complex and would avoid any halide scrambling. With complications in accurately dispensing the requisite stoichiometric amount as well as the somewhat indiscriminate nature of chlorine gas, the small molecule crystalline iodobenzene dichloride ($PhICl_2$) was used. This reagent is commonly employed in the mild chlorination of alkenes but can also be used as a Cl_2 source for transition metal-based oxidative addition.

Initial monitoring of the reaction by $^{31}P\{^1H\}$ NMR spectroscopy indicated the development of a new symmetrical doublet resonance (34.10 ppm, $^1J_{RhP}$ = 119 Hz). The doublet environment at 34.10 ppm perfectly matches the known carbonyl complex **[RhCl(CO)(PPh$_3$)$_2$]**. The origin of this carbonyl formation can perhaps be explained through the generation *in situ* of the dichlorocarbene species **[RhCl(=CCl$_2$)(PPh$_3$)$_2$]**, which though only the fluorine analogue is known,[133] is a reactive and likely intermediate to the hydrolysis at the chlorocarbene to form the more stable carbonyl complex. The hydrolysis of dichlorocarbene complexes to the corresponding carbonyls is well-documented.[134] This is, however, complete conjecture. A second resonance of equal intensity at 37.56 ppm ($^1J_{RhP}$ = 120 Hz) was identified and though unable to be separated, was presumed to be the remaining rhodium moiety as **[RhCl$_3$(PPh$_3$)$_2$]**.

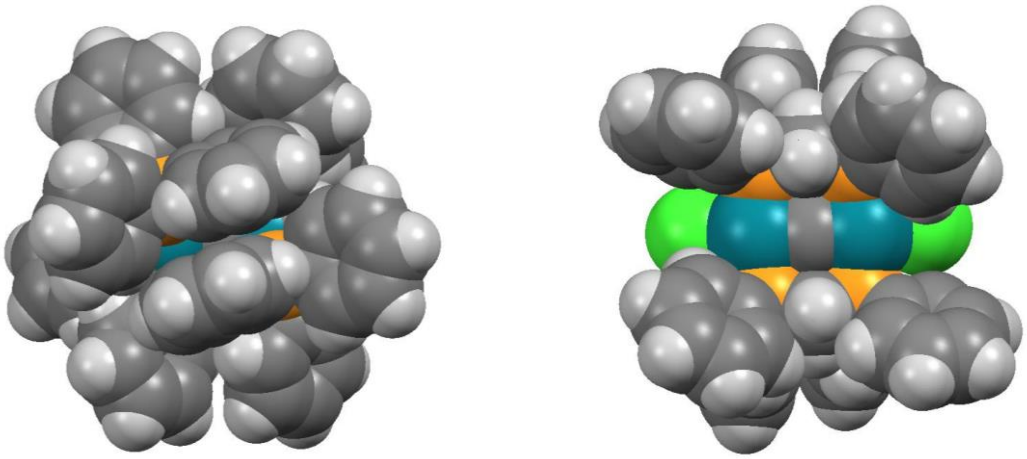

Figure 2.4: Space-filling representations of (left) **[$Rh_2(\mu$-C)$Cl_2(PPh_3)_4$]** and (right) **1**

The apparent failures in the oxidative addition reactions can perhaps be explained when examining the space-filling representation of **[$Rh_2(\mu$-C)$Cl_2(PPh_3)_4$]** (**Figure 2.4**). Whilst *trans*-triphenylphosphine ligands themselves do not completely encompass a metal centre (Tolman angle = 145°), the four phosphine ligands situated in close proximity and orthogonal to each other completely occlude most of the inner atoms, including the Rh=C=Rh spine. The steric hindrance and kinetic protection provided by these phosphine ligands would perhaps render the anticipated higher coordinate (vertex-shared bioctahedral) carbido complex relatively unstable and more susceptible to cleavage of the Rh=C=Rh unit.

When examining the space-filling diagrams of the recently synthesised A-frame complexes, the dppm analogue **1** remarkably showed the phenyl rings facing away from the metal centres to provide two clefts that expose the Cl–Rh=C=Rh–Cl core. It was surmised that the exposed reactive sites in **1** would be the more accessible for reactivity studies, and in addition to that, the dppm co-ligand may provide stability by constraining the two rhodium centres to remain proximal.

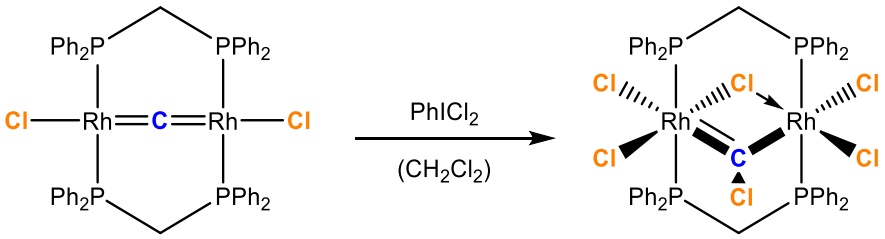

Scheme 2.9: Oxidative addition of chloride to **1**, forming a μ_2-halocarbyne ligand

The reaction of $PhICl_2$ with **1** was investigated under identical conditions to those above: A red dichloromethane solution of **1** immediately turned yellow upon addition of $PhICl_2$ and the reaction was complete almost immediately ($^{31}P\{^1H\}$ NMR). A yellow precipitate formed upon addition of alkane solvents (**Scheme 2.9**). Unlike the reaction with its triphenylphosphine analogue, the solution showed a single rhodium-phosphorus doublet resonance at 3.38 ppm in the $^{31}P\{^1H\}$ NMR spectrum. The doublet showed a decreased $^1J_{RhP}$ coupling constant of 95 Hz, which is suggestive of moving from a four- to six-coordinate rhodium species (based on the % *s* character between sp^2d and sp^3d^2).

The ESI-MS of the yellow precipitate supported the addition of two equivalents of Cl_2, with the $[M\text{-}Cl]^+$ fragment detected at 1162.8810 *m/z* (Calcd. for $C_{51}H_{44}{}^{35}Cl_5P_4Rh_2$ = 1162.8911 *m/z*). The presumed product, **$[Rh_2(\mu\text{-}C)Cl_6(\mu\text{-}dppm)_2]$**, displayed an interesting feature in the ^1H NMR spectra. In the starting material **1**, the methylene hydrogens on dppm appear as a single environment, however, the NMR spectra now displayed two distinct multiplet resonances at 3.56 and 3.20 ppm. This suggests that the two hydrogens are now in different enough chemical environments, unable to undergo site exchange. If the oxidative addition resulted in the symmetrical product **$[Rh_2(\mu\text{-}C)Cl_6(\mu\text{-}dppm)_2]$** there should be the expected single (time-averaged) environment (idealised D_{2h} symmetry). The infrared spectrum included a conspicuous band at 852 cm^{-1} and whilst this would be consistent with a ν_{RhCRh} oscillator, it should also be noted, as became apparent, that this region (850-1000 cm^{-1}) is also host to vinylic ν_{CCl} bands.

The molecular structure was determined using X-ray crystallography (**Figure 2.5**) revealing the true outcome of the oxidative addition reaction to be the formation of a μ_2-chlorocarbyne complex **$[Rh(\mu\text{-}CCl)(\mu\text{-}Cl)Cl_4(\mu\text{-}dppm)_2]$ (18)**.

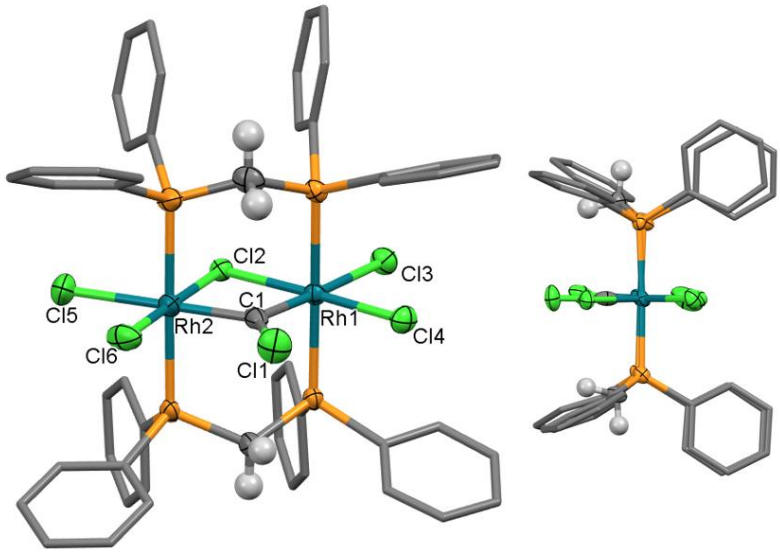

Figure 2.5 Molecular structure of **[Rh(μ-CCl)(μ-Cl)Cl$_4$(μ-dppm)$_2$] (18)** (50% displacement ellipsoids, some hydrogen atoms omitted, phenyl groups simplified). Selected bond lengths (Å) and angles (°): Rh1···Rh2 3.1866(7), Rh2-C1 1.948(6), Rh2-C1 1.912(6), C1-Cl1 1.674(7), Rh1-Cl2 2.403(1), Rh1-P1 2.381(2), Cl1-H91A 2.983, Rh1-C1-Rh2 111.3(3), C1-Rh1-Cl2 83.0(2)

The C_{2v} complex **18** contains two (*cf.* 3 for D_{2h}) internal (non-crystallographic) mirror planes along and perpendicular to the Cl_5Rh_2CCl plane, which explains the symmetry implicit from the ^{1}H and ^{31}P{^{1}H} NMR spectra. Two chlorine atoms have undergone migration, one into a bridging position between the two rhodium atoms, and the second has undergone migratory insertion onto the carbido ligand. This insertion reaction takes the cumulenic carbido species and transforms it into a μ^2-halocarbyne ligand in **[Rh(μ-CCl)(μ-Cl)Cl$_4$(μ-dppm)$_2$]** (**18**). The formal metal-carbon bond order of the halocarbyne ligand is decreased, which is seen in the elongation of the two Rh-C bond lengths (1.948(6) and 1.912(6) Å), notwithstanding the increased coordination number at rhodium, and a shift in the Rh-C-Rh angle (111.3(3) °) to reflect the sp^2 hybridised carbon atom. Although there are four terminal chloride ligands on **18**, the two chlorine atoms that are located *trans*- to the chlorocarbyne ligand are noticeably elongated (*e.g.*, Rh1-Cl3 = 2.444(1) *cf.* Rh1-Cl4 = 2.307(1) Å), highlighting the carbyne *trans* influence.

With the presence of a new functional group, the infrared spectra of **18** was of significant importance. The prominent absorption at 852 cm^{-1} in the infrared spectrum corresponds to the ν_{CCl} mode of the chlorocarbyne, which falls in a region similar to terminal chlorocarbynes and

chlorocarbenes,[135] and within reasonable distance to the calculated value[xxxvii] of 914 cm^{-1} studies on the structurally similar **[Rh(μ-CCl)(μ-Cl)Cl$_4$(μ-dmpm)$_2$]**).

Because of its significance, the ^{13}C resonance of the μ_2-chlorocarbyne was pursued. Under identical reaction conditions, the isotopologue **[Rh$_2$(μ-^{13}CCl)Cl$_4$(μ-dppm)$_2$]** (**18'**) could be synthesised from **1'**. The 1D $^{13}C\{^1H\}$ NMR spectrum detected a broad environment downfield at 410.1 ppm, which is interestingly upfield of the μ-carbido complexes despite the presence of the electronegative chloride, suggesting that the multiple bonding character to rhodium plays a dominant role in its chemical shift.

Reactions with [pyH][Br$_3$]

In order to examine the feasibility in completing the halocarbyne library, the halogenation switched from chlorine to bromine. In order to add a stoichiometric amount of Br_2 in a mild form, pyridinium tribromide [pyH][Br_3] was used. However, to prevent possible halide scrambling from occurring, the two terminal chloride ligands on **[Rh$_2$(μ-C)Cl$_2$(μ-dppm)$_2$]** had to first be replaced. The susceptibility of silver to abstract chloro ligands from metals due to the high lattice energy of AgCl and associated insolubility was exploited, with a slight excess of AgOTf added to a MeCN solution of **1**, to form the *in-situ* species **[Rh(μ-C)(OTf)$_2$(μ-dppm)$_2$]**. Following removal of AgCl by filtration, excess LiBr was then added, and the orange product **[Rh$_2$(μ-C)Br$_2$(μ-dppm)$_2$] (1b)** was isolated upon filtration. The $^{31}P\{^1H\}$ NMR spectra appeared identical to **1**, highlighting the small effect the change in terminal halide has on the relative dppm chemical shift.

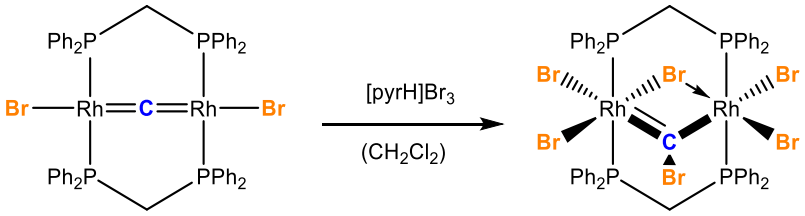

Scheme 2.10: Oxidative addition of halogens to **1**, forming a μ_2-halocarbyne ligand

[xxxvii] (a) DFT: ωB97X-D/6-31G*/LANL2Dζ (b) For computational economy the dppm ligands were replaced with dmpm however in practice attempts to prepared **[Rh(μ-C)Cl$_2$(μ-dmpm)$_2$]** *via* the reaction of **[Rh$_2$(μ-C)Cl$_2$(PPh$_3$)$_4$]** with dmpm resulted in extensive degradation.

Following an identical procedure for chlorination, a dichloromethane solution of the bromine analogue **1b** immediately turned red following addition of [pyH]Br_3 (**Scheme 2.10**). Monitoring the reaction by $^{31}P\{^1H\}$ NMR spectroscopy showed a slower reaction rate than the chlorination, but after a few hours the starting material was completely absent from the ^{31}P NMR spectra. Instead, a new phosphorus resonance centred at -5.73 ppm displayed the expected doublet multiplicity with a smaller observed coupling constant $^1J_{RhP}$ of 96 Hz. Under the initial assumption that the bromocarbyne analogue had been synthesised, the spectral data were examined for similar patterns. The ^1H NMR spectra once again did not show the single, broad hydrogen environment for the methylene group like **18**, however, the separation of the two environments (3.18 and 3.13 ppm) is not as pronounced as for the chlorocarbyne species. The addition of four bromine atoms was confirmed in the ESI-MS, with the extensive envelope of the $[M\text{-}Br]^+$ fragment centred at 1386.6341 *m/z* (*cf.* 1386.6370 *m/z* for $C_{51}H_{44}{}^{79}Br_2{}^{81}Br_3P_4Rh_2$).

Whilst the $\nu_{C\text{-}Cl}$ stretch was detectable in the IR spectra, the equivalent $\nu_{C\text{-}Br}$ was expected to appear in the heavily populated fingerprint region (Redlich-Teller Product Rule: ~571 cm^{-1}) and was not able to be discerned with confidence. That being said, the molecular structure from X-ray crystallography analysis confirmed the synthesis of the μ^2-bromocarbyne complex, **[Rh(μ-CBr)(μ-Br)Br_4(μ-dppm)$_2$] (19)**.

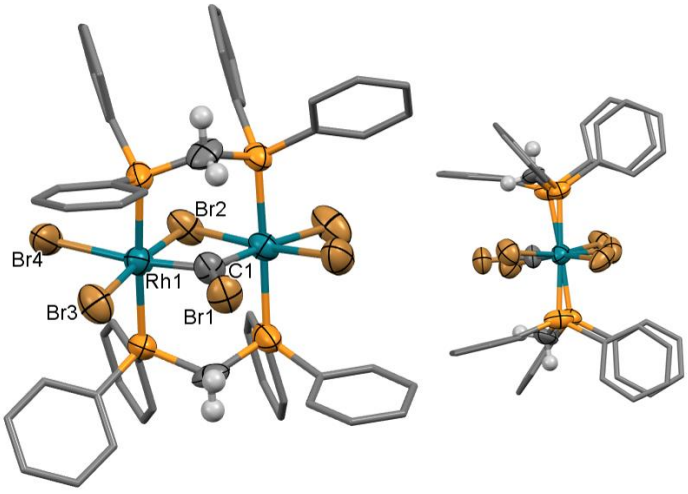

Figure 2.6 Molecular structure of **[Rh(μ-CBr)(μ-Br)Br_4(μ-dppm)$_2$] (19)** (50% displacement ellipsoids, some hydrogen atoms omitted, phenyl groups simplified). Selected bond lengths lengths (Å) and angles

(°): Rh1-C1 2.09(4), C1-Br1 1.60(6), Rh1-Rh1 3.220(3), Rh1-Br2 2.494(4), Rh1-P1 2.382(7), Rh1-Br4 2.458(5), Rh1-C1-Rh1 103(2), Br2-Rh1-C1 88.5(13)

The structural features of the bromocarbyne complex **19** are similar to **18**, with the exception that the tetragonal unit cell contains, *inter alia*, a two-fold rotation axis (z = 0.2500) that includes C1, Br1 and Br2 (space group, $P4_32_12$). The Rh-C bond length is longer again, at 2.09(4) Å. The bromine ligands *trans*- to the bromocarbyne are longer than those *trans*- to the bridging bromide (2.579(4) and 2.460(5) Å respectively). The Rh–C bond length is significantly shorter (0.112 Å, approximately 28 e.s.d.) for **18**, which is consistent with the bromide being a more effective π-donor than chloride, requiring less retrodonation from rhodium into the antibonding π^* orbital.

In an effort to see if the halide metathesis prior to bromination to form **19** is required, excess [pyH][Br_3] was added directly to **[Rh_2(μ-C)Cl_2(μ-dppm)$_2$]** and stirred for 15 hours. Based on the $^{31}P\{^1H\}$ NMR spectra of the resulting solution, the complete bromination product **19** was formed as the major product, but it wasn't the sole product. A new environment at -3.90 ppm had a similar $^1J_{RhP}$ coupling constant of 98 Hz and was formed in a 1:3 ratio to **19** based on signal integration. Examining the ESI-MS of the final orange/red powder, the second product was determined to be the mixed halogenation product, with four bromine and two chloride ligands on the complex ([M-Br]$^+$ at 1294.7416 m/z *cf.* 1294.7410 for $C_{51}H_{44}{}^{79}Br_2{}^{81}Br^{35}Cl_2P_4Rh_2$, [M-Cl]$^+$ at 1340.6932 m/z *cf.* 1340.6879 for $C_{51}H_{44}{}^{79}Br_2{}^{81}Br_2{}^{35}ClP_4Rh_2$). The diagnostic $\nu_{C\text{-}Cl}$ stretch was absent in the IR spectra, so it was determined that the halogen that apparently underwent migration were the added bromine atoms. This was supported with the molecular structure derived from X-ray crystallography, with the complex formula **[Rh(μ-CBr)(μ-Br)Br_2Cl_2(μ-dppm)$_2$] (20)**. It must be noted that due to their almost identical characteristics, the mixed halide species **20** was never able to be separated from the perbromocarbyne complex **19**, making NMR characterisation beyond $^{31}P\{^1H\}$ NMR spectroscopy difficult. Based on simple bond enthalpy arguments (Br–Rh=C–Cl vs Cl–Rh=C–Br), the chlorocarbyne isomer should be thermodynamically favoured and hence selective formation of the bromocarbyne **20** is presumably a kinetic phenomenon, i.e., addition of 'Br^+' *cis* to the carbido ligand means the chloro ligand is always *trans* and unable to migrate to the carbido. The regiochemistry of the product also retains *trans* disposition of chloro and chlorocarbyne ligands.

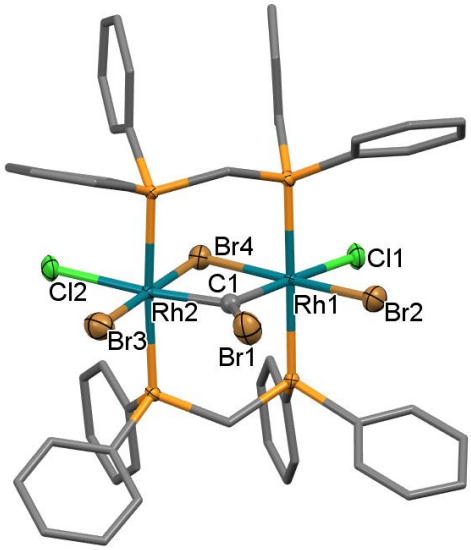

Figure 2.7: Molecular structure of **[Rh(μ-CBr)(μ-Br)Br_2Cl_2(μ-dppm)$_2$] (20)** (50% displacement ellipsoids, hydrogen atoms omitted, phenyl groups simplified). Selected bond lengths lengths (Å) and angles (°): Rh1-C1 2.03(1), Rh2-C1 1.91(1), Rh1-Rh2 3.236(1), C1-Br1 1.72(2), Rh1-Br2 2.422(2), Rh1-Cl1 2.40(1), Rh1-Br4 2.504(2), Rh1-C1-Rh2 107.7(6)

Interestingly, the two chloride ligands that have remained on the metal centre ultimately reside *trans*- to the bromocarbyne ligand (**Figure 2.7**). The longer nature of the Rh-Br bonds means now the terminal Rh-Cl and Rh-Br bonds are approximately the same length (2.40(1) and 2.422(2) Å, respectively). The comparably long Rh-Cl bond lengths (Rh1-Cl1 = 2.40(1), Rh1-Br2 = 2.422(2) Å) is due to the strong *trans* effect of the carbyne ligand. Unfortunately, the μ-carbido atom proved exceptional difficult to model anisotropically, even when attempting to solve for disorder of the μ-Br and μ-CBr, compromising the precision of derived Rh-C bond lengths and angles. Leaving the mixture of **19** and **20** in excess [pyH][Br_3] for an extended period of time (>24 hours) saw the complete bromination of **19** into **20**.

One feature to note for all the molecular structures **18**-**20**, is that the modelling software (Mercury®) includes a Rh-Rh 'bond', which is incorrect to describe as a formal bonding interaction (3.1866(7) Å for **18**, and 3.220(3) Å for **19**). Despite their unavoidable proximity, the effective atomic number requirements (EAN Rules) of the rhodium centres do not call for the invocation of metal-metal bonding.

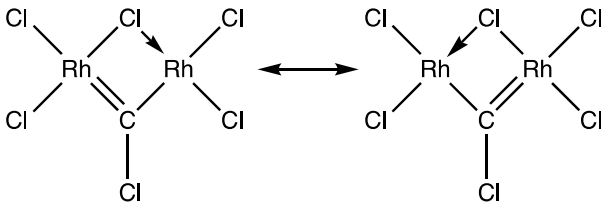

Figure 2.8: Alternate bonding representations for the μ-Cl and μ_2-chlorocarbyne ligand

Taking a single rhodium centre, the addition of two halide and two phosphine ligands brings the total electron count to 15. It is here that for electronic inventory the bridging halogen and halocarbyne ligand must be considered in their electron-allocated resonance forms and not the delocalised hybrid (**Figure 2.8**). The sp^2 hybridised halocarbyne can be considered to be a two-electron donor to one rhodium and a single donor to the other. The halogen is conversely considered to have a single bond to one rhodium and a lone pair donation to the other, giving each rhodium atom the requisite three valence electrons. Structural data are only available for a single example of a dirhodium μ-carbyne complex, **[Rh$_2$(μ-CC$_6$H$_4$Me-4)(μ-CO)(η-C$_5$Me$_5$)$_2$]BPh$_4$**, which has a mean Rh–C separation of 1.903(10) Å across what must be described as a Rh–Rh bond (2.568(1)Å) of multiple character,[136] as it is notably shorter than the covalent radii of the rhodium atoms ($2r_{cov}$(Rh) = 2.96 Å). Taken together, the dimensions of the Rh$_2$(μ-C) halocarbyne cores are rather similar with almost crystallographically identical (difference = 0.0334 Å, 11 esd) Rh···Rh separations, consistent with their proximity being dictated by the geometric constraints of four bridging ligands rather than any formal bonding.

μ_2-halocarbyne complexes are exceptionally scarce in the literature, and the complexes **18-20** represent the first structurally characterised examples of a small molecule μ_2-halocarbyne species.

2.3.2 μ_2-halocarbyne reactivity

The novelty of synthesising a new ligand class, in this case the μ_2-halocarbyne, quickly becomes replaced by the prospects of exploring unknown reactivity. Whilst terminal halocarbyne reactivity is well-studied and has demonstrated impressive versatility, it remains to be seen if such utility might extend to bimetallic examples.

Attempted coordination of AuCl

The first reaction of the halocarbyne to be explored involved the possible addition of a gold(I) unti across the remaining Rh-C multiple bond. Stone has previously demonstrated the addition of metal centres to pre-formed heterbimetallic μ-carbyne complexes as a means of strategically constructing heterotrimetallic (trimetallatetrahedranes).[132] As has been previously discussed, Au(I) complexes have a strong affinity for multiple bonds, be it carbon-carbon or metal-carbon bonds. Transfer of AuCl units using synthons with labile thioether ligands **[AuCl(SR$_2$)]** (SR$_2$ = THT, SMe$_2$) across MC multiple bonds has been shown to occur readily including addition to the W≡C bond of the bromocarbyne complex **[W(≡CBr)(CO)$_2$(Tp*)]**.[137] It was therefore of interest whether a similar reaction would take place with the bromocarbyne species **19** (**Scheme 2.11**), the caveat being the Rh–C–Rh multiple bonding in the chlorocarbyne complex involves orbitals orthogonal to the dimetallacarbyne plane, access to which is somewhat prevented by the proximal dppm phenyl groups.

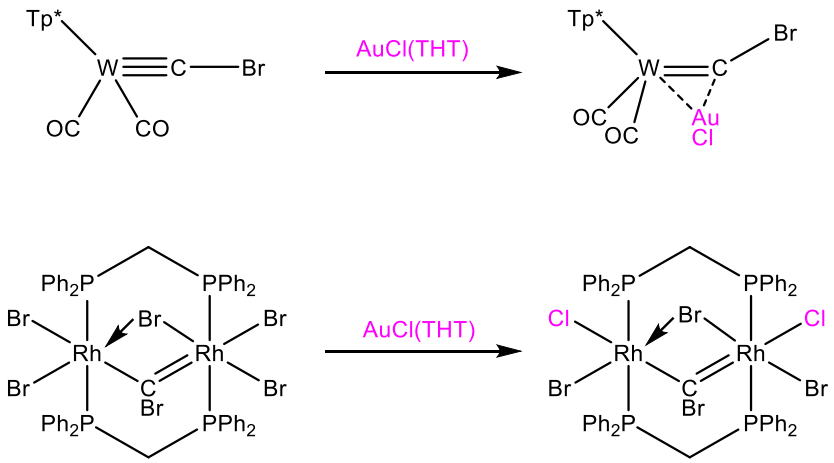

Scheme 2.11: Contrasting reactivity of **[W(≡CBr)(CO)$_2$(Tp*)]** and **19** to **[AuCl(THT)]**

When a dichloromethane solution of **19** was treated with **[AuCl(THT)],** no obvious colour changes occurred, however, the resonance due to the starting material in the $^{31}P\{^1H\}$ NMR spectrum had vanished after an hour. In its place was a phosphorus environment at -3.89 ppm, with a $^1J_{RhP}$ coupling of 98 Hz. This rather disappointingly matched the resonance for the previously synthesised complex **20**, which consists of the bromocarbyne complex with two terminal bromide and two chloride ligands, *i.e.*, the **[AuCl(THT)]** reagent achieved a transformation that might equally be achieved with common salt. Crystallographic data were

analogous to **21**, confirming that the two bromine ligands to undergo replacement were *trans*- to the bromocarbyne ligand, manifesting as a kinetic *trans* effect the thermodynamic *trans* influence reflected in the elongation of the *trans* Rh-Br bonds. Unfortunately, aside from a minute fragmentation pattern observed in the ESI-MS, there was no substantial evidence to indicate the addition of AuCl to the Rh=C bond, which was primarily dismissed due to steric hindrance from dppm phenyl groups being proximal to the bromocarbyne ligand. This was further supported with the chlorocarbyne species **18**, which failed to display any reactivity with **[AuCl(THT)]** under identical reaction.

Reaction with 4-methyl thiophenol

The reactions of dichlorocarbene and terminal chlorocarbyne complexes with thiols typically proceed via simple halide/thiolate substitution to afford thiolatocarbene or carbyne complexes.[138] Thiol addition to electrophilic bridging carbyne centres also has precedent, e.g., the diiron toluidyne salt **[Fe$_2$(μ-CO){μ-CC$_6$H$_4$Me-*p*}(CO)$_2$(η-C$_5$H$_5$)$_2$][BBr$_4$]**, when treated with sodium thiolates undergo nucleophilic addition to provide complexes with bridging aryl mercaptocarbene ligands μ-C(SR)C$_6$H$_4$Me-*p* (**Scheme 2.12** below).[139]

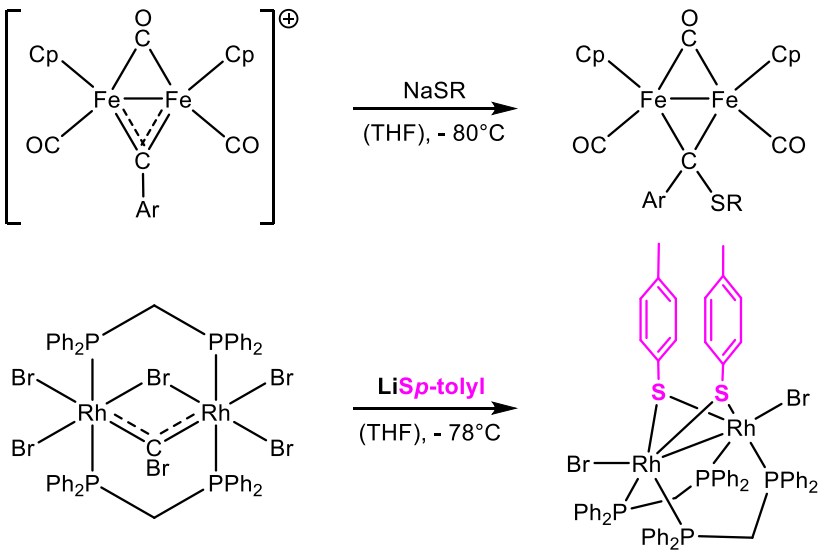

Scheme 2.12: Thiolate addition to **[Fe$_2$(μ-CO){μ-CC$_6$H$_4$Me-*p*}(CO)$_2$(η-C$_5$H$_5$)$_2$][BBr$_4$]** and attempted nucleophilic substitution using **19**

When a THF solution of the lithium toluenethiolate was added to the bromocarbyne in the same solvent at –78 °C, the solution gradually turns red upon warming to room temperature. The ^{1}H NMR spectrum of the red product shows the expected aliphatic resonance of the thiol at 2.15 ppm, suggesting an inclusion of the thiolate group. However, integration of the peaks suggest that two thiols had added. The ^{31}P{^{1}H} NMR spectra showed a symmetrical Rh-P doublet at 4.57 ppm, with the second order coupling effects common to dppm. The value of $^{1}J_{RhP}$ was however significantly larger than for the bromocarbyne precursor, increasing from 95 Hz to 128 Hz. The increased coupling constant is indicative of a decrease in coordination number.

The ESI-MS of the product failed to show any fragments that supported a simple substitution of the thiol at the bromocarbyne, however, the major fragment identified at 1301.1091 m/z corresponded to the $[M–Br]^{+}$ fragment of a curious substitution product, losing the elements of CBr_4, and addition of two toluene thiolate groups.

The complexity of the reaction was confirmed with the molecular structure that followed from a crystallographic analysis (**Figure 2.9**). It confirms that not only were the two terminal bromine ligands substituted for thiol ligands, the bromocarbyne and bridging bromide ligand have been lost from the complex, forming [**$Rh_2(\mu\text{-}4\text{-}SC_6H_4Me)_2Br_2(dppm)_2$] (21)**.

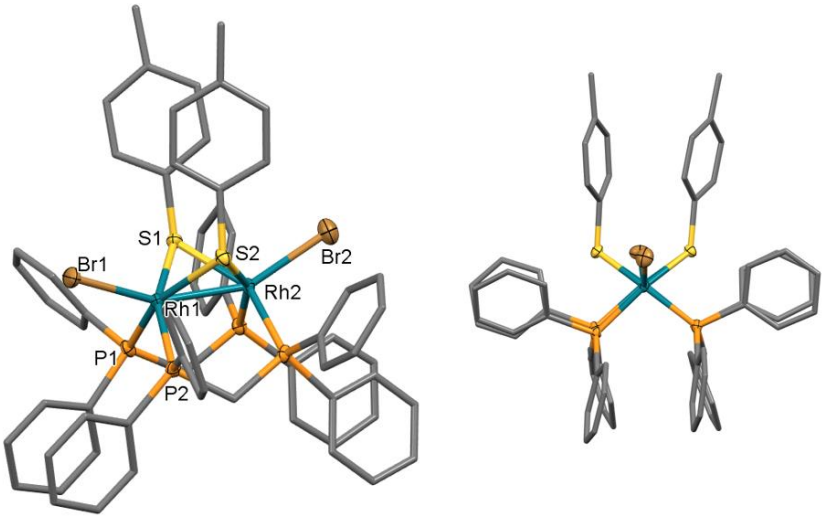

Figure 2.9: Simplified molecular structure of **[$Rh_2(\mu\text{-}4\text{-}SC_6H_4Me)_2Br_2(dppm)_2$] (21)**. 50% displacement ellipsoid, phenyl rings and hydrogen atoms removed. Selected bond lengths lengths (Å) and angles (°): Rh1-Rh2 2.5605(6), Rh2-S2 2.363(1), Rh1-S2 2.373(1), Rh2-Br2 2.5821(8), P4-Rh2-P3 98.50(5)

Complex **21** retains two terminal bromine ligands, and the bridging dppm ligands. The phosphines have been shifted into a *cis* geometry (P-Rh-P angle of 98.50(5)°), allowing a degree of overlap and π stacking of the phenyl rings. The two thiols have coordinated as bridging ligands, retaining their effective tetrahedral geometry, and octahedral coordination sphere of the rhodium(II) centres. The most intriguing feature of the complex is the complete loss of the bromocarbyne ligand. The shorter Rh-Rh distance (2.5605(6) Å, shorter than $2r_{cov}$(Rh)), with is now close enough to consider a formal Rh-Rh bond being present. Treating the bonding mode of the bridging thiols as a σ coordinated ligand to one rhodium and a dative coordination to the other through the lone pairs, both rhodium centres would be 17 electron species without inclusion of the Rh-Rh bond, which justifies it being classified as a formal d^7-d^7 interaction (*cf.* singly bound **[Rh$_2$(OAc)$_4$]**), consistent with the diamagnetism.

Attempts to optimise conditions to allow successful nucleophilic substitution to be observed were unsuccessful, however alternative successful approaches to dirhodium thiolatocarbynes are discussed elsewhere in this thesis.

Reactivity with TMS-imidazole

Examining a different reagent class, nitrogen-based systems were chosen. TMS-imidazole was tested first, selected because the imidazole ring was expected to direct it modest steric bulk away from the complex core, while its planar nature might make it easier to slot in between the dppm rings and still conjugate its π-system with the RhCRh unit. Trimethylsilylimidazole has been previously seen to react with the terminal bromocarbyne species **[Mo(≡CBr)(CO)$_2$(Tp*)]** to furnish the imidazolyl carbyne complex **[Mo(≡C-Im)(CO)$_2$(Tp*)]** (**Scheme 2.13**).[140]

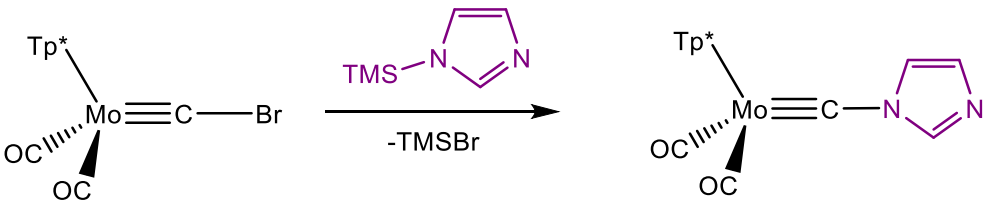

Scheme 2.13: Reactivity of **[Mo(≡CBr)(CO)$_2$Tp*]** with TMS-imidazole

Taking the bromocarbyne complex **[Rh$_2$(μ$_2$-CBr)(μ-Br)Br$_4$(μ-dppm)$_2$]**, addition of excess TMS-imidazole resulted in no discernible reactivity over 24 hours under ambient conditions in dichloromethane. The same yellow reaction mixture of the bromocarbyne complex and TMS-imidazole in dichloroethane, however, turned slightly green upon heating for two hours. Interestingly, removal of solvent resulted in the product turning a deep purple in colour. Separation through chromatography revealed further colour changes, with the complex eluting as a green solution with THF before again reverting to purple when concentrated. The $^{31}P\{^1H\}$ NMR spectrum of the purple complex shows only a very broad resonance around 13.0 ppm. Removal excess imidazole was achieved through a two-phase dichloromethane/water separation, which produced dark red/purple crystals of somewhat dubious quality. Unfortunately, the imidazolyl-carbyne was only stable in the presence of excess imidazole in solution and decomposed during attempts to purify through chromatography or selective crystallisation.

Attempting to use ^1H NMR spectroscopy to characterise the complex proved difficult with the presence of excess TMS-imidazole, and because the imidazole peaks of interest fall within the aromatic region. The two dppm methylene linker environments could be located at new chemical positions of 3.48 and 3.92 ppm, and a potential imidazole peak was identified upfield of the aromatic region at 6.89 ppm. Unfortunately, the remainder of the imidazole peaks were clustered within the aromatic region heavily populated by dppm resonances.

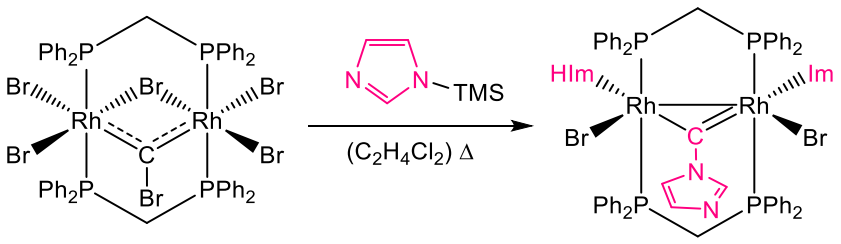

Scheme 2.14: Synthesis of imidazolyl-carbyne complex
[Rh$_2$(μ$_2$-C-*N*-Im)Br$_2$(Im)(Him)(μ-dppm)$_2$] (22)

Though the complex remained stable in solution, a very small number of crystals suitable for analysis could be formed through gradual concentration under reduced pressure. The molecular structure of the purple compound (**Figure 2.10**) remarkably displayed the anticipated imidazolyl-carbyne ligand on **[Rh$_2$(μ$_2$-C-*N*-Im)Br$_2$(Im)(Him)(μ-dppm)$_2$] (22)**. The excess

TMS-imidazole had resulted in further ligand replacement, with two terminal bromine ligands being replaced with imidazole (HIm) and imidazolyl (Im) ligand.

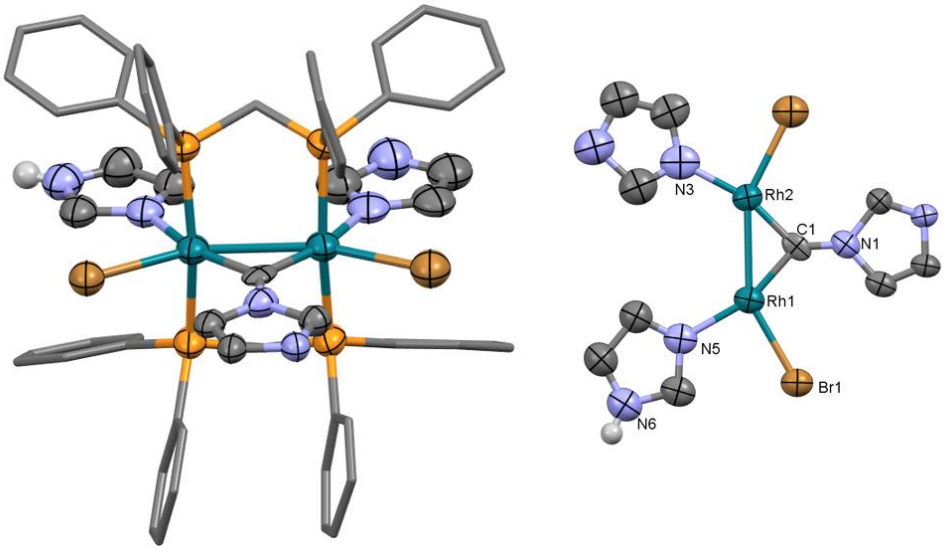

Figure 2.10: Molecular structure of **[Rh_2(μ_2-C-*N*-Im)Br_2(Im)(HIm)(μ-dppm)$_2$] (22)**. (30% displacement ellipsoids, hydrogen atoms omitted, phenyl and imidazole/yl groups simplified). Selected bond lengths lengths (Å) and angles (°): Rh1-Rh2 2.773(2), Rh1-C1 1.934(19), Rh1-Br1 2.591(3), Rh2-C1 1.88(2), C1-N1 1.33(2), Rh1-N5 2.14(2), Rh2-N3 2.06(1), Rh1-C1-Rh2 93.2(10)

Though to a lower degree of accuracy than would be ideal, the bond lengths in **23** are consistent with an imidazolyl carbyne. The imidazolyl carbyne complex **[Mo{≡C-*N*-Im}$(CO)_2${$HB(pzMe_2)_3$}]** was not structurally characterised, the amino and pyridine carbyne complexes contain C-N bond lengths (1.394(5) Å for DMAP, 1.316(4) Å for NEt_2) that fall in the same vicinity observed for the imidazolyl carbyne (1.35(4) Å). The angle of the μ_2-carbyne ligand undergoes significant contraction from the bromocarbyne precursor at 91.5(17) °, in a similar manner to the μ_2-chalcocarbonyl species described elsewhere. The two Rh-C bond lengths are crystallographically identical (1.91(4) Å) and fall within the ranges seen for the μ_2-carbyne/chalcocarbonyl ligands.

Of the two presumed imidazolyl ligands *trans* to the carbyne, the structural data and EAN requirements both support one undergoing protonation to HIm. The protonated imidazole ligand has a longer Rh-N bond (Rh1-N5 = 2.14(2) Å, Rh2-N3 = 2.06(1)) which is consistent with literature findings.[141] Electron density mapping could accurately determine the nitrogen positions

on the rings and supported the protonation at only a single nitrogen site (N6 in **Figure 2.10**). The presence of a single, broad resonance in the ^{31}P NMR spectrum suggests an exchange of imidazole and imidazolyl ligands in solution. The diagnostic ν_{NH} stretch could be identified in the IR spectrum at 3247 cm^{-1}, though the corresponding hydrogen resonance unfortunately could not be unambiguously identified in the ^{1}H NMR spectrum.

In an attempt to better purify the complex without the use of water, the reaction was repeated, and the red/purple complex was thoroughly washed with diethyl ether to leave behind a yellow solid. Initial hopes that this yellow solid might be the stable imidazole-carbyne complex were quickly dashed when the $^{31}P\{^{1}H\}$ NMR spectrum revealed only decomposition products and free phosphine. It seems that the presence and coordination of the excess imidazole groups on **22** are necessary for its stability.

Given the peculiarities attending the identification of the imidazolylcarbyne complex, a same reaction was investigated using *N*-methyl imidazole under comparable conditions. The methyl group present makes the remaining imidazole nitrogen significantly more nucleophilic and basic. As such, it might have been expected to form the cationic imidazolium carbyne ligand, as in the case of **[Mo(≡CBr)(CO)$_2$(Tp*)]** reacting to provide **[Mo(≡CImMe)(CO)$_2$(Tp*)]Br**.[140] A dichloromethane solution of the bromocarbyne complex **[Rh$_2$(μ$_2$-CBr)(μ-Br)Br$_4$(μ-dppm)$_2$]** and *N*-methyl imidazole, however, shows no reactivity over the course of 24 hours. Attempts to thermally induce reactivity by heating under reflux in dichloroethane ultimately proved futile. Removal of solvent under vacuum, and separation through column chromatography only yielded a yellow oil which failed to precipitate out a solid under any conditions investigated. The $^{31}P\{^{1}H\}$ NMR spectrum of the yellow oil only showed ligand decomposition peaks, and no signs of a rhodium complex.

Reactivity with Phosphines

The reactions of terminal halocarbynes with various phosphines have provided access to phosphonio-, phosphino- and phosphido (phosphaisonitrile) carbynes[142] and it was hoped that a similarly rich chemistry of CPRx (x = 1-3) ligands might emerge from the binuclear platform provided by the μ-halocarbynes. Due to the pyrophoricity and potentially indiscriminate reactivity of PMe_3, the more ammenable analogue PMe_2Ph was chosen. Once again, the rationale can also be traced to terminal bromocarbyne chemistry, where PMe_2Ph undergoes a nucleophilic substitution of bromide to form a phosphoniocarbyne (**Scheme 2.15**).[15] Bridging

phosphoniocarbynes have been described by Schmidbauer as arising from the reactions of high-valent metal halides with phosphane ylides,[143] suggesting such species might be viable.

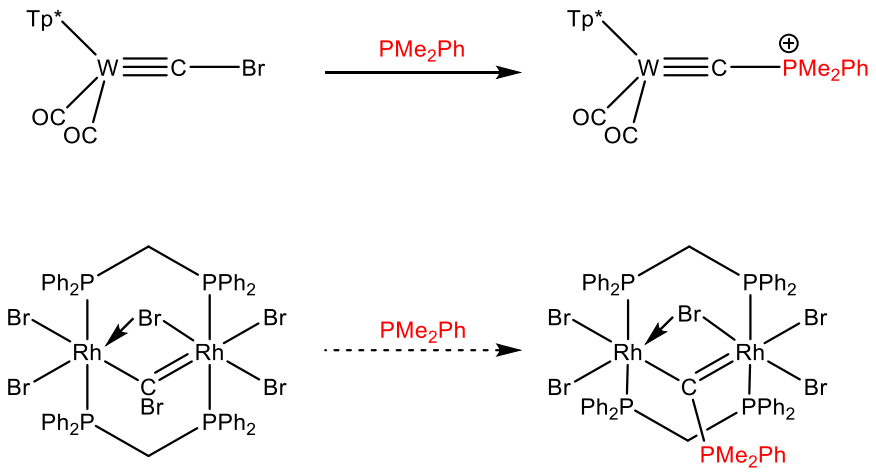

Scheme 2.15: PMe_2Ph reactivity to **[W(≡CBr)(CO)$_2$(Tp*)]** and attempted substitution to **19**

A cooled (-78 °C) THF solution of the bromocarbyne complex **19** was treated with a slight excess of PMe_2Ph. The orange solution turns red when the solution was allowed to warm to room temperature. A $^{31}P\{^1H\}$ NMR spectra of the solution showed a plethora of multiplet environments, implying a variety of products had formed. Column chromatography on silica gel eluting with dichloromethane/hexane elute furnished an orange/gold band. The $^{31}P\{^1H\}$ NMR spectrum of the product indicated two distinct phosphine environments, one as a doublet of doublets, and the other as a doublet of triplets consistent with a *mer*-$Rh(PMe_2Ph)_3$ unit. The ESI-MS of the gold crystals that formed unfortunately did not match any anticipated bimetallic species, but did however, correspond to the mononuclear rhodium complex *mer*-**[RhBr$_3$(PMe$_2$Ph)$_3$]**. This octahedral complex would contain two phosphine environments in a 2:1 ratio, explaining the observed NMR data.

The meridional geometry of the octahedral species was confirmed through crystallographic analysis (**Figure 2.11**), which shows a single rhodium centre with three halide and three phosphine ligands.

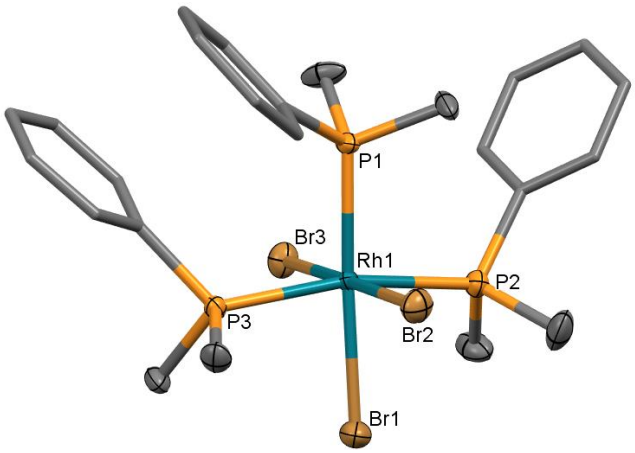

Figure 2.11: Simplified molecular structure of **[RhBr$_3$(PMe$_2$Ph)$_3$]**. Phenyl rings simplified and hydrogen atoms removed. Selected bond lengths lengths (Å) and angles (°): Rh1-P1 2.303(2), Rh1-P3 2.363(1), Rh1-Br1 2.5314(8)), Rh1-Br2 2.4816(6)

The molecular structure confirms the loss of the bromocarbyne ppm ligand to form the single rhodium species. Furthermore, the alkyl phosphine has also completely replaced the bidentate, chelating dppm ligands, indeed only four of the original atoms remain. To do this under mild conditions was unexpected. Further subsequent reactions under different conditions yielded the same product **[RhBr$_3$(PMe$_2$Ph)$_3$]** which has been previously synthesised.[144] No remaining complexes were identified following chromatography, and hence phosphines were abandoned as potential nucleophiles.

2.3.3 Mechanistic Conjecture

Although the synthesis of novel halocarbyne complexes were an unexpected success, the issue arises as to the intimate mechanistic pathway leading to their formation. Because the reactions take place too quickly to monitor accurately using NMR studies, identifying any key intermediates of perhaps a single oxidative addition reaction have been frustratingly futile. Unfortunately, both direct halogenation of a carbyne ligand, and halogenation away from a carbyne ligand have been reported in the literature (**Scheme 2.16**), supporting a number of alternate pathways.[145]

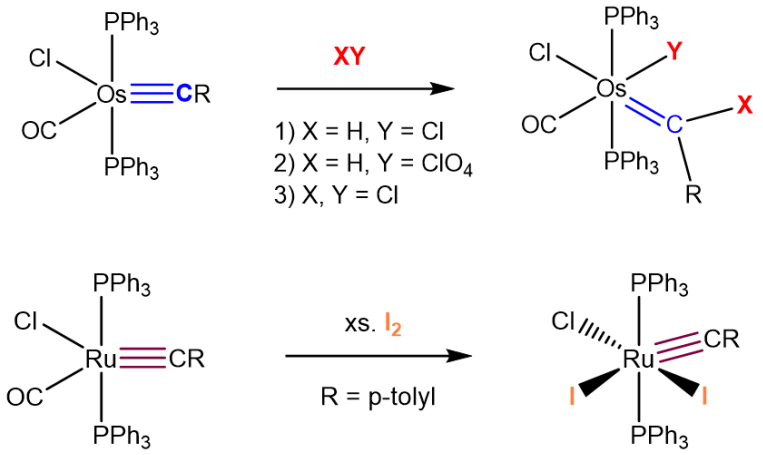

Scheme 2.16 (Top) Carbyne centred oxidative addition of **[Os(≡CAr)Cl(CO)(PPh$_3$)$_2$]** (Ar = *p*-tolyl).[145a] (Bottom) halogenation of a ruthenium carbyne complex away from the M≡C bond[145e]

Two proposed rhodium-centred addition pathways have been suggested, which are presented the below **Scheme 2.17**. The 1,3 – addition pathway (in pink), as it involves an initial symmetrical addition of one halogen to each rhodium centre (in the 1 and 3 positions respectively). The proposed intermediate raises fundamental questions regarding how best to describe the bonding within the RhCRh spine and these will be discussed in more detail below. The addition of the second equivalent of X_2 would again add to both rhodium centres, leading to the migration of two halides into their respective and distinct bridging positions.

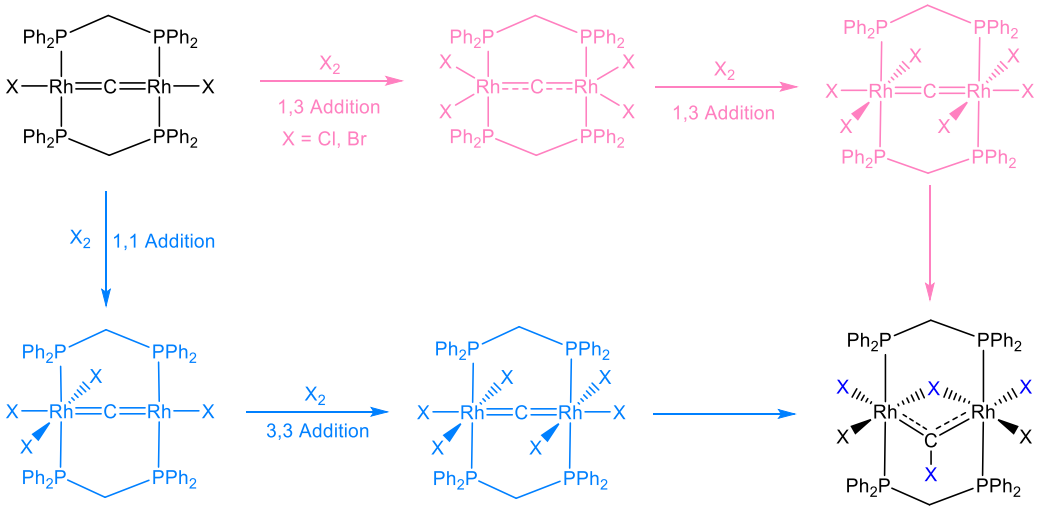

Scheme 2.17: Proposed halogenation pathways of the bridging carbido ligand. (X = Cl, Br); proposed intermediate complexes depicted in pink or blue were not observed

The second proposed pathway in blue is the "1,1 – addition", as it conversely involves the oxidative addition of both halogen units initially onto the same rhodium centre. This would lead to an intermediate species of *metallacarbyne* nature, containing the 18-electron octahedral Rh(III) and the 16-electron square planar Rh(I) centres. This asymmetrical nature of the intermediate can be rationalised when remembering that the asymmetric cumulenic (Class A) species **[Rh$_2$(μ-C)H(κC-2-C$_6$H$_4$PPh$_2$)(Tp*)$_2$]** relies on a similar motif as does, more precisely, the metallacarbyne (Class B) species **[Ru$_2$(μ-C)HCl$_3$(IMesH$_2$)$_2$]** reported by Grubbs.[10] The addition of the second source of X_2 would add to the remaining Rh(I) centre, which in a similar fashion led to the bridged halocarbyne species.

Halogenation of [Rh$_2$(μ-C)Cl$_2$(μ-dppf)$_2$]

Unfortunately, as mentioned, the intermediates for the halogenation of **1** were never observed, even when using a deficiency of halogenating reagents. It was postulated however, that using a bulkier phosphine co-ligand might potentially impede incoming halogen sources or embiggen the lifetime of any proposed intermediates due to the steric crowding of the rhodium centres. Armed with this hypothesis, the recently synthesised **[Rh$_2$(μ-C)Cl$_2$(μ-dppf)$_2$] (6)** was used as an alternative starting material, with the larger dppf co-ligands providing both ample flexibility and sheathing of the complex.

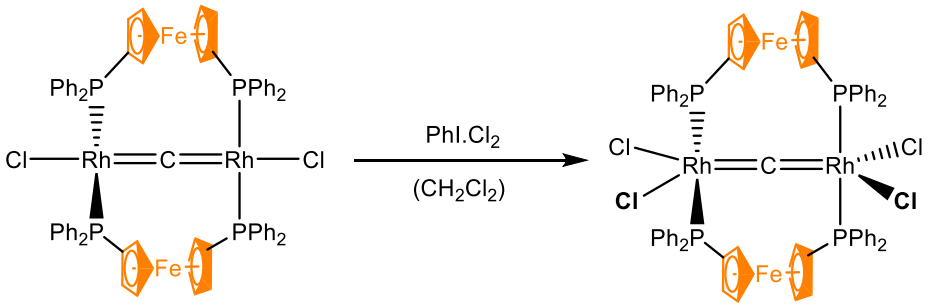

Scheme 2.18: Halogenation of **6** to give **[Rh$_2$(μ-C)Cl$_4$(μ-dppf)$_2$] (23)**

An initially bright orange dichloromethane solution of **6** immediately turns a dark green upon addition of $PhICl_2$ (**Scheme 2.18**). This initial colour change is dramatically different to the

typical colour range of yellow-red complexes seen previously in these studies. In a similar fashion to the chlorination of **1**, the reaction is extremely rapid and complete in a matter of minutes. Addition of ethanol led to the formation of dark green hexagonal crystals overnight, which were suitable for spectroscopic and crystallographic studies. The ^{1}H and ^{13}C NMR spectra were of limited diagnostic use aside from confirming the presence of the dppf ligands with both phenyl and cyclopentadienyl environments. The $^{31}P\{^{1}H\}$ NMR spectra, however, comprised a lone phosphorus environment downfield at 28.49 ppm, which relative to that of the precursor is the opposite to the upfield shift seen with the halogenations of **1**. The value of the $^{1}J_{RhP}$ coupling constant (95 Hz) is similar to the six-coordinate complexes **18 — 19** (95-96 Hz). In the ESI-MS, the $[M]^{+}$ ion peak of 1467.8862 *m/z* corresponds to the addition of a single equivalent of Cl_2, *i.e.,* **[Rh$_2$(μ-C)Cl$_4$(μ-dppf)$_2$]** (Calc. for $C_{69}H_{56}P_4{}^{35}Cl_3{}^{37}Cl^{56}Fe_2{}^{103}Rh_2$: 1467.8866 *m/z*). The deviation from the typically seen $[M\text{-}Cl]^{+}$ fragment can be rationalized when considering the ease of a one electron oxidation of the ferrocenyl ligands. The analytical data combined suggest the oxidative addition reaction stopped after the single addition, which perhaps could be akin to one of the possible intermediate species identified earlier. Considering the $^{31}P\{^{1}H\}$ NMR spectrum, if the "1,1 – addition" intermediate had been formed there would be two distinct rhodium environments, one six coordinate and the other four, which would lead to two disparate phosphine environments and $^{1}J_{PRh}$ couplings. Given that a single, symmetrical resonance is observed, the inferred molecular symmetry lends support to the synthesis of the 1,3 – addition isomer.

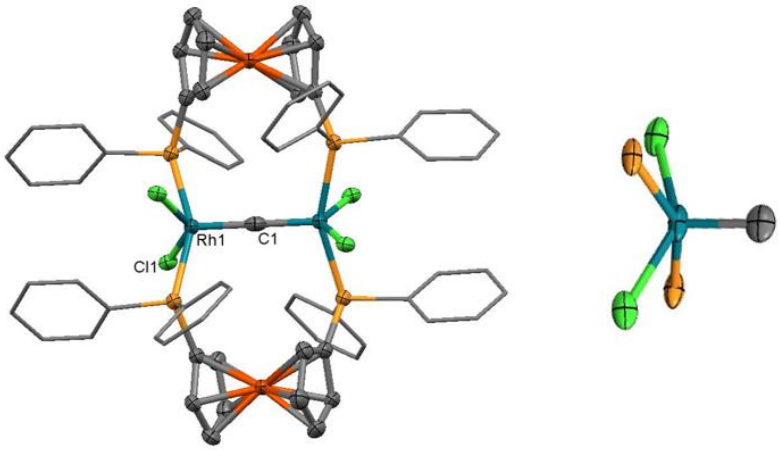

Figure 2.12: Molecular structure of **[Rh(μ-C)Cl$_4$(μ-dppf)$_2$] (23)** (50% displacement ellipsoids, hydrogen atoms omitted, phenyl groups simplified). Selected bond lengths lengths (Å) and angles (°): Rh1-C1 1.7945(4), Rh1-Cl1 2.425(1), Rh1-P1 2.3596(9), Rh1-C1-Rh2 180

The product **[Rh(μ-C)Cl$_4$(μ-dppf)$_2$] (23)** was confirmed by a single crystal molecular structure determination (**Figure 2.12**). The orthorhombic space group of the crystal structure causes the carbido atom to reside on an inversion centre ($^3/_8$, $^3/_8$, $^3/_8$) where three proper axes intersect such that only one quarter of the molecule is crystallographically unique with the enantiomer generated by glide planes. This requires the Rh=C=Rh bond angle to be perfectly 180°. Because of this symmetry, the two Rh=C bond lengths are also identical (1.7945(4) Å), which is consistent with a cumulenic (Class A) carbido description.

In classifying this as a cumulenic species based on symmetric crystal structure, the perennially thorny issue of metal oxidation states arises, as if the vagaries with carbenes and carbynes were not enough. Using electron counting principles, the rhodium centres would be 17-electron, rhodium(II) if we are to assume two Rh=C bonds. This causes problems with not only the electron count being neither 18 nor 16, but also that d^7-Rh(II) should be paramagnetic. Whilst the ^{31}P{^{1}H} NMR spectrum indicates modest line-broadening (hhw = 20 Hz) due to fluxional vibration, the ^{1}H and ^{13}C{^{1}H} NMR spectra show sharp resonances within conventional ranges indicating that the complex is entirely diamagnetic with no indication of a paramagnetic shift effect. The μ-carbido resonance itself could still be detected, albeit with some difficulty, using ^{13}C enrichment, detected as a broad singlet at 466.0 ppm, slightly but not dramatically downfield of the rhodium(I) precursor.

This phenomenon may be considered from two perspectives. One possible reason is the delocalisation of the cumulenic bonding mode with a metallacarbyne. It was recently demonstrated that a Class C μ-carbido complex, **[RuPt(μ-C)Cl$_4$(py)$_2$(PCy$_3$)]**, reacted with dppm to afford the Class B complex **[RuPt(μ-C)Cl$_4$(dppm)$_2$]** (**Scheme 2.19,** see also **Chapter 1**). The octahedral d^6-ruthenium(II) and square planar d^8-platinum(II) centres respectively form triple and single bonds to the bridging carbido ligand, entirely consistent with the characteristic EAN requirements of the disparate metal centres.

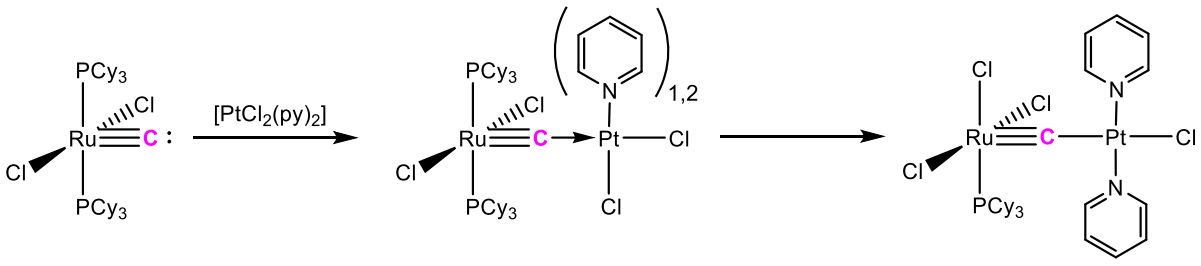

Scheme 2.19: Class C to Class B μ-carbido transformation

This transformation provided the first demonstration of the interconversion of two classes of μ-carbido complex (C → B). The treating the carbido ligand as a metallacarbyne, the EAN rules for Fisher carbyne ligand would lead to 18 and 16 electron rhodium (V) and (III) respectively, both of which are diamagnetic. Considering equal contributions from mirror-image canonical descriptions $Rh^{V}{\equiv}C–Rh^{III}$ and $Rh^{III}–C{\equiv}Rh^{V}$ accounts for a symmetrical geometry akin to a cumulenic Class A carbido (**Figure 2.13**).

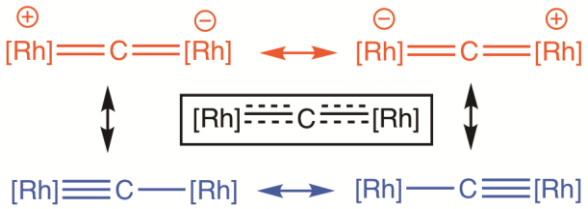

Figure 2.13: Possible delocalisation of μ-carbido ligand between Classes A and B

Alternatively, computational interrogation of the simplified analogue **$[Rh_2(\mu\text{-}C)Cl_4(\mu\text{-}dmpf)_2]$** (dmpf = 1,1'-bis(dimethylphosphino)ferrocene) reveals deep within the molecular orbital manifold, a pair of approximately orthogonal orbitals (HOMO-33, HOMO-36) that are fully π-bonding along the Rh–C–Rh spine (**Figure 2.14**) the occupation of which fully accounts for the spin-pairing and resulting diamagnetism of the complex.

The isolation of **23** it provides tangible evidence in support of the 1,3 – addition pathway for the previous oxidative addition reactions. The addition of a single stoichiometric amount of the X_2 species does indeed end up placing the halogen ligands on adjacent rhodium centres, rather than on one alone. Unfortunately, the steric encumbrance of the dppf ligands that allowed the single addition product to be isolated also presumably deters the addition of a second equivalent of Cl_2, preventing the synthesis of the analogous chlorocarbyne from this intermediate species.

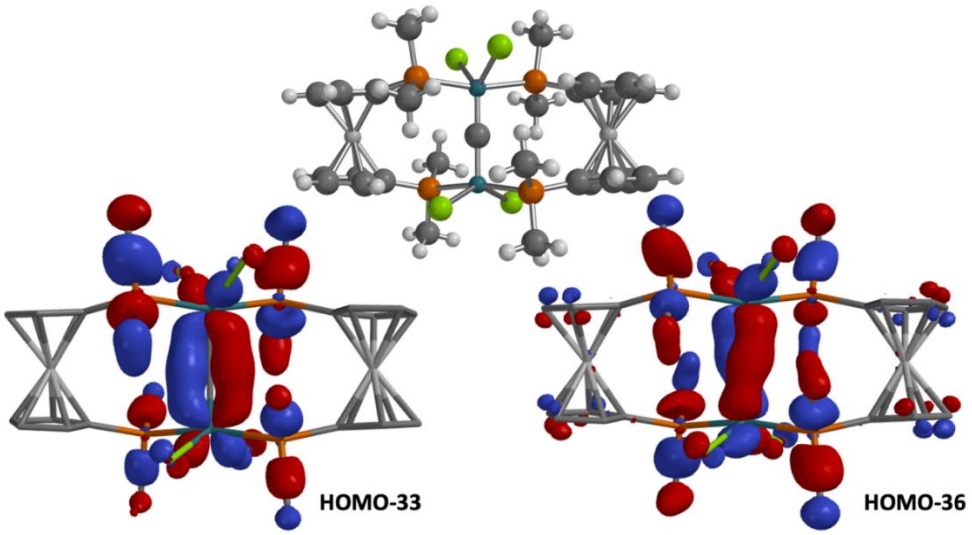

Figure 2.14: Optimised geometry and Rh-C-Rh π-bonding orbitals for the complex **[Rh_2(μ-C)Cl_4(μ-dmpf)$_2$]**. (DFT: B3LYP/6-31G*/LANL2D)

2.3.4 Summary

This chapter explored the synthesis and reactivity of the μ_2-halocarbyne ligand, which had been absent from the literature prior to this work. The μ-carbido complexes **[Rh_2(μ-C)X_2(μ-dppm)$_2$]** (where X = Cl, Br) underwent oxidative addition with mild halogenating agents iodobenzene dichloride and pyridinium tribromide. The oxidative addition pathway results in the migration of a halo ligand onto the μ-carbido, forming μ_2-chloro- and bromocarbyne complexes **[Rh_2(μ_2-CX)(μ-X)X_4(μ-dppm)$_2$]**.

Although the intimate mechanism for formation failed to be elucidated, the chlorination of the sterically larger dppf-bridged species **[Rh_2(μ-C)Cl_2(μ-dppf)$_2$]** resulted in a single oxidative addition step, forming the rhodium(II) μ-carbido complex **[Rh_2(μ-C)Cl_2(μ-dppf)$_2$]**. This supported the 1,3-addition mechanism. Although the symmetrical $Rh^{II}CRh^{II}$ geometry is superficially reminiscent of a conventional dimetallacumulenic Class A carbido description, simple electron counting arguments point to distinctive subtleties in the bonding.

Unfortunately, difficulties were encountered when testing the reactivity of the μ_2-halocarbyne complexes. The presence of five halide ligands and steric bulk of the dppm co-ligands around a sterically encumbered edge-shared bioctahedral core resulted in many processes leading to complex decomposition. One notable success is the formation of an unprecedented bridging

imidazolyl-carbyne species **[$Rh_2(\mu_2$-CIm)Br_2(Im)(HIm)(μ-dppm)$_2$]** through substitution with TMS-imidazole.

The field of μ_2-halocarbyne chemistry is far from developed and may benefit from refinements in the ancillary ligand-set may provide a more suitable candidate for future reactivity studies.

As of this date, results from this Chapter have contributed to the following publications:

1. H. J. Barnett, A. F. Hill, *Chem. Commun.,* **2019**, 55, 1734
2. H. J. Barnett, A. F. Hill, *Chem. Commun.*, **2020**, 56, 7738

2.4 EXPERIMENTAL

Synthesis of $[Rh_2(\mu_2\text{-}CCl)(\mu_2\text{-}Cl)Cl_4(dppm)_2]$ (18)

A mixture of $[Rh_2(\mu\text{-}C)Cl_2(dppm)_2]$ (30 mg, 0.028 mmol) and $PhICl_2$ (31 mg, 0.112 mmol) was dissolved in dry CH_2Cl_2 (10 mL). The orange solution immediately turned yellow and was stirred at room temperature for 15 hours. The solution was concentrated under reduced pressure and purified by chromatography using a silica gel column (CH_2Cl_2 eluent). A yellow band was collected and diluted with n-hexane. Slow removal of the dichloromethane under reduced pressure afforded yellow crystals that were isolated by filtration and dried in vacuo. Yield: 27 mg (0.022 mmol, 80%). ^{1}H NMR (400 MHz, $CDCl_3$) δ_H = 3.20 (d, $^2J_{PH}$ = 12 Hz, 2 H, PCH_2), 3.56 (d, $^2J_{HP}$ = 17 Hz, 2 H, PCH_2), 7.03 (t J_{PH} = 7 Hz, 7 H, C_6H_5), 7.18 (t, J_{PH} = 7 Hz, 3 H, C_6H_5), 7.31-7.36 (m, 7 H, C_6H_5), 7.52 (br. s, 8 H, C_6H_5), 7.91 (br. s, 7 H, C_6H_5). ^{13}C{^{1}H} NMR (192.5 MHz, $CDCl_3$) δ_C = 410.1 (br., μ_2-CCl), 135.9 (t^v, J_{PC} = 5 Hz, C_6H_5), 132.1 (t^v, J_{PC} = 5 Hz, C_6H_5), 131.1 (s, C_6H_5), 130.7 (s, C_6H_5), 130.1(br., C_6H_5), 128.1(t^v, J_{PH} = 5 Hz, C_6H_5), 127.9 (t^v, J_{PH} = 5 Hz, C_6H_5), 125.9 (t^v, J_{PH} = 25 Hz, C_6H_5), 24.9 (p^v,J_{PC} = 10 Hz, CH_2). ^{31}P{^{1}H} NMR (162 MHz, $CDCl_3$) δ_P = 3.38 (ddd, $^1J_{RhP}$ = 95 Hz, $^3J_{RhP}$ = 14 Hz, $^2J_{PP}$ = 2 Hz). IR ν_{max} (ATR, cm^{-1}): 3060, 2987, 1434, 852 (ν_{CCl}). MS (ESI, *m/z*): Accurate mass: Found 1162.8861 [M-Cl]$^+$. Calcd for $C_{51}H_{44}{}^{35}Cl_5P_4Rh_2$: 1162.8911. Anal. Found: C, 49.77; H, 3.76%. Calcd for $C_{51}H_{44}Cl_6P_4Rh_2.0.5(CH_2Cl_2)$: C, 49.65; H, 3.76%. A crystal for analysis could be grown from a chloroform solution. *Crystal data for* $C_{51}H_{44}Cl_6P_4Rh_2.CHCl_3$ (M_w = 1318.63 g.mol^{-1}): triclinic, space group *P*-1 (no. 2), a = 10.9452(5), b = 14.1036(7), c = 23.4931(8) Å, α = 81.467(4)°, β = 76.544(3)°, γ = 69.731(4)°, V = 3299.5(3) Å^3, Z = 2, T = 150.0(1) K, μ(Mo Kα) = 0.99 mm^{-1}, D_{calcd} = 1.327 Mg.m^{-3}, 70868 reflections measured (7.4° ≤ 2Θ ≤ 57.4°), 16211 unique (R_{int} = 0.122) which were used in all calculations. The final R_1 was 0.080 ($I > 2\sigma(I)$) and wR_2 was 0.223 (all data) for 592 refined parameters. CCDC 1880642.

Synthesis of $[Rh_2(\mu_2\text{-}CBr)(\mu_2\text{-}Br)Br_4(dppm)_2]$ (19)

A mixture of $[Rh_2(\mu\text{-}C)Cl_2(dppm)_2]$ (78 mg, 0.074 mmol) and AgOTf (46.8 mg, 0.182 mmol) was dissolved in dry CH_2Cl_2 (10 mL). The orange solution was stirred at room temperature for one hour, during which time a white precipitate formed. Excess KBr (61.5 mg, 0.517 mmol) was added, and the solution stirred for a further half hour. The solution was cannula filtered into a dry Schlenk tube, and pyridinium tribromide (63.0 mg, 0.197 mmole) added to the filtrate. The

red solution was stirred for 15 hours at room temperature. Ethanol was added, resulting in the deposition of an orange precipitate upon removal of solvent under reduced pressure. The orange precipitate was isolated *via* vacuum filtration and dried in vacuo. Yield: 72.0 mg (0.049 mmol, 67%). ^{1}H NMR (400 MHz, $CDCl_3$) δ_H = 3.13, 3.18 (m x 2, 2 H x 2, PCH_2), 7.00 (br., 7 H, C_6H_5), 7.15 (t, $^{3}J_{HH}$ = 7 Hz, 6 H, C_6H_5), 7.33 (br., 12 H, C_6H_5), 7.55 (br., 8 H, C_6H_5), 7.94 (br., 7 H, C_6H_5). ^{13}C{^{1}H} NMR (192.5 MHz, $CDCl_3$) δ_C = 136.3 (t^{v}, J_{PH} = 5 Hz, C_6H_5), 134.3 (t^{v}, J_{PH} = 5 Hz, C_6H_5), 132.2 (br. s, C_6H_5), 131.2 (br. s, C_6H_5), 130.8 (br. s, C_6H_5), 130.7 (br. s, C_6H_5), 128.0 (t^{v}, J_{PH} = 5 Hz, C_6H_5), 127.9 (t^{v}, J_{PH} = 5 Hz, C_6H_5), 127.8 (br. s, C_6H_5), 24.9 (p^{v}, J_{PC} = 10 Hz, PCH_2). ^{31}P{^{1}H} NMR (162 MHz, $CDCl_3$) δ_P = –5.73 (ddd, $^{1}J_{RhP}$ = 96 (*86*) Hz, $^{3}J_{RhP}$ = (*10*) Hz, $^{4}J_{PP}$ = (*2.3*) Hz). IR ν_{max} (ATR, cm^{-1}): 3053, 2963, 1433. MS (ESI, *m*/*z*): Accurate mass: Found 1386.6341 [M-Br]$^{+}$. Calcd for $C_{51}H_{44}{}^{79}Br_3{}^{81}Br_2P_4Rh_2$: 1386.6370. Anal. Found: C, 41.62; H, 3.10%. Calcd for $C_{51}H_{44}Br_6P_4Rh_2$: C, 41.78; H, 3.03%. Crystals for analysis could be grown from a CH_2Cl_2/toluene solution. *Crystal data for* $C_{51}H_{44}Br_6P_4Rh_2$ (M_w = 1466.02 g.mol^{-1}): tetragonal, space group $P4_32_12$ (No. 96), a = 15.3383(2), c = 25.9466(5) Å, V = 6104.3(2) Å^3, Z = 4, T = 150.0(1) K, μ(Cu Kα) = 10.19 mm^{-1}, D_{calcd} = 1.595 Mg.m^{-3}, 41974 reflections measured (9.0° ≤ 2Θ ≤ 142.4°), 5390 unique (R_{int} = 0.093) which were used in all calculations. The final R_1 was 0.094 ($I > 2\sigma(I)$) and wR_2 was 0.322 (all data) for 366 refined parameters with 414 restraints. CCDC 1880643.

Synthesis of [Rh$_2$(μ$_2$-CBr)(μ$_2$-Br)Br$_2$Cl$_2$(dppm)$_2$] (20)

An orange solution of [Rh_2(μ-CBr)(μ-Br)Br_4(dppm)$_2$] (0.051 g, 0.035 mmol) and [AuCl(SMe_2)] (0.031 g, 0.10 mmol) in dry CH_2Cl_2 (15 mL) was stirred at room temperature for 5 hours, with no observable colour changes. The solvent was removed under reduced pressure, and the orange residue subjected to silica gel chromatography. An orange band was eluted with neat CH_2Cl_2, and an orange precipitate was obtained upon addition of petrol and dried in vacuo. Phosphorus-31 NMR spectroscopy confirmed an approximately 3:1 ratio with **19**. Yield: 33.5 mg (0.024 mmol, 70%). ^{1}H NMR (400 MHz, $CDCl_3$) δ_H = 3.64 (br., 2 H, PCH_2), 7.00 (br., 8 H, C_6H_5), 7.13 (br., 4 H, C_6H_5), 7.33 (br., 8 H, C_6H_5), 7.45-7.53 (br. m, 10 H, C_6H_5), 7.66 (br., 4 H, C_6H_5), 7.83-7.95 (br. m, 6 H, C_6H_5). Remaining PCH_2 environment unable to be distinguished from **19**. ^{13}C{^{1}H} NMR (192.5 MHz, $CDCl_3$) δ_C = 136.2 (t^{v}, J_{PH} = 5 Hz, C_6H_5), 134.4 (t^{v}, J_{PH} = 5 Hz, C_6H_5), 132.1 (br. s, C_6H_5), 131.0 (br. s, C_6H_5), 130.7 (br. s, C_6H_5), 130.5 (br. s, C_6H_5), 128.1 (t^{v}, J_{PH} = 5 Hz, C_6H_5), 127.9 (t^{v}, J_{PH} = 5 Hz, C_6H_5), 127.6 (br. s, C_6H_5), 23.6 (p^{v}, J_{PC} = 10 Hz, PCH_2). ^{31}P{^{1}H} NMR (162 MHz, $CDCl_3$) δ_P = –3.90 (d, $^{1}J_{RhP}$ = 99 Hz). IR ν_{max} (ATR, cm^{-1}): 3052, 1435. MS (ESI, *m*/*z*):

Accurate mass: Found 1294.7416 [M-Br]$^+$. Calcd for $C_{51}H_{44}{}^{79}Br_2{}^{81}Br^{35}Cl_2P_4Rh_2$: 1294.7410. A crystal of suitable quality was grown from a CH_2Cl_2 evaporation but was Found to co-crystallise with **19** in a 3:1 ratio. *Crystal data for* $C_{51}H_{44}Br_{4.5}Cl_{1.5}P_4Rh_2$ (M_w = 1400.00 g.mol^{-1}): monoclinic, space group $P2_1/n$, a = 16.3889(7), b = 15.8545(8), c = 19.5530(11) Å, β = 93.167(4) °, V = 5072.8(4) Å^3, Z = 4 T = 150.0(1) K, μ(Cu Kα) = 4.45 mm^{-1}, D_{calcd} = 1.833 Mg.m^{-3}, 55823 reflections measured (7.4° ≤ 2Θ ≤ 46.0°), 10259 unique (R_{int} = 0.151) which were used in all calculations. The final R_1 was 0.094 ($I > 2\sigma(I)$) and wR_2 was 0.344 (all data) for 565 refined parameters with 61 restraints.

Synthesis of [Rh$_2$(μ$_2$-*p*-SC$_6$H$_4$Me)$_2$Br$_2$(dppm)$_2$] (21)

The complex [Rh$_2$(μ$_2$-CBr)(μ-Br)Br$_4$(dppm)$_2$] (20 mg, 0.014 mmol) was dissolved in 10 mL of THF and cooled to -78°C. In a separate Schlenk tube, 4-methylbenzenethiol (120 mg, 0.97 mmol) was dissolved in THF (6 mL) and cooled to -78 °C. A solution of ^{n}BuLi (1.6 M in hexanes, 0.13 mL, 0.16 mmol) was added to the thiol solution and left to stir for half an hour, during which time the temperature was slowly raised to 0 °C and then back down to -78 °C. A 2.0 mL aliquot of the lithium thiolate solution (ca 0.24 mmol, excess) was added dropwise to the orange bromocarbyne solution, and the mixture left to stir at -78 °C for two days. The deep red solution was gradually brought up to room temperature, and volatiles removed under reduced pressure. The red powder was dissolved in dichloromethane and subjected to silica gel chromatography. A red band was collected using neat dichloromethane, and a dark red precipitate formed upon addition of hexane, which was isolated and dried *in vacuo*. Yield: 6.2 mg (0.0045 mmol, 32%). ^{1}H NMR (400 MHz, $CDCl_3$) δ: 2.15 (br. s, 6 H, CH_3), 3.25 (br. s, 2 H, PCH_2), 4.44 (br. s, 2 H, PCH_2), 6.55 (d, J_{PH} = 7 Hz, 4 H, SC_6H_4), 6.89-6.97 (m, 24 H, C_6H_5 + SC_6H_4), 7.37-7.43 (m, 12 H, C_6H_5), 7.97 (br. s, 8 H, C_6H_5). Satisfactory ^{13}C NMR data were not acquired due to insufficient amounts. ^{31}P{^{1}H} NMR (162 MHz, $CDCl_3$) δ: 4.57 (d, $^1J_{RhP}$ = 128 Hz). IR ν_{max} (ATR, cm^{-1}): 3048, 1436. MS (ESI, *m/z*): Accurate mass: Found 1301.0151 [M-Br]$^+$. Calc. for $C_{64}H_{58}{}^{81}BrP_4Rh_2S_2$: 1301.0203. A crystal of a dichloromethane solvate suitable for analysis was grown from a CH_2Cl_2/toluene solution. *Crystal data for* $C_{64}H_{58}Br_2P_4Rh_2S_2{\cdot}CH_2Cl_2$ (M_w = 1465.67 g.mol^{-1}): monoclinic, space group $P2_1/c$, a = 12.9444(3), b = 22.1253(4), c = 22.4355(4) Å, β = 95.490(2)°, V = 6396.0(2) Å^3, Z = 4, T = 150.0(1) K, μ(Cu Kα) = 8.26 mm^{-1}, D_{calcd} = 1.522 Mg.m^{-3}, 21910 reflections measured (8.8° ≤ 2Θ ≤ 146.4°), 12054 unique (R_{int} = 0.031) which were used in all calculations. The final R_1 was 0.058 ($I > 2\sigma(I)$) and wR_2 was 0.172 (all data) for 696 refined parameters.

Synthesis of $[Rh_2(\mu\text{-C-Im})(Im)(HIm)Br_2(\mu\text{-dppm})_2]$ (22)

A flask containing **$[Rh_2(\mu\text{-CBr})Br_4(\mu\text{-dppm})_2]$** (40 mg, 0.029 mmol) was charged with 1,2-dichloroethane (20 mL) and TMS-imidazole (TMS-Im, 1.0 mL, 0.956 g.mL^{-3}, 6.8 mmol). The orange solution was heated to 50 °C for three hours during which time it turned dark pink in colour. The solution was concentrated under reduced pressure and the organic band extracted using CH_2Cl_2 and washed with H_2O. A dark purple solution was isolated and concentrated under reduced pressure to give a purple residue of **23** which retained excess imidazole as indicated by ^{1}H NMR analysis. Complex **23** was unable to be isolated entirely from the imidazole without the onset of decomposition. ^{1}H NMR (400 MHz, $CDCl_3$) δ: 3.48 (br. m, 2 H, PCH_2), 3.92 (br. m, 2 H, PCH_2), 6.89 (br. s, 2 H, Im), 7.08 (br. s, 11 H, C_6H_5 + Im), 7.18 (br. s, 11 H, C_6H_5 + Im), 7.39 (br. s, 27 H, C_6H_5 + Im), 7.54-7.65 (m, 25 H, C_6H_5 + Im), 7.95 (br. s, 19 H, C_6H_5 + Im). HIm NH environment not detected unambiguously. Useful ^{13}C NMR data could not be acquired due to excess imidazole obscuring peaks of interest. ^{31}P{^{1}H} NMR (162 MHz, $CDCl_3$) δ: 13.01 (br. m). IR ν_{max} (ATR, cm^{-1}): 3247 ν_{NH}, 1586 $\nu_{CN,}$ 1435 ν_{CC}. MS (ESI, *m/z*): Accurate mass: Found 1199.0256 $[M\text{-HIm-Br}]^+$, Calc. for $C_{57}H_{50}{}^{79}BrN_4P_4Rh_2$: 1199.0279. Crystals of poor analytical quality could be grown from the CH_2Cl_2 solution, with one molecule in the unit cell displaying extensive disorder. *Crystal data for* $^2/_3(C_{61}H_{40}Br_2N_5P_4Rh_2)\cdot{}^4/_3(C_{60}H_{42}Br_2N_6P_4Rh_2)$ (M_w = 2557.83 g.mol^{-1}): orthorhombic, space group *Imma* (No. 74), a = 44.653(4) Å, b = 21.6762(16) Å, c = 32.723(3) Å, V = 31,672(5) Å^3, Z = 6, T = 150.0(1) K, μ(Cu Kα) = 4.17 mm^{-1}, D_{calcd} = 0.805 Mg.m^{-3}, 50052 reflections measured (8.4° ≤ 2Θ ≤ 69.4°), 11851 unique (R_{int} = 0.257) which were used in all calculations. The final R_1 was 0.175 ($I > 2\sigma(I)$) and wR_2 was 0.522 (all data) for 470 refined parameters with 256 restraints.

Synthesis of $[Rh_2(\mu\text{-C})Cl_4(\mu\text{-dppf})_2]$ (23)

The complex $[Rh_2(\mu\text{-C})Cl_2(dppf)_2]$ (40 mg, 0.029 mmol) and $PhICl_2$ (17 mg, 0.062 mmol) were dissolved in CH_2Cl_2 (10 mL). The orange solution immediately turned dark green and was left stirring at room temperature for 1 hour. The solution was concentrated under reduced pressure and subjected to silica gel chromatography. A green band was isolated using neat CH_2Cl_2 as eluent, an diluted with *n*-hexane resulting in precipitation of the dark green product. This was isolated *via* filtration and washed with ethanol and hexane and dried in vacuo. Yield: 34 mg (0.023 mmol,

81%). ^{1}H NMR (400 MHz, $CDCl_3$) δ: 3.84 (br. s, 4 H, C_5H_4), 4.01 (br. s, 4 H, C_5H_4), 4.20 (br. s, 4 H, C_5H_4), 5.69 (br. s, 4 H, C_5H_4), 6.88 (br. s, 8 H, C_6H_5), 7.10 (br. s, 4 H, C_6H_5), 7.30 (br. s, 8 H, C_6H_5), 7.48-7.53 (m, 12 H, C_6H_5), 8.23 (br. s, 8 H, C_6H_5). ^{31}P{^{1}H} NMR (162 MHz, $CDCl_3$) δ: 28.49 (d, $^{1}J_{RhP}$ = 95 Hz).^{13}C{^{1}H} NMR (101 MHz, $CDCl_3$) δ: 137.6, 136.6, 133.8, 130.8, 130.4, 129.5, 128.0, 126.7 (8 x br., C_6H_5), 81.7 (C_α), 73.1 (br., C_β), 71.9 (br., C_γ). IR ν_{max} (ATR, cm^{-1}): 3050, 1433, 688 ν_{FeC}. MS (ESI, *m*/*z*): Accurate mass: Found 1467.8862 $[M]^+$, Calc. for $C_{69}H_{56}P_4{}^{35}Cl_3{}^{37}Cl^{56}Fe_2Rh_2$: 1467.8866. Anal. Found: C, 53.22; H, 3.37 %. Calcd for $C_{69}H_{56}Cl_4Fe_2P_4Rh_2.CHCl_3$: C, 52.95; H, 3.62%. Crystals suitable for analysis were grown in a chloroform solution. *Crystal data for* $0.5(C_{69}H_{56}Cl_4Fe_2P_4Rh_2)\cdot 5/4(CHCl_3)$ (M_w = 884.55 $g.mol^{-1}$): orthorhombic, space group *Fddd* (No. 70), *a* = 13.1949(4), *b* = 31.0550(6), *c* = 40.4621(7) Å, *V* = 16580.1(7) $Å^3$, *Z* = 16, *T* = 150.0(1) K, μ(Cu Kα) = 10.36 mm^{-1}, D_{calcd} = 1.417 $Mg.m^{-3}$, 22852 reflections measured (9.8° ≤ 2Θ ≤ 147.2°), 4177 unique (R_{int} = 0.032) which were used in all calculations. The final R_1 was 0.060 ($I > 2\sigma(I)$) and wR_2 was 0.191 (all data) for 222 refined parameters with 24 restraints. CCDC 1921282.

EPISODE THREE – REVENGE OF THE NHCS

CLASS D CARBIDO: THE FIRST STABLE *METALLA*-HETEROCYCLIC CARBENE COMPLEX

3.1 PREFACE

Published in "Chemistry in Australia" (Royal Australian Chemical Institute, May/June 2020 Issue)

Binuclear μ-carbido complexes feature a single atom of carbon "held" between two metal centres, and to date, all examples involve a linear MCM geometry. N-Heterocyclic Carbenes (NHCs), e.g., imidazolylidenes, are now ubiquitous ancillary ligands in coordination chemistry, enjoying extensive use in homogeneous catalysis. This raises the question of whether the two classes of compound might be combined by replacing the NCN component of the imidazolylidene with isolobal metal-ligand MCM fragments. This would in turn require the geometry at the intervening carbido atom to be bent. This has now been achieved with the first isolation, by H. J. Barnett and A. F. Hill at the Australian National University, of a transition metal analogue of an NHC (an MHC), in which the μ-carbido is indeed bent (A Dirhoda-Heterocyclic Carbene. *Angew. Chem. Int. Ed.*, doi:10.1002/anie.201912650).

The addition of an activated alkyne (DMAD = dimethylacetylenedicarboxylate) to a linear cumulenic (Rh=C=Rh) μ-carbido complex **$[Rh_2(\mu_2\text{-}C)Cl_2(\mu\text{-}dppm)_2]$** occurs across both rhodium centres to form a metalla-aromatic C_2Rh_2C core in which the μ-carbido ligand is by necessity bent (124°). The frontier orbitals of this metallacycle are remarkably similar in topology to those of an NHC suggesting nucleophilic character at the carbido carbon which would allow coordination of further metal centres. This could be demonstrated by coordination of the bent carbido to coinage metal chlorides to provide trigonal μ_3-carbido complexes **$[Rh_2M(\mu_3\text{-}C)(\mu\text{-}DMAD)Cl_3(\mu\text{-}dppm)_2]$** (M = Au, Cu). The coordination to metal centres thus confirms the dirhodium species to be the first isolated, stable example of a Metalla-Heterocyclic Carbene.

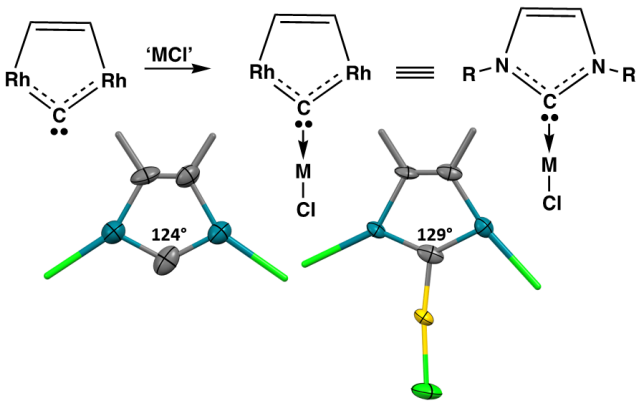

Figure 3.0: Overview of Rhodium-Heterocyclic Carbene reactivity and NHC comparison

3.2 INTRODUCTION

3.2.1 Arduengo Carbenes

The eponymous Arduengo carbenes, presaged by Wänzlick some 30 years earlier, are by and large the most commonly synthesised form of persistent carbenes. The synthesis of the stable free carbene species in 1991 started the explosion in carbene research that would continue to the present day.[146] Based on an imidazole C_2N_2C core, the steric bulk of the adamantyl groups in Arduengo's first carbene, in conjunction with the π-donation from the nitrogen lone-pairs into the carbene unoccupied *p*-orbital, help stabilise the free carbene species both sterically and electronically and allow the central carbon atom to use its radially directed lone pair in reactivity (**Figure 3.1**).

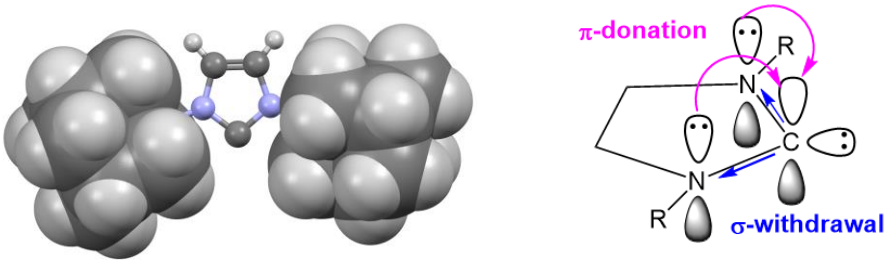

Figure 3.1: (left) Arduengo's isolated persistent carbene with adamantyl groups in space filling. (right) Frontier orbitals showing the stabilisation of the carbene singlet state through positively mesomeric (***M***$^+$) nitrogen π-donation

The stabilisation of this singlet state allows the carbene lone pair to act as a neutral two-electron donor of strong but tuneable σ-basicity in transition metal chemistry, and because of this, they have become a fashionable alternative to phosphine ligands. All of these factors combined have resulted in thousands of publications on NHCs, and a simple CCDC structural search of the NHC archetype bound to a transition metal returns around 11,000 results.[147]

N-Heterocyclic Carbenes (NHCs) have for some decades now been an extensively investigated topic of coordination chemistry, emerging as the ubiquitous ancillary ligand for tailoring metal centres for homogeneous catalysis. The NCN motif allows for both unprecedented mastery of the steric and electronic properties of the ligand and consequently the metal centre to which it is coordinated. NHCs have found success in catalysis as both stand-alone organic catalysts

or coordinated as a transition metal catalyst and have been widely deployed for *inter alia* olefin metathesis,[148] amination reactions,[149] alkene reduction,[150] and C–C cross-coupling processes.[151] As a result of their popularity, multiple important reviews have been published on their uses and properties, and it is not the place of this work to delve into them, but rather to show in the coming pages how NHC molecules can be altered to form "abnormal" or non-classical NHC species, with the inclusion of transition metals.

3.2.2 Main Group Abnormal NHCs

The continued strive to design new NHC ligands with unique steric and electronic properties logically developed into a shift from the archetypal or "normal" C_2N_2C imidazolium core. In the first instance, variation of the carbene carbon substituents according to their π-basicity has afforded stable P, S, and O-heterocyclic carbenes. An alternative route that has been taken has involved examining persistent carbenes on non-imidazolium rings, such a pyridine or perimidine.[152] However, the modification of particular relevance for this work considers substitution within the imidazolium ring for other heteroatoms (**Figure 3.2**). There are two key positions where this might take place and the obvious site for replacement is at the nitrogen position. It has been shown that one of the nitrogen atoms can be replaced by selective quaternary carbon groups (forming cyclic alkyl amino carbenes, or CAACs),[153] oxygen and sulfur (forming oxazol/thiazol-2-ylidenes),[154] and finally phosphorous (simply P-heterocyclic carbenes, PHCs).[155] In the case of oxygen and sulfur derivatives, complexes of these ligands long pre-dated their isolation as free carbenes. In addition to the nitrogen position, limited work has also been devoted to replacing one or both of the olefinic carbon units in the backbone of the NHC ligand, with results largely focused on the immediate neighbours to carbon: boron and nitrogen.[156]

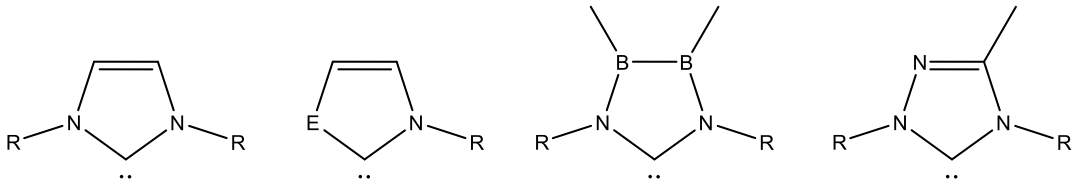

Figure 3.2: from left to right – standard imidazolium NHC template, *N*-substituted (E = O, S, PR, CR_2), and *C*-substituted for both boron and nitrogen

Given the superlative modularity, the potential for tailoring and creating "abnormal" NHCs are almost limitless.[xxxviii] The electronic character of the abnormal NHCs can extend far beyond that of the standard NHC ligands, including enhanced σ-donicity and π-acceptor character.

3.2.3 Metalla-*N*-Heterocyclic Carbenes (MNHCs)

N-tethered *M*NHCs

The logical pathway for functionalising an NHC with a transition metal is the incorporation of the metal complex as a substituent for one or both of the N-junctions in the imidazole framework. Despite the increasing interest in NHC ligand development towards catalysis, and the well-established imidazole ligand chemistry, there has been comparatively little done to blend these two fields together and examine the conversion of metal-imidazole complexes into potential metal tethered NHC complexes (**Figure 3.3**). Functionalising the NHC ligand with a transition metal as an integral component of the ring architecture would provide a class of compounds that we will refer to as *Metalla* N-Heterocyclic Carbenes, or MNHCs.

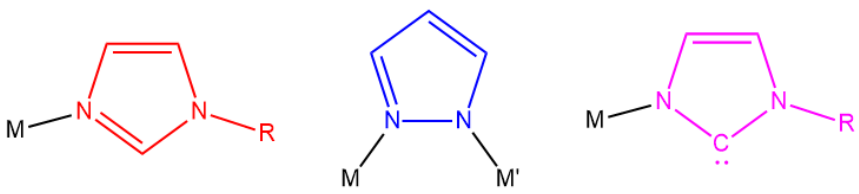

Figure 3.3: (left-centre) typical bonding modes of an imidazole- and pyrazolide-based ligands; (right) archetypical structure of an *N*-bound *M*NHC complex

One of the intricacies of imidazole reactivity that is apparent with the inclusion of an N-bound transition metal is the tautomerisation of the imidazole ligand between being N-bound or C-bound. The ammine N-bound and carbene C-bound tautomers have been seen to coexist when bound to a variety of transition metal complexes. It is also worth noting that this tautomerisation exists not only for imidazole ligands but has also been observed with pyridine to carbene

[xxxviii] The term 'abnormal' is used here with reference to the diversity of ring atom replacements as distinct from the class of mesoionic abnormal carbenes, for which only zwitterionic valence bond descriptions are valid.

transformations. The earliest example of this comes from Taube and Clarke, who in 1973 showed the acid-catalysed conversion of an N-bound imidazole ligand on ruthenium to the C-bound NHC complex (**Scheme 3.1**).[157] The ligand set on the ruthenium (II) complex contains purely σ-donor ligands (ammine and water), and the acid-promoted tautomerisation allows the imidazole ligand to transform into the NHC ligand, which has albeit modest π-acceptor character, hence alleviating the electron density build up on the d^6 (t_{2g}^6)ruthenium centre. Although the reverse tautomerisation was not observed in this case, more recent examples using the same transition metal prove this conversion is possible.[158] In this example, the ruthenium (II) centre, **[RuHCl(CO)(Im)(PPh$_3$)$_2$]**, contains ligands with noticeable π-acceptor character (specifically a *trans*-coordinated CO ligand). Because of this, the tautomerisation to the hard-donor nitrogen atom as an imidazole ligand obviates competition for retrodonation.

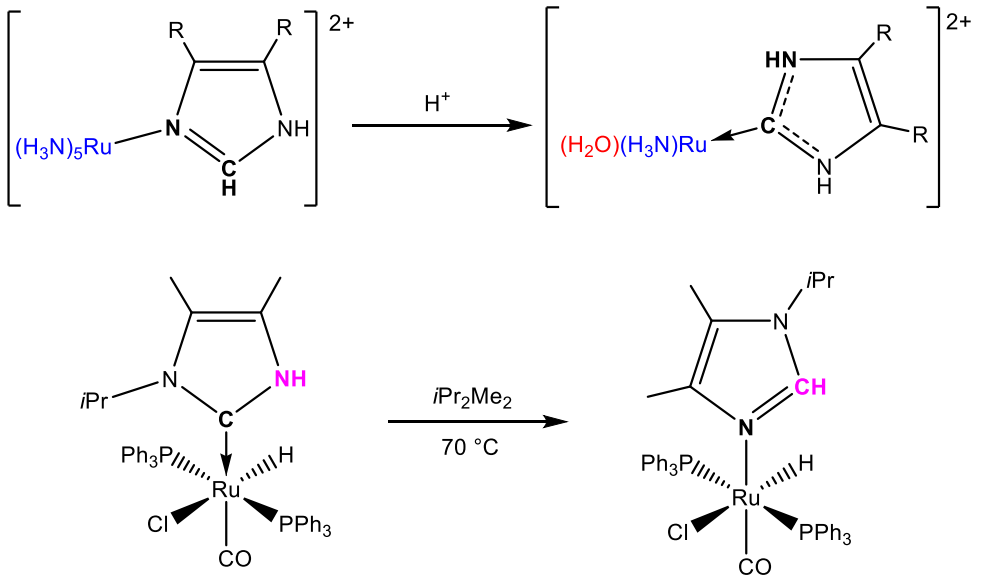

Scheme 3.1: (above) acid-catalysed N-C tautomerisation of a ruthenium complex; (below) base-promoted C-N tautomerisation of a ruthenium complex

Theoretical studies have been carried out on the ability of the transition metal complex to stabilise both the N and C tautomers in order to delineate factors that might favour a preferential binding mode. The limited results, however, show that rather expectedly, the preference of binding is heavily dependent on the transition metal and ligand set.[159] The results did show a proclivity for the heavier transition metals to favour the C-bound coordination, though the inclusion of a competitive π-acceptor ligand such as CO appeared to stabilise the N tautomer. Carbenes are

typically assigned as soft ligands in HSAB paradigm with a strong trans influence, with a lower electronegativity and stronger bond covalency. The more electronegative N-bound imidazole or pyridine ligands are conversely considered to be conventionally hard donor ligands with a low trans influence, which better suited to smaller metals with higher charge density.

An exemplary step in the field came in 2007 from Ruiz and co-workers, which saw a rather elegant tautomerisation of an N-bound NHC complex to form bimetallic MNHC species (**Scheme 3.2**).[160] Starting from the manganese N-bound imidazole species *fac*-**[Mn(Im)(CO)$_3$(bipy)]$^+$**, the base-promoted tautomerisation causes the manganese to migrate from the N-terminus to the central carbene position, forming a classical NHC carbene complex. What separates this work from the others is this tautomerisation could be reversed upon addition of a second metal, notably **[AuCl(PPh$_3$)]**. Upon deprotonation of the amine, coordination of the MNHC carbene to the gold centre takes place, as the manganese returns to the nitrogen position once again, forming a bimetallic MNHC species.

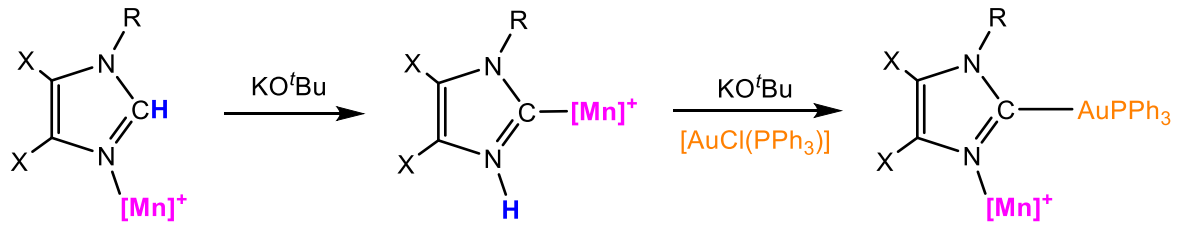

Scheme 3.2: Tautomerisation of N-bound manganese complex to a C-bound NHC, and further coordination to gold as an m-MNHC species. [Mn] = *fac*-**[Mn(CO)$_3$(bipy)]** (R = Me, Ph, X = Cl, H)

Transition Metals Incorporated Within the NHC Scaffold

The replacement of the backbone carbon atoms has been predominately accomplished with non-metallic heteroatoms, including boron and nitrogen (**Figure 3.2** above). Although transition metal complexes such as ferrocene and molybdenum have been combined with NHC ligands or atypical NHC architectures, only relatively recently was the first example of the incorporation of a transition metal centre in the imidazolium ring itself reported.

Wachter and co-workers in 1989 were successful in the remarkable cleavage of diphenyl carbodiimide by the molybdenum dimeric species **[CpMo(CO)$_2$]$_2$**, forming a bridging isocyanide ligand between the two molybdenum centres.[161] Upon sequential addition of carbon monoxide, the bridging isocyanide and imido ligands underwent insertion in between the Mo-Mo bond,

forming a MoN_2C core with the second molybdenum centre remaining bound to the carbene-like carbon atom (**Scheme 3.3**). This formed what might be considered to be a metalla-NHC, with the molybdenum centre replacing the two olefinic carbons, though the unbound MNHC was never isolated.

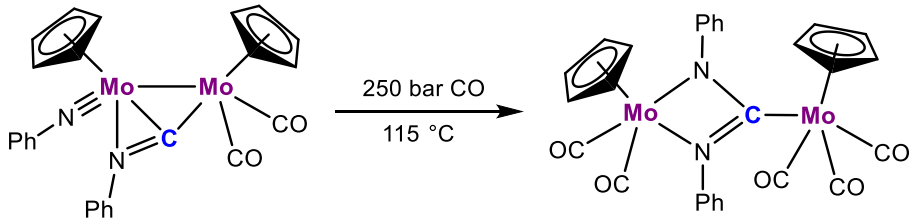

Scheme 3.3: Synthesis of a molybdenum based MNHC species

Including a metal into a traditional NHC archetype came much later, and the work has been largely carried out by Ruiz and co-workers since. The initial synthesis of the MNHC relied on the cyclisation and transmetallation of an acyclic diaminocarbene. The manganese complex *fac*-**[Mn{C(NHPh)(NHMe)}(CO)$_3$(bipy)]$^+$** undergoes an unusual reaction with **[AuCl(PPh$_3$)]** and KOH, affording an NHC-type ligand bound to the 'AuPPh$_3$' moity. The deprotonation and transmetallation of the diaminocarbene into an NHC is believed to proceed through a formamidinyl intermediate, with ultimate incorporation of the manganese centre into the newly formed imidazolium ring, replacing one of the traditional olefinic carbons.[162]

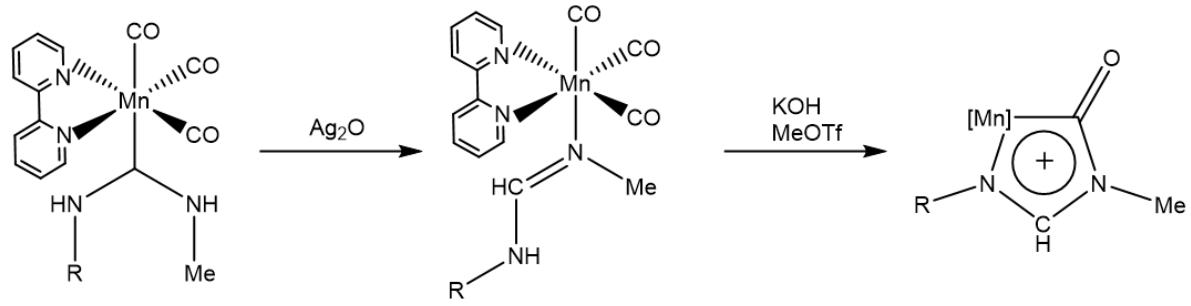

Scheme 3.4: Base promoted incorporation of a manganese centre to an MNHC precursor.
[Mn] = **[Mn(CO)$_2$bipy]**

The use of the manganese scaffold was revisited in 2015, however, with the notable difference of Ag_2O (a common reagent for metalating imidazolium salts) being used in conjunction with KOH to deprotonate and transmetallate the diaminocarbene ligand (**Scheme 3.4**).[163] The addition of Ag_2O results in the C-N shift of the diaminocarbene ligand, with the retention of the amino proton now transferring to the carbon atom. Following the sequential cyclisation to the MNHC, the carbon retains the bound hydrogen which is reminiscent of NHC imidazolium salt precursors. Like their organic counterparts, the MNHC precursors could be deprotonated selectively at the NHC-carbon using a non-nucleophilic base, and the free carbene could further coordinate to metal centres such as CuCl, **[AuClPPh$_3$]** and **[Rh(COD)Cl]$_2$**, furnishing bimetallic MNHC species. Once again, the free carbene species was not directly isolated, even at low temperatures with added trapping agents, illustrating its instability.

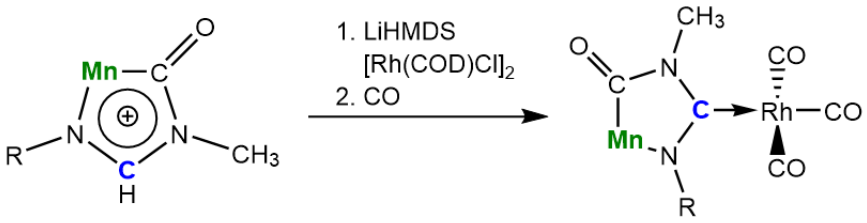

Scheme 3.5: Coordination of a manganese MNHC to **[RhCl(CO)$_2$]**, allowing for the calculation of TEP from the average ν_{CO}. Mn = **[Mn(CO)$_2$bipy]**

Results obtained for the manganese MNHC included the coordination of the MNHC initially to **[Rh(COD)Cl]$_2$**, followed by the addition of carbon monoxide to form *cis*-**[RhCl(CO)$_2$(MNHC)]** (**Scheme 3.5**).[163] The presence of two carbonyl ligands on the rhodium allowed the calculation of the Tolman electronic parameter (TEP = 2039 cm^{-1}), which lies towards the lower end of TEPs for NHCs (which typically range from 2035 to 2061 cm^{-1}), demonstrating the strong net electron donating ability of an MNHC.

A more systematic synthesis was also undertaken and involved the gradual incorporation of two bridging amino ligands between iron (**[CpFe(CO)(CNR)$_2$]** (R = xylyl)) and ruthenium (**[Ru(*p*-cymene)Cl$_2$]$_2$**) centres (**Scheme 3.6**).[164] Coordination of a terminal isocyanide ligand onto the ruthenium centre results in cyclisation through nucleophilic addition of the bridging amino ligands to the isocyanide ligand, forming again a traditional NHC archetype with the ruthenium centre occupying a position instead of a carbon atom.

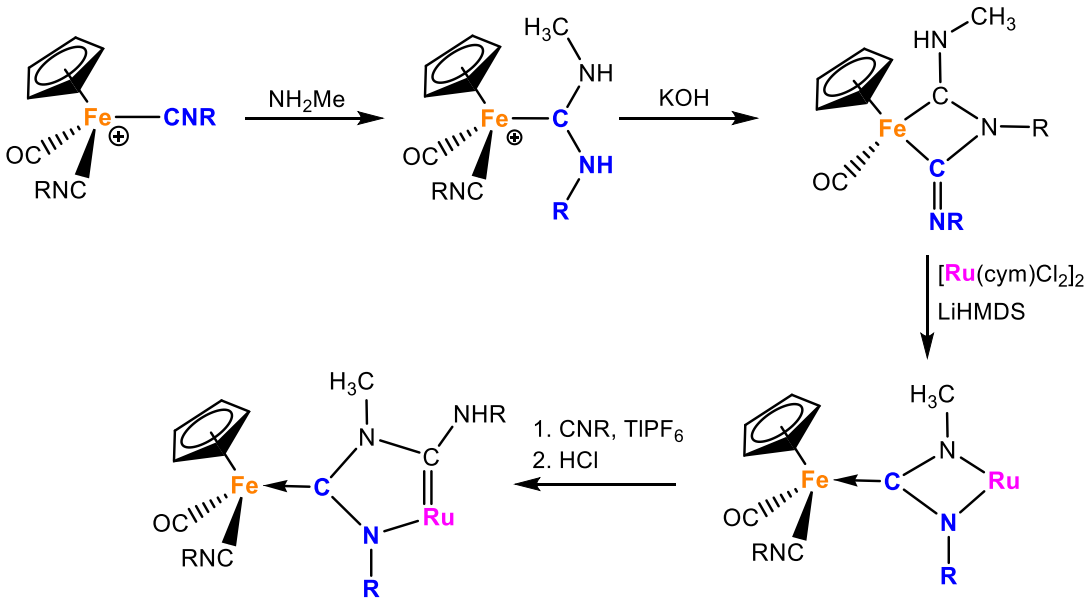

Scheme 3.6: Stepwise construction of a heterometallic MNHC complex from a diaminocarbene ligand (R = xylyl, Ru = **[RuCl(Cym)]**)

This systematic approach again contains the caveat of the coordinated metal centre being predetermined prior to MNHC synthesis, and the 'free' carbene species unbound to the iron complex was not formed. Unfortunately, the limited number of examples means that an analysis of the effect a transition metal has on the electronic properties of the MNHC ligand has yet to be addressed.

Fortunately, the work carried out on the iron-ruthenium MNHC complex also included a comparison to a purely organic NHC-iron analogue. The iron NHC complex **[CpFe(CO)(CNR)(NHC)]**$^+$ contains one important bond length deviation when the ruthenium centre replaces one of the backbone carbons (**Figure 3.4**). The nitrogen atom adjacent to the ruthenium has a slightly shorter bond length to the carbene carbon (1.362(9) for the NHC *cf.* 1.315(5) Å for the MNHC), suggesting a stronger π-contribution from the nitrogen atom when the ruthenium centre is present. The coordinated iron centre has both carbonyl and isonitrile co-ligands, and a comparison of the MNHC and NHC show a decrease in both υ_{CO} and υ_{CN} stretching frequencies when the ruthenium centre is included in the imidazolium ring. This gives credence to MNHCs having a stronger electron donicity than their organic counterparts, and it is important to note that inclusion of the metal centre has a more profound effect on the stretching frequencies than does functionalising of the NHC at one of the N-termini.

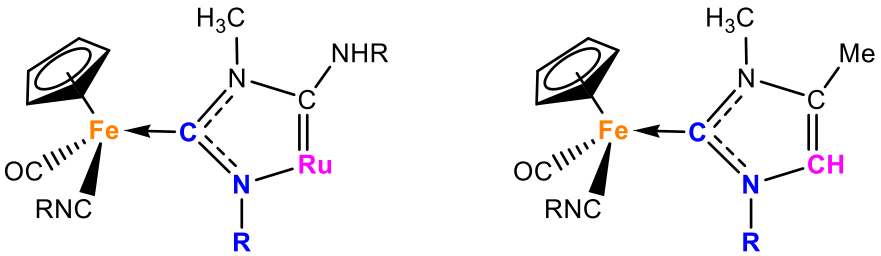

υ_{CN} = 2114
υ_{CO} = 1975

υ_{CN} = 2125
υ_{CO} = 1980

Figure 3.4: Comparison of iron MNHC (left) and NHC (right) complexes, with Fe-CN and CO IR stretches provided below. Ru = **[RuCl(Cym)]**

The most recent example of a metalla-NHC appeared in 2020 when Copéret, Goodpaster and Tonks generated titanocene adducts of carbodiimides **[Ti(κ²-*N,N'*-RNCNR)(η-C₅H₅)₂]** (R = *t*Bu, Cy) to furnish the first examples of a monometallic complex with a κ²-*N,N'* bound heterocumulene.[165] These complexes was theoretically predicted to be too high in energy to be isolable, though ambient conditions resulted in the clean and high-yielding conversion of **[Ti(Cp)₂(TMS-CC-TMS)]** into the four-membered metallocycle **[Ti(Cp)₂(κ²-*t*BuNCN*t*Bu)]** (**Scheme 3.6**).

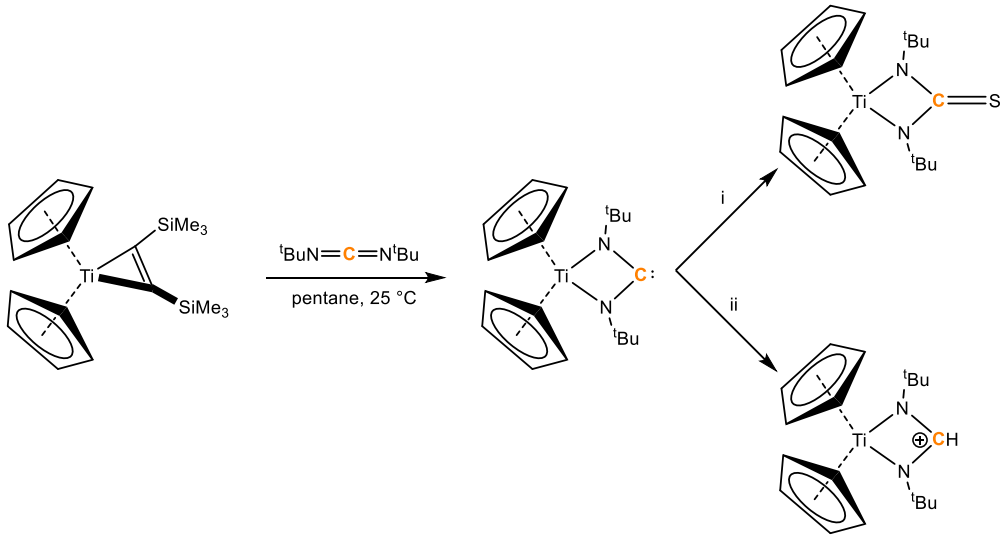

Scheme 3.7: Synthesis and reactivity of the MNHC **[Ti(Cp)₂(κ²-*t*BuNCN*t*Bu)]** (i = $^1/_8$ S_8, ii = [LuH]I)

Calculations performed on the metallacycle suggested nucleophilic character for the cyclic carbon, in a similar fashion to an Arduengo carbene or, more perhaps precisely, Betrand's borametallacyclic carbene ($^{i}Pr_2NB(ND^{i}PP)_2C$:).[167] This was demonstrated experimentally by the coordination of both sulfur and a proton through the reaction of the metallacycle with S_8 and 2,6-Dimethylpyridinium, respectively. Though only a brief exploration of reactivity has appeared, the titanacyclic carbene species presents an elegant metalla-*N*-heterocyclic carbene.

3.2.5 *Metalla*-Heterocyclic Carbenes (*M*HCs)

With the incorporation of a transitional metal into the backbone of the NHC scaffold having a profound influence on the electronics of the 'ligand,' the next step in the journey to combine metals and NHCs is to utilise transition metal complexes to *directly* stabilise the carbene in place of the imino groups bound to the carbene carbon. The replacement of the NCN archetype with metals would in theory create a *Metalla*-Heterocyclic Carbene, or MHC (**Figure 3.5**).

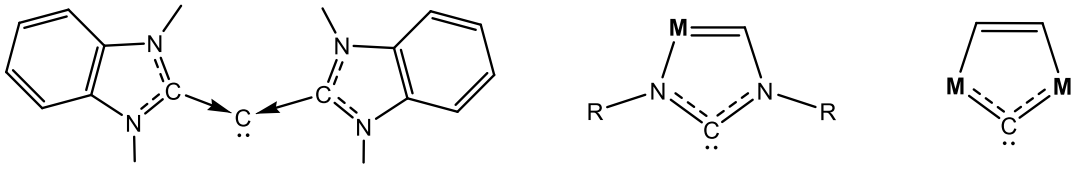

Figure 3.5: Example of a bent allene species,[167] an MNHC and a theoretical MHC

The only example to date of a metal complex pertaining MHC-like behaviour was first reported in 2014 by Takemoto and Matsuzaka.[168] The di-ruthenium species **[(Cp*Ru)$_2$(μ-NPh)(μ-CH)]BF$_4$** contains a bridging methylidyne unit, which was envisioned to undergo deprotonation to form the free bridging carbene species in a RuCRu motif. Although the methylidyne ligand could be deprotonated and coordinate to small organic molecules such as CO_2 *in situ*, the free carbene species could never be isolated following deprotonation. Even when the deprotonation was performed under extremely mild conditions, including temperatures of -90–70 °C, the Arduengo-esque carbene species (or potassium halide adduct) could only be inferred as an intermediate in the reaction.

Caveats aside, the di-ruthenium species has shown that the bridging methylidyne ligand when deprotonated can coordinate to main group atoms (forming μ_2-thio- and selenocarbonyls) and a variety of late transition metal centres (**[PtMe(PMe$_3$)$_2$]$^+$**, CuCN, AgOTf and AuCl) to form trimetallic μ_3-carbido ligands (**Scheme 3.8**).[169] The presence of the two adjacent transition metals have a remarkable effect on the carbene evident in the ^{13}C NMR spectrum. The resonance for the methylidyne precursor appears downfield at δ_C = 379 (identified using ^{13}C enrichment), while that for the presumed free carbene intermediate is exceptionally deshielded, being identified at 675 ppm, due presumably to the paramagnetic contribution which metal-carbene complexes are known to display. (See **Section 6.2**). The downfield shift of the free carbene indicates a strong π-interaction between the transition metals and the carbene, in a similar fashion to the nitrogen stabilisation of Arduengo carbenes.

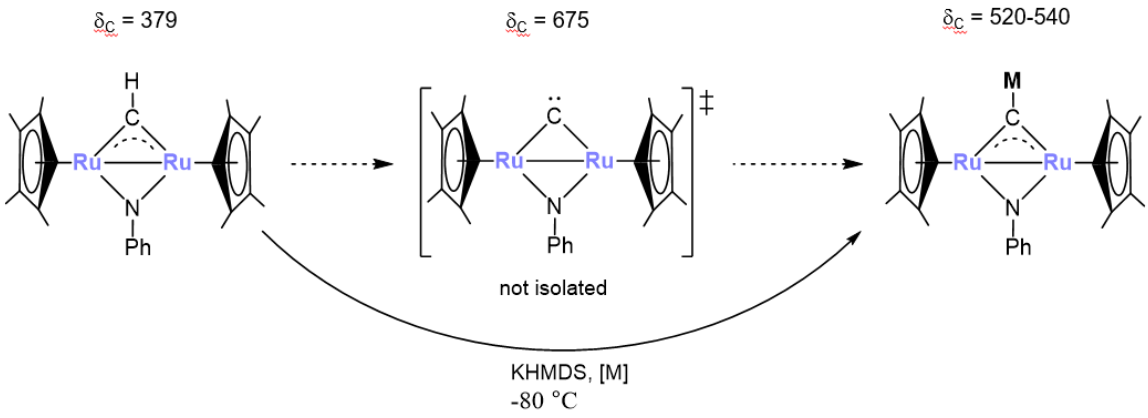

Scheme 3.8: Synthesis of μ_3-carbido complexes through a presumed but unstable carbene intermediate ([M] = CuCl, AgOTf, AuCl, **[PtMe(PMe$_3$)$_2$]$^+$**)

The work detailed above tantalisingly indicates the nascent field of MHC chemistry is potentially rich. The fact remains, however, that the incorporation of transition metals into the NHC scaffold has yet to provide stable and isolable Arduengo-type free carbene species. If free, stable MHC complexes could be isolated and characterised, it would establish a fourth class of carbido complexes which have up until now been divided into three classes (See **Section 1.2**).

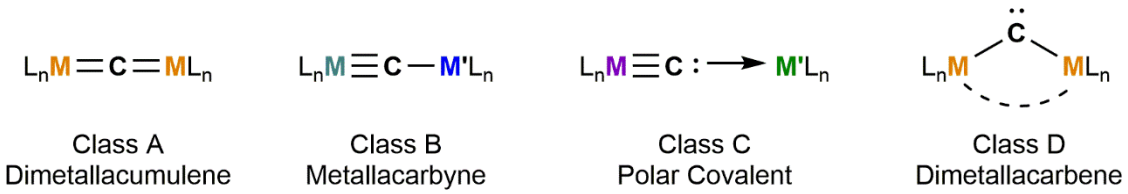

Figure 3.6: Updated classification convention of μ-carbido complexes, including the newly synthesised Class D complexes to be described herein

3.2.5 Rationale for this work

The introduction presented here tells the story of the gradual combination between organometallic and NHC chemistry. Though typically the two fields are combined through the incorporation of an NHC ligand to a metal complex, the incorporation of metals *into* NHC ligands is still in its infancy, and the generation of a stable Arduengo-type "*metalla*-heterocyclic carbene" is a feat yet to be accomplished. The work in this coming chapter addresses this challenge.

3.3 RESULTS AND DISCUSSION

3.3.1 The alkyne that could – Reaction with DMAD

The choice to revisit rhodium acetylene chemistry followed naturally from the interesting cycloaddition processes that ensue between CS_2 and **[$Rh_2(\mu\text{-}C)Cl_2(PPh_3)_4$]** or **[$Rh_2(\mu\text{-}C)Cl_2(dppm)_2$]** (**Section 1.3**). Although attempts to install an alkynyl ligand in place of the terminal chloride ligand in either of these complexes were unsuccessful, the reactivity of free alkynes was of interest in the context of cyclo-addition of Rh–C and C–C multiple bonds, akin to the celebrated olefin metathesis reaction.[170]

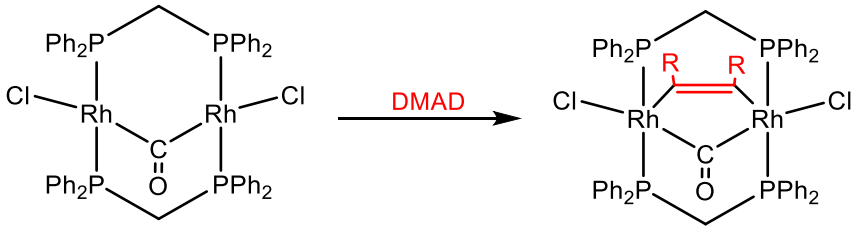

Scheme 3.9: Coordination of DMAD across a dirhodium A-frame complex (R = CO_2Me)

The first acetylene to be tested was rather obviously dimethylacetylene dicarboxylate (DMAD). Being an extremely electrophilic acetylene due to the two ***M*** ester substituents, DMAD is a highly activated dienophile and is ubiquitous in cycloaddition chemistry, and often results in atypical reactivity compared to common acetylenes. This distinctive reactivity relative to simple alkynes is also a recurrent feature of the organometallic chemistry of DMAD. Drawing from literature precedent, DMAD has been seen to readily undergo alkyne addition to bridge two metal centres in dirhodium A-frame complexes, though it must be noted that the species in question each contained an already bent, bridging ligand (carbonyl, chloride, or methylidene) which required no geometric rearrangement (**Scheme 3.9**).[171] Given the μ-carbido ligand was presumed to not 'bend' out of the Rh-Rh vector, it was though that DMAD would react with one of the Rh=C bonds (**Scheme 3.8**) or a single coordinatively unsaturated rhodium centre.

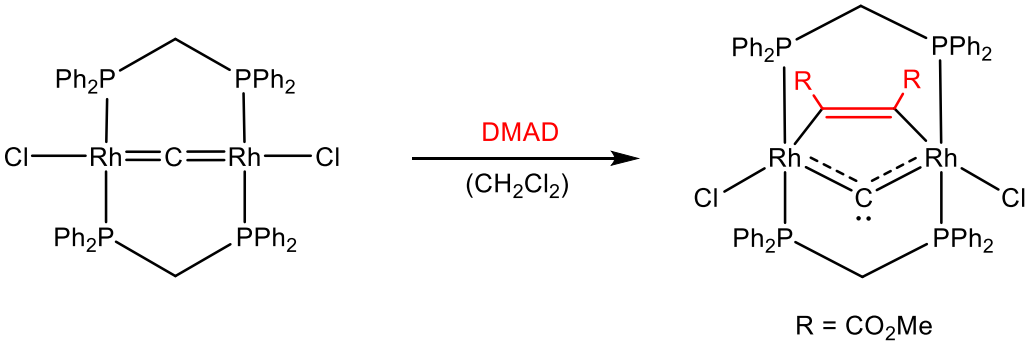

Scheme 3.10: Synthesis of **[Rh₂(μ-C)(μ-DMAD)Cl₂(μ-dppm)₂]** (**24**, R = CO_2Me) from **1**

Due to the same issues that have been encountered previously with steric hindrance of the carbido core, **[Rh₂(μ-C)Cl₂(dppm)₂] (1)** was chosen as the starting complex due to the enhanced accessibility of the Rh=C bonds. A yellow CH_2Cl_2 solution of **1** immediately turns red upon addition of DMAD, and reaction monitoring through $^{31}P\{^1H\}$ NMR spectroscopy confirms that the reaction is complete within 5 minutes. The NMR spectra of the red solution shows complete loss of the starting material environment, and the presence of a single, new environment (δ_P = 12.5 ppm). The phosphorus environment displays the typical doublet from the $^1J_{RhP}$ coupling (137 Hz), and yet, shows no signs of a distinct $^3J_{RhP}$ which is quite pronounced in the starting material (~40 Hz). What is immediately noteworthy is what the single, symmetrical environment implies, i.e., that the reaction with DMAD produces a symmetrical product where once again all four phosphine atoms are chemically equivalent. The reduction in $^1J_{RhP}$ suggests an increase in coordination number at the rhodium centres (due to lower s-character), though remains significantly larger than observed for the six-coordinate halocarbyne species previously identified (130 Hz *cf.* 95 Hz for the six-coordinate halocarbynes *vide supra*). As with the μ²-halocarbyne complexes, the ^1H NMR spectrum shows two distinct environments for the dppm methylene hydrogens (δ_H = 2.29, 3.60 ppm), which suggests that the complex contains two internal mirror planes (C_{2v}), but not three (D_{2h}).

The ^1H NMR spectrum also showed only a single environment for what was found to be the DMAD methoxy hydrogens at 2.39 ppm, integrating to six hydrogens. The $^{13}C\{^1H\}$ NMR spectra under standard conditions showed the expected environments for the dppm co-ligands, but also broad environments (δ_C = 50.3, 80.4) for the DMAD methoxy and (previously) acetylenic environments respectively. Although the expected ester carbon on DMAD was unable to be located directly from $^{13}C\{^1H\}$ NMR spectra, the strong correlation between the methoxy

hydrogens and the ester carbon resulted in a strong cross peak being observed in the 2D ^{1}H-^{13}C HMBC NMR spectrum, appearing downfield at 166.1 ppm. Unfortunately, the same issues arose when attempting to locate the μ-carbido environment in the 1D ^{13}C NMR spectra, with the expected triplet of pentet splitting making the resonance elusive.

The high-resolution ESI-MS confirmed the installation of a single moiety of DMAD, with the major fragmentation appearing at 1163.04340 *m/z* ($C_{57}H_{50}{}^{35}ClO_4P_4{}^{103}Rh_2$ $[M–Cl]^+$ = 1163.04527 *m/z*) corresponding to the typically seen loss of a chloride ligand. Through X-ray crystallography, the molecular structure was able to be confirmed (**Figure 3.7**) showing remarkably the alkyne incorporation of DMAD across the Rh=C=Rh linkage in a formal [2+3] cyclo-addition.

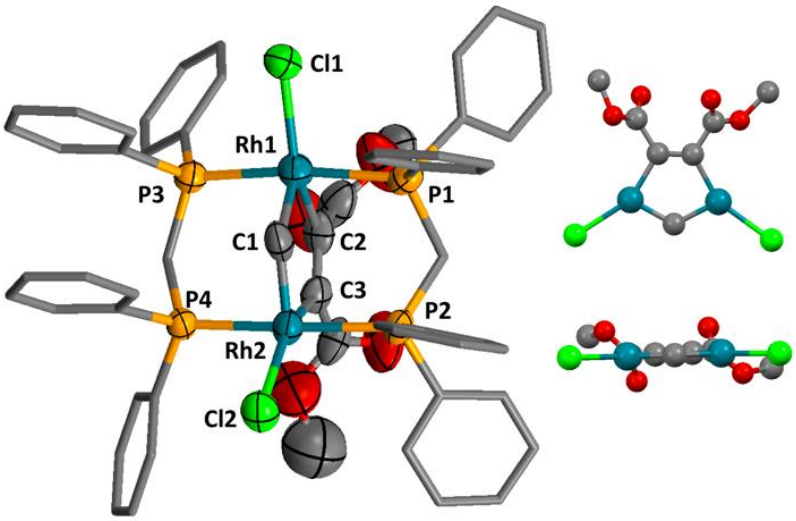

Figure 3.7: Molecular structure of **[Rh_2(μ-C)(μ-DMAD)Cl_2(μ-dppm)$_2$] (24)** (50% displacement ellipsoids, hydrogen atoms omitted and phosphine substituents simplified). Selected distances [Å] and angles [°]: Rh1–Cl1 2.451(4), Rh1–C2 2.008(14), Rh1–C1 1.851(19), Rh2–Cl2 2.447(4), Rh2–C1 1.860(16), Rh2–C3 2.006(17), C2-Rh1-Cl1 154.3(5), C1-Rh1-Cl1 117.3(5), C1-Rh1-C2 88.4(7), C1-Rh2-Cl2 118.3(6), C1-Rh2-C3 88.6(8), C3-Rh2-Cl2 153.0(5), Rh1-C1-Rh2 = 124.7(10)

Because of the sterically encumbering nature of the dppm ligands, the unit cell of **24** is isomorphous to its precursor **1**. The DMAD ligand binds symmetrically (μ:σ,σ' fashion) across the Rh=C=Rh plane, accounting for the high symmetry implicit in the NMR spectra. Both rhodium centres are now five-coordinate, as suggested by the reduction in the $^{1}J_{RhP}$ value relative to the precursor. The Rh-C-C-Rh geometry would not be able to also accommodate a linear RhCRh carbido linkage and the μ-carbido ligand is found to be displaced substantially the Rh···Rh

vector to form a five-membered bimetallacycle. The DMAD ligand coordination is reminiscent of the previously described carbonyl complex **[Rh$_2$(μ-CO)(μ-DMAD)Cl$_2$(μ-dppm)$_2$]**, with the two rhodium-carbon bonds (2.008(14), 2.006(17) Å) and vinylic C=C (1.30(2) Å) being comparable (2.004(6) and 1.32(1) Å, respectively).[172] The Rh-C bond lengths to the bent carbido are shorter than expected for Rh-C single bonds (1.851(19) and 1.860(16) *cf.* ~2.1 Å) and combined with the essentially sp^2 hybridized geometry at the carbide carbon (Rh1-C1-Rh2 = 124.7(10)°), suggests a retention of multiple-bond character. In a similar fashion to the halocarbyne complexes, the two rhodium atoms are situated too far apart to invoke any formal bonding interaction (Rh1-Rh2 = 3.279(2) Å, $2r_{cov}$(Rh) = 2.84 Å).

Comparing the structure of **24** with the closely related ketonic species **[Rh$_2$(μ-CO)(μ-DMAD)Cl$_2$(μ-dppm)$_2$]**, there are a number of similarities. The terminal chloride ligands in both cases are positioned on the same face as the carbonyl/carbido ligand, rather than the face of the added DMAD or colinear with the Rh···Rh vector. The geometry of the rhodium centres is therefore best described as a distorted square-based pyramid, with the bridging ligand taking the apical position. The dppm co-ligands are both folded in a geometry that overlaps the methylene linker unit with the more crowded face of the complex where DMAD has inserted, which allows for the phenyl rings to occupy space on the more open face. This is also the case seen in the μ$_2$-halocarbyne complexes (in **Section 2.3**) and gives rise to the two distinct hydrogen environments in the ^{1}H NMR spectra. The Rh···Rh separation is slightly shorter in **24** (3.279(2) *cf.* 3.3542(9) Å) possibly due to the higher π-character of the μ-carbido linkage (*vide infra*).

One of the recurrent issues to plague characterisation of the linear μ-carbido complexes discussed previously is the weak nature of asymmetric $\upsilon_{Rh=C=Rh}$ stretching mode in the IR spectra. Competing with more prominent stretches and bends from the phenyl rings, the expected absorption around 1000 cm^{-1} is rarely detected with confidence. However, with the μ-carbido ligand now bent out of plane, theoretical studies (*vide infra*) show a much stronger stretch that corresponds to the symmetric Rh=C=Rh stretch, which was predicted to appear around 800 cm^{-1}. Because the metallacycle **24** is largely identical in structure to its precursor, the 'fingerprint' regions of the IR spectra of the two complexes are largely identical. Taking a difference spectra, the appearance of a new band at 798 cm^{-1} can be confidently assigned to the μ-carbido ligand. The presence of the two ester groups on the μ-DMAD ligand are manifest with typical strong absorptions at 1732 and 1700 cm^{-1}.

Although analogous complexes have been formed with bridging carbonyl, methylidene or methylidyne units, the DMAD installation on **[Rh$_2$(μ-C)(μ-DMAD)Cl$_2$(μ-dppm)$_2$]** provides the first characterised example of a stable bent μ-carbido complex.

^{13}C Labelling

Because of the rather unique chemical environment that the bent μ-carbido was in, it seemed important to try and identify the associated resonance using ^{13}C NMR spectroscopy. Due to the relative insolubility of the complex, and the broadness of the peaks in the ^{31}P NMR spectrum, the carbon environment was unable to be detected using the 2D ^{31}P-^{13}C HMQC protocol designed for revealing the resonances of other recalcitrant μ-carbido complexes (see **Chapter 6**). However, the ^{13}C enriched isotopologue **[Rh$_2$(μ-^{13}C)(μ-DMAD)Cl$_2$(μ-dppm)$_2$] (24')** could be successfully synthesised under identical conditions. The ^{13}C{^{1}H} NMR spectrum of this enriched sample revealed a broad resonance far downfield at 563.0 ppm (**Figure 3.8**), displaying coupling to both ^{103}Rh ($^1J_{RhC}$ = 30 Hz) and ^{31}P ($^2J_{PC}$ = 10 Hz) nuclei. The downfield shift of the bent carbido environment, even relative to the linear μ-carbido complexes, is the most downfield shift for an isolated carbido complex to date.

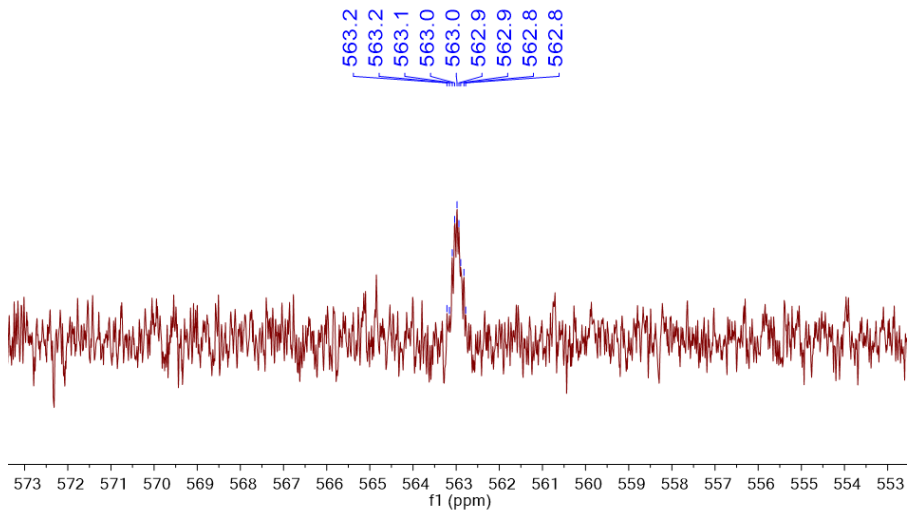

Figure 3.8: ^{13}C{^{1}H} NMR spectrum extract of **[Rh$_2$(μ-^{13}C)(μ-DMAD)Cl$_2$(μ-dppm)$_2$]**

3.3.2 Studies on Bonding

The metallacycle compound presents a similar electronic quandary that a few dirhodium compounds in this work have already encountered. Without the inclusion of formal Rh–Rh bonding character, the two rhodium centres would be paramagnetic rhodium (II), however, the diamagnetic nature of the complex implicit in the NMR spectra calls for an explanation. The planar nature along the five-membered ring (maximum deviation = 0.011 Å) and geometrical data are consistent with the formation of a *pseudo*-metalla-aromatic complex, consisting of a delocalised π-system across the CRh_2C_2 ring. The bonding of the metallacycle may be described using the canonical modes in **Figure 3.9**, some of which place negative charge(s) on the carbido carbon. The issue of 'metalla-aromaticity' is somewhat clouded by the number of electrons provided by the metal to an overall Hückel-type electron inventory, i.e., two occupied orbitals of π-symmetry with respect to the ring are available on each rhodium.

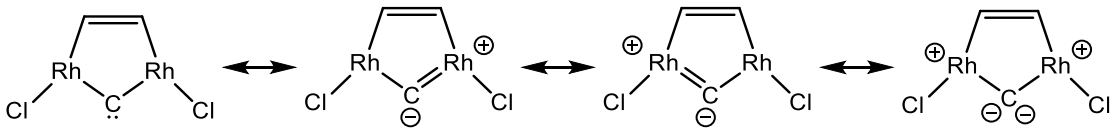

Figure 3.9: Possible canonical descriptions of the delocalised bonding of the CRh_2C_2 ring

The delocalised π-system accounts for the diamagnetic rhodium centres evident from experimental data. The electron delocalisation across the ring is further supported through computational interrogation. Modelling of the simpler analogue **$[Rh_2(\mu\text{-}C)Cl_2(\mu\text{-}HCCH)(\mu\text{-}dmpm)_2]$** shows extensive delocalisation across the metalla-aromatic system, but what is more interesting, is the comparison between this system and those of a free NHC (**Figure 3.10**).

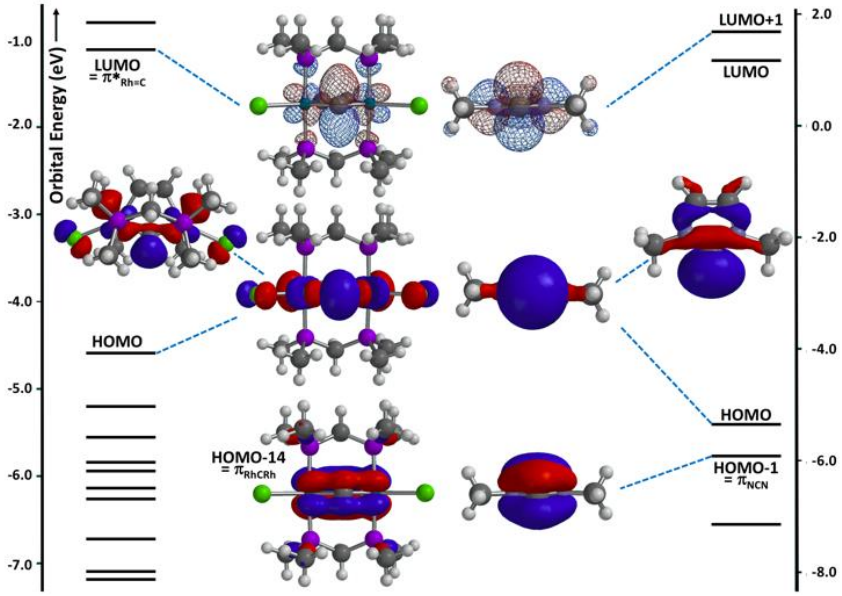

Figure 3.10: Frontier orbitals of interest for **[Rh_2(μ-C)Cl_2(μ-HCCH)(μ-dmpm)$_2$]** and *N,N'*-dimethylimidazolylidene (DFT: ωB97X-D/6-31G*/LANL2Dζ)

The HOMO is completely in the plane of the metallacycle, of σ-symmetry and includes contribution from an e_g-type orbital on each metal, in addition to a large region facing outwards from the bent carbido atom. Similarly, the LUMO, with π-symmetry with respect to the ring plane, is primarily localised on the carbido atom but with notable contribution, in a Rh-C π* antibonding manner, of a t_{2g}-type orbital on each rhodium. The μ-carbido atom was calculated to carry a substantial negative charge (Natural = -0.41, Mulliken = -0.24, Electrostatic = -0.87). The rhodium-carbon interactions have considerable multiple bond character (Löwdin B.O. 1.71) relative to those of the Rh-alkenyl carbons (0.98).

Absolute Hardness

There are multiple theoretical measures that can be used in an attempt to quantify aromatic behaviour, which has been one of the most enduring challenges in theoretical chemistry. The most straightforward measure is absolute hardness (η), which simply takes the energy gap between the HOMO and LUMO and halves the value for a good approximation.[173] In theory the greater the value of η, the greater aromatic character the system presents. In comparison to benzene, it has been seen that metallabenzene complexes often have values of 25-70%, suggesting a weaker but present aromaticity.[174] The HOMO-LUMO energy difference calculated for the metallacycle **24**

came to 7.9 eV using DFT studies (ωB97X-D/6-31G*/LANL2DZ)), which gives an absolute hardness value of 3.95. The accepted absolute hardness for benzene using DFT methods is 6.47, meaning that the metallacycle contains approximately 60% aromatic behaviour relative to benzene, which lies well above the 20% threshold deemed for there to be considered aromatic character and in a similar range to NHC ligands.[175]

3.3.2 On the nature of alkynes

Attempted reactivity with carbodiimides

Following on from the successful coordination of *t*-butyl carbodiimide to **[Ti(Cp)$_2$(TMS-CC-TMS)]** to form **[Ti(Cp)$_2$(κ^2-*N,N'*-^{t}BuNCN^{t}Bu)]** by Coperet and co-workers, the brief reactivity of carbodiimides was examined (**Scheme 3.9**), noting that carbodiimides form betaine adducts with more conventional NHCs[176] and that carbodiimides are isolobal with CS_2 (**Chapter 1.3**). Both the trimethylsilyl- and cyclohexyl carbodiimide were investigated, however, neither displayed any reactivity when mixed in excess with **[Rh$_2$(μ-C)Cl$_2$(μ-dppm)$_2$]**, under ambient or forced (specify) conditions (**Scheme 3.11**). The rhodium μ-carbido species in comparison to the titanocene species present two very different electron systems, so it is perhaps not unsurprising that the reactions failed.

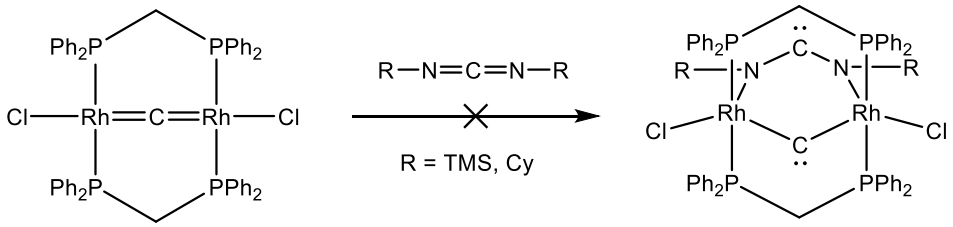

Scheme 3.11: Failed reactivity of **1** to carbodiimides

Attempts to form an inorganic betaine analogue were also unsuccessful, with the carbodiimides displaying no reactivity with the MHC species **24.**

Alkynes with Electron-Donating-Groups

With the success of DMAD and failure of the carbodiimides, the next step in developing a library of bent-carbido complexes was to determine the range and types of common alkynes that could potentially undergoe [3+2] cycloadditions with the linear cumulenic carbido unit. Within the A-frame class of compounds, previous alkyne coordination to dirhodium complexes are limited to DMAD and hexafluoro-2-butyne (HFB) by Cowie,[172a] though the latter encounters problems in the modern world as a restricted fluorocarbon. Extensive studies by Dixon on dirhodium HFB complexes, e.g., **[Rh$_2$(μ-HFB)(CO)$_n$(η-C$_5$H$_5$)$_2$]** (n = 1,2) have been described previously.[177]

To determine if the alkyne needs to be a potent dienophile (containing electron withdrawing substituents), common electron rich alkynes were tested in comparison. The alkynes diphenylacetylene, bis(trimethylsilyl)-2-butyne and 4-octyne were all treated with **[Rh$_2$(μ-C)Cl$_2$(μ-dppm)$_2$]**, and even under more forcing conditions (specify), there was no observable reactivity with either visual or ^{31}P NMR spectroscopic monitoring. None of the alkynes tested were thought to present any restrictive steric issues, and therefore the failure to observe any reactivity must originate from the electron-rich alkyne and rhodium centres being incompatible.

Reaction with ethyl-4,4,4-trifluoro-2-butynoate

To confirm this hypothesis, our attention returned to other common alkynes that typically act as strong dienophiles. With CoVid-19 related difficulties in acquiring hexafluoro-2-butyne hampering progress, commercially available unsymmetric alkynes were instead investigated. The alkyne ethyl-4,4,4-trifluoro-2-butynoate (ETFB) combines one CF_3 unit of hexafluoro-2-butyne with an ester substituent similar to the methyl ester group of DMAD, which makes the alkyne electron deficient and presumably well-disposed towards coordination and metallacycle formation.

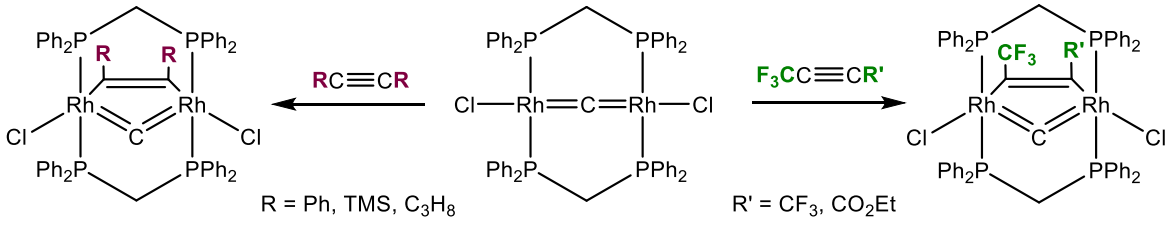

Scheme 3.12: Synthetic routes to potential metalla-aromatics using alkynes with Electron Donating Groups (left) and Electron Withdrawing Substituents (right)

Taking a yellow CH_2Cl_2 solution of **1**, there was no instant colour change when ethyl-4,4,4-trifluoro-2-butynoate was added. However, within minutes the solution turns red in colour, and in an identical manner, a red product begins to precipitate from the solution. The ESI-MS of the red powder confirms the coordination of the alkyne, with the expected $[M\text{-}Cl]^+$ fragmentation at 1198.0452 *m/z* (*cf.* $C_{57}H_{49}{}^{35}ClF_3O_4P_4{}^{103}Rh_2$: 1187.0434 *m/z*) and the dicationic $[M\text{-}2Cl]^{2+}$ fragment at 576.0 *m/z* matching the simulated patterns perfectly. Unfortunately, the extreme insolubility of **$[Rh_2(\mu_2\text{-}C)(\mu\text{:}\sigma,\sigma'\text{-}F_3C\text{-}CC\text{-}CO_2Et)Cl_2(\mu\text{-}dppm)_2]$ (25)** rendered NMR analysis decidedly problematic. The single CF_3 group can be detected in the ^{19}F NMR spectrum at -49.15 ppm, and the ethyl ester hydrogens are distinct as a triplet at 0.25 ppm (J = 7 Hz), and a quartet at 3.01 ppm (J = 7 Hz). The facial asymmetry is reflected again in two distinct methylene environments on dppm at 2.38 and 3.55 ppm, all of which could be confirmed through $^1H\text{-}^1H$ COSY correlation studies. Because of the introduced asymmetry, the previously equivalent phosphine ligands would be split into an AA'BB'XX' system, and two heavily coupled environments at 10.96 and 11.54 ppm in the $^{31}P\{^1H\}$ NMR spectrum support the installation of ETFB ($^1J_{RhP}$ = 134 Hz) with adoption of C_s molecular symmetry. The key functional group differences, namely the single ester group and new CF_3 group, were expected to be easily identifiable in the infrared spectra. Without the second ester group, the carbonyl region was notably simpler with only a single band at 1699 cm^{-1} being assigned to ν_{CO}. The CF_3 group showed a strong ν_{CF} absorption at 1220 cm^{-1}, a region which contains no bands in the DMAD analogue. What is, however, noticeable is the negligible shift in the key bent carbido Rh=C=Rh stretch, which now appears only three wavenumbers from the DMAD species at 800 cm^{-1}.

The confirmation of the unsymmetrical alkyne coordination was provided by the results of a crystallographic study. Presumably, because neither the ester nor the trifluoromethyl groups protrude significantly from the octaphenyl cavity, their impact on crystal packing is minimal such that there is no site preference for the alkyne within the crystal and the coordinated ligand is equally disordered across both positions, with the CF_3 and CO_2Et groups overlapping. Changing the coordinated alkyne had no effect on the unit cell of the lattice, being isomorphous again to both the DMAD species and the μ-carbido precursor.

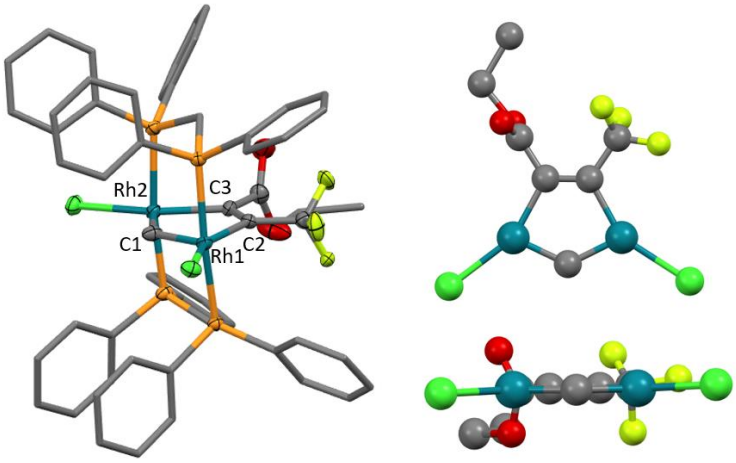

Figure 3.11: Molecular structure of **[$Rh_2(\mu_2$-C)(μ:σ,σ'-F_3C-CC-CO_2Et)$Cl_2(\mu$-dppm)$_2$] (25)** (50% displacement ellipsoids, hydrogen atoms omitted, phosphine substituents and ethyl group simplified). Selected distances [Å] and angles [°]: Rh1-C1 1.818(8), Rh1-C2 2.019(6), Rh1-Cl1 2.456(2), Rh2-C1 1.834(8), Rh2-C3 2.046(7), C2-C3 1.333(9), Rh1-C1-Rh1 128.2(4)

The geometry of the C_2Rh_2C core is virtually unchanged when comparing the unsymmetrical alkyne to the symmetrical DMAD species. The two carbido bond lengths are not perfectly symmetric, though are still crystallographically equivalent (Δ = 0.016, 2 e.s.d.), and the same conclusion follows when comparing these bond lengths to the DMAD structure. Thus, the nature of the electron withdrawing substituents has a very minor geometric effect on the metallacycle geometry. This is supported when comparing the remaining bond lengths in the core (i.e., Rh2-C3, Rh1-C2, C2-C3), which all fall within precision limits (6 e.s.d.) between the structures considered. The bent carbido ligand retains much of the presumed π-character, with the Rh1-C1-Rh2 bond angle still pronounced at 128.2(4) ° and short Rh–C bond lengths (1.818(8), 1.834(8) Å).

Reaction with methyl-propiolate

The second unsymmetrical electrophilic alkyne examined was methyl-propiolate with a single ester substituent and a purely σ-bonding hydrogen terminus. This lack of symmetry in terms of both steric and electronic considerations was anticipated to potentially present a challenge, however, it was hoped that the single ester group would still sufficiently activate the alkyne. Methyl propiolate has in some instances been found to undergo identical cycloaddition reactions to

DMAD, suggesting it contains comparable electrophilicity. A dichloromethane reaction mixture of **[Rh_2(μ-C)Cl_2(μ-dppm)$_2$]** and excess methyl propiolate rapidly turned red in colour, which was initially considered a promising sign. Unfortunately, the red colour was in fact due to complex degradation, which was reflected in the ^{31}P NMR spectrum as only unbound and oxidised dppm was detected. Whether through coordination to form an unstable species, or just degradation of the phosphine ligand, methyl propiolate unfortunately fails to undergo the sought after [3+2] cycloaddition.

Reaction with hexafluoro-2-butyne

The final activated alkyne examined was the fluorocarbon hexafluoro-2-butyne. Being a restricted fluorocarbon, the compressed gas was unable to be shipped to Australia (typical), however, remarkably a sole cannister that had been in storage longer than the author had been alive was found. Being of somewhat unknown quality, a CH_2Cl_2 solution of **1** was evacuated and backfilled with an atmosphere of hexafluoro-2-butyne. When left overnight the solution changes to a red colour and a precipitate is formed as expected.

What was anticipated to be a simple spectroscopic characterisation of **[Rh_2(μ-C)(μ-HFB)Cl_2(dppm)$_2$] (26)** proved to be deceptively curious. The ESI-MS displayed the coordination of one equivalent of HFB (1183.0096. *m/z cf.* 1183.0111 for $C_{55}H_{44}{}^{35}ClF_6P_4{}^{103}Rh_2$ $[M–Cl]^+$), and the complex was expected to be highly symmetrical. What immediately challenged this expectation was an examination of the $^{31}P\{^1H\}$ and $^{19}F\{^1H\}$ NMR spectra. The $^{19}F\{^1H\}$ NMR spectrum *in chloroform* showed three environments, two more than expected. Two of these resonances (at -51.68 and -50.01 ppm) appeared as quartets ($^5J_{FF}$ = 18 Hz), which implied the two environments of the alkyne were in fact distinct with the nuclei coupling to each other. The remaining minor resonance appeared as a singlet at -49.60 ppm, which was expected if the alkyne was coordinated in a symmetrical manner. This anomaly was also reflected in the phosphorous environments. The major two environments at 0.85 and -0.21 ppm ($^1J_{RhP}$ = 104 and 120 Hz) imply two distinct rhodium centres, with the different coupling constants implying a ligand differential. The minor symmetrical product is also seen at 9.27 ppm ($^1J_{RhP}$ = 136 Hz), of which the chemical shift and coupling constant closely align to the remaining two previous MHC complexes. The 'slippage' of an alkyne to act as a σπ ligand has been seen previously for hexafluoro-2-butyne,[172] and may explain the multiple environments present in solution.

What became intriguing was that the equilibrium between coordinated and slippage complexes could be dictated by solvent choice. Measuring the same sample in dichloromethane instead of chloroform completely switches the appearance of the two environments. As **Figure 3.12** shows, the $^{19}F\{^{1}H\}$ NMR spectrum of **26** in dichloromethane now shows the predominant signal being the singlet peak corresponding to the symmetrical species, with much smaller quartet peaks for the slippage complex. The ^{31}P NMR spectrum also displayed the same shift, with the major environment now the symmetrical product.

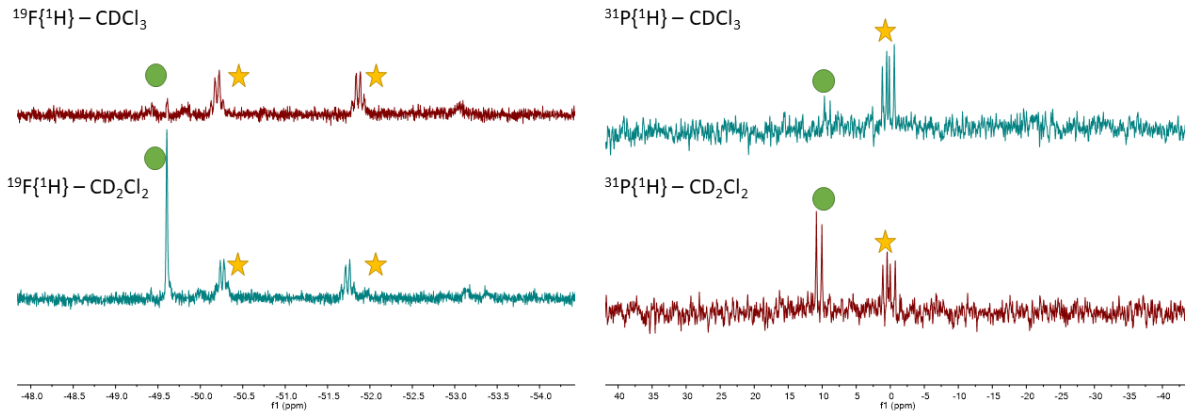

Figure 3.12: $^{19}F\{^{1}H\}$ and $^{31}P\{^{1}H\}$ NMR spectra of **$[Rh_2(\mu\text{-}C)(\mu\text{-}HFB)Cl_2(dppm)_2]$ (26)** in $CDCl_3$ (top) and CD_2Cl_2 (bottom)

Although the solution-state structure showed a clear 'slippage' of the coordinated alkyne, diffraction studies on the solid-state structure showed only the clear olefinic coordination mode of HFB in a tetragonal unit cell. The molecular structure (**Figure 3.13**) shows a symmetrical coordination of HFB, with equivalent Rh-C bond lengths (2.034(6) and 2.050(7) Å). Once again, the coordination of the alkyne results in the μ-carbido ligand bending (Rh-C-Rh = 127.4(4) °), and although the unit cell (Space group = $P4_3$) doesn't contain a crystallographic mirror plane, the two Rh=C bonds are equivalent (1.830(7) and 1.830(6) Å). The geometry of the C_2Rh_2C core is effectively unchanged when compared to the DMAD the ETFB complexes as expected.

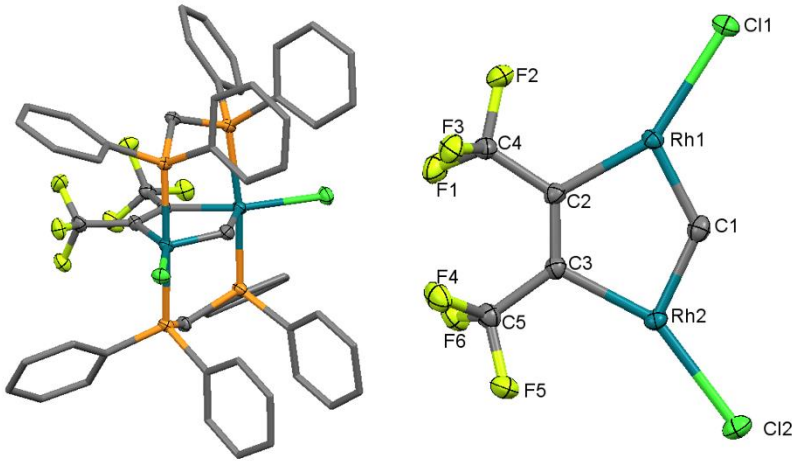

Figure 3.13: Molecular structure of of **[$Rh_2(\mu_2$-C)(μ-HFB)Cl_2(μ-dppm)$_2$] (26)** (50% displacement ellipsoids, hydrogen atoms omitted, phosphine substituents and ethyl group simplified). Selected distances [Å] and angles [°]: Rh1-C1 1.830(7), Rh1-C2 2.034(6), Rh2-C1 1.830(6), Rh2-C3 2.050(7), C2-C3 1.339(9), Rh1-C1-Rh1 127.4(4)

It has become clear that the alkyne insertion onto the dirhodium species requires an alkyne with electron deficient character, and the most important outcome of this reaction is the bending of the μ-carbido ligand. The question that immediately followed these reactions was "is there an electronic consequence that impacts on reactivity"?

3.3.3 An *M*HC?

Reactions with [AuCl(SMe_2)]

Based on the computational data and canonical bonding modes presented for the metallacycle species **24**, the possibility of a more or less 'lone' pair of electrons residing on the bent carbido atom needed to be experimentally examined. When solving the molecular structures for **24-26**, there is noticeable electron density situated in-plane to the bent carbido ligand but modelling the ligand as a methylidyne unit was unsuccessful and would be inconsistent with the NMR and MS data, which is also inconsistent with the μ-methylene species from Cowie.[178] If a lone pair of electrons could be localised on the carbon, the μ-carbido ligand could be treated as a persistent carbene species, with the two rhodium atoms stabilising the carbene centre. This complex could be the vanguard of a new wave of *Metalla*-Heterocyclic Carbenes, or an MHC.

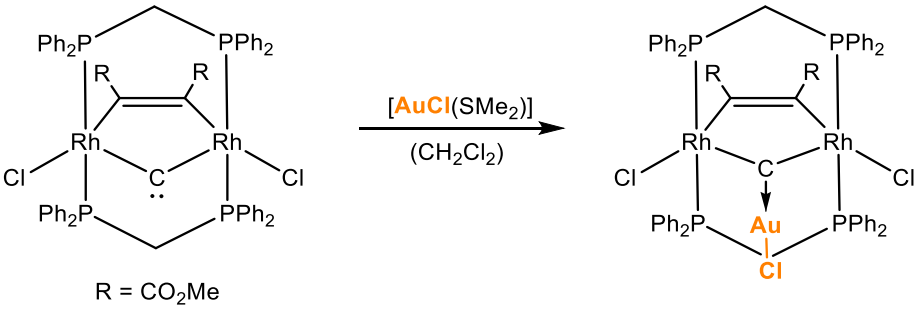

Scheme 3.13: Synthesis of **[$Rh_2Au(\mu_3\text{-}C)(\mu\text{-}DMAD)Cl_2(\mu\text{-}dppm)_2$] (27)**

The first logical choice to test the validity of the NHC/*M*HC analogy was to attempt to coordinate it to a simple metal species. The simple, linear metal complex **[$AuCl(SMe_2)$]** was chosen, as the labile SMe_2 ligand can be lost to access the 'AuCl' moiety (**Scheme 3.13**). The red solution of **24** gradually turns a gold/orange colour after addition of **[$AuCl(SMe_2)$]**, and through silica gel column chromatography a single yellow band was isolated. The orange precipitate showed a single, symmetrical P(III) environment in the $^{31}P\{^1H\}$ NMR spectrum (δ_P = 7.8 ppm), which displayed a similar $^1J_{RhP}$ value to the precursor (130 *cf.* 137 Hz). There were no new ^1H environments in the NMR spectra, and the environments of the methoxy and methylene units remain relatively unchanged. The NMR data suggests the retention of molecular C_{2v} symmetry as in the precursor, supporting the reactivity taking place at the bent carbido ligand.

The ESI-MS found a single major fragmentation at 1394.98169 *m*/*z*, which was entirely consistent with the $[M\text{-}Cl]^+$ fragment (Calc. for $C_{57}H_{50}Au^{35}Cl_2O_4Rh_2$ = 1394.98067 *m*/*z*) and the installation of an AuCl moiety. The addition of AuCl to the bent carbido ligand was crystallographically confirmed in the molecular structure determination of **[$Rh_2Au(\mu_3\text{-}C)(\mu_2\text{-}DMAD)Cl_3(\mu\text{-}dppm)_2$] (27)** (**Figure 3.14**). Resorting to ^{13}C enrichment, the μ_3-carbido resonance was detected at 471.1 ppm, which is surprisingly upfield of the carbene starting material, suggesting that the paramagnetic deshielding effect is stronger for the bent carbene.

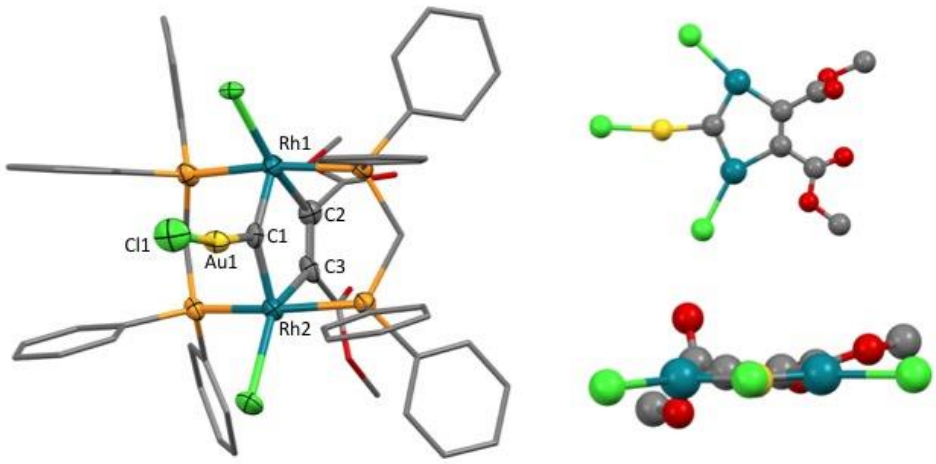

Figure 3.14: Molecular structure of **[$Rh_2Au(\mu_3\text{-}C)(\mu\text{-}DMAD)Cl_3(\mu\text{-}dppm)_2$] (27)** (50% displacement ellipsoids, hydrogen atoms omitted and phosphine substituents simplified). Selected distances [Å] and angles [°]: Rh1-C1 1.870(9), Rh1-C2 1.99(1), Rh1-Cl2A 2.488(3), Rh2-C1 1.877(9), Rh2-C3 2.00(1), Rh2-Cl3 2.487(3), Au1-C1 1.937(9), Au1-Cl1 2.303(4), C2-C3 1.32(1), Rh1-C1-Rh1 126.9(5), Rh2-C1-Au1 109.4(4), C1-Au1-Cl1 171.7(3)

The ring undergoes negligible geometrical change in relation to the precursor, with only the rhodium-carbido bonds experiencing slight elongation (Rh1,2-C1 = 1.870(9)/1.877(9) *cf.* 1.851(19) and 1.860(16), Rh1-C2 = 1.99(1) *cf.* 2.008(14), Rh2-C3 = 2.00(1) *cf.* 2.006(17) Å, Rh1-C1-Rh2 = 126.9(5) *cf.* 124.7(10)°), which attests to lone pair on the carbon atom being used for coordination. The addition of AuCl to the bent carbido results in a new *M*HC-Au bond length of 1.937(9) Å which is comparable to conventional gold(I)-NHC species.[179]

The fast, simple, and clean reaction with the AuCl synthon to produce the NHC-like adduct is a testament to the nucleophilicity of the lone pair that resides predominately on the bent carbido ligand. This reinforces the perspective that the bent-carbido metallacycle is best viewed as a heterocyclic carbene stabilised by two adjacent metal centres, *i.e.*, a true M_2HC. Although single metal centres have been included in the backbone of conventional N-donor NHC complexes (referred to as MNHCs), they have never been the atoms in a stable heterocyclic ring of an Arduengo-type carbene.

To extend this principle, the unsymmetric complex **[$Rh_2(\mu_2\text{-}C)(\mu\text{:}\mu'\text{-}F_3C\text{-}CC\text{-}CO_2Et)Cl_2(\mu\text{-}dppm)_2$]** was also treated with **[$AuCl(SMe_2)$]**. In an identical manner, the solution gradually turns yellow in colour as the insoluble red starting material dissolves. The orange compounded isolated by chromatography displayed an upfield shift in the two ^{31}P resonances (4.44

and 6.64 ppm), though the ^{19}F resonance showed minimal change (-51.08 ppm). The AuCl adduct was detected by high-resolution mass spectra as the $[M\text{-}Cl]^+$ fragment (1418.97871 *m/z cf.* 1418.97823 for $C_{57}H_{49}Au^{35}Cl_2F_3O_2P_4Rh_2$). Though the ethyl ester resonances (CH_3: 0.00, OCH_2: 2.80 ppm) undergo minor changes in the ^1H NMR spectrum, the PCH_2P signals (now 2.88 and 3.62 ppm) replicate what was seen for gold coordination to the previous carbene.

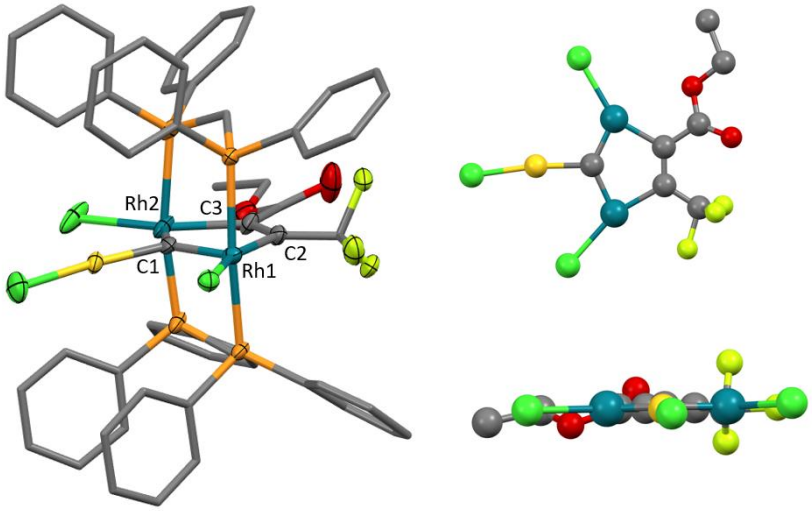

Figure 3.15: Molecular structure of **[$Rh_2Au(\mu_3\text{-}C)(\mu{:}\sigma,\sigma'\text{-}F_3C\text{-}CC\text{-}CO_2Et)Cl_3(\mu\text{-}dppm)_2$] (28)** (50% displacement ellipsoids, hydrogen atoms and solvent omitted, and phosphine substituents simplified). Selected distances [Å] and angles [°]: Rh1-C1 1.87(1), Rh1-C2 2.03(1), Rh1-Cl2 2.459(3), Rh2-C1 1.81(1), Rh2-C3 2.01(1), Rh2-Cl3 2.467(4), Au1-C1 1.99(1), Au1-Cl1 2.306(4), C2-C3 1.35(1), Rh1-C1-Rh2 129.5(6), C2/C3 centroid-C1-Au1 176.42

The molecular structure of **[$Rh_2Au(\mu_3\text{-}C)(\mu{:}\mu'\text{-}F_3C\text{-}CC\text{-}CO_2Et)Cl_3(\mu\text{-}dppm)_2$] (28)** (**Figure 3.15**) displayed the same linear coordination of the carbene to AuCl (176.42 °). The geometry of the dirhodacycle remains consistent with its DMAD analogue, further substantiating the singlet-carbene type reactivity of the bent μ-carbido precursor

The reactivity of the final dimetallacarbene species, **[$Rh_2(\mu\text{-}C)(\mu\text{-}HFB)Cl_2(\mu\text{-}dppm)_2$]**, followed the same pattern. The reaction with **[$AuCl(SMe_2)$]** caused an instant yellow/orange colour change, and the yellow species could be cleanly isolated through column chromatography. Interestingly, the solvent-dependent nature of the hexafluoro-2-butyne coordination that was detected for the carbene species is not evident in the μ_3-carbido complex **[$Rh_2(\mu_2\text{-}C\text{-}AuCl)(\mu$-**

HFB)Cl_2(μ-dppm)$_2$] (29), the NMR data for which indicate C_{2v} molecular symmetry. The $^{31}P\{^1H\}$ NMR spectra of the complex now indicate only a single environment with a resonance at 4.71 ppm ($^1J_{RhP}$ = 125 Hz), and the $^{19}F\{^1H\}$ NMR spectrum consists of a singlet at -50.58 ppm, further confirming that the coordination of the hexafluoro-2-butyne bridge is symmetrical.

The crystal structure of **29** was significantly more demanding to model, as four crystallographically independent units appeared in the asymmetric unit cell, though variations in geometric parameters between molecules was negligible (**Figure 3.16**). The Rh–C multiple bonding character is retained in the now trigonally coordinated μ-carbido ligand (Rh1/2-C1: 1.859(6), 1.824(8) Å, Rh1-C1-Rh2: 128.2(4) °). There is no coordinated aquo ligand present, which suggests it is a feature only in the DMAD ligated complexes.

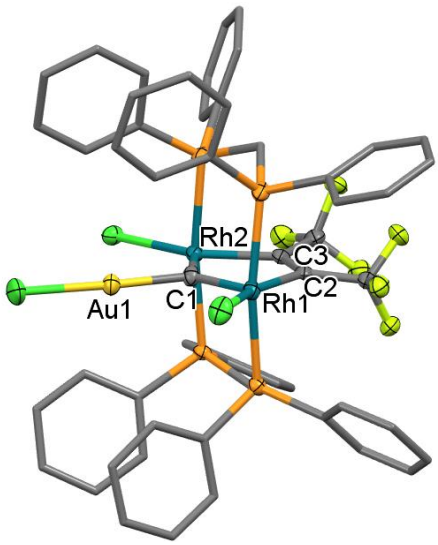

Figure 3.16: Molecular structure of **[Rh_2Au(μ$_3$-C)(μ:σ,σ'-HFB)Cl_3(μ-dppm)$_2$] (29)** (50% displacement ellipsoids, hydrogen atoms and solvent omitted, and phosphine substituents simplified). Selected distances [Å] and angles [°]: Rh1-C1 1.859(6), Rh1-C2 2.036(7), Rh1-Cl1 2.405(2), Rh2-C1 1.824(8), Rh2-C3 2.019(6), Au1-C1 1.949(7), Au1-Cl3 2.280(2), C2-C3 1.326(9), Rh1-C1-Rh2 128.2(4)

3.3.4 Buried Volume Analysis

With the successful appending of the linear gold(I)-chloride moiety onto each of the various analogues of the MHC, determining the versatility of the MHC as a ligand was important. In order to explore this, the original DMAD-derived metallacycle was chosen for more detailed

investigation, as its synthetic pathway contained the most readily available alkyne and the product is highly symmetrical.

Although gold halide addition provided the necessary proof of concept and more conventional complexes of the form **[AuCl(NHC)]** represent an extensive field of study in their own right, not least in catalysis,[180] the small, linear nature of the addend is rather simple in comparison to the potential addition of bulkier metal-ligand fragments. In steric terms, the key issue of interest relates to topology of the surrounding cavity provided by the dppm and chloride co-ligands on the complex. The phenyl rings are arranged around the complex to minimise repulsion against the coordinated DMAD ligand, which causes them to fold forward over the bent carbido ligand. The rings remain in this geometry even after coordination of the carbene to gold, causing them to 'envelop' the coordinated metal. Using the recently developed percent buried volume calculation ($\%V_{Bur}$),[181] the space occupied by the MHC ligand around the coordinated gold can be quantified (**Figure 3.17**). The $\%V_{Bur}$ gives a more accurate indication of a ligands' encapsulating capacity around a metal centre and is not restricted to a single set of compounds as in the case of the Tolman cone angle commonly used for phosphines.

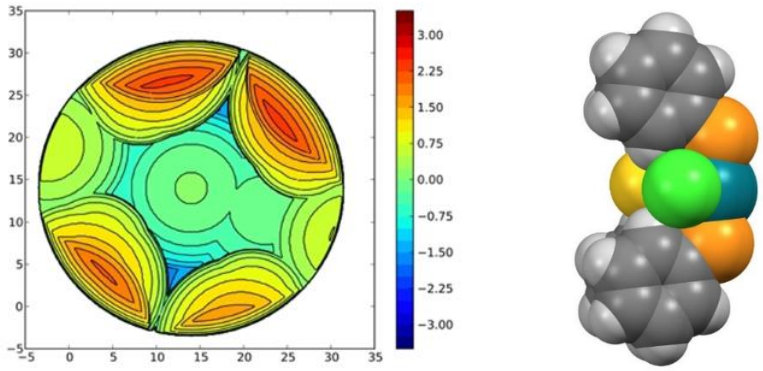

Figure 3.17: $\%V_{Bur}$ steric map of **[$Rh_2Au(\mu_3\text{-}C)(\mu\text{-}DMAD)Cl_3(\mu\text{-}dppm)_2$]** at the gold atom (left), and phenyl ring enveloping of the Au unit (right – looking down the Rh-Rh axis)

The calculated buried volume for the *M*HC of 63.8% is significantly greater than commonly found for phosphines and NHC ligands (PCy_3 = 29.6, NHC^{iPr} = 36.0%) and correlates to values associated with polydentate binding ligands such as pincer ligands.[182] The significantly higher $\%V_{Bur}$ of the *M*HC compared to regular phosphine and NHC ligands may present a steric barrier when attempting to coordinate larger metal complexes. Indeed, the very isolation of these species is itself no doubt a reflection, in part, of the substantial kinetic protection provided by this tetraphenyl

wall. To investigate this potential issue, a range of synthons for metal-ligand fragments with varying steric and electronic features were examined.

3.3.5 Further Coordination to Coinage Metals

Reactions with [AuCl(PCy$_3$)] and [AuCl(AsPh$_3$)]

With the success of the AuCl coordination, a similar reaction was repeated with the analogous gold(I) phosphine complex **[AuCl(PCy$_3$)]**, to determine whether the MHC is capable of replacing the phosphine ligand, or, to form the cationic complexes **[Au(MHC)$_2$][Cl]** or **[Au(MHC)(PCy$_3$)][Cl]**. An NMR scale investigation of **[Rh$_2$(μ-C:)(μ-DMAD)Cl$_2$(μ-dppm)$_2$]** with excess **[AuCl(PR$_3$)]** (R = Ph, Cy) in $CDCl_3$ revealed no change in the $^{31}P\{^1H\}$ chemical shift nor the generation of free phosphine, confirming that no reaction had ensued over a period of 24 hours. The replacement of the phosphine by the MHC was considered unlikely given the strong σ-donating nature of the phosphine and the steric congestion attending an associative substitution. Replacement of the chloride ligand may well have also been encumbered by the sterics of the dppm phenyl rings.

Although the phosphine ligand was not substituted presumably due to its strong donicity, the MHC complex was successful in replacing a weaklier coordinating arsine. Combining the gold-arsine complex **[AuCl(AsPh$_3$)]** with the free MHC resulted in replacement the arsenic ligand and over a matter of hours led to complete conversion to the MHC-AuCl complex.

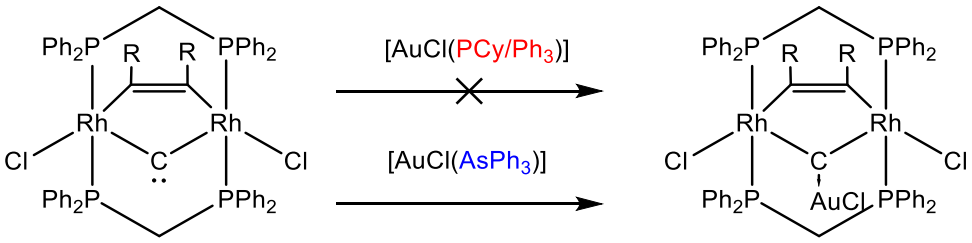

Scheme 3.14: Failed phosphine but successful arsine replacement of [AuCl] moiety (R = CO_2Me)

Reaction with [CuCl(SMe$_2$)]

Continuing with the trend of simple linear metallic species, the same reaction was repeated with the analogous copper species, **[CuCl(SMe$_2$)]** which serves as a soluble synthon for 'CuCl'. It was expected that either the identical MHC species with CuCl would form, or, a dimeric (MHC)$_2$Cu$_2$(μ-Cl)$_2$ species with bridging chloride ligands between the two Cu centres, reflecting the greater propensity for copper to form complexes of increased coordination number. Upon combination with **[CuCl(SMe$_2$)]** the red solution showed a similar colour change to yellow as observed for AuCl adduct formation and monitoring of the reaction progress by ^{31}P{^{1}H} NMR spectroscopy showed complete conversion within minutes. The new symmetrical environment (δ_P = 8.7) lies near the AuCl adduct and shows the same slight reduction in the $^1J_{RhP}$ value (132 Hz) upon coordination of the MHC. The complex was again able to be purified by column chromatography under identical conditions, reflecting the enduring stability of these species.

The ^{1}H NMR spectrum of the presumed CuCl species **[Rh$_2$Cu(μ$_3$-C)(μ:σ,σ'-DMAD)Cl$_3$(μ-dppm)$_2$] (30)** was almost identical to the analogous gold species. The methoxy environment on DMAD remains in a similar position as a singlet at 2.31 ppm, but the methylene units of dppm undergo slight chemical shifts. One appears as a broad resonance centred at 2.47 ppm, but the other comprises the expected well-resolved doublet of virtual pentets (δ_H = 3.64, J = 12, 6 Hz). The ^{13}C{^{1}H} NMR spectrum again solely consistent of aromatic dppm and DMAD resonances, little changed from those for the AuCl adduct. The high-resolution ESI-MS displayed a fragmentation pattern at 1262.0100 m/z consistent with the [M-Cl]$^+$ fragment (Calc. for $C_{57}H_{50}{}^{35}Cl_2{}^{63}CuO_4P_4Rh_2$ = 1261.9476 m/z). The crystallographically determined molecular structure (**Figure 3.18**) shows the CuCl behaving in an identical manner to AuCl, forming a linear C-Cu-Cl species.

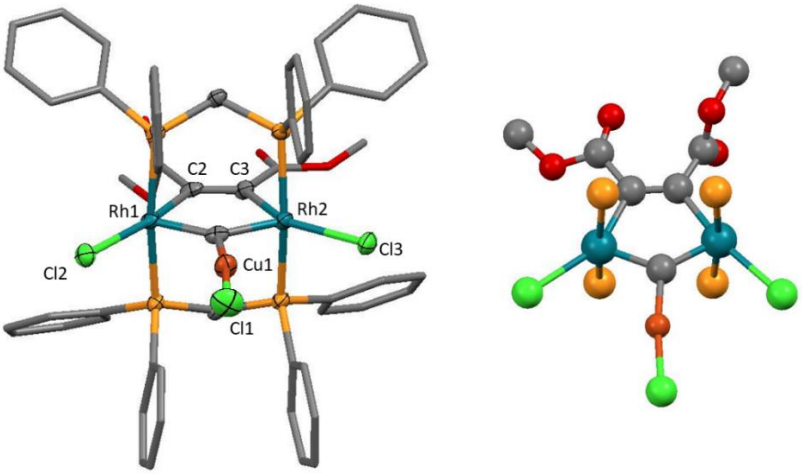

Figure 3.18: Molecular structure of **[$Rh_2Cu(\mu_3\text{-}C)(\mu{:}\sigma,\sigma'\text{-}DMAD)Cl_3(\mu\text{-}dppm)_2$] (30)** (50% displacement ellipsoids, solvent, ligated water and hydrogen atoms omitted; phosphine substituents simplified). Selected distances [Å] and angles [°]: Rh1-C1 1.866(9), Rh1-C2 2.023(9), Rh1-Cl2 2.492(2), Rh2-C1 1.862(9), Rh2-C3 2.029(9), Rh2-Cl3 2.487(3), Cu1-C1 1.836(9), Cu1-Cl1 2.119(4), C2-C3 1.31(1), Rh1-C1-Rh1 126.7(5), Rh2-C3-C2 119.6(7), C1-Au1-Cl1 173.9(3)

As has been seen in the previous MHC structures, the visualisation software presented default bonds between the two rhodium centres and between the copper and rhodium centres. The Rh—Rh distance of 3.3320(9) Å is, however, longer than $2r_{cov}$(Rh) of 2.84 Å, and electron counting rules dictate that no formal metal-metal interaction is required. The same arguments preclude describing the Cu—Rh distances of 3.014(2) and 3.271(2) Å as involving any formal bonding component. The distinct difference in Cu-Rh separations (Δ = >100 e.s.d) is due to the coordinated aqua ligand in the solid-state structure, causing deviation from linearity (C1-Cu1-Cl1 = 173.9(3)°), however, the solid-state distortion is in no way representative of the coordinated CuCl fragment having any interactions with either Rh=C multiple bonds.

When comparing the CuCl and AuCl molecular structures, the two are as anticipated almost identical. Other than having shorter C-Cu and Cl-Cu bonds than Au (1.836(9) *cf.* 1.937(9), 2.119(4) *cf.* 2.303(4) Å respectively – r_{cov} = 1.32(4) (Cu), 1.36(6) (Au)[xxxix]), the geometry of the metallacyclic

[xxxix] Covalent radii for metals are typically with reference to statistical analysis of the CCDC which is problematic for copper, even when Jahn-Teller distorted structures are excluded due to the very different coordination behaviours of closed-shell d^{10}-Cu(I) and d^9-Cu(II) species in the population – described as "*coordination sphere plasticity*".[183] The population of gold(I) structures is in contrast dominated by linear 2-coordinate geometries with bond lengths being typically shorter than for higher coordination numbers.

CRh_2C_2 ring remains essentially unperturbed, with the two rhodium-carbido bond lengths showing minimal change (Rh1-C1 = 1.866(9) and Rh2-C1 = 1.862(9) Å) from the MHC precursor.

Coordination of Au(C_6F_5)

Before attempting to move on to larger systems, the synthesis of a linear complex with a larger *trans* group was attempted and for this purpose the pentafluorophenyl substituent was chosen. Initial attempts to form this species took the MHC-AuCl complex **27** in combination with LiC_6F_5. Monitoring the reaction through $^{31}P\{^1H\}$ NMR spectroscopy revealed resonances for a mixture of multiple new compounds, none of which were unable to be isolated or separated through flash chromatography. The presence of three metal-chloride bonds which could in principle undergo lithium-halogen exchange most likely accounts for this plethora, and the desired species could not be cleanly isolated *via* this approach.

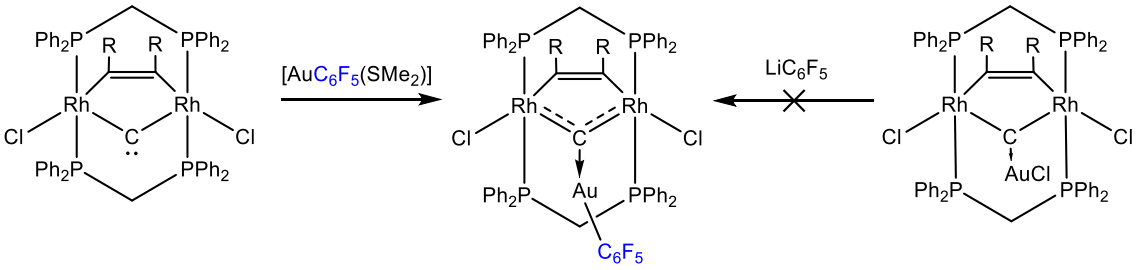

Scheme 3.15: Synthesis of **[$Rh_2Au(\mu_3\text{-}C)(C_6F_5)(\mu{:}\sigma,\sigma'\text{-}DMAD)Cl_2(dppm)_2$] (31)**. R = CO_2Me

Moving to an alternative convergent approach, the gold(I) complex **[Au(C_6F_5)(SMe_2)]** is available from the reaction between LiC_6F_5 and **[AuCl(SMe_2)]**.[184] The reaction of this complex with the dimetallacarbene species proceeds in an identical manner to AuCl addition, and the yellow species formed manifested all the spectroscopic details expected for the installation of an AuC_6F_5 unit **(Scheme 3.15)**. The single ^{31}P resonance for the product is centred at 8.78 ppm, slightly downfield of the AuCl analogue, with a similar coupling constant $^1J_{RhP}$ of 130 Hz. The three discernible ^{19}F multiplet resonances due to the C_6F_5 group are all shifted from the gold precursor, appearing at -112.9, -158.6 and -162.8 ppm respectively. Hydrogen bonding is implicit between the C_6F_5 ring and one of the hydrogens on the methylene unit in dppm given the significant downfield shift to 3.71 ppm (*cf.* 2.67 ppm for the remaining environment). As expected, the coordination of one equivalent of Au(C_6F_5) was supported by the major $[M\text{-}Cl]^+$ fragment in the

mass spectrum at 1527.0067 *m/z* (Calcd. for $C_{63}H_{50}Au^{35}ClF_5O_4P_4Rh_2$ = 1527.0044 *m/z*). The molecular structure of **[$Rh_2Au(\mu_3$-C)(C_6F_5)(μ:σ,σ'-DMAD)Cl_2(dppm)$_2$] (31)** (**Figure 3.19**) confirmed that even the bulkier C_6F_5 ligand *trans* to the MHC is capable of fitting into the phenyl ring pocket, just. The PC–H···F hydrogen-bonding inferred from solution ^{1}H NMR data above is however obviated by the conformation of the dppm ligands adopted in the solid state.

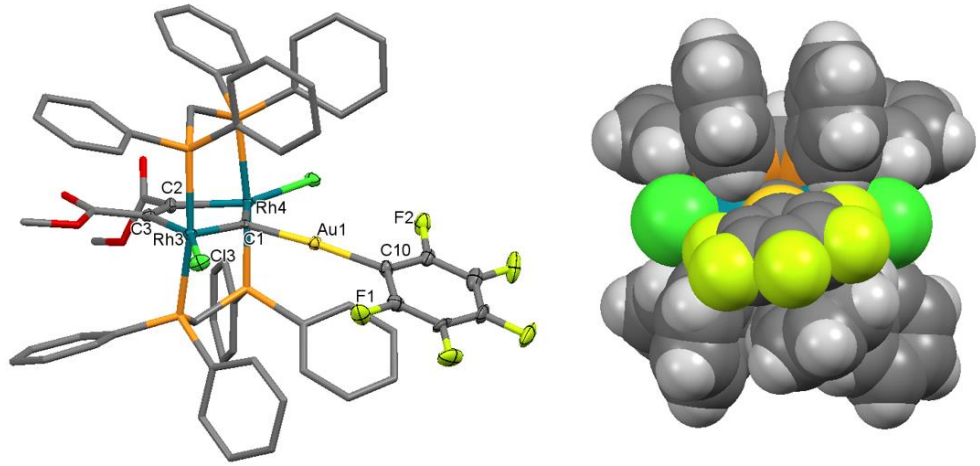

Figure 3.19: Molecular structure of **[$Rh_2Au(\mu_3$-C)(C_6F_5)(μ:σ,σ'-DMAD)Cl_2(dppm)$_2$] (31)** (50% displacement ellipsoids, solvent and hydrogen atoms omitted; phosphine substituents simplified). Selected distances [Å] and angles [°]: Rh3-C1 1.83(1), Rh4-C1 1.87(1), Rh3-Cl3 2.443(3), Rh4-C2 2.03(1), Rh3-C3 2.02(1), Au1-C1 2.00(1), Au1-C10 2.05(1), C2-C3 1.35(2), Rh3-C1-Rh4 130.5(6), C1-Au1-C10 174.7(5)

With the spectroscopic data for the desired complex in hand, the crude $^{31}P\{^1H\}$ NMR spectrum of the product mixture arising LiC_6F_5 and **[$Rh_2Au(\mu_3$-C)(μ-DMAD)Cl_3(μ-dppm)$_2$]** was revisited, analysis of which confirmed that **31** was absent.

Unexpected reactivity with [$AuCl_3$(THT)]

Given the high percent buried volume, it was assumed that appending metal-ligand unit with atom density abutting the carbene would be strongly disfavoured, as it would clash with the chloride and phenyl rings. That said, the cleft that is evident in the topology of Figure 3.15 suggested that perhaps a thin flat metal-ligand fragment might be accommodated. Because of its simple d^8-sqaure planar nature, and the successful coordination to **[AuCl(THT)]**, **[$AuCl_3$(THT)]** was chosen to test this hypothesis.

Visually, the reaction with the gold(III) species proceeds in an identical manner to that with **[AuCl(SMe$_2$)]**, with the dichloromethane reaction solution rapidly turning yellow in colour. Though a reaction had clearly taken place, the spectroscopic data were not consistent with formation of the desired product. The *positive-ion* high-resolution mass spectrum was devoid of any fragments incorporating gold. Instead, a major envelope at 1234.9821 *m/z* corresponds to the $[M]^+$ of the cationic chlorocarbyne complex **[Rh$_2$(μ$_2$-CCl)(μ$_2$-DMAD)Cl$_2$(dppm)$_2$]$^+$** (*cf.* 1234.9987 *m/z*) and the $[M\text{-}Cl]^{2+}$ dication at 599.0070 *m/z*.

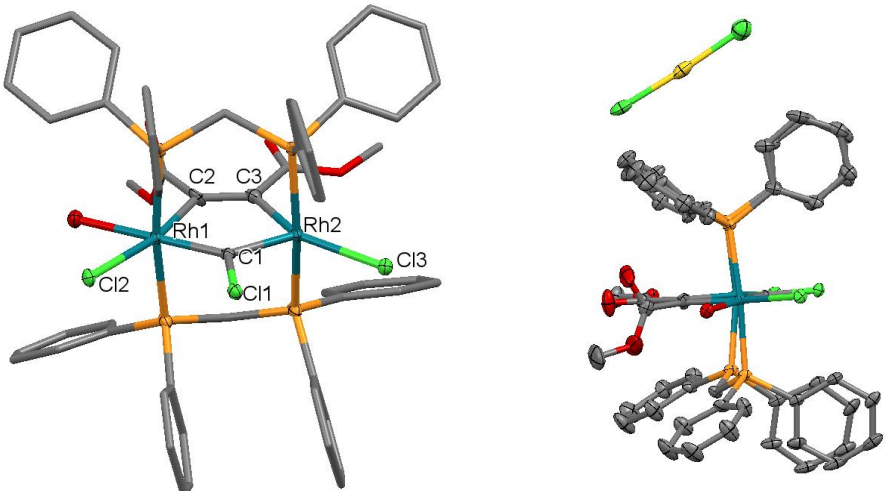

Figure 3.20: Molecular structure of **[Rh$_2$(μ$_2$-CCl)Cl$_2$(OH$_2$)(μ-DMAD)(μ-dppm)$_2$][AuCl$_2$] (32a)**. (50% displacement ellipsoids, hydrogen atoms omitted; phosphine substituents simplified). Selected distances [Å] and angles [°]: Rh1-C1 1.905(8), Rh1-C2 2.01(1), Rh1-Cl2 2.474(2), Rh2-C1 1.881(8), Rh2-C3 1.991(1), Cl1-C1 1.715(9), C2-C3 1.36(1), Rh1-C1-Rh1 127.2(5)

The molecular structure of the aqua adduct **[Rh$_2$(μ$_2$-CCl)(μ$_2$-DMAD)Cl$_2$(dppm)$_2$][AuCl$_2$] (32a) (Figure 3.20)** highlights that a redox reaction has taken place, rather than carbene coordination. The presence of the cationic chlorocarbyne ligand, in addition to the $[Au^ICl_2]$ anion, supports the theory that the MHC is too bulky to coordinate as a ligand to $AuCl_3$ or easily enter into nucleophile/electrophile processes when outer-sphere electron transfer processes may compete. Instead, in this case an atom-transfer redox reaction takes place, forming the more sterically accessible chlorocarbyne complex.

Unfortunately, the chlorocarbyne salt **32** remains to date one of the least soluble complexes encountered in this work, which made NMR characterisation exceptionally difficult. Metathesis of

the counter ion with PF_6 was successful but unfortunately failed to usefully increase the solubility. Interestingly, the ^1H NMR spectrum showed only a single resonance for the dppm methylene linkers at 2.55 ppm, unlike the two usually seen. Since there is no obvious low-energy means for the two protons to undergo site-exchange without dppm chelate ring-opening, this most likely reflects coincidental chemical equivalence. The DMAD methyl groups were manifest as a sngle resonance at 3.34 ppm, while ^1H-^{13}C HMQC studies detected the corresponding ester methylene and methyl carbon environment at 15.7 and 50.8 ppm, respectively. The $^{31}P\{^1H\}$ NMR spectrum was not as expected, comprising two doublets at 2.15 ($^1J_{RhP}$ = 107 Hz) and 8.85 ($^1J_{RhP}$ = 115 Hz) suggesting a loss of symmetry. It has been observed above that for A-frame complexes with apparently pentacoordinate rhodium geometries based on spectroscopic data, on occasion the solid-state structures include an aquo ligand coordinated to one, but not two of the rhodium centres. This was attributed to either the rapid coordination/dissociation of adventitious water to the nominally 16-electron rhodium centres occurring rapidly in solution on the $^{31}P\{^1H\}$ NMR timescale so as to not be evident, or complete dissociation such that entrapment of an aquo ligand was a solid-state phenomenon. Arguably, the cationic nature of the chlorocarbyne complex might be expected to enhance aquo binding, however the caveat would be that the presence of adventitious water to any significant extent would be expected to eventually lead via hydrolysis of the chlorocarbyne ligand to the carbonyl complex **$[Rh_2(\mu\text{-}CO)Cl_2(\mu\text{-}DMAD)(\mu\text{-}dppm)_2]$**. This complex was described previously by Cowie but was *not* observed here. Thus. it has been presumed that the coordinated aqua solvent plays no role in the solution state, however, it may remain bound in this cationic example, causing this facial asymmetry. Utilising ^{13}C enrichment, the μ_2-chlorocarbyne resonance of interest could be detected at 395.3 ppm in the ^{13}C NMR spectrum, with a distinct triplet coupling to the two rhodium centres ($^1J_{RhC}$ = 35 Hz).

This complex is the second structurally characterised example of a μ_2-chlorocarbyne, the first being recently published[130] and described in **Section 2.2**. Comparing the two structures **(Figure 3.21)** leads to some interesting spectroscopic differences. The ^{13}C chemical shifts are both upfield of the μ-carbido environments, though the present example is shifted further upfield compared to the hexachlorido complex at 410.2 ppm. Both resonances, however, fall within the region previously observed for μ_2-carbynes.

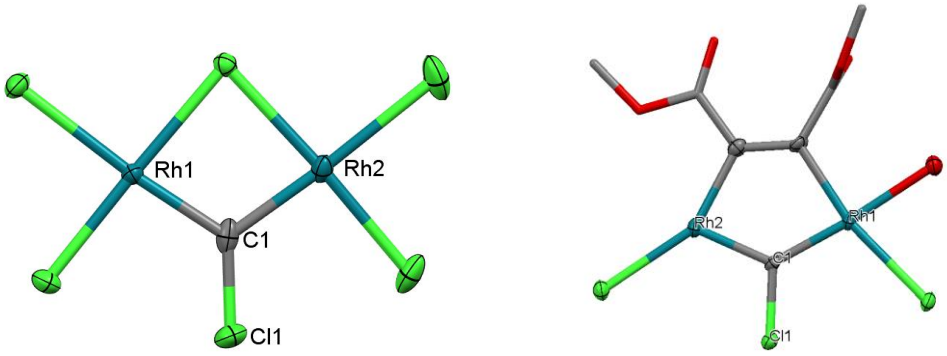

Figure 3.19: Simplified equatorial core structures of the two structurally characterised chlorocarbynes

The key bond lengths and angles are collated below in **Table 3.1**. The key differences stem from the 5-membered ring arising from the MHC compared to the four-membered ring of the halo-bridged species. The steric strain of the four-membered ring causes a contraction of the Rh-C-Rh bond angle, from 127.2(5) down to 111.3(3) °. Though the angle changes, the bond lengths for the rhodium centres to the chlorocarbyne ligand are almost the same. The MHC bond lengths are slightly shorter (average of 1.893(8) Å) compared to the chloro-bridged species (average of 1.930(6) Å), however, the difference is approximately only 5 e.s.d.

Length (Å) / Angle (°)	**$[Rh_2(\mu_2\text{-}CCl)Cl_2(\mu\text{-}DMAD)(\mu\text{-}dppm)_2]^+$**	**$[Rh_2(\mu_2\text{-}CCl)(\mu\text{-}Cl)Cl_4(\mu\text{-}dppm)_2]$**
Rh1-C1	1.905(8)	1.912(5)
Rh2-C1	1.881(8)	1.948(6)
Rh1-C1-Rh2	127.2(5)	111.3(3)
C1-Cl1	1.72(1)	1.674(6)
Rh1···Rh2	3.3907(8)	3.1866(7)

Table 3.1: Selected bond lengths and angles of μ_2-chlorocarbyne complexes

Conversely, the chlorocarbyne C-Cl bond length appears to be marginally longer for the **32**, but once, again, this difference is within the precision of the structural models (<5 e.s.d.). The largest bond difference, as would be expected on simple geometric grounds, is between the two rhodium centres. While both are beyond the covalent radii of two rhodium atoms and should not contain formal bonding character, the five-membered ring in **32** has less steric strain and positions the rhodium centres 0.2 Å further away.

Though the geometric changes are minor and not expected to alter the chlorocarbyne chemistry, its extreme insolubility and late-stage synthesis into this work meant that detailed studies into the reactivity of the new μ_2-chlorocarbyne were not pursued, but it presents an additional avenue for future research into this field.

3.3.6 Halogenation Reactions

Attempted Chlorination of MHC-AuCl

Although the gold(III) complex could not be made from the direct addition of **[$AuCl_3$(THT)]**, it was thought that perhaps the chlorination of the gold(I) adduct could lead to the desired product.

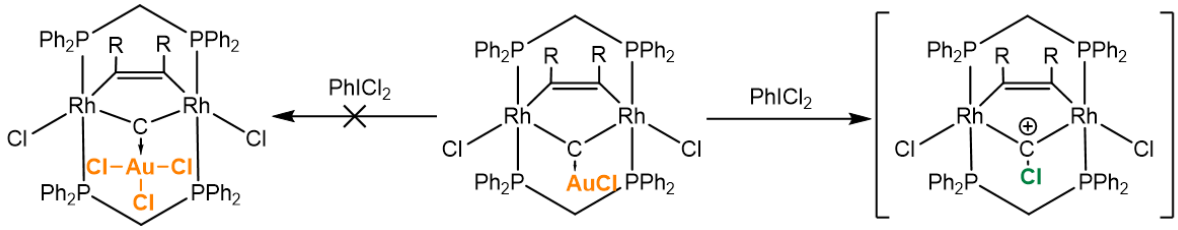

Scheme 3.16: Chlorination of MHC-AuCl with $PhICl_2$ forming the μ_2-halocarbyne **32**. R = CO_2Me

For this purpose, $PhICl_2$ was considered as a mild chlorinating agent, given that it had proven to be quite successful in earlier work in oxidising the rhodium centres. The orange/gold solution of the MHC-AuCl complex rapidly turns yellow upon addition of $PhI.Cl_2$, and the reaction is complete almost immediately as evident from $^{31}P\{^1H\}$ NMR spectroscopy. As partly expected, the NMR spectra matched those of the chlorocarbyne salt **[$Rh_2(\mu_2$-CCl)$Cl_2(\mu$-DMAD)(μ-dppm)$_2$][$AuCl_2$] (Scheme 3.16)**. Once again, the longevity of the **[$AuCl_3$(MHC)]** species, if actually formed, would appear to be sterically disfavoured.

Reaction with $PhI.Cl_2$

Given the formation above of the cationic chlorocarbyne complex **$[Rh_2(\mu_2\text{-}CCl)Cl_2(\mu\text{-}DMAD)(\mu\text{-}dppm)_2]^+$** *via* two serendipitous gold-mediated routes, its synthesis directly from the free MHC and $PhICl_2$ seemed feasible.[xl] The red solution of the MHC immediately turns yellow upon addition of $PhICl_2$ and the $^{31}P\{^1H\}$ NMR spectrum of the resulting yellow product revealed the identical resonances as seen previously for the dichloroaurate salt. It is expected that the counterion present in solution is the remaining chloride ion, however the reluctance of this halide to coordinate to the unsaturated rhodium centre(s) is noteworthy, suggesting a pronounced trans-effect by the μ-chlorocarbyne ligand. (**Scheme 3.17**).

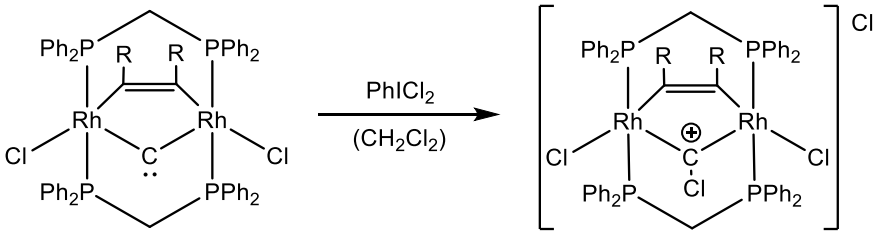

Scheme 3.17: C–Chlorination with $PhICl_2$ to form the μ_2-halocarbyne **32**. R = CO_2Me

3.3.7 Coordination with Mercury(II) Species

Reaction with $[Hg(CF_3)_2]$

A further metal of interest for coordination was divalent mercury, not least because the coordination of NHC ligands to Hg^{II} dates back to Wänzlick's pioneering studies.[185] Mercury(II) complexes, being d^{10}, have no geometric preferences arising from crystal field stabilisation energies, and could therefore change geometry upon coordination of the carbene. The first species chosen was **$[Hg(CF_3)_2]$**, as the electron-withdrawing trifluoromethyl groups should favour coordination of the carbene to the mercury. The Lewis acidity of $[Hg(CF_3)_2]$ towards halides, pseudo-halides,

[xl] Though anonymous, it is of interest to note that a referee for the original μ-chlorocarbyne publication mused whether C-chlorination of the linear cumulenic carbido ligand might actually proceed *via* initial bending to general a nucleophilic carbene. *"...is it possible that 8 is actually a symmetric Rh(III)-Rh(III) complex $[Rh_2(\mu\text{-}C)X_4(\mu\text{-}dppm)_2]$ with a bent Rh-C-Rh arrangement and a lone pair on carbon (sterically protected and stabilized like a free NHC)? The carbene would certainly be susceptible to the observed halogen addition."* Given that this insight pre-dated our discovery of just such a species, the referee should be applauded.

crown ethers, amines and even water is well documented[186] although these studies pre-dated the emerging recognition of spodium bonding.[187] A key feature of the weak coordination of Lewis bases to the 'Hg$(CF_3)_2$' unit is the retention of an essentially linear *trans*-HgC_2 spine.

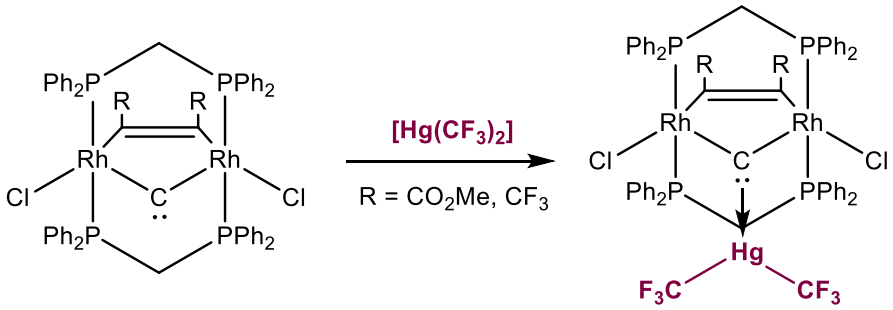

Scheme 3.18: Proposed reaction of an MHC with **[Hg$(CF_3)_2$]**

In an NMR vial, addition of excess **[Hg$(CF_3)_2$]** to a solution of the MHC **24** in $CDCl_3$ causes the insoluble carbene to dissolve, suggesting the formation of a more soluble adduct (**Scheme 3.18**). Monitoring the $^{31}P\{^1H\}$ NMR spectrum saw a slight change (*ca* 1.2 ppm) in the carbene environment, which was now centred at 13.81 ppm but still displayed the same $^1J_{RhP}$ coupling constant of 137 Hz, in contrast to the reduction typically seen during carbene coordination. The ^{19}F NMR spectrum only displayed a single environment at -36.01 ppm, straddled by ^{199}Hg satellites ($^2J_{FHg}$ = 1258 Hz, ^{199}Hg I = ½ 16.9% abundant).

Any attempt to isolate the presumed adduct **[$Rh_2Hg(\mu_3$-C)$(CF_3)_2(\mu$:σ,σ'-DMAD$)Cl_2(\mu$-dppm$)_2$] (33)** failed. Addition of petrol precipitated a red powder that was confirmed to be the unbound carbene complex and attempts to separate out any products through silica gel chromatography also failed. The coordination that seems to operate in the solution phase must be a weak or dynamic process, readily dissociating on attempted trapping.

To confirm this weak coordination, the same reaction was repeated with the hexafluoro-2-butyne analogue. The $CDCl_3$ NMR solution of **[$Rh_2(\mu$-C$)(\mu$-HFB$)Cl_2(\mu$-dppm$)_2$]** remains orange and insoluble until **[Hg$(CF_3)_2$]** is added, which causes the solution to turn red and translucent. The ^{31}P NMR spectrum displays a new major symmetrical environment at 12.02 ppm, with a similar $^1J_{RhP}$ value (132 Hz) to that of the precursor. The ^{19}F NMR spectrum interestingly does not show a new environment for the Hg-CF_3 groups (δ_F = -35.91), but the CF_3 groups on the metallacarbene are shifted slightly to a *single* resonance at -49.06 ppm *cf.* -51.68 and -50.01 ppm

in the free MHC. Notably, the chemical shifts of the dppm methylene hydrogen resonances are changed to 2.37 and 3.39 ppm, suggesting a formal modification of the carbene species to most likely give **[$Rh_2Hg(\mu_3\text{-}C)(CF_3)_2(\mu\text{:}\sigma,\sigma'\text{-}HFB)Cl_2(\mu\text{-}dppm)_2$] (34)**. Given the fluxional nature of the hexafluro-2-butyne that was apparent in $CDCl_3$ the presence of a symmetrical species implies coordination of the carbene to the mercury. Once again, attempts to work up the complex in any form causes the species to revert to the constituent Rh_2HC and organomercurial components.

Reaction with [$HgCl_2$]

Mercury(II) chloride has been found to react with NHC compounds to form complex mercury-NHC adducts, often resulting in halo-bridged dimercury species (**Figure 3.20**).[188]

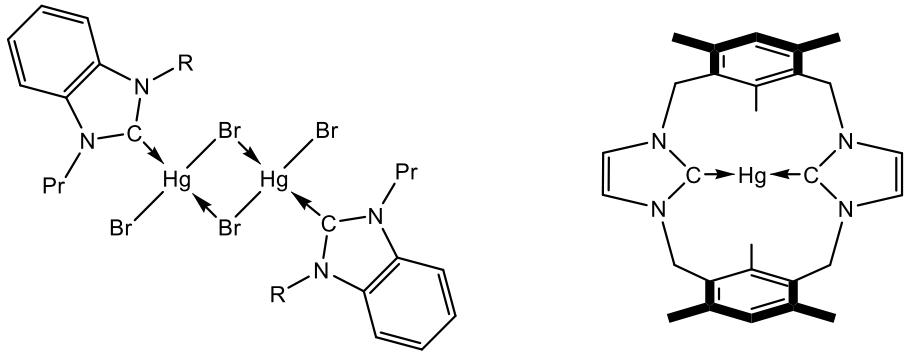

Figure 3.20: Examples of mercury NHC complexes

Taking a $CDCl_3$ solution of the MHC complex **24**, addition of **[$HgCl_2$]** resulted in the expected increased solubility of the carbene complex into solution, as observed for **[$Hg(CF_3)_2$]** above. Curiously, the ^{31}P NMR spectra displayed a new doublet environment centred at 8.82 ppm, which follows the upfield trend seen when the carbene coordinates to a third metal. The $^1J_{RhP}$ coupling constant of 115 Hz is however significantly smaller than expected, and the peaks are rather broad in comparison to the sharp signals seen for the coinage metal adducts. The ^1H NMR spectra clearly displayed one dppm methylene environment at 4.03 ppm, with the expected doublet of virtual pentet splitting ($^2J_{HH}$ = 12 Hz, $^2J_{PH}$ = 5 Hz).

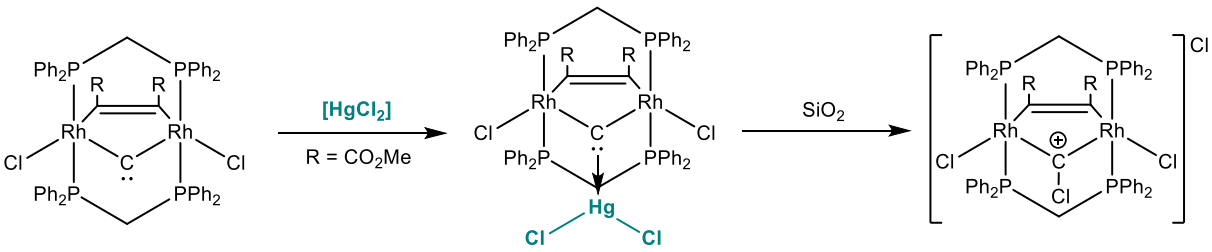

Scheme 3.19: Reaction of MHC **24** with **[$HgCl_2$]**

Unfortunately, attempts to work up or isolate the presumed mercury adduct **[$Rh_2Hg(\mu_3$-C)(μ:σ,σ'-DMAD)$Cl_4(\mu$-dppm)$_2$] (35)** led to immediate decomposition, reflected in the evolution of multiple broad resonances. The major species present after chromatography was identified as the chlorocarbyne salt **[$Rh_2(\mu$-CCl)(μ-DMAD)$Cl_2(\mu$-dppm)$_2$]Cl** with white insoluble mercury biproducts remaining above the silica.

3.3.8 Unsuccessful but Notable Coordination Attempts

Reactivity with H^+

One of the simpler reactions that was examined for the metallacarbene was with acids and methylating agents. Protonation, in particular, was important because the pathway into NHC chemistry typically begins from the deprotonation of an imidazolium salt, so formation of the dirhodium analogue is of interest (**Scheme 3.20**).

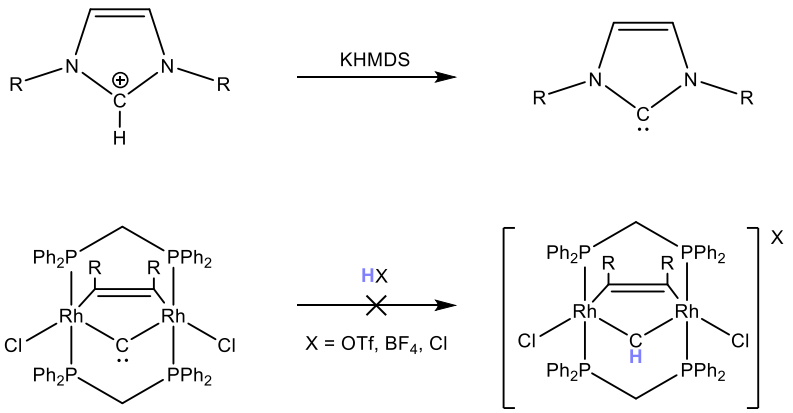

Scheme 3.20: Top: deprotonation of an imidazolium salt to form an NHC. Bottom: failed attempts at protonation of **24** to form a dirhodaimidazolium salt. R = CO_2Me

Unfortunately, the reactivity of the metallacarbene with various Brønsted acids was difficult to decipher. The reaction of the metallacarbene **24** with anhydrous tetrafluoroboric acid results in the expected yellow colour change and increased solubility of the product. The $^{31}P\{^{1}H\}$ NMR spectrum of the reaction mixture displays a slightly shifted resonance centred on 12.9 ppm, with a reduced $^{1}J_{RhP}$ coupling constant of 117 Hz. No resonance could, however, be identified in the ^{1}H NMR spectrum that would be consistent with the proton of a μ-methylidyne ligand, which would not only be expected to appear at a low field chemical shift, but also present distinct coupling to the ^{103}Rh and ^{31}P nuclei. Neither was there any evidence in the high-field region of the ^{1}H NMR spectrum (0 – -30 ppm) for the occurrence of direct protonation at one rhodium to afford a terminal hydrido ligand

Attempts to separate *via* column chromatography or isolate this species through crystallisation in petrol or toluene all failed, leading to largely decomposition of the ligand set or the reformation of the precursor **24**.

Attempts to change the acid to triflic or concentrated hydrochloric acid resulted in decomposition of the carbene species when the reactions were attempted. Though the carbene is the ideal protonation location, the presence of co-ordinately unsaturated rhodium centres and methyl ester groups on DMAD all present alternate sites for initial protonation.

Reactivity with carbon monoxide

One of the benchmark reactions that helps determine the nucleophilicity of a carbene is with carbon monoxide. It has been reported in the literature that strongly nucleophilic NHC species or abnormal NHCs (such as CAACs), are capable of coordinating to CO in solution to form the ketene species (**Scheme 3.21**).[189] Furthermore, there is precedent for the anticipated μ_2-ketenylidene ligand within A-frame chemistry, e.g., **[OsRhH(μ-CCO)(CO)$_3$(μ-dppm)$_2$]**.[190]

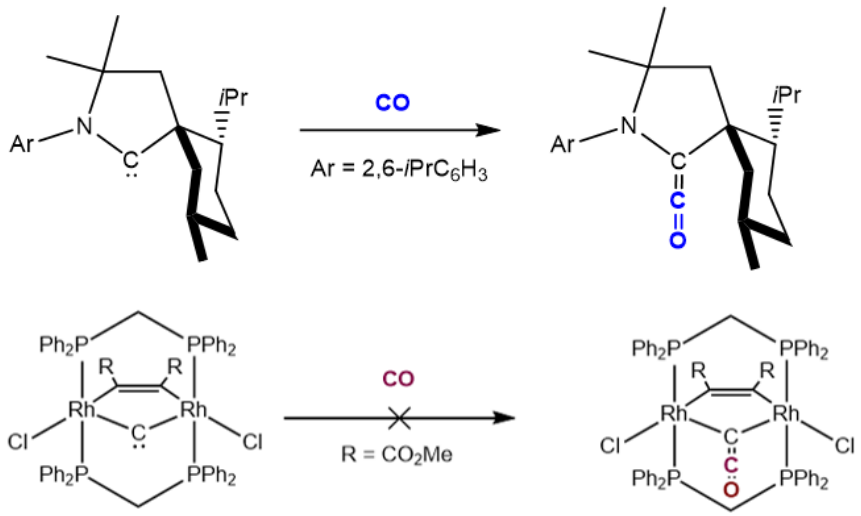

Scheme 3.21: (top) CAAC coordination to CO to form ketene. (Bottom) unsuccessful reaction between MHC **24** and carbon monoxide. R = CO_2Me

When CO was bubbled through a red suspension of **24** in either CH_2Cl_2 or THF no changes to the appearance of the solution were observed over 15 hours, while the $^{31}P\{^1H\}$ NMR spectra of the red solutions comprised only the resonance corresponding to the carbene starting material, suggesting no reaction had taken place. Similarly, heating a THF solution to *ca* 50 °C under an atmosphere of CO also failed to induce any reaction between the two species over a period of 3 hours. The DFT calculated HOMO of the simplified species **[Rh$_2$(μ-C)(μ-DMAD)Cl$_2$(μ-dmpm)$_2$]** is lower in energy (-0.6 eV) than those of CAACs, suggesting the MHC presents less nucleophilic character than a CAAC, perhaps explaining the failure to couple with carbon monoxide, despite the formally 16-electron rhodium centres.

3.3.9 Thio-, seleno- and tellurocarbonyls

The dirhodametallacyclic carbenes are topologically reminiscent of the Cowie's carbonyl complex **[Rh$_2$(μ-CO)(μ-DMAD)Cl$_2$(μ-dppm)$_2$],** in which the bridging carbide is replaced by a conventional bridging carbonyl. Although the carbonyl ligand was present on the dirhodium complex *prior* to installation of the alkyne, and no subsequent reactivity was described, 'on paper' one might imagine converting the carbido to a carbonyl simply by oxidation with an oxygen transfer agent. More interestingly, it could also be conjectured that the carbene character of the bent carbido ligand could react with the heavier chalcogens to provide the corresponding

chalcocarbonyl ligand. Because the carbonyl was already characterised, work would be focussed on completing the chalcogen series, with sulfur, selenium and tellurium. If successful, it would be the first examples of rhodium seleno- and tellurocarbonyl ligands. Such processes would be of fundamental intrigue but also attended by some irony in that the reverse reaction, abstraction of chalcogens from chalcocarbonyls, has been a fruitful strategy in the *formation* of carbido ligands.

Reactions with sulfur

Descending the chalcogen group, the thiocarbonyl complex was the first to be targeted. The benefit of attempting to make this thiocarbonyl complex was there were in fact two synthetic routes that could be attempted. Earlier in this work (**Section 1.3**), the first bridging thiocarbonyl species of rhodium was reported **[Rh$_2$(μ-CS)Cl$_2$(μ-dppm)$_2$]**. This thiocarbonyl complex is pre-arranged to be susceptible to coordination by DMAD, having one face of the molecule exposed, in a similar fashion to the process by which is formed the carbonyl complex **[Rh$_2$(μ-CO)(μ-DMAD)Cl$_2$(μ-dppm)$_2$]**. If the same reaction could be repeated with the thiocarbonyl preinstalled, it would lead to the same motif with the thiocarbonyl being retained.

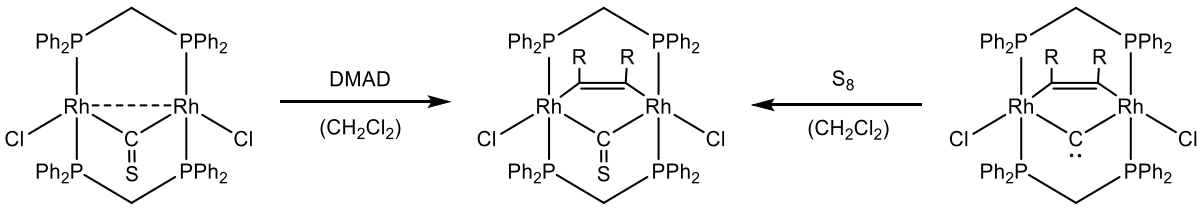

Scheme 3.22: Proposed synthetic pathways to the thiocarbonyl MHC complex **36** (R = CO_2Me)

Taking the dark green thiocarbonyl species **[Rh$_2$(μ-CS)Cl$_2$(μ-dppm)$_2$]**, addition of DMAD resulted in no immediately apparent reaction, in contrast to the addition of DMAD to [Rh$_2$(μ-C)Cl$_2$(μ-dppm)$_2$] which is complete in a matter of minutes. However, over the course of an hour, the green solution slowly decolourised to yellow, and monitoring the reaction by $^{31}P\{^1H\}$ NMR spectroscopy confirmed complete consumption of the starting material and the appearance of a new doublet at 7.08 ppm ($^1J_{RhP}$ = 133 Hz), in a region similar to that of the MHC-AuCl adduct. The crude solution could be effectively purified through silica gel chromatography, which eluted a pink band in a CH_2Cl_2/THF solution. The ESI-MS supported the formulation of the pink

product as being **[Rh$_2$(μ$_2$-CS)(μ-DMAD)Cl$_2$(μ-dppm)$_2$] (36)** with the appearance of a characteristic [M-Cl]$^+$ peak at 1195.0172 *m/z* (*cf.* calc. 1195.0179 *m/z*), supporting the installation of a single DMAD moiety. The IR spectra quite clearly showed the expected strong band of the carbonyl groups on DMAD, appearing as a broad band at 1720 cm^{-1}, and a shift in the CS stretch to 1249 cm^{-1}. The shift to a lower wavenumber suggests a lower bond order of the CS bond, which is logical given it is now involved in what might be described as a dimetallathiourea (imidazolylidene thione).

Once again, interrogating the NMR spectra in search of the ^{13}C resonance of interest (Rh$_2$*C*S) was confounded by the divaricate couplings arising from the Rh$_2$P$_4$ spin system present, such that the thiocarbonyl resonance was unable to be directly detected in this way. The ^{1}H NMR spectrum saw the usual splitting of the methylene bridge hydrogens on dppm, appearing at 2.88 and 3.95 ppm.

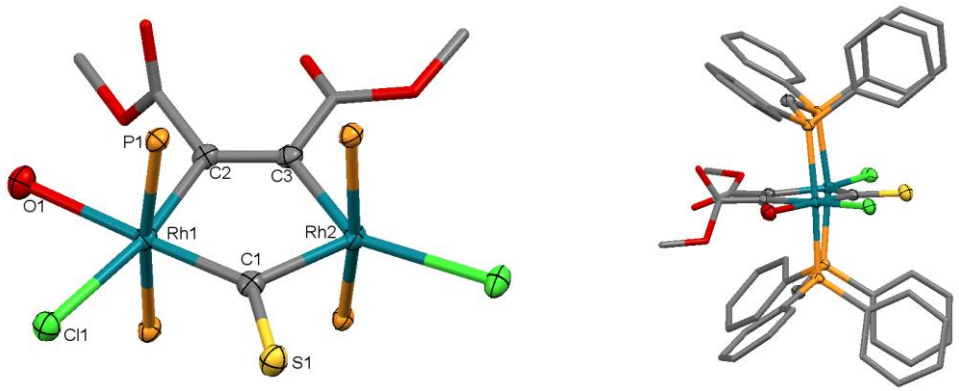

Figure 3.21: Molecular structure of **[Rh$_2$(μ$_2$-CS)(μ-DMAD)Cl$_2$(μ-dppm)$_2$] (36)** (50% displacement ellipsoids, solvent, hydrogen atoms omitted; phosphine substituents simplified). Selected distances [Å] and angles [°]: Rh1-C1 1.935(5), Rh1-C2 2.020(4), Rh1-Cl1 2.474(1), Rh1-O1 2.299(3), Rh2-C1 1.953(5), Rh2-C3 2.000(4), C1-S1 1.625(5), C2-C3 1.350(6), Rh1-C1-Rh1 122.0(2), Rh1/2 Centroid-C1-S1 168.3(1)

Once again, the molecular structure of an MHC-derived complex with DMAD crystallises with a single unit of H$_2$O which coordinates to a single rhodium centre (**Figure 3.21**). Superficially, its coordination has no gross effect on the geometry of the structure of **36** except that for the 5-coordinate rhodium the C3-Rh2–Cl2 angle is more clearly obtuse. This apparently minor compression seems sufficient to preclude coordination of a second aquo ligand – effectively an inverse cooperativity between the two potential binding sites. Data arising from NMR spectra of

the complex in solution are not consistent with the reduced (C_s) molecular symmetry arising from this coordination, suggesting that it is purely a solid-state packing effect from the slow crystallisation under less than scrupulously anhydrous conditions.[xli] Packing effects can also explain the marginal bend along the thiocarbonyl C-S bond (approximately 168.3 ° to the centre of the Rh1-Rh2 plane) such that C2, C1 and S1 are close to colinear, as a solvent unit of $CHCl_3$ is present in the unit cell, nestled in the space between Cl1 and S1, though not close enough to either for formal hydrogen bonding to be present.

The addition of sulfur to the bent carbido ligand in **36** does have a measurable effect on the geometry of the metallacycle. Specifically, the Rh–C(S) bonds are substantially lengthened (ca 0.1 Å) upon conversion to the thiocarbonyl (Rh1/2-C1 = 1.935(5) and 1.953(5) Å respectively) providing indirect support for the inferred Rh–C multiple bonding in the μ-carbido (MHC) complex. This can be attributed to net π-bonding capacity of the carbon now being also shared with sulfur at the expense of the bond order of this carbon to the rhodium centres. The remainder of the core bond lengths remain crystallographically identical to the other MHC complexes and their derivatives. Comparing the structure to the thiocarbonyl precursor, the Rh-C bond lengths of the thiocarbonyl ligand are essentially unchanged (Rh1/2-C1 = 1.913(4) and 1.915(4) Å, approximately 4 e.s.d. longer). The Rh-C-Rh angle of the μ_2-thiocarbonyl is exceptionally different, with **[Rh$_2$(μ_2-CS)Cl$_2$(μ-dppm)$_2$]** bent to a near perfect 90 ° (90.0(2)), which increases rather dramatically to 122.0(2) ° in **[Rh$_2$(μ_2-CS)(μ_2-DMAD)Cl$_2$(μ-dppm)$_2$]**.

Given that the thiocarbonyl complex **36** could be synthesised and was found to be air-stable, the alternative synthetic route was explored beginning with the free MHC complex to investigate its reactivity towards elemental sulfur. Taking a CH_2Cl_2 solution of the MHC, the suspension shows no immediate reaction when S_8 is added. Leaving the mixture overnight, however resulted in a dark red, clear solution with no visible suspended sulfur particles remaining. A red band was eluted from a silica gel chromatography column with CH_2Cl_2/THF as eluent, and the $^{31}P\{^1H\}$ NMR spectrum found to comprise the expected doublet for the thiocarbonyl product at 7.08 ppm, but also the presence of multiple phosphine decomposition products, including dppm-S and dppm-S_2. The ring-opening of S_8 can be initiated by nucleophiles, electrophiles, or single-electron transfer formation of diradical species making conjecture as to the intimate mechanistic detail exceptionally difficult to substantiate or predict. Once oxidative sulfurisation of a pendant

[xli] The possibility that aquo association/dissociation is rapid on the $^{31}P\{^1H\}$ NMR timescale could not be excluded; however intentional use of moist NMR solvents did not result in variations in the chemical shift.

phosphine to a phosphine sulfide occurs, its ability to recoordinate is significantly diminished. That being said, the synthesis of the thiocarbonyl species nevertheless confirms the conversion of the bent carbido ligand to a thiocarbonyl.

In an attempt to optimise the synthetic protocol, the sulfur source propylene sulfide was also briefly examined to circumvent the unpredictable and somewhat indiscriminate S_8 reactivity. An NMR-scale reaction with the MHC complex and propylene sulfide initially showed no reactivity when monitoring through $^{31}P\{^{1}H\}$ NMR spectroscopy. When the solution was left overnight, the red suspension evolved to orange which initially looked promising, however, the $^{31}P\{^{1}H\}$ NMR spectrum revealed complete consumption of the coordinated dppm ligands to form free sulfide adducts, with no residual peaks indicating Rh-P coordination.

Reactions with selenium

With oxygen and sulfur accounted for, the next chalcogen to be examined was selenium. The selenium reaction was expected to be more problematic than the lighter two chalcogens, as there is no precedent for a rhodium selenocarbonyl complex to date and excess (??) elemental (grey) selenium is exceedingly insoluble in common organic solvents. A CH_2Cl_2 mixture of the MHC and selenium was a near black suspension due to the low solubility of both reactants. Vigorous stirring overnight still showed the presence of suspended selenium, however, recourse to column chromatography gave an orange and pink band.

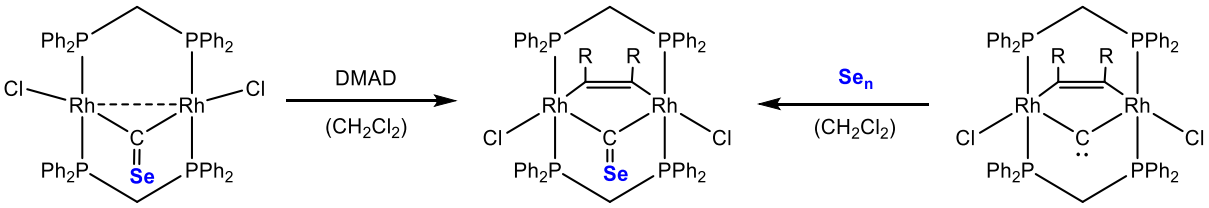

Scheme 3.23: Proposed synthetic pathways to the MHC-derived selenocarbonyl complex **37** (R = CO_2Me)

The orange band contained residual MHC starting material and a parade of phosphorus resonances analogous to the sulfur reaction. The pink band comprised a pure single compound, which provided the necessary dppm and DMAD hydrogen resonances in the ^{1}H NMR spectrum, and a single symmetrical ^{31}P environment at 4.11 ppm ($^{1}J_{RhP}$ = 131 Hz). Although the isolated yield

of this pink species was a disappointing 11%, and the reaction largely formed the decomposition/unidentifiable side reaction products, the synthesis was repeatable and reliable (**Scheme 3.23**).

The high-resolution ESI-MS data gave a perfect match for the $[M\text{-}Cl]^+$ fragment at 1242.9637 m/z (Calcd. for $C_{57}H_{50}{}^{35}ClO_4P_4Rh_2{}^{80}Se$ $[M\text{-}Cl]^+$ = 1242.9629 m/z), with the characteristically wide envelope of isotopes[xlii] associated with selenium inclusion in **[Rh$_2$(μ$_2$-CSe)(μ$_2$-DMAD)Cl$_2$(μ-dppm)$_2$] (37)**. The C-Se stretch even could be identified in the infrared spectrum at 893 cm^{-1}, however, no comparison can be made with the only other known symmetrically bridging selenocarbonyl complex **[Ru$_2$(μ-CSe)(μ-N^{t}Bu)(η-C$_5$Me$_5$)$_2$]**, as it was not reported by the authors.[77]

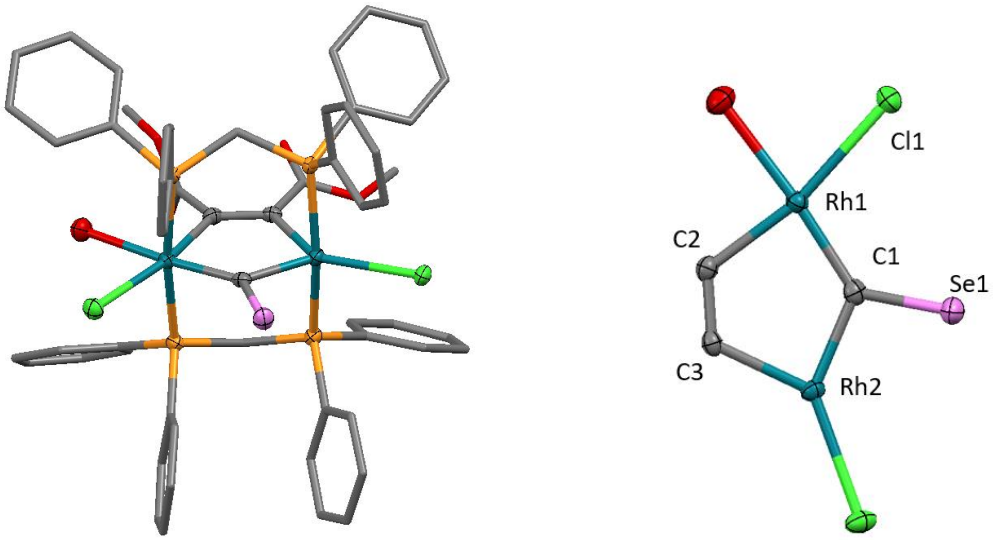

Figure 3.22: Molecular structure of **[Rh$_2$(μ$_2$-CSe)(μ:σ,σ'–DMAD)Cl$_2$(μ-dppm)$_2$] (37)** (50% displacement ellipsoids, solvent and hydrogen atoms omitted; phosphine substituents simplified). Selected distances [Å] and angles [°]: Rh1-C1 1.927(6), Rh1-C2 2.017(6), Rh1-Cl1 2.478(2), Rh1-O1 2.289(5), Rh2-C1 1.935(6), Rh2-C3 2.008(6), C1-Se1 1.785(6), C2-C3 1.345(8), Rh1-C1-Rh1 124.2(3), Rh1/2 Centroid-C1-Se1 164.0(1), C2-Rh1-C1 86.2(2), C3-Rh2-C1 87.7(2)

[xlii] Selenium has six isotopes that occur naturally in significant abundances, five of which are stable (^{74}Se, ^{76}Se, NMR-active ^{77}Se, ^{78}Se and ^{80}Se).

The molecular structure of **37** (**Figure 3.22**) follows the patterns observed for the thiocarbonyl analogue. The selenium is slightly bent (C2/C3 centroid-C1-Se1 = 164.0(1) °), due to the coordinated aquo ligand on a single rhodium centre. The two Rh-C bonds to the selenocarbonyl ligand show insignificant deviation from the thiocarbonyl analogue (1.927(6) and 1.935(6) Å *cf.* 1.935(5) and 1.953(5) Å for sulfur, max Δ = 4 e.s.d), though the carbon-chalcogen bond is significantly longer for selenium than sulfur, as expected with the heavier element (1.785(6) *cf.* 1.625(5) Å; r_{cov} = 1.05(3) (S), 1.20(4) Å (Se)).

The synthesis of **$[Rh_2(\mu_2\text{-CSe})(\mu\text{:}\sigma,\sigma'\text{-DMAD})Cl_2(\mu\text{-dppm})_2]$ (37)** provides the first known example of a rhodium selenocarbonyl complex, and only the second report for a Group 9 element beyond a single paper on the selenocarbonyl analogue of Vaska's Complex **$[IrCl(CSe)(PPh_3)_2]$**, which is yet to be structurally characterised. Because of its significance, the ^{13}C enriched isotopologue was prepared under identical conditions, and the selenocarbonyl resonance was located at 318.3 ppm, further upfield than expected provided the previously identified selenocarbonyl resonance in **$[Rh_2(\mu_2\text{-CSe})Cl_2(\mu\text{-dppm})_2]$** located at 341.3 ppm. The significance of bridging selenocarbonyl ligands and their NMR properties will become apparent in a subsequent Chapter.

With the success of forming the MHC/chalcocarbonyl analogues, a synthetic manifold can be constructed which demonstrates the interconnectivity between the carbido and chalcocarbonyl ligands (**Scheme 3.24**).

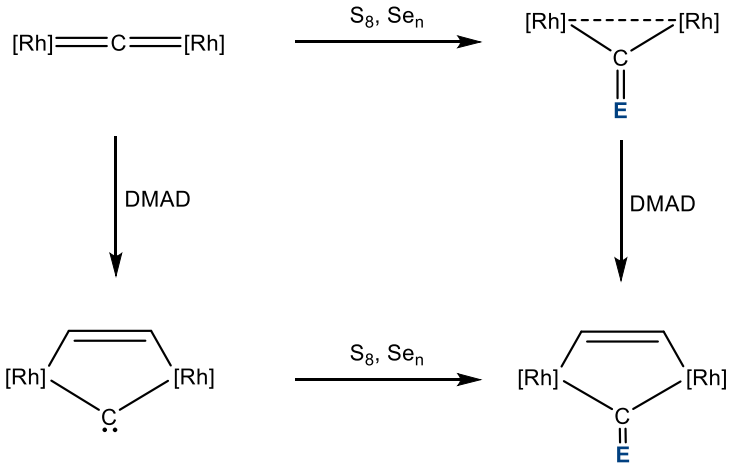

Scheme 3.24: The interplay between the carbido, carbene, and chalcocarbonyl ligands (E = S, Se)

Attempted construction of a tellurocarbonyl

Moving down Group 16, tellurium – the element Chivers has described as the 'maverick amongst chalcogens' – was finally attempted.[191] The range of tellurocarbonyl complexes is even more scarce than thio- and selenocarbonyl complexes. Unfortunately, tellurium is even less soluble than selenium and sulfur and the tellurocarbonyl ligand considerably less stable due to poor π-orbital overlap between a light and heavy element.

Under the same reaction conditions that proved successful for sulfur and selenium, no observable reaction ensued when monitoring both colour change and the ^{31}P NMR spectrum. Attempts to thermally encourage the reaction in dichloroethane merely resulted in the decomposition of the metallacarbene species. Unfortunately, the chalcocarbonyl series stops at selenium for now.

3.3.9 Summary

This Chapter started by exploring the reactivity of the μ-carbido ligand with acetylenes. Though the expected [2+2] cycloaddition did not take place, it was found with the activated alkyne DMAD that a [3+2] cycloaddition across the Rh-C-Rh linkage was possible, with the alkyne adopting a *cis*-vinylic μ:σ,σ' bridging mode to the two rhodium centres. The complex **[Rh_2(μ-C)(μ:σ,σ'-DMAD)Cl_2(μ-dppm)$_2$]** contains a bent μ-carbido ligand, which was calculated to pertain carbene-like characteristics. The bent μ-carbido class of complex could be broadened with metallacycles derived from hexalfluoro-2-butyne and ethyl 4,4,4-trifluoro-2-butynoate, but not simple terminal or internal hydrocarbon alkynes. The ^{13}C NMR chemicals shift of the bent carbido nucleus appears dramatically downfield at 563.0 ppm.

The persistent carbene character could be experimentally confirmed through reactivity with synthons for linear metal-ligand fragments, forming μ_3-carbido complexes of the general formula **[Rh_2M(μ_3-C)(μ-DMAD)RCl_2(μ-dppm)$_2$]**, where MR = AuCl, CuCl, Au(C_6F_5). The MHC complexes were also observed to undergo a weak coordination in solution with mercury(II) electrophiles, namely $HgCl_2$ and **[$Hg(CF_3)_2$]**.

The μ_2-chlorocarbyne complex **[Rh_2(μ_2-CCl)(μ-DMAD)Cl_2(μ-dppm)$_2$]$^+$** could be formed through a variety of pathways. Attempts to coordinate '$AuCl_3$' resulted in a redox process providing instead the chlorocarbyne and **[$AuCl_2$]$^-$** counter ion, while direct halogenation using $PhICl_2$ formed the same chlorocarbyne complex as a chloride salt.

Unfortunately, due to a combination of steric hindrance, vacant coordination sites on rhodium and low carbene donicity, many of the inorganic and organic reagents explored were unsuccessful in coordination or simply led to decomposition of the carbene species.

The metallacarbene complex successfully reacted with sources of both sulfur and selenium to afford the corresponding μ_2-thio- and selenocarbonyl complexes **[$Rh_2(\mu_2$-CE)(μ:σ,σ'-DMAD)$Cl_2(\mu$-dppm)$_2$]** (E = S, Se).

The work in this chapter provides the first example of a stable *Metalla*-Heterocyclic Carbene, and has been published in the following works:

1. H. J. Barnett, A. F. Hill, *Angew. Chem. Int. Ed.,* **2020**, 59, 4274
2. H. J. Barnett, A. F. Hill, *Chem. Commun.,* **2020**, 56, 12593

3.4 EXPERIMENTAL

Synthesis of $[Rh_2(\mu_2\text{-}C)(\mu_2\text{-}DMAD)Cl_2(\mu\text{-}dppm)_2]$ (24)

To a flask containing $[Rh_2(\mu\text{-}C)Cl_2(\mu\text{-}dppm)_2]$ (0.018 g, 0.017 mmol) was added CH_2Cl_2 (15 mL). To this yellow solution, DMAD (0.10 mL, 1.156 $Mg.m^{-3}$, 0.81 mmol) was added, and the resulting red solution was stirred for 30 min. After this time the volatiles were removed *in vacuo* and the residue was subjected to column chromatography (10 x 1 cm silica gel column), eluting initially with neat CH_2Cl_2 and then with 1:19 THF:CH_2Cl_2. A red band was collected, and the volatiles were removed under reduced pressure to give a red microcrystalline solid of pure **24**. Yield: 0.019 g (0.016 mmol, 93%). ^{1}H NMR (400 MHz, $CDCl_3$, 298 K): δ_H = 1.99 (br. s, 2 H, PCH_2), 2.40 (s, 6 H, CH_3), 3.54 (br. s, 2 H, PCH_2), 6.96 (s, 2 H, C_6H_5), 7.05–7.09 (m, 8 H, C_6H_5), 7.17–7.21 (m, 4 H, C_6H_5), 7.36 (br. s, 10 H, C_6H_5), 7.86 (br. s, 8 H, C_6H_5), 8.00-8.05 (m, 8 H, C_6H_5). ^{13}C{^{1}H} NMR (151 MHz, $CDCl_3$, 298 K): δ_C = 563.0 (tp, $^1J_{RhC}$ = 30 Hz, $^2J_{PC}$ = 9 Hz, μ-C), 152.3 (CO_2), 135.1, 134.0, 132.0, 130.4, 128.6, 128.3 (2C), 128.2 (8 x br. s, C_6H_5), 74.8 (RhC=CRh), 50.3 (OCH_3), 15.5 (PCH_2). ^{31}P{^{1}H} NMR (162 MHz, $CDCl_3$, 298 K): δ_P = 12.5 (d, $^1J_{RhP}$ = 137 Hz). IR (ATR, cm^{-1}): 1732s, 1700s ν_{CO}, 1435s $\nu_{C=C}$, 1206s ν_{C-O}, 798s $\nu_{Rh=C=Rh}$. MS (ESI, *m/z*): Accurate mass: Found 1163.04340. Calcd for $C_{57}H_{50}{}^{35}ClO_4P_4Rh_2$ $[M–Cl]^+$: 1163.04527. Anal. Found: C, 51.75; H, 3.97%. Calcd for $C_{57}H_{50}Cl_2O_4P_4Rh_2.2CH_2Cl_2$: C, 51.18; H, 4.59%. A crystal suitable for structure determination was grown by slow evaporation of a CH_2Cl_2/hexane mixture. *Crystal data for* $C_{57}H_{50}Cl_2O_4P_4Rh_2$ (M_w =1199.57 $g.mol^{-1}$): tetragonal, space group $P4_3$ (No. 78), a = 21.2191(3), c = 14.2033(3) Å, V = 6395.0(2) $Å^3$, Z = 4, T = 150.0(1) K, μ(Cu Kα) = 22.258 mm^{-1}, D_{calcd} = 1.246 $Mg.m^{-3}$, 34755 reflections measured (7.6° ≤ 2Θ ≤ 133.2°), 11255 unique (R_{int} = 0.065) which were used in all calculations. The final R_1 was 0.070 ($I > 2\sigma(I)$) and wR_2 was 0.193 (all data) for 619 refined parameters with 67 restraints. CCDC 1955250.

Synthesis of $[Rh_2(\mu_2\text{-}C)(\mu_2\text{-}F_3C\text{-}CC\text{-}CO_2Et)Cl_2(\mu\text{-}dppm)_2]$ (25)

To a flask containing $[Rh_2(\mu\text{-}C)Cl_2(\mu\text{-}dppm)_2]$ (0.080 g, 0.072 mmol) was added CH_2Cl_2 (10 mL). To this yellow solution, ethyl-4,4,4-trifluoro-2-butynoate (0.020 mL, 1.162 $Mg.m^{-3}$, 0.14 mmol) was added, and the resulting solution turned red over the course of 30 min. After this time,

petroleum spirits (10 mL) were added, and the resulting red precipitate isolated *via* vacuum filtration to give a red microcrystalline solid of pure $[Rh_2(\mu_2\text{-}C)(\mu_2\text{-}F_3C\text{-}CC\text{-}CO_2Et)Cl_2(\mu\text{-}dppm)_2]$. Yield: 0.080 g (0.066 mmol, 91%). ^{1}H NMR (400 MHz, $CDCl_3$, 298 K): δ_H = 0.25 (t, $^3J_{HH}$ = 7 Hz, 3 H, CH_3), 2.38 (br., 2 H, PCH_2), 3.01 (q, $^3J_{HH}$ = 7 Hz, 2 H, OCH_2), 3.54-3.57 (m, 2 H, PCH_2), 6.99-7.08 (m, 8 H, C_6H_5), 7.38, 7.57, 7.66 (3 x m, 24 H, C_6H_5), 7.99 (br. s, 8 H, C_6H_5). $^{13}C\{^1H\}$ NMR (151 MHz, $CDCl_3$, 298 K): δ_C =135.1, 133.5, 132.1, 132.1, 131.0, 130.7, 130.6, 128.7, 128.4, 127.7, 126.9 (C_6H_5), 59.9 (OCH_2), 15.4 (PCH_2), 13.5 (CH_3). Carbon-13 resonances identified through ^{1}H-^{13}C HSQC/HMBC studies. μ-carbido and CF_3 groups unable to be identified due to low solubility. $^{31}P\{^1H\}$ NMR (162 MHz, $CDCl_3$, 298 K): δ_P = 10.96 (m), 11.54 (m). $^{19}F\{^1H\}$ NMR (376.5 MHz, CD_2Cl_2, 298K): δ_F = -49.15 (s). IR (ATR, cm^{-1}): 1699s ν_{CO}, 1435s $\nu_{C=C}$, 1220s $\nu_{C\text{-}F}$, 800s $\nu_{Rh=C=Rh}$. MS (ESI, *m/z*): Accurate mass: Found 1187.0452. Calcd for $C_{57}H_{49}{}^{35}ClF_3O_2P_4Rh_2$ $[M–Cl]^+$: 1187.0434. A crystal suitable for structure determination was grown by slow evaporation of a $CHCl_3$/hexane mixture. *Crystal data for* $C_{57}H_{49}Cl_2F_3O_2P_4Rh_2$ (M =1223.56 g.mol^{-1}): tetragonal, space group $P4_1$ (No. 76), a = 21.1663(1), c = 14.1382(2) Å, V = 6334.09(11) Å^3, Z = 4, T = 150.0(1) K, μ(Cu Kα) = 6.31 mm^{-1}, D_{calcd} = 1.283 Mg.m^{-3}, 36741 reflections measured (8.4° ≤ 2Θ ≤ 141.6°), 11459 unique (R_{int} = 0.035) which were used in all calculations. The final R_1 was 0.042 ($I > 2\sigma(I)$) and wR_2 was 0.116 (all data) for 695 refined parameters with 77 restraints.

Synthesis of $[Rh_2(\mu_2\text{-}C)(\mu_2\text{-}HFB)Cl_2(\mu\text{-}dppm)_2]$ (26)

To a flask containing **$[Rh_2(\mu\text{-}C)Cl_2(\mu\text{-}dppm)_2]$** (0.053 g, 0.050 mmol) was added CH_2Cl_2 (10 mL). The argon was evactuated under reduced pressure, and back filled with one atmosphere of hexafluoro-2-butyne (HFB). The solution left to stir under an atmosphere of HFB for 48 hours. After this time, hexane (10 mL) was added to the red solution, and the resulting red precipitate isolated *via* vacuum filtration to give a red microcrystalline solid of pure $[Rh_2(\mu_2\text{-}C)(\mu_2\text{-}HFB)Cl_2(\mu\text{-}dppm)_2]$. Yield: 0.057 g (0.047 mmol, 94%). The ^{31}P and $^{19}F\{^1H\}$ NMR spectra were recorded in both $CDCl_3$ and CD_2Cl_2. ^{1}H NMR (400 MHz, $CDCl_3$, 298 K): δ_H = 2.79-2.84 (m, 2 H, PCH_2), 3.74 (dp^v, $^2J_{PH}$ = 13, $^2J_{HH}$ = 6 Hz, 2 H, PCH_2), 6.88 (t, $^3J_{HH}$ = 8 Hz, 3 H, C_6H_5), 7.02 (t, $^3J_{HH}$ = 8 Hz, 5 H, C_6H_5), 7.33-7.39 (m, 15 H, C_6H_5), 7.61 (m, 4H, C_6H_5), 7.71 (t, $^3J_{HH}$ = 7 Hz, 2 H, C_6H_5), 7.81 (q J = 7 Hz, 3 H, C_6H_5), 7.94 (m, 4 H, C_6H_5), 8.01 (q, J = 6 Hz, 3 H, C_6H_5). $^{13}C\{^1H\}$ NMR (151 MHz, $CDCl_3$, 298 K): δ_C = 136.0, 134.2, 133.2, 131.6, 131.2, 130.8, 128.8, 127.6 (C_6H_5), 16.0 (PCH_2). ^{13}C peaks identified through ^{1}H-^{13}C HSQC and ^{1}H-^{13}C HMBC studies. HFB and μ-carbido resonances

not found. $^{31}P\{^1H\}$ NMR (162 MHz, $CDCl_3$, 298 K): δ_P = -0.22 (d, $^1J_{RhP}$ = 120 Hz), 0.85 (d, $^1J_{RhP}$ = 104 Hz), 9.27 (d, $^1J_{RhP}$ = 136 Hz). $^{31}P\{^1H\}$ NMR (162 MHz, CD_2Cl_2, 298 K): δ_P = -0.36 (d, $^1J_{RhP}$ = 119 Hz), 0.78 (d, $^1J_{RhP}$ = 103 Hz), 10.46 (d, $^1J_{RhP}$ = 131 Hz). $^{19}F\{^1H\}$ NMR (376 MHz, $CDCl_3$, 298K): δ_F = -49.43 (s), -50.01 (q, $^5J_{FF}$ = 18 Hz), -51.67 (q, $^5J_{FF}$ = 18 Hz). $^{19}F\{^1H\}$ NMR (376.5 MHz, CD_2Cl_2, 298K): δ_F = -49.60 (s), -50.25 (q, $^5J_{FF}$ = 18 Hz), -51.73 (q, $^5J_{FF}$ = 18 Hz). IR (ATR, cm^{-1}): 1435s $\nu_{C=C}$, 1207, 1219 ν_{CF}, 804s $\nu_{Rh=C=Rh}$. MS (ESI, *m/z*) Accurate mass: Found 1183.0096. Calcd for $C_{55}H_{44}{}^{35}ClF_6P_4Rh_2$ $[M–Cl]^+$: 1183.0111. A crystal suitable for structure determination was grown by slow evaporation of a CH_2Cl_2/C_6H_6 mixture. *Crystal data for* $C_{55}H_{44}Cl_2F_6P_4Rh_2.0.33(C_6H_6)$ (M_w =1245.54 g.mol^{-1}): tetragonal, space group $P4_3$ (No. 78), a = 21.1471(1), c = 14.2797(2) Å, V = 6385.88(11) Å^3, Z = 4, T = 150.0(1) K, μ(CuKα) = 6.31 mm^{-1}, D_{calcd} = 1.296 Mg.m^{-3}, 25511 reflections measured (8.4° ≤ 2Θ ≤ 147.0°), 9475 unique (R_{int} = 0.043) which were used in all calculations. The final R_1 was 0.035 (I > 2σ(I)) and wR_2 was 0.085 (all data) for 664 refined parameters with 49 restraints.

Synthesis of [Rh$_2$Au(μ$_3$-C)(μ$_2$-DMAD)Cl$_3$(μ-dppm)$_2$] (27)

To a flask containing [Rh$_2$(μ$_2$-C)(μ$_2$-DMAD)Cl$_2$(μ-dppm)$_2$] (0.019 g, 0.016 mmol) and [AuCl(SMe$_2$)] (0.007 g, 0.02 mmol) was added CH_2Cl_2 (10 mL). The resulting red solution was stirred for 30 min, turning orange in colour. After this time the volatiles were removed *in vacuo* and the residue was subjected to silica gel chromatography, eluting initially with neat CH_2Cl_2 and then with 1:19 THF:CH_2Cl_2. A yellow band was collected, and the volatiles were removed under reduced pressure to give an orange microcrystalline solid of pure **[Rh$_2$Au(μ$_3$-C)(μ$_2$-DMAD)Cl$_3$(μ-dppm)$_2$] (27)**. Yield: 0.025 g (0.014 mmol, 90%). ^1H NMR (400 MHz, $CDCl_3$, 298 K): δ_H = 1.99 (br. s, 2 H, PCH_2), 2.40 (s, 6 H, CH_3), 3.54 (br. s, 2 H, PCH_2), 6.96 (s, 2 H, C_6H_5), 7.05–7.09 (m, 8 H, C_6H_5), 7.17–7.21 (m, 4 H, C_6H_5), 7.36 (br s, 10 H, C_6H_5), 7.86 (br s, 8 H, C_6H_5), 8.00-8.05 (m, 8 H, C_6H_5). $^{13}C\{^1H\}$ NMR (151 MHz, $CDCl_3$, 298 K): δ_C = 471.1 (tp, $^1J_{RhC}$ = 20 Hz, $^2J_{PC}$ = 8 Hz, μ$_3$-C), 165.4 (br., CO_2), 134.8 (t^v, J = 7 Hz, C_6H_5), 133.6 (t^v, J = 7 Hz, C_6H_5), 132.1 (t^v, J = 5 Hz, C_6H_5), 131.6 (s, C_6H_5), 130.8 (s, C_6H_5), 129.7 (t^v, J = 6 Hz, C_6H_5), 128.7 (t^v, J = 5 Hz, C_6H_5), 128.6 (t^v, J = 5 Hz, C_6H_5), 50.8 (s, CH_3), 14.7 (p^v, J = 14 Hz, PCH_2). DMAD alkyne resonance not detected due to overlap with $CDCl_3$ signal. $^{31}P\{^1H\}$ NMR (162 MHz, $CDCl_3$, 298 K): δ_P = 7.8 (d, $^1J_{RhP}$ = 130 Hz). IR (ATR, cm^{-1}): 1726 br s ν_{CO}, 1435s $\nu_{C=C}$, 1208s ν_{C-O}. MS (ESI, *m/z*)

Accurate mass: Found 1394.98169. Calcd for $C_{57}H_{50}Au^{35}Cl_2O_4P_4Rh_2$ $[M–Cl]^+$: 1394.98067. Despite multiple attempts, satisfactory analytical elemental data were not obtained due to sample decomposition in transit, best is presented here. Anal. Found: C, 33.91; H, 3.32%. Calcd for $C_{57}H_{50}AuCl_3O_4P_4Rh_2$: C, 47.81; H, 3.52%. A crystal suitable for structure determination was grown by slow evaporation of a CH_2Cl_2/hexane mixture. *Crystal data for* $C_{57}H_{50}AuCl_3O_4P_4Rh_2.CHCl_3$ (M_w =1516.91 g.mol^{-1}): monoclinic, space group $P2_1/c$ (No. 14), a = 12.5998(1), b = 15.7877(1), c = 30.5760(3) Å, β = 92.147(1)°, V = 6077.96(9) Å^3, Z = 4, T = 150.0(1) K, μ(Cu Kα) = 22.258 mm^{-1}, D_{calcd} = 1.658 Mg.m^{-3}, 76036 reflections measured (8.0° ≤ 2Θ ≤ 147.6°), 12199 unique (R_{int} = 0.045) which were used in all calculations. The final R_1 was 0.059 ($I > 2\sigma(I)$) and wR_2 was 0.153 (all data) for 666 refined parameters with 30 restraints. CCDC 1955249.

Synthesis of $[Rh_2Au(\mu_3\text{-}C)(\mu_2\text{-}F_3CCCO_2Et)Cl_3(\mu\text{-}dppm)_2]$ (28)

To a flask containing $[Rh_2(\mu\text{-}C)(\mu_2\text{-}F_3CCCCO_2Et)Cl_2(\mu\text{-}dppm)_2]$ (0.030 g, 0.025 mmol) and $[AuCl(SMe_2)]$ (0.011 g, 0.037 mmol) was added CH_2Cl_2 (10 mL). The resulting red solution was stirred for 30 min, turning gold in colour. After this time the volatiles were removed *in vacuo* and the residue was subjected to column chromatography (10 x 1 cm silica gel column), eluting initially with neat CH_2Cl_2 and then with 1:19 THF:CH_2Cl_2. An orange band was collected, and the volatiles were removed under reduced pressure to give a yellow microcrystalline solid of pure $[Rh_2Au(\mu_3\text{-}C)(\mu_2\text{-}F_3CCCCO_2Et)Cl_3(\mu\text{-}dppm)_2]$. Yield: 0.034 g (0.024 mmol, 95%). ^{1}H NMR (400 MHz, $CDCl_3$, 298 K): δ_H = 0.00 (t, $^3J_{HH}$ = 7 Hz, 3 H, CH_3), 2.77-2.80 (m, 2 H, PCH_2), 2.80 (q, $^3J_{HH}$ = 7 Hz, 2 H, OCH_2), 3.58-3.67 (m, 2 H, PCH_2), 7.09 (d, J_{HH} = 7 Hz, 2 H, C_6H_5), 7.11 (d J_{HH} = 7 Hz, 2 H, C_6H_5), 7.16-7.21 (m , 16 H, C_6H_5), 7.28-7.30 (m, 6 H, C_6H_5), 7.78 (br. m, 4 H, C_6H_5), 8.02 (br. q, $^3J_{HH}$ = 7 Hz, 4 H, C_6H_5), 8.14 (dq, $^3J_{HH}$ = 14, $^5J_{HH}$ = 7 Hz, 6 H, C_6H_5). ^{13}C{^{1}H} NMR (151 MHz, $CDCl_3$, 298 K): δ_C = 134.3, 134.0, 132.8, 131.2, 131.0, 128.5, 128.0, 127.8, 124.7 (C_6H_5), 61.4 (OCH_2), 14.7 (PCH_2), 13.1 (-CH_3). ^{13}C peaks identified through HSQC and HMBC studies. μ_3-carbido, carboxylate, CF_3 and alkenyl environments not detected. ^{31}P{^{1}H} NMR (162 MHz, $CDCl_3$, 298 K): δ_P = 4.52 (d x m, $^1J_{RhP}$ = 124 Hz), 6.46 (d x m, $^1J_{RhP}$ = 127 Hz). ^{19}F{^{1}H} NMR (376 MHz, $CDCl_3$, 298K): δ_F = -51.08. IR (ATR, cm^{-1}): 1704 s ν_{CO}, 1435 $\nu_{C=C}$, 1219, $\nu_{C\text{-}F}$. MS (ESI, *m/z*) Accurate mass: Found 1418.97871. Calcd for $C_{57}H_{49}Au^{35}Cl_2F_3O_4P_4Rh_2$ $[M–Cl]^+$: 1418.97823. A crystal suitable for structure determination was grown by slow evaporation of a CH_2Cl_2/hexane mixture. *Crystal data for* $C_{57}H_{50}AuCl_3F_3O_{2.5}P_4Rh_2{\cdot}0.5CH_2Cl_2$ (M_w =1507.45 g.mol^{-1}): monoclinic,

space group $P2_1/c$ (No. 14), a = 12.9893(3), b = 15.9264(4), c = 30.6470(8) Å, β = 93.797(2)°, V = 6326.1(3) Å^3, Z = 4, T = 150.0(1) K, μ(Cu Kα) = 11.35 mm^{-1}, D_{calcd} = 1.583 Mg.m^{-3}, 197089 reflections measured (8.8° ≤ 2Θ ≤ 141.0°), 11772 unique (R_{int} = 0.030) which were used in all calculations. The final R_1 was 0.063 ($I > 2\sigma(I)$) and wR_2 was 0.164 (all data) for 746 refined parameters with 204 restraints.

Synthesis of [Rh$_2$Au(μ$_3$-C)(μ$_2$-HFB)Cl$_3$(μ-dppm)$_2$] (29)

To a flask containing [Rh$_2$(μ-C)(μ$_2$-HFB)Cl$_2$(μ-dppm)$_2$] (0.029 g, 0.024 mmol) and [AuCl(THT)] (0.011 g, 0.036 mmol) was added CH_2Cl_2 (10 mL). The resulting red solution was stirred for one hour, turning gold in colour. After this time the volatiles were removed *in vacuo* and the residue was subjected to silica gel chromatography, eluting initially with neat CH_2Cl_2 and then with 1:19 THF:CH_2Cl_2. An orange band was collected, and the volatiles were removed under reduced pressure to give a yellow microcrystalline solid of pure **[Rh$_2$Au(μ$_3$-C)(μ$_2$-HFB)Cl$_3$(μ-dppm)$_2$] (29)**. Yield: 0.033 g (0.023 mmol, 96%). ^{1}H NMR (400 MHz, $CDCl_3$, 298 K): δ_H = 2.88, 3.54 (2 x m, 4 H, PCH_2), 7.08-7.11 (m, 8 H, C_6H_5), 7.18-7.22 (m, 7 H, C_6H_5), 7.42 (br. s, 12 H, C_6H_5), 7.96 (br. s, 7 H, C_6H_5), 8.10-8.13 (m, 6 H, C_6H_5). ^{13}C{^{1}H} NMR (151 MHz, $CDCl_3$, 298 K): δ_C = 134.8, 133.6, 132.1, 131.8, 131.4, 129.8, 128.9, 125.7 (C_6H_5), 14.7 (PCH_2). μ$_3$-C and CF_3 environments not detected. Carbon-13 resonances detected using ^{1}H-^{13}C HSQC and HMBC studies due to low solubility.^{31}P{^{1}H} NMR (162 MHz, $CDCl_3$, 298 K): δ_P = 4.71 (d, $^1J_{RhP}$ = 124 Hz). ^{19}F{^{1}H} NMR (376.5 MHz, $CDCl_3$, 298K): δ_F = -50.58 (s). IR (ATR, cm^{-1}): 1435s $\nu_{C=C}$, ,1219 ν_{C-F}. MS (ESI, *m/z*): Accurate mass: Found 1456.0024. Calcd for $C_{55}H_{44}Au^{35}Cl_2F_6P_4Rh_2$ [M–Cl+MeCN]$^+$: 1455.9716. A crystal suitable for structure determination was grown by slow evaporation of a CH_2Cl_2/hexane mixture. *Crystal data for* 4($C_{55}H_{44}AuCl_3F_6P_4Rh_2$) ($M$ =5807.66 g.mol^{-1}): monoclinic, space group $P2_1/c$ (No. 14) a = 46.8295(5), b = 13.0711(1), c = 43.5964(5) Å, β = 109.821(1)°, V = 25105.0(5) Å^3, Z = 4, T = 150.0(1) K, μ(Cu Kα) = 11.07 mm^{-1}, D_{calcd} = 1.537 Mg.m^{-3}, 81,758 reflections measured (8.6° ≤ 2Θ ≤ 141.6°), 46,788 unique (R_{int} = 0.038) which were used in all calculations. The final R_1 was 0.051 ($I > 2\sigma(I)$) and wR_2 was 0.119 (all data) for 2,557 refined parameters.

Synthesis of [Rh$_2$Cu(μ$_3$-C)(μ$_2$-DMAD)Cl$_3$(μ-dppm)$_2$] (30)

To a flask containing [Rh$_2$(μ$_2$-C)(μ$_2$-DMAD)Cl$_2$(μ-dppm)$_2$] (0.020 g, 0.017 mmol) and [CuCl(SMe$_2$)] (0.006 g, 0.04 mmol) was added CH_2Cl_2 (10 mL). The resulting red solution

was stirred for 30 minutes, turning gold in colour. After this time the volatiles were removed *in vacuo* and the residue was subjected to column chromatography (10 x 1 cm silica gel column), eluting initially with neat CH_2Cl_2 and then with 1:19 THF:CH_2Cl_2. A yellow band was collected, and the volatiles were removed under reduced pressure to give a yellow solid of **30**. Yield: 0.020 g (0.014 mmol, 97%). ^{1}H NMR (400 MHz, $CDCl_3$, 298 K): δ_H = 2.37 (s, 6 H, OCH_3), 2.54 (br. s, 2 H, PCH_2), 3.71 (dp^v, $^2J_{HH}$ = 12 Hz, $^2J_{PH}$ = 6 Hz, 2 H, PCH_2), 6.98-7.07 (m, 4 H, C_6H_5), 7.07–7.16 (m, 10 H, C_6H_5), 7.36–7.39 (m, 12 H, C_6H_5), 7.89-7.95 (m, 14 H, C_6H_5). ^{13}C{^{1}H} NMR (151 MHz, $CDCl_3$, 298 K): δ_C = 165.0 (br. s, CO_2), 134.8 (t^v, J = 7 Hz, C_6H_5), 131.9 (t^v, J = 5 Hz, C_6H_5), 131.6 (s, C_6H_5), 130.8 (s, C_6H_5), 129.1 (t^v, J = 6 Hz, C_6H_5), 128.8 (t^v, J = 6 Hz, C_6H_5), 128.5 (s, C_6H_5), 127.8 (s, C_6H_5), 50.6 (br. s, OCH_3), 14.9 (br. m, PCH_2). μ_3-C and DMAD alkyne environment not detected due to low solubility. ^{31}P{^{1}H} NMR (162 MHz, $CDCl_3$, 298 K): δ_P = 8.7 (d, $^1J_{RhP}$ = 132 Hz). IR (ATR, cm^{-1}): 1708, 1687 s ν_{CO}, 1435s $\nu_{C=C}$, 1216s ν_{C-O}. MS (ESI, *m/z*): Accurate mass: Found 1262.00996 $[M–Cl]^+$, 565.04527 $[M–CuCl_3]^{2+}$. Calcd for $C_{57}H_{50}Cu^{35}Cl_2O_4P_4Rh_2$ $[M–Cl]^+$: 1260.94372, $C_{57}H_{50}O_4P_4Rh_2$ $[M–CuCl_3]^{2+}$: 564.03793. Anal. Found: C, 45.89; H, 3.28%. Calcd for $C_{57}H_{50}CuCl_3O_4P_4Rh_2.2CHCl_3$: C, 46.10; H, 3.41%. A crystal suitable for structure determination was grown by slow evaporation of $CHCl_3$. *Crystal data for* $C_{57}H_{52}Cl_3CuO_5P_4Rh_2.2(CHCl_3)$ (M_w =1555.31 g.mol^{-1}): monoclinic, space group $P2_1/c$ (No. 14), a = 12.8040(3), b = 15.9061(4), c = 30.3291(7) Å, β = 92.704(2)°, V = 6170.0(3) Å^3, Z = 4, T = 150.0(1) K, μ(Cu Kα) = 22.258 mm^{-1}, D_{calcd} = 1.674 Mg.m^{-3}, 19231 reflections measured (8.8° ≤ 2Θ ≤ 140.8°), 11507 unique (R_{int} = 0.046) which were used in all calculations. The final R_1 was 0.077 ($I > 2\sigma(I)$) and wR_2 was 0.226 (all data) for 724 refined parameters with 18 restraints. CCDC 1966846.

Synthesis of [Rh$_2$Au(μ$_3$-C)(μ$_2$-DMAD)(C$_6$F$_5$)Cl$_2$(μ-dppm)$_2$] (31)

To a flask containing [Rh$_2$(μ$_2$-C)(μ$_2$-DMAD)Cl$_2$(μ-dppm)$_2$] (0.029 g, 0.024 mmol) and [Au(C$_6$F$_5$)(SMe$_2$)] (0.008 g, 0.03 mmol) was added CH_2Cl_2 (10 mL). The resulting red solution was stirred for 30 min, turning orange in colour. After this time the volatiles were removed *in vacuo* and the residue was subjected to silica gel chromatography, eluting initially with neat CH_2Cl_2 and then with 1:19 THF:CH_2Cl_2. An orange band was collected, and the volatiles were removed under reduced pressure to give a red microcrystalline solid of pure **[Rh$_2$Au(μ$_3$-C)(μ$_2$-DMAD)(C$_6$F$_5$)Cl$_2$(μ-dppm)$_2$] (31).** Yield: 0.034 g (0.022 mmol, 91%). ^{1}H NMR (400 MHz,

$CDCl_3$, 298 K): δ_H = 2.45 (s, 6 H, OCH_3), 2.67, 3.71 (2x m, 4 H, PCH_2), 6.89 (t, $^3J_{HH}$ = 8 Hz, 8 H, C_6H_5), 7.06 (t, $^3J_{HH}$ = 8 Hz, 4 H, C_6H_5), 7.37 (br. s, 12 H, C_6H_5), 7.89 (br. s, 8 H, C_6H_5), 8.07 (d, $^3J_{HH}$ = 7 Hz, 8 H, C_6H_5). $^{13}C\{^1H\}$ NMR (151 MHz, $CDCl_3$, 298 K): δ_C = 505.3 (br. m, μ_3-C), 165.6 (CO_2Me), 165.3 (d, J = 34 Hz, C_6F_5), 149.4 (m, C_6F_5), 148.1 (t, J = 32 Hz, C_6F_5), 135.1, 132.2, 132.1, 131.3, 130.7, 128.7, 128.7, 128.2 (8 x br., C_6H_5), 126.5 (t, J = 68 Hz, C_6F_5), 50.8 (s, OCH_3), 14.4 (p^v, J_{PC} = 13 Hz, PCH_2). $^{31}P\{^1H\}$ NMR (162 MHz, $CDCl_3$, 298 K): δ_P = 8.8 (d, $^1J_{RhP}$ = 130 Hz). $^{19}F\{^1H\}$ (376 MHz, $CDCl_3$, 298K): δ_F = -112.90 (m, *ortho*), -158.58 (t, $^3J_{FF}$ = 20 Hz, *meta*), -162.8 (t, $^3J_{FF}$ = 20 Hz, *para*). IR (ATR, cm^{-1}): 1726 br s ν_{CO}, 1435s $\nu_{C=C}$, 1208s ν_{C-O}, 984 ν_{C-F}. MS (ESI, *m/z*): Accurate mass: Found 1527.0067. Calcd for $C_{63}H_{50}Au^{35}ClF_5O_4P_4Rh_2$ $[M–Cl]^+$: 1527.0044. A crystal suitable for structure determination was grown by slow evaporation of a CH_2Cl_2/hexane mixture. *Crystal data for* $C_{63}H_{50}AuCl_2F_5O_4P_4Rh_2$ (M_w =1563.59 $g.mol^{-1}$): orthorhombic, space group $P2_12_12_1$ (No. 19), a = 16.3512(4), b = 27.4127(4), c = 29.9209(4) Å, V = 13411.5(4) $Å^3$, Z = 8, T = 150.0(1) K, μ(Cu Kα) = 10.07 mm^{-1}, D_{calcd} = 1.549 $Mg.m^{-3}$, 26465 reflections measured (8.0° ≤ 2Θ ≤ 141.6°), 17770 unique (R_{int} = 0.027) which were used in all calculations. The final R_1 was 0.043 ($I > 2\sigma(I)$) and wR_2 was 0.118 (all data) for 1,497 refined parameters with 74 restraints.

Synthesis of $[Rh_2(\mu\text{-}CCl)(\mu\text{-}DMAD)Cl_2(\mu\text{-}dppm)_2]A^-$ (32)

Method A: A = $AuCl_2$

To a flask containing $[Rh_2(\mu\text{-}C)(\mu\text{-}DMAD)Cl_2(\mu\text{-}dppm)_2]$ (0.020 g, 0.017 mmol) and $[AuCl_3(THT)]$ (0.009 g, 0.02 mmol) was added CH_2Cl_2 (10 mL). The resulting yellow solution was stirred for 30 minutes. After this time the volatiles were removed *in vacuo* and the residue was subjected to silica gel chromatography, eluting initially with neat CH_2Cl_2 and then with 1:1 THF:CH_2Cl_2. A yellow band was collected, and the volatiles were removed under reduced pressure to give a red microcrystalline solid of $[Rh_2(\mu\text{-}CCl)(\mu\text{-}DMAD)Cl_2(\mu\text{-}dppm)_2][AuCl_2]$. Yield: 0.021 g (0.014 mmol, 83%). ^1H NMR (400 MHz, $CDCl_3$, 298 K): δ_H = 2.54 (br., 4 H, PCH_2), 3.34 (s, 6 H, CH_3), 6.86 (t, $^3J_{HH}$ = 8 Hz, 2 H, C_6H_5), 7.00 (t, $^3J_{HH}$ = 8 Hz, 2 H, C_6H_5), 7.05 (t, $^3J_{HH}$ = 8 Hz, 2 H, C_6H_5), 7.18 (t, $^3J_{HH}$ = 8 Hz, 2 H, C_6H_5), 7.25-7.36 (m, 8 H, C_6H_5), 7.44-7.61 (m, 10 H, C_6H_5), 7.63-7.72 (m, 10 H, C_6H_5), 7.73-7.78 (m, 4 H, C_6H_5). $^{13}C\{^1H\}$ NMR (151 MHz, $CDCl_3$, 298 K): δ_C = 395.3 (t, $^1J_{RhC}$ = 35 Hz, μ_2-CCl), 170.6 (CO_2), 134.9, 134.1, 132.2, 130.7, 129.1, 128.6, 127.0 (C_6H_5), 50.8 (CH_3), 15.7 (PCH_2). ^{13}C peaks identified through ^1H-^{13}C HSQC and HMBC studies. $^{31}P\{^1H\}$ NMR (162 MHz, $CDCl_3$, 298 K): δ_P = 8.85 (d, $^1J_{RhP}$ = 116 Hz). IR (ATR, cm^{-1}):

1722s br. ν_{CO}, 1434s $\nu_{C=C}$. ν_{CCl} not unambiguously identified. MS (ESI, *m/z*): Accurate mass: Found 1234.9821. Calcd for $C_{57}H_{52}{}^{35}Cl_3O_4P_4Rh_2$ $[M]^+$: 1234.9987. A crystal suitable for structure determination was grown by slow evaporation of a CH_2Cl_2/toluene mixture, though contained both the mono- and di-aqua adducts and disorder of a $AuCl_2$ anion over a special position. *Crystal data for* $AuCl_2 \cdot C_{57}H_{54}Cl_3O_6P_4Rh_2 \cdot C_{57}H_{52}Cl_3O_5P_4Rh_2 \cdot Au_{0.5}Cl_{1.5} \cdot Au_{0.5}Cl_2 \cdot 4(CHCl_3)$ (M =3590.46 g.mol^{-1}): triclinic, space group *P*1 (No. 1), a = 17.6098(5), b = 18.4743(5), c = 26.9004(9) Å, α = 73.622(3), β = 78.866(3), γ = 72.078(2), V = 7934.6(4) Å^3, Z = 2, T = 150.0(1) K, μ(Cu Kα) = 11.46 mm^{-1}, D_{calcd} = 1.503 Mg.m^{-3}, 43471 reflections measured (8.0° ≤ 2Θ ≤ 141.4°), 27743 unique (R_{int} = 0.042) which were used in all calculations. The final R_1 was 0.078 ($I > 2\sigma(I)$) and wR_2 was 0.228 (all data) for 1528 refined parameters with 2 restraints.

Method B: A = PF_6

The reaction was performed in an identical manner in Method A. The yellow powder of $[Rh_2(\mu_2\text{-CCl})(\mu_2\text{-DMAD})Cl_2(\mu\text{-dppm})_2][AuCl_2]$ was further dissolved in a 1:1 DCM MeOH solution (50 mL total volume) with excess $NaPF_6$ (0.55 g, 0.33 mmol) and stirred for one hour for anion exchange, before being subject to a silica gel column under identical conditions to isolate $[Rh_2(\mu_2\text{-CCl})(\mu_2\text{-DMAD})Cl_2(\mu\text{-dppm})_2]PF_6$ (0.027 g, 0.020 mmol, 78%). All spectroscopic data matched **32**, except for those associated with the PF_6 counter ion. $^{31}P\{^1H\}$ NMR (162 MHz, $CDCl_3$, 298 K): δ_P = -144.24 (sep, $^1J_{PF}$ = 713 Hz). $^{19}F\{^1H\}$ (376 MHz, $CDCl_3$, 298K): δ_F = -72.85 (d, $^1J_{PF}$ = 713 Hz). IR (ATR, cm^{-1}): 863 ν_{PF}. A crystal suitable for structure determination was grown by slow evaporation of a CH_2Cl_2/toluene mixture. *Crystal data for* $C_{57}H_{52}Cl_3O_5P_4Rh_2 \cdot F_6P$ (M_w =1430.40 g.mol^{-1}): monoclinic, space group $P2_1/c$ (no. 14) a = 12.6154(6), b = 15.6209(7), c = 30.4092(12) Å, V = 5991.2(5) Å^3, Z = 4, T = 150.0(1) K, μ(Cu Kα) = 7.82 mm^{-1}, D_{calcd} = 1.586 Mg.m^{-3}, 19206 reflections measured (9.0° ≤ 2Θ ≤ 137.4°), 10467 unique (R_{int} = 0.088) which were used in all calculations. The final R_1 was 0.077 ($I > 2\sigma(I)$) and wR_2 was 0.192 (all data) for 706 refined parameters with 36 restraints.

Observation of $[Rh_2Hg(\mu_3\text{-C})(\mu\text{-DMAD})(CF_3)_2Cl_2(\mu\text{-dppm})_2]$ (33)

To a $CDCl_3$ solution of $[Rh_2(\mu_2\text{-C})(\mu_2\text{-DMAD})Cl_2(\mu\text{-dppm})_2]$ (0.010 g, 0.009 mmol) was added $[Hg(CF_3)_2]$ (0.010 g, 0.031 mmol). The solution immediately changed colour to red. Monitoring by ^{31}P NMR spectroscopy shows complete consumption of starting material (δ_P =

12.5) after 5 minutes to form [$Rh_2Hg(\mu_3$-C)(μ-DMAD)$(CF_3)_2Cl_2(\mu$-dppm$)_2$]. Due to lability issues, the complex was not successfully isolated from the NMR solution and only limited spectroscopic data are provided below. ^{1}H NMR (400 MHz, $CDCl_3$, 298 K): δ_H = 2.37 (s, 6 H, OCH_3), 3.52 (tp^v, $^2J_{PH}$ = 13, $^2J_{HH}$ = 6 Hz, 2 H, PCH_2), 7.03 (t, $^3J_{HH}$ = 8 Hz, 8 H, C_6H_5), 7.12 (t, $^3J_{HH}$ = 7 Hz, 4 H, C_6H_5) 7.33-7.38 (m, 12 H, C_6H_5), 7.61 (br. d, $^3J_{HH}$ = 6 Hz, 8 H, C_6H_5), 7.86 (br. s, 8 H, C_6H_5). ^{31}P{^{1}H} NMR (162 MHz, $CDCl_3$, 298 K): δ_P = 13.8 (d, $^1J_{RhP}$ = 137 Hz). ^{19}F{^{1}H} (376 MHz, $CDCl_3$, 298K): δ_F = -36.01 (s, $^2J_{HgF}$ = 1264 Hz, Hg-CF_3). MS, IR, and elemental analysis performed on **33** returned data matching [$Rh_2(\mu_2$-C)(μ_2-DMAD)$Cl_2(\mu$-dppm$)_2$] due to the labile coordination of [$Hg(CF_3)_2$].

Synthesis of [$Rh_2(\mu_2$-C-Hg{CF_3}$_2$)(μ-HFB)$Cl_2(\mu$-dppm$)_2$] (34)

To a $CDCl_3$ solution of [$Rh_2(\mu_2$-C)(μ_2-HFB)$Cl_2(\mu$-dppm$)_2$] (0.010 g, 0.008 mmol) was added [$Hg(CF_3)_2$] (0.010 g, 0.031 mmol). The solution immediately changed colour to red. Monitoring by ^{31}P NMR spectroscopy shows complete consumption of starting material (δ_P = -0.22, 0.85) after 5 minutes to form [$Rh_2Hg(\mu_3$-C)(μ-HFB)$(CF_3)_2Cl_2(\mu$-dppm$)_2$]. Due to lability issues, the complex was not successfully isolated from the NMR solution and only limited spectroscopic data are presented below. ^{1}H NMR (400 MHz, $CDCl_3$, 298 K): δ_H = 2.37 (br. s, 2 H, PCH_2), 3.36-3.39 (m, 2 H, PCH_2), 7.02-7.07 (m, 14 H, C_6H_5), 7.40-7.42 (m, 10 H, C_6H_5), 7.61 (br. s, 8 H, C_6H_5), 7.89 (br. s, 8 H, C_6H_5). ^{31}P{^{1}H} NMR (162 MHz, $CDCl_3$, 298 K): δ_P = 12.0 (d, $^1J_{RhP}$ = 132 Hz). ^{19}F{^{1}H} (376 MHz, $CDCl_3$, 298K): δ_F = -35.91 (s, $^2J_{HgF}$ = 1248 Hz, Hg-CF_3), -49.06 (s, HFB CF_3). MS, IR, and elemental analysis performed on **34** returned data matching [$Rh_2(\mu_2$-C)(μ_2-HFB)$Cl_2(\mu$-dppm$)_2$] due to the labile association of [$Hg(CF_3)_2$].

Synthesis of [$Rh_2(\mu_2$-C-$HgCl_2$)(μ-DMAD)$Cl_2(\mu$-dppm$)_2$] (35)

To a $CDCl_3$ solution of **[$Rh_2(\mu_2$-C)(μ_2-DMAD)$Cl_2(\mu$-dppm$)_2$]** (0.010 g, 0.008 mmol) was added **[$HgCl_2$]** (0.010 g, 0.031 mmol). The solution immediately changed colour to red. Monitoring by ^{31}P NMR spectroscopy shows complete consumption of starting material after 5 minutes to form primarily **[$Rh_2Hg(\mu_3$-C)(μ-DMAD)$Cl_4(\mu$-dppm$)_2$]**. Due to stability issues, the complex was not successfully isolated from the NMR solution and only limited spectroscopic data

are available. ^{1}H NMR (400 MHz, $CDCl_3$, 298 K): δ_H = 2.50 (br. s, 2 H, PCH_2), 4.03 (dp^v, $^{2}J_{PH}$ = 13, $^{2}J_{HH}$ = 6 Hz, 2 H, PCH_2), 7.04 (br. t, $^{3}J_{HH}$ = 7 Hz, 8 H, C_6H_5), 7.20-7.24 (m, 4 H, C_6H_5), 7.38-7.42 (m, 13 H, C_6H_5), 7.72-7.79 (m, 15 H, C_6H_5). ^{31}P{^{1}H} NMR (162 MHz, $CDCl_3$, 298 K): δ_P = 8.82 (d, $^{1}J_{RhP}$ = 117 Hz). Attempts to purify or isolate **35** led to the synthesis of **32** as the chloride salt through monitoring the ^{31}P NMR spectrum of the product (δ_P = 8.87).

Synthesis of [Rh$_2$(μ-CS)(μ-DMAD)Cl$_2$(μ-dppm)$_2$] (36)

Method A: To a flask containing **[Rh$_2$(μ-CS)Cl$_2$(dppm)$_2$]** (0.050 g, 0.047 mmol) was added CH_2Cl_2 (10 mL) followed by DMAD (0.10 mL, 1.156 g.cm^{-3}, 1.7 mmol). The resulting green solution was stirred for 60 minutes at room temperature, turning red in colour. Over this time a red precipitate formed, and this was isolated by filtration and washed with hexane to remove unreacted DMAD. Drying *in vacuo* gave a red powder of pure [Rh$_2$(μ-CS)(μ-DMAD)Cl$_2$(μ-dppm)$_2$] (**36**). Yield: 0.046 g (0.037 mmol, 79%). ^{1}H NMR (400 MHz, $CDCl_3$, 298 K): δ_H = 2.41 (s, 6 H, OCH_3), 2.88 (br. d, $^{2}J_{PH}$ = 12 Hz, PCH_2), 3.95 (dp^v, = $^{2}J_{PH}$ = 18 Hz, $^{2}J_{HH}$ = 6 Hz, PCH_2), 7.01 (t, $^{3}J_{HH}$ = 8 Hz, 9 H, C_6H_5), 7.17 (t, $^{3}J_{HH}$ = 7 Hz, 5 H, C_6H_5), 7.30–7.35 (m, 16 H, C_6H_5), 7.73 (q, $^{3}J_{HH}$ = 5 Hz, 8 H, C_6H_5) 7.83 (br. d, $^{3}J_{HH}$ = 6 Hz, 2 H, C_6H_5). ^{13}C{^{1}H} NMR (151 MHz, $CDCl_3$, 298 K): δ_C = 164.5 (*C*O_2Me); HMBC with δ_H = 2.43), 135.2, 132.4, 130.6, 130.2 2C, 128.5, 128.1, 125.7 (C_6H_5), 50.3 (s, OCH_3), 16.6 (p^v, J_{PC} = 11 Hz, PCH_2). ^{31}P{^{1}H} NMR (162 MHz, $CDCl_3$, 298 K): δ_P = 7.09 (d, $^{1}J_{RhP}$ = 133 Hz). IR (ATR, cm^{-1}): 1720 br, s ν_{CO}, 1249 br, s ν_{CS}. MS (ESI, *m/z*): Accurate mass: Found 1195.0172. Calcd for $C_{57}H_{50}{}^{35}ClO_4P_4Rh_2S$ [M–Cl]$^+$: 1195.0179. A crystal of a chloroform solvate of the aquo adduct suitable for structure determination was grown by slow evaporation of a wet $CHCl_3$/petrol mixture. *Crystal data for* $C_{57}H_{52}Cl_2O_5P_4Rh_2S{\cdot}CHCl_3$ (M_w = 1369.01 g.mol^{-1}): monoclinic, space group $P2_1/c$ (no. 14), a = 12.7306(2), b = 15.6417(3), c = 30.6406(4) Å, β = 92.455(1)°, V = 6095.81(17) Å^3, Z = 4, T = 150.0(1) K, μ(Cu Kα) = 22.258 mm^{-1}, D_{calcd} = 1.492 Mg.m^{-3}, 11380 reflections measured (8.0° ≤ 2Θ ≤ 142.2°), 9442 unique (R_{int} = 0.028) which were used in all calculations. The final R_1 was 0.049 ($I > 2\sigma(I)$) and wR_2 was 0.128 (all data) for 679 refined parameters without restraints. CCDC 2013310.

Method B: To a flask containing **[Rh$_2$(μ$_2$-C)(μ$_2$-DMAD)Cl$_2$(dppm)$_2$]** (0.040 g, 0.033 mmol) was added CH_2Cl_2 (10 mL) followed by S_8 (0.023 g, 0.090 mmol). The resulting red suspension was stirred for 15 hours at room temperature, turning dark red as the starting material dissolved to give a clear solution. The solution was concentrated under reduced volume and subjected to a

silica gel column (10 x 1 cm). Eluting with a with 5% mixture of THF in CH_2Cl_2 provided a red band which was freed of volatiles to afford the desired product (0.018 g, 0.015 mmol, 44%). The product was identified comparison of ESI-MS and ^{31}P NMR spectroscopic data with those for a sample prepared as described above.

Synthesis of [Rh$_2$(μ-CSe)(μ-DMAD)Cl$_2$(μ-dppm)$_2$] (37)

Method A: To a flask containing [Rh$_2$(μ$_2$-C)(μ$_2$-DMAD)Cl$_2$(μ-dppm)$_2$] (0.100 g, 0.083 mmol) was added CH_2Cl_2 (10 mL) followed by grey selenium (0.009 g, 0.11 mg.atom). The resulting red suspension was stirred for 24 hours at room temperature. The supernatant was decanted to remove excess suspended selenium, and the red solution concentrated under reduced pressure to *ca* 1 mL. Subjecting the solution to a silica gel column (1 x 10 cm), a pink band was eluted using a mixture of 5% THF in CH_2Cl_2. A pink powder precipitated upon addition of petroleum spirits and drying *in vacuo* gave a pink powder of pure [Rh$_2$(μ-CSe)(μ-DMAD)Cl$_2$(μ-dppm)$_2$] (**37**). Yield: 0.015 g (0.012 mmol, 14%). ^1H NMR (400 MHz, $CDCl_3$, 298 K): δ_H = 2.46 (s, 6 H, OCH_3), 2.79-2.86 (m, 2 H, PCH_2), 3.79-3.85 (m, 2 H, PCH_2), 7.03, 7.34, 7.72, 7.83, 8.04 (m x 5, 40 H, C_6H_5). $^{13}C\{^1H\}$ NMR (151 MHz, $CDCl_3$, 298 K): δ_C = 318.3 (tp, $^1J_{RhC}$ = 28 Hz, $^2J_{PC}$ = 8 Hz, μ$_2$-CSe), 164.7 (*C*O$_2$Me; HMBC with δ_H = 2.48), 135.9, 135.3, 132.7, 130.6, 130.2, 128.4, 128.1, 125.7 (C_6H_5), 50.4 (s, OCH_3), 16.7 (p^v, *J* = 14 Hz, PCH_2). $^{31}P\{^1H\}$ NMR (162 MHz, $CDCl_3$, 298 K): δ_P = 4.11 (d, $^1J_{RhP}$ = 131 Hz). $^{77}Se\{^1H\}$ NMR (134 MHz, $CDCl_3$, 298 K) δ_{Se} = 1433.1 (br.). IR (ATR, cm^{-1}): 1718 br, s ν_{CO}, 893, s ν_{CSe}. MS (ESI, *m*/*z*): Accurate mass: Found 1242.9637. Calcd for $C_{57}H_{50}{}^{35}ClO_4P_4Rh_2{}^{80}Se$ $[M–Cl]^+$: 1242.9629. A crystal suitable for structure determination was grown by slow evaporation of a wet CH_2Cl_2/toluene mixture. *Crystal data for* $C_{57}H_{52}Cl_2O_5P_4Rh_2Se\cdot0.5(CH_2Cl_2)\cdot C_7H_8$ (M_w = 1431.14 g.mol^{-1}): monoclinic, space group $P2_1/c$ (No. 14), a = 12.4786(2), b = 15.7365(2), c = 31.0651(4) Å, β = 91.657(1)°, V = 6097.69(15) Å^3, Z = 4, T = 150.0(1) K, μ(Cu Kα) = 22.258 mm^{-1}, D_{calcd} = 1.559 Mg.m^{-3}, red plate 0.305 x 0.179 x 0.066, 11460 reflections measured (7.0° ≤ 2Θ ≤ 141.8°), 9756 unique (R_{int} = 0.035) which were used in all calculations. The final R_1 was 0.058 ($I > 2\sigma(I)$) and wR_2 was 0.152 (all data) for 734 refined parameters without restraints. CCDC 2013307.

Method B: To a flask containing **[Rh$_2$(μ$_2$-CSe)Cl$_2$(dppm)$_2$]** (0.040 g, 0.035 mmol) was added CH_2Cl_2 (20 mL). To this green solution was added DMAD (0.05 mL, 1.156 g.cm^{-3}, 0.4 mmol). The resulting dark green solution was stirred for 24 hours at room temperature, turning

pink in colour. The solution was concentrated under reduced volume and subjected to a silica gel chromatography column. Eluting a red band with 5% THF in CH_2Cl_2 provided the pink product (0.038 g, 0.030 mmol, 84%). The identity of the product was confirmed through comparison of ESI-MS and $^{31}P\{^1H\}$ NMR data with those for **37** presented above.

EPISODE FOUR – A NEW CLASS

QUANTIFYING THE *METALLA*-HETEROCYCLIC CARBENE

4.1 PREFACE

From: H. J. Barnett, A. F. Hill, H. MacDermott-Opeskin (*written for publication*)

The Class D μ-carbido complexes **[Rh_2(μ-C:)(μ-RCCR)Cl_2(μ-dppm)$_2$]** (R = CO_2alkyl, CF_3) represent the first examples of stable, isolable *Metalla*-Heterocyclic Carbenes. Their reactions with selenium furnish μ_2-selenocarbonyl complexes, of which the ^{77}Se NMR chemical shifts in conjunction with computational modelling provide new insights into the **strong** π-acidity of the unique metallacarbene species.

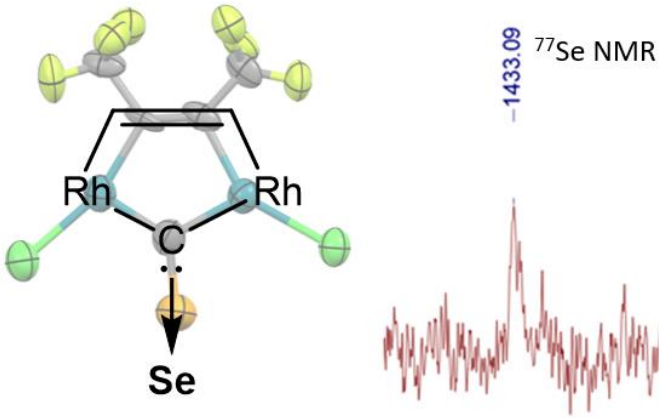

Figure 4.0: Abstract graphic

4.2 INTRODUCTION

4.2.1 Quantifying NHC Properties

Much like their counterpart phosphine ligands, the range of functionalisation possible for NHC ligands leads to incredibly diverse steric and electronic properties. In order to sufficiently gauge and understand how tailoring these ligands affect the transition metal complex when coordinated, a range of spectroscopic techniques have been developed in order to quantify these properties. This has become an increasingly important issue as NHC chemistry develops, as they have become a foundation for metal-catalysed industrial processes.

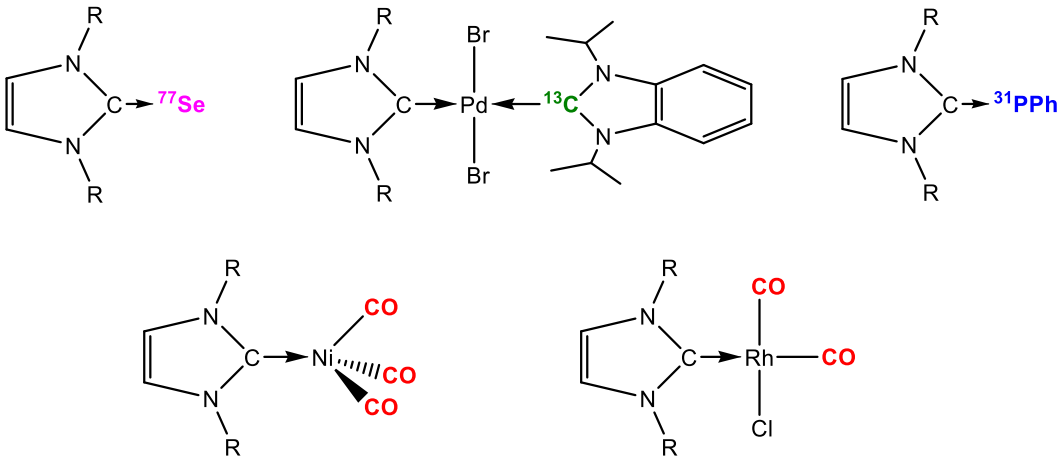

Scheme 4.1: Overview of current popular metrics for quantifying NHC properties. The top row is based on NMR; the bottom row is based on infrared data

The Tolman Electronic Parameter

The earliest of these properties followed from phosphine chemistry and correspond to the Tolman parameters of the ligand. The Tolman parameters consist of a steric component (more commonly described as the cone angle), and an electronic parameter (the TEP). The TEP was measured through reaction of the phosphine ligand with **[Ni(CO)$_4$]**, forming the nickel tricarbonyl species **[Ni(CO)$_3$L]** (L = PR$_3$).[192] Utilizing the now-present IR handle, the carbonyl ligands, the TEP is simply the stretching frequency of the symmetric carbonyl stretch (the A$_1$ stretch). This relies on the tenet that the electron density transferred from the NHC to the metal is further transferred into the π* orbitals of the carbonyl ligand. The more strongly donating the

phosphine is, the lower the CO bond order, which is reflected in a lower wavenumber in the IR spectrum. Though initially studied and referenced for phosphines, it had been found that the acidity of Arduengo type carbenes could also be quantified using this method.[193]

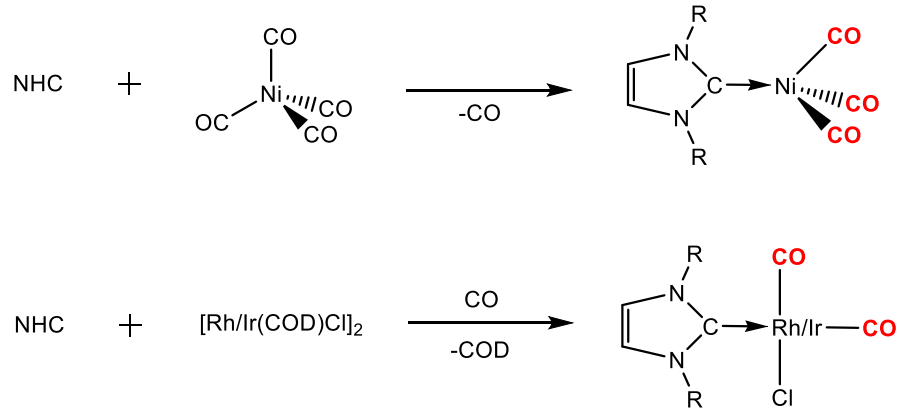

Scheme 4.2: Reaction pathways to **[Ni(CO)$_3$(NHC)]** and ***cis*-[Rh/Ir(CO)$_2$Cl(NHC)]**

One of the issues commonly associated with using the classical Tolman parameter is the toxicity of nickel(0) tetracarbonyl. Because of this issue, there are limited examples in the literature of NHC ligands bound to the nickel tricarbonyl unit which makes broad comparisons difficult. To obviate this limitation, the nickel centre can be effectively replaced with the isolation of complexes of the form *cis*-**[M(CO)$_2$Cl(NHC)]** (M = Rh, Ir). The synthesis of the carbonyl species is not too dissimilar from the nickel analogues, where the NHC typically first breaks apart the **[M(COD)Cl]$_2$** dimeric species before carbon monoxide displaces the labile COD ligand.[194]

The square-planar rhodium or iridium(I) centres also contain two *cis*-disposed carbonyl ligands, which again have been used as a measure of net-acidity of the carbene towards the metal centre. The similarity of values obtained from both the rhodium and iridium complexes have been seen to form a linear dependency with the TEP values, allowing for an accurate data comparison across metal complexes.[195] Being a significantly safer synthetic route, the Group 9 carbene complexes have flourished and even include NHC analogues such as cyclic(alkyl)(amino)carbene complexes.[196]

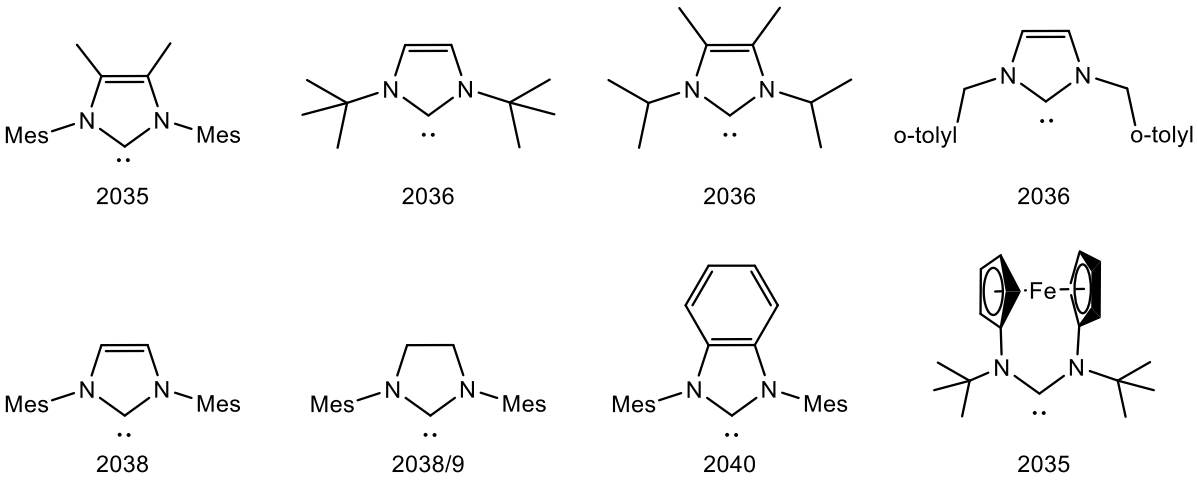

Figure 4.1: Narrow range of TEP values for selected NHCs with *N*-substituted and backbone modifications (data from [196-198])

There arise three caveats from these infrared-based processes. The first is the rather narrow range of stretching frequencies for the carbonyl vibrations (typically less than 60 cm^{-1}; Tolman initially reported a range of 2056 to 2111 cm^{-1} for **[Ni(CO)$_3$L]**),[199] which makes detailed comparisons between modifications difficult (see **Figure 4.1**). The second issue is the solvent- and state-dependent nature of IR spectroscopy, which in conjunction with the first issue, raises questions over the ability to accurately distinguish features.[200] Finally, the third issue of the Tolman parameter is the rather basic interpretation of the values, which correspond to a single electronic property of the ligand (i.e., the *net* electron density), i.e., the TEP is not separable into σ-acidity, π-acidity and π-acidity components.[201] This was initially overlooked as an issue because carbenes were assumed to have insignificant π-acidity, a view that has since been revised resulting in the need for a better system.

The Huynh Electronic Parameter

One of the more recent methods of NHC quantitative analysis attempts to include the disparity between σ and π acidity using NMR spectroscopy. The palladium complex *trans*-**[PdBr$_2$(*i*Pr$_2$-bimy)(NHC)]** developed by Huynh (where *i*Pr$_2$-bimy = 1,3-diisopropylbenzimidazolin-2-ylidene), contains the ^{13}C NMR chemical shift on the *trans*-*i*Pr$_2$-bimy ligand.[202] The chemical shift of the carbon atom is called the HEP (Huynh Electronic Parameter), and can be applied to NHCs in addition to other monodentate ligands such as phosphines.

However, examining the (limited) carbene-derived data reveals that the spectral dispersion of ^{13}C chemical shifts when comparing different carbene species is rather modest (<10 ppm in the original work), and much like the TEP, interrogating minor modifications becomes difficult.[203] What is even more curious is that the ^{13}C NMR data fail to agree with the TEP values for identical ligands, which plays into the comparison of electron density around spin active nuclei bound to a metal centre compared to the relative back-donation of a metal centre onto a carbonyl ligand.

NHC Phosphinidenes

A large step in quantifying the π-component for NHC acidity was through ^{31}P NMR spectroscopy. The spin active nucleus is known to be sensitive to the electronic environment of the phosphorus and covers a relatively large chemical shift range, potentially allowing for more accurate comparisons. The phosphorous nuclei to be examined come from the phosphinidene adducts of carbenes, which can be represented in two possible canonical extremes; a phospha-alkene with a formal P=C double bond, or a mercaptoimidazolium zwitterion with a C-P single bond (**Figure 4.2**).[204]

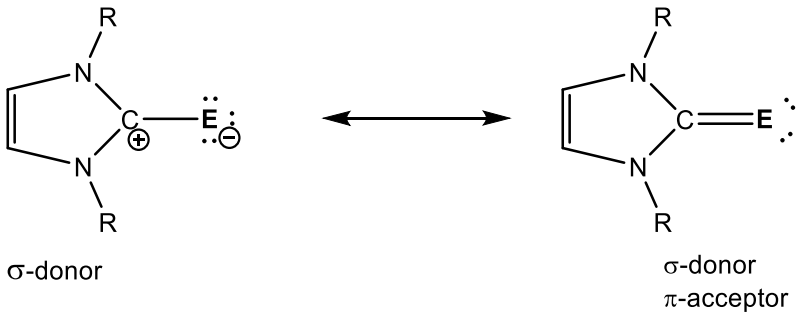

Figure 4.2: Alternate bonding descriptions for phosphinidene and selenide adducts of NHCs. (E = PPh, Se)

The zwitterionic canonical form on the left is largely comprised of a σ-donation from the carbene to the heteroatom, with little or no π-character. As the π-acidity of the carbene increases, the hetero-olefin bonding mode involves significant π-retrodonation from a heteroatom p-orbital. This retrodonation back into the NHC gives, unlike the TEP, an indication of its π-acidity. The data taken from Bertrand and Nolan's initial work show a wide ^{31}P NMR range from -75 to +130

ppm and display a linear relationship with the ^{13}C NMR shift of the carbene carbon.[205] The further downfield the ^{31}P NMR chemical shift is the stronger is the π-accepting nature of the NHC.

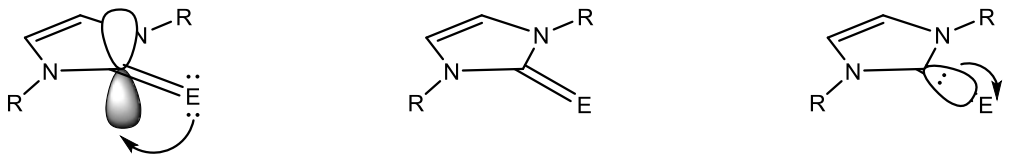

Figure 4.3: Phosphinidene and selenide adducts of NHCs. (left) π-retrodonation to the NHC, (right) σ-donation to the chalcogen. (E = PPh, Se)

Once again, shifting from an infrared based metric to NMR reveals inconsistencies with the data. The phosphinidene complexes were found to be exceptional metrics for measuring the π-acidity of the carbenes, whereas the TEP values give a net value. Due to this, there was a poor correlation between an NHC-phosphinidene ^{31}P NMR shift and its corresponding TEP value.

NHC Selenoureas

In a similar fashion to the phosphinidene/phospha-alkene π-acceptor relationship, selenium has been used as a spectroscopic tool to quantify NHC electronic properties. The selenium adducts of NHC species can be described by the same two-extreme canonical forms; either with an NHC dative bond to the selenium atom (which retains three lone pairs), or a selenourea C=Se double bond through back donation of a selenium lone pair to the carbene. The higher the degree of olefinic character corresponds to π-acidic NHCs, which have been found to manifest low field ^{77}Se NMR shifts.[206]

The ^{77}Se NMR shifts recorded for selenourea compounds have the largest range of any metric, currently spanning -56 to +1180 ppm. The most downfield environment (recorded in acetone) corresponds to an *unstable* cyclic (alkyl)(amino)carbene, which generally have small singlet-triplet gaps and lead to a strong paramagnetic deshielding effect.[207] It was found that there was a strong linear relationship ($R^2 = 0.9051$) between the ^{77}Se NMR shifts and their corresponding ^{31}P NMR shifts for the NHC selenide and phosphinidene compounds, highlighting that both NMR analyses are capable of probing the π-acidity of a carbene.[208] The ^{77}Se nuclei is sufficiently sensitive

to changes in its electronic environment, that installation of two ketone groups on the backbone of the IMes NHC causes a shift of ~700 ppm in the ^{77}Se NMR spectrum (**Figure 4.4**).

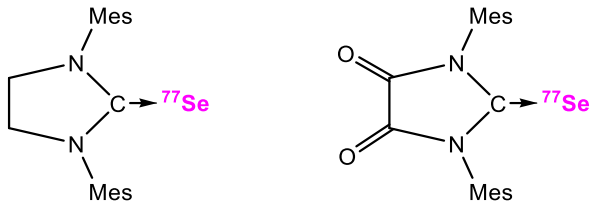

Figure 4.4: ^{77}Se NMR shift for two NHC selenocarbonyl compounds[209]

Nolan and Ganter went one step further and utilised molecular orbital theory to explain the differences in the ^{77}Se environments. It was proposed that a relationship exists between the ^{77}Se chemical shift and the paramagnetic shielding of the nuclei. Theoretical calculations performed on three NHC selenourea compounds saw almost no change to the diamagnetic shielding values of the selenium nucleus, but a large change along one direction of the paramagnetic shielding tensor, specifically along the C=Se bond, the origin of which was attributed to the transition between the occupied selenium p orbital and the π* antibonding orbital of the CSe bond.[210] Plotting the energy difference between these two orbitals against the ^{77}Se NMR shifts revealed a linear dependency (R^2 = 0.8617), and the transition was calculated to be the primary electronic transition across all NHC compounds (**Figure 4.5**).

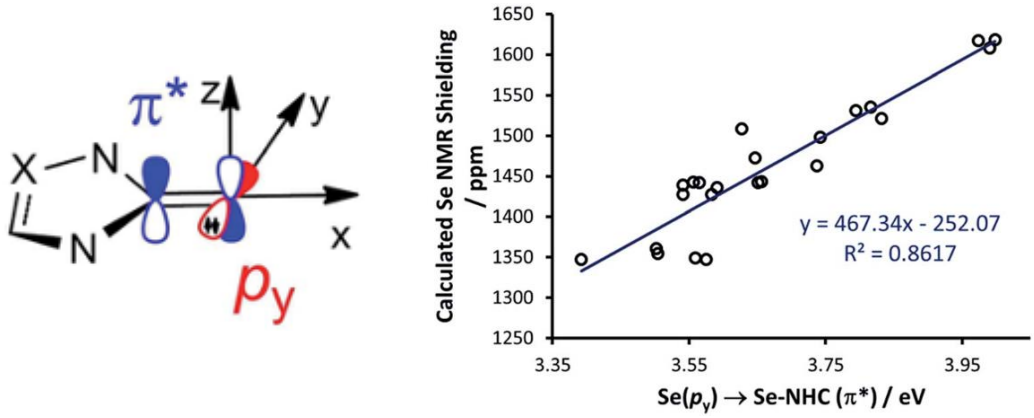

Figure 4.5: (left) Observed transition from selenium p-orbital into C=Se π* orbital. (right) Comparison of observed NHC-Se ^{77}Se NMR shifts and Se p→ C=Se π*orbital energy gap (from [210])

The ^{77}Se NMR studies on selenourea compounds has even been applied to NHC compounds with weakly binding anionic substituents on the carbon backbone (**Scheme 4.3**).[211] Tamm and co-workers examined the popular IMes (1,3-bis(2,4,6-trimethylphenyl)imidazolin-2-ylidene) and and IDipp (1,3-bis(2,6-diisopropylphenyl)imidazolin-2-ylidene) NHC systems, however, a weakly coordinated Group 13 anion was tethered to one of the backbone carbon atoms. Measuring the effect of the $E(C_6F_5)_3^-$ (E = B, Al, Ga) anion on the selenourea ^{77}Se NMR shift saw minimal change (within 20 ppm of the neutral species).

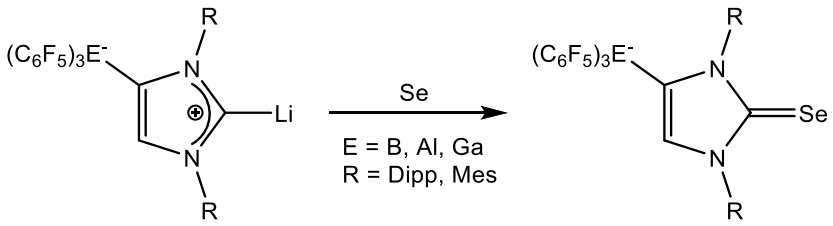

Scheme 4.3: Coordination of weak anionic groups to NHC selenourea compounds

Furthermore, attempts to use the selenourea ^{77}Se chemical shift as a metric for catalytic behaviour were made recently by Coperet *et al.*[212] Examining 29 ruthenium benzylidene complexes with an NHC co-ligand, which are employed in olefin metathesis, it was found that enhancing the π-acceptor property of the NHC ligand led to not only the increased rate of degenerate metathesis, but also the diene selectivity. This helps confirm the ^{77}Se metric as a potentially powerful quantitative tool for carbene chemistry.

4.2.2 Rationale for this Chapter

The synthesis of the first stable MHC complex allowed the subsequent coordination of various inorganic and main group moieties. However, one of the key pieces of information missing is a formal quantification of the electronic properties, including the π-nature of the metallacarbene. The synthesis of the selenocarbonyl complex **$[Rh_2(\mu\text{-CSe})(\mu\text{-DMAD})Cl_2(\mu\text{-dppm})_2]$** provided the impetus for addressing this challenge.

4.3 RESULTS AND DISCUSSION

4.3.1 ^{13}C and ^{77}Se NMR

One of the key reactions of the MHC complex was with selenium to furnish the selenocarbonyl complex **[Rh$_2$(μ-CSe)(μ-DMAD)Cl$_2$(μ-dppm)$_2$] (37)**. The μ$_2$-selenocarbonyl complex represented a key building block for the quantification of the MHC acidity. Early experimental results had shown that the carbene is nucleophilic enough to replace the arsenic ligand of **[AuCl(AsPh$_3$)]** but not the corresponding phosphine. With the synthesis of a stable organometallic analogue of a selenourea, the ^{77}Se NMR shift could potentially be used as a metric to quantify the MHC π-acidity more accurately.

Unfortunately, initial NMR studies on the selenocarbonyl complex proved as complex as usual. The addition of the ^{77}Se nuclei added an extra degree of coupling to the μ-carbido ligand (now a triplet of pentet with satellites) and measuring the ^{77}Se nuclei itself is made more difficult with the aforementioned splitting to ^{103}Rh and ^{31}P. Because there was no benchmark to narrow down the NMR range, scanning the entire ^{77}Se spectral width from -1000 to 2000 ppm unfortunately failed to reveal any definitive resonance.

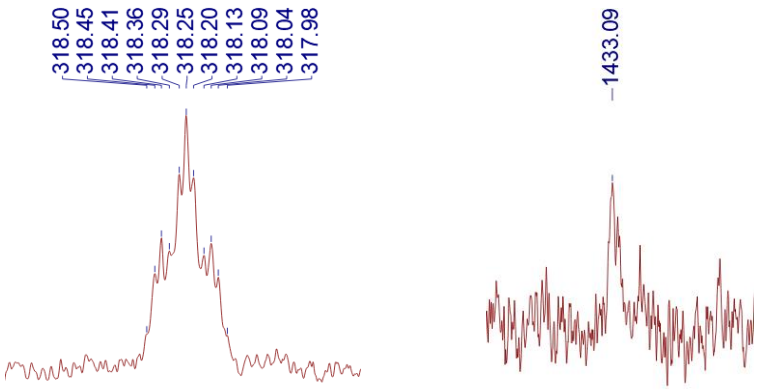

Figure 4.6: ^{13}C and ^{77}Se NMR shifts of **[Rh$_2$(μ-^{13}CSe)(μ-DMAD)Cl$_2$(μ-dppm)$_2$] (37')**

To help narrow the search, the computational expertise of Hugo MacDermott-Opeskin at the ANU was enlisted. Performing solution-state geometry and energy calculations on **[Rh$_2$(μ-CSe)(μ-DMAD)Cl$_2$(μ-dppm)$_2$]** (see *Experimental Section* for computational details), the theoretical ^{77}Se NMR shift in $CHCl_3$ was calculated at 1406.0 ppm. Performing a high scan

$^{77}Se\{^{1}H\}$ NMR experiment with a narrow spectral range finally revealed a broad peak at 1433.09 ppm (**Figure 4.6**). The location is almost 600 ppm further downfield than the lowest field environment for a stable selenourea compound.

Because of its significance, the ^{13}C chemical shift of the μ_2-selenocarbonyl became a key piece of information. Using ^{13}C enrichment, the isotopologue **[Rh$_2$(μ-^{13}CSe)(μ-DMAD)Cl$_2$(μ-dppm)$_2$]** was successfully obtained under identical reaction conditions. The $^{13}C\{^{1}H\}$ NMR spectrum for the isotopologue displayed a clear downfield environment at 318.3 ppm, displaying the unique triplet of pentet splitting of the AA'A"A'"MM'X spin system.

Reaction with hexafluoro-2-butyne

Because of the unexpected location of the ^{77}Se and ^{13}C NMR shifts for the MHC selenocarbonyl complex, more analogues of the MHC selenocarbonyl complex were required if accurate trends were to be discerned.

The remaining two MHC complexes yet to be tested contained the alkynes hexafluoro-2-nutyne and the asymmetric ethyl 4,4,4-trifluoro-2-butynoate. There are two synthetic routes towards the selenocarbonyl complexes: addition of the alkyne to **[Rh$_2$(μ-CSe)Cl$_2$(μ-dppm)$_2$]** or addition of selenium to **[Rh$_2$(μ-C)(μ-alkyne)Cl$_2$(μ-dppm)$_2$]** (**Scheme 4.4**).

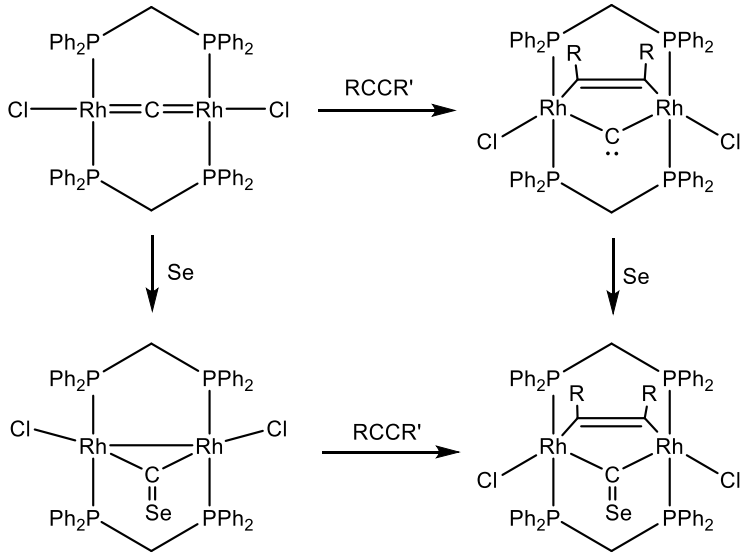

Scheme 4.4: Synthetic routes to two further MHC selenocarbonyl complexes
(R = CF_3, R' = CF_3, CO_2Et)

Addition of grey selenium to **[Rh$_2$(μ-C)(μ-HFB)Cl$_2$(μ-dppm)$_2$]** results in the dichloromethane solution turning dark red over 48 hours. Filtering out the excess selenium allowed for the separation of a dark pink complex through column chromatography. Both the $^{31}P\{^1H\}$ and $^{19}F\{^1H\}$ NMR spectra reflected the symmetric nature of the complex, in contrast to the slippage seen for the free carbene species (see **Chapter 3.3**). The phosphorous resonance, centred at -0.07 ppm, displays a reduction in $^1J_{RhP}$ to 127 Hz attending the selenium coordination to the carbene. The symmetrical nature of the hexafluoro-2-butyne is reflected in the singlet peak in the $^{19}F\{^1H\}$ NMR at -51.92 ppm, displaying none of the fluxional nature seen in the carbene precursor. The selenium adduct was evident in the ESI-MS at 613.9796 m/z (Calcd. for $C_{55}H_{44}F_6P_4{}^{103}Rh_2{}^{77}Se$ [M–2Cl]$^{2+}$: 613.9790). The IR spectrum displayed the C-F stretch at 1097 and 1053 cm^{-1}, though the C=Se stretch could not be unambiguously identified. The molecular structure of **[Rh$_2$(μ-CSe)(μ-HFB)Cl$_2$(μ-dppm)$_2$] (38)** was confirmed through X-ray diffraction studies (**Figure 4.7**).

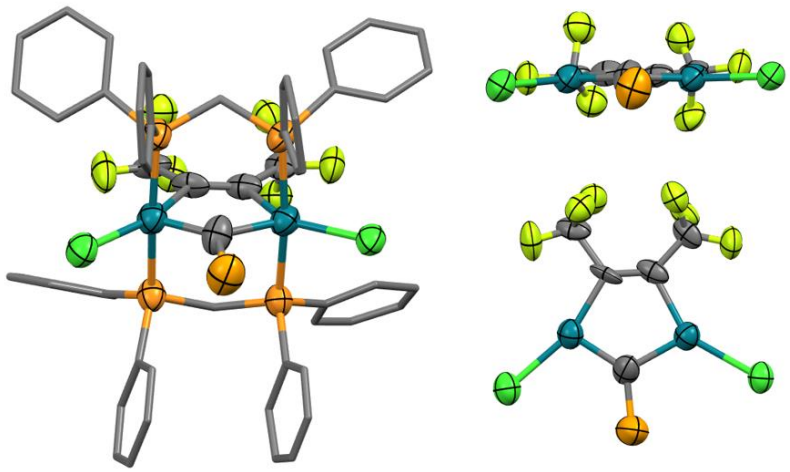

Figure 4.7: Molecular structure of **[Rh$_2$(μ-CSe)(μ-HFB)Cl$_2$(μ-dppm)$_2$] (38)** (50% displacement ellipsoids, solvent, disorder and hydrogen atoms omitted, dppm groups simplified). Selected bond lengths (Å) and angles (°): Rh1-C1 1.99(5), Rh2-C1 1.90(4), C1-Se1 1.75(5), Rh1-C2 2.09(4), Rh2-C3 1.99(3), C2-C3 1.34(6), Rh1-C1-Rh2 118(2)

Reaction with ethyl 4,4,4-trifluoro-2-butynoate

The asymmetric nature of ethyl 4,4,4-trifluoro-2-butynoate is retained upon coordination of the selenium. The ^{31}P NMR spectra displayed two similar but distinct environments with

resonances centred at 1.01 and -0.25 ppm ($^1J_{RhP}$ = 129 and 125 Hz respectively). The single CF_3 group give rise to a resonance in the $^{19}F\{^1H\}$ NMR spectrum, only 0.3 ppm shifted from the hexafluoro-2-butyne complex at -51.60 ppm. The ESI-MS spectrum again displayed the $[M\text{-}2Cl]^{2+}$ dication at 615.9969 *m/z* (*cf.* 615.9959 for $C_{57}H_{47}F_3O_24P_4{}^{103}Rh_2{}^{77}Se$). The molecular structure of **$[Rh_2(\mu\text{-}CSe)(\mu\text{-}ETFB)Cl_2(\mu\text{-}dppm)_2]$ (39)** (**Figure 4.8**) confirmed the coordination of selenium to the carbene complex. The aqua ligand is present in the solid-state structure, coordinated to the rhodium centre adjacent to the ester functional group rather than the CF_3, which supports its presence and absence in the DMAD and HFB complexes, respectively. The five-membered ring undergoes minimal geometric deviation, with the Rh-C bond lengths of 1.932(6) and 1.912(6) Å and the bent carbido ligand of 124.4 °.

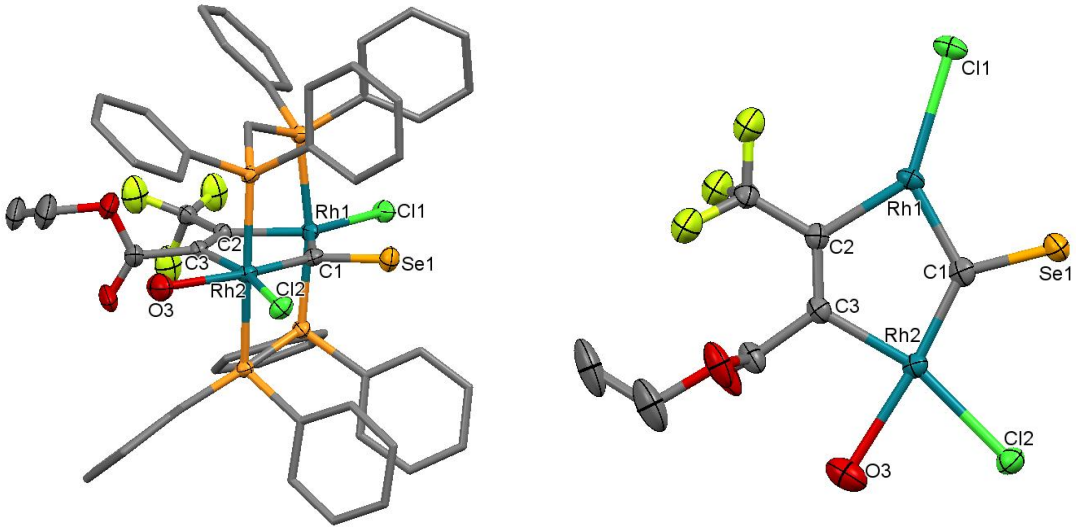

Figure 4.8: Molecular structure of **$[Rh_2(\mu\text{-}CSe)(\mu\text{-}ETFB)Cl_2(\mu\text{-}dppm)_2].H_2O$ (39)** (50% displacement ellipsoids, solvent, disorder and hydrogen atoms omitted, dppm groups simplified). Selected bond lengths (Å) and angles (°): Rh1-C1 1.932(6), Rh2-C1 1.912(6), C1-Se1 1.782(6), Rh1-C2 2.005(6), Rh2-C3 2.023(6), C2-C3 1.337(9), Rh1-C1-Rh2 124.4(3), C2/3-C1-Se1 165.82(1)

With the library of MHC selenocarbonyl complexes now at three, the remaining two ^{77}Se NMR shifts were vital to the studies. Using the same computational modelling as before, the theoretical ^{77}Se shifts for **38** and **39** were calculated to be 1525.7 and 1504.8 ppm respectively. The replacement of the ester group with the stronger electron withdrawing group CF_3 causes a stronger paramagnetic deshielding of the selenium atom, moving the ^{77}Se resonance to higher frequency.

Running exceptionally concentrated samples using a high field NMR instrument (^{1}H: 700 MHz; ^{77}Se: 134 MHz) led to the discovery of the two remaining selenocarbonyl environments. The ETFB complex **39** with one CF_3 group saw a downfield shift to 1504.8 ppm, and then the bis(trifluoromethyl) derivative **38** even further to 1525.7 ppm. The CF_3 group (σ_P = +0.54) is marginally more electron withdrawing than the ester group (σ_P = +0.45), which increases the π-acidity of the carbene, and consequently the deshielding effect to the ^{77}Se nuclei.

4.3.2 Efforts Towards other Metrics

The Tolman Parameter

Although work on the selenocarbonyl front was proving successful, the development of the other key metric species was attempted in order to have a more complete picture of the MHC electronics. The obvious choice to examine is the classical Tolman Parameter, utilising nickel(0) carbonyl and examining the carbonyl stretch in the infrared spectrum.

The standard pathway to these species (**Scheme 4.2**) forms **[Ni(CO)$_4$]** *in situ* by bubbling carbon monoxide through a THF solution of **[Ni(COD)$_2$]**, followed by the addition of the NHC species to replace one of the carbonyl ligands on nickel.

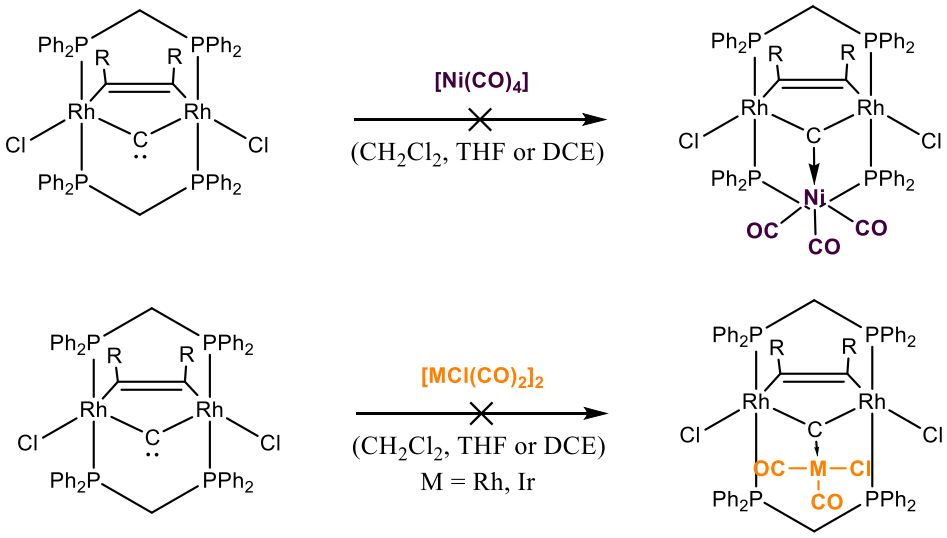

Scheme 4.5: Coordination attempts of **37** to **[Ni(CO)$_4$]** and **[Rh/IrCl(CO)$_2$]$_2$.** (R = CO_2Me)

Addition of the MHC species **37** to either a THF or CH_2Cl_2 solution of **[Ni(CO)$_4$]** results in absolutely no change to the complex when measuring the ^{31}P NMR spectrum of the solution. In an effort to encourage the reaction, the solvent system was replaced with dichloroethane and heated over a period of 24 hours. Even after these more forceful conditions, the MHC **37** displayed no reactivity with **[Ni(CO)$_4$]**. The 64% buried volume of the MHC as a ligand would simply not accommodate the three remaining carbonyl ligands around the nickel centre, and from a steric point of the view, the expected product **[Rh$_2$(μ-C-Ni{CO}$_3$)(μ-DMAD)Cl$_2$(μ-dppm)$_2$]** was unlikely to be formed. It has been seen with some bulky NHCs and phosphines that the dicarbonyl complex **[Ni(NHC)(CO)$_2$]** could be formed,[213] but not in this case.

Attempts to replace nickel(0) carbonyl with the more commonly used rhodium and iridium carbonyl complexes **[MCl(CO)$_2$]$_2$** also proved unsuccessful (**Scheme 4.5**). The square-planar nature of the Group 9 metals would likely point two co-ligands directly into the chloride or dppm ligands on the dirhodium carbene, making this synthetic pathway unlikely. Starting from the cyclooctadiene precursors, the reaction between **37** and both **[MCl(COD)]$_2$** (M = Rh, Ir) fails to display any measurable reactivity when monitoring the reaction mixture with ^{31}P NMR. Bubbling carbon monoxide through the reaction mixture to form the carbonyl species **[MCl(CO)$_2$]$_2$** *in* situ could be tracked using infrared monitoring, though these species still did not exhibit any reactivity with **37**. Heating the reaction mixture in THF or dichloroethene for 24 hours only led to the decomposition of **37**.

Attempted Phosphinidene Synthesis

One of the other metrics that was attempted is the phosphinidene species, the bonding of which can also be represented by two alternate canonical forms depending on the π-acidity of the carbene (**Figure 4.2**).

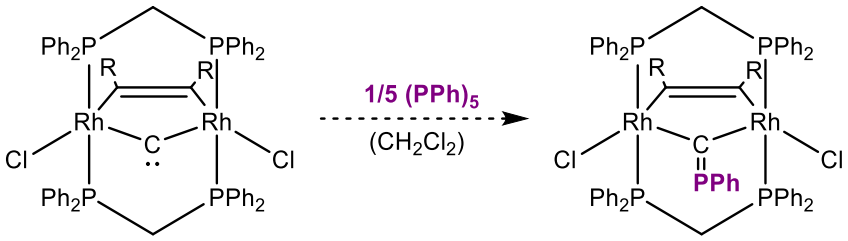

Scheme 4.6: Attempted synthesis of **[Rh$_2$(μ-CPPh)(μ-DMAD)Cl$_2$(μ-dppm)$_2$]** (R = CO_2Me)

Though considered here from the perspective of a MHC derivative, it should be noted that phospha-isonitrile (phosphaisocyanide) ligands are exceedingly rare being limited to two reports of terminal examples,[15, 214] and two of bridging CPR ligands.[215] Thus the successful synthesis of a further example would be of fundamental significance in its own right.

The synthesis of an MHC phosphinidene species was attempted using the standard literature method developed for the reactions of NHCs with the oligomer $(PPh)_5$. The reaction mixture of the carbene species **$[Rh_2(\mu\text{-}C{:})(\mu\text{-}DMAD)Cl_2(\mu\text{-}dppm)_2]$** with 1/5 equivalent of $(PPh)_5$ turns red over the course of 2 hours. Monitoring the reaction through ^{31}P NMR unfortunately saw the generation of at least a dozen new resonances, suggesting a remarkably unclean reaction had taken place. Unfortunately, no manner of selective crystallisation or chromatography could separate the products, which were also exceptionally susceptible to decomposition.

Although a clean product could not be isolated or unambiguously solved, there was a promising sign detected in the ^{31}P NMR spectrum. When comparing NHC phosphinidene and selenourea compounds, it was found that a linear relationship occurred between the NHC ^{31}P and ^{77}Se NMR chemical shifts (**Equation 4.1**, $R^2 = 0.918$).

$$\delta_P = 0.133(\delta_{Se}) + 205.021$$

Equation 4.1: Calculation of NHC phosphinidene ^{31}P chemical shifts from selenourea ^{77}Se shifts

Based on the formulation, the phosphinidene adduct for the MHC complex **$[Rh_2(\mu\text{-}CPPh)(\mu\text{-}DMAD)Cl_2(\mu\text{-}dppm)_2]$** (**Scheme 4.5**) is calculated to appear around 95 ppm (considering the authors did not include subtraction from the reference values in their calculations), which is suitably downfield as expected from the ^{77}Se chemical shift. Examining the crude ^{31}P NMR spectrum of the reaction, there is indeed two resonances centred near 95 ppm (**Figure 4.9**), displaying coupling to multiple spin-active nuclei. Though unable to be confirmed, the presence of these downfield, coupled environment supports the synthesis of an MHC-phosphinidene adduct.

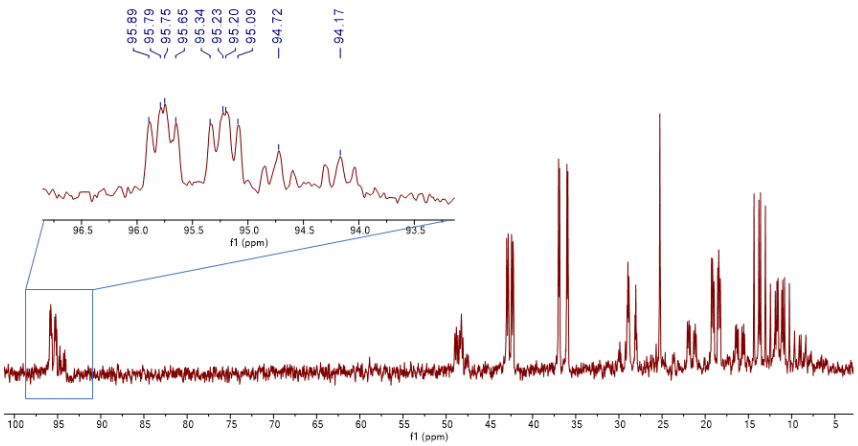

Figure 4.9: ^{31}P NMR spectrum of **[Rh$_2$(μ-CPPh)(μ-DMAD)Cl$_2$(μ-dppm)$_2$]** reaction mixture

4.3.2 Crystallographic Analysis

One key component that emerged from the solid-state studies of the metallacarbene complexes was the short C=Se bond. Provided carbenes with strong π-acceptor properties were more accurately described by the hetero-olefin canonical form, the C=Se bond length may be used as a metric for π-acidity. To help support the high π-acceptor capability of the *Metalla*-Heterocyclic Carbenes, the crystallographic C=Se bond lengths were compared to all NHC selenourea compounds present in the CCDC (98 in total as of 09/2021).

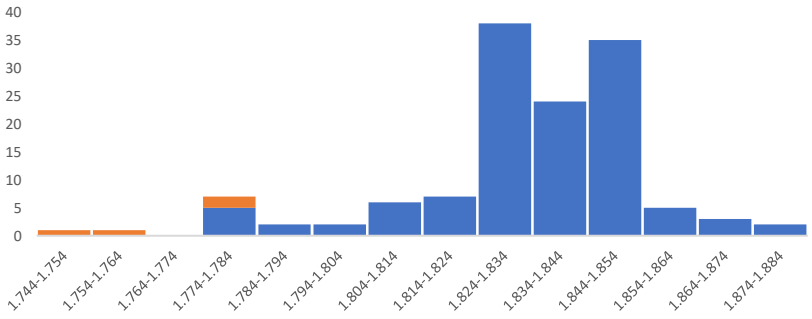

Figure 4.10: Histogram of NHC C=Se bond lengths (Data taken from CCDC).
Blue: CCDC Data, Orange: this work

The stacked histogram of the C=Se bond lengths (**Figure 4.10**) shows a large cluster (accounting for 75%) for NHC compounds between 1.824 and 1.854 Å. The few selenourea

compounds that contain significantly higher degrees of multiple bonding contain strong electron withdrawing substituents. The selenourea with the shortest C-Se bond recorded (1.774 Å) contains the π-acidic oxalamide backbone and also has the lowest field shift in the ^{77}Se NMR range for a stable NHC (876 ppm).[216]

The bond lengths for the MHC selenocarbonyl complexes are considerably shorter when comparing to the NHC species. The symmetrically bridging selenocarbonyl **[$Rh_2(\mu_2$-CSe)$Cl_2(\mu$-dppm)$_2$]** has the shortest C=Se bond length recorded at 1.747(6) Å, and the three MHC selenium adducts fall within the range of 1.75(5) to 1.785(6) Å. The shorter C=Se bond lengths imply a higher bonding order, the result from coordination to a carbene with strong π-accepting properties.

4.3.3 Nucleophilicity Studies

Carbenes of higher π-acidity are better described by the seleno-olefin canonical form. With increased multiple bonding character, the nucleophilicity of the selenium is decreased (moving from three lone pairs to two), which is reflected by the difference in reactivity of two selenourea compounds with methyl iodide to form seleno-ethers (**Scheme 4.7**).[217] The π-acidic NHC with the oxalamide backbone displayed no reactivity after 24 hours, in contrast to the ethyl backbone going to completion in 10 minutes.

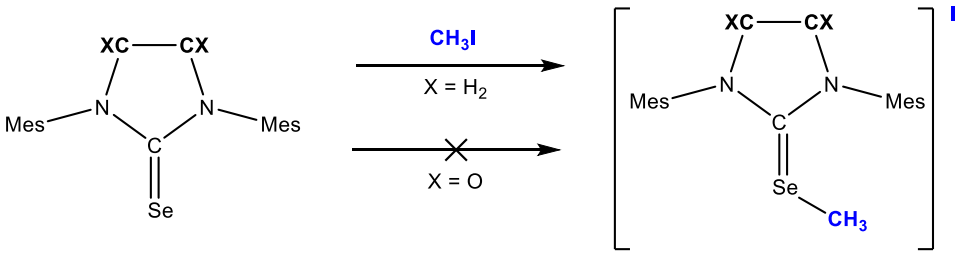

Scheme 4.7: Synthesis of a selenoether complex

Examining the theoretical charge of selenium, there is a clear relationship with the ^{77}Se chemical shift (see **Table 4.1**). Internally, the change in Hirshfeld charge has a strong linear correlation with the MHC ^{77}Se NMR shifts (R^2 = 0.9984). The more positive charge on the selenium corresponds to less electron density around it, due to the higher π-acidity of the carbene.

Though calculated to a different level of theory, the inclusion of Ganter and Nolan's selenourea compounds retain the direct correlation (**Figure 4.11**, $R^2 = 0.9713$). This supports the use of ^{77}Se NMR as a universal metric for carbene π-acidity.

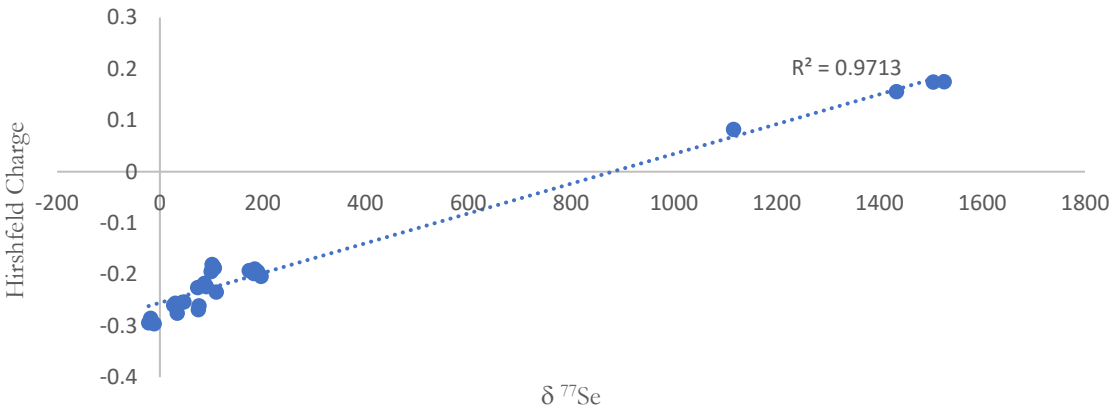

Figure 4.11: Calculated Hirshfeld Charges as a function of experimental ^{77}Se chemical shifts. Note: Data on NHC compounds taken from [210]

The low nucleophilicity of the selenocarbonyl species can be visualised using electrostatic potential maps, which give an indication of charge distribution along the C=Se bond. The calculated electrostatic potential maps for the selenocarbonyl complexes show the potential localised on the selenium atom is largely neutral, indicating the that the olefinic canonical form is a more apt description of the bonding taking place. This is in stark comparison to π-basic NHC IMes, which presents a substantial negative potential on the selenium atom (**Figure 4.12**). This neutral electrostatic potential also suggests that the nucleophilic character of the selenium will be lower due to the π-acidic carbene coordination.

In **Section 1.3**, the selenocarbonyl complex **$[Rh_2(\mu\text{-}CSe)Cl_2(\mu\text{-}dppm)_2]$** failed to display any reactivity with the weak methylating agent methyl iodide, but with the stronger methyl triflate the selenoether species **$[Rh_2(\mu\text{-}CSe\text{-}CH_3)Cl_2(\mu\text{-}dppm)_2](OTf)$** was formed in high yields. The failure of methyl iodide can be attributed to the low nucleophilic character of the selenium.

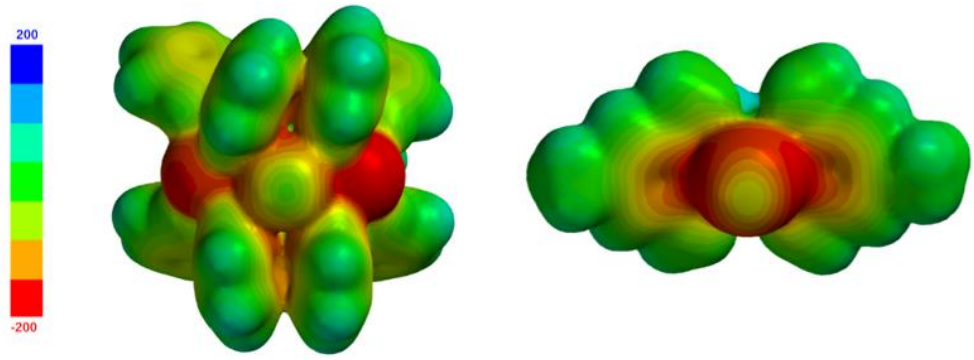

Figure 4.12: Electrostatic Potential Maps of **[$Rh_2(\mu_2$-CSe)(μ-DMAD)Cl_2(μ-dppm)$_2$]** and IMes, looking along the Se=C bond

Stirring the three metallacarbene selenocarbonyl complexes in solution with excess methyl iodide shows no observable reaction taking place after 24 hours, as expected. Exchanging to a stronger methylating agent, the metallacarbene complex **[$Rh_2(\mu_2$-CSe)Cl_2(μ-HFB)(μ-dppm)$_2$]** was treated with methyl triflate in a dichloromethane solution. Even with the significantly stronger methylating agent, the reaction did not show any significant colour changes over the course of 24 hours. Subjecting the reacting mixture to silica gel chromatography provided only the selenocarbonyl starting complex, and there were no changes detected in the $^{31}P\{^1H\}$ NMR spectrum. It is plausible that there is a steric issue with the chloride co-ligands present that would cause 'crowding' around the selenium nucleus, however, the failed reactivity with methyl triflate cannot solely be attributed to steric factors. The π-acidity of the carbene can, however, be attributed to lowering the nucleophilicity of the selenium through increased multiple bonding character.

4.3.4 Paramagnetic Deshielding and Tensors

Comparison of experimental and SR-DFT studies

To compare the theoretical studies performed on the metallacarbene complexes, the calculated chemical shifts were compared to the experimental values found from NMR studies. The accuracy of the calculations could be confirmed from a strong linear dependence ($R^2 = 0.9979$) between the two data sets (**Figure 4.13**), and the individual NMR percentage error on the values were all ≤ 1 %. The high accuracy of the SR-DFT NMR studies provided confidence that more in-depth analysis could be possible.

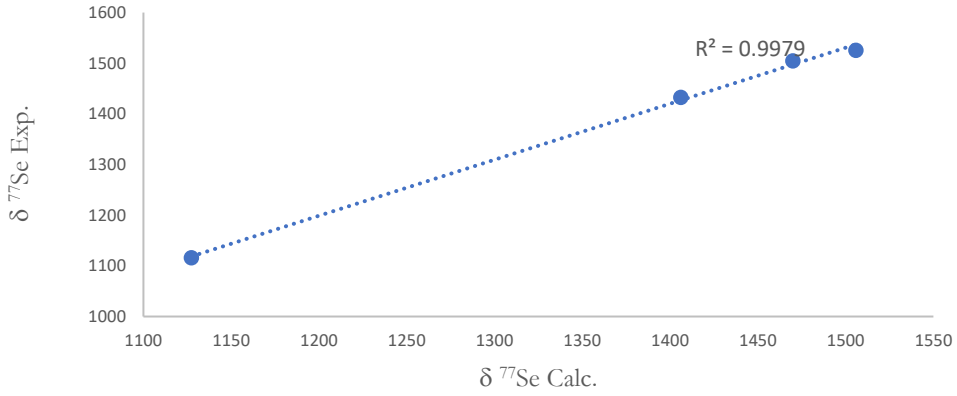

Figure 4.13: Comparison of SR-DFT and experimental ^{77}Se NMR shifts

Paramagnetic Deshielding and ^{77}Se NMR

After calculating the theoretical ^{77}Se NMR shifts for a range of the selenocarbonyl complexes, the next challenge was to examine which factors were primarily responsible for these changes in the ^{77}Se NMR shift. Based on the work of Nolan and Ganter for NHC-selenourea compounds, the magnetic environment of the ^{77}Se nuclei was strongly sensitive to changes in the paramagnetic shielding tensor.

Examining the calculated shielding of the selenium atom, it can be broken down into its diamagnetic (DSO) and paramagnetic (PSO) terms. The diamagnetic shielding value across all of the selenocarbonyl complexes remained effectively unchanged (standard deviation of merely 1.32) which was to be expected. The diamagnetic shielding is due to the core electrons around the nucleus, which should remain unchanged. Though calculated to a different level of theory, the diamagnetic shielding values calculated for the organic NHC selenourea compounds fall in a similar range.

Complex	δ^{77}Se (DFT)	DSO	PSO	Hirshfeld charge
$[Rh_2(\mu\text{-CSe})Cl_2(dppm)_2]$	1127.30	3025.89	-2395.23	0.08196
$[Rh_2(\mu\text{-CSe})(\mu\text{-HCCH})Cl_2(dppm)_2]$	1378.83	3025.69	-2646.57	0.11431
$[Rh_2(\mu\text{-CSe})(\mu\text{-DMAD})Cl_2(dppm)_2]$	1406.00	3027.38	-2675.42	0.15538
$[Rh_2(\mu\text{-CSe})(\mu\text{-ETFB})Cl_2(dppm)_2]$	1475.81	3027.06	-2744.92	0.17419
$[Rh_2(\mu\text{-CSe})(\mu\text{-HFB})Cl_2(dppm)_2]$	1505.88	3027.09	-2775.02	0.17471

Table 4.1: Calculated ^{77}Se NMR shifts and their corresponding shielding parameters

The paramagnetic deshielding, however, changes quite dramatically even between selenocarbonyl complexes. The paramagnetic deshielding parameter (which is a negative value as opposed to the positive diamagnetic shielding value) undergoes significant change between complexes, which is reflected by a change in both the selenium Hirshfeld charge and the ^{77}Se chemical shift. As **Figure 4.14** highlights, plotting both the paramagnetic shielding values and Hirshfeld charge against the experimental ^{77}Se NMR shifts provide strong linear dependencies. As the carbene π-acidity changes, it influences the paramagnetic deshielding of the selenium nuclei, and the change in electronic environment as reflected in its Hirshfeld charge. The changing paramagnetic shielding values supports the ongoing validation that the ^{77}Se chemical shift is a good metric for measuring the π-effects of carbenes, unlike the TEP.

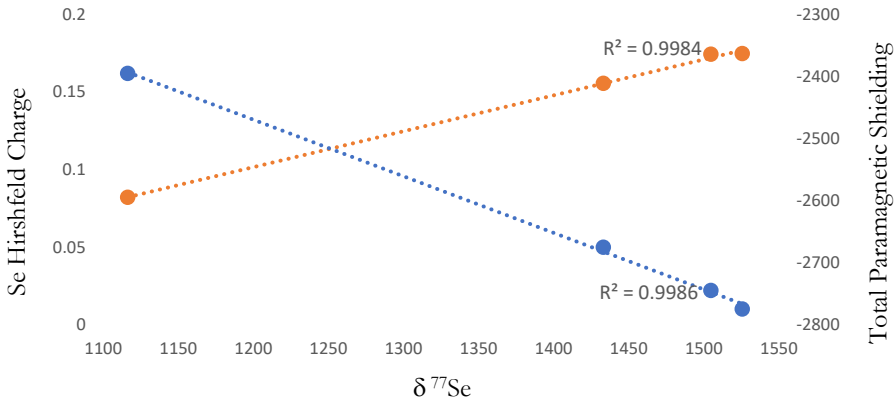

Figure 4.14: Plot of Hirshfeld charge (orange) and paramagnetic shielding (blue) obtained from SR-DFT calculations as a function of experimental ^{77}Se chemical shifts

Breaking Down the Shielding Tensor

The key to quantifying the metallacarbene complexes came down to breaking down the key orbital transitions that underpin the paramagnetic deshielding tensors. The work on selenourea species discovered the key orbital transition involves the occupied selenium p-orbital coupling to the C=Se π* orbital. If the MHC complexes behaved as organometallic Arduengo carbene analogues, the orbital transitions should be similar.

System	δ ^{77}Se (Calc.)	σ_{xx}	σ_{yy}	σ_{zz}
No alkyne	1127.3	-1932.7	-3153.5	-2099.5
HCCH	1378.3	*-3717.3*	-3052.7	*-1169.8*
DMAD	1406.0	*-3513.9*	-3096.3	*-1714.8*
ETFB	1470.0	*-3406.2*	-3060.3	*-1768.3*
HFB	1505.9	*-3456.3*	-3060.5	*-1509.4*

Table 4.2: Paramagnetic shielding tensors for MHC complexes

Breaking down the total paramagnetic shielding into its directional components, the deshielding effect is most notable along the xx axis, which is along the C=Se bond (**Table 4.2**). Examining the contribution of orbital-pair couplings to the ^{77}Se shifts across all complexes revealed that the dominant contributor to the paramagnetic deshielding is the occupied selenium p-orbital (HOMO, or HOMO-1) and the C=Se π* virtual orbital (LUMO+1 or LUMO+2), the same orbital coupling seen for the NHC compounds (**Figure 4.15**). The coupling of the selenium p_z orbital is detected along the xx axis, supporting the change in shielding tensor values.

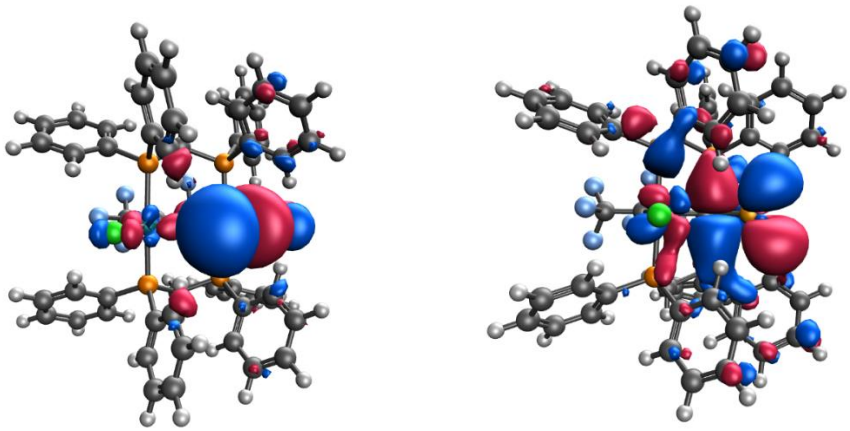

Figure 4.15: (left) HOMO and (right) LUMO +1 of **[Rh$_2$(μ$_2$-CSe)Cl$_2$(μ-HFB)(μ-dppm)$_2$]**

Plotting the energy gap between these two orbitals against the theoretical ^{77}Se chemical shift (**Figure 4.16**) revealed a good linear relationship between the two (R^2 = 0.8816). As the energy gap between the orbitals decreases, the paramagnetic deshielding effect is more pronounced, resulting in higher frequency ^{77}Se NMR shifts. This is the same trend and primary transition seen for NHC compounds, supporting the comparison of these species to a 'metal NHC'.

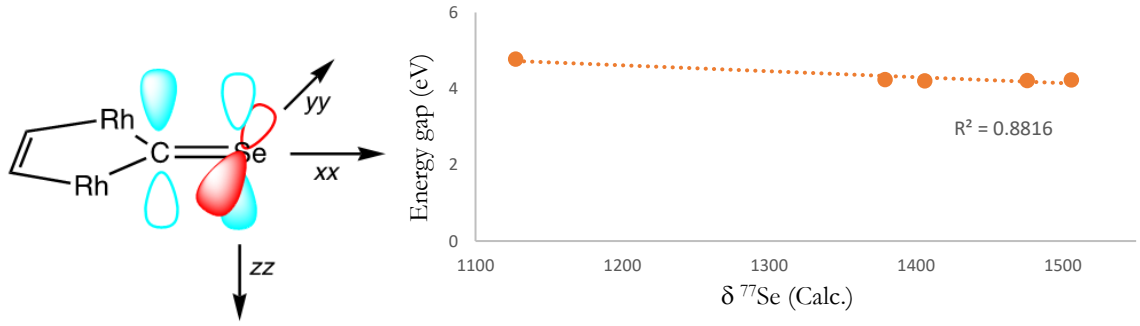

Figure 4.16: (left) orbital diagram for the coupling between occupied selenium p_y (red) and the C=Se π* orbital (blue). (right) Plot of calculated ^{77}Se NMR shifts against the p_y-π* orbital energy gap

Although the p-π* coupling was calculated to be the primary transition for all carbene species, and internally consistent with the change in MHC ^{77}Se NMR shifts, the difference in orbital energies (3.5 to 4.5 eV) is comparable to the NHC selenourea compounds, and therefore cannot solely account for the significantly lower field ^{77}Se chemical shifts the metallacarbenes exhibit.

Unlike the NHC species, the MHC complexes displayed a second significant paramagnetic shielding change detected along the *zz* axis. Though neithetr of the individual shielding components along *xx* or *zz* axes could not give an accurate ^{77}Se shift-dependence, the summation of the two values did (R^2 = 0.9967), suggesting that the chemical shift was in fact dependent upon two orbital couplings, not one.

The deshielding effect along the *zz* axis was strongest for the non-ringed species **[Rh_2(CSe)Cl_2(dppm)$_2$]**. Breaking down the orbital couplings, the third most prominent was calculated to be between the HOMO-1 (selenium p_y orbital) and the LUMO+2. Although substantially involving contributions from co-ligand orbitals (dppm, alkyne, Cl), the virtual orbital of relevance in the vicinity of the selenocarbonyl has distinct C–Se σ* character (**Figure 4.17**). This p_y-σ* coupling would be detected in the *zz* axis. Unfortunately, attempts to identify suitable molecular orbitals containing strong C-Se σ* character that couple with the selenium p_y orbital has proved unsuccessful.

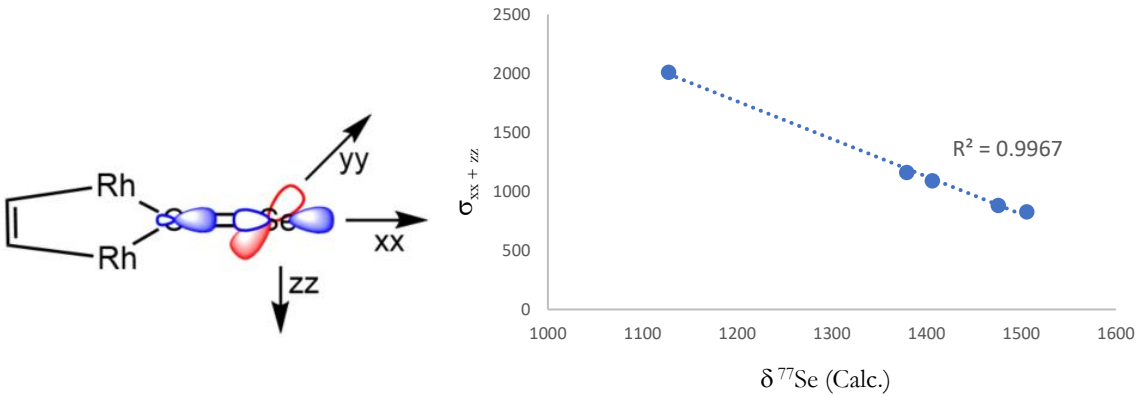

Figure 4.17: (left) Visual of calculated transition between occupied selenium p_y (red) to C-Se σ* (blue). (right) Summation of *xx* and *zz* total shielding tensors as a function of calculated ^{77}Se shifts

The primary transition associated with the σ_{yy} component for NHC compounds is the occupied selenium p_z orbital coupling with the C-Se σ* virtual orbital. However, this transition was not detected in the MHC examples. Instead, the second strongest coupling for all species was between the occupied Rh-Se σ* orbital and the C=Se π* orbital, which would be detected along the *yy* tensor (**Figure 4.18**). Though this value is unchanging between complexes, the heavy d-orbital character of the rhodium nuclei in this coupling highlights the significant differences for these metallacarbene complexes.

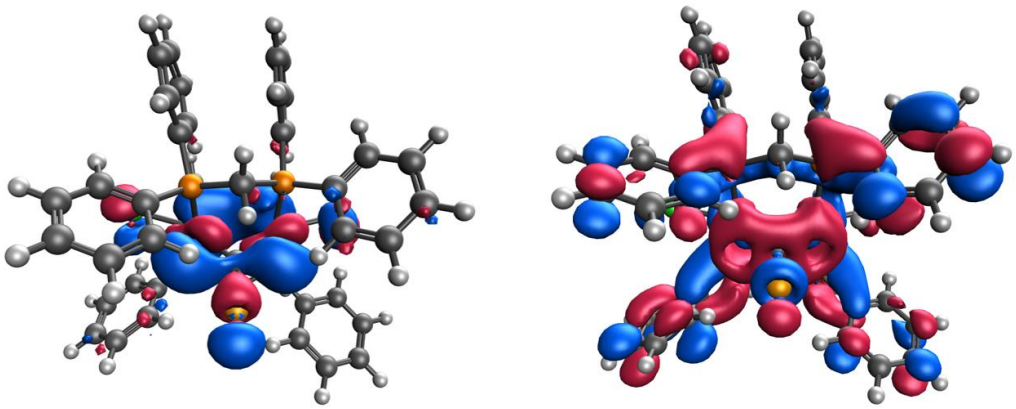

Figure 4.18: (left) visualization of Rh-C-Se σ* orbital. (right) visualization of C-Se σ* orbital

Provided the metallacarbene selenocarbonyl complexes show a strong dependence between the paramagnetic deshielding and the ^{77}Se NMR shift, and that the primary transition is between the selenium p_y to the C=Se π* orbital, the Class D μ-carbido complexes show significant similarities to *N*-Heterocyclic Carbenes. The significantly enhanced π-acidity in comparison to the nitrogen heterocycles can be attributed to the heavy involvement of the rhodium d-orbitals in the π-system of the selenocarbonyl species, which leads to extremely downfield ^{77}Se NMR shifts.

4.3.6 Summary

This chapter explored the possible quantification of the electronic nature of *Metalla*-Heterocyclic Carbene complexes. Due to the significance of the MHC complex **[Rh$_2$(μ-CSe)(μ-DMAD)Cl$_2$(μ-dppm)$_2$]**, two additional analogues were formed based on the alkynes ethyl 4,4,4-trifluoro-2-butynoate (ETFB) and hexafluoro-2-butyne (HFB). These two additional metallacarbene complexes react with selenium in an analogous fashion to furnish the corresponding μ_2-selenocarbonyl complexes.

The ^{77}Se NMR studies performed on the three metallacarbene complexes revealed exceptionally downfield chemical shifts. The DMAD complex contains a selenium environment at 1433.09 ppm, with the ETFB and HFB complexes at lower fields still (1504.8 and 1525.7 ppm respectively).

The MHC complex **[Rh$_2$(μ-C:)(μ-DMAD)Cl$_2$(μ-dppm)$_2$]** failed to display any reactivity with both **[Ni(CO)$_4$]** and **[Rh/IrCl(CO)$_2$]** to furnish the Tolman Parameter metric complexes. The attempted synthesis of the phosphinidene species **[Rh$_2$(μ-C-PPh)(μ-DMAD)Cl$_2$(μ-dppm)$_2$]** with $(PPh)_5$ ultimately failed to provide an isolable product, though promising signs were identified in the ^{31}P NMR spectrum for a phosphinidene adduct.

Computational SR-DFT studies were performed on the three MHC complexes, in addition to **[Rh$_2$(μ-CSe)Cl$_2$(μ-dppm)$_2$]** and the hypothetical species **[Rh$_2$(μ-CSe)(μ-HCCH)Cl$_2$(μ-dppm)$_2$]**. The downfield ^{77}Se chemical shifts could be attributed to an increase in the paramagnetic deshielding in comparison to NHC compounds, and the primary orbital transition responsible is the selenium p_y orbital coupling to the C=Se π* virtual orbital.

The theoretical and experimental studies combine to paint a picture that quantifies the metallacarbene complexes as exceptionally π-acidic NHC analogues.

4.4 EXPERIMENTAL

Computational Details

^{13}C, ^{31}P and ^{77}Se chemical shifts were calculated using scalar-relativistic all-electron DFT calculations in the ORCA suite of programs.[218] Structures of compounds **37-39** were first optimised, starting from their respective crystal structures where available. Optimisations were conducted using the TPSS-D3BJ functional[219,220] and zeroth-order regular approximation (ZORA) scalar relativistic Hamiltonian.[221,222] The relativistically recontracted ZORA-def2-TZVP[223] basis set was used for all elements except Rh, for which the ZORA-SARC-TZVP[7] basis set was used. The RI-J resolution of the identity approach was employed in conjunction with the SARC/J auxiliary basis set[224-226] to speed up computation of the Coulomb integrals. A large angular grid (ORCA Grid 7, NoFinalGrid) and radial grid (ORCA IntAcc=12) were selected to ensure accuracy when calculating properties of heavy elements using scalar-relativistic all-electron DFT. The SCF convergence threshold was set to 10^{-8} (ORCA TightSCF). Solvent effects were included using the CPCM continuum solvation model[227] with chloroform as the solvent, to best match the experimental NMR setup. Numerical frequencies were calculated at each optimised geometry to ensure a stationary point on the potential energy surface was obtained. Chemical shifts were calculated from the optimised geometries with the ORCA gauge-invariant atomic orbital (GIAO) code.[228] The PBE0 hybrid functional[229] was employed along with the ZORA-def2-TZVP(P) and ZORA-SARC-TZVP(P) basis sets for all elements apart from Rh and Rh respectively. The same RI-J, grid, SCF and solvent configuration used for geometry optimisations were applied in the calculation of chemical shifts. Quantification of relative charges on nuclear centres was achieved by calculation of Hirshfeld charges. To allow comparison of chemical shifts to experiment, chemical shifts of reference compounds tetramethylsilane (C^{13}), phosphoric acid (P^{31}), and dimethylselenide (Se^{77}) were computed at the same level of theory. Chemical shifts of compounds **37-39** were then obtained by subtracting the chemical shift of the target molecule from the chemical shift of the reference. Molecular orbital plots were constructed using PyMol.[230] Coordinates of optimised geometries and sample input files are available at https://github.com/OMaraLab/Rh_NHCs_NMR.

Synthesis of $[Rh_2(\mu_2\text{-}CSe)(\mu_2\text{-}HFB)Cl_2(\mu\text{-}dppm)_2]$ (38)

To a flask containing $[Rh_2(\mu_2\text{-}C)(\mu_2\text{-}HFB)Cl_2(\mu\text{-}dppm)_2]$ (0.080 g, 0.033 mmol) was added CH_2Cl_2 (10 mL) followed by grey selenium (0.023 g, 0.090 mg.atom). The resulting dark red suspension was stirred for 48 hours at room temperature, turning pink/red as the starting material dissolved to give a clear solution. The solution was concentrated under reduced volume and subjected to silica gel column chromatography (10 x 1 cm). Eluting with a 5% mixture of THF in CH_2Cl_2 provided a pink band which was freed of volatiles to afford the desired product $[Rh_2(\mu_2\text{-}CSe)(\mu_2\text{-}HFB)Cl_2(\mu\text{-}dppm)_2]$ as a dark pink powder. Yield: 0.018 g (0.015 mmol, 44%). ^{1}H NMR (400 MHz, $CDCl_3$, 298 K): δ_H = 3.11 (br. d, $^2J_{PH}$ = 14 Hz, 2 H, PCH_2), 3.74 (dp^v, J_{PH} = 14, $^2J_{HH}$ = 6 Hz, 2 H, PCH_2), 7.04 (t, $^3J_{HH}$ = 8 Hz, 8 H, C_6H_5), 7.20 (t, $^3J_{HH}$ = 8 Hz, 4 H, C_6H_5), 7.38 (br. s, 14 H, C_6H_5), 7.82 (q, $^3J_{HH}$ = 6 Hz, 8 H, C_6H_5), 7.91-7.93 (m, 8 H, C_6H_5). ^{13}C{^{1}H} NMR (151 MHz, $CDCl_3$, 298 K): δ_C = 134.9, 132.0, 130.6, 130.4, 128.6, 128.2, 128.0, 125.7 (C_6H_5 – identified accurately through HSQC studies due to low solubility), 16.6 (p^v, J_{CP} = 11 Hz, PCH_2). Remaining environments not detected. ^{31}P{^{1}H} NMR (162 MHz, $CDCl_3$, 298 K): δ_P = -0.06 (d, $^1J_{RhP}$ = 127 Hz). ^{19}F{^{1}H} NMR (370 MHz, $CDCl_3$, 298 K): δ_F = -51.92. ^{77}Se{^{1}H} NMR (370 MHz, $CDCl_3$, 298 K): δ_{se} = 1525.5 (br. s). IR (ATR, cm^{-1}): 1097, 1053 ν_{CF}. ν_{CSe} not unambiguously identified. MS (ESI, *m/z*): Accurate mass: Found 613.9796. Calcd for $C_{55}H_{44}F_6P_4Rh_2{}^{80}Se$ $[M–2Cl]^{2+}$: 613.9790. A crystal suitable for structure determination was grown by slow evaporation of a CH_2Cl_2/petrol mixture. *Crystal data for* $C_{55}H_{44}Cl_2F_6P_4Rh_2Se$ (M_w = 1298.46 g.mol^{-1}): tetragonal, space group $P4_1$ (No. 76) a = 21.4117(12), c = 14.2580(13) Å, V = 6536.7(9) Å^3, Z = 4, T = 150.0(1) K, μ(Cu Kα) = 6.80 mm^{-1}, D_{calcd} = 1.319 Mg.m^{-3}, 27791 reflections measured (7.4° ≤ 2Θ ≤ 132.2°), 11462 unique (R_{int} = 0.157) which were used in all calculations. The final R_1 was 0.127 ($I > 2\sigma(I)$) and wR_2 was 0.418 (all data) for 571 refined parameters with 414 restraints.

Synthesis of $[Rh_2(\mu_2\text{-}CSe)(\mu_2\text{-}ETFB)Cl_2(\mu\text{-}dppm)_2]$ (39)

To a flask containing $[Rh_2(\mu_2\text{-}C)(\mu_2\text{-}ETFB)Cl_2(\mu\text{-}dppm)_2]$ (0.050 g, 0.041 mmol) was added CH_2Cl_2 (10 mL). To this solution was added grey selenium (0.020 g, 0.25 mg.atom^{-1}). The resulting red suspension was stirred for 24 hours at room temperature. The solution was decanted to remove excess suspended selenium, and the red solution concentrated under reduced pressure. Subjecting the solution to silica gel column chromatography, a pink band was eluted using 5% THF in CH_2Cl_2. A pink powder precipitated upon addition of petroleum spirits and drying *in vacuo* gave a pink

powder of pure [$Rh_2(\mu_2$-CSe)(μ_2-ETFB)$Cl_2(\mu$-dppm)$_2$] (**39**). Yield: 0.033 g (0.025 mmol, 62%). ^{1}H NMR (400 MHz, $CDCl_3$, 298 K): δ_H = 0.05 (t, $^3J_{HH}$ = 7 Hz, 3 H, CH_3), 2.71 (q, $^3J_{HH}$ = 7 Hz, 2 H, OCH_2), 2.96 (d, $^2J_{PH}$ = 13 Hz, 2 H, PCH_2), 3.78 (dp^v, J_{PH} = 14 Hz, $^2J_{HH}$ = 6 Hz, 2 H, PCH_2), 6.97 (t, $^3J_{HH}$ = 7 Hz, 4 H, C_6H_5), 7.08 (t, $^3J_{HH}$ = 7 Hz, 4 H, C_6H_5), 7.13 (t, $^3J_{HH}$ = 7 Hz, 2 H, C_6H_5), 7.22 (t, $^3J_{HH}$ = 7 Hz, 2 H, C_6H_5), 7.34–7.36 (m, 16 H, C_6H_5), 7.73 (m, 6 H, C_6H_5), 7.94 (m, 6 H, C_6H_5). ^{13}C{^{1}H} NMR (151 MHz, $CDCl_3$, 298 K): δ_C = 136.2, 134.8, 132.2, 130.8, 130.4, 128.3, 127.9, 125.7 (C_6H_5), 60.2 (OCH_2-), 16.4 (PCH_2), 13.2 (CH_3). All ^{13}C resonances identified through HSQC studies due to low solubility. Remaining environments not detected. ^{31}P{^{1}H} NMR (162 MHz, $CDCl_3$, 298 K): δ_P = 1.08 (d, $^1J_{RhP}$ = 131 Hz), -0.26 (d, $^1J_{RhP}$ = 125 Hz). ^{19}F{^{1}H} NMR (370 MHz, $CDCl_3$, 298 K): δ_F = -51.60. ^{77}Se{^{1}H} NMR (370 MHz, $CDCl_3$, 298 K): δ_{se} = 1504.8. IR (ATR, cm^{-1}): 1693 ν_{CO}, 1097, 1050 ν_{CF}. ν_{CSe} not unambiguously identified. MS (ESI, *m*/*z*): Accurate mass: Found 615.9969. Calcd for $C_{57}H_{47}F_3O_24P_4Rh_2{}^{80}Se$ [M–2Cl]$^{2+}$: 615.9950. A crystal suitable for structure determination was grown by slow evaporation of a CH_2Cl_2/toluene mixture. *Crystal data for* $C_{57}H_{51}Cl_2F_3O_3P_4Rh_2Se{\cdot}C_7H_8$ (M_w = 1412.67 g.mol^{-1}): monoclinic, space group $P2_1/c$ (no. 14), a = 12.7778(2), b = 15.5941(2), c = 31.0896(4) Å, β = 90.788(1)°, V = 6194.27(15) Å^3, Z = 4, T = 150.0(1) K, μ(Cu Kα) = 7.19 mm^{-1}, D_{calcd} = 1.515 Mg.m^{-3}, 19580 reflections measured (8.0° ≤ 2Θ ≤ 133.2°), 9,353 unique (R_{int} = 0.029) which were used in all calculations. The final R_1 was 0.062 ($I > 2\sigma(I)$) and wR_2 was 0.191 (all data) for 767 refined parameters and 144 restraints.

EPISODE FIVE – THE ALKYNE STRIKES BACK

SYNTHESIS OF METALLACYCLES FROM THE μ-CARBIDO LIGAND

5.1 PREFACE

Abstract taken from H.J. Barnett, A.F. Hill, *Dalton Trans.,* **2021**, 50, 9383.

The linear μ-carbido complex **[$Rh_2(\mu\text{-}C)Cl_2(dppm)_2$]** (dppm = bis(diphenylphosphino)methane) reacts with a benzyne equivalent ($Me_3SiC_6H_4OTf\text{-}2/F^-$) to afford **[$Rh_2(\mu\text{-}CC_6H_4)(\mu\text{-}Cl)(C_6H_5)Cl_2(\mu\text{-}dppm)_2$]**, in which the benzyne moiety adds across one of the two metal–carbon double bonds.

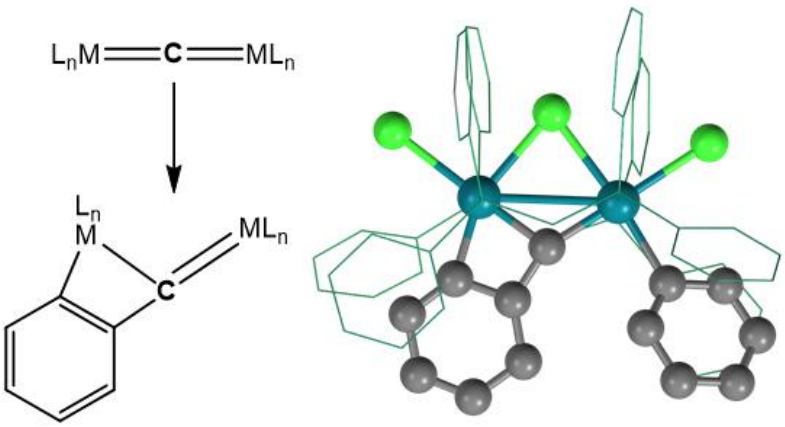

Figure 5.0: Simplified transformation of the μ-carbido ligand into a metallacyclobutadiene

5.2 INTRODUCTION

5.2.1 Metals in Alkyne Metathesis

The disproportionation or dismutation of alkynes, more commonly known as alkyne metathesis, is at its core underpinned by the involvement of a transition metal catalyst. Even before mechanistic insights emerged, the first reported case of alkyne disproportionation by Pannella *et al.* in 1968 required a heterogenous tungsten oxide on silica catalyst.[231] Homogenous catalysis of alkyne metathesis was achieved not long after, with Mortreux utilising molybdenum hexacarbonyl and resorcinol for the metathesis of *p*-tolylphenylacetylene in 1977.[232]

One year later, mechanistic studies on alkyne metathesis were put presented by Katz and supported a similar process to the recently suggested alkene metathesis involving a metal-carbon multiple bond.[233] It was suggested (**Figure 5.1**) that the reaction between a metal-carbon triple bond and an alkyne would initially go through a metallacyclobutadiene intermediate, which would break up to form the new alkyne and metal alkyne complex.

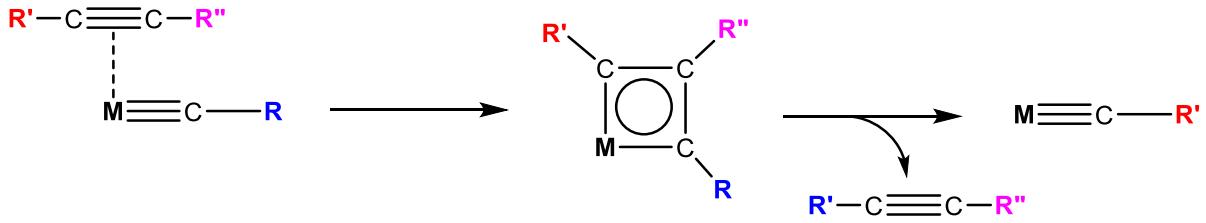

Figure 5.1: Proposed mechanism of alkyne metathesis through a metallacyclobutadiene intermediate

This tidy mechanistic picture was initially confounded by the failure of known carbyne complexes, e.g., those discovered by Fisher, to effectively metathesise alkynes, in contrast to the success of Fisher-esque carbenes in alkene and enyne metathesis.[234] It was not until the development by Schrock of rather different carbynes, specifically the high oxidation state tungsten complex **[W(≡C^{t}Bu)(O-^{t}Bu)$_3$]**, that the first reported example of a metal carbyne complex catalysing the metathesis of an asymmetric alkynes could be demonstrated.[235-237]

Though the development of alkyne metathesis has not shared the same glory as its alkene counterpart, alkyne metathesis still plays a strong and emerging role in organic synthesis. The organometallic foundations of this process remain a relevant area of investigation, as highlighted

by Schrock himself in 2013[238] and more recently in reviews by Tamm,[239] Fürstner,[240] and others[241] that explore this chemistry in great detail.

5.2.2 Metallacyclobutadiene Complexes

The key intermediate that underpins the alkyne metathesis process is a metallacyclobutadiene, a four-membered metallocycle comprising the metal and three sp^2 carbon centres. A review on the chemistry of metallacyclobutadienes has been recently published by Cui *et. al.*,[242] and this introduction will only serve to provide an oversight into their synthetic pathways. This alkyne metathesis intermediate may in some cases undergoes further rearrangement to reform a much more stable metal alkyne species in the catalytic process, or through a further polyhedral cyclisation form the three-membered *trihapto*-cyclopropenium ligand (a *'metallatetrahedrane'*), which in some instances may terminate the catalytic processes (**Figure 5.2**).[242]

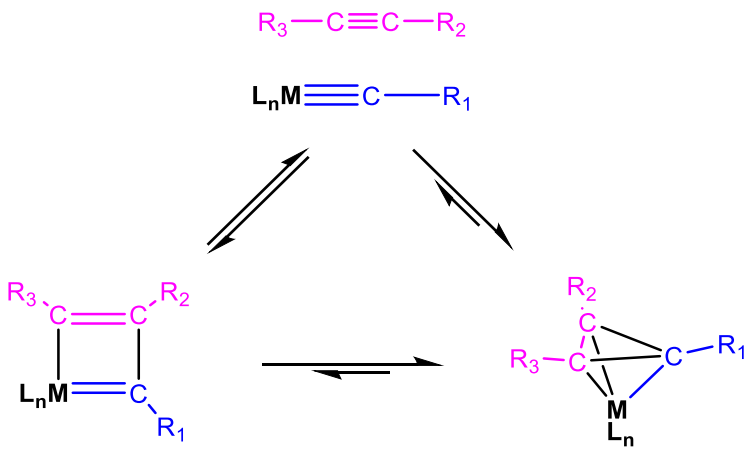

Figure 5.2: Interconversion of alkyne metathesis species

The organic isolobe, cyclobutadiene, is a textbook example of a Hückel antiaromatic compound, with only 4 electrons in the π system. Due to this electronic instability, and the high ring strain of planar sp^2 carbons forming bonds at 90° to each other, even sterically encumbered derivatives of these molecules have proven highly reactive and only isolable with the use of trapping agents. Formally replacing one of the carbon vertices in cyclobutadiene with an isolobal transition metal fragment gives metallacyclobutadiene complexes. The involvement of the transition metal d-orbitals in the π-system of the ring results in the organometallic analogues often

being far more stable and isolable. [xliii] The first reported example appeared in 1970 and involved the addition of the triphenylcyclopropenium cation to the iridium square planar complex **[IrCl(CO)(PMe$_3$)$_2$]**, forming the metallacyclobutadiene species **[Ir(C$_3$Ph$_3$)Cl(CO)(PMe$_3$)$_2$]BF$_4$** (**Scheme 5.1**).[243] This process was repeated with a rhodium analogue, **[RhCl(CO)(PMe$_2$Ph)$_2$]**, though in this example the carbonyl ligand is lost and replaced with a chloride.[244] This process of insertion of a metal into a cyclopropenium ring is believed to proceed through a η^3-cyclopropenyl intermediate, which was supported through the synthesis of an iridacyclobutadiene species by heating the cyclopropenyl complex **[Ir$_2$(μ-CO)(CO)$_2$(C$_3$^{t}Bu$_3$)$_2$]**.[245]

Because the metal presents two *d*-orbitals of π-symmetry, it could be argued that metallacyclobutadienes are more usefully described as 6π systems and as such satisfy the Hückel criteria. In any event, the isolobal analogy is of only superficial use.

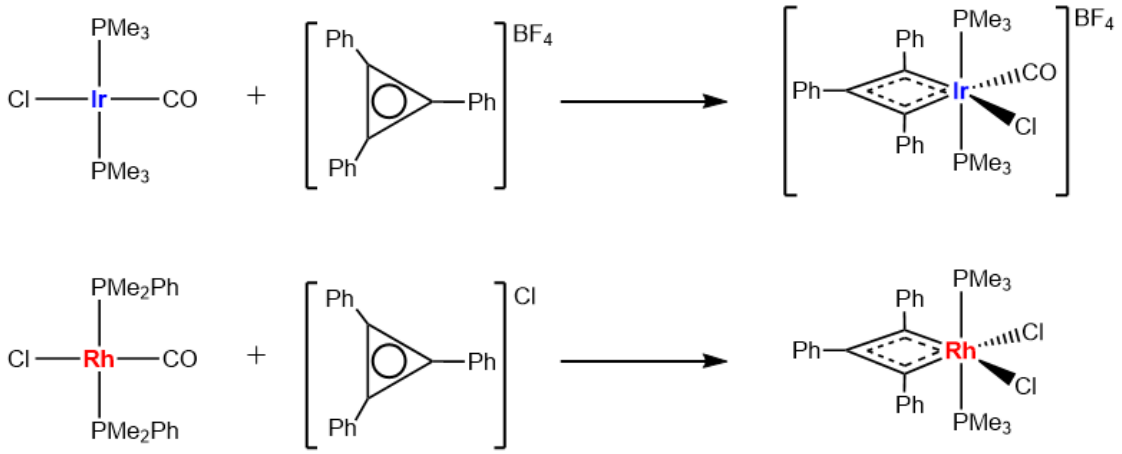

Scheme 5.1: Synthesis of Group 9 metallacyclobutadiene species using triphenylcyclopropenium

Other methods for the synthesis of metallacyclobutadiene complexes include alkylation of metallacyclobutenones,[246] and thiones , electrophilic addition to iminometallacyclobutenes,[247] and cleaving M-M and M-N multiple bonds.[248] The most relevant reaction pathway for this current work though, is however the 2+2 cycloaddition of alkynes to a metal-carbon multiple bond.

[xliii] Because the metal presents two *d*-orbitals of π-symmetry, it can be argued that metallacyclobutadienes are more usefully described as 6π systems to satisfy the Hückel criteria. In any event, the isolobal analogy is of only superficial use.

The first example of a 2+2 cycloaddition forming a metallacyclobutadiene complex was centred around the osmium thiocarbonyl species **[Os(CS)(CO)(PPh$_3$)$_3$]**, which reacts with diphenylacetylene across the Os-CS multiple bond to furnish the intermediate osmacyclobutenethione which could further react with methyl iodide to methylate the exocyclic sulfur and furnish the osmacyclobutadiene species (**Scheme 5.2**).[249]

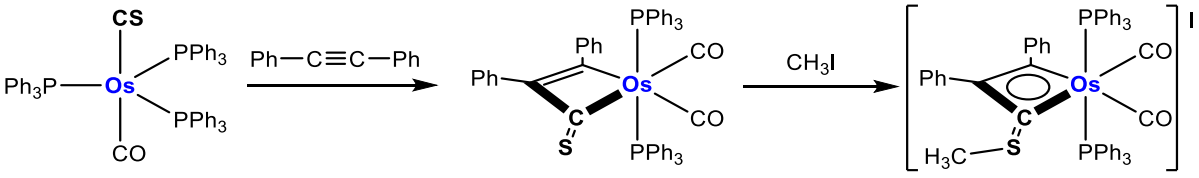

Scheme 5.2: Synthesis of an osmium metallacyclobutadiene from alkyne 2+2 cycloaddition

In a similar fashion, alkynes bearing both electron donating (phenylacetylene, acetylene) and withdrawing groups (methyl propiolate) were successfully installed across the Ir-C multiple bond in the thiocarbonyl complex **[IrX(CS)(PPh$_3$)$_2$]** (X = Cl, I), forming the iridacyclobutadiene fused to a five-membered heterocycle arising from a 1,3-dipolar cycloaddition of a second equivalent of alkyne to the sulfur and iridium (**Scheme 5.3**).[250] The carbyne/alkyne cycloaddition has been extensively explored with tungsten and molybdenum Schrock carbyne complexes, furnishing a library of Group 6 metallacyclobutadiene complexes.[251] The alkynes by and large contain alkyl or aliphatic groups, in contrast to the activated alkynes such as DMAD which have been seen in **Chapter 4.3** to perform a 3+2 cycloaddition to electron rich low-valent dirhodium complexes. This is due to the electronic nature of the Schrock carbynes, which contain a high-valent tungsten(VI) centre, which readily coordinates further electron donating groups to stabilise its high oxidation state.

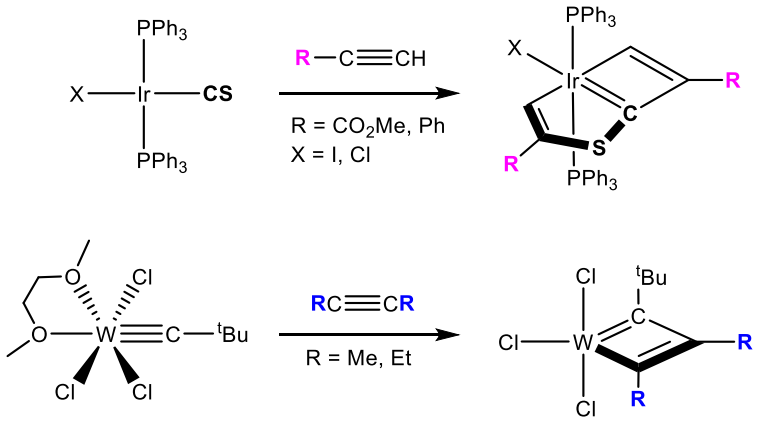

Scheme 5.3: Examples of 2+2 cycloadditions of alkynes to metal-carbon multiple bonds

This cycloaddition pathway has proven quite versatile for alkynes of various electrodative capacities, and for a range of transition metals from high-valent tantalum and rhenium,[252] to low-valent iron and osmium.[253] The alkynes used in these metathesis and cycloaddition addition usually contain two carbon-based R groups, and terminal alkynes are largely avoided. This is due to the generation of acetylene in the metathesis process, which can destructively interact with the metal centre, and typically is removed with molecular sieves during the reaction.[254]

5.2.3 Synthesis of benzyne complexes

Benzyne, or 1,2-dehydrobenzene, is the parent compound of the aryne (dehydroarene) class. Arynes present an unusual and highly reactive class of organic molecules, derived from the *ortho* abstraction of two substituents of an aromatic ring, forming a highly reactive triple bond. Though postulated as early as 1927,[255] reactivity-based evidence in support of their intermediacy did not appear until almost 40 years later, when Roberts *et al.* used ^{14}C enriched chlorobenzene with sodium amide forming a 50:50 mixture between enriched *ipso* and *ortho* sites (**Scheme 5.4**).[256]

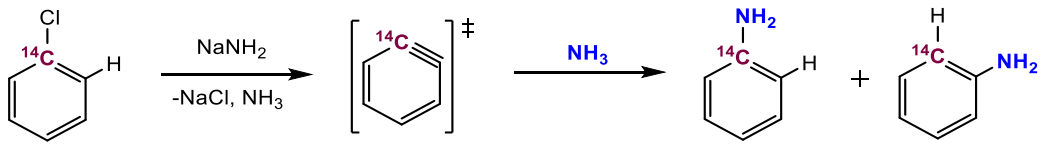

Scheme 5.4: ^{14}C labelled reaction of chlorobenzene and sodium amine, with presumed benzyne intermediate

The first structurally characterised transition metal complex bearing a benzyne ligand appeared in 1979. Schrock showed (molecular structure later published by Churchill) that thermolysis of tantalum(V) and niobium(V) complexes with the general formula **[M(Ph)Me$_3$Cp]** leads to the elimination of methane and conversion of the σ-phenyl ligand into a benzyne unit.[257] Thermolytic C-H activation was continued with a range of early transition metal complexes, using complexes with aryl or alkyl ligands. One particular example took a vanadium PNP pincer complex **[(PNP)V(CH$_2$*t*Bu)$_2$]** (PNP = N[2-P{CHMe$_2$}$_2$-4-methylphenyl]$_2$) and upon addition of d$_6$-benzene, led to the two-fold elimination of the alkyl ligands to form the μ$_2$-benzyne complex (**Scheme 5.5**).[258] This elimination pathway has been the entry point for benzyne complexes of early and middle transition metals, including molybdenum, niobium, ruthenium, tantalum, , vanadium, and zirconium.[259]

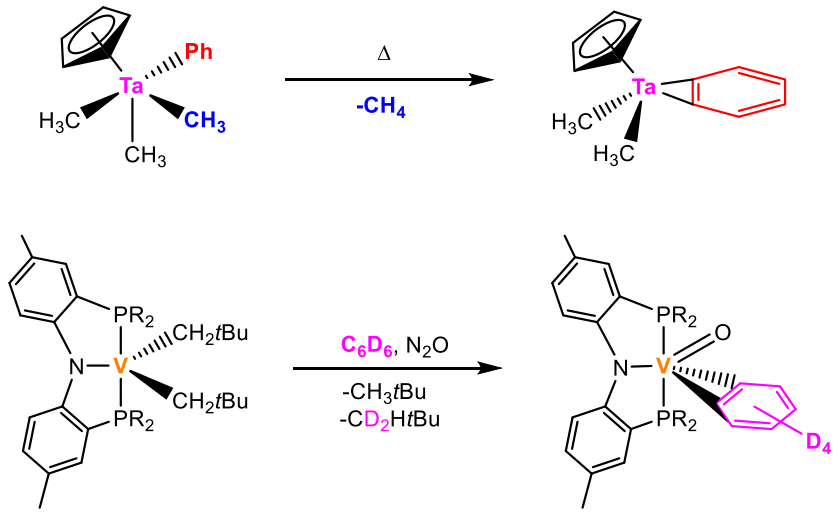

Scheme 5.5: Thermolytic C-H activation to form early benzyne complexes (R =*i*Pr$_2$)

The entry into late transition metal benzyne chemistry was pioneered by Bennett in the 1980s. Prior to this, many failed attempts to uncover Group 10 benzyne chemistry had failed.[260] The first reported example within the nickel triad came in 1985 from Bennett and co-workers, where reduction of a preinstalled *ortho*-bromobenzene ligand with sodium amalgam or KC$_8$ dehalogenates the phenyl ligand and forms the benzyne ligand (**Scheme 5.6**).[261] This same procedure has been used for platinum and for a variety of substituted or larger aromatic

analogues.[262] Accessing Group 9 benzyne complexes was first achieved through defluorination of a fluorophenyl ligand on **[MH(C$_6$F$_4$H)(PMe$_3$)(Cp*)]** (M = Ir, Rh) using butyllithium.[263]

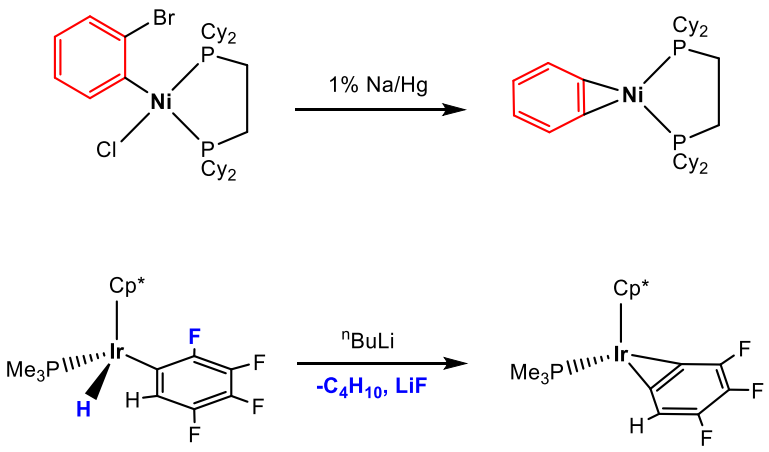

Scheme 5.6: Accessing late transition metal benzyne complexes through dehalogenation

5.2.4 Reactivity of benzyne complexes

Examining the crystallographic data available, the key carbon-carbon bond length of the coordinated benzyne fragment reveals a lot about the metal-ligand bonding. The bond length of the alkyne in free benzyne was first calculated in 1996 to be 1.24(2) Å, which is significantly close to the alkyne bond length in acetylene (*ca.* 1.20 Å).[264]

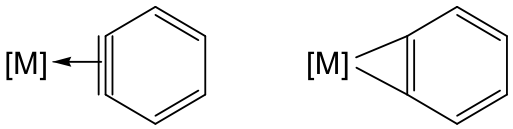

Figure 5.3: Bonding descriptions of the η^2-benzyne ligand

In valence-bond terms, as a ligand bound to a metal complex, benzyne may be canonically viewed as either an alkyne datively coordinating to the metal, or as an *ortho*-phenylene-diyl ligand with two formal M-C bonds and a C=C double bond (**Figure 5.3**). The bond lengths (taken from the CCDC) for the 11 available structures all contain a C=C bond length in the range of 1.312 – 1.422 Å, which is significantly elongated compared to the estimated free state triple bond. This

reflects the fact that the benzyne ligand cannot be treated as a pure aryne, with delocalisation forms both in the ring and to the metal lowering the C-C bond order in a manner reminiscent of the Dewar-Chatt-Duncanson description of alkene π-coordination.

Though benzyne in the "free state" could be considered to be a strong electrophile and is best known for cycloaddition and Diels-Alder reactions, the chemistry changes when coordinated to a metal centre. The benzyne ligand itself is notably susceptible to insertion reactions with electrophiles across one of the M-C bonds. Taking the nickel benzyne complex **[Ni(η²-C₆H₄)(dcpe)]**, insertion reactions with MeI, DMAD, alkenes, and CO_2 all furnish the corresponding substituted phenyl ligand (**Scheme 5.7**).[265]

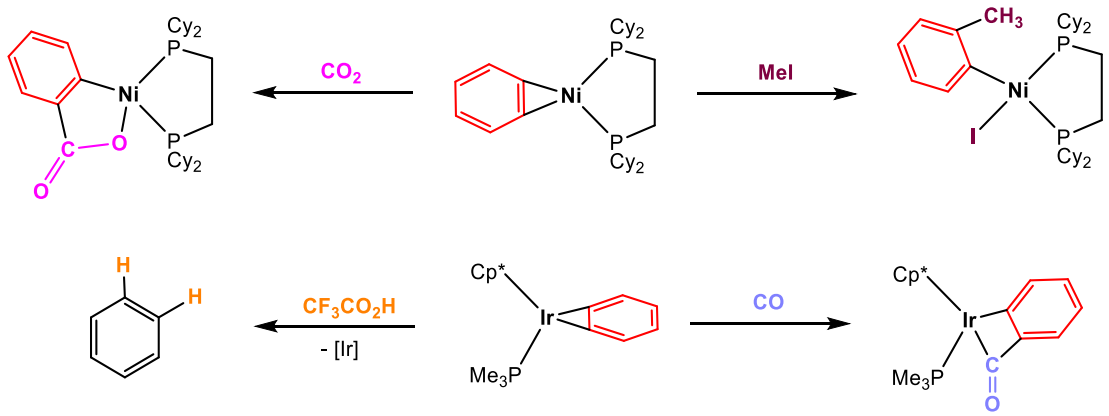

Scheme 5.7: Insertion reactions of MeI and CO_2 into **[Ni(η²-C₆H₄)(dcpe)]**

These insertion reactions are ubiquitous across both early and late transition metal benzyne complexes. Of particular note, the iridium benzyne complex **[Ir(Cp*)(PMe₃)(η²-C₆H₄)]** can be protonated using trifluoroacetic acid to regenerate benzene, and uniquely reacts with carbon monoxide to form the monoinsertion product **[Ir(Cp*)(PMe₃){κ²-C(=O)C₆H₄}]** (**Scheme 5.7**), whereas the rhodium and iridium fluorobenzyne complexes showed no reactivity with CO.[266]

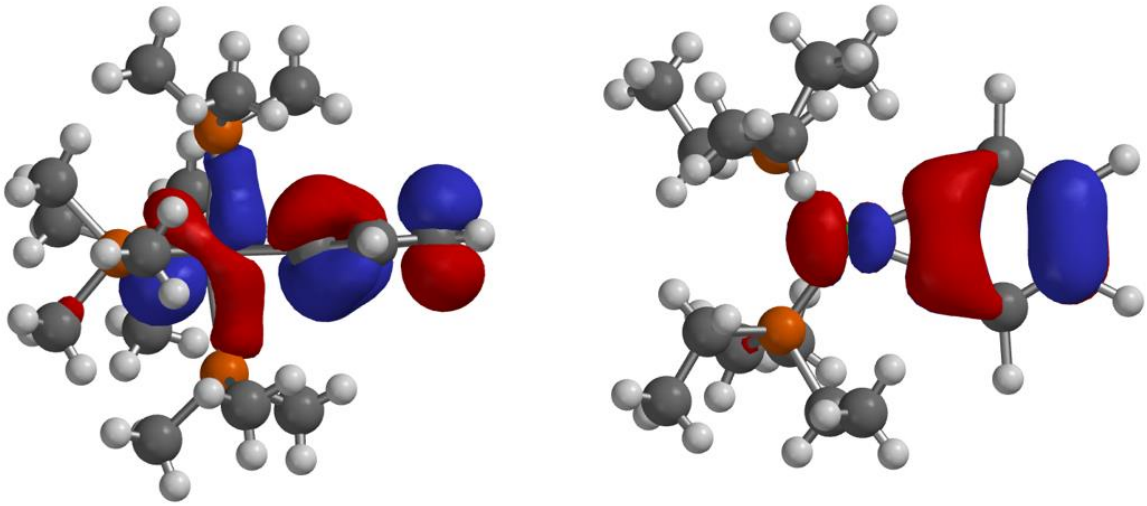

Figure 5.4: (left) Calculated HOMO of **[Ru(PMe$_3$)$_4$(η^2-C$_6$H$_4$)]** looking along benzyne C≡C bond. (right) Calculated HOMO of **[Ni(PEt$_3$)$_2$(η^2-C$_6$H$_4$)]** looking down on benzyne C≡C bond (DFT: ωBP96X-D/6-31G*/LANL2Dζ)

Although there are no reports of the computational interrogation of benzyne complexes, **Figure 5.4** presents the calculated HOMO of the simplified benzyne complexes **[Ni(PEt$_3$)$_2$(η^2-C$_6$H$_4$)]** and **[Ru(PEt$_3$)$_4$(η^2-C$_6$H$_4$)]**. Addition of an electrophile would likely react across the alkyne bond of benzyne. Because this orbital is antibonding with respect to the benzyne-metal ligation, insertion of this electrophile would break one of these bonds while strengthening the remaining M–C bond, thereby forming a substituted σ-phenyl ligand, consistent with experimental observations.

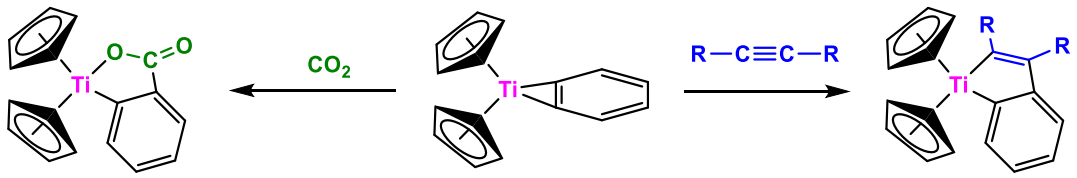

Scheme 5.8: Selected reactivity of a titanocene μ$_2$-benzyne complex

The benzyne complexes based on titanocene and zirconocene, **[M(Cp)$_2$(η^2-C$_6$H$_4$)]**, have rich and developed reactivity studies. Insertion reactions with chalcogens,[267] hetero-olefins,[268] metal carbonyl complexes,[269] alkenes,[270] carbon dioxide, nitriles, and even dinitrogen have all been

recorded (**Scheme 5.8**).[271] Benzyne complexes have been put forward as a key building block in organic synthesis for substituted aromatic compounds because of their high and specific reactivity. Although many of these transformations pre-dated Buchwald's isolation of stable zirconocene benzyne complexes, it was really only with the advent of the latter that the organic synthetic potential was more widely embraced.

5.2.5 Generation of Benzyne

Though many of the examples of μ_2-benzyne complexes begin with the preinstallation of a substituted phenyl ligand on the metal centre, the generation of benzyne *in situ* presents an alternative pathway to these species.

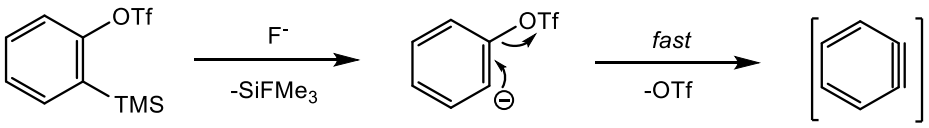

Scheme 5.9: Kobayashi generation of benzyne *in situ*

One of the modern approaches that is becoming heavily employed in organic chemistry is the method developed by Kobayashi.[272] The Kobayashi protocol utilises the disubstituted benzene species 2-(trimethylsilyl)phenyl trifluoromethanesulfonate (**Scheme 5.9**). The desilation of the TMS group leads to the *ortho*- elimination of the triflate, which is believed to generate benzyne *in situ*. The benefit of this procedure is its use under more mild conditions, without the need for harsh lithium reagents or reducing agents. The Kobayashi protocol has been well developed and employed in organic aryne chemistry, with a review recently published by Li and co-workers.[273]

5.2.6 Rationale for this work

The development of aryne chemistry has been pioneered by the preinstallation of the substituted phenyl ligand onto the metal centre followed by modification. Though various methods allow the generation of free benzyne in solution, it is by no means clear that the short lifetime (*ca* 20 ns in the gas phase) is compatible with the rates of, e.g., ligand substitution. Accordingly, there are no reports of the synthesis of benzyne complexes via generation and

subsequent coordination of the free ligand. It is nevertheless plausible that a metal complex that is already coordinatively unsaturated, i.e., not in need of pre-activation through ligand dissociation, might serve as a precursor for benzyne installation.

Given the heavy use of the Kobayashi protocol in organic chemistry, the work in this chapter aimed to blend the two areas and focus on the reactivity of generated benzyne, or its synthetic equivalent, with square-planar rhodium(I) μ-carbido complexes.

5.3 RESULTS AND DISCUSSION

5.3.1 Benzyne

Reaction of $[Rh_2(\mu\text{-}C)Cl_2(\mu\text{-}dppm)_2]$ with benzyne

Following on from the successful installation of DMAD and other simple activated alkynes across the Rh-Rh linkage, our attention turned towards the reactivity of the μ-carbido complexes towards more 'exotic' acetylenes. One of the basic tenets of organotransitionmetal chemistry is the ability of an otherwise unstable organic molecule to be stabilised as a ligand on a transition metal; and one such classical example deserving of note is benzyne.

Treating benzyne as a highly reactive acetylenic species, the question arises as to whether coordination to one or both of the rhodium centres in an analogous fashion to DMAD (dimethylacetylene dicarboxylate) would be possible (**Scheme 5.10**).

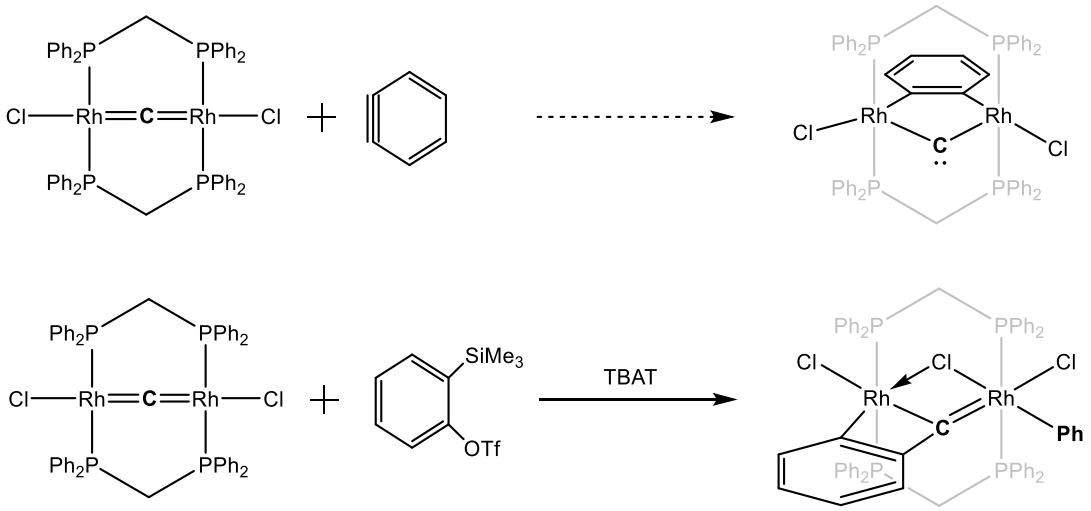

Scheme 5.10: Addition of benzyne across Rh=C bond

The protocol chosen was developed by Kobayashi and co-workers, as it has been noted to be stable under ambient conditions and avoids harsh lithium reagents. The procedure has been used previously for benzyne insertion into a Pd-C single bond by Vicente and co-workers.[274]

Taking a dichloromethane solution of **$[Rh_2(\mu\text{-}C)Cl_2(\mu\text{-}dppm)_2]$**, there is no reaction observed upon addition of the benzyne precursor 2-(trimethylsilyl)phenyl

trifluoromethanesulfonate. Using the conventional TBAF solution as the source of fluoride ions, the reaction mixture immediately turns dark red upon addition. Monitoring the reaction by $^{31}P\{^{1}H\}$ NMR spectroscopy, the starting material completely disappears after a matter of minutes, with the formation of new peaks and a large amount of free and oxidised dppm. The decomposition due to TBAF has been seen previously when attempting to perform desilylations, and because of this, a more anhydrous[xliv] and manageable source of fluoride was investigated.

The switch from TBAF to TBAT (tetrabutylammonium difluorotriphenylsilicate), meant that more accurate equivalents could be measured on a very small scale, and avoids any water that inevitably contaminates TBAF solutions. Addition of two equivalents of TBAT saw the colour change to dark red happen over a matter of hours, though monitoring the reaction revealed a much cleaner conversion to the same product peaks seen previously with TBAF. The product could be successfully separated through column chromatography on silica gel and was isolated as a pink/red powder identified as **$[Rh_2(\eta^2\text{-}CC_6H_4)(\mu\text{-}Cl)(Ph)Cl_2(\mu\text{-}dppm)_2]$ (40)**.

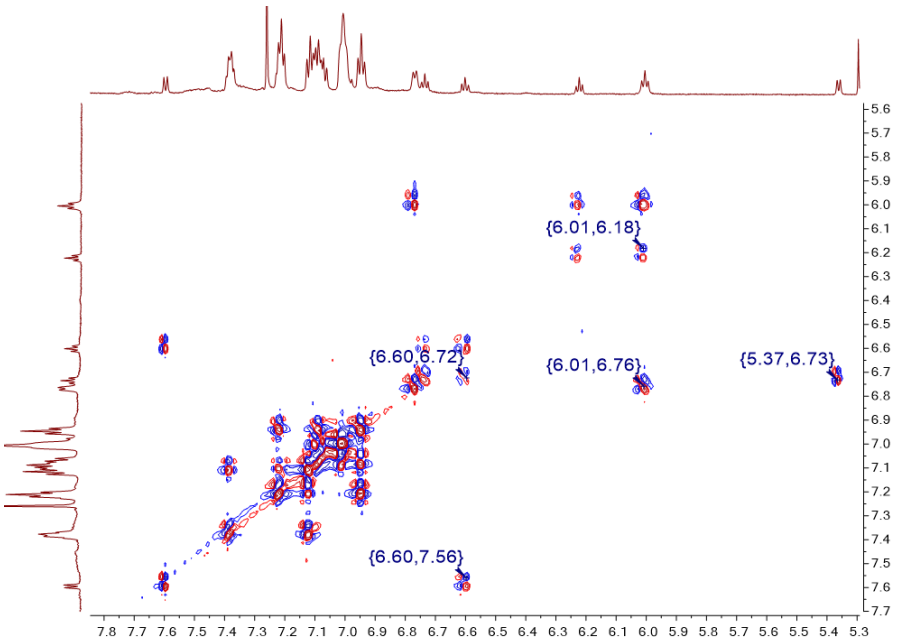

Figure 5.5: Extract of the ^{1}H-^{1}H COSY NMR spectra of **40**, focussing on the aryl region

[xliv] TBAF is available as a 1.0 M solution in THF from commercial suppliers (e.g., Adrich-216143) that the suppliers indicate contains 1-2% water. Entirely anhydrous TBAF is not available as decomposition accompanies dehydration due to the onset of Hoffmann elimination processes.

The NMR analysis of the product proved deceptively difficult. The ^{31}P NMR spectra showed two heavily split environments, which inferred a loss of two of the three internal mirror planes present in the (D_{2h}) precursor and reduced symmetry. The AA'BB'XY spin system showed two environments of equal integration. Modelling the spin system using gNMR yielded two doublet of doublet of doublets, with the primary one bond $^{1}J_{RhP}$ coupling for the environments at 119 and 125 Hz, indicating an increase in coordination number.

The ^{1}H NMR spectrum showed the consequence of extra aryl rings and asymmetry. What immediately stood out was the presence of hydrogens in regions outside the standard dppm range, with numerous small well-dispersed multiplet peaks appearing between 5 and 6 ppm. The shielding of a hydrogen environment is apparent for groups in close proximity to a transition metal, with the most obvious example being hydride groups that typically have chemical shifts to lower frequency of $SiMe_4$ ($\delta_H = 0$). If an aromatic ring were directly bound to the rhodium centre, the shielding could be rationalised. Curiously, using 2D COSY correlation (**Figure 5.5**), the shielded hydrogens (totalling to 9) pertained to two different spin systems, suggesting a benzyne ligand (four hydrogens, δ_H = 5.36, 6.66, 7.74, 7.60) and potentially a σ-phenyl ligand (five hydrogens, δ_H = 6.00, 6.22, 6.77) on the same complex.

The presence of the additional two aromatic groups was confirmed in the high-resolution mass spectrum, with the expected [M-Cl]$^+$ major fragment appearing at 1209.0574 m/z for the addition of C_6H_4 but also unexpectedly the elements of C_6H_5Cl. This was ultimately confirmed through the single crystal X-ray diffraction molecular structure (**Figure 5.6**).

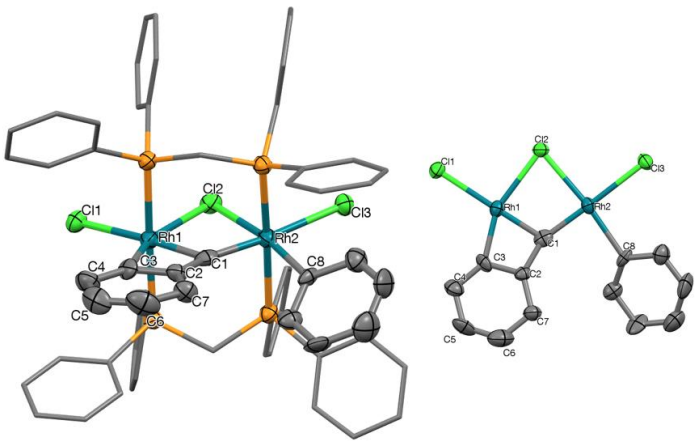

Figure 5.6: Molecular structures of **40** (50% displacement ellipsoids, disordered atoms omitted, solvent and hydrogen atoms omitted, phenyl groups simplified). Selected bond lengths (Å) and angles (°): Rh1-C1

1.916(8), Rh2-C1 1.922(8), Rh1-C3 1.94(2), Rh2-C8 2.19(2), C1-C2 1.44(2), C2-C3 1.41(3), Rh1-Rh2 3.1760(7), Rh1-C1-Rh2 111.7(4), Rh1-C1-C2 93.0(7). Inset shows view orthogonal to the Rh-Rh plane, phosphine ligands omitted

The most notable feature of **[$Rh_2(\mu:\kappa^2\text{-}CC_6H_4\text{-}2)(\mu\text{-}Cl)(Ph)Cl_2(\mu\text{-}dppm)_2$] (40)** is the fate of the benzyne addenda. Rather than coordinating to a single metal centre, or across the Rh-Rh spine as might have been expected, the 'alkyne' has undergone a [2+2] cycloaddition reaction with one of the Rh=C multiple bonds to form a metallacyclobutadiene. Cycloaddition reactions with alkynes and late transition metal carbyne complexes are exceptionally rare but has been previously achieved with propiolic acid and an osmium pentalyne species (**Scheme 5.11**).[275]

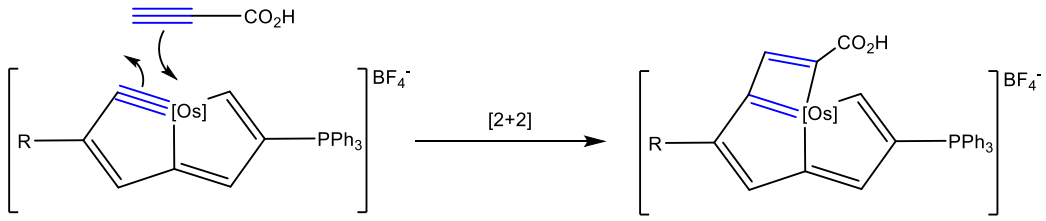

Scheme 5.11: 2+2 cycloaddition of propynoic acid across an osmium carbyne ligand. [Os] = [$OsCl(PPh_3)_2$], R = CO_2Me

The incorporation of a second aryl group is manifest in the form of a σ-bound phenyl ligand, coordinated to the remaining rhodium centre. Examining the rhodium centres themselves, the now six-coordinate centres are separated by 3.1760(7) Å which, in an analogous fashion to the μ_2-halocarbynes, is beyond the conventional distance ($2r_{cov}$(Rh) = 2.96 Å) for there to be any formal metal-metal interactions and none need be invoked to satisfy the EAN requirements of either rhodium centre. The change in coordination number at the μ-carbido atom results in it being drawn from between the two rhodium atoms (Rh-C-Rh = 111.7(4) °), with an additional chloride ligand assuming the bridging position on the opposite face of the complex.

The asymmetry evident in the $^{31}P\{^1H\}$ NMR spectrum is now seen to be consistent with the benzyne ligand across one Rh=C bond, and the phenyl ligand in the other rhodium coordination sphere. The addition of two aryl groups can be explained using electronic arguments, as the remaining rhodium centre would be electron deficient with only the addition of the benzyne unit.

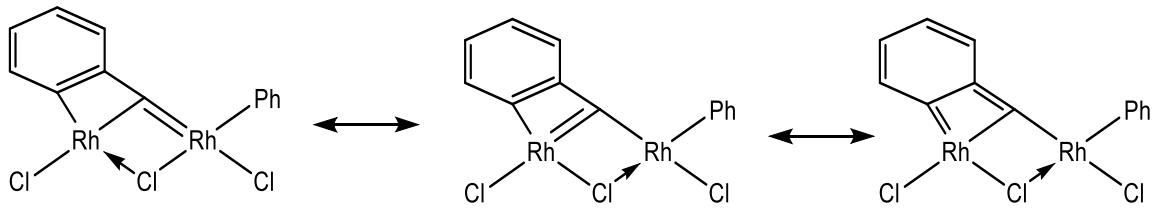

Scheme 5.12: Possible valence bond forms of the metallacycle in **40**

Although the metallacyclobutadiene species **40** contains two additional aromatic ligands, the bonding descriptions are more complicated. The σ-phenyl ligand contains a conventional Rh-C single bond length (Rh2-C8 = 2.19(2) Å), however, the Rh-C phenylene bond length is significantly shorter (Rh1-C3 = 1.94(2) Å), which might imply delocalisation effects and is more comparable with the two rhodium-μ-carbido bond lengths (1.916(8) and 1.922(8) Å). Some alternative valence bonding descriptions are outlined in **Scheme 5.12**, which may account for the solid-state measurements.

Despite the presumed ring strain, the multiple bonding present in the rhodacycle can be considered akin to that of a cyclometallated μ-benzylidyne ligand. The only example of a symmetrically bridging rhodium benzylidyne ligand, in **[Rh$_2$(μ-CC$_6$H$_4$Me-4)(CO)(Cp*$_2$)]BPh$_4$**, contains rhodium-carbon bonds unconstrained by cyclometallation and of comparable length (1.903(10) Å)[276] to **40** and the μ-halocarbyne complexes seen in **Chapter 2**.

The presence of multiple bonding in the four-membered metallacycle can be further inferred from inspection of the relevant molecular orbitals derived for the hypothetical, model complex **[Rh$_2$(μ:κ^2-CC$_6$H$_4$)(Ph)(μ-Cl)Cl$_2$(μ-dmpm)$_2$]** (**Figure 5.7**). Though many valence bond forms can be entertained for **40** (**Scheme 5.12**), the calculated molecular orbitals portray a far more complex scenario that isn't adequately conveyed by simple two-centre, two-electron localised bonding scenarios. Notably, the π framework between C1-C2 and Rh1-C3 can be seen in numerous occupied molecular orbitals, which taken to gether would account for the respective shortness of the bonds, such that the *ortho*-quinoidal bonding scenario presented above may provide a useful perspective of the bonding scenario. The π-bonding across the Rh-C-Rh carbido unit can still be seen, in addition to a complete delocalisation across the benzyne ligand and associated metallacycle. No occupied orbitals involve any significant Rh-Rh interactions, supporting earlier EAN-based conclusions that there is no formal bond between the two centres.

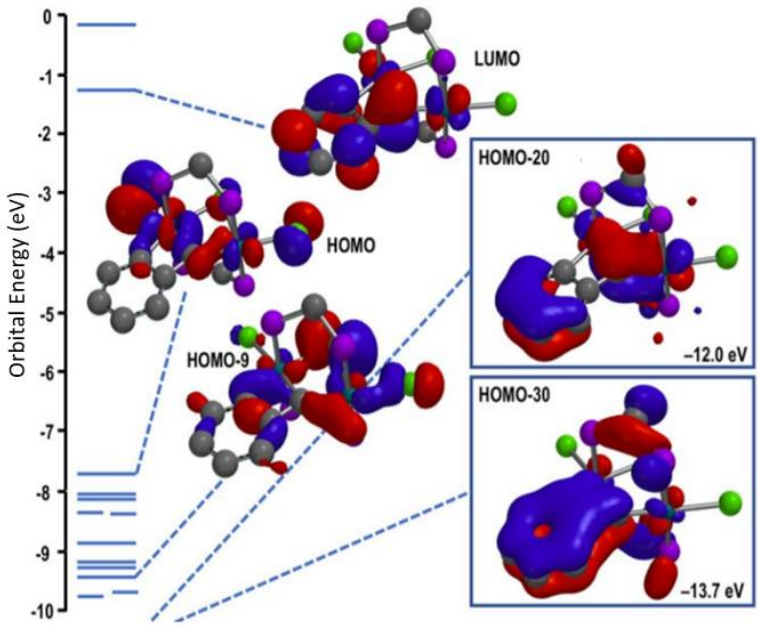

Figure 5.7: Selected molecular orbitals for **$[Rh_2(\eta^2\text{-}CC_6H_4)(Ph)(\mu\text{-}Cl)Cl_2(\mu\text{-}dmpm)_2]$** (DFT: ωBP96X-D/6-31G*/LANL2Dζ)

The juxtaposition of the benzylidyne and phenyl ligand bound directly to the rhodium centres presents interesting spectroscopic features. The hydrogen on C7 of the phenylene unit in shows a strong ROESY correlation to the *ortho* hydrogens on the nearby phenyl ligand, allowing for accurate assignments of benzyne hydrogens. Because of the molecular weight, the NOESY NMR spectrum showed none of the expected cross peaks, due to the intermittent zero phasing issue. As the ^{13}C NMR features of the phenylene unit were of particular interest, the reaction was repeated with the ^{13}C enriched isotopologue of **40** to synthesise **$[Rh_2(\mu\text{:}\kappa^2\text{-}^{13}CC_6H_4)(\mu\text{-}Cl)(Ph)Cl_2(\mu\text{-}dppm)_2]$ (40')**. The $^{13}C\{^1H\}$ NMR spectra for **40'** revealed the μ-carbido resonance in the expected low field range at 394.9 ppm, interestingly appearing as a broad doublet ($^1J_{RhC}$ = 35.6 Hz, **Figure 5.8**). It could even be detected in the $^1H\text{-}^{13}C$ HMBC spectrum, correlating with the phenylene resonance at 7.60 ppm and the dppm methylene hydrogens at 2.8 ppm. The rhodium-bound *ipso* positions on the benzylidyne and σ-phenyl ligands were also identified at comparatively high frequency 171.3 and 144.9 ppm, respectively. The higher frequency of the benzyne carbon resonance compared to that of the phenyl carbon might perhaps reflect stronger paramagnetic deshielding due to the multiple bonding character presumed to be present.

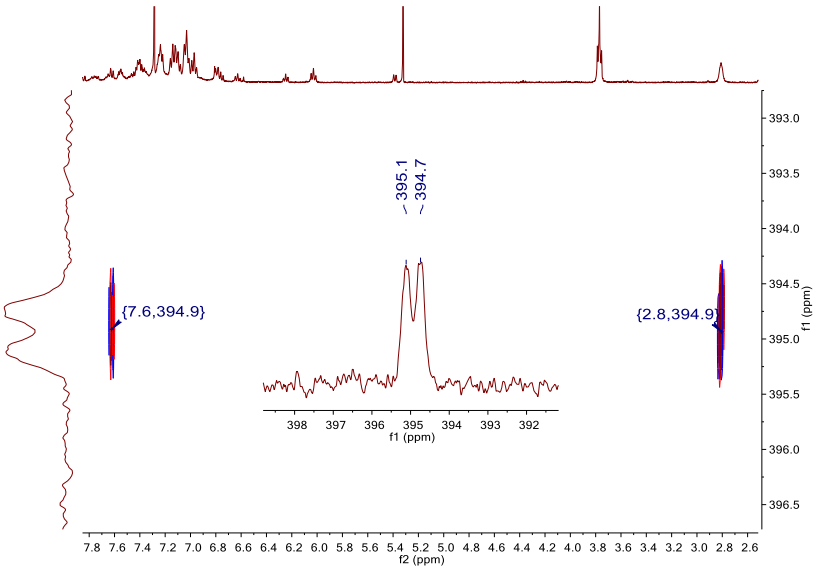

Figure 5.8: Extracts of the ^{13}C NMR and ^{1}H-^{13}C HMBC spectra of **40'**, focussing on the μ-carbido carbon nuclei

The yield for the reaction was consistently only *ca* 30%, though no other stable complexes were detected in the reaction mixture (NMR) nor isolated by column chromatography. The stoichiometric addition of HCl can be explained if one equivalent of the starting material **[Rh$_2$(μ-C)Cl$_2$(μ-dppm)$_2$]** serves to scavenge 'HCl', decomposing in the process, consistent with the observation of unbound dppm in the $^{31}P\{^{1}H\}$ NMR spectrum. In an attempt to increase the yield of **40**, extraneous HCl was added to optimise the stoichiometry. Initially, small amounts of anhydrous HCl were added into the reaction mixture along with the TBAT, though the reaction mixture instead turns yellow and the major product isolated was the μ$_2$-chlorocarbyne species **[Rh$_2$(μ$_2$-CCl)(μ$_2$-Cl)Cl$_4$(μ-dppm)$_2$]**. Evidently the presence of concentrated HCl instead, leads to the oxidation of the rhodium centres, presumably with loss of H_2. Using $[NH_4]Cl$ as a milder source unfortunately also failed to increase the yield of **40**, however, the new reaction conditions also lead to the synthesis of the closely related complex **[Rh(μ:κ^2-CC$_6$H$_4$)(μ-Cl)Cl$_3$(μ-dppm)$_2$] (41)**. The presence of excess chloride ions in solution appears to partially but not completely preclude installation of the σ-phenyl ligand such that equal amounts of **[Rh(μ:κ^2-CC$_6$H$_4$)(μ-Cl)Cl$_2$X(μ-dppm)$_2$]** (X = Cl, Ph) are obtained.

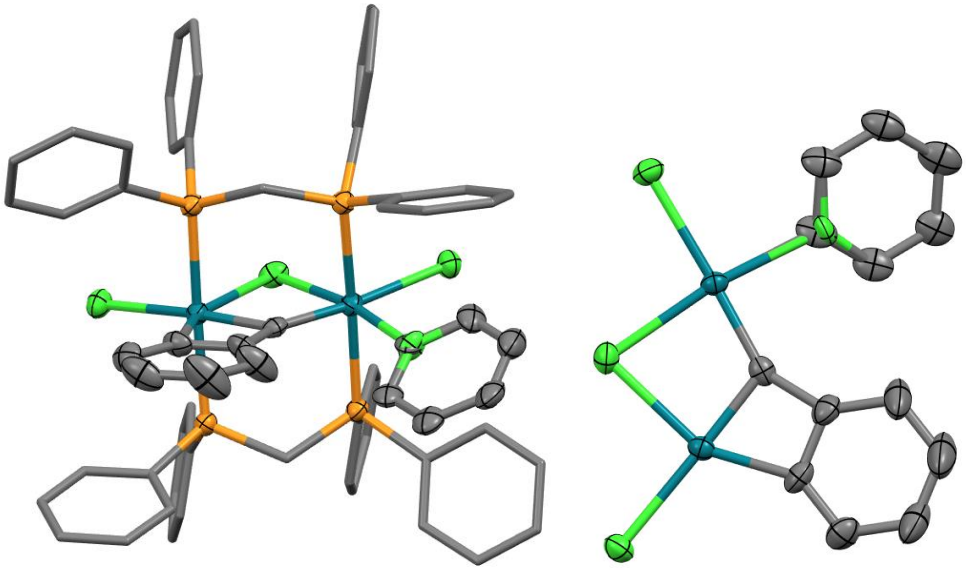

Figure 5.9: Overlaying molecular structures of **[Rh_2(μ:κ²-CC_6H_4)(μ-Cl)Cl_2(L)(μ-dppm)$_2$]** (L = Cl, Ph). (50% displacement ellipsoids, disordered atoms omitted, solvent and hydrogen atoms omitted, phenyl groups simplified). Selected bond lengths (Å) and angles (°): Rh1-C1 1.909(4), Rh1-C3 1.945(7), Rh1-C8 2.198(12), C1-C2 1.435(9), C2-C3 1.390(1), Rh1-C1-Rh2 112.7(4), Rh1-C1-C2 95.6(3)

Unfortunately, the tetrachlorido analogue was formed in equal amounts to the original trichlorophenyl complex (based on NMR data and crystallographic modelling), and because of their close structural similarities, these complexes could not be separated by chromatography and even co-crystallised in the same unit cell (**Figure 5.9**). This severely compromised complete spectroscopic data acquisition and satisfactory interpretation of the ^{1}H and ^{13}C NMR spectra of the mixture. That being said, the slight change in chemical environment for the phenylene unit enabled identification of the associated resonances in the ^{1}H NMR spectra, with the four environments now appearing at 5.23, 6.73, 6.84 and 8.03 ppm. Both [M-Cl]$^{+}$ fragments could be identified in the HR-MS (chloride analogue major peak at 1169.0522 *m/z cf.* 1168.9853 *m/z*). Because the chloride analogue was unable to be isolated in greater yields or as a sole product, it was not pursued further.

Mechanistic Conjecture

At its heart, the cycloaddition of benzyne across a metal-carbon bond is the first of its kind. The issue that arose from this unprecedented outcome, in addition to the installation of a second phenyl ligand invites conjecture in search of a mechanistic understanding. The Kobayashi protocol

for the synthesis of benzyne from 2-(trimethylsilyl)phenyl trifluoromethanesulfonate and fluoride ions proceeds through the carbanionic aryl triflate, though it is noted that the subsequent *ortho* elimination of the triflate ion is sufficiently rapid so as to prevent protonation that would afford phenyltriflate (PhOTf). Because of this, the likely method of installation of the benzyne unit is a classical [2+2] cycloaddition reaction with one of the Rh=C double bonds, perhaps *via* initial coordination to rhodium as a *pseudo*-alkyne (**Scheme 5.13**). It is however possible that the carbanion species coordinates to the unsaturated rhodium centre first. This anionic species could then undergo a nucleophilic addition reaction with the proximal μ-carbido ligand.

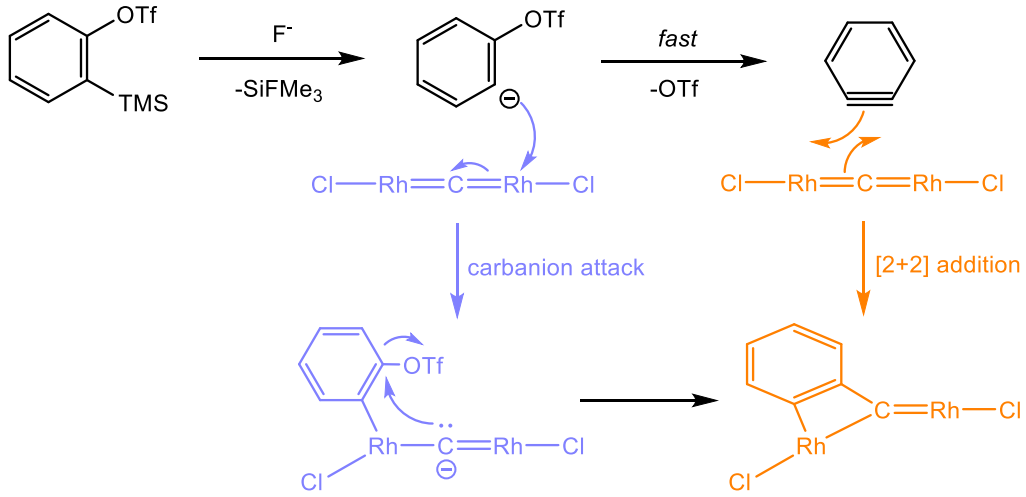

Scheme 5.13: Mechanistic conjecture for initial η^2-C_6H_4 coordination

The origin of the σ-phenyl ligand is more difficult to rationalise. The proton source was originally believed to come from residual H_2O in the TBAF solution but using anhydrous TBAT ($[^nBu_4N][SiF_2Ph_3]$) yielded the same result. The decomposition of one equivalent of **$[Rh_2(\mu\text{-}C)Cl_2(\mu\text{-}dppm)_2]$** is believed to provide the scavenged chloride ligands, and it is possible this is also the proton source. The question remains whether a μ_2-benzyne ligand initially is formed which undergoes protonation, or direct addition of phenyl triflate followed by triflate/chloride metathesis.

A number of reactions were carried out to (in)validate one theory or the other.

First, the rhodium μ-carbido complex does not react with 2-(trimethylsilyl)phenyl trifluoromethanesulfonate until a fluoride source is added. Therefore, oxidative addition or nucleophilic substitution at the triflate site can be ruled out as the first step.

The rhodium μ-carbido complex also fails to react with phenyl triflate. This, however, does not rule out the reaction of phenyl triflate or 2-(trimethylsilyl)phenyl trifluoromethanesulfonate with the rhodium complex at a later stage after the initial benzyne incorporation.

The combination of trimethyl(phenyl)silane with **[Rh_2(μ-C)Cl_2(μ-dppm)$_2$]** in the presence of TBAT also fails to result in any observed reactivity. The presence of the *ortho* triflate group is key to the reactivity.

The possibility of a benzyne μ:η^2 coordination across the Rh-Rh linkage, followed by protolysis to form the σ-phenyl ligand has been ruled out as a possibility as the previously made MHC complexes (**Chapter 3**) do not exhibit this behaviour in their reactions with acids such as HCl, and the yield is unchanging without the addition of extraneous NH_4Cl.

One of the possible reactive pathways for **40** might involve the migratory insertion of the σ-phenyl ligand onto the μ-carbido ligand, forming a μ_2-diphenylcarbene ligand. The diphenylcarbene ligand has been studied extensively for dirhodium complexes by Werner,[276] though **40** showed no such reactivity during any of the reactivity studies or upon heating.

Finally, the $^{31}P\{^1H\}$ NMR spectra of both phenyl and chloride complexes does not change before and after column chromatography (i.e., the crude and purified complex are the same). This suggests there is no reactivity with the mildly acidic silica oxide medium during purification. Unfortunately, being unable to isolate any intermediates makes detailed suppositions hard to substantiate.

The μ:κ^2 phenylene ligand is chemically distinct from a benzyne ligand and does not exhibit similar reactivity. Addition of methyl iodide or even an anhydrous hydrochloric acid solution results in no observable reaction taken place, as the 18-electron rhodium(III) metallacyclobutadiene complex has no discernible reactive sites, in contrast to a benzyne complex.

5.3.2 Cyclopropenium Incorporation

Reaction of $[Rh_2(\mu\text{-}C)Cl_2(\mu\text{-}dppm)_2]$ with $[C_3Ph_3]X$ (X =Br, PF_6)

The inclusion of the carbido ligand in the novel metallacycles discussed above raises the challenge of constructing other types of metallacycles, e.g., metallacyclobutadienes or metalla-arenes. One of the earliest methods for the synthesis of metallacyclobutadiene complexes (including on rhodium) involved utilising cyclopropenium salts. Thus **Scheme 5.1** presents the oxidative addition of the cyclopropenium ring to an unsaturated rhodium(I) centre with formation of a four-membered rhodium(III) metallacyclobutadiene species.

The cyclopropenium cation can be stabilised by a number of counter anions, though the bromide was initially chosen because of its synthetic ease and ability to coordinate as a ligand if needed to satisfy EAN rules. A dichloromethane solution of **$[Rh_2(\mu\text{-}C)Cl_2(\mu\text{-}dppm)_2]$** and $[C_3Ph_3]Br$ turns dark red when stirred at room temperature and monitoring the reaction by ^{31}P NMR spectroscopy revealed the generation of a large number of new environments. The profusion of products were unable to be cleanly separated or simply decomposed when subjected to column chromatography. It was suspected that the coordinative potential of bromide might allow not only halide scrambling, but also by conferring neutrality on a product open up further pathways for reactivity towards the cyclopropenium, electrophile. To obviate such processes, the bromide counter ion was replaced with a non-coordinating anion.

The relative insolubility of $[C_3Ph_3]PF_6$ allowed for the addition of excess and easy separation by filtering of unreacted starting material. Early signs were already more promising when the dichloromethane reaction solution turns a dark green in colour (*cf.* red above).

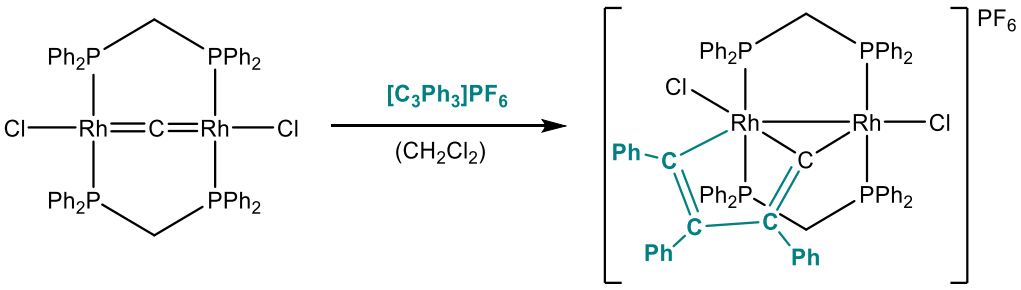

Scheme 5.14: Synthesis of a metallacyclopentadiene from cyclopropenium addition

Attempts to separate the reaction mixture through silica gel chromatography proved somewhat difficult, with the dark green species eluting exceedingly slowly with neat dichloromethane. The $^{31}P\{^{1}H\}$ NMR spectrum of the dark green powder indicated two chemically and magnetically inequivalent environments with two heavily coupled resonances being observed in addition to the PF_6 counter ion (1:1:1, **Figure 5.10**). The two environments both had clear doublet of triplet fine-structure (δ_P = 17.17, $^{1}J_{RhP}$ = 97 Hz, $^{3}J_{RhP}$ = 37 Hz, and δ_P = 22.40, $^{1}J_{RhP}$ = 126 Hz, $^{3}J_{RhP}$ = 37 Hz), and the vastly different values in the primary coupling constant suggested six- and five-coordinate rhodium centres (**Scheme 5.14**). ESI-MS of the complex supported a cationic species with the addition of C_3Ph_3 at 1323.1072 *m/z* (*cf.* 1323.1049 for $C_{72}H_{59}{}^{35}Cl_2P_4Rh_2^+$).

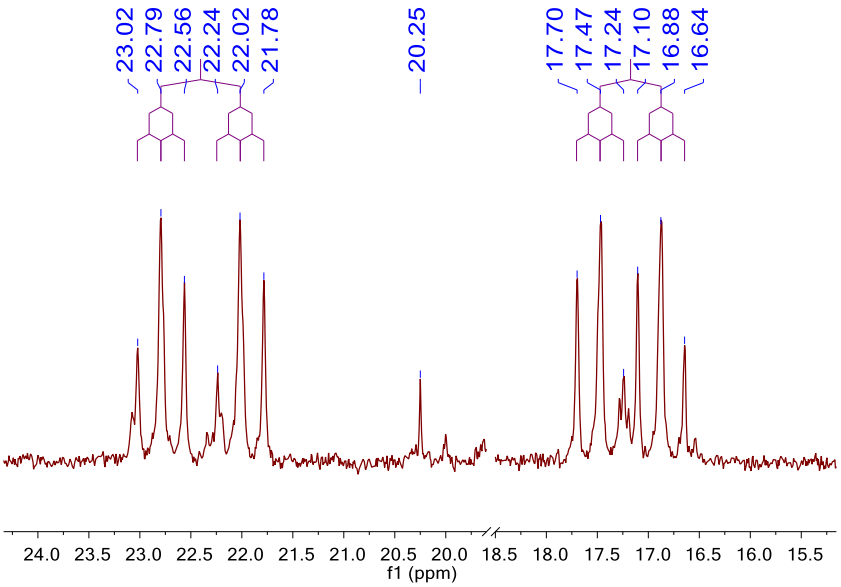

Figure 5.10: $^{31}P\{^{1}H\}$ NMR snippet of **$[Rh_2(\kappa^2\mu_2\text{-}CC_3Ph_3)Cl_2(\mu\text{-dppm})_2]PF_6$ (42)**. NB: decomposition product environment at ~19 ppm omitted for clarity

The ^{1}H and ^{13}C NMR spectrum were both more complex to analyse than the benzyne products discussed above. Exhaustive analysis of the two-dimensional spectra (summarised here) suggested that all three phenyl rings of the added triphenyl cyclopropenium were in distinct chemical environments. The ^{1}H-^{1}H COSY spectrum detected three separate spin systems (H_{ABC} = 6.04, 6.57, 6.81; H_{DEF} = 6.31, 6.98, 7.18; H_{GHI} = 5.87, 6.71, 6.86 ppm), all supporting the characteristic AA'BB'C system of distinct phenyl rings. The presence of aromatic environments at a higher field than expected most likely reflects the close proximity of one of the rings to a metal centre (**Figure 5.11**).

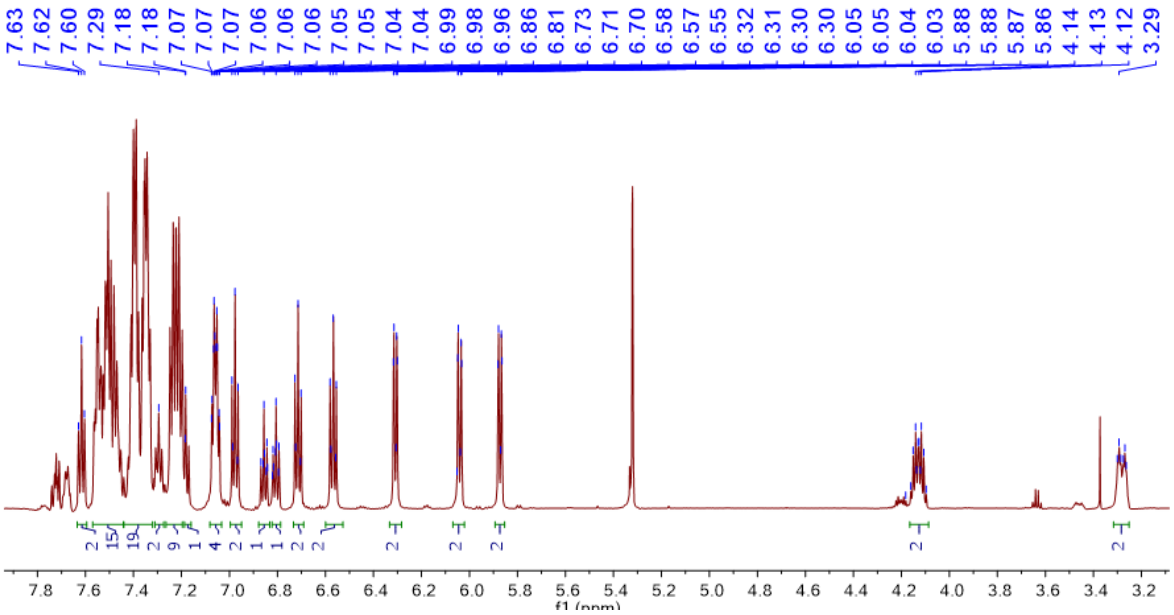

Figure 5.11: ^{1}H NMR spectrum of **[Rh$_2$(κ^{2}μ$_2$-CC$_3$Ph$_3$)Cl$_2$(μ-dppm)$_2$]PF$_6$**

Using the two-dimensional ^{1}H-^{13}C HMBC spectrum, the three key carbon environments arising from the original cyclopropenium ring were identified at 166.5 (C_1), 144.1 (C_2) and 143.4 (C_3) ppm. Of these, the downfield resonance at 166.5 ppm was considered most likely to be directly bound to a rhodium centre. This was confirmed by its splitting in the ^{13}C{^{1}H} spectrum, displaying a broad doublet of triplets ($^{1}J_{RhC}$ = 35 Hz, $^{2}J_{PC}$ = 6 Hz). In order to have three distinct CPh chemical environments, and only one carbon bound to a rhodium, a ring opening product along one Rh=C bond was perhaps one of the only logical solutions.

Due to its presumed significance, the ^{13}C enriched isotopologue was formed from the identical reaction with **[Rh$_2$(μ-^{13}C)Cl$_2$(μ-dppm)$_2$]**. Employing a broad spectral width, the ^{13}C{^{1}H} NMR spectrum included a low-field broad resonance which was was detected at 411.5 ppm (**Figure 5.12**). The environment is importantly nearby to the location of the μ-C resonance for the cyclometallated benzylidyne complex **[Rh$_2$(η$_2$-CC$_6$H$_4$)(Ph)Cl$_3$(μ-dppm)$_2$]**, potentially supporting a similar formation of a metallacyclic species. Though in a similar environment to the precursor **[Rh$_2$(μ-^{13}C)Cl$_2$(μ-dppm)$_2$]**, its absence was confirmed (^{31}P NMR) prior to acquisition of the ^{13}C{^{1}H} NMR spectrum.

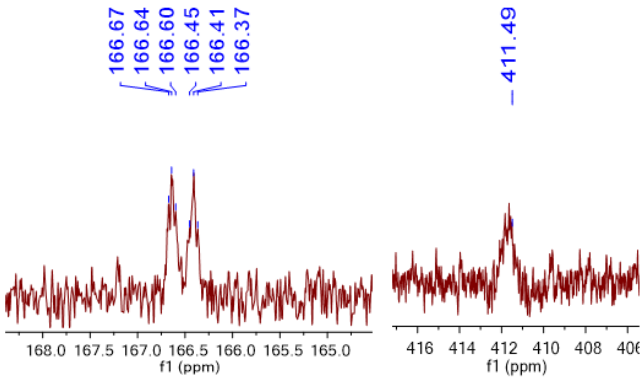

Figure 5.12: ^{13}C NMR snippets of **[Rh$_2$(κ^{2}μ$_2$-CC$_3$Ph$_3$)Cl$_2$(μ-dppm)$_2$]PF$_6$ (42')**

Group 9 metallacyclopentadiene complexes are well known, with rhodium examples emerging primarily from the group of Marder. The synthesis of these rhodacyclopentadienes have been achieved through oxidative coupling of alkynes by low-valent rhodium(I) complexes. The first synthesis in 2001 employed the rhodium(I) complex **[Rh(CCSiMe$_3$)(PMe$_3$)$_4$]** in combination with two equivalents of 1,4-bis(*p*-tolyl)buta-1,3-diyne forming the 2,5-bis(arylethynyl)rhodacyclopentadiene complex.[277a] The two Rh-C bond lengths (2.087(5), 2.110(5) Å) align well with largely Rh-C single bond lengths. A more general synthesis could be achieved with addition of various diynes to **[Rh(CCR)(PMe$_3$)$_4$]** (**Scheme 5.15**).[277b,c]

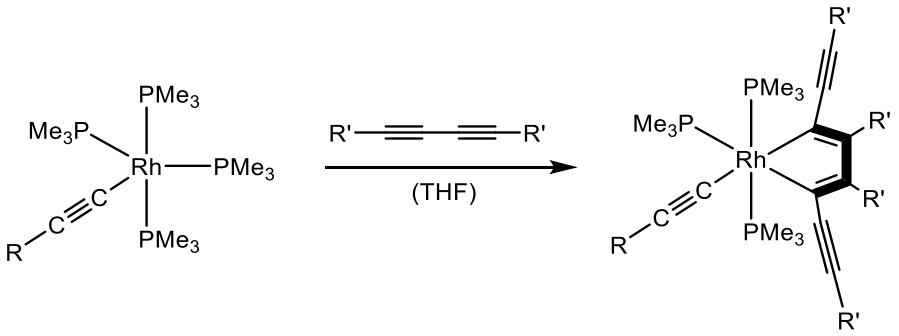

Scheme 5.15: Marder and co-workers' general synthesis of rhodium metallacyclopentadiene complexes

Unfortunately, the green complex displays remarkable sensitivity to both solvents and atmospheric conditions, gradually decomposing into a dark grey complex with no observable NMR handles. The complex decomposes rapidly in the presence of coordinating solvents such as acetonitrile and THF, and even dichloromethane solutions stored under N_2 slowly decompose.

Rather unfortunately, **42** also exhibits exceptionally poor crystallisation properties. Attempts to exchange to counter ion with OTf, BPh_4 and BF_4 did not lead to crystallographic grade crystals. Although the molecular structure was unable to be unambiguously confirmed crystallographically, the data gathered are sufficient to confidently suggest the metallacyclopentadiene formulation.

Decomposition Product

Taking the crude green solution, separation *via* column chromatography also resulted in a yellow band that eluted slowly with dichloromethane. The bright yellow powder contained a new symmetrical phosphorous environment in the ^{31}P NMR spectrum (δ ^{31}P = 19.3, $^{1}J_{RhP}$ = 114 Hz), which was unexpected if the metallacyclobutadiene or metallacyclopentadiene had formed. The PF_6 counterion could also be detected in both ^{31}P and ^{19}F NMR spectrum. The ^{1}H NMR spectrum was devoid of any resonances that might have originated from the cyclopropenium cation however, the resonances for the dppm methylene linkers indicated two distinct chemical environments (3.57 and 4.17 ppm), suggesting one face of the complex was chemically distinct from the other. Examining the infrared spectra proved more valuable than anticipated, with two distinct bands at 1993 and 1974 wavenumbers suggesting the presence of carbonyl ligands. Provided the starting material **1** does not decompose in the presence of the silica medium or ambient conditions to form oxygen adducts, the yellow product is likely a decomposition product of the cyclopropenium complex.

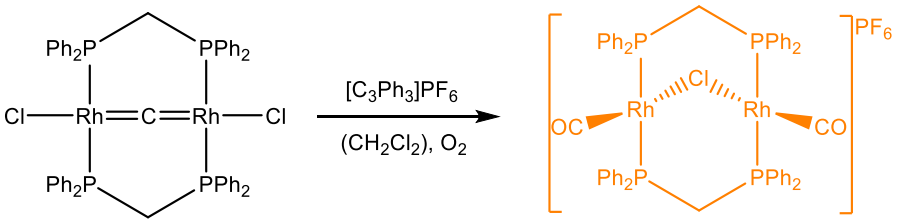

Scheme 5.16: Decomposition of **40** to form **$[Rh_2(\mu\text{-}Cl)(CO)_2(\mu\text{-}dppm)_2]PF_6$**

The ESI-MS detected the monocationic species cleanly at 1065.01 *m/z* (*cf.* 1065.01 *m/z* for $C_{52}H_{44}{}^{35}ClO_2P_4Rh_2^+$), which supported the presence of two carbonyl ligands. Based on their higher wavenumber bands in the infrared spectrum, neither carbonyl ligand adopted a bridging position. The decomposition of the enriched isotopologue detected a new environment at 185.8 ppm in the

^{13}C NMR spectrum, as a doublet of triplet with strong $^{1}J_{RhC}$ coupling (90 Hz), suggesting multiple bonding character to a single rhodium centre, thereby confirming that the CO ligands arose via oxidation of the bridging carbido ligand. The presence of two terminal carbonyl ligands and a symmetrical complex was confirmed in the molecular structure (**Figure 5.13**).

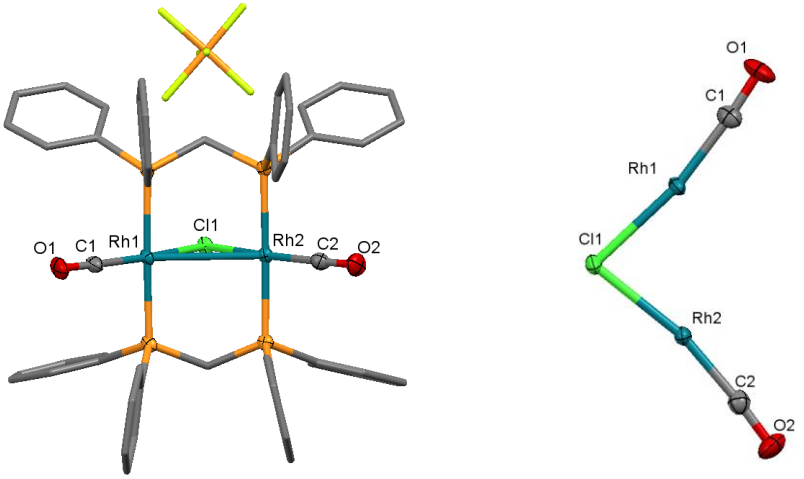

Figure 5.13: Molecular structure of **[Rh$_2$(μ-Cl)(CO)$_2$(μ-dppm)$_2$]PF$_6$**. (50% displacement ellipsoids, disordered atoms omitted, solvent and hydrogen atoms omitted, phenyl groups simplified). Selected bond lengths (Å) and angles (°): Rh1-Rh2 3.1285(5), Rh1-C1 1.816(3), Rh1-Cl1 2.3880(7), Rh2-C2 1.813(3), C2-O2 1.141(4), Rh1-Cl1-Rh2 81.82(2), Cl1-Rh1-C1 170.26(9)

Fortunately, the complex **[Rh$_2$(μ-Cl)(CO)$_2$(μ-dppm)$_2$]BF$_4$** has been previously reported by Cowie and co-workers.[278] Though an interesting complex in its own right, as a low yielding decomposition and known product, further analysis of the complex or conjecture as to its mode of formation was not warranted.

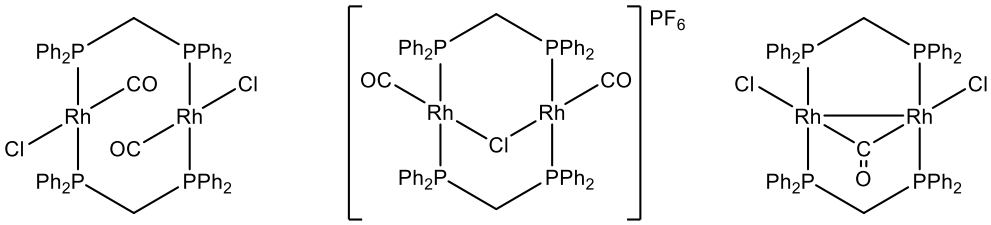

Chart 5.1: This work and Cowie's previous work on dirhodium A-frame carbonyl complexes

5.3.3 Summary

This smaller chapter examined the project centred around the reactivity of benzyne and triphenyl cyclopropenium. The reactivity of benzyne, formed through the Kobayashi protocol *in situ*, was observed to involve addition one of the Rh=C double bonds in **[Rh_2(μ-C)Cl_2(μ-dppm)$_2$]**, forming the metallacyclobutadiene complex **[Rh_2(η_2-CC_6H_4)(μ-Cl)(Ph)Cl_2(μ-dppm)$_2$]** in contrast to other activated alkynes that undergo [3+2] cycloadditions to afford rhodacyclic carbenes. The X-ray crystallographic analysis supported the presence of multiple bonding and delocalisation occurring across the four-membered benzorhodacyclobutadiene, which was supported through DFT studies showing highly conjugated molecular orbitals. Though the reaction also installs a second σ-phenyl ligand onto one rhodium centre, its mechanism for formation remains unclear, though some pathways could be excluded through experimental studies with aryl triflates and silanes. The μ-carbon could be detected in the ^{13}C NMR spectrum of the enriched isotopologue, appearing at 394.6 ppm.

Addition of extraneous H^+ and Cl^-, in the form of NH_4Cl, resulted in the formation of the tetrachloro analgue **[Rh_2(η_2-CC_6H_4)(μ-Cl)Cl_3(μ-dppm)$_2$]**, which unfortunately formed in equal amounts to the phenyl analogue and failed to be separated under any conditions.

The reactivity of the rhodium-carbon bond was also explored with the cyclopropenium cation. Known for the formation of metallacyclobutadiene complexes, the reaction of **[Rh_2(μ-C)Cl_2(μ-dppm)$_2$]** and triphenyl cyclopropenium led to ring opening along one of the Rh=C bonds to form the metallacyclopentadiene complex **[Rh_2($\kappa^2\eta_2$-CC_3Ph_3)Cl_2(μ-dppm)$_2$]PF_6**. The μ-carbon of the enriched isotopologue could be detected at 411.5 ppm, in a similar environment to the metallacyclobutadiene complex.

These reactions represent the first examples of the μ-carbido undergoing ligand transformation to form metallacycles.

As of this date, work in this chapter is currently published in:

1. H.J. Barnett, A.F. Hill, *Dalton Trans.,* **2021**, 50, 9383

5.4 EXPERIMENTAL

Synthesis of $[Rh_2(\mu_2\text{-}C)(\mu\text{-}Cl)(\kappa_2\text{-}C_6H_4)(C_6H_5)Cl_2(\mu\text{-}dppm)_2]$ (40)

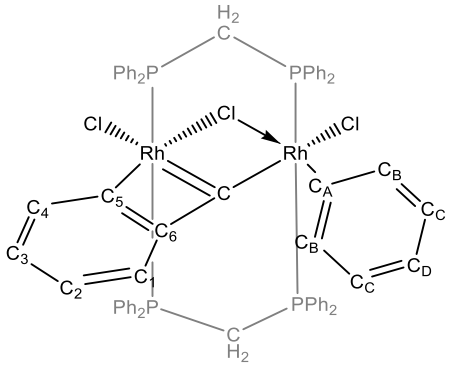

To a flask containing **$[Rh_2(\mu_2\text{-}C)Cl_2(\mu\text{-}dppm)_2]$** (0.050 g, 0.047 mmol) and 2-(trimethylsilyl)phenyl trifluoromethanesulfonate (0.023 mL, 0.095 mmol) was added acetonitrile (25 mL). To this yellow solution was added TBAF (1 M solution in THF, 0.10 mL, 0.10 mmol). The solution immediately turned dark red in colour and was stirred for 2 hours at room temperature. After this time the volatiles were removed *in vacuo* and the residue was subjected to column chromatography (10 x 1 cm silica gel column), eluting initially with neat CH_2Cl_2 and then with 1:19 THF:CH_2Cl_2. An orange/pink band was collected, and the volatiles were removed under reduced pressure to give a beige microcrystalline solid of pure **40** (0.019 g, 0.015 mmol, 32%). ^{1}H NMR (400 MHz, $CDCl_3$, 298 K): δ_H = 2.78 (s, 4 H, PCH_2), 5.36 (d, $^3J_{HH}$ = 7 Hz, 1 H, H_1), 6.00 (dd, $^3J_{HH}$ = 7, 7 Hz, 2 H, H_C), 6.22 (t, $^3J_{HH}$ = 7 Hz, 1 H, H_D), 6.60 (dd, $^3J_{HH}$ = 8, 8 Hz, 1 H, H_3), 6.74 (dd, $^3J_{HH}$ = 7, 7 Hz, 1 H, H_2), 6.77 (d, $^3J_{HH}$ = 8 Hz, 2 H, H_B), 6.95 (t, $^3J_{HH}$ = 8 Hz, 4 H , C_6H_5), 7.00-7.02 (m, 9 H, C_6H_5), 7.06-7.13 (m, 12 H, C_6H_5), 7.20-7.23 (m, 6 H, C_6H_5), 7.37-7.40 (m, 4 H, C_6H_5), 7.60 (d, $^3J_{HH}$ = 8 Hz, 1 H, H_4), 7.88-7.91 (m, 4 H, C_6H_5), 8.23-8.25 (m, 4 H, C_6H_5). ^{13}C{^{1}H} NMR (151 MHz, $CDCl_3$, 298 K): δ_C = 394.8 (m, μ_2-C), 171.3 (m, C_5), 144.9 (dt, $^1J_{RhC}$ = 35 Hz, $^2J_{RhP}$ = 7 Hz, C_A), 141.6 (s, C_B), 138.7-139.0 (m, C_6), 138.1 (s, C_2), 136.5, 136.2 (2 x m, C_6H_5), 135.8 (s, C_1), 133.9, 133.4 (2 x m, C_6H_5), 131.8 (s, C_6H_5), 130.8 (m, C_6H_5), 130.5 (s, C_6H_5), 129.8 (s, C_6H_5), 129.5 (s, C_6H_5), 128.0 (m, C_6H_5), 127.8 (m, C_6H_5), 127.5 (m, C_6H_5), 127.1 (t, J_{PH} = 25 Hz, C_6H_5), 124.5 (s, C_C), 124.2 (s, C_3), 121.7 (s, C_D), 120.7 (s, C_4), 22.9-23.0 (m, PCH_2) . All ^{13}C environments identified based on ^{1}H-^{13}C HSQC/HMBC couplings to the bonded H environments. ^{31}P{^{1}H} NMR (162 MHz, CDCl3, 298 K): δ_P = 1.93 (ddd, $^1J_{RhP}$ = 119 Hz, $^3J_{RhP}$ = (21) Hz, $^4J_{PP}$ = (11) Hz), 6.92 (ddd, $^1J_{RhP}$ = 125 Hz, $^3J_{RhP}$ = (21) Hz, $^4J_{PP}$ = (11) Hz). IR (ATR, cm^{-1}): 3050, 2935 ν_{CH}, 1434 $\nu_{C=C}$. MS (ESI, *m/z*): Accurate mass: Found 1209.0574. Calcd for $C_{63}H_{53}{}^{35}Cl_2P_4Rh_2$ $[M–Cl]^+$:

1209.0585. Anal. Found: C, 59.89; H, 4.74%. Calcd for $C_{63}H_{53}Cl_3P_4Rh_2$: C, 59.95; H, 4.37%. A crystal suitable for structure determination was grown by slow evaporation of a CH_2Cl_2/toluene mixture. *Crystal data for* $C_{63}H_{53}Cl_3P_4Rh_2$ (M_w = 1246.10 g.mol^{-1}): tetragonal, space group $P4_12_12$ (No. 92) a = 15.01727(5), c = 26.39108(12) Å, V = 5951.67(5) Å^3, Z = 4, T = 150.0(1) K, μ(Cu Kα) = 7.03 mm^{-1}, D_{calcd} = 1.391 Mg.m^{-3}, 108169 reflections measured (8.2° ≤ 2Θ ≤ 147.2°), 6006 unique (R_{int} = 0.034) which were used in all calculations. The final R_1 was 0.029 ($I > 2\sigma(I)$) and wR_2 was 0.075 (all data) for 408 refined parameters with 183 restraints. CCDC 2035999 (see CCDC 2036000 for orthorhombic solution).

The synthesis could also be achieved with replacement of TBAF with two equivalents of TBAT (tetrabutylammonium difluorotriphenylsilicate) with similar yields recorded.

Synthesis of $[Rh_2(\mu_2\text{-}C)(\mu\text{-}Cl)(\kappa^2\text{-}C_6H_4)Cl_3(\mu\text{-}dppm)_2]$ (41)

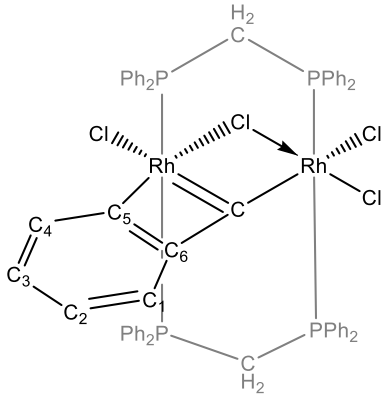

To a flask containing $[Rh_2(\mu_2\text{-}C)Cl_2(\mu\text{-}dppm)_2]$ (0.033 g, 1.229 g.cm^{-3}, 0.031 mmol), ammonium chloride (0.055 g, 1.0 mmol, 33 eq.), and 2-(trimethylsilyl)phenyl trifluoromethanesulfonate (0.050 mL, 0.21 mmol) was added acetonitrile (25 mL). To this yellow solution was added TBAT (0.039 g, 0.072 mmol). The solution remained yellow in colour while it was stirred for 15 hours at room temperature. After this time the volatiles were removed *in vacuo* and the residue was subjected to column chromatography (10 x 1 cm silica gel column), eluting initially with neat CH_2Cl_2 and then with 1:19 THF:CH_2Cl_2. A yellow band was collected, and the volatiles were removed under reduced pressure to give a beige powder comprising of **40** and **41** in equal amounts (combined yield 0.012 g). ^{1}H NMR (400 MHz, $CDCl_3$, 298 K): δ_H = 2.74, 3.01 (2 x m, 4 H, PCH_2), 5.23 (d, $^3J_{HH}$ = 7 Hz, 1 H, H_1), 6.74 (dd, $^3J_{HH}$ = 7, 7 Hz, 1 H, H_3), 6.84 (dd, $^3J_{HH}$ = 7, 7 Hz, 1 H, H_2), 6.95 (t, $^3J_{HH}$ = 8 Hz, 4 H, C_6H_5), 7.42-7.53 (m, 12 H, C_6H_5), 7.62-7.65 (m, 3 H, C_6H_5), 7.68-7.73 (m, 4 H, C_6H_5), 8.03 (d, $^3J_{HH}$ = 8 Hz, 1 H, H_4), 8.06-8.11 (m, 4 H, C_6H_5). Remaining

aromatic resonances were unable to be clearly distinguished from those of **40**. $^{13}C\{^1H\}$ NMR spectrum was unable to be usefully distinguished from that of **40**. $^{31}P\{^1H\}$ NMR (162 MHz, $CDCl_3$, 298 K): δ_P = 0.74 (dt, $^1J_{RhP}$ = 96 Hz, $^3J_{RhP}$ = 14 Hz), 7.14 (m). The relative proportions of **40** (50%) and **41** (50%) were established by integration of the $^{31}P\{^1H\}$ spectrum. IR (ATR, cm^{-1}): 3052, 2937 ν_{CH}, 1434 $\nu_{C=C}$. MS (ESI, *m/z*): Accurate mass: Found 1209.0574. Calcd for $C_{57}H_{48}{}^{35}Cl_3P_4Rh_2$ $[M–Cl]^+$: 1166.9882. Anal. Found: C, 59.90; H, 4.75%. Calcd for $0.5(C_{63}H_{53}Cl_3P_4Rh_2)$ + $0.5(C_{57}H_{48}Cl_4P_4Rh_2)$: C, 60.57; H, 4.28%. A crystal suitable for structure determination was grown by slow evaporation of a CH_2Cl_2/toluene mixture. *Crystal data for* $C_{60}H_{50.5}Cl_{3.5}P_4Rh_2$ (M_w = 1225.28 $g.mol^{-1}$): tetragonal, space group $P4_12_12$ (No. 92), a = 14.9951(1), c = 26.1521(4) Å, V = 5880.38(12) $Å^3$, Z = 4, T = 150.0(1) K, μ(Cu Kα) = 7.31 mm^{-1}, D_{calcd} = 1.384 $Mg.m^{-3}$, 10253 reflections measured (8.4° ≤ 2Θ ≤ 141.6°), 5,538 unique (R_{int} = 0.028) which were used in all calculations. The final R_1 was 0.034 ($I > 2\sigma(I)$) and wR_2 was 0.100 (all data) for 365 refined parameters with 97 restraints. CCDC 2069151.

Synthesis of $[Rh_2(\kappa^2\mu_2\text{-}C\text{-}C_3Ph_3)Cl_2(\mu\text{-}dppm)_2]PF_6$ (42)

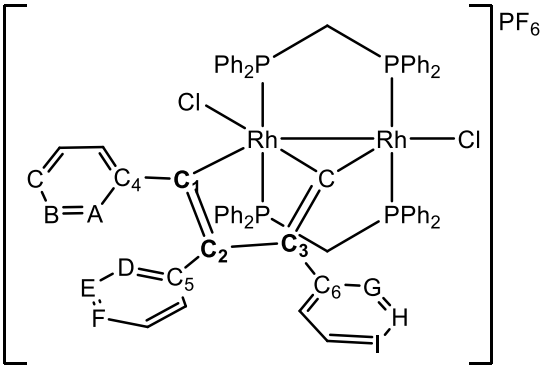

To a yellow dichloromethane solution containing $[Rh_2(\mu\text{-}C)Cl_2(\mu\text{-}dppm)_2]$ (0.030 g, 0.028 mmol) was added excess triphenyl cyclopropenium hexafluorophosphate (0.108 g, 0.262 mmol). The resulting solution turns green over the course of two hours at room temperature. Subjecting the solution to silica gel chromatography eluted a green band slowly in neat CH_2Cl_2. Addition of petrol and removal of solvent under vacuum produced a light-green powder of pure $[Rh_2(\kappa^2\mu_2\text{-}C\text{-}C_3Ph_3)Cl_2(\mu\text{-}dppm)_2]PF_6$ (33 mg, 0.022 mmol, 80 %). ^1H NMR (600 MHz, CD_2Cl_2, 298 K): δ_H = 3.28 (dp^v, $^2J_{HH}$ = 14 Hz, $^2J_{PH}$ = 4 Hz, 2 H, PCH_2), 4.13 (dp^v, $^2J_{HH}$ = 14 Hz, $^2J_{PH}$ = 6 Hz, 2 H, PCH_2), 5.87 (dd, $^3J_{HH}$ = 8 Hz, $^5J_{HH}$ = 1 Hz, 2 H, H_G), 6.04 (dd, $^3J_{HH}$ = 8 Hz, $^5J_{HH}$ = 1 Hz, 2 H, H_A), 6.31 (dd, $^3J_{HH}$ = 8 Hz, $^5J_{HH}$ = 1 Hz, 2 H, H_D), 6.57 (dd, $^3J_{HH}$ = 8, 8 Hz, 2 H, H_B), 6.71 (dd, $^3J_{HH}$ = 8, 8 Hz, 2 H, H_H), 6.81 (tt, $^3J_{HH}$ = 8 Hz, $^5J_{HH}$ = 1 Hz, 1 H, H_C), 6.86 (tt, $^3J_{HH}$ = 8 Hz, $^5J_{HH}$ = 1 Hz, 1 H,

H_I), 6.98 (t, $^3J_{HH}$ = 8 Hz, 2 H, H_E), 7.06 (ddt, J = 7, 5, 1 Hz, 4 H, C_6H_5), 7.18 (tt, $^3J_{HH}$ = 8 Hz, $^5J_{HH}$ = 1 Hz, 1 H, H_F), 7.19-7.25 (m, 8 H, C_6H_5), 7.29 (t, $^3J_{HH}$ = 8 Hz, 2 H, C_6H_5), 7.33 – 7.41 (2 x m, 16 H, C_6H_5), 7.47-7.56 (m, 14 H, C_6H_5), 7.62 (t, $^3J_{HH}$ = 8 Hz, 2 H, C_6H_5). $^{13}C\{^1H\}$ NMR (151 MHz, CD_2Cl_2, 298 K): δ_C = 411.5 (br., μ-C), 166.5 (d, $^1J_{RhC}$ = 35 Hz, C_1), 144.1 (s, C_4), 143.4 (s, C_3), 139.3 (s, C_6), 138.1 (d, $^2J_{RhC}$ = 9 Hz, C_2), 136.5 (s, C_5), 135.7 (t^v, J = 6 Hz, C_6H_5), 134.2 (dt^v, J = 13, 6 Hz, C_6H_5), 133.8 (t^v, J = 6 Hz, C_6H_5), 132.9, 132.7, 132.7, 132.6 (4 x s, C_6H_5), 132.4 (s, C_D), 132.0 (s, C_6H_5), 130.6 (s, C_G), 130.4 (s, C_6H_5), 130.3 (s, C_A), 130.1 (t^v, J = 5 Hz, C_6H_5), 129.8 (t^v, J = 5 Hz, C_6H_5), 129.6 (t^v, J = 5 Hz, C_6H_5), 129.4 (t^v, J = 5 Hz, C_6H_5), 128.2 (s, C_B), 127.6 (s, C_E), 127.3 (s, C_H), 127.2 (s, C_F), 126.6 (s, C_C), 126.2 (s, C_I), 25.6 (p^v, J_{PC} = 10 Hz, PCH_2). $^{31}P\{^1H\}$ NMR (162 MHz, CD_2Cl_2, 298 K): δ_P = 17.17 (dt, $^1J_{RhP}$ = 97 Hz, $^3J_{RhP}$ = 37 Hz), 22.40 (dt, $^1J_{RhP}$ = 126 Hz, $^3J_{RhP}$ = 37 Hz), -142.3 (hept., $^1J_{PF}$ = 707 Hz, PF_6). IR (ATR, cm^{-1}): 3079, 3047, 2989 ν_{CH}, 1440, 1426, $\nu_{C=C}$, 894 ν_{PF}. MS (ESI, m/z): Accurate mass: Found 1323.1072. Calcd for $C_{72}H_{59}{}^{35}Cl_2P_4Rh_2$ $[M]^+$: 1323.1049.

Further elution of the above chromatography column with neat CH_2Cl_2 resulted in elution of a yellow band. Addition of petrol and removal of solvent under vacuum produced a yellow powder of pure **$[Rh_2(\mu\text{-}Cl)(CO)_2(\mu\text{-}dppm)_2]PF_6$** (5 mg, 0.004 mmol, 15 %). Limited spectroscopic data (IR, ^{1}H NMR) are reported here for comparison with those published for the corresponding salt **$[Rh_2(\mu\text{-}Cl)(CO)_2(\mu\text{-}dppm)_2]BF_4$**.[278] IR (ATR, cm^{-1}): 1993, 1974 ν_{CO}, 894 ν_{PF}. ^{1}H NMR (600 MHz, CD_2Cl_2, 298 K): δ_H = 3.57 (dp^v, $^2J_{HH}$ = 11 Hz, J_{PH} = 4 Hz, 4 Hz, 2 H, PCH_2), 4.17 (dp^v, $^2J_{HH}$ = 10 Hz, J_{PH} = 4 Hz, 4 Hz, 2 H, PCH_2). $^{31}P\{^1H\}$ NMR (162 MHz, CD_2Cl_2, 298 K): δ_P = 19.3 (d, $^1J_{RhP}$ = 114 Hz), -142.3 (hept., $^1J_{PF}$ = 708 Hz, PF_6). MS (ESI, m/z): Found 1065.01. Calcd for $C_{52}H_{44}{}^{35}ClO_2P_4Rh_2^+$ $[M]^+$: 1065.01 m/z. A crystal suitable for structure determination was grown by slow evaporation of a CH_2Cl_2/toluene mixture. *Crystal data for* $C_{52}H_{44}ClO_2P_4Rh_2.F_6P$ (M_w = 1210.99 g.mol^{-1}): monoclinic, space group $P2_1/n$ (No. 14) a = 14.88706(7), b = 16.69242(7), c = 23.74501(9) Å, β = 96.1333(4)°, V = 5866.88(4) Å^3, Z = 4, T = 150.0(1) K, μ(Cu Kα) = 6.72 mm^{-1}, D_{calcd} = 1.371 Mg.m^{-3}, 117588 reflections measured (9.2° ≤ 2Θ ≤ 146.2°), 10558 unique (R_{int} = 0.042) which were used in all calculations. The final R_1 was 0.030 ($I > 2\sigma(I)$) and wR_2 was 0.080 (all data) for 650 refined parameters with 48 restraints.

EPISODE VI– RETURN OF THE RESONANCE

^{13}C AND ^{103}Rh RESONANCE DETECTION THROUGH LABELLING AND MULTIDIMENSIONAL NMR STUDIES

6.1 PREFACE

The recent expansion of dirhodium μ–carbido complexes described herein has led to the discovery of significantly deshielded ^{13}C chemical shifts. The development of ^{1}H-^{31}P-^{13}C triple relay NMR and ^{31}P-X HMQC NMR (X = ^{13}C, ^{103}Rh) techniques have resulted in the rapid indirect detection of previously 'hidden' μ-carbido ^{13}C NMR resonances but present opportunities for broad applicability as a generalisable technique for organometallic phosphine complexes. The scarcely detected ^{103}Rh chemical shifts have allowed for in-depth analysis of the paramagnetic deshielding effect for these metal-carbon multiple bond complexes.

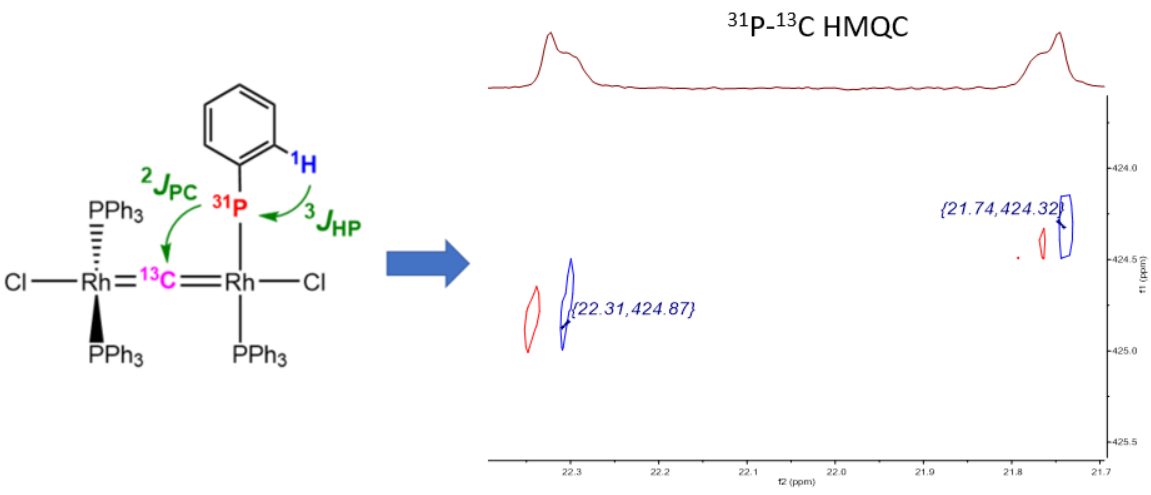

Figure 6.0: ^{31}P-^{13}C HMQC Spectrum

6.2 INTRODUCTION

6.2.1 Previous Studies Resorting to ^{13}C Labelling

The complexes presented in this, and previous work, present a complex and challenging nature for their characterisation through NMR studies. The 100% abundance of ^{31}P and ^{103}Rh, both of which are spin ½ nuclei, results in the carbon coupling with up to six spin active nuclei. Quaternary carbons themselves are difficult to detect in the ^{13}C NMR spectra due to a lack of NOE enhancement from bound hydrogens, and if the expected AMM'XX'YY' system is included, the carbido resonance is next to impossible to detect using standard NMR conditions.[xlv]

Previous work by the author had been successful in detecting two of these bridging carbon nuclei, namely those of key complexes **[$Rh_2(\mu\text{-}C)Cl_2(PPh_3)_4$]** and **[$Rh_2(\mu\text{-}C)H(\kappa C\text{-}2\text{-}C_6H_4PPh_2)(Tp^*)_2$]**. Utilising $^{13}CS_2$ generated enriched isotopologues of the two compounds, which allowed the direct detection of the μ-carbido ligand nucleus in the $^{13}C\{^1H\}$ NMR spectra (**Figure 6.1**). The resonances appear far downfield in the accepted μ-carbido range, at 426.4 and 447.2 ppm, respectively.[279]

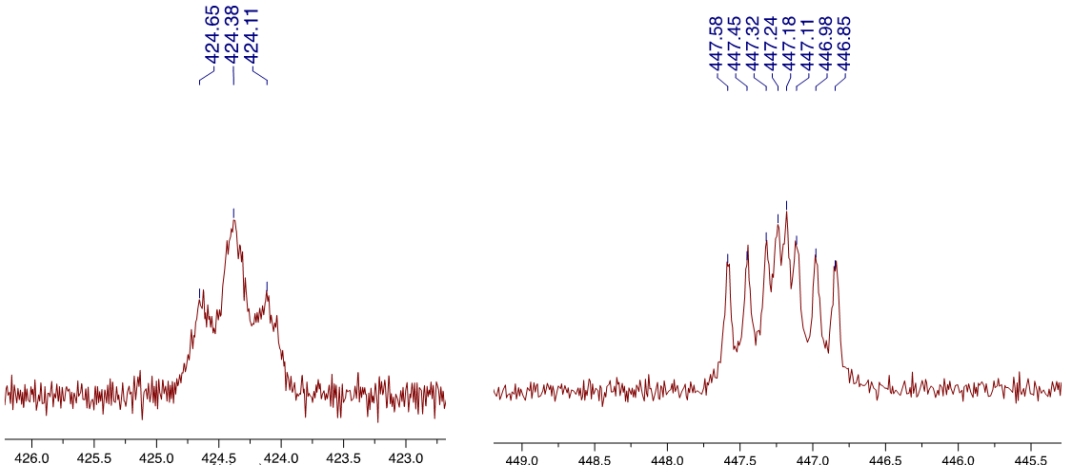

Figure 6.1: $^{13}C\{^1H\}$ NMR spectra of the carbido region of **[$Rh_2(\mu\text{-}C)Cl_2(PPh_3)_4$]** (left) and **[$Rh_2(\mu\text{-}^{13}C)H(\kappa C\text{-}2\text{-}C_6H_4PPh_2)(Tp^*)_2$]** (right)

[xlv] The maximum field strength available for this study was 201.2 MHz (cryoprobe). Limitations to sample solubility often precluded increased sensitivity with temperature reduction.

Although this demonstrated that ^{13}C labelling provided a viable approach, it was not the first method attempted. Though the bridging carbon atom was not identified in the standard $^{13}C\{^{1}H\}$ NMR spectrum, employing even the strongest magnetic field instruments available, more elaborate NMR pulse sequences were explored to enhance the direct detection of the carbido resonance.

One pulse sequence in particular, which was initially thought to have been promising involved utilising a phosphorus-decoupled carbon spectrum, i.e., a $^{13}C\{^{31}P\}$ NMR study. If the $^{2}J_{PC}$ coupling to the four phosphorus ligands could be removed,[xlvi] then the bridging carbon would only appear as a triplet due to the $^{1}J_{RhC}$ coupling, and perhaps be intense enough to detect. Unfortunately, even using broad-band decoupling to remove all traces of $^{2}J_{PC}$, the carbon resonances were never detected directly. This may have been a result of using a lower field instrument, as the only available NMR instrument capable of dual pulsing ^{31}P (106.0 MHz) and ^{13}C (100.6 MHz) at the time was a Varian 400, and the quaternary carbon was still coupled to the two ^{103}Rh nuclei.

6.2.2 μ-carbido Complexes and ^{13}C Labelling

One of the common detection techniques used for elusive carbon nuclei involves selective ^{13}C labelling. Carbon-13 enrichment can help shed light on mechanisms and major products of reactions, but it also has a use for detection of previously unseen resonances. The use of ^{13}C labelling for metal-carbon ligands (carbidos, carbenes, carbynes) is not novel, however, the source of the carbon ligand plays a huge role in determining the ease and cost of forming the isotopologue.

The first isolated terminal carbido $[K(benzo\text{-}15\text{-}crown\text{-}5)_2]$**[Mo(≡C){NᵗBu(C$_6H_3Me_2$)}$_3$]** arose from a synthetic sequence in which the carbido source molecule, ^{13}CO, was introduced early in the pathway, ultimately allowing direct observation of the carbon resonance at 482.8 ppm, in the absence any coupling to spin active metal or ligand nuclei. One of the key starting materials which has led to the rather rapid development of Class C carbido complexes is **[Ru(≡C:)Cl$_2$(PCy$_3$)$_2$]**, which is discussed in **Chapter 1.2**. Containing the free, stable carbido ligand allows ease of coordination to a variety of metal complexes to furnish μ-carbido complexes. What is quite endearing about this complex is that the free carbido ligand can also be readily enriched with ^{13}C. The synthetic pathway to the ruthenium carbido complex stars from the well-

[xlvi] Attempts to prepare arsine analogues of key compounds by substitution with $AsPh_3$, $Ph_2AsCH_2AsPh_2$ or $Ph_2AsCH_2CH_2AsPh_2$ failed due to the lower nucleophilicity and metal binding strength of arsines relative to phosphines.

known Grubbs' Catalyst, which undergoes alkene metathesis with vinyl acetate to form the acetato carbene derivative (see **Scheme 6.1** below). The acetato carbene is short-lived with clean conversion to the free carbido species proceeding through spontaneous geminal elimination of acetic acid. Replacing the vinyl acetate with ^{13}C enriched vinyl acetate, $^{13}CH_2{}^{13}CHOAc$, forms the isotopologue **[Ru(≡^{13}C)Cl$_2$(PCy$_3$)$_2$]**,[280] with the advantage of introducing the expensive ^{13}C label late in the synthetic sequence.

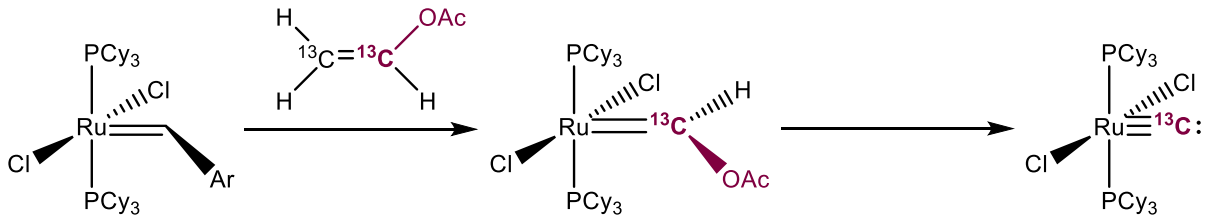

Scheme 6.1: Synthesis of ^{13}C-enriched free carbide complex **[Ru(≡^{13}C:)Cl$_2$(PCy$_3$)$_2$]** from labelled vinyl acetate and Grubbs' Catalyst

The financial setback of ^{13}C enrichment ($1500 AUD for 1 gram), is offset when considering the small molecular weight of vinyl acetate and the 1:1 stoichiometric ratio which can be used to form the free carbido. Therefore, 1 gram of enriched vinyl acetate can produce a significant amount of the enriched free carbido species. The ease of installation of the ^{13}C atom in this case outweighs the expense of the purchasing the labelled reagent. The ^{13}C resonance of the free carbido ligand was observed downfield at 472 ppm, owing to the significant paramagnetic contribution from the ruthenium multiple bond.[281]

Using this isotopologue, the ^{13}C NMR shifts for the bimetallic Class C carbido complexes could be easily detected, including the coupling and satellites from spin active transition metals (see **Section 1.2** for details) and spin-active ligand nuclei, e.g., $^{31}PCy_3$. Coordination of the metal centre to form μ-carbido complexes has a profound effect on the location of the carbido resonances in ^{13}C NMR spectra, which so far appear in the range of 346.7 to 433.5 ppm for all 12 coordinated d^8/d^{10} metals (**Table 6.1**).[19-20]

Complex	δ ^{13}C
$(AsPh_4)[(Cy_3P)_2Cl_2Ru{\equiv}C{-}PtCl_3]$	344.7
$[(Cy_3P)_2Cl_2Ru{\equiv}CPtCl_2(dmso\text{-}S)]$	349.0
$[(Cy_3P)_2Cl_2Ru{\equiv}C{-}PtCl_2(py)]$	350.3

$[(Cy_3P)Cl_3RuR{\equiv}C–PtCl(py)_2]$	354.6
$(PNP)[(Cy_3P)_2Cl_2Ru{\equiv}C–PdCl_3]$	380.9
$[(Cy_3P)_2Cl_2Ru{\equiv}C–IrCl(COD)]$	387.6
$[(Cy_3P)_2Cl_2Ru{\equiv}C–AuCl]$	395.3
$[\{(Cy_3P)_2Cl_2Ru{\equiv}C\}_2Au]OTf$	395.3
$[(Cy_3P)_2Cl_2Ru{\equiv}C–RhCl(CO)_2]$	396.4
$[\{(Cy_3P)_2Cl_2Ru{\equiv}C\}_2IrCl(CO)]$	397.4
$[(Cy_3P)_2Cl_2Ru{\equiv}C–RhCl(COD)]$	411.7
$[(Cy_3P)_2Cl_2Ru{\equiv}C–Ag(4'\text{-}Ph\text{-}terpy)]OTf$	433.1
$[(Cy_3P)_2Cl_2Ru{\equiv}C–Ag(terpy)]OTf$	433.5

Table 6.1: ^{13}C NMR shifts for the carbide carbon in Class B and C μ-carbido complexes from **$[Ru(\equiv^{13}C)Cl_2(PCy_3)_2]$**

Closer to this research, the work of Braun on the rhodium cumulenic μ-carbido complex, **$[Rh_2(\mu\text{-}C)(SBpin)_2(PEt_3)_4]$**, included the synthesis of the ^{13}C enriched isotopologue (Discussed in **Section 1.2**). Utilising $^{13}CS_2$ as the source of enriched carbon is an expensive process (> $1000 AUD per gram), but once again the use of this reagent in a stoichiometric manner, as a late-stage modification, enables ample conversion to the isotopologue.

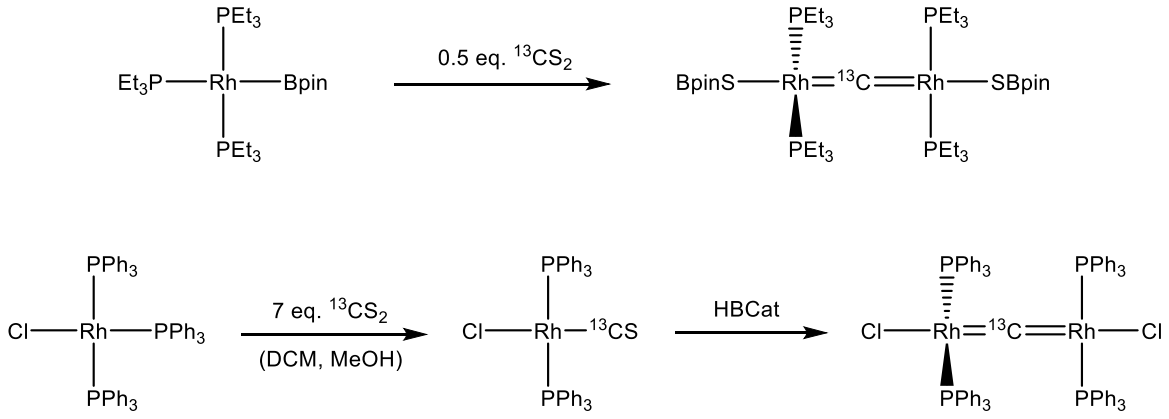

Scheme 6.2: (top) use of $^{13}CS_2$ to stoichiometry form a labelled cumulenic μ-carbido complex. (bottom) current synthesis of **$[Rh(^{13}CS)Cl(PPh_3)_2]$**

Through the ^{13}C enrichment, the furcated μ-carbido resonance could be detected at 439.4 ppm and the fine-structure resolved sufficiently to measure both the rhodium ($^1J_{RhC}$ = 45 Hz) and phosphorus ($^2J_{PC}$ = 11 Hz) coupling as a triplet of pentets.[282]

The issue previously presented with ^{13}C enrichment in this work is the nature of the early use of carbon disulfide in the reaction, *as a cosolvent* with methanol. The scale of the reaction using 1 mL of $^{13}CS_2$ generates less than 100 milligrams of **[RhCl(^{13}CS)(PPh$_3$)$_2$]**, which is not a feasible solution provided the subsequent μ-carbido synthesis affords yields of *ca* 50%.

6.2.3 Diamagnetic and Paramagnetic Shielding

The large chemical shift range for the carbido carbon nuclei reflects a combination of the diamagnetic and paramagnetic shielding effects on the nucleus. The diamagnetic shielding, or shielding contribution from the core electrons, contributes typically only a few ppm for light elements, but become a scalable property with Z when looking at the transition metals and post-TM chemistry. However, the diamagnetic shielding of a nucleus cannot explain chemical shift changes of heavy elements, as the nature of the core electrons remain fairly consistent. As the core electrons are not involved in any bonding, the diamagnetic values cancel out in chemical shift calculations of post-hydrogen elements such as ^{13}C and ^{103}Rh.

The paramagnetic contribution is considerably more difficult to interpret as it not only includes the ground state wavefunction, but also excited states. This paramagnetic effect does, however, play the major contributing role in chemical shift and shielding values.[283] The paramagnetic term, which is often a deshielding effect, is centred around the electron density of non-spherical orbitals of a nucleus (i.e., non *s*-orbital contributions). For ^{13}C, the paramagnetic deshielding effect is dominated by *p*-orbital components, however for larger elements this also includes higher angular momentum orbitals (importantly the *d*-orbitals of transition metal nuclei). The deshielding effect arises from the mixing or 'coupling' of two orbitals in the presence of an external magnetic field. A minor effect arises from the coupling of two occupied orbitals; however the dominant coupling is between occupied and virtual orbitals.

The accepted relationship between the range of chemical shifts and the core electron shell radius of an element is an inverse cube relationship (i.e. $\frac{1}{r^3}$). With the inclusion of ligand field splitting, the imbalance of charge density, and the delocalisation of electrons in molecular orbitals (Q_{ij}), the modelling of the paramagnetic vector contribution to NMR shift (σ_{ii}) can be simplified to **Equation 6.1**.[284]

$$-\sigma_{ii} \propto (\Delta E)^{-1} \cdot < r^{-3} > \cdot \sum Q_{ij}$$

Equation 6.1: Simplified Ramsey model for calculating paramagnetic contribution to NMR shifts

What **Equation 6.1** really tells us is that the paramagnetic contribution is related to:

(i) The accessible excitation energies ΔE. This becomes increasingly important with the inclusion of transition metal orbitals or more generally the smaller the energy difference between occupied orbitals and virtual orbitals, the greater the contribution. In a molecule, it might be anticipated that the HOMO-LUMO gap (axiomatically the smallest value of ΔE) will be of particular interest.

(ii) The distance from the nucleus to the electron ($<r^{-3}>$), which generally increases with principle quantum number, and

(iii) The relative populations of higher angular momentum orbitals, which is simplified to ΣQ_N and better known as the angular momentum operators.[285]

An early appreciation of the significance of paramagnetic shielding effects on carbon π-acid ligands was the recognition that for series of chalcocarbonyl complexes L_nMCA (A = O, S, Se)[xlvii] the chemical shift of the chalcocarbonyl carbon resonance correlates inversely with the HOMO-LUMU gap (π-π*) of the free diatomic.[286]

6.2.4 Comments on ^{13}C NMR

Paramagnetic Deshielding of Carbene Complexes

Arguably the most interesting piece of characterisational data for an organometallic ligand is the ^{13}C NMR resonance of the donor carbon. One of the largest studies performed for organometallic complexes is the deshielding of transition metal carbene and carbyne complexes relative to their organic counterparts. Eisenstein and co-workers have recently published detailed and insightful articles studying a range of Fischer and Schrock carbyne and carbene complexes and the molecular orbital theory that accounts for their remarkably downfield chemical shifts.[287] One of the key pieces of information to note is that in comparison to alkene/yne compounds, isolobal transition metal carbene (M=C) and carbyne (M≡C) complexes have pronounced lower field ^{13}C

[xlvii] Unfortunately, the work pre-dated the isolation of the first tellurocarbonyl complex, however a similar trend is observed for **$[OsCl_2(CA)(CO)(PPh_3)_2]$** (A = O, S, Se, Te).

shifts. Both the incorporation of a transition metal, and the degree of multiple bonding, have a profound effect on the ^{13}C chemical shift.

Because the paramagnetic deshielding tensor is a property for non-spherical orbital interactions, it is dominated by *p*-orbital interactions in alkene compounds and *p-d* interactions for transition metal carbene complexes. Theoretical studies have identified the two key occupied-virtual orbital couplings for alkene/carbene compounds; the major component consists of the σ^b to π^* transition,[xlviii] with a secondary π^b to σ^* transition having a minor effect (depicted in **Figure 6.2**).

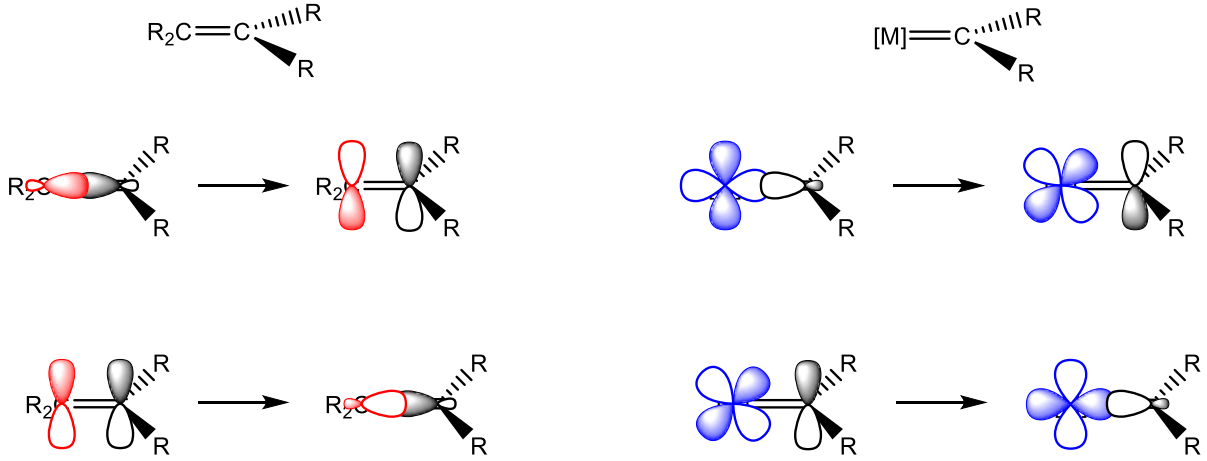

Figure 6.2: Relevant orbitals for alkenes and carbene complexes for the σ^b to π^* transition (above) and the π^b to σ^* transition (below)

The dominant effect that the incorporation of a transition metal has is the reduction in energy gap between the coupled occupied and virtual orbitals. This greatly reduces the ΔE component of **Equation 6.1**, which in turn causes large perturbations in the paramagnetic shielding tensor. The relative orbital energies are such an important feature of the paramagnetic deshielding that the distinction between Fisher and Schrock carbenes can be meaningfully described and quantified. Fisher carbenes have a stronger paramagnetic deshielding component due to the stronger coupling between the M-C σ^b to M=C π^* orbitals. The presence of π-acceptor ligands on the Fisher carbenes lower the energy of the π^* orbital (and hence electrophilicity of the carbon), which increases the coupling strength. The donor ligands typically seen on a Schrock

[xlviii] ^{b} refers to a bonding molecular orbital, * refers to an anti-bonding molecular orbital.

carbene instead destabilise the π^* orbital, thereby increasing the energy gap. The Schrock carbenes are partially compensated with a stronger coupling for the secondary M=C π^b to M-C σ^* transition, however this effect is less pronounced. Hence Schrock carbenes display comparatively upfield ^{13}C NMR shifts relative to those of Fischer carbenes.

One of the noticeable effects of the carbene ^{13}C chemical shift tensor is the valence shell of the transition metal used in bonding. Carbene complexes of *3d* transition metals contain a stronger paramagnetic deshielding component than their corresponding *4d* and *5d* counterparts, due to the increased importance of σ-donation due to relativistic stabilisation.[288]

The ^{13}C chemical shift of carbene complexes and alkenes are both dominated by the paramagnetic tensor σ_p, which in turn is dominated by the coupling of the occupied M-C σ^b to virtual M=C π^* orbitals.

Heavy Atom to Light Atom Effect

A simple account of paramagnetic deshielding fails to incorporate relativistic effects of heavy atoms. What is significant for the ^{13}C NMR analysis of organometallic complexes is the HALA effect, i.e., the Heavy Atom to Light Atom coupling (For example, ^{103}Rh to ^{13}C). The NMR active *p*- and *d*-type atomic orbitals on the metal are split by spin orbit (SO) coupling, and this energy difference is propagated through the metal-ligand bond *via* Spin-Dipolar or Fermi Contact mechanisms.[289] Unlike paramagnetic deshielding, the effects of SO coupling on the light atom have been well documented and comprise a number of factors including the *s*-orbital character of the bond,[290] the FMO energy gaps,[291] oxidation state and covalency of the bond.[292] More specifically for transition metal chemistry, the covalency of the M-L bond, *d*/*p* orbital character, and the *trans* influence correlate quantitatively with the SO coupling.

6.2.5 ^{103}Rh NMR

Rhodium plays an important role in organometallic chemistry, as many large industrial processes rely on rhodium catalysed reactions (reduction of hydroformylation of alkenes for example), and because of this, detection and analysis of the ^{103}Rh nucleus through NMR studies has the potential to be an important tool.[293] For example, it was discovered through in situ ^{103}Rh NMR studies that the two diastereomeric intermediates that form through the hydrogenation of L-DOPA precursors do so at different rates and could be correlated to the different electronic

environments of the two rhodium nuclei.[294] Rhodium-103 NMR chemical shifts have been correlated in a similar manner to catalytic activity for CO_2 hydrogenation.[295]

The 100% abundant, spin active (I = ½) ^{103}Rh nuclei for the most part is an extremely useful feature, e.g., analysis of the $^{1}J_{RhP}$ coupling constants instantly reveal the decomposition of the complex (ligand dissociation) or a change in coordination number(*s*-character)/ligand sphere.

The main issues with direct detection of the ^{103}Rh nuclei are (i) the rather broad spectral range encompassing signals (~12500 ppm – see **Figure 6.3**), (ii) long T_1 relaxation times, (iii) narrow linewidths, and (iv) low sensitivity (0.186 receptivity compared to ^{13}C). This means that direct detection is often an unreliable method for locating and accurately observing these signals.[296] The low frequency required for detecting ^{103}Rh (Ξ = 3.16 MHz) also means conventional NMR probes often cannot be used. Because of all of these issues, the first published direct detection of the ^{103}Rh nucleus only appeared in 1979 and the published research since has been comparatively sparse.[297]

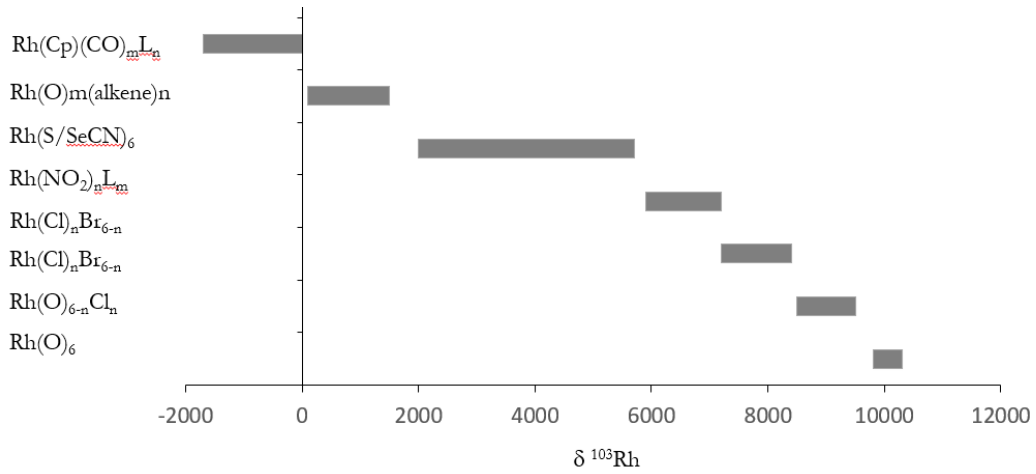

Figure 6.3: Chemical shift ranges for a range of rhodium complexes (adapted from Elsevier[298])

^{103}Rh Chemical Shifts

The exceptionally large spectral dispersion of ^{103}Rh NMR shifts highlights how responsive the nuclei are to minor changes in the metal coordination sphere, especially the π-donor/acceptor nature of the ligands. This is best exemplified in **Figure 6.3**, which shows that variation in the values of *n* for the complex $\mathbf{[RhCl_nBr_{6-n}]^{3-}}$ results in a spectral range of ~1000 ppm by simple chloride/bromide replacement. Similar effects have also been seen when comparing phosphine

ligands of differing bite angles and substituents,[299] counterion exchange,[300] κ-coordination number of polydentate ligands,[301] and even switching from a coordinated COD ligand to NBD, the latter changing the ^{103}Rh chemical shift by up to 500 ppm (**Figure 6.4**).[302]

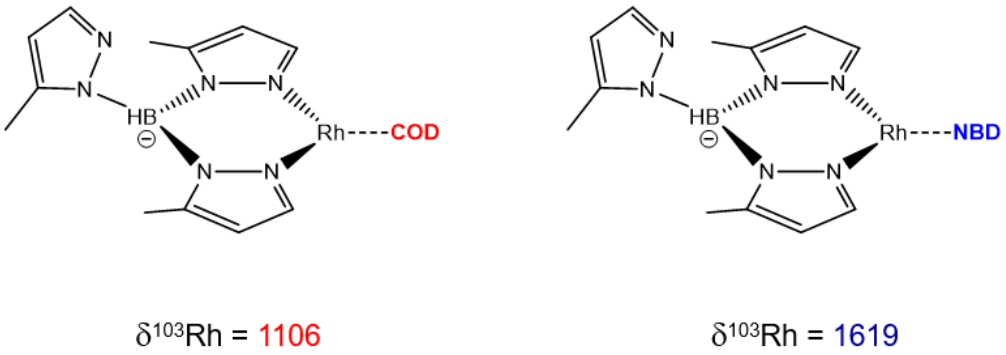

Figure 6.4: **[Tp'RhL]** (L = COD, NBD) and their corresponding ^{103}Rh NMR shifts

Fortunately, there have been a number of previous studies that have attempted to delineate factors contributing to the chemical response of the ^{103}Rh NMR shift. One such study from Szczecinski and co-workers considered rhodium(I) complexes with the same butene-amine ancillary ligand ($Me_2NCH_2CMe_2CH{=}CH_2$).[303] By substituting the coordinated ethene ligand for acetonitrile and pyridine derivatives, the change in ^{103}Rh chemical shift could be shown to directly reflect the π-donicity of the ligand (**Table 6.2**). A similar study undertaken at the same time saw the effect changing the R group on the six-coordinate complexes *trans*-**[RhI(R)(CN^{t}Bu)$_4$]$^+$**, the ^{103}Rh chemical shift of which changed by more than 70 ppm by simply moving from a methyl to an ethyl ligand.[304]

Complex	δ^{103}Rh
[RhCl(L)(**ethylene**)]	652.4 [a]
[RhCl(L)(**acetonitrile**)]	1696.3 [a]
[RhCl(L)(**4-cyanopyridine**)]	2029.5 [a]
[RhCl(L)(**pyridine**)]	2050.9 [a]
[RhCl(L)(**4-dimethylaminopyridine**)]	2095.1 [a]
[RhI(**Me**)(CN^{t}Bu)$_4$]$^+$	107 [b]
[RhI(**Et**)(CN^{t}Bu)$_4$]$^+$	183 [b]
[RhI(**^{n}Pr**)(CN^{t}Bu)$_4$]$^+$	174 [b]
[RhI(**^{n}Bu**)(CN^{t}Bu)$_4$]$^+$	175 [b]

[Rh(COD)(**dppb**)]PF_6	-8576 [c]
[Rh(COD)(**dppe**)]PF_6	-8809 [c]
[Rh(COD)(**S,S-DIOP**)]PF_6	-8555 [c]
[Rh(COD)(**R-BINAP**)]PF_6	-8379 [c]
[Rh(COD)(**R-TolBINAP**)]PF_6	-8389 [c]
[Rh(COD)(**S,S-MeDUPHOS**)]PF_6	-8756 [c]
[Rh(COD)(**S,S-MeBPE**)]PF_6	-8799 [c]

Table 6.2: Data ([a] taken from [303], [b] taken from [304], [c] taken from [299]) of ^{103}Rh NMR resonances (where L = $Me_2NCH_2CMe_2CH{=}CH_2$)

The successful direct detection of the ^{103}Rh nuclei helped shed light on the significance of the interactions between the ligand and metal. The ^{103}Rh environment clearly shows a downfield trend when changing the ligand from a good π-acceptor in ethylene through to a strong σ-donor for the pyridine examples. The decrease of π-retrodonation back to the ligands is the cause of this downfield shift.

A similar study undertaken in 1987 by Pregosin and Anklin examined rhodium(III) complexes with the same cyclometallated Schiff base co-ligand (**Table 6.3**).[305] This rather detailed study was able to vary the substituted Schiff base ligand, in addition to the phosphine and halide co-ligands, to give a rather elegant overview on the changes each made at the rhodium centre.

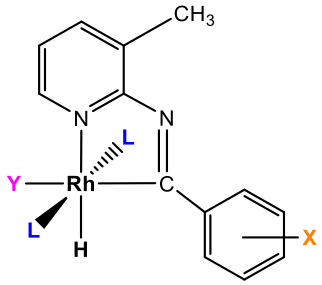

Entry	X	L	Y	δ ^{103}Rh	δ ^{1}H
1	3-NO_2	PPh_3	Cl	830.2	-11.23
2	3-NO_2	PPh_3	Br	739.2	-11.43
3	3-NO_2	PPh_3	$P(OCH_3)_3$[a]	125.5	-12.58
4	3-NO_2	$AsPh_3$	Cl	981.5	-11.88
5	3-NO_2	$AsPh_3$	SCN	947.4	-12.09
6	4-NO_2	PPh_3	Cl	830.1	-11.21
7	4-NO_2	PPh_3	CN(Cy)[a]	198.7	-11.78
8	2-OH	PPh_3	$P(OCH_3)_3$[a]	106.0	-13.07
9	2-OH	PPh_3	^{13}CN	238.1	-12.52

10	2-OH	$SbPh_3$	Cl	799.6	- 12.22
11	2-OH, 3-OCH_3	PPh_3	Cl	821.9	-11.37
12	2-OH, 3-OCH_3	$AsPh_3$	Cl	968.0	-12.02

Table 6.3: Data (taken from [305]) of ^{103}Rh and corresponding hydride ^{1}H NMR environments. [a] cationic complex

Comparing entries 1 and 2 shows the upfield shift in the rhodium environment of nearly 100 ppm when shifting from a chloride to bromide ligand. A shift downfield is seen when replacing PPh_3 with the poorer σ-donor $AsPh_3$ (entry 1 to 4, Δ = -151.3 ppm; entry 11 to 12, Δ = -146.1 ppm). The three cationic complexes (entries 3, 7 and 8) all have a significant upfield shifts from the neutral complexes. Interestingly, alternating the X group on the Schiff base ligand had minor effects on the ^{103}Rh shift. Comparing the nitro group at the 3 and 4 position had almost no measurable difference, and even the disubstituted ring (entries 11 and 12) differ by less than 30 ppm from their corresponding nitro analogues. The most interesting piece of comparison though is the change in ^{103}Rh when compared to the corresponding hydride ^{1}H NMR environments. The ^{103}Rh resonances span almost 800 ppm, but the hydride environment changes by as little as 1.86 ppm, even when comparing the cationic complexes. This difference is due to the large paramagnetic deshielding parameter of the ^{103}Rh nuclei, resulting in considerable fluctuations with minor changes to the ligand field.

Spin Orbital Coupling

Spin orbit coupling (SO) falls under the relativistic effects that aren't included in the simple Ramsey formulation for paramagnetic deshielding. To define spin orbit coupling, we must take our perspective of the atom and tell it from the side of the electron. Rather than considering the nucleus as frozen in space with electrons orbiting, if we instead consider the electron motionless, then the nucleus becomes the object that is in orbit. Because the nucleus is a charged particle moving in a circular motion, the magnetic field B that it creates acts on the electron in accordance with the right-hand rule. One of the intrinsic properties of the electron is their spin magnetic moment, μ_s, which also creates a small magnetic field (μ_s). In the presence of the external magnetic field B, the total energy of the magnetic moment that the electron experiences can be defined by the dot product between the magnetic moment and the external field. To reduce the energy of this dot product, the orientation of the electron changes to align itself parallel to the external magnetic

field, which changes the energy levels of the relevant MOs. This mixing of MOs induces a spin polarization on the nuclei, which can then interact with neighbouring atoms to induce either a shielding or deshielding effect at the atom in the presence of an external magnetic field.

The spin-orbit coupling values of ^{103}Rh for a range or rhodium complexes have been calculated by Saielli and co-workers in a detailed experimental and theoretical study.[306] The shielding analysis of the ^{103}Rh nuclei concluded that the spin-orbit coupling values played a large contribution to the chemical shifts (~10% the value of the paramagnetic shielding), however, the values remained relatively consistent, and could largely be ignored as a changing effect on the chemical shift (See **Table 6.4**).

Complex	σ_{calcd}	σ_{SO}
$[Rh(Cp)(CO)_2]$	807	388
$[Rh(CO)_4]$	286	409
$[Rh(CO)_2Cl]_2$	-522	405
$[Rh(cod)_2]^+$	-1185	407
$[Rh(acac)(C_2H_4)_2]$	-1548	390
$[RhI_4(SMe_2)]_2^-$	**-3374**	**793**
$[RhBr_4(SMe_2)]_2^-$	**-4785**	**639**
$[RhCl_4(SMe_2)]_2^-$	**-5290**	**596**
$[Rh(acac)_3]$	-7478	508

Table 6.4: Calculated ^{103}Rh chemical shift (Relativistic spin-orbit ZORA/TZ2P all-electrons) and contributions from spin-orbit coupling for a range of rhodium complexes. Data from [306]

What did play a significant role on the spin-orbit coupling was the inclusion of multiple heavy atoms bound to rhodium. Examining the complexes studied, the spin-orbit coupling values of **$[RhX_4(SMe_2)]_2^-$** (X = Cl, Br, I) were significantly higher than the complexes with one or no heavy elements. Even among these three complexes, there is a clear trend down Group 17 (δ_{SO} Cl = 596, Br = 639, I = 793 ppm), which is reflected by the increase in halide spin-density. Similar trends were seen by Ziegler and Gilbert when examining the ^{195}Pt NMR chemical shifts of dihalide complexes.[307]

The first example solely examining this halogen dependence came in 1993 from Heaton, Jacob and Moffet, studying anionic rhodium(I) complexes of the general formula ***cis*-$[RhX_2(CO)_2]^-$**, where one or both X units could be either Cl, Br or I.[308] The expected trend based on ligand field theory placed the dichloride complex **$[RhCl_2(CO)_2]^-$** the furthest downfield with

δ_{103Rh} = 73 and the diiodo complex **[RhI$_2$(CO)$_2$]$^-$** the furthest upfield at δ_{103Rh} = -221. Theoretical studies performed more recently by Mirzaeva and Kozlova revealed a linear dependency between the calculated HOMO-LUMO gap of the anionic complexes and their corresponding ^{103}Rh NMR shift (see **Figure 6.5**), which was supported by a noticeable change in the paramagnetic component to the total shielding parameter.[309]

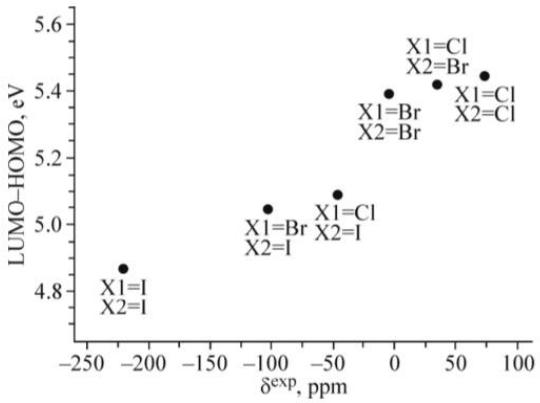

Figure 6.5: Linear dependency of the HOMO-LUMO energy gap for **[RhX$_2$(CO)$_2$]$^-$** and the ^{103}Rh NMR shift. (from [309])

A similar study on spin-orbit effects of halogens was performed more recently on the di-rhodium complexes **[Rh(Cp*)X]$_2$(μ-X)$_2$**.[310] An identical trend was observed as the ^{103}Rh NMR environment shifts upfield with heavier halide ligands, from 2303 ppm for X =Cl through 2068 (Br) to 1426 ppm for I. The spin orbit effects of the halogen are reflected in changing HOMO-LUMO energy gaps as the increase in π-donor capacity of the halogen elevates the energies of d_{xy}, d_{xz} and d_{yz} orbitals, giving different paramagnetic deshielding values.

Curiously, the role oxidation state plays on the ^{103}Rh chemical shift has been debated over for some time. Though it might be simple to try and join the dots between a higher oxidation state and change of charge density of the rhodium centre, the noticeable effect in fact came from the ligands. High oxidation state complexes were typically associated with weak-field ligands, and conversely for low oxidation state rhodium complexes. However, taking a high oxidation state rhodium(III) complex with strong-field ligands, such as **[RhH$_2$(Si(OEt$_3$))(PMe$_3$)$_3$]**, the negative chemical shift of -1222 ppm lies in a similar region to rhodium(I) silyl complexes and would suggest the ligand field effects outweigh the presumed effect of the oxidation state.[311] An often-overlooked contribution assigned incorrectly to oxidation state effects is the difference in coordination

number at the metal centre, for example the typically observed square-planar rhodium(I) *cf.* octahedral rhodium(III) species.

6.2.6 Indirect Detection Methods

Though high-field spectrometers are occasionally able to directly detect nuclei like ^{103}Rh, the main method of detection has become indirect. Indirect detection, in the same way a HSQC or HMBC experiment would, utilises coupled nuclei with high gyromagnetic ratios and receptivity (such as ^{1}H, ^{19}F or ^{31}P) to enhance the signal of the low gyromagnetic nucleus, which for the purpose of this work are ^{103}Rh and ^{13}C. There are two available pathways that utilise a sensitive nucleus; enhancement of the signal thorough polarisation transfer (an INEPT pulse sequence, or Insensitive Nuclei Enhanced by Polarization Transfer), or through a back-and-forth INEPT pulse sequence that allows for indirect detection in the dimension of the more sensitive nucleus, which is more commonly known as HMQC NMR (Heteronuclear Multiple Quantum Coherence).

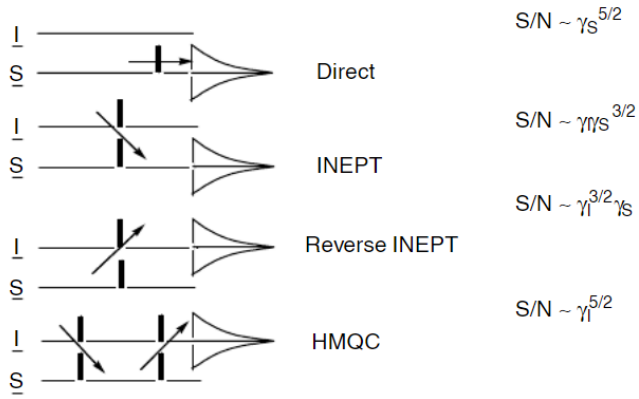

Figure 6.6: (taken from Elsevier[311]) (left) Basic pulse sequence representations for INEPT and HMQC NMR experiments. (right) The respective signal to noise ratios based on sensitivity (γ) (I = high γ nucleus, S = low γ nucleus). Note: The black blocks in the pulse sequences represent a 90° pulse for the respective nuclei

As **Figure 6.6** shows, utilising the nucleus with high sensitivity has a profound effect on the signal to noise ration of the nucleus with low sensitivity, with the HMQC pulse sequence being reliant on only the more sensitive nucleus. Polarisation transfer from ^{1}H to ^{103}Rh can increase enhancement 32-fold for an INEPT pulse sequence, and in theory 5680-fold using a HMQC NMR

experiment. This is however a theoretical maximum enhancement, and in reality, the low gyromagnetic ratio for rhodium means that the overall enhancement can be particularly low. The general equation that represents a change in signal to noise using enhancement techniques can be described as follows (**Equation 6.3**).[312]

$$\frac{S}{N} \propto \gamma_{exc}\, \gamma_{obs}^{3/2}\, B_0^{3/2} [1 - \exp\left(-\frac{t}{T_1^{exc}}\right)]$$

Equation 6.3: Signal to noise enhancement based on relaxation time (T_1), NMR field strength (B_0), and the sensitivity of the direct and indirect nuclei (γ) (exc = excited nuclei, obs = observed nuclei)

With an increase in magnetic field strength and sensitivity of the coupled nucleus, the signal to noise undergoes its greatest enhancement. What makes this enhancement effect so profound is the T_1, or relaxation time, is that of the excited nucleus, not the one being observed. To put it into context, the HMQC experiments between ^{1}H and ^{103}Rh are largely reliant on the sensitivity and relaxation time of ^{1}H, not ^{103}Rh, which overcomes two rather large obstacles.

^{31}P-^{103}Rh NMR

Though early developments of two-dimensional ^{103}Rh NMR was based on employing the ^{1}H nuclei,[313] the advantage in using an alternative nucleus of high sensitivity is that nucleus is not restricted to ^{1}H. Although two-dimensional NMR spectra such as ^{1}H-^{103}Rh HMQC and para hydrogen induced polarisation (PHIP) enhancement have proven extremely useful for indirect detection, hydrogen itself has noticeable shortcomings in this respect. The presence of a hydride ligand represents the ideal situation, with a large $^{1}J_{RhH}$ and strong coupling allowing for easy polarisation transfer. However, hydride ligands are relatively uncommon, and often thermodynamically unfavourable for coordination. In addition, relying on hydrogens that branch off ancillary ligands reduces the INEPT effect on the metal, as the $^{n}J_{RhH}$ drops off dramatically with increased values of n and the delay for polarization transfer can lead to excessive loss of magnetisation.[314]

Nucleus (% abundance)	γ^{13C}	Δ^{1H}	Δ^{31P}
^{103}Rh (100)	0.186	5680[a]	580[a]
^{109}Ag (48)	0.290	2143[a]	219
^{57}Fe (2)	0.00425	5329[a]	544
^{31}P (100)	37.7		
^{1}H (100)	5870		

Table 6.5: Comparison of selected transition metal enhancement using INEPT pulse sequences with both ^{1}H and ^{31}P. Note: γ^{13C} corresponds to the relative receptivity of the nucleus in comparison to ^{13}C. $\Delta^{1H/31P}$ is the enhancement factor theoretically possible for detection. [a] taken from [314, 315]

It is because of this that the ^{31}P nuclei has been explored for some time as an alternative source of polarisation enhancement. Phosphorus-31, like hydrogen, is a 100% abundant, spin ½ nucleus. Having a high value of γ, the enhancement factor for ^{31}P-^{103}Rh transfer can still reach acceptable levels of ~580, though it is theoretically still 10 times less than ^{1}H (see **Table 6.5**). What tips the scale in favour of using ^{31}P is its heavy presence in organometallic chemistry. Countless rhodium complexes, including almost all in this work, rely on phosphine ligands to stabilise the transition metal, and with large scalar coupling $^{1}J_{RhP}$ values (generally > 80 Hz), the tuning of pulse sequences and $T_{1,2}$ can be effectively achieved.

Phosphorus may present the added bonus of often having more than one equivalent nucleus on the metal complex, making polarization transfer more effective. Two-dimensional ^{31}P-TM pulse sequences have been successfully used to indirectly detect a number of difficult to detect transition metals, such as ^{103}Rh, ^{183}W, ^{61}Ni, and even ^{57}Fe, which contains both low sensitivity and low abundance of a spin-active nuclei.[314]

Complex	δ^{103}Rh
[Rh^{I}**Cl**(PPh$_3$)$_3$]	-1291
[Rh^{I}**Br**(PPh$_3$)$_3$]	-1230
[Rh^{I}**I**(PPh$_3$)$_3$]	-1104
[Rh^{I}**(CO)Cl**(PPh$_3$)$_3$]	-1003
[Rh^{III}**Cl$_3$**(PPh$_3$)$_3$]	-4146
[Rh^{III}**Br$_3$**(PPh$_3$)$_3$]	-3709
[Rh$_2^{III}$**Cl$_6$**(PPh$_3$)$_4$]	-4354

Table 6.6: Data (taken from [316]) of ^{31}P-^{103}Rh HMQC NMR environments for various rhodium(I) and (III) phosphine complexes.

Two-dimensional enhancement utilising the ^{31}P nucleus actually began prior to the direct detection of ^{103}Rh. In 1969 Brown and Green examined a range of known rhodium(I) and (III) phosphine complexes related to Wilkinson's Catalyst, **[RhCl(PPh$_3$)$_3$]**.[316] The rhodium resonances were all identified using indirect detection, and the resonances provided in **Table 6.6** show the strong correlations between minor changes in the ligand field and location of the ^{103}Rh resonance in the NMR spectrum. Once again, the spin-orbit coupling of the halide has a strong effect on the chemical shift, with chloride ligands leading to the lowest field shifts.

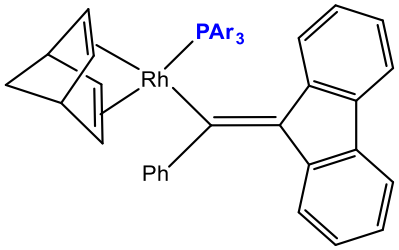

Ar = 4-FC_6H_4 — δ ^{103}Rh = -7862

Ar = 4-$(CF_3)C_6H_4$ — δ ^{103}Rh = -7870

Ar = 3,5-$(CF_3)_2C_6H_3$ — δ ^{103}Rh = -7861

Figure 6.7: ^{103}Rh chemical shifts of three rhodium phenylvinylfluorenyl complexes

More recent work again utilised the comparatively rapid acquisition of ^{103}Rh NMR data using indirect ^{31}P-^{103}Rh HMQC NMR. Investigating the stereospecific polymerisation of phenylacetylene, three rhodium-fluorene complexes were synthesised with the generic formula **[Rh(NBD)(CPh=Fluorene)(PAr$_3$)]** (Ar = C_6H_4F, C_6H_4-CF_3, C_6H_3-$(CF_3)_2$ – **Figure 6.7**).[317] It was found using a combination of direct and indirect methods that the ^{103}Rh environments for the three complexes all fell within ~10 ppm of each other (-7861, -7862, -7870 ppm). This close chemical shift range implies that the alteration of the fluorine group on the phosphine ligand has an almost negligible effect on the electronic properties of the rhodium centre. This was confirmed experimentally, as all three rhodium catalysts gave similar values for the *cis* content, dispersity, and molecular weights for the synthesised polymers. The use of indirect methods to detect the ^{103}Rh resonances once again demonstrated utility in understanding the chemistry that the rhodium complexes mediate.

6.2.7 Rationale for this Chapter

The work presented in this coming chapter will focus on a variety of multi-dimensional NMR studies on μ-carbido complexes. Notably, the success with the two-dimensional ^{31}P-^{13}C and three-dimensional ^{1}H-^{31}P-^{13}C correlation sequences to detect μ-carbido environments, in addition to the detection of the rhodium chemical shifts through two-dimensional ^{31}P-^{103}Rh HMQC NMR. The work in this chapter also provides alternative means of addressing the previous issues associated with ^{13}C labelling. The insights gathered on the chemical environments and couplings of Class A μ-carbido complexes and its relation to their metal environment are the first of their kind.

6.3 RESULTS AND DISCUSSION

6.3.1 μ-carbido Paramagnetic Deshielding

Paramagnetic Deshielding of Allenes

Before examining the deshielding of the linear μ-carbido complexes, comparison to the organic allene system is instructive. In an identical manner to the comparison of alkenes and carbene complexes by Eisenstein and co-workers presented earlier, the more complicated bonding model of the μ-carbido complexes might be expected to show relatable orbital transitions when compared to the allene species.

The shielding of carbon nuclei in allenes and higher cumulenes were studied in 1999 by Zilm and Cheeseman.[318] Examining the parent allene, the central quaternary carbon exhibits a significantly lower field shift than those of the termini, which was attributed to a stronger paramagnetic deshielding across all directional vectors (δ_P = -288 for $=CH_2$ and -715 for =C=). For the central carbon, the molecular orbital analysis revealed that three occupied MOs were responsible for the deshielding effect. The largest contribution came from the in-phase σ^b orbital, which consists of overlapping p_z [xlix]orbitals of the three carbon atoms (**Figure 6.8**). This occupied σ^b orbital was calculated to couple with the two degenerate C=C=C π^* virtual orbitals ($\sigma \rightarrow \pi^*$ transition). Because the π^* bonding system along each axis involves minimal overlap with one terminal carbon *p* orbital, the deshielding effect is most pronounced for the central carbon.

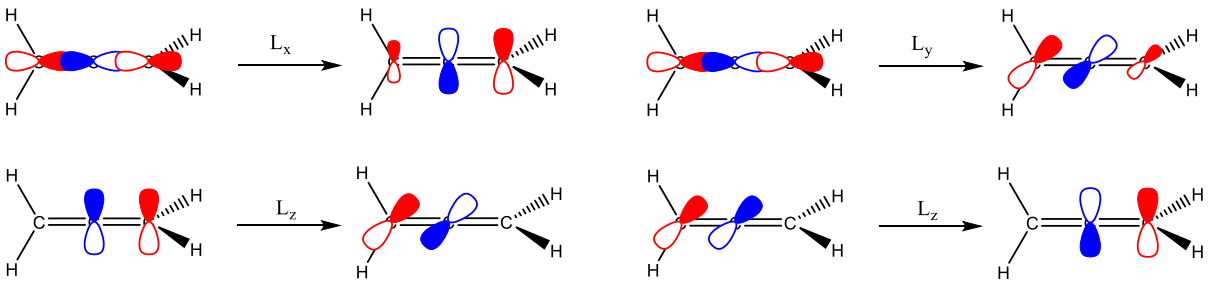

Figure 6.8: Calculated orbital transitions for the allene system[l]

[xlix] The allene spine is denoted as the *z*-axis

[l] Though the π^* and π^b molecular orbitals display evidence of a helical coarctate, the orbitals presented here are as described by Zilm and Cheeseman in their study.

The second orbital coupling of relevance is the $\pi \rightarrow \pi^*$ transitions, and there are two degenerate couplings present due to the spacial arrangement of the allene. This spacial degeneracy of the π-system is the difference between examining the allene and alkene system. Although the two π-bonds are energetically degenerate, they are spatially non-degenerate. This non-degeneracy increases the paramagnetic deshielding effect of the central carbon. Unlike the alkene compounds, the virtual orbitals of relevance do not include the σ^b orbital. The primary component to the deshielding of the allene central carbon is the $\sigma \rightarrow \pi^*$ transition.

μ-carbido Paramagnetic Shielding Tensors

In order to properly analyse the chemical shift breakdown of the μ-carbido ligand, natural chemical shift and shielding tensor calculations were performed by Hugo MacDermott-Opeskin at the ANU. Theoretical calculations were performed on two μ-carbido complexes, D_{2d}-**[Rh$_2$(μ-C)Cl$_2$(PPh$_3$)$_4$]** and D_{2h}-**[Rh$_2$(μ-C)Cl$_2$(μ-dppm)$_2$]**. Scalar Relativistic (SR) DFT calculations returned chemical shifts of 504.5 and 484.5 ppm for the two complexes respectively, which is slightly downfield of their experimentally determined chemical shifts (424.4 and 411.8, respectively). The agreement of the ^{13}C chemical shifts was seen the be lower when analysing the selenocarbonyl compounds in **Chapter 4**, even though the calculated ^{77}Se and ^{31}P chemical shifts closely matched experimentally derived data.

Though DFT methods have proven to be an attractive basis for quantum chemical calculations of heavier elements, the second and third row transition metals also contain significant relativistic effects.[319] In order to properly account for these relativistic effects (such as spin orbit coupling), a popular inclusion is an effective core potential (ECP), which implicitly treats the core electrons as a pseudopotential and can be adjusted to account for scalar relativistic (SR) effects. SR-DFT methods are routinely used in theoretical modelling of transition metal species.[320]

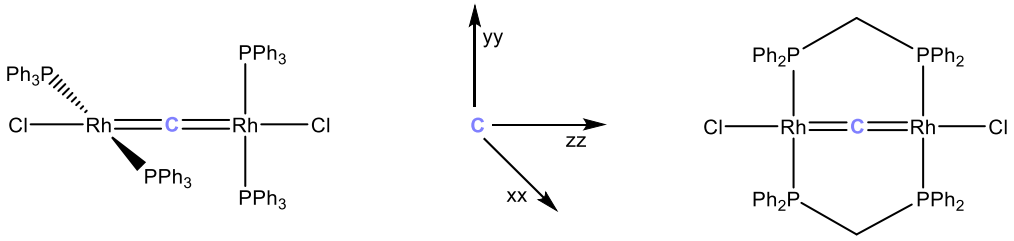

Figure 6.9: Directional tensors for **[Rh$_2$(μ-C)Cl$_2$(PPh$_3$)$_4$]** and **[Rh$_2$(μ-C)Cl$_2$(μ-dppm)$_2$]**

The anisotropic chemical environment of the carbido nucleus means that the three components that constitute the isotropic chemical shift are markedly distinct. Examining the shielding tensors of the μ-carbido atom, similarities to allene chemistry appear. As expected, the diamagnetic shielding tensor is approximately equal for both complexes and is invariant across all three directional vectors since filled sub-valence shells have isotropic electronic distributions. The paramagnetic shielding tells a different story that intimately reflects subtleties in the valence/frontier orbitals. For the parent D_{2d} μ-carbido species, **$[Rh_2(\mu\text{-}C)Cl_2(PPh_3)_4]$**, the paramagnetic deshielding is smallest along the plane of the Rh=C=Rh bond (σ_{zz} in **Figure 6.9**, δ_P = -75.39), but has dominant and equal contributions along the planes parallel with the two orthogonal P-Rh-P vectors (σ_{xx} and σ_{yy} in **Figure 6.9**). The value of these shifts ($\sigma_{yy} = \sigma_{xx}$ = -964) is a whole order of magnitude larger than σ_{zz} (**Table 6.7**). The deshielding effect for allenes is similarly dominant orthogonal to the C=C=C axis, though not by as significant a margin.

Complex	σ_D	σ_P	σ_{zz}	σ_{yy}	σ_{xx}
$[Rh_2(\mu\text{-}C)Cl_2(PPh_3)_4]$	351.7	-668.0	-75.39	-963.79	-964.70
$[Rh_2(\mu\text{-}C)Cl_2(\mu\text{-}dppm)_2]$	312.8	-608.9	-58.86	-737.27	-1030.71

Table 6.7: SR DFT calculated shielding tensors for μ-carbido complexes

The coplanar (D_{2h}) species **$[Rh_2(\mu\text{-}C)Cl_2(\mu\text{-}dppm)_2]$** exhibits similar behaviour. The deshielding present along the Rh=C-Rh axis is again minor in comparison to that with respect to the orthogonal axes. However, because the rhodium coordination spheres are coplanar, there is a distinction between the deshielding values along the P-Rh-P plane (σ_{yy} = -737.27) and orthogonal to it (σ_{xx} = -1030.71). This is due to the molecular orbitals being non-degenerate for the D_{2h} symmetric $P_2RhCRhP_2$ core. The total paramagnetic deshielding values are comparable at -668.0 and -608.9 for PPh_3 and μ-dppm respectively, which correlates with the lower field shift in the ^{13}C NMR spectrum for the former.

Molecular Orbital Coupling Analysis

Breaking down the paramagnetic deshielding tensor into their orbital coupling components, it was discovered that the orbitals of relevance were, in terms of topology,

surprisingly close to the allene system. The major components of the deshielding couplings were centred around a single occupied orbital for **[Rh_2(μ-C)Cl_2(PPh_3)$_4$]** and two for **[Rh_2(μ-C)Cl_2(μ-dppm)$_2$]**. All three orbitals of relevance are heavily associated with the σ^b interaction of the Rh-C-Rh linkage, consisting of the in-plane carbon *p*-orbital interacting in phase with two rhodium *d*-orbitals (**Figure 6.10**).

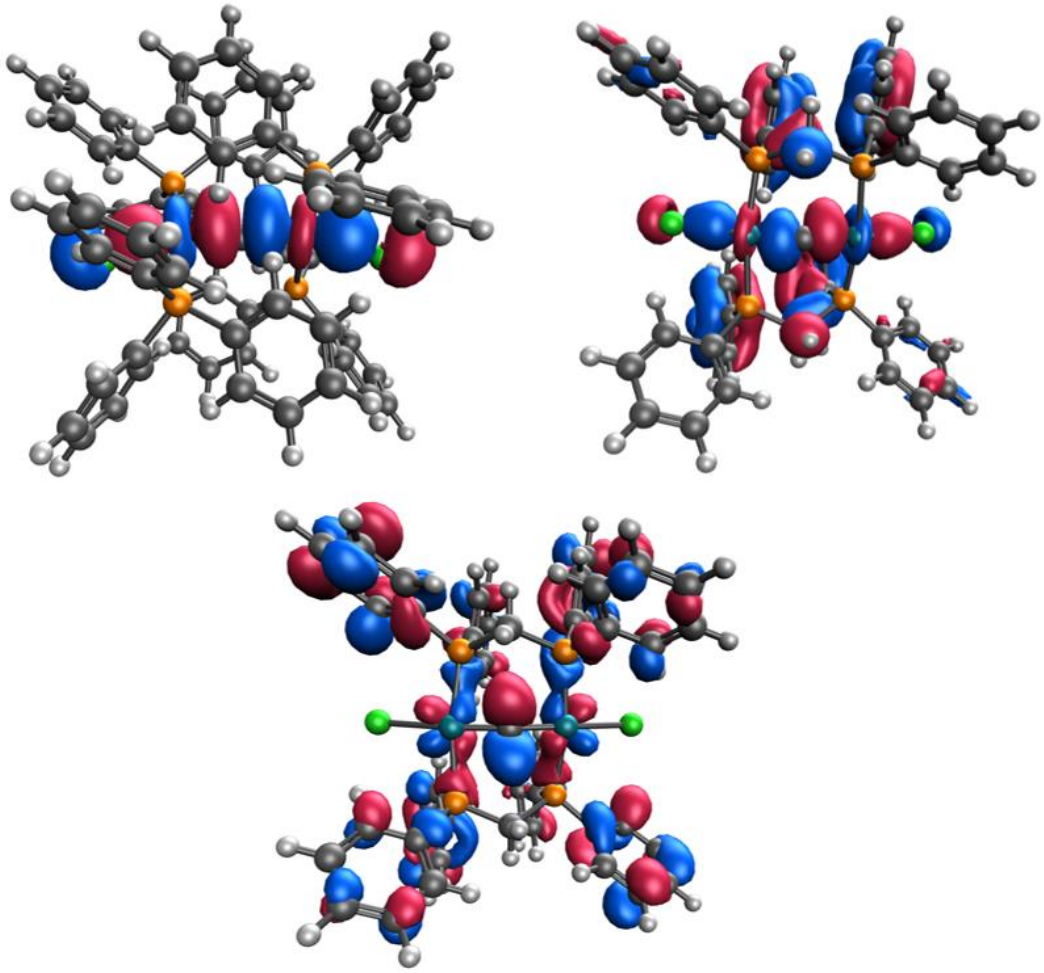

Figure 6.10: (top) Rh-C-Rh occupied σ^b molecular orbital of **[Rh_2(μ-C)Cl_2(PPh_3)$_4$]** (left) and **[Rh_2(μ-C)Cl_2(μ-dppm)$_2$]*** (right). NB*: only one of two MOs displayed

(bottom) Rh-C-Rh virtual π* molecular orbital for **[Rh_2(μ-C)Cl_2(μ-dppm)$_2$]**

The σ^b orbitals are calculated to couple with multiple virtual orbitals, each leading to a significant contribution to the deshielding tensor. Plotting the virtual orbitals of relevance, the C_1

symmetry of the gas-phase complexes results in minor changes to the aromatic rings occupancies, but all virtual orbitals contain distinct Rh=C=Rh π* character (**Table 6.8**).

Complex	Occupied Orbital (symmetry)	Virtual Orbital (symmetry)	Shielding Component
$[Rh_2(\mu\text{-}C)Cl_2(PPh_3)_4]$	265 (σ^b)	341 (π*)	-52.74
		343 (π*)	-49.26
		362 (π*)	-36.79
$[Rh_2(\mu\text{-}C)Cl_2(\mu\text{-}dppm)_2]$	208 (σ^b)	267 (π*)	-37.42
		280 (π*)	-36.75
		271 (π*)	-17.77
	210 (σ^b)	267 (π*)	-20.58
		280 (π*)	-17.05

Table 6.8: Major components to the deshielding coupling orbitals and values for **$[Rh_2(\mu\text{-}C)Cl_2(PPh_3)_4]$** and **$[Rh_2(\mu\text{-}C)Cl_2(\mu\text{-}dppm)_2]$**

As **Table 6.8** highlights, the primary couplings behind the μ-carbido deshielding are all centred around this $\sigma^b \rightarrow \pi^*$ transition. The two non-degenerate σ^b orbitals of **$[Rh_2(\mu\text{-}C)Cl_2(\mu\text{-}dppm)_2]$** both display coupling to the same virtual orbitals, though with different magnitudes due to the differences in respective energy levels.

In order to properly compare the energy levels of this σ to π* coupling, the parent allene species ($H_2C=C=CH_2$) and a simplified carbido complex **$[Rh_2(\mu\text{-}C)Cl_2(PMe_3)_4]$** were both analysed using DFT studies to identical levels of theory (ωB97X-D / 6-31G*). Examining the orbitals of interest, it can be clearly seen that the inclusion of the transition metals greatly reduces the energy gap upon which this orbital coupling inversely depends (ΔE^{-1}). As highlighted in **Figure 6.11**, the energy gap is significantly reduced in the μ-carbido complex than the allene. Though a simplified example, this reinforces the SR-DFT calculations and supports the exceptional downfield ^{13}C shifts seen in the NMR spectra.

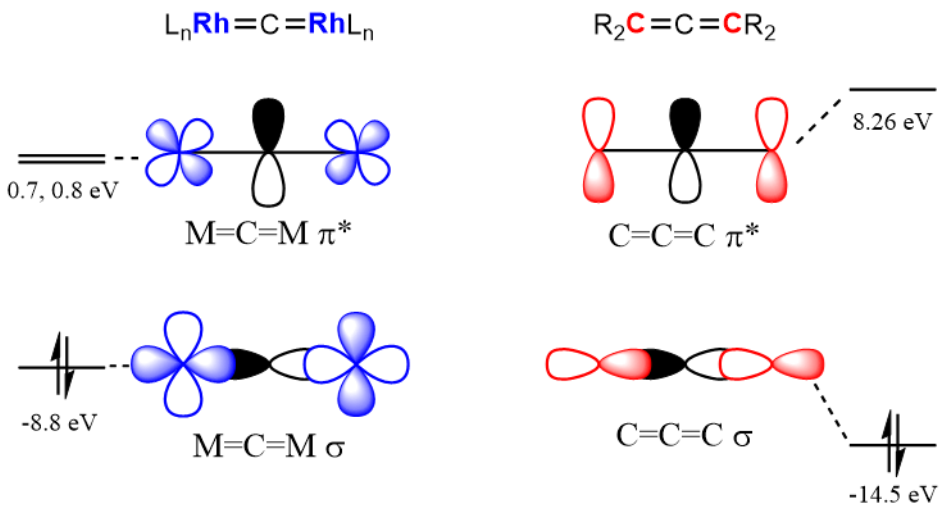

Figure 6.11: DFT calculated MOs of relevance for the $\sigma^{b}\rightarrow\pi^{*}$ coupling of D_{2d}-**[Rh$_2$(μ-C)Cl$_2$(PMe$_3$)$_4$]** (left) and allene (right), and their associated energy levels (DFT: ωB97X-D / 6-31G*)

6.3.2 Optimisation of ^{13}C-Labelling

Before multidimensional NMR studies were explored in detail, the immediate challenge in need of addressing related to the problems with ^{13}C enrichment. The issue that persisted with ^{13}C enrichment is the expense and time delay, exacerbated by CoVid-19 disruptions, in acquiring $^{13}CS_2$ and the use of it as a solvent in Wilkinson's original synthetic protocol (**Scheme 6.3**). Thus despite the eight-fold increase in the cost of rhodium during this research peaking at AU$1350/g, the precious metal was not as it transpired the cost-limiting factor.

Following the labelling experiments used in earlier work, it was considered essential to develop a refined synthesis for the rhodium thiocarbonyl complex **[RhCl(CS)(PPh$_3$)$_2$]** that removed the reliance of carbon disulfide as a solvent. If the carbon disulfide could be used instead as a reagent (albeit presumably in modest excess), the economy of the thiocarbonyl labelling could be significantly increased allowing for improved access to the requisite enriched isotopomer.

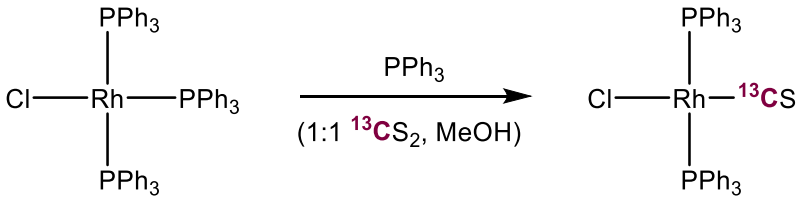

Scheme 6.3: Original synthesis for **[RhCl(^{13}CS)(PPh$_3$)$_2$]**

To replace volatile carbon disulfide (b.p. 46.3 °C[li]) as a solvent, the replacement would ideally also be aprotic, and have a low polarity index to keep the overall polarity of the mixture similar.[lii] Though more polar than carbon disulfide, dichloromethane appeared to be the best candidate. Due to the decreased solubility of Wilkinson's Catalyst in dichloromethane, the 1:1 solution of CH_2Cl_2/methanol was unable to completely dissolve the solid. However, addition of 1 equivalent of carbon disulfide as a reagent slowly turns the maroon solution green as the coordination of CS_2 to the rhodium takes place, indicating that the first half of the reaction was seemingly successful. The next main difference encountered is during the heating process, which had to be extended from one hour using CS_2 as a solvent to an overnight reaction. One surprising benefit in utilising dichloromethane as the solvent was that upon addition of ethanol to the orange/brown solution, the thiocarbonyl complex immediately begins precipitating from solution and can be cleanly isolated upon concentration under vacuum, due to the lower solubility of the thiocarbonyl species in dichloromethane.

What emerged from this process is the 1:1 solvent ratio between dichloromethane and methanol allows for the addition of a *single* equivalent of $^{13}CS_2$ (**Scheme 6.4**). Because the carbon disulfide is now being used as a reagent, a 0.5 mL aliquot of $^{13}CS_2$ could be used in combination with *ca* three grams of Wilkinson's catalyst rather than the milligram scale conducted previously.

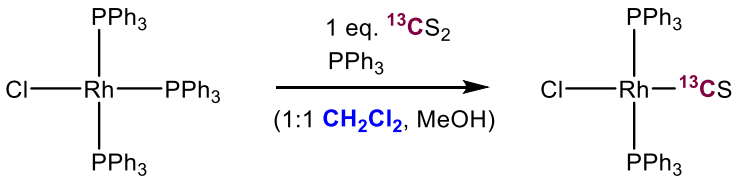

Scheme 6.4: Modified synthesis for **[RhCl(^{13}CS)(PPh$_3$)$_2$]** using dichloromethane as solvent

Because of the high yield of the isotopologue, many of the key complexes from **Chapters 1-5** were successfully enriched with ^{13}C. The ^{13}C chemical shifts for enriched complexes are

[li] *ca* 44 °C corrected for altitude of Canberra (570 m).

[lii] Ionisation of the Rh–Cl bond in highly polar media allow for the formation of phosphoniodithiocarboxylate complexes which needs to be discouraged.[321]

summarised in **Table 6.9**. In all cases, a 1:3 dilution of 100% enriched **[RhCl(^{13}CS)(PPh$_3$)$_2$]** with natural abundance **[RhCl(CS)(PPh$_3$)$_2$]** afforded a material that was 25% enriched, thereby still allowing for a 25-fold increase in ^{13}C NMR sensitivity.

Complex	δ ^{13}C	$^{1}J_{RhC}$	$^{2}J_{PC}$
[Rh$_2$(μ-^{13}C)Cl$_2$(μ-dppm)$_2$]	412.0	40	14
[Rh$_2$(μ-^{13}C)Cl$_2$(μ-dppf)$_2$][liii]	418.6	-	-
[Rh$_2$(μ-^{13}C)Cl$_4$(μ-dppf)$_2$]	465.9	59	-
[Rh$_2$(μ-^{13}CCl)(μ-Cl)Cl$_4$(μ-dppm)$_2$]	410.2	-	-
[Rh$_2$(μ-^{13}CS)Cl$_2$(μ-dppm)$_2$]	322.1	38	7
[Rh$_2$(μ-^{13}CSe)Cl$_2$(μ-dppm)$_2$]	341.3	-	-
[Rh$_2$(μ-^{13}C)(μ-DMAD)Cl$_2$(μ-dppm)$_2$]	563.0	30	9
[Rh$_2$(μ-^{13}CCl)(μ-DMAD)Cl$_2$(μ-dppm)$_2$]Cl	395.3	33	6
[Rh$_2$(μ-^{13}CSe)(μ-DMAD)Cl$_2$(μ-dppm)$_2$]	318.3	28	8
[Rh$_2$(μ-^{13}CAuCl)(μ-DMAD)Cl$_2$(μ-dppm)$_2$]	471.1	20	6
[Rh$_2$(η$_2$-^{13}CC$_6$H$_4$)(Ph)Cl$_3$(μ-dppm)$_2$]	394.9	36	-
[Rh$_2$(η$_2$-^{13}C-C$_3$Ph$_3$)Cl$_2$(μ-dppm)$_2$]PF$_6$	411.8	-	-

Table 6.9: ^{13}C NMR data derived from enriched complexes. Note: due to the proximity and broadness of the peaks, some couplings were not adequately resolved

The chemical shifts all appear in the expected downfield environment due to the strong paramagnetic deshielding caused by the by the unsaturated Rh$_2$C systems. Though not all of the coupling values could be abstracted from the NMR resonances, there exhibits a clear trend that the high coordination rhodium complexes possess a smaller $^{1}J_{RhC}$ coupling, due to the reduced *s*-character of the five- (sp^3d) and six-coordinate (sp^3d^2) rhodium centres compared to their square planar (sp^2d) counterparts. The $^{2}J_{PC}$ coupling remains within a few Hz across all complexes, regardless of coordination number and ligand set.

The use of ^{13}C enrichment as a "necessary evil", proved extremely useful in the detection of some rather significant μ-carbido and chalcocarbonyl complex chemical shifts.

[liii]The presumed onset of fluxionality for the dppf ligands resulted in broadening of the ^{31}P and ^{13}C resonances obscuring fine structure.

6.3.3 2D and 3D ^{31}P-^{13}C Correlation NMR

Although the ^{13}C enrichment was successful and rewarding in the detection of multiple new μ-carbido environments, the reliance upon $^{13}CS_2$, which is both expensive and on occasion time-critical to transport to Australia, called for a more effective long-term solution. Because of this, using indirect detection became increasingly attractive.

There were two solutions that were considered (**Figure 6.12**). The first was to attempt a relatively simple 2D HMQC NMR experiment, but instead of using the somewhat distal ^{1}H nuclei as the direct detection nuclei, the ^{31}P nuclei of the ancillary phosphine ligands seemed. This strategy would exploit both a strong, reasonably sharp signal in the ^{31}P 1D NMR, and an approximation of the $^{2}J_{PC}$ coupling constant(s), which could be obtained from this work and other ^{13}C labelled studies performed previously. The ^{31}P-^{13}C HMQC pulse sequence is a well-defined NMR tool, though only unpublished results from Berger have applied this NMR tool to an inorganic system.[322]

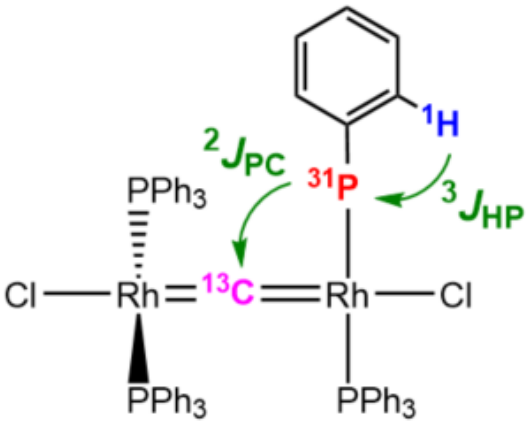

Figure 6.12: Visualization of the ^{1}H and ^{31}P nuclei used for indirect ^{13}C detection

The second method is somewhat more intricate, and in essence is a three-dimensional ^{1}H-^{31}P-^{13}C NMR relay (3D HPC). The principle is the same as the HMQC NMR presented above, except the direct detection takes place in the ^{1}H dimension, with magnetisation sequentially transferred to the ^{31}P and ^{13}C and back. Though a significantly longer experiment, utilising the many (16-24) *ortho*-phenyl hydrogen environments on the phosphine ligands might be expected to provide an alternative detection method.

3D ^{1}H-^{31}P-^{13}C NMR

The 3D HPC pulse sequence was first optimised for the thiocarbonyl precursor **[RhCl(CS)(PPh$_3$)$_2$]**, as the ^{13}C resonance (276.5 ppm) and coupling $^{2}J_{PC}$ = 67 Hz) are known and the complex has relatively high solubility in chlorinated solvents, giving the required high concentrations to run the experiments. Using the strongest magnetic field instrument available, a Bruker 800 NMR, the phosphorus doublet detected in the 1D ^{31}P{^{1}H} NMR spectra for both complexes had a signal to noise ratio of 32:1 after only a single scan, boding well for the identification of correlation peaks in the 2D spectra.

A correlation was found between the phenyl hydrogens (δ_H of 7.79) and two carbon peaks centred on 276.5 ppm (**Figure 6.13**). The thiocarbonyl carbon of **[RhCl(^{13}CS)(PPh$_3$)$_2$]** is detected in the 1D ^{13}C{^{1}H} NMR spectra at 276.5 ppm, a perfect match for the environment.

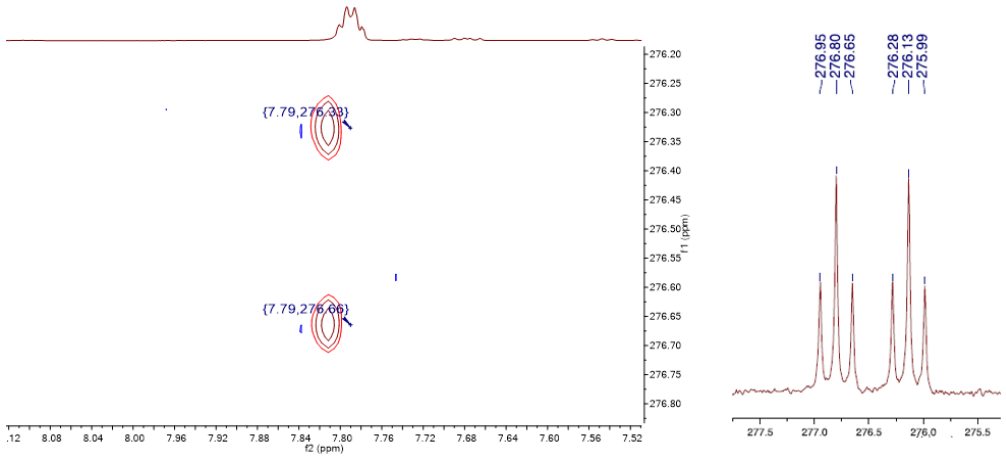

Figure 6.13: (left) Extract of the 3D ^{1}H-^{31}P-^{13}C NMR spectrum of **[Rh(CS)Cl(PPh$_3$)$_2$]** focussing on the thiocarbonyl resonance. (right) Extract of the conventional 1D ^{13}C NMR spectrum of **[Rh(^{13}CS)Cl(PPh$_3$)$_2$]**

The cross peak in the ^{13}C dimension appears as a doublet of J = 66 Hz. The ^{13}C enriched spectra of **[Rh(^{13}CS)Cl(PPh$_3$)$_2$]** displays the $^{1}J_{RhC}$ coupling constant of 67 Hz. The accuracy of the multidimensional study compared to ^{13}C enrichment data supports the use of the 3D NMR protocol.

Although the 3D HPC NMR was successful in using the phenyl hydrogens to indirectly detect the quaternary carbon atom, the nature of the longer and more complicated pulse sequence meant that the acquisition time was considerably protracted (>>24 hours). In order to find the

ideal NMR method, a shorter one was examined next, and this pulse sequence was never trialled on a μ-carbido species.

2D ^{31}P-^{13}C HMQC NMR

In an effort to reduce acquisition time, the shorter ^{31}P-^{13}C HMQC was tested. By removing the ^{1}H dimension and relying on strong ^{31}P signals, the 2D NMR would be substantially faster and hopefully achieve satisfactory high signal to noise.

The 2D HMQC NMR was tested on the carbido complex **[Rh$_2$(μ-C)Cl$_2$(PPh$_3$)$_4$]**, as it contains four magnetically equivalent ^{31}P nuclei. As expected, the 2D NMR acquisition was substantially faster, with cross peak clearly distinguishable and resolved after only five hours (**Figure 6.14** below). In comparison to acquiring a 1D ^{13}C NMR spectra on expensive ^{13}C enriched samples over 12-18 hours, the 2D NMR method is both time and cost effective. The bridging cumulenic carbido resonance for **[Rh$_2$(μ-^{13}C)Cl$_2$(PPh$_3$)$_4$]** was located at 424.4 ppm in the 1D ^{13}C{^{1}H} NMR spectra, and is extremely close in the 2D NMR spectra, appearing at 424.6 ppm.

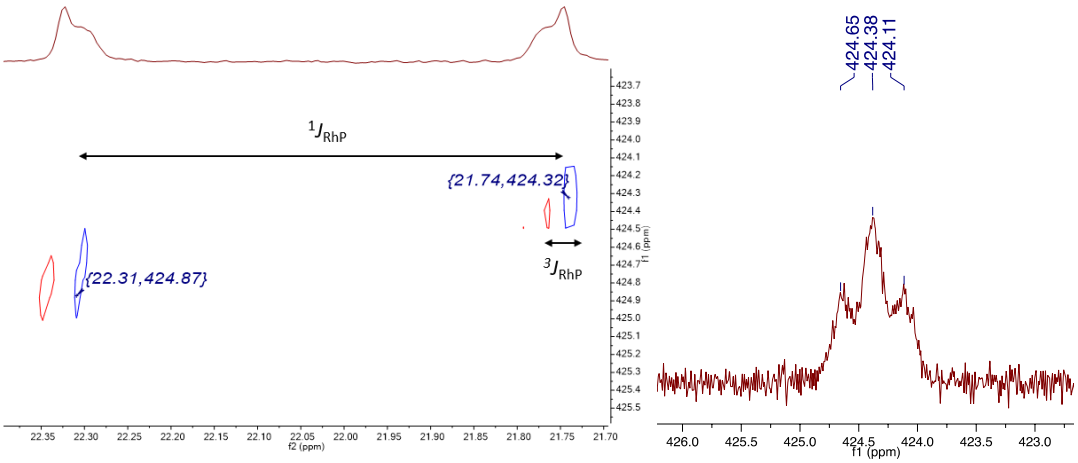

Figure 6.14: (left) Extract of 2D ^{31}P-^{13}C NMR spectrum of **[Rh$_2$(μ-C)Cl$_2$(PPh$_3$)$_4$]**, focussing on the carbido correlation peak. (right) 1D ^{13}C{^{1}H} NMR spectrum extract of enriched **[Rh$_2$(μ-^{13}C)Cl$_2$(PPh$_3$)$_4$]**

The appearance of the ^{13}C correlation peaks in the 2D NMR is considerably more complicated. The direct detection in the ^{31}P dimension means the $^{1}J_{RhP}$ and $^{1}J_{RhC}$ splitting are not removed. Interrogating the correlation peaks, the appearance is that of a doublet of doublets. The doublet of doublets aligns with the environment seen in the 1D ^{31}P NMR and correspond quite

well to the experimental $^{1}J_{RhP}$ and $^{3}J_{RhP}$ values. One of the intricacies of the HMQC NMR spectrum was the dispersion of cross peaks along the ^{13}C dimension. The spacing of the cross peaks along the ^{31}P dimension matched cleanly with the expected $^{1}J_{RhP}$ and $^{3}J_{RhP}$ values, however, the vertical coupling did not directly correspond directly to the obvious $^{1}J_{RhC}$ coupling. The *observed* coupling in the 2D spectrum was calculated to be approximately 85 Hz, which is double the value of the $^{1}J_{RhC}$ coupling of 43 Hz found through ^{13}C enrichment. This potentially provides a means to indirectly measure the $^{1}J_{RhC}$ coupling without the need of expensive ^{13}C enrichment.

Work continued on the coplanar species **$[Rh_2(\mu\text{-}C)Cl_2(dppm)_2]$** (**1**). One issue that emerged for **1** was a combination of broader peaks which are also further apart in the $^{31}P\{^{1}H\}$ NMR spectra. The ^{31}P-^{13}C HMQC spectrum could be acquired over a similar timeframe (*ca* 5 hours), during which correlation peaks centred at 411.7 ppm appeared. Once again, the chemical shift is reassuringly close to the chemical shift determined from the 1D $^{13}C\{^{1}H\}$ NMR of the enriched **1'** (412.0 ppm).

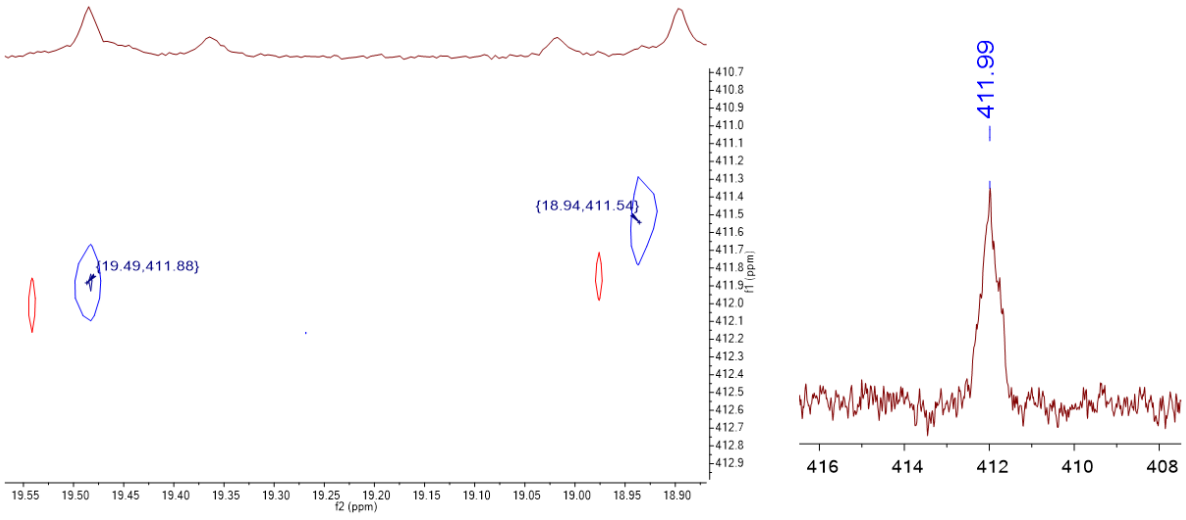

Figure 6.15: (left) 2D ^{31}P-^{13}C NMR extract of **1**. (right) $^{13}C\{^{1}H\}$ NMR extract of enriched **1'**

One difference that arose (**Figure 6.15**) is the lower signal to noise of the smaller cross peaks that correspond to the $^{3}J_{RhP}$ coupling, which is likely due to the broader signals leading to a lower signal to noise factor. Fortunately, the remaining two cross peaks are split along the ^{13}C dimension, and following the same process, the *observed* coupling can be calculated to be 79 Hz, which would give a $^{1}J_{RhC}$ value of *ca* 40 Hz. This again corresponds accurately with the value of 40 Hz obtained from ^{13}C enrichment studies. This coupling value is slightly smaller than the

orthogonal complex **[Rh$_2$(μ-C)Cl$_2$(PPh$_3$)$_4$]** ($^1J_{RhC}$ = 43 Hz), despite **1** containing larger $^{1,3}J_{RhP}$ couplings.

Attention then turned towards the remaining μ-carbido complexes that has not been subject to ^{13}C enrichment. The dcpe species **[Rh$_2$(μ-C)Cl$_2$(μ-dcpe)$_2$]** (**4**) retained excellent solubility in d^2-DCM, and the smaller value of $^3J_{RhP}$ meant that the four peaks are quite close together in the ^{31}P{^{1}H} NMR spectrum, providing good signal to noise. Attempts to detect the μ-carbido ligand utilising a ^{1}H-^{13}C HMBC sequence was unsuccessful. The ^{31}P-^{13}C HMQC NMR spectrum of **4** provided a strong correlation peak again after only a few hours. The ^{13}C resonance appeared at 415.1 ppm, which lies in an almost identical environment to **1** despite the presence of the cyclohexyl groups on the phosphine ligand.

The orthogonal dppp complex **[Rh$_2$(μ-C)Cl$_2$(μ-dppp)$_2$]** (**5**) was investigated next. If there was an angular dependence on the chemical shift of the bridging carbon resonance or associated scalar couplings in the NMR, it would be most diagnostically discriminating between this orthogonal complex and the coplanar complex **1**, as the ligand architectures are as close as possible. The correlation peak for the carbido nucleus was detected at a very similar field as expected to the previous complexes, appearing at 411.5 ppm in the ^{31}P-^{13}C HMQC spectrum (**Figure 6.16**). The difference of merely 3-4 ppm between the complexes **1**, **4** and **5** appears to support a negligible effect by the relative geometry of the rhodium centres on the chemical environment of the bridging carbon atom.

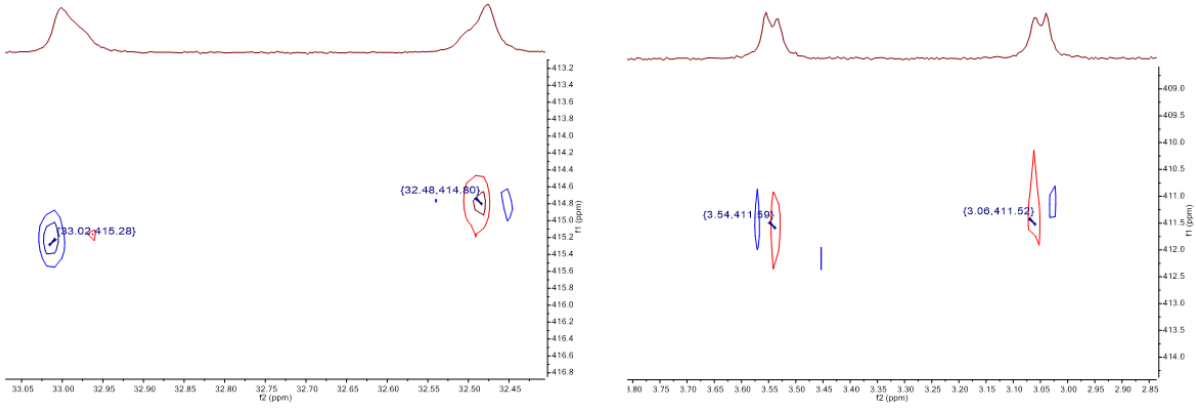

Figure 6.16: Extracts of the 2D ^{31}P-^{13}C HMQC NMR spectra of (left) **[Rh$_2$(μ-C)Cl$_2$(μ-dcpe)$_2$]** and (right) **[Rh$_2$(μ-C)Cl$_2$(μ-dppp)$_2$]**, focussing on the carbido cross peaks

The $^{1}J_{RhC}$ coupling constants could again be calculated from the dispersion of peaks along the ^{13}C dimension. This coupling in the dcpe species **4** was found to be 42 Hz, and in the dppp complex **5** was calculated to be 45 Hz using this method.

Complex	δ μ-C	P-Rh—Rh-P (°)	$^{1}J_{RhC}$ (Hz)	$^{1}J_{RhP}$
$[Rh_2(\mu\text{-}C)Cl_2(PPh_3)_4]$	424.4	90.09(2)	43	177
$[Rh_2(\mu\text{-}C)Cl_2(\mu\text{-}dppm)_2]$	412.0	2.95(6)	40	191
$[Rh_2(\mu\text{-}C)Cl_2(\mu\text{-}dcpe)_2]$	415.1	42.93(5)	42	172
$[Rh_2(\mu\text{-}C)Cl_2(\mu\text{-}dppp)_2]$	411.5	69.55(3)	45	161

Table 6.10: Comparison of key NMR coupling data for rhodium(I) μ-carbido complexes

Examining the calculated $^{1}J_{RhC}$ values, all fall within a 5 Hz range and correspond well to values calculated through ^{13}C enrichment studies (See **Chapter 1.2**). The coupling values are all larger than the corresponding chalcocarbonyl, halocarbyne and dimetallacarbene complexes, which reflects the higher % *s*-character of the four-coordinate rhodium. It is difficult to confidently assign a relationship between the relative geometries of the rhodium coordination spheres and the $^{1}J_{RhC}$ coupling (**Table 6.10**), though the coplanar species **1** does possesses a smaller value than the corresponding orthogonal complexes. This matches what has been noted experimentally, as there is seemingly no barrier needed to be overcome to install a bidentate phosphine ligand at any dihedral angle across the μ-carbido framework.

Limitations of ^{31}P-^{13}C HMQC NMR

Unfortunately, it was at this point that the current limitations of the 2D ^{31}P-^{13}C HMBC protocol were encountered. It had been clear so far that any decrease in the signal to noise ratio or increase in peak width required the acquisition of many more scans to achieve satisfactory correlation peak intensity. Whilst this issue had not been overly limiting for the complexes studied so far, the first problem was encountered with the bridging dppf species **6**. The free dppf molecule has quite a broad ^{31}P resonance in the 1D NMR spectra, and this characteristic is featured again in the metal bound complex. The broad signals (h.h.w. = 90 Hz) unfortunately resulted in a much lower signal to noise ratio, and accordingly no clear cross peaks were detected in the ^{31}P-^{13}C HMQC spectrum, even after an extended acquisition time (24 hrs). This feature of the dppf co-ligand also meant that the protocol failed for the tetrachloride species **$[Rh_2(\mu\text{-}C)Cl_4(\mu\text{-}dppf)_2]$**.

The broadness is presumed to be due to arrested or retarded inversion of the helical $Rh_2(\mu\text{-dppf})_2$ core and signal sharpening might be expected to attend heating or cooling to arrive at fast or slow exchange regimes, respectively.[liv] Whilst heating is generally an unattractive option for thermolabile organometallics, the alternative of cooling the sample, whilst in principle increasing signal/noise, introduces the second limiting factor, that of solubility.

One of the notable features of the μ^2-halocarbyne and dimetallacarbene complexes that have been made so far is their rather low solubility in any readily available NMR solvents (deuterated $CHCl_3$, CH_2Cl_2, MeCN, DMSO, …). Because of this, even saturated solutions of the complexes **18, 19** and **24** gave signals in the ^{31}P NMR spectra that were far too weak in terms of signal to noise. Again, the 2D ^{31}P-^{13}C HMQC NMR spectra were measured for all of these complexes for extended periods of time, and yet, no clear correlation peaks could be identified. These two caveats of the 2D ^{31}P-^{13}C HMQC NMR protocol although frustrating are completely reasonable and, in the future, may yield to either fine tuning of the pulse sequence or complexes.

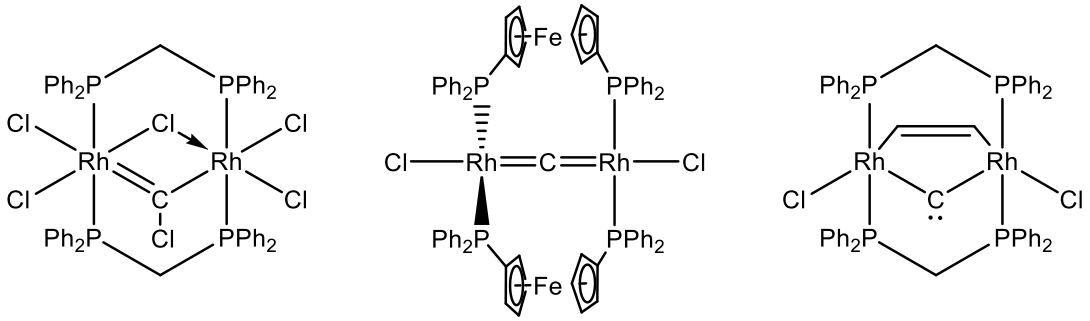

Figure 6.17: Selection of recalcitrant complexes (**6**, **18**, **19**, **23**, **24**) for ^{31}P-^{13}C HMQC NMR studies

Largely due to the significance of the μ_2-halocarbyne and metalla-heterocyclic carbene complexes, the ^{13}C chemical shifts were considered too valuable a piece of information to avoid resorting to ^{13}C labelling for their characterisation.

[liv] Given the high molecular weights, heating might also accelerate molecular tumbling with an attendant increase in T_2.

6.3.5 ^{103}Rh Detection

Following the successful detection of the μ-carbido ligand, it was mooted that a similar method might be implemented to detect the ^{103}Rh resonances. Though the ^{103}Rh nucleus is 100% abundant, the exceedingly large chemical shift range and low sensitivity make direct detection difficult.

Tuning a Bruker 800 MHz NMR for ^{103}Rh detection allowed for direct detection to be attempted. To pre-empt optimism, nothing was found. The extensive spectral width and typically narrow line widths meant that a composite of multiple constituent runs was required over smaller ranges, however, at no point in the experiments did anything resembling a genuine peak appear. Following the publication of the synthesis of Rhodium(I)-α-Phenylvinylfluorenyl complexes, the ^{103}Rh NMR specialist expertise of Dr Gareth Nealon at the University of Western Australia was highlighted.[317] The work in question was able to use a ^{31}P-^{103}Rh HMQC NMR experiment to indirectly detect the rhodium chemical shift. Because of the relatively close proximity by Australian standards of UWA (3,800 km), a collaboration was established, with provision of samples to Dr. Nealon for NMR analysis.

The first data related the key reactive complex **[Rh$_2$(μ-C)Cl$_2$(μ-dppm)$_2$]**. The two-dimension ^{31}P-^{103}Rh HMQC spectrum displayed a cluster of cross peaks correlating to the phosphorus resonance (**Figure 6.18**), which were centred on -7970.7 ppm in the ^{103}Rh dimension. The same environment could be directly detected by running a doubly decoupled ^{103}Rh{^{31}P}{^{1}H} experiment, with the singlet appearing at -7951.0 ppm. Though detectable, the direct approach was significantly longer and was aided by narrowing down the spectral width to the known area and would not be a pragmatic approach to detecting unknown environments.

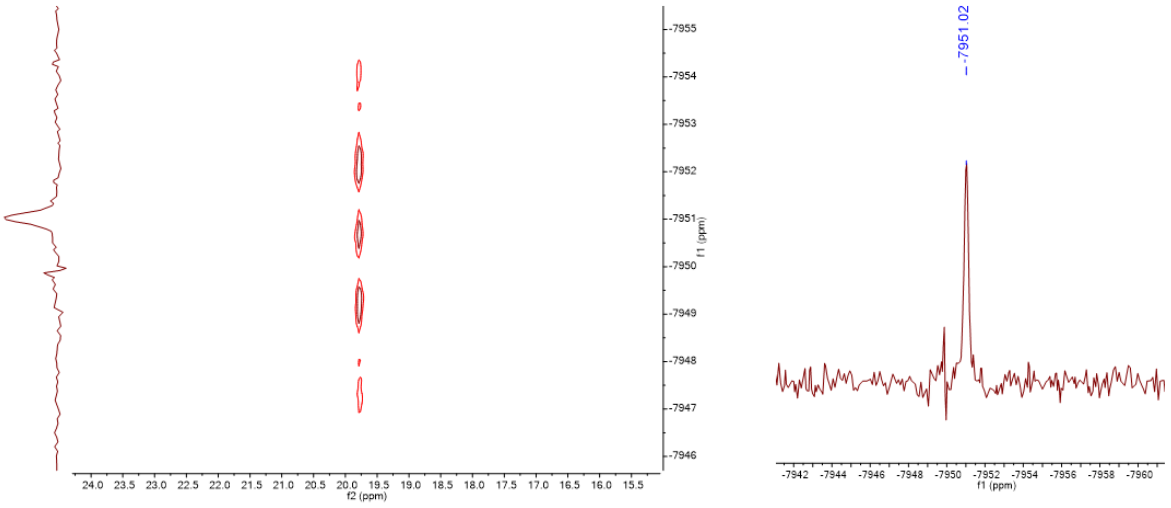

Figure 6.18: (left) Correlation peak of ^{31}P-^{103}Rh HMQC spectrum for **[Rh$_2$(μ-C)Cl$_2$(μ-dppm)$_2$]** (8 scans). (right) corresponding peak in the ^{103}Rh{^{31}P}{^{1}H} NMR spectrum (17255 scans)

The fine structure evident in the correlation peaks in the ^{31}P-^{103}Rh HMQC spectrum were unexpected, as peaks due to the $^{1}J_{RhP}$ and $^{3}J_{RhP}$ couplings should not appear in this experiment. It was considered that the cross peaks might come from isotopic distribution, however, the coupling value (28 Hz) is considerably larger than have been reported for $^{35/37}$Cl distribution and the presence of five peaks cannot be explained using this method.[323] Regardless, this presented the first example of a ^{103}Rh NMR chemical shift observation for a μ-carbido complex.

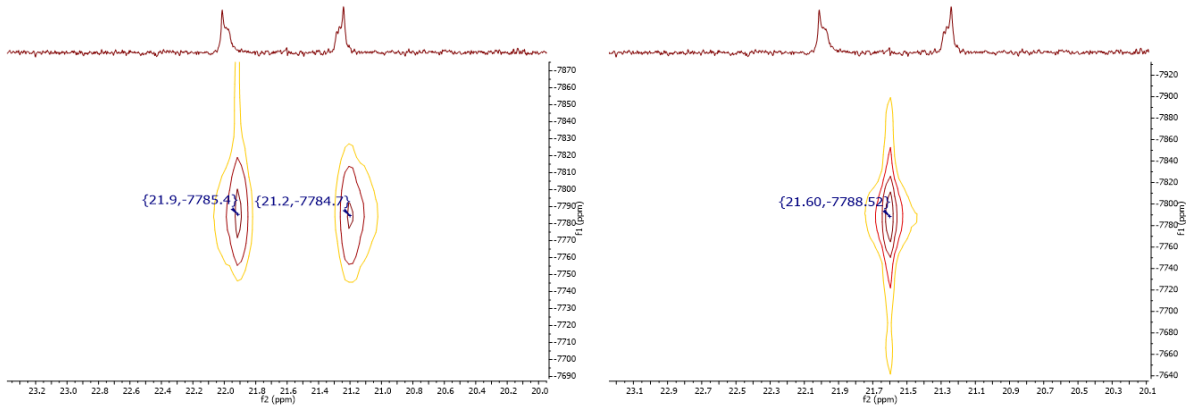

Figure 6.19: ^{31}P-^{103}Rh HMQC spectra of **[Rh$_2$(μ-C)Cl$_2$(PPh$_3$)$_4$]**, focussed on the cross peaks. (left) no ^{31}P decoupling. (right) ^{31}P decoupling present

The two-dimensional procedure was repeated with a number of the cumulenic μ-carbido complexes, and the remainder of the two-dimensional spectra visually matched what was expected (dependent on the nature of decoupling); either a singlet peak centred on the ^{31}P chemical shift, or two cross-peaks appearing along the ^{31}P dimension due to the $^{1}J_{RhP}$ coupling. This can be clearly seen with the parent carbido complex **[Rh$_2$(μ-C)Cl$_2$(PPh$_3$)$_4$]** (**Figure 6.19**), with the distance between cross peaks corresponding to a coupling constant of 177 Hz, perfectly matching the value obtained from the 1D ^{31}P{^{1}H} NMR spectrum and validated by gNMR simulation.

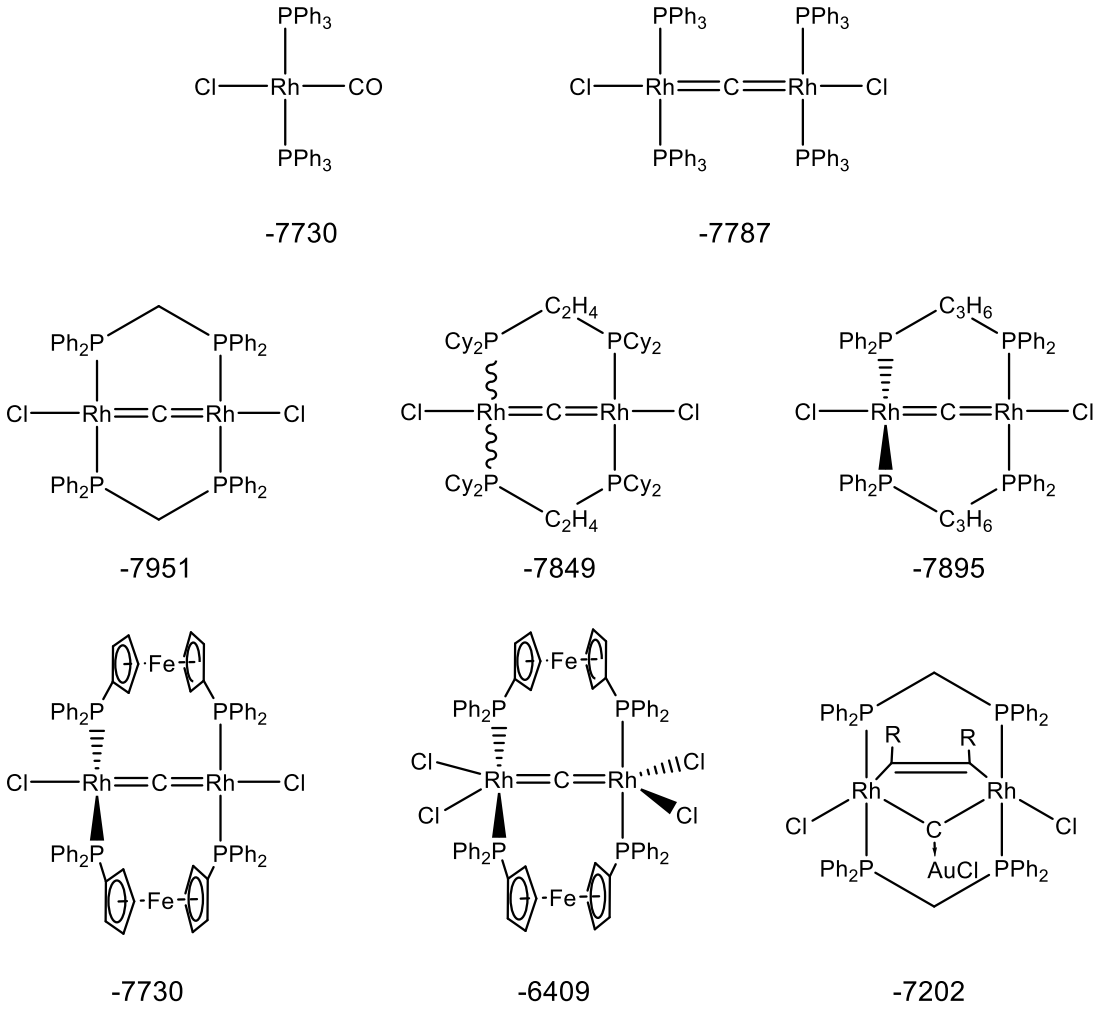

Figure 6.20: Detected ^{103}Rh chemical shifts (ppm) for μ-carbido complexes

The remaining complexes studied are presented above in **Figure 6.20** and cover a range of linear μ-carbido complexes, in addition to the carbonyl complex **[RhCl(CO)(PPh$_3$)$_2$]** and the μ$_3$-carbido complex **[Rh$_2$(μ-CAuCl)(μ-DMAD)Cl$_2$(μ-dppm)$_2$]**. Unfortunately, due to solubility

issues, resonances for the thiocarbonyl complex **[RhCl(CS)(PPh$_3$)$_2$]** and the MHC complex **[Rh$_2$(μ-C:)(μ-DMAD)Cl$_2$(μ-dppm)$_2$]** were not detected.

Looking at the chemical shifts acquired, there are a number of trends which are important to note. As expected, all of the linear μ-carbido complexes vary by a range of 200 ppm, highlighting that even minor chemical changes in the phosphine ligand cause significant differences for the ^{103}Rh chemical shift. As **Table 6.11** highlights, the ^{13}C NMR data for the rhodium(I) μ-carbido complexes fall within a narrow range of 13 ppm as one might expect, and yet the ^{103}Rh chemical shifts are significantly more diverse.

Complex	δ ^{13}C	δ ^{31}P	δ ^{103}Rh
[Rh$_2$(μ-C)Cl$_2$(μ-dppm)$_2$]	411.8	19	-7951
[Rh$_2$(μ-C)Cl$_2$(μ-dppp)$_2$]	411.5	3	-7895
[Rh$_2$(μ-C)Cl$_2$(μ-dcpe)$_2$]	415.1	27	-7849
[Rh$_2$(μ-C)Cl$_2$(μ-dppf)$_2$]	418.6	19	-7730
[Rh$_2$(μ-C)Cl$_2$(PPh$_3$)$_4$]	424.4	20	-7787
[Rh$_2$(μ-C)Cl$_4$(μ-dppf)$_2$]	465.9	28	-6409

Table 6.11: Comparison of ^{13}C, ^{31}P, and ^{103}Rh NMR data for linear μ-carbido complexes

What is interesting is the comparison between the carbonyl species **[Rh(CO)Cl(PPh$_3$)$_2$]** and μ-carbido complex **[Rh$_2$(μ-C)Cl$_2$(PPh$_3$)$_4$]**. The change in chemical environment when shifting from a terminal carbonyl ligand to the μ-carbido ligand was expected to cause large changes in the ^{103}Rh NMR shifts, as the ^{13}C and ^{31}P chemical shifts are distinctly different. What was rather unusual was the rather modest change of 57 ppm in the ^{103}Rh chemical shift, which is around the magnitude observed for μ-carbido complexes with differing phosphine ligands. Taking the substantial change between the two dppf examples discussed below as an indication of oxidation state dependence, variations in coordination number notwithstanding, and the general sensitivity of metal NMR data to σ-donor/π-acceptor effects, these data provide perhaps the best indication that considering the Class A carbido as a neutral ligand (*cf.* CO) coordinated to rhodium(I) is valid.

One interesting feature is the difference between the dppm and dppp complexes. The ^{13}C chemical shift for the μ-carbido environments are almost identical at 411.8 and 411.5 ppm, as the

co-ligands have very similar steric and electronic properties. Nevertheless, the ^{103}Rh NMR shifts (-7951 and -7895 ppm respectively) are almost 60 ppm apart, owing to the enhanced sensitivity of ^{103}Rh chemical shifts in response to minor chemical changes, in this case most likely the dihedral relationship of the rhodium coordination planes.

The largest difference comes when comparing the ferrocene backbone complexes, as they represent the rhodium nuclei in two different oxidation states. Oxidation causes the rhodium chemical shift to dramatically move downfield from -7730 to -6409 ppm. The change in oxidation and addition of an extra halide ligand has been documented previously to lead to large upfield chemical shifts (see **[RhCl(PPh$_3$)$_3$]** *cf.* **[RhCl$_3$(PPh$_3$)$_3$]** in **Table 6.6**), however, the oxidised rhodium(II) complex has a significantly lower field shift than its lower-valent precursor. This shift is attributed to the change in geometry from square-planar to a five-coordinate species, which has been seen from published ^{103}Rh NMR data to cause large downfield chemical shifts due to a smaller FMO energy gap.[324]

Examining the μ_3-carbido complex **[RhAu(μ_3-C)(μ-DMAD)Cl$_3$(μ-dppm)$_2$]**, because the ligand set is completely different with the introduction of the alkyne DMAD and coordinated AuCl, the change in chemical shift for the μ_3-carbido complex at -7202 ppm is not unexpected. Unfortunately, the lack of data for the parent MHC complex due to solubility issues makes any comparison difficult.

^{13}C and ^{103}Rh NMR

What emerged from this combined study of ^{103}Rh and ^{13}C chemical shifts is a more complete picture about the electronics of the μ-carbido system. In an attempt to compare the different spin-active nuclei on the carbido complexes, there was no dependency or relationship found between ^{31}P and ^{13}C chemical shifts, which was initially disappointing as the phosphine ligand was the only changing variable for the rhodium(I) μ-carbido complexes.

Based on the previous work on carbenes by Eisenstein, and the work on *Metalla*-Heterocyclic Carbene quantification (**Chapter 4**), an intricate relationship between the ^{13}C and ^{77}Se chemical shifts and the strong paramagnetic deshielding effect of the metal centres has been developed. What emerges is the energy levels for the relevant molecular orbitals that underpins deshielding would be directly related to the electronic environment of the rhodium nuclei, i.e., that the co-ligands and geometry of the rhodium complexes would have a direct impact on the magnitude of deshielding exhibited in the ^{13}C NMR spectra of the μ-carbido nucleus.

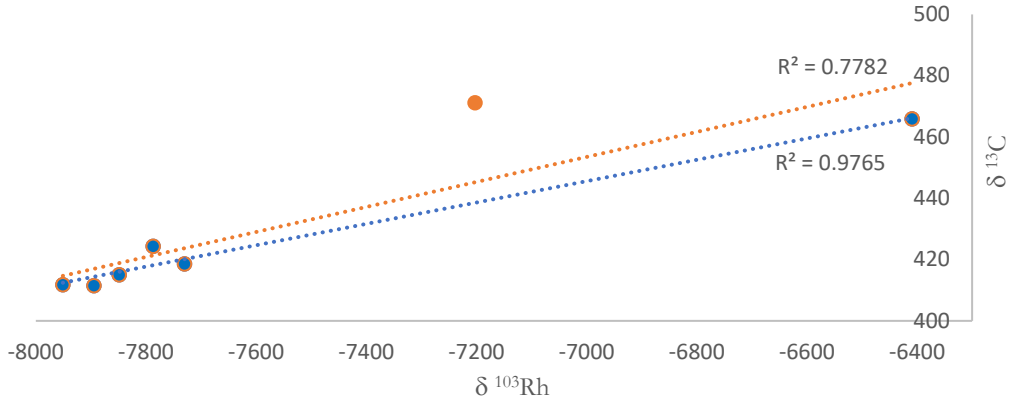

Figure 6.21: (blue) Plot of observed ^{103}Rh chemical shifts against ^{13}C chemical shifts for linear μ-carbido complexes. (orange) inclusion of the μ_3-carbido complex **[Rh$_2$(μ-CAuCl)(μ-DMAD)Cl$_2$(μ-dppm)$_2$]**

Comparing the linear μ-carbido complexes, the change in the μ-carbido ^{13}C chemical shift is proportional to the change in the ^{103}Rh dimension (blue in **Figure 6.21**). This even accounts for the oxidative addition complex **[Rh$_2$(μ-C)Cl$_4$(μ-dppf)$_2$]**, which changes both oxidation state and coordination number. Notably, the complexes which deviate from this geometry have not been included in this plot. The carbonyl complex **[RhCl(CO)(PPh$_3$)$_2$]**, though containing a square planar rhodium(I) centre, does not possess the second metal centre which causes the extreme deshielding of the μ-carbido ligand. Although the ^{103}Rh environment of -7730 ppm is within the ballpark of the μ-carbido complexes, the paramagnetic deshielding effect that affects that ^{13}C resonance is not directly comparable.

The μ_3-carbido species **[Rh$_2$(μ-CAuCl)(μ-DMAD)Cl$_2$(μ-dppm)$_2$]** now contains a third metal centre, which will also have shielding effects on the μ_3-carbido ligand due to increased coordination number, which may not be reflected in the ^{103}Rh NMR. Including this data point drops the R^2 value to 0.7782 (orange in **Figure 6.21**), and this is reflected by the ^{13}C shift being more deshielding than the electronic environment of the rhodium atoms would suggest, which is likely caused by the deshielding effect of the third metal.

6.3.6 Summary

This final chapter explored the electronic nature of the μ-carbido complexes through recourse to data available from 1- and 2-dimensional NMR data. The presence of downfield ^{13}C chemical shifts of the μ-carbido ligand warranted investigation into the origin of its strong deshielding. SR-DFT studies performed on both **[Rh_2(μ-C)Cl_2(PPh_3)$_4$]** and **[Rh_2(μ-C)Cl_2(μ-dppm)$_2$]** saw a significant deshielding effect of the μ-carbido nuclei in comparison to the organic allene counterparts, which were attributed to the coupling between the Rh=C=Rh σ-bonding orbital(s) to the π* antibonding orbital. The orbital energy gap for this transition was found, as expected, to be significantly smaller for the organometallic species in comparison to an allene, accounting for the low field ^{13}C NMR chemical shifts.

In order to develop the ^{13}C NMR studies on the dirhodium complexes, the ^{13}C enrichment process was refined in order to minimise the stoichiometry of $^{13}CS_2$ needed and maximise economy. The use of a 1:1 dichloromethane and methanol solution allowed for the installation of the enriched thiocarbonyl ligand in **[Rh(^{13}CS)Cl(PPh_3)$_2$]** using a single equivalent of $^{13}CS_2$ and achieving respectable yields (76%).

In addition to enrichment studies, multidimensional NMR studies were performed, utilising both ^{31}P-^{103}Rh HMQC and a three-dimensional relay ^{1}H-^{31}P-^{103}Rh INEPT NMR analysis. The indirect detection of the carbido resonances was successful for the bidentate phosphine complexes of dcpe, dppp and dppm, however, the insolubility and/or broad ^{31}P peaks of many complexes meant that ^{13}C enrichment remained the most appropriate approach.

To complete the NMR picture, the ^{103}Rh chemical shifts were indirectly detected using the ^{31}P-^{103}Rh HMQC technique. The chemical shifts of the μ-carbido complexes fell just shy of -8000 ppm when referenced to **[Rh(acac)$_3$]** (δ_{Rh} = 0.0), and minor chemical changes such as differing phosphine ligands and geometry were seen to lead to changes of multiple hundred ppm.

An intimate linear relationship (R^2 = 0.9767) between the rhodium and μ-carbido chemical shifts was demonstrated. The strong paramagnetic deshielding effect of the two rhodium nuclei upon the μ-carbido ligand is the dominant feature behind its chemical shift.

6.4 EXPERIMENTAL

NMR Considerations

Both ^{1}H-^{31}P-^{13}C HPC and ^{31}P-^{13}C HMQC NMR were acquired on a Bruker Avance (800 MHz for ^{1}H equipped with a cryoprobe). $^{13}C\{^{1}H\}$ NMR spectra were acquired on Bruker Avance instruments (^{1}H = 600, 700 or 800 MHz). ^{31}P-^{103}Rh HMQC NMR were acquired at 298K on a Bruker Avance IIIHD (600 MHz for ^{1}H) instrument at 19.1 MHz using a commercial 5 mm triple resonance broadband probe (doubly tuned $^{1}H/^{31}P$ outer coil, with inner broadband coil) with 90° pulses of 27.5 μs and 18.4 μs for ^{103}Rh and ^{31}P respectively. ^{103}Rh chemical shifts, δ, are given in ppm relative to Ξ = 3.186447 for $[Rh(acac)_3]$[325] and were determined by four pulse ^{31}P-^{103}Rh HMQC experiments. The transmitter frequency offset and t_1 increments were varied to ensure that no signals were folded. All ^{103}Rh data were processed using MestReNova®. NMR simulations were modelled using the gNMR software. Exponential line broadening of 10 Hz was applied to 1D ^{103}Rh data, with 2D data zero filled, Gaussian broadened by 10 Hz and treated with sine-squared window function during processing.

Computational Details

^{13}C, and ^{31}P chemical shifts were calculated using scalar-relativistic all-electron DFT calculations implemented in the ORCA suite of programs.[218] Structures of compounds were first optimised, starting from their respective crystal structure coordinates where available. Optimisations were conducted using the TPSS-D3BJ functional[219,220] and zeroth-order regular approximation (ZORA) scalar relativistic Hamiltonian.[221,222] The relativistically recontracted ZORA-def2-TZVP[223] basis set was used for all elements except Rh, for which the ZORA-SARC-TZVP[7] basis set was used. The RI-J resolution of the identity approach was employed in conjunction with the SARC/J auxiliary basis set[224-226] to speed up computation of the Coulomb integrals. A large angular grid (ORCA Grid 7, NoFinalGrid) and radial grid (ORCA IntAcc=12) were selected to ensure accuracy when calculating properties of heavy elements using scalar-relativistic all-electron DFT. The SCF convergence threshold was set to 10^{-8} (ORCA TightSCF). Solvent effects were included using the CPCM continuum solvation model[227] with chloroform as the solvent, to best match the experimental NMR setup. Numerical frequencies were calculated at each optimised geometry to ensure a stationary point on the potential energy surface was

obtained. Chemical shifts were calculated from the optimised geometries with the ORCA gauge-invariant atomic orbital (GIAO) code.[228] The PBE0 hybrid functional[229] was employed along with the ZORA-def2-TZVP(P) and ZORA-SARC-TZVP(P) basis sets for all elements apart from Rh respectively. The same RI-J, grid, SCF and solvent configuration used for geometry optimisations were applied in the calculation of chemical shifts. To allow comparison of chemical shifts to experiment, chemical shifts of reference compounds tetramethylsilane (C^{13}) and phosphoric acid (P^{31}) were computed at the same level of theory. Chemical shifts of compounds were then obtained by subtracting the chemical shift of the target molecule from the chemical shift of the reference. Molecular orbital plots were constructed using PyMol.[230] Coordinates of optimised geometries and sample input files are available at https://github.com/OMaraLab/Rh_Carbido_NMR.

Optimised Synthesis of [Rh(^{13}CS)Cl(PPh$_3$)$_2$]

A flask containing [RhCl(PPh$_3$)$_3$] (3.00 g, 3.24 mmol) was charged with a 1:1 solution of CH_2Cl_2 and methanol (50 mL total volume). To this maroon mixture, $^{13}CS_2$ was added (0.50 mL, 8.4 mmol), and the solution gradually turns dark green upon stirring. The solution as left to stir at room temperature for 1 hour. After this time, the solution was heated and stirred under reflux for 15 hours. The orange/brown solution was concentrated under reduced pressure, and 100 mL of ethanol added to precipitate out the bright orange product, which was isolated *via* filtration and washed with ethanol and *n*-hexane. Yield: 1.75 g (2.48 mmol, 76%). This compares with the yield of 72% typically obtained using the original synthesis. $^{31}P\{^1H\}$ NMR (162 MHz, $CDCl_3$): δ 30.98 (dd, $^1J_{RhP}$ = 142 Hz, $^2J_{PC}$ = 15 Hz). IR ν_{max} (ATR, cm^{-1}): 1302 ν_{CS}. (*cf.* 1304 cm^{-1} for ^{12}C isotopomer).

7.1 APPENDIX

7.1.1 Published Manuscripts

Significant parts of this work have already been published in peer reviewed journals and have been appropriately referenced throughout this work. For completeness, the manuscripts for each of the published articles are attached in the **Supporting Information** document but are listed here in chronological order of publication.

They are as follows:

1. H. J. Barnett, L. K. Burt, A. F. Hill, *Dalton Trans.,* **2018**, 47, 9570
2. H. J. Barnett, A. F. Hill, *Chem. Commun.*, **2019**, 55, 1734
3. H. J. Barnett, A. F. Hill, *Angew. Chem. Int. Ed.,* **2020**, 59, 4274
4. H. J. Barnett, A. F. Hill, *Chem. Commun.*, **2020**, 56, 7738
5. H. J. Barnett, A. F. Hill, *Chem. Commun.*, **2020**, 56, 12593
6. H. J. Barnett, A. F. Hill, *Dalton Trans.,* **2021**, 50, 9383

8.1 REFERENCES

1. A. Reinholdt, J. Bendix, *Chem. Rev.,* **2022**, 122, 830.
2. (a) F. Fischer, H. Tropsch, *Berichte der deutschen chemischen Gesellschaft (A and B Series),* **1926**, 59, 830. (b) F. Fischer, H. Tropsch, *Berichte der deutschen chemischen Gesellschaft (A and B Series)*, **1926**, 59, 832. (c) S. L. Latesky, J. P. Selegue, *J. Am. Chem. Soc.,* **1987**, 109, 4731. (d) S. R. Caskey, M. H. Stewart, J. E. Kivela, J. R. Sootsman, M. J. A. Johnson, J. W. Kampf, *J. Am. Chem. Soc.,* **2005**, 127, 16750.
3. (a) K. M. Lancaster, M. Roemelt, P. Ettenhuber, Y. Hu, M. W. Ribbe, F. Neese, U. Bergmann, S. DeBeer, *Science,* **2011**, 334, 974. (b) T. Spatzal, M. Aksoyoglu, L. Zhang, S. L. A. Andrade, *Science,* **2011,** 334, 940. (c) J. A. Wiig, Y. Hu, M. W. Ribbe, *Science*, **2012**, 337, 1672. (d) K. M. Lancaster, Y. Hu, U. Bergmann, M. W. Ribbe, S. DeBeer, *J. Am. Chem. Soc.,* **2013**, 135, 610. (e) J. A. Wiig, C. C. Lee, Y. Hu, M. W. Ribbe, *J. Am. Chem. Soc,* **2013**, 135, 4982.
4. S. L. Latesky, J. P. Selegue, *J. Am. Chem. Soc.,* **1987**, 109, 4731.
5. (a) M. Etienne, P. S. White, J. L. Templeton, *J. Am. Chem. Soc.,* **1991**, 113, 2324. (b) T. Desmond, F. J. Lalor, G. Ferguson, M. Parvez, *J. Chem. Soc., Chem. Commun.*, **1983**, 457.
6. Selected examples: (a) R. L. Cordiner, A. F. Hill, J. Wagler, *Organometallics*, **2008**, 27, 5177. (b) A. F. Hill, R.Shang, *Organometallics,* **2012**, 31, 4635. (c) B. J. Frogley, A. F. Hill, *Chem. Commun.,* **2019**, 55, 12400.
7. E. S. Borren, A. F. Hill, R. Shang, M. Sharma, A. C. Willis, *J. Am. Chem. Soc.*, **2013**, 135, 494.
8. I. A. Cade, A. F. Hill, C. M. A. McQueen, *Organometallics,* **2009**, 28, 6639.
9. W. Knauer, W. Beck, *Z. Anorg. Allg. Chem.*, **2008**, 634, 2241.
10. S. H. Hong, M. W. Day, R. H. Grubbs, *J. Am. Chem. Soc.,* **2004**, 126, 7414.
11. M. Etienne, P. S. White, J. L. Templeton, *J. Am. Chem. Soc.,* **1991**, 113, 2324.
12. A. F. Hill, M. Sharma, A. C. Willis, *Organometallics,* **2012**, 31, 2538.
13. L. K. Burt, R. L. Cordiner, A. F. Hill, R. A. Manzano, J. Wagler, *Chem. Commun.,* **2020**, 56, 5673.
14. A. F. Hill, R. A. Manzano, *Dalton Trans.,* **2019**, 48, 6596.
15. A. L. Colebatch, A. F. Hill, *J. Am. Chem. Soc.*, **2014**, 136, 17442.
16. (a) B. J. Frogley, A. F. Hill, A. Seitz, *Chem. Commun.,* **2020**, 56, 3265. (b) B. J. Frogley, A. F. Hill, *Eur. J. Chem.,* **2020**, 26, 12125.
17. L. K. Burt, A. F. Hill, *Chem. Commun.*, 2021, 57, 8480.
18. (a) A. Krapp, G. Frenking, *J Am. Chem. Soc.*, **2008**, 130, 16646. (b) A. Hejl, T. M. Trnka, M. W. Day, R. H. Grubbs, *Chem. Commun.*, **2002**, 2524. (c) R. G. Carlson, M. A. Gile, J. A. Heppert, M. H. Mason, D. R. Powell, D. V. Velde, J. M. Vilain, *J. Am. Chem. Soc.*, **2002**, 124, 1580.
19. (a) Y. Chen, W. Petz, G. Frenking, *Organometallics,* **2000**, 19, 2698. (b) A. Reinholdt, J. E. Vibenholt, T. J. Morsing, M. Schau-Magnussen, N. E. A. Reeler, J. Bendix, *Chem. Sci.,* **2015**, 6, 5815. (c) A. Reinholdt, K. Herbst, J. Bendix, *Chem. Commun.,* **2016**, 52, 2015.
20. A. Reinholdt, J. Bendix, *Inorg. Chem.*, **2017**, 56, 12492.

21. K. Tatsumi, R. Hoffmann, M. -H. Whangbo, *J. Chem. Soc. Chem. Commun.,* **1980**, 509.
22. I. Noda, S. Kato, M. Mizuta, N. Yasuoka, N. Kasai, *Angew. Chem. Int .Ed.,* **1979**, 18, 83.
23. (a) D. Mansuy, *Pure and Applied Chem.*, **1980**, 52, 681. (b) D. Mansuy, J. P. Lecomte, J. C. Chottard, J. F. Bartoli, *Inorg. Chem.,* **1981**, 20, 3119.
24. V. Goedken, M. Deakin, L. Bottomly, *J. Chem Soc. Chem. Commun.,* **1982**, 11, 607.
25. D. R. English, D. N. Hendrickson, K. S. Suslick, *Inorg. Chem.,* **1983**, 22, 367.
26. G. Rossi, V. Goedken, C. Ercolani, *J. Am. Chem. Soc. Chem. Commun.,* **1988**, 1, 46.
27. A. Kienast, C. Bruhn, H. Homborg, *Z. Anorg. Allg. Chem.,* **1997**, 623, 967.
28. A. Kienast, L. Galich, K. Murray, B. Moubaraki, G. Lazarev, J. D. Cashion, H. Homborg, *J. Porphyr. Phthalocya.,* **1997**, 1, 141.
29. A. M. Paoletti, G. Pennesi, G. Rossi, C. Ercolani, *Inorg. Chem.,* **1995,** *34*, 4780.
30. A. Kienast, C. Bruhn, H. Homborg, *Z. Anorg. Allg. Chem.,* **1997,** 623, 967.
31. A. Kienast, L. Galich, K. S. Murray, B. Moubaraki, G. Lazarev, J. D. Cashion, H. Homborg, *J. Porphyr. Phthalocya.,* **1997,** 1, 141.
32. A. Kienast, H. Homborg, *Z. Anorg. Allg. Chem.,* **1998,** 624, 107.
33. L. Galich, A. Kienast, H. Hückstädt, H. Homborg, *Z. Anorg. Allg. Chem.,* **1998,** 624, 1235.
34. B. Floris, M. P. Donzello, C. Ercolani, In *The Porphyrin Handbook*; K. M. Kadish, K. M. Smith, R. Guilard, Eds.; Academic Press: Amsterdam, **2003**.
35. W. Beck, W. Knauer, C. Robl, *Angew. Chem. Int. Ed.*, **1990**, 29, 318.
36. W. Knauer, W. Beck, *Z. Anorg. Allg. Chem.,* **2008**, 634, 2241.
37. C. Colomban, E. V. Kudrik, D. V. Tyurin, F. Albrieux, S. E. Nefedov, P. Afanasiev, A. B. Sorokin, *Dalton Trans.,* **2015**, 44, 2240.
38. A. P. Kroitor, L. P. Cailler, A. G. Martynov, Y.G. Gorbunova, A. Y. Tsivadzec, A. B. Sorokin, *Dalton Trans.,* **2017**, 46, 15651.
39. P. J. Dyson, *Adv. Organomet. Chem.*, **1998**, 44, 43.
40. R. Miller, P. Wolczanski, A. Rheingold, *J. Am. Chem. Soc.*, **2002**, 115, 10422.
41. A. Caselli, E. Solari, R. Scopelliti, C. Floriani, *J. Am. Chem. Soc.,* **2000**, 122, 538.
42. E. Solari, S. Antonijevic, S. Gauthier, R. Scopelliti, K. Severin, *Eur. J, Inorg. Chem.,* **2007**, 3, 367.
43. I. S. Butler, N. J. Coville, D. Cozak, *J. Organomet. Chem.*, **1977**, 133, 59.
44. M. C. Baird, G. Wilkinson, *Chem. Commun.*, **1967**, 267.
45. R. Young, A. F. Hill, G. Cavigliasso, R. Stranger, *Angew. Chem. Int. Ed.,* **2013**, 52, 3699.
46. S. Kallane, T. Braun, M. Teltewskoi, B. Braun, R. Hermann, R. Laubenstein, *Chem. Commun.,* **2015**, 51, 14613.
47. T. Ahrens, B. Schmiedecke, T. Braun, R. Hermann, R. Laubenstein, *Eur. J. Inorg. Chem.,* **2017**, 3, 713.
48. S. A. Westcott, T. B. Marder, R. T. Baker, J. C. Calabrese, *Can. J. Chem.*, **1993**, 71, 930.
49. R. B. Bedford, A. F. Hill, A. J. P. White, D. J. Williams, *Angew. Chem., Int. Ed.*, **1996**, 35, 95.
50. I. R. Crossley, A. F. Hill, A. C. Willis, *Organometallics,* **2007**, 26, 3891.

51. H. J. Barnett, L. K. Burt, A. F. Hill, *Dalton Trans.,* **2018**, 47, 9570.

52. A. F. Hill, L. J. Watson, *Chem. Commun.,* **2020**, 56, 2356.

53. T. Takao, T. Seki, *Organometallics,* **2021**, 471, 40.

54. C. P. Kubiak, R. Eisenberg, *J. Am. Chem. Soc.,* **1977**, 99, 6129.

55. A. Sacco, R. Ugo, *J. Chem. Soc.*, **1964**, 3274.

56. R. Fornika, C. Six, H. Gorls, M. Kessler, C. Kruger, W. Leitner, *Can. J. Chem.,* **2001**, 79, 642.

57. (a) Y. Pan, J. T. Mague, M. J. Fink, *J. Am. Chem. Soc.*, **1993**, 115, 3842. (b) W. P. Schaefer, R. E. Marsh, T. M. McCleskey, H. B. Gray, *Acta Crystallogr., Sect. C: Cryst. Struct. Commun.*, **1991**, 47, 2553.

58. M. H. Garner, R. Hoffmann, S. Rettrup, G. C. Solomon, *ACS Cent. Sci.*, **2018**, 4, 688.

59. (a) J. Diez, M. Pilar Gamasa, J. Gimeno, A. Aguirre, S. Garcia-Granda, J. Holubova, L. R. Falvello, *Organometallics*, **1999**, 18, 662. (b) C. D. Effendy, C. Pettinari, B. W. Skelton, N. Somers, A. H. White, *Inorg. Chim. Acta,* **2005**, 358, 695. (c) T. S. A. Hor, S. P. Neo, C. S. Tan, T. C. W. Mak, K. W. P. Leung, R. -J. Wang, *Inorg. Chem.*, **1992**, 31, 4510. (d) M. Trivedi, R. Nagarajan, A. Kumar, N. P. Rath, P. Valegra, *Inorg. Chim. Acta*, **2011**, 376, 549.

60. A. M. Gallego, M. N. Penas-Defrutos, G. Marcos-Ayuso, J. M. Martin-Alvarez, J. M. Martinez-Ilarduya, P. Espinet, *Dalton Trans.*, **2020**, 49, 11336.

61. L. K. Burt, A. F. Hill, *Dalton Trans.,* **2020**, 49, 8143.

62. J. Emerson-King, R. Knighton, M. Gyton, A. B. Chaplin, *Dalton Trans.,* **2017**, 46, 11645.

63. (a) S. C. Rawle, R. Yagbasan, K. Prout, S. R. Cooper, *J. Am. Chem. Soc.,* **1987**, 109, 6181. (b) A. J. Blake, M. A. Halcrow, M. Schroder, *Acta Cryst.,* **1993**, C49, 85

64. A. F. Hill, J. D. E. T Wilton-Ely, *Organometallics,* **1997**, 16, 4517.

65. J. C. Cannadine, A. F. Hill, A. J. P. White, D. J. Williams, J. D. E. T. Wilton-Ely, *Organometallics*, **1996**, 15, 5409.

66. (a) B. Cetinkaya, P. Dixneuf, M. F. Lappert, *J. Chem. Soc., Dalton Trans.*, **1974**, 1827. (b) R. D. Dewhurst, A. F. Hill, A. C. Willis, *Organometallics,* **2004**, 23, 5903.

67. For transition metals: (a) P. Collman, J. W. Kang, *J. Am. Chem. Soc.*, **1967**, 89, 844. (b) D. Seyferth, D. P. Ruschke, W. M. Davis, M. Cowie, A. D. Hunter, *Organometallics*, **1994**, 13, 3834. (c) B. F. G. Johnson, J. Lewis, P. R. Raithby, D. A. Wilkinson, *J. Organomet. Chem.*, **1991**, 408, C9. (d) X. L. R. Fontaine, S. J. Higgins, C. R. Langrick, B. L. Shaw, *Dalton Trans.,* **1987**, 777. (e) Z. Dauter, R. J. Mawby, C. D. Reynolds, D. R. Saunders, *Dalton Trans.,* **1986**, 433. (f) R. J. Cross, M. F. Davidson, *Dalton Trans.*, **1986**, 1987. For lanthanides: (g) G. Lin, R. McDonald, J. Takats, *Organometallics*, **2000**, 19, 1814. (h) G. B. Deacon, D. L. Wilkinson, *Inorg. Chim. Acta*, **1988**, 142, 155. For main-group: (i) D. J. Cook, A. F. Hill, *Dalton Trans.*, **1998**, 1171.

68. R. A. Manzano, A. F. Hill, R. L. Georgelin, *Chem. Commun.,* **2020**, 56, 14597.

69. (a) A. F. Hill, M. C. J. Harris, R. P. Melling, *Polyhedron,* **1992**, 11, 781. (b) A. F. Hill, R. P. Melling, *J. Organomet. Chem.,* **1990**, 396, C22. (c) R. B. Bedford, A. F. Hill, A. R. Thompsett, A. J. P. White, D. J. Williams, *J. Chem. Soc., Chem. Commun.*, **1996**, 1059.

70. (a) M. Cowie, S. Dwight, *J. Organomet. Chem.,* **1981**, 214, 233.

71. Carbynes: (a) G. R. Clark, K. Marsden, W. R. Roper, L. J. Wright *J. Am. Chem. Soc.* **1980**, 102, 6570. (b) D. S. Gill, M. Green, K. Marsden, I. Moore, A. G. Orpen, F. G. A. Stone, I. D. Williams, P. Woodward, *J. Chem. Soc., Dalton Trans.,* **1984**, 1343. (c) P. G. Byrne, M. E. Garcia, J. C. Jeffery, P. Sherwood, F. G. A. Stone, *J. Chem. Soc., Dalton Trans.,* **1987**, 1215; (d) A. F. Hill, B. A. Nasir, F. G. A. Stone, *Polyhedron*, **1989**, 8, 179; (e) S. Anderson, D. J. Cook, A. F. Hill, *Organometallics*, **2001**, 20, 2468. (f) A. J. Hulkes, A. F. Hill, B. A. Nasir, A. J. P. White, D. J. Williams, *Organometallics,* **2004**, 23, 679. (g) D. J. Cook, A. F. Hill *Chem. Commun.,* **1997**, 955. (h) D. J. Cook, A. F. Hill, *Organometallics*, **2003**, 22, 3502. Carbenes: (a) A. F. Hill, W. R. Roper, J. M. Waters, A. H. Wright, *J. Am. Chem. Soc.,* **1983**, 105, 18, 5939. (b) H. Fischer, S. Zeuner, *Z. Naturforschung. B,* **1985**, 40, 954. (c) W. E. Buhro, M. C. Etter, S. Georgiou, J. A. Gladysz, F. B. McCormick, *Organometallics*, **1987**, 6, 1150. Vinylidenes: (h) H Werner, J. Wolf, R. Zolk, U. Schubert, *Angew. Chem., Int. Ed. Engl.,* **1983**, 22, 981-982.

72. A. R. Cowley, A. L. Hector, A. F. Hill, A. J. P. White, D. J. Williams, J. D. E. T. Wilton-Ely, *Organometallics,* 2007, 26, 6114.

73. H. Werner, O. Kolb, U. Schubert, K. Ackermann, *J. Organomet. Chem.,* **1982**, 240, 421.

74. (a) L. Gelmini, D. W. Stephan, S. J. Loeb, *Inorg. Chim. Acta,* **1985**, 98, L3. (b) M. Cowie, S. K. Dwight, *Inorg. Chem.*, **1980**, 19, 2500.

75. B. Cordero, V. Gomez, A. E. Platero-Prats, M. Reves, J. Echeverria, E. Cremades, F. Barragan, S. Alvarez, *Dalton Trans.,* **2008**, 2832.

76. W. Petz, *Coord. Chem. Rev.*, **2008**, 252, 1689.

77. S. Takemoto, J. Ohata, K. Umetani, M. Yamaguchi, H. Matsuzaka., *J. Am. Chem. Soc.,* **2014**, 136, 15889.

78. (a) R. H. Lam, C. M. A. McQueen, I. Pernik, R. T. McBurney, A. F. Hill, B. A. Messerle, *Green Chem.*, **2019**, 21, 538. (b) M. Doux, N. Mezailles, L. Ricard, P. Le Floch, *Organometallics*, **2003**, 22, 4624. (c) C. Bianchini, D. Masi, C. Mealli, A. Meli, M. Sabat, *Organometallics*, **1985**, 4, 1014. (d) E. Lindner, B. Keppeler, H. A. Mayer, K. Gierling, R. Fawzi, M. Steimann, *J. Organomet. Chem.*, **1996**, 526, 175.

79. P. Leoni, M. Pasquali, L. Fadini, A. Albinati, P. Hofmann, M. Metz, *J. Am. Chem. Soc.,* **1997**, 119, 8625.

80. (a) P. W. Schrier, P. E. Fanwick, R. A. Walton, *Inorg. Chem.*, **1992**, 31, 3929. (b) J. -S. Qi, P. W. Schrier, P. E. Fanwick, R. A. Walton, *Inorg. Chem.*, **1992**, 31, 258.

81. L. M. Caldwell, A. F. Hill, R. Stranger, R. N. L. Terrett, K. M. von Nessi, J. Ward, A. C. Willis, *Organometallics,* **2015**, 34, 328.

82. (a) R. W. Wilson, A. A. Penzias, P. G. Wannier, R. A. Linke, *Astrophys. J.*, **1976**, 204, L135. (b) J. -H. Chou, T. B. Rauchfuss, *J. Am. Chem. Soc.,* **1997**, 199, 4537.

83. B. J. Frogley, A. F. Hill, L. J. Watson, *Chem. Commun.,* **2019**, 55, 14450.

84. M. Cowie, T. G. Southern, *J. Organomet. Chem.,* **1980**, 193, C46.

85. B. Sutherland, M. Cowie, *Inorg. Chem.,* **1984**, 23, 1290.

86. (a) H. -N. Adams, G. Fachinetti, J. Strahle, *Angew. Chem. Int. Ed.*, **1981**, 20, 125. (b) J. R. Galsworthy, C. E. Housecroft, R. L. Ostrander, A. L. Rheingold, *J. Organomet. Chem.,* **1995**, 492, 211.

87. R. F. Jordan, J. R. Norton, *J. Am. Chem. Soc.*, **1982**, 104, 1263.

88. R. M. P. Veenboer, A. Collado, S. Dupuy, T. Lebl, L. Falivene, L. Cavallo, D. B. Cordes, A. M. Z. Slawin, C. S. J. Cazin, S. P. Nolan, *Organometallics*, **2017**, 36, 2861.

89. L. M. Caldwell, A. F. Hill, A. D. Rae, A. C. Willis, *Organometallics*, **2008**, 27, 341.

90. (a) R. E. Wagner, R. A. Jacobson, R. J. Angelici, M. H. Quick, *J. Organomet. Chem.,* **1978**, 148, C35. (b) E. Ma, G. Semelhago, A. Walker, D. H. Farrar, R. G. Gukathasan, *J. Chem. Soc. Dalton Trans.*, **1985**, 2595. (c) V. G. Albano, S. Bordoni, L. Busetto, C. Camiletti, M. Monari, A. Palzzi, F. Prestopino, V. Zanotti, *J. Chem. Soc. Dalton Trans.*, **1997**, 4665. (d) V. G. Albano, S. Bordoni, L. Busetto, A. Palazzi, P. Sabatino, V. Zanotti, *J. Organomet. Chem.*, **2002**, 659, 15. (e) A. R. Manning, C. J. McAdam, A. J. Palmer, J. Simpson, *Acta Crystallogr., Sect. E: Struct. Rep.*, **2008**, 64, m635. (f) A. R. Manning, L. O'Dwyer, P. A. McArdle, D. Cunningham, *J. Organomet. Chem.*, **1998**, 551, 139. (g) A. R. Manning, C. J. McAdam, A. J. Palmer, B. H. Robinson, J. Simpson, *Dalton Trans.*, **2003**, 4472. (h) N. L. Cromhout, A. R. Manning, A. J. Palmer, C. J. McAdam, B. H. Robinson, J. Simpson, *Inorg. Chim. Acta*, **2003**, 354, 54.

91. B. J. Frogley, A. F. Hill, C. S. Onn, *Dalton Trans.,* **2019**, 48, 11715.

92. K. A. Johnson, W. L. Gladfelter, *Organometallics*, **1990**, 9, 2101. Further examples, see: M. K. Reinking, P. E. Fanwick, C. P. Kubaik, *Angew. Chem. Int. Ed.,* **1989**, 28, 1377.

93. (a) H. -N. Zhang, W. -G. Jia, Q. -T. Xu, C. -C. Ji, *Inorg. Chim. Acta*, **2016**, 450, 315. (b) M. Fettouhi, M. I. M. Wazeer, S. Ahmad, A. A. Isab, *Polyhedron*, **2004**, 23, 1. (c) A. Bredenkamp, X. Zeng, F. Mohr, *Polyhedron,* **2012**, 33, 107. (d) F. Nahra, S. R. Patrick, D. Bello, M. Brill, A. Obled, D. B. Cordes, A. M. Z. Slawin, D. O'Hagan, S. P. Nolan, *Chem. Cat. Chem.*, **2015**, 7, 240. (e) D. J. Nelson, F. Nahra, S. R. Patrick, D. B. Cordes, A. M. Z. Slawin, S. P. Nolan, *Organometallics*, **2014**, 33, 364.

94. D. Nelson, F. Nahra, S. Patrick, D. Cordes, A. Slawin, S. P Nolan, *Organometallics*, **2014**, 33, 3640.

95. D. A. Khobragade, S. G. Mahamulkar, L. Pospoisil, I. Cisarova, L. Rulisek, U. Jahn, *J. Eur. Chem.,* **2012**, 18, 12267.

96. X. -F. Zhao, C. Zhang, *Synthesis,* **2007**, 4, 551.

97. J. Holz, M. A. Garcia, W. Frey, F. Krupp, R. Peters, *Dalton Trans.,* **2018**, 47, 3880.

98. A. Luquin, E. Cerrada, M. Laguna, in *Gold Chemistry: Applications and Future Directions in the Life Sciences*, Wiley, **2009**.

99. W. E. Tyrra, *J. Flu. Chem.,* **2001**, 112, 149.

100. P. W. Jolly, in *Comprehensive Organometallic Chemistry,* Pergamon Press, **1982**.

101. (a) H. F. Luecke, R. G. Bergman, *J. Am. Chem. Soc.*, **1998**, 120, 11008. (b) C. J. Pell, Y. Zhu, R. Huacuja, D. E. Herbert, R. P. Hughes, O. V. Ozerov, *Chemical Science,* **2017**, 8, 3178.

102. (a) E. O. Fischer, U. Schubert, *J. Organomet. Chem.,* **1975**, 100, 59. (b) B. D. Dombek, R. J. Angelici, *Inorg. Chem.,* **1976**, 15, 2397. (c) L. J. Guggenberger, R. R. Schrock, *J. Am. Chem. Soc.* **1975**, 97, 10, 2935.

103. (a) R. R. Schrock, *Science*, **1983**, 219, 18. (b) R. R. Schrock, *J. Organomet. Chem.*, **1986**, 300, 249. Recent work heavily developed by Tamm, see: (b) H. Ehrhorn, D. Bockfield, M. Freytag, T. Bannenberg, C. Kefalidis, L. Maron, M. Tamm, *Organometallics*, **2019**, 38, 1627. (c) B. D. Dombek, R. J. Angelici, *Inorg. Chem.*, **1976**, 15, 2397.

104. (a) H. U. Schubert, E, O, Fischer, D. Wittmann, *Angew. Chem. Int. Ed.,* **1980**, 19, 643. (b) R. R. Schrock, A. H. Hoveyda, *Angew. Chem. Int. Ed.,* **2003**, 42, 4592.

105. E. O. Fischer, M. Schluge, J. O. Besenhard, P. Friedrich, G. Huttner, F. R. Kreibl, *Chem. Ber.,* **1978**, 111, 3530.

106. G. R. Clark, K. Marsden, W. R. Roper, L. J. Wright, *J. Am. Chem Soc.,* **1980**, 102, 6570.

107. G. R. Clark, N. R. Edmonds, R. A. Pauptit, W. R. Roper, J. M. Waters, A. H. Right, *J. Organomet. Chem.,* **1983**, 244, C57.

108. CCDC as of 09/21 update

109. (a) B. J. Frogley, A. F. Hill, A. Seitz, *Chem. Commun.,* **2020**, 56, 3265. (b) M. P. Yin Yu, K. -K. Cheung, A. Mayr, *J. Chem. Soc. Dalton Trans.,* **1998**, 2373. (c) K. J. Ahmed, M. H. Chisholm, J. C. Huffman, *Organometallics,* **1985**, 4, 1168. (d) R.L. Cordiner, A.F. Hill, R. Shang, A.C. Willis, *Organometallics,* 2011, 30, 139. (e) R. A. Manzano, R. L. Georgelin, A. F. Hill, *Chem. Commun.*, **2020**, 49, 12731.

110. (a) S. J. Holmes, R. R. Schrock, M. R. Churchill, H. J. Wasserman, *Organometallics*, **1984**, 3, 476. (b) G. M. Jamison, P. S. White, J. L. Templeton, *Organometallics*, **1991**, 10, 1954. (c) R. L. Cordiner, P. A. Gugger, A. F. Hill, A. C. Willis. *Organometallics*, **2009**, 28, 6632. (d) A. K. List, G. L. Hillhouse, A. L. Rheingold, *Organometallics*, **1989**, 8, 2010. (e) A. L. Colebatch, A.F. Hill, R. M. Sharma, *Organometallics*, **2015**, 34, 2165. (f) M. Kamitani, B. Pinter, K. Searles, M. G. Crestani, A. Hickey, B. C. Manor, P. J. Carroll, D. J. Mindiola, *J. Am. Chem. Soc.,* **2015**, 137, 11872. (g) B. Frogley, A. F. Hill, *Chem. Commun.,* **2018**, 54, 12373. (h) A. L. Colebatch, B. J. Frogley, A. F. Hill, *Dalton Trans.,* **2019**, 48, 10628.

111. (a) L. M. Caldwell, A. F. Hill, J. Wagler, A. C. Willis, *Dalton Trans.,* **2008**, 3538. (b) A. F. Hill, C. M. A. McQueen, *Organometallics*, **2012**, 31, 2482. (c) B. J. Frogley, A. F. Hill, R. A. Manzano, M. Sharma, *Chem. Commun.,* **2018**, 54, 1702. (d) B. J. Frogley, T. L. Genet, A. F. Hill, C. S. Onn, *Dalton Trans.,* **2019**, 48, 7632. (e) B. J. Frogley, A. F. Hill, L. J. Watson, *Dalton Trans.,* **2019**, 48, 12598.

112. (a) B. S. Bronk, J. D. Protasiewicz, L. E. Pence, S. J. Lippard, *Organometallics,* **1995**, 14, 2177. (b) K. C. Stone, P. S. White, J. L. Templeton, *J. Organomet. Chem.,* **2003**, 684, 13.

113. (a) M. M. Deegan, J. C. Peters, *Chem. Commun.,* **2019**, 55, 9531. (b) D. L. M. Suess, J. C. Peters, *J. Am. Chem. Soc.*, **2013**, 135, 12580.

114. E. F. van der Eide, W. E. Piers, P. E. Romero, M. Parvez, R. McDonald, *Organometallics*, **2004**, 23, 314.

115. (a) J. C. Peters, A. L. Odom, C. C. Cummins, *Chem Commun.,* **1997**, 1995. (b) A. Hejl, T. M. Trnka, M. W. Day, R. H. Grubbs, *Chem. Commun.,* **2002**, 2524. (c) M. H. Stewart, M. J. A. Johnson, J. W. Kampf, *Organometallics*, **2007**, 26, 5102. (d) T. J. Morsing, A. Reinholdt, S. P. A. Sauer, J. Bendix, *Organometallics*, **2016**, 35, 100.

116. G. Huttner, A. Frank, E. O. Fischer, W. Kleine, *J. Organomet. Chem.*, **1977**, 141, C17.

117. (a) T. Desmond, F. J. Lalor, G. Ferguson, M. Parvez, *J. Chem. Soc. Chem. Commun.*, **1983**, 457. (b) F. J. Lalor, T. Desmond, G. M. Cotter, C. A. Shanahan, G. Ferguson, M. Parvez, B. Ruhl, *J. Chem. Soc. Dalton Trans.,* **1995**, 1709.

118. T. Desmond, F. J. Lalor, G. Ferguson, M. Parvez, *J. Chem. Soc. Chem. Commun.*, **1983**, 55.

119. A. E. Enriquez, P. S. White, J. L. Templeton *J. Am. Chem. Soc.,* **2001**, 123, 21, 4992.

120. R. L. Cordiner, A. F. Hill, J. Wagler, *Organometallics*, **2008**, 27, 5177.

121. B. F. Frogley, A. F. Hill, *Chem. Commun.*, **2018**, 54, 2126.

122. (a) A. F. Hill, M. Sharma, A. C. Willis, *Organometallics*, **2012**, 31, 2538. (b) B. J. Frogley, A. F. Hill, *Chem. Commun.,* **2019**, 55, 12400.

123. K. Bartl, R. Boese, G. Schmid, *J. Organomet. Chem.,* **1981**, 206, 331.

124. R. Ercoli, E. Santambrogio, G. T. Casagrande, *Chimica e l'Industria,* **1962**, 44, 1244.

125. (a) D. Seyferth, J. E. Hallgren, P. L. K. Hung, *J. Organomet. Chem.,* **1973**, 50, 265. (b) D. Seyferth, G. H. Williams, C. L. Nivert, *Inorg. Chem.,* **1977**, 16, 758.

126. (a) M. I. Bruce, K. A. Kramarczuk, G. J. Perkins, B. W. Skelton, A. H. White, N. N. Zaitseva, *J. Cluster Sci.,* **2004**, 15, 119. (b) H. Huang, R. P. Hughes, A. L. Rheingold, *Dalton Trans.,* **2011**, 40, 47. (c) D. N. Duffy, M. M. Kassis, A. D. Rae, *Acta Crystallogr.,* 1991, 47, 2054. (d) D. Lent, I. Brudgam, H. Hartl, *Angew. Chem. Int. Ed.,* **1985**, 24, 119. (e) D. Y. Jan, D. P. Workman, L. -Y. Hsu, J. A. Krause, S. G. Shore, *Inorg. Chem.,* **1992**, 31, 5123. (f) R. Vilar, S. E. Lawrence, D. M. P. Mingos, D. J. Williams, *Chem. Commun.,* **1997**, 285. (g) W. Schulze, H. Hartl, K. Seppelt, *J. Organomet. Chem.,* **1987**, 319, 77. (h) T. Kurogi, K. Irifune, T. Enoki, K. Takai, *Chem. Commun.,* **2021**, 57, 5199.

127. V. Batzel, G. Schmid, *Chem. Ber.,* **1976**, 109, 3339.

128. E. Muetterties, T. Rhodin, E. Band, C. F. Brucker, W. R. Pretzer, *Chem. Rev.,* **1979**, 79, 91.

129. G. Demitras, E. Muetterties, *J. Am. Chem. Soc.,* **1977**, 99, 2876.

130. J. Beck, F. Wolf, *Z. Anorg. Allg. Chem.,* **2002**, 628, 1453.

131. W. Knauer, W. Beck, *Z. Anorg. Allg. Chem.,* **2008**, 634, 2241.

132. (a) F. G. A. Stone, *Angew. Chem. Int. Ed. Engl.,* **1984**, 23, 89. (b) M. R. Awang, J. C. Jeffery. F. G. A. Stone, *J. Chem. Soc. Dalton Trans.,* **1986**, 165. (c) M. Green, J. A. K. Howard. A. P. James, C. M. Nunn, F. G. A. Stone, *J. Chem Soc. Dalton Trans.,* **1986**, 187.

133. J. Goodman, V. V. Grushin, R. B. Larichev, S. A. Macgregor, W. J. Marshall, D. C. Roe, *J. Am. Chem. Soc.*, **2009**, 131, 4236-4238.

134. (a) W. R. Roper, A. H. Wright, *J. Organomet. Chem.,* **1982**, 233, C59. (b) G. R. Clark, K. Marsden, W. R. Roper, L. J. Wright, *J. Am. Chem. Soc.,* **1980**, 102, 1206.

135. P. J. Brothers, W. R. Roper, *Chem. Rev.,* **1988**, 88, 1293.

136. S. A. Benyunes, P. A. Chaloner, P. B. Hitchcock, *J. Chem. Soc. Chem. Comm.,* **1989**, 1491.

137. Selected examples: (a) G. A. Carriedo, V. Riera, G. Sanchez, X. Solans, M. Labrador, *J. Organomet. Chem.,* **1990**, 391, 431. (b) B. J. Frogley, A. F. Hill, *Chem. Commun.,* **2019**, 55, 15077. (c) A. F. Hill, R. A. Manzano, *Dalton Trans.,* **2019**, 48, 6596.

138. W. R. Roper, A. H. Wright, *J. Organomet. Chem.,* **1982**, 233, C59.

139. Y. Liu, R. Wang, J. Sun, J. Chen, *Organometallics,* **2000**, 19, 3498.

140. R. L. Cordiner, A. F. Hill, J. Wagler, *Organometallics,* **2008**, 27, 4532.

141. J. Long, M. Ebihara, *Acta Crystallogr. E*, **2014**, 70, 362.

142. A. L. Colebatch, B. J. Frogley, A. F. Hill, C. S. Onn, *Chem. Eur. J.*, **2021**, 27, 5322.

143. H. Schmidbaur, R. Pichl, G. Muller, *Angew. Chem. Int. Ed.,* **1986**, 25, 574.

144. R. B. English, *Cryst. Struct. Commun.,* **1979**, 8, 167.

145. (a) G. R. Clark, K. Marsden, W. R. Roper, L. J. Wright, *J. Am. Chem. Soc.,* **1980**, 102, 6570. (b) G. R. Clark, C. M. Cochrane, K. Marsden, W. R. Roper, L. J. Wright, *J. Organomet. Chem.,* **1986**, 315, 211. (c) T. B. Wen, S. M. Ng, W. Y. Hung, Z. Y. Zhou, M. F. Lo, L. -Y. Shek, I. D. Williams, Z. Lin, G. Jia, *J. Am. Chem. Soc.,* **2003**, 125, 884. (d) W. Bai, K. -H. Lee, W. Y. Hung, I. D. Williams, Z. Lin, G. Jia, *Organometallics*, **2017**, 36, 657. (e) M. A. Gallop, W. R. Roper, *Adv. Organomet. Chem.*, **1986**, 25, 121.

146. A. Arduengo, R. Harlow, M. Kline, *J. Am. Chem. Soc.,* **1991**, 113, 361.

147. CCDC as of 09/21

148. (a) G. C. Vougioukalakis, R. H. Grubbs, *Chem. Rev.*, **2010**, 110, 1746. (b) O. M. Ogba, N. C. Warner, D. J. O'Leary, R. H. Grubbs, *Chem. Soc. Rev.,* **2018**, 47, 4510.

149. H. Jang, F. Romiti, S. Torker, A. H. Hoveyda, *Nat. Chem.,* **2017** 9, 1269.

150. D. M. Flanigan, F. R-Michailidis, N. A. White, T. Rovis, *Chem. Rev.*, **2015**, 115, 9307.

151. E. Alvarez, S. Conejero, M. Paneqye, A. Petronilho, M. L. Poveda, O. Serrano, E. Carmona, *J. Am. Chem. Soc.,* **2006**, 128, 13060.

152. P. J. Fraser, W. R. Roper, F. G. A. Stone, *J. Chem. Soc. Dalton Trans.*, **1974**, 760. (b) A. Tukov, A. Normand, M. Nechaev, *Dalton Trans.,* **2009**, 35, 7015.

153. M. Melaimi, R. Jazzar, M. Soleilhavoup, G. Bertrand, *Angew. Chem. Int. Ed.,* **2017**, 56, 10046.

154. For sulfur, see: E. S-Grobler, O. Schuster, C. E. Strasser, M. Albrecht, S. Cronje, H. G. Raubenheimer, *Polyhgedron*, **2011**, 30, 2776. For oxygen, see: J. Ruiz, G. Garcia, M. E. G. Mosquera, B. F. Perandones, M. P. Gonzalo, M. Vivanco, *J. Am. Chem. Soc.,* **2005**, 127, 8584.

155. J. D. Masuda, D. Martin, C. L-Saunier, A. Baceiredo, H. Gornitzka, B. Donnadieu, G. Bertrand, *Chem. Asian J.*, **2007**, 2, 178.

156. For nitrogen, see as example: S. Guo, H. V. Huynh, *Organometallics,* **2014**, 33, 2004. For boron, see: K.E. Krahulic, G.D. Enright, M. Parvez, R. Roesler, *J. Am. Chem. Soc.,* **2005**, 127, 4142.

157. M. Clarke, H. Taube, *J. Am. Chem. Soc.,* **1975**, 97, 1397.

158. S. Burling, M. F. Mahon, R. E. Powell, M. K. Whittlesey, J. M. J. Williams, *J Am. Chem. Soc.,* **2006**, 128, 13702.

159. (a) M. A. Esteruelas, F. J. Fernandex-Alvarez, E. Onate, *J. Am. Chem. Soc.,* **2006**, 128, 13044. (b) G. Sini, O. Esisenstein, R. H. Crabtree, *Inorg. Chem.,* **2002**, 41, 602.

160. J. Ruiz, B. F. Perandones, *J. Am. Chem. Soc.,* **2007**, 129, 9298.

161. H. Brunner, W. Meier, J. Wachter, I. Bernal, E. Raabe, *J. Organomet. Chem.,* **1989**, 362, 95.

162. J. Ruiz, L. Garcia, B. F. Perandones, M. Vivanco, *Angew. Chem. Int. Ed.,* **2011**, 50, 3010.

163. (a) J. Ruiz, L. Garcia, M. Vivanco, A. Berros, J. Francisco, J. F. Va der Maelen, *Angew. Chem. Int. Ed.,* **2015**, 54, 4212. (b) Theoretical studies performed by S. S. Rohman, B. Ghosh, A. K. Phukan, *Dalton Trans.,* **2019**, 48, 11772.

164. J. Ruiz, L. Garcia, C. Mejuto, M. Vivanco, M. Rosario Diaz, S. Garcia-Granda, *Chem. Commun.,* **2014**, 50, 2129.

165. E. P. Beaumier, C. P. Gordon, C. Copéret, R. P. Harkins, M. E. McGreal, X. Wen, J. D. Goodpaster, I. A. Tonks, *J. Am. Chem Soc.,* **2020**, 142, 8006.

166. Y. Ishida, B. Donnadieu, G. Bertrand, *Proc. Nat. Acad. Sci. USA.*, **2006**, 103, 13585.

167. C. A. Dyker, V. Lavallo, B. Donnadieu, G. Bertrand, *Angew. Chem. Int. Ed.*, **2008**, 47, 3206.

168. S. Takemoto, J. Ohata, K. Umetani, M. Yamaguchi, H. Matsuzaka, *J. Am. Chem. Soc.,* **2014**, 136, 15889.

169. (a) S. Takemoto, M. Tsujita, H. Matsuzaka, *Organometallics,* **2017**, 36, 3686. (b) S. Takemoto, T. Kobayashi, T. Ito, A. Inui, K. Karitani, S. Katagiri, Y. Masuhara, H. Matsuzaka, *Organometallics*, **2011**, 30, 2160.

170. (a) J. J. Davidson, W. Harrison, D. W. A. Sharp, G. A. Sim, *J. Organomet. Chem.,* **1972**, 46, C47. (b) E. J. Forbes, N. Goohand, T.A Hamor, M. Iranpoor, *J. Fluorine Chem.,* **1980**, 16, 339.

171. M. Cowie, T. G. Southern, *J. Organomet. Chem.,* **1980**, 193, C46.

172. (a) M. Cowie, R. Dickson, *Inorg. Chem.,* **1981**, 20, 2682. (b) For unsymmetric RhMo: L. Wang, M. Cowie, *Can. J. Chem.,* **1995**, 73, 1058.

173. (a) R. G. Pearson, *Proc. Natl. Acad. Sci. U.S.A.*, **1986**, 83, 8440. (b) Z. Zhou, R. G. Parr, *J. Am. Chem. Soc.,* **1989**, 111, 7371.

174. (a) I. Fernandez, G. Frenking, G. Merino, *Chem. Soc. Rev.,* **2015**, 44, 6452. (b) D. Chen, Y. Hua, H. Xia, *Chem. Rev.,* **2020**, 120, 12994.

175. S. G. Patra, N. Mandal, *Quantum Chem.,* **2020**, 120, e26152.

176. J. R. Lamb, C. M. Brown, J. A. Johnson, *Chem. Sci.,* **2021**, 12, 2699.

177. G. R. County, R. S. Dixon, G. D. Fallon, S. M. Jenkins, J. Johnson, *J. Organomet. Chem.,* **1996**, 526, 279.

178. I. R. McKeer, S. J. Sherlock, M. Cowie, *J. Organomet. Chem.,* **1988**, 352, 205.

179. I. J. Lin, C. S. Vasam, *Can. J. Chem.,* **2005**, 83, 6.

180. A. S. K. Hashmi, Y. Yu, F. Rominger, *Organometallics,* **2012**, 31, 895.

181. L. Falivene, Z. Cao, A. Petta, K. Serra, A. Poater, R. Oliva, V. Scarano, L. Cavallo, *Nat. Chem.*, **2019**, 11, 872.

182. D. Roddick, *Organometallic Pincer Chemistry,* **2012**, 49.

183. J. Gazao, I. B. Bersuker, J. Garaj, M. Kabesova, J. Kohout, H. Langfelderova, M. Melnik, S. F. Valach, *Coord. Chem. Rev.,* **1976**, 19, 253.

184. A. Luquin, E. Cerrada, M. Laguna, in *Gold chemistry: Applications and future directions in the life sciences*, **2009**, 93.

185. H. -W. Wanzlick, H. -J. Schonherr, *Angew. Chem. Int. Ed.,* **1968**, 7, 141.

186. (a) F. Schulz, I. Pantenburg, D. Naumann, Z. Anorg, Allg, Chem., 2005, 631, 649. (b) B. Korpar-Colig, Z. Popovic, M. Bruvo, I. Vickovic, *Inorg. Chim. Acta.*, **1988**, 150, 113. (c) D. Naumann, F. Schulz, I. Pantenburg, W. Tyrra, *Z. Anorg. Allg. Chem.*, **2004**, 630, 529. (d) M. Nolte, I. Pantenburg, G. Meyer, *Z. Anorg. Allg. Chem.*, **2005**, 631, 649.

187. A. Bauza, I. Alkorta, J. Elguero, T. J. Mooibroek, A Frontera, *Angew. Chem. Int. Ed.*, **2020**, 59, 17482.

188. (a) M. V. Baker, D. H. Brown, R. A. Haque, P. V. Simpson, B. W. Skelton, A. H. White, C. C. Williams, *Organometallics,* **2009**, 28, 3793. (b) M. Atif, H. N. Bhatti, M. A. Iqbal, Y. Jamil, *J. Coord. Chem.,* **2020**, 73, 1377.

189. V. Lavallo, Y. Canac, B. Donnadieu, *Angew. Chem. Int. Ed.,* **2006**, 45, 3488.

190. K. D. Wells, R. McDonald, M. J. Ferguson, M. Cowie, *Inorg. Chem.,* **2011**, 50, 3523.

191. T. Chivers, R. S. Laitinen, *Chem. Soc. Rev.,* **2015**, 44, 1725.

192. (a) C. A. Tolman, *J. Am. Chem. Soc.,* **1970**, 92, 2953. (b) C. A. Tolman, *Chem. Soc. Rev.,* **1972**, 1, 337.

193. (a) J. A. Anthony, *Acc. Chem. Res.,* **1999**, 32, 913. (b) A. Roodt, S. Otto, G. Steyl, *Coord. Chem. Rev.,* **2003**, 245, 121. (c) O. Kuhl, *Coord. Chem. Rev.,* **2005**, 249, 693. (d) D. Cremer, E. Kraka, *Dalton Trans.,* **2017**, 46, 8323. (e) S. Diez-Gonzalez, S. P. Nolan, *Coord. Chem. Rev.,* **2007**, 251, 874.

194. (a) A. R. Chianese, X. Li, C. Janzen, J. W. Faller, R. H. Crabtree, *Organometallics*, **2003**, 22, 1663. (b) S. Wolf, H. Plenio, *J. Organomet. Chem.,* **2009**, 694, 1487.

195. (a) for iridium, see: R. A. Kelly III, H. Clavier, S. Giudice, N. M. Scott, E. D. Stevens, J. Bordner, I. Samardjiev, C. D. Hoff, L. Cavallo, S. P. Nolan, *Organometallics*, **2004**, 23, 2461. (b) for rhodium: T. Droge, F. Glorius, *Angew. Chem. Int. Ed.,* **2010**, 49, 6940.

196. A summary of iridium-NHC complexes used for the data studies can be found at D. J. Nelson, S. P. Nolan, *Chem. Soc. Rev.,* **2013**, 42, 6723.

197. V. Lavallo, Y. Canac, C. Prasang, B. Donnadieu, G. Bertrand, *Angew. Chem. Int. Ed.,* **2005**, 44, 5705

198. H. Huynh, *Chem. Rev.,* **2018**, 118, 9457.

199. C. A. Tolman, *Chem. Rev.,* **1977**, 77, 313.

200. (a) B. M. Neilson, V. M. Lynch, C. W. Bielawski, *Angew. Chem. Int. Ed.,* **2011**, 50, 10322. (b) A. B. Powell, C. W. Bielawski, A. H. Cowley, *J. Am. Chem. Soc.,* **2010**, 132, 10184. (c) S. Chessa, N. J. Clayden, M. Bochmann, J. A. Wright, *Chem. Commun.,* **2009**, 797.

201. S. Fantasia, J. L. Petersen, H. Jacobsen, L. Cavallo, S. P. Nolan, *Organometallics*, **2007**, 26, 5880.

202. H. Huynh, Y. Han, R. Jothibasu, J. Yang, *Organometallics*, **2009**, 28, 5395.

203. Q. Teng, H. Huynh, *Dalton Trans.,* **2017**, 46, 614.

204. First published in: A. Decken, C. J. Carmalt, J. A. C. Clyburne, A. H. Cowley, *Inorg. Chem.,* **1997**, 36, 3741.

205. O. Back, M. Henry-Ellinger, C. D. Martin, D. Martin, G. Bertrand, *Angew. Chem., Int. Ed.*, **2013**, 52, 2939.

206. A. Liske, K. Verlinden, H. Buhl, C. Ganter, *Organometallics,* **2013**, 32, 5269.

207. Z. McCarty, D. Lastovickova, C. Bielawski, *Chem. Commun.,* **2016**, 52, 5447.

208. K. Verlinden, H. Buhl, W. Frank, C. Ganter, *Eur. J. Inorg. Chem.,* **2015**, 2416.

209. A. Liske, K. Verlinden, H. Buhl, K. Schaper, C. Ganter, *Organometallics,* **2013**, 32, 5269.

210. S. Vummaleti, D. Nelson, A. Poater, A. Gomez-Suarez, D. Cordes, A. Slawin, S. P. Nolan, L. Cavallo, *Chem. Sci.,* **2015**, 6, 1895.

211. L. P. Ho, M. Koneczny, T. Bannenberg, M. Tamm, *Inorg. Chem.,* **2021**, 60, 9019.

212. P. Engl, C. Santiago, C. Gordon, W. Liao, A. Fedorov, C. Copéret, M. S. Sigman, A. Togni, *J. Am. Chem. Soc.*, **2017**, 139, 13117.

213. R. Dorta, N. Scott, C. Constabbbile, L. Cavallo, C. Hoff, S. P. Nolan, *J. Am. Chem. Soc.,* **2005**, 127, 2485.

214. T. Agapie, P. L. Diaconescu, C. C. Cummins, *J. Am. Chen. Soc.,* **2002**, 124, 2412.

215. (a) H. Jun, V. G. Young Jr, R. J. Angelici, *J. Am. Chem. Soc.,* **1991**, 113, 9379. (b) L. Weber, I. Schumann, T. Schmidt, H. -G. Stammler, B. Neumann, *Z. Anorg. Allg. Chem.,* **1993**, 619, 1759.

216. M. Braun, W. Frank, C. Ganter, *Organometallics,* **2012**, 31, 1927.

217. H. Buhl, K. Verlinden, C. Ganter, S. Novakovic, C. Bogdanovic, *Eu. J. Inorg. Chem.,* **2016**, 21, 3389.

218. F. Neese, *Wiley Interdiscip. Rev. Comput. Mol. Sci.*, **2018**, 8, e1327.

219. J. Tao, J. P. Perdew, V. N. Staroverov, G. E. Scuseria, *Phys. Rev. Lett.*, , DOI:10.1103/PhysRevLett.91.146401.

220. S. Grimme, S. Ehrlich, L. Goerigk, *J. Comput. Chem.*, **2011**, 32, 1456.

221. C. Van Wüllen, *J. Chem. Phys.*, **1998**, 109, 392.

222. E. Van Lenthe, A. Van Der Avoird, P. E. S. Wormer, *J. Chem. Phys.*, **1998**, 108, 4783.

223. F. Weigend, R. Ahlrichs, *Phys. Chem. Chem. Phys.*, **2005**, 7, 3297.

224. J. D. Rolfes, F. Neese , D. A. Pantazis, *J. Comput. Chem.*, **2020**, 41, 1842.

225. D. A. Pantazis, F. Neese, *J. Chem. Theory Comput.*, **2009**, 5, 2229.

226. D. A. Pantazis, F. Neese, *J. Chem. Theory Comput.*, **2011**, 7, 677.

227. V. Barone and M. Cossi, *J. Phys. Chem. A*, **1998**, 102, 1995.

228. R. Bouten, E. J. Baerends, E. Van Lenthc, L. Visscher, G. Schreckenbach, T. Ziegler, *J. Phys. Chem. A*, **2000**, 104, 5600.

229. C. Adamo, V. Barone, *J. Chem. Phys.*, **1999**, 110, 6158.

230. *The PyMOL Molecular Graphics System*, version 1.8; L. C. C. Schrodinger, New York.

231. F. Pannella, R. Banks, G. Bailey, *Chem. Commun. (London),* **1968**, 1548.

232. A. Montreux, J. C. Delgrange, M. Blanchard, B. Labochinsky, *J. Mol. Catal.*, **1977**, 181, 99.

233. T. J. Katz, *Adv. Organomet. Chem.*, **1979**, 16, 283.

234. R. H. Grubbs, *Prog. Inorg. Chem.*, **1978**, 24, 1.

235. R. R. Schrock, J. H. Wengrovious, J. Sancho, *J. Am. Chem. Soc.*, **1981**, 103, 3932.

236. I. Ibrahem, R. R. Schrock, A. H. Hoveyda, *J. Am. Chem. Soc.*, **2009**, 131, 3844. See review on E/Z olefin metathesis: K. M. Dawood, K. Nomura, *Adv. Synth. Catal.,* **2021**, 363, 1970.

237. (a) R. R. Schrock, S. F. Pedersen, M. R. Churchill, J. W. Ziller, *Organometallics*, **1984**, 3, 1574. (b) R. R. Schrock, S. F. Pedersen, L. Mcullough, M. R. Churchill, J. W. Ziller, *Organometallics*, **1983**, 2, 1046. (c) M. R. Churchill, J. W. Ziller, S. F. Perderson, R. R. Schrock, *J. Chem. Soc. Chem. Commun.*, **1984**, 485.

238. R. R. Schrock, *Chem. Commun.,* **2013**, 49, 5529.

239. (a) H. Ehrhorn, M. Tamm, *Chem. Euro. J.*, **2019**, 25, 3190. (b) X. Wu, M. Tamm, *Beilstein J. Org. Chem.,* **2011**, 7, 82.

240. (a) A. Fürstner, *Acc. Chem. Res.*, **2021**, 54, 861. (b) A. Fürstner, in *Modern Alkyne Chemistry*, Wiley-VCH, **2014**, 69. (c) A. Fürstner, *Angew, Chem. Int. Ed.,* **2013**, 52, 2794.

241. (a) S. Huang, Z. Lei, Y. Jin, W. Zhang, *Chem. Sci.,* **2021**, 12, 9591. (b) B. N. Bhawal, B. Morandi, *Angew. Chem. Int. Ed.,* **2019**, 58, 10074. (c) A. Gradillas, J. Perez-Castells, in *Topics in Heterocycle Chemistry*, Springer, **2017**, 245. H. Yang, Y. Jin, Y. Du, W. Zhang, *J. Mater. Chem. A,* 2014, 2, 5986

242. M. Cui, R. Lin, G. Jia, *Chem. Asian. J.*, **2018**, 13, 895.

243. (a) R. M. Tuggle, D. Weaver, *J. Am. Chem. Soc.,* **1970**, 92, 5523. (b) R. M. Tuggle, D. L. Weaver, *Inorg. Chem.,* **1972**, 11, 2237.

244. (a) P. D. Frisch, G. P. Khare, *Inorg. Chem.,* **1979**, 18, 781. (b) P. D. Frisch, G. P. Khare, *J. Organomet. Chem.,* **1977**, 142, C61.

245. R. P. Hughes, D. S. Tucker, A. L. Rheingold, *Organometallics,* **1994**, 13, 4664.

246. (a) L. L. Padolik, J. Gallucci, A. Wojcicki, *J. Organomet. Chem.,* **1990**, 383, C1. (b) L. L. Padolik, J. Gallucci, A. Wojcicki, *J. Organomet. Chem.,* **1993**, 115, 9986. (c,d) V. Plantevin, A. Wojcicki, *J. Organomet. Chem.,* **2004**, 689, 2000, *ibid,* 2013.

247. (a) Y. Wakatsuki, S. Miya, H. Yamazaki, *J. Chem. Soc. Dalton Trans.,* **1986**, 1201. (b) Y. Wakatsuki, S. Miya, H. Yamazaki, *J. Chem. Soc. Dalton Trans.,* **1986**, 1207. (c) J. Torres-Alacan *et. al.*, *Chem. Eur. J.,* **2015**, 21, 17184. (d) B. Wezisla, J. Lindner, U. Das, A. C. Filippou, P. Voehringer, *Angew. Chem. Int. Ed.,* **2017**, 56, 6901. (e) C. J. Adams, K. M. Anderson, I. M. Bartlett, N. G. Connelly, A. G. Orpen, T. J. Paget, H. Phetmung, D. W. Smith, *J. Chem. Soc. Dalton Trans.,* **2001**, 1284.

248. (a) I. A. Latham, L. R. Sita, R.R. Schrock, *Organometallics*, **1986**, 5, 1508. (b) A. M. Geyer, R. L. Gdula, E. S. Wiedner, M. J. Johnson. *J. Am. Chem. Soc.*, **2007**, 129, 3800.

249. G. P. Elliott, W. R. Roper, *J. Organomet. Chem.,* **1983**, 250, C5.

250. G. R. Clark, G. L. Lu, W. R. Roper, L. J. Wright, *Organometallics*, **2007**, 26, 2167.

251. (a) R.R. Schrock, S. F. Pedersen, M. R. Churchill, *Organometallics*, **1984**, 270, 201. (b) M. R. Curchill, H. J. Easserman, *J. Organometal. Chem.*, **1984**, 270, 201. (c) J. H. Freudenberger, R. R. Schrock, M. R. Churchill, A. L. Rheingold, J. W. Ziller, *Organometallics,* **1984**, 3, 1554. (d) S. A. Krouse, R. R. Schrock, *Macromolecules*, **1989**, 22, 2589. (e) M. R. Churchill, J. W. Ziller, J. H. Freudenberger, R. R. Schrock, *Organometallics,* **1984**, 3, 1554.

252. (a) H. Van der Heijden, A. W. Gal, P. Pasman, *Organometallics*, 1985, 4, **1847**. (b) R. Ramirex-Contreras, N. Bhuvanesh, O. V. Ozerov, *Organometallics*, **2015**, 34, 1143.

253. (a) C. Zhu, Y. Yang, M. Luom C. Yang, J. Wu, L. Chen, G. Liu, T. Wen, J. Zhu, H. Xai, *Angew. Chem. Int. Ed.,* **2015**, 54, 6181. (b) U. Das, Dissertation Thesis, University of Bonn (ISBN: 978-973-86387-551-0), **2014**.

254. B. Haberlag , M. Freytag , C. G. Daniliuc , P. G. Jones, M. Tamm , *Angew. Chem., Int. Ed.*, **2012**, 51 , 13019.

255. W. E. Bachmann, H. T. Clarke, *J. Am. Chem. Soc.,* **1927**, 49, 2089.

256. J. D. Roberts, H. E. Simmons, L. A. Carlsmith, C. W. Vaughan, *J. Am. Chem. Soc,* **1953**, 75, 3290.

257. S. McLain, R. R. Schrock, P. Sharp, M. Churchill, W. Youngs, *J. Am. Chem. Soc.*, **1979**, 101, 263.

258. J. G. Andino, U. J. Kilgore, M. Pink, A. Ozarowski, J. Krzystek, J. Tesler, M. -H. Baik, D. J. Mindiola, *Chem. Sci.,* **2010**, 1, 351.

259. (a) C. Boulho, P. Oulie, L. Vendier, M. Etienne, V. Pimienta, A. Locati, F. Bessac, F. Maseras, D. A. Pantazis, J. E. McGrady, *J. Am. Chem. Soc.,* **2010**, 132, 14239. (b) K. Wada, C. B. Pamplin, P. Legzdins, *J. Am. Chem. Soc.,* **2002**, 124, 9680. (c) L. Giannini, A. Caselli, E. Solari, C. Floriani, A. Chiesi-Villa, C. Rizzoli, N. Re, A. Sgamelloti, *J. Am. Chem. Soc.,* **1997**, 119, 9198. (d) J. K. F. Bujink, K. R. Kloetstra, A. Meetsma, J. H. Tueben, W. J. J. Smeets, A. L. Spek, *Organometallics,* **1996**, 15, 2523. (e) K. Mashima, Y. Tanaka, A. Nakamura, *Organometallics,* **1995**, 14, 5642. (f) M. I. Bruce, G. A. Koutsantonis, M. J. Liddell, E. R. T. Tiekink, *J. Organomet. Chem.* **1991**, 420, 253.

260. (a) (a) H. J. S. Winkler, G. Wittig, *J. Org. Chem.* **1963**, 28, 1733. (b) C. D. Cook, G. S. Jauhal, *J. Am. Chem. Soc.,* **1968**, 90, 1464. (c) T. L. Gilchrist, F. J. Graveling, C. W. Rees, *J. Chem. Soc.*, **1971**, C, 977

261. M. A. Bennett, T. W. Hambley, N. K. Roberts, G. B. Robertson, *Organometallics*, **1985**,4, 1992

262. M. A. Bennett, T. Dirnberger, D. C. R. Hockless, E. Wenger, A. C. Willis, *J. Chem Soc. Dalton Trans.,* **1998**, 271.

263. R. Hughes, R. B. Laritchev, A. Williamson, C. D. Incarvito, L. N. Zakharov, A. L. Rheingold, *Organometallics*, **2002**, 21, 4873.

264. A. M. Orendt, J. C. Facelli, J. G. Radziszewski, W. J. Horton, D. M. Grant, J. Michl, *J. Am. Chem. Soc.*, **1996**, 118, 846.

265. M. A. Bennett, T. W. Hambley, N. K. Roberts, G. B. Robertson, *Organometallics*, **1985**, 4, 1992.

266. R. Hughes, R. Laritchev, A. Williamson, C. Incarvito, L. Zakharov, A. Rheingold, *Organometallics*, **2003**, 22, 2134.

267. (a) G. Gautheron, G. Tainturier, S. Pouly, *Organometallics,* **1984**, 38, 1495. (b) G. Erker, P. Czisch, R. Mynott, Y. -H. Tsay, C. Kruger, *Organometallics*, **1985**, 4, 1310.

268. H. J. R. deBoer, O. S. Akkerman, F. Bickelhaupt, G. Erker, P. Czisch, R. Mynott, J. M. Wallis, C. Kruger, *Angew. Chem. Int. Ed.*, **1986**, 25, 639.

269. G. Erker, U. Dorf, R. Mynott, Y. -H. Tsay, C. Kruger, *Angew. Chem. Int. Ed.*, **1985**, 97, 572.

270. (a) J. Mattia, M. B. Humphrey, R. D. Rogers, J. L. Atwood, M. D. Rausch, *Inorg. Chem.,* **1978** 17, 3257. (b) M. D. Rausch, E. A. Mintz, *J. Orgamoet. Chem.*, **1980**, 190, 65.

271. E. G. Berkovich, V. B. Shur, M. E. Vol'pin, B. Lorenz, S. Rummel, M. Wahren, *Chem. Ber.,* **1980** 113, 70.

272. Y. Himeshima, T. Sonoda, H. Kobayashi, *Chem. Lett.*, **1983**, 12, 1211.

273. J. Shi, L. Li, Y. Li, *Chem. Rev.*, **2021**, 121, 3892.

274. (a) J. Garcia-Lopez, M. Oliva-Madrid, I Saura-Llamas, D. Bautista, J. Vicente, *Chem. Commun.*, **2012**, 48, 6744. (b) M. Oliva-Madrid, I Saura-Llamas, D. Bautista, J. Vicente, *Chem. Commun.*, **2013**, 49, 7997.

275. C. Zhu, S. Li, M. Luo, X. Zhou, Y. Niu, M. Lin, J. Zhu, Z. Cao, X. Lu, T. Wen, Z. Xie, P. R. Schleyer, H. Xia, *Nat. Chem.,* **2013**, 5, 698.

276. E. Bleuel, O. Gevert, A. M. Laubender, H. Werner, *Organometallics*, **2000**, 19, 3109.

277. (a) J. Rourke, A. Batsanov, J. Howard, T. Marder, *Chem. Commun.,* **2001**, 1, 2626. (b) A. Steffen, R. Ward, M. G. Tay, R. M. Edkins, F. Seeler, M. van Leeuwen, L. -O. Palsson, A. Beeby, A. S. Batsanov, J. A. K. Howard, T. B. Marder, *Chem. Eur. J.,* **2014**, 20, 3652. (c) C. Sieck, M. G. Tay, M. -. Thibault, R. M. Edkins, K. Costuas, J. -F. Halet, A. S. Batsanov, M. Haehnel, K. Edkins, A. Lorbach, A. Steffen, T. B. Marder, *Chem. Eur. J.,* **2016**, 22, 10523.

278. M. Cowie, S. K. Dwight, *Inorg. Chem.,* **1979**, 18, 2700.

279. Published as part of H. J. Barnett, L. K. Burt, A. F. Hill, *Dalton Trans.,* **2018**, 47, 9570.

280. J. C. Peters, A. L. Odom, C. C. Cummins, *Chem. Commun*., **1997**, 1995.

281. A. Reinholdt, K. Herbst, J. Bendix, *Chem. Commun.,* **2016**, 52, 2015.

282. S. Kallane, T. Braun, M. Teltewskoi, B. Braun, R. Herrmann, R. Laubenstein, *Chem. Commun.,* **2015**, 51, 15613.

283. For a much more in-depth review of shielding tensors, see: J. C. Facelli, *Prog. Nucl. Magn. Reson. Spectrosc.*, **2011**, 58, 176.

284. (a) N. F. Ramsey, *Phys. Rev.,* **1952**, 86, 243. (b) P. Pyykkö, *Theor. Chem. Acc.,* **2000**, 103, 214.

285. C. Widdifield, R. Schurko, *Concepts in Magnetic Resonance Part A,* **2009**, 34, 91.

286. D. Cozaklan, S. Butlerlone, M. Baibich, *J. Organomet. Chem.,* **1979**, 169, 381.

287. (a) K. Yamamoto, C. P. Gordon, W. -C. Liao, C. Coperet, C. Raynaud, O. Eisenstein, *Angew. Chem., Int. Ed.,* **2017**, 56, 10127. (b) C. Gordon, C. Raynaud, R. Anderson, C. Coperet, O. Eisenstein, *Acc. Chem. Res.,* **2019**, 52, 2278.

288. A. Ehlers, Y. Ruiz-Morales, E. Baerends, T. Ziegler, *Inorg. Chem.,* **1997**, 26, 5031.

289. J. Vicha, M. Straka, M. L. Munzarova, R. Marek, *J. Chem. Theory Comput.,* **2014**, 10, 1489.

290. M. Kaupp, O. L. Malkina, V. G. Malkin, P. Pyykkö, *Chem. Eur. J.*, **1998**, 4, 118.

291. (a) S. Wolff, T. Ziegler, *Chem. Phys.*, **1998**, 109, 895. (b) M. Hyvärinen, J. Vaara, A. Goldammer, B. Kutzky, K. Hegetschweiler, M. Kaupp, M. Straka, *J. Am. Chem. Soc.*, **2009**, 131, 11909.

292. (a) L. A. Truflandier, E. Brendler, J. Wagler, J. Autschbach, *Angew. Chem., Int. Ed.,* **2011**, 50, 255. (b) T. Pawlak, M. L. Munzarová, L. Pazderski, R. J. Marek, *Chem. Theory Comput.*, **2011**, 7, 3909.

293. For a detailed overview of ^{103}Rh NMR, see: L. Carlton, *Annual Reports on NMR Spectroscopy,* **2008**, 63, 49.

294. B. Bender, M. Koller, D. Nanz, W. von Philipsborn, *J. Am. Chem Soc.,* **1993**, 115, 5889.

295. R. Fornika, H. Gorls, B. Seemann, W. Leitner, *J. Chem. Soc., Chem Commun.,* **1995**, 14, 1479.

296. E. Maurer, S. Rieker, M. Schollbach, A. Schwenk, T. Egolf, W. von Philipsborn, *Helv. Chim. Acta*, **1982**, 65, 26.

297. D. Gill, O. Gansow, F. Bennis, K Ott, *J. Mag. Res.,* **1979**, 35, 459.

298. J. Ernsting, S. Gaemers, C. Elsevier, *Mag. Reson. Chem.,* **2004**, 42, 721.

299. (a) J. M. Ernsting, C. J. Elsevier, W. G. J. de Lange, K. Timmer, *Magn. Reson. Chem.*, **1991**, 29, S118. (b) W. Leitner, M. Buhl, R. Fornika, C. Six, W. Baumann, E. Dinjus, M. Kessler, C. Kruger, A. Rufinska, *Organometallics*, **1999**, 18, 1196. (c) F. R. Bregman, J. M. Ernsting, F. Muller, M. D. K. Boele, L. A. van der Veen, C. J. Elsevier, *J. Organomet. Chem.*, **1999**, 592, 306.

300. T. G. Cherkasova , Y. S. Varshavsky, I. S. Podkorytov, L. V. Osetrova, *Rhodium Express*, **1993**, 21.

301. U. E. Bucher, A. Currao, R. Nesper, H. Ruegger, L. M. Venanzi, E. Younger, *Gaz. Chim. Ital.*, **1995**, 125, 181.

302. U. E. Bucher, A. Currao, R. Nesper, H. Ruegger, L. M. Venanzi, E. Younger, *Inorg. Chem.,* **1995**, 34, 66.

303. M. Cocivera, A. J. McAlees, R. McCrindle, P. Szczecinski, *J. Organomet. Chem.,* **1982**, 235, 97.

304. B. Akermark, K. Warnmark, K. Zetterberg, M. Blomberg, J. Glaser, L. Ohrstrom, S. Wahlberg, *Organometallics*, **1991**, 10, 733.

305. C. Arz, P. Pregosin, C. Anklin, *Mag. Reson. Chem.,* **1987**, 25, 158.

306. L. Orian, A. Bisello, S. Santi, A. Ceccon, G. Saielli, *Chem. Eur. J.,* **2004**, 10, 4029.

307. T. M. Gilbert, T. Ziegler, *J. Phys. Chem. A,* **1999**, 103, 7535.

308. B. Heaton, C. Jacob, S. Moffet, *J. Organomet. Chem.,* **1993**, 462, 347.

309. I. Mirzaeva, S. Kozlova, *J. Struct. Chem.,* **2019**, 60, 1750.

310. I. Mirzaeva, D. Mainichev, S. Kozlova, *J. Phys. Chem. A,* **2016**, 120, 1944.

311. D. Milstein, C. Elsevier, J. Ott, M. Aizenberg, *J. Organomet. Chem.,* **1998**, 551, 81.

312. P. Mandal, A. Majumdar, *Concepts in Magnetic Resonance,* **2004**, 20A, 1.

313. C. Brevard, G. van Stein, G. van Koten, *J. Am. Chem. Soc.,* **1981**, 103, 6746.

314. E. Kolehmainen, *Encyclopedia of Spectroscopy and Spectrometry*, **2017**, 366.

315. R. Benn, C. Brevard, *J. Am. Chem. Soc.,* **1986**, 108, 5622.

316. (a) T. Brown, P. Green, *J. Am. Chem. Soc.,* **1969**, 91, 3378. (b) T. Brown, P. Green, *J. Am. Chem. Soc.,* **1970**, 92, 2359.

317. N. Tan, P. V. Simpson, G. L. Nealon, A. N. Sobolev, P. Raiteri, M. Massi, M. I. Ogden, A. B. Lowe, *Eur. J. Inorg. Chem.,* **2019**, 5, 592.

318. K. B. Wiberg, J. D. Hammer, K. W. Zilm, J. R. Cheeseman, *J. Org. Chem.,* **1999**, 64, 6394.

319. M. Buhl, C. Reimann, D. A. Pantazis, T. Bredow, F. Neese, *J. Chem. Theory Comput.*, **2008**, 4, 1449.

320. (a) G. Schreckenbach, T. Ziegler, *Int. J. Quantum Chem.,* **1997**, 61, 899. (b) D. A. Pantazis, Z. -Y. Chen, C. R. Landis, F. Neese, *J. Chem. Theory Comput.*, **2008**, 4, 908. (c) F. Aquino, N. Govind, J. Austchbach, *J. Chem. Theory Comput.*, **2011**, 7, 3278.

321. G. R. Clark, T. J. Collins, S. M. James, W. R. Roper, K. G. Town, *J. Chem. Soc. Chem. Commun.*, **1976**, 475.

322. Mentioned in: P. Bast, S. Berger, H. Gunther, *Magn. Reson. Chem.,* **1992**, 30, 587.

323. K. Koch, L. Engelbrecht, *Dalton Trans.,* **2017**, 46, 9303.

324. E. Lindner, B. Keppeler, R. Fawzi, M. Steimann, *Chem. Ber.*, **1996**, 129, 1103.

325. R. K. Harris, E. D. Becker, S. M. Cabral de Menezes, P. Granger, R. E. Hoffman, K. W. Zilm, *Pure Appl. Chem.*, **2008**, 80, 59.